frontiers | Research Topics

Next generation MSC therapy manufacturing, potency and mechanism of action analysis

Edited by
Raghavan Chinnadurai, Guido Moll and Sowmya Viswanathan

Published in
Frontiers in Immunology

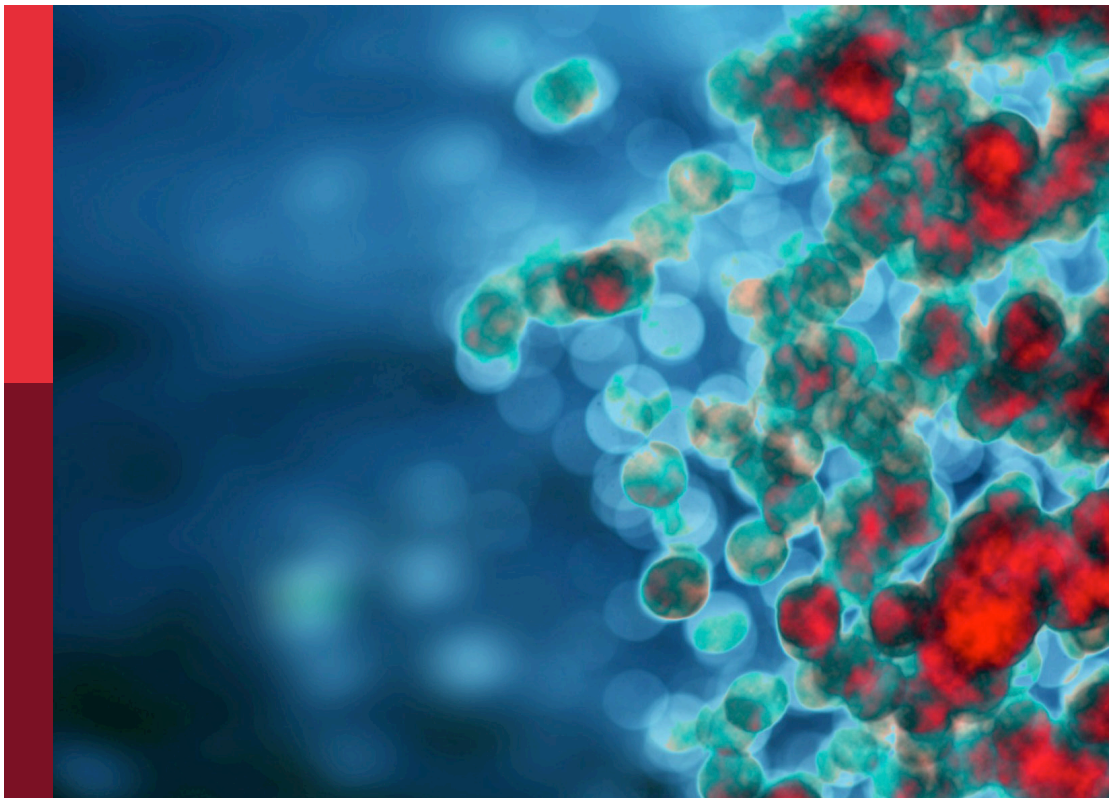

ISSN 1664-8714
ISBN 978-2-8325-2359-9
DOI 10.3389/978-2-8325-2359-9

About Frontiers

Frontiers is more than just an open access publisher of scholarly articles: it is a pioneering approach to the world of academia, radically improving the way scholarly research is managed. The grand vision of Frontiers is a world where all people have an equal opportunity to seek, share and generate knowledge. Frontiers provides immediate and permanent online open access to all its publications, but this alone is not enough to realize our grand goals.

Frontiers journal series

The Frontiers journal series is a multi-tier and interdisciplinary set of open-access, online journals, promising a paradigm shift from the current review, selection and dissemination processes in academic publishing. All Frontiers journals are driven by researchers for researchers; therefore, they constitute a service to the scholarly community. At the same time, the *Frontiers journal series* operates on a revolutionary invention, the tiered publishing system, initially addressing specific communities of scholars, and gradually climbing up to broader public understanding, thus serving the interests of the lay society, too.

Dedication to quality

Each Frontiers article is a landmark of the highest quality, thanks to genuinely collaborative interactions between authors and review editors, who include some of the world's best academicians. Research must be certified by peers before entering a stream of knowledge that may eventually reach the public - and shape society; therefore, Frontiers only applies the most rigorous and unbiased reviews. Frontiers revolutionizes research publishing by freely delivering the most outstanding research, evaluated with no bias from both the academic and social point of view. By applying the most advanced information technologies, Frontiers is catapulting scholarly publishing into a new generation.

What are Frontiers Research Topics?

Frontiers Research Topics are very popular trademarks of the *Frontiers journals series*: they are collections of at least ten articles, all centered on a particular subject. With their unique mix of varied contributions from Original Research to Review Articles, Frontiers Research Topics unify the most influential researchers, the latest key findings and historical advances in a hot research area.

Find out more on how to host your own Frontiers Research Topic or contribute to one as an author by contacting the Frontiers editorial office: frontiersin.org/about/contact

Next generation MSC therapy manufacturing, potency and mechanism of action analysis

Topic editors
Raghavan Chinnadurai — Mercer University, United States
Guido Moll — Charité University Medicine Berlin, Germany
Sowmya Viswanathan — University Health Network, Canada

Citation
Chinnadurai, R., Moll, G., Viswanathan, S., eds. (2023). *Next generation MSC therapy manufacturing, potency and mechanism of action analysis*.
Lausanne: Frontiers Media SA. doi: 10.3389/978-2-8325-2359-9

SV has 60% ownership in Regulatory Cell Therapy Consultants Inc. which does not pose real or perceived conflict of interest.

The remaining authors declare that the research was conducted in the absence of any commercial or financial relationships that could be construed as a potential conflict of interest

Table of contents

frontiers | Frontiers in Immunology

TYPE Editorial
PUBLISHED 21 April 2023
DOI 10.3389/fimmu.2023.1192636

OPEN ACCESS

EDITED AND REVIEWED BY
Denise L. Doolan,
James Cook University, Australia

*CORRESPONDENCE
Raghavan Chinnadurai
chinnadurai_r@mcercer.edu
Sowmya Viswanathan
sowmya.viswanathan@uhnresearch.ca
Guido Moll
guido.moll@charite.de

†These authors have contributed equally to this work

SPECIALTY SECTION
This article was submitted to Vaccines and Molecular Therapeutics, a section of the journal Frontiers in Immunology

RECEIVED 23 March 2023
ACCEPTED 04 April 2023
PUBLISHED 21 April 2023

CITATION
Chinnadurai R, Viswanathan S and Moll G (2023) Editorial: Next generation MSC therapy manufacturing, potency and mechanism of action analysis. *Front. Immunol.* 14:1192636. doi: 10.3389/fimmu.2023.1192636

Editorial: Next generation MSC therapy manufacturing, potency and mechanism of action analysis

Raghavan Chinnadurai [1*†], Sowmya Viswanathan [2,3,4*†] and Guido Moll [5,6,7*†]

[1]Department of Biomedical Sciences, Mercer University School of Medicine, Savannah, GA, United States, [2]Osteoarthritis Research Program, Division of Orthopedic Surgery, Schroeder Arthritis Institute, University Health Network, Toronto, ON, Canada, [3]Krembil Research Institute, University Health Network, Toronto, ON, Canada, [4]Institute of Biomedical Engineering, Division of Hematology, Department of Medicine, University of Toronto, Toronto, ON, Canada, [5]BIH Center for Regenerative Therapies (BCRT), Berlin, Germany, [6]Berlin-Brandenburg School for Regenerative Therapies (BSRT), Berlin, Germany, [7]Department of Nephrology and Internal Intensive Care Medicine, all Charité Universitätsmedizin Berlin, corporate member of Freie Universität Berlin, Humboldt-Universität zu Berlin, Berlin Institute of Health (BIH), Berlin, Germany

KEYWORDS

mesenchymal stromal/stem cells (MSC), cell product manufacturing, mechanism of action (MOA), safety and efficacy, potency analysis, cell therapy, immunomodulation, and regeneration

Editorial on the Research Topic
Next generation MSC therapy manufacturing, potency and mechanism of action analysis

Introduction

Mesenchymal stromal/stem cells (MSCs) are non-hematopoietic cells found in vascularized tissues and organs, that possess profound immunomodulatory and regenerative properties, which warrant their application in cellular and regenerative therapy (1–7). Regulatory authorities have already approved MSC therapies for several clinical conditions, such as Graft-versus-Host Disease (GvHD), Perianal Fistula in Crohn's Disease, and Critical Limb Ischemia (6, 7). However, there are still some limitations with this novel type of cell therapy that need to be understood and addressed, and thus form the basis for this and other earlier Research Topics (2, 3). These concerns are mainly due to contradictory results on MSCs' therapeutic efficacy profile in preclinical models compared to real-world experience in different clinical indications (7–9). In addition, there are also some minor safety concerns related to systemic infusion that should not be overlooked (4, 5, 10). However, both efficacy and safety limitations may be overcome through improved

understanding of MSC product properties, handling, and function (2, 4, 5, 9, 11–19). Indeed, any remaining limitations with this novel type of therapy may be largely due to variations in MSC products, their manufacturing practices, a lack of understanding on their optimal clinical delivery, their *in vivo* mechanism of action (MoA), and the concomitant clinical indications, and in particular the insufficient clinical potency assessment (4, 5, 9, 11–23). In this Research Topic, we have collected 13 original research and review articles that address new strategies for improved manufacturing, and MoA and potency assessment in clinical trials, for the design of next-generation MSC therapies with optimal clinical efficacy and safety Figure 1.

Fresh vs frozen thawed MSCs

Clinical use of cryopreserved "off-the-shelf" MSC products is a feasible strategy in which cryopreserved cells are thawed near the bedside and infused immediately into the patients (11). This strategy has been discussed as a potential confounder of MSC efficacy since preclinical data have shown a discrepant functionality of MSCs immediately post thawing (11, 16, 24–31). These prompted insights on the clinical testing of "fresh MSCs" either derived from actively growing culture or post thaw culture rescued from cryopreservation. Stenger et al. tested the safety of autologous "fresh MSCs" in 11 patients with GvHD (n=4 Acute; n=7 Chronic). Culture rescue was deployed in a multi-dosing strategy where bone marrow (BM)-MSCs were expanded and cryobanked from a single BM aspiration. Subsequently, the cells were thawed and culture rescued for 72 hours prior to infusion. Intravenous (IV) infusions of fresh MSCs were well tolerated in these patients and no dose associated toxicity was observed. Three out of four acute GvHD patients displayed partial to complete responses to fresh MSCs. In chronic GvHD, three-month overall responses were partial (n=5), stable (n=1) and progressive (n=1). Although this study's primary endpoint is safety, the efficacy data, particularly for acute GvHD, are encouraging, since the responses are equivalent to FDA approved second line treatments for steroid resistant GvHD. Ekpo et al. put forth an opinion paper on cryopreservation of cell-based drug delivery systems. The authors emphasize, when stem cells (ex. MSCs) are utilized as a vehicle for drug delivery, cryopreservation formulations need to be well researched, since the cryopreservation process could negatively impact the functionality of drug formulations and their therapy efficacy. Fernandez-Santos et al. provided a general guide, including rules and legislation, for homogenous MSC manufacturing, cell banks, optimal cryopreservation and post thaw potency assessments for improved therapy. In support, Willer et al. demonstrated that pooled human BM-MSCs during cell

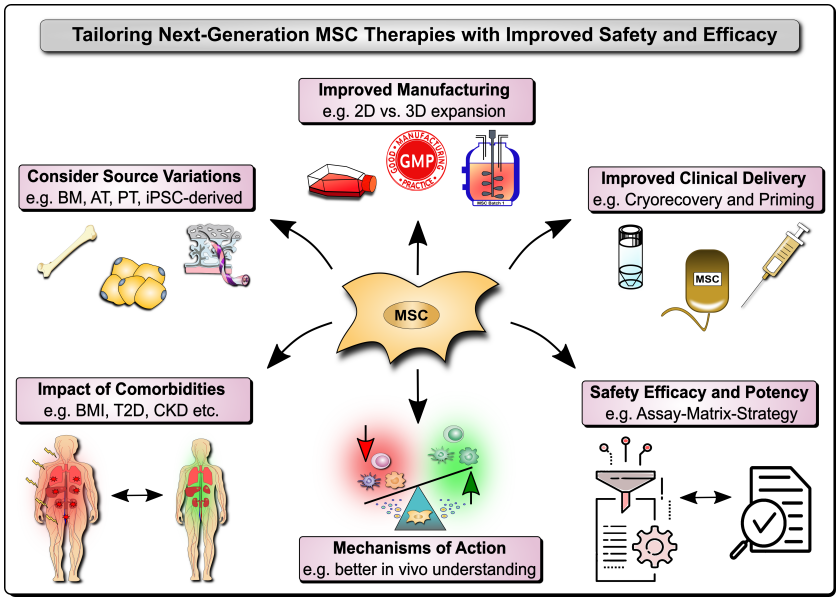

FIGURE 1
Next Generation MSC Therapy Manufacturing, MoA and Potency Analysis. Next-generation MSC therapy improvements to safety and efficacy include among others: 1) Considerations on variations in the MSC source material, e.g. typically including bone marrow (BM), adipose tissue (AT), perinatal tissue (PT), and induced pluripotent stem cell (iPSC)-derived MSC products; 2) The relevant impact of donor comorbidities, e.g. the role of the body mass index (BMI), obesity, and the typically associated common comorbidities that are increasing in the population, such as type 2 diabetes (T2D) and chronic kidney disease (CKD); 3) Improved MSC product manufacturing, e.g. 2D vs. 3D expansion and in particular the anticipation of the degree of cell expansion and respective loss of potency, but also concomitant safety considerations; 4) Improved clinical delivery of MSC products, e.g. anticipating the role of cryopreservation and freeze-thawing, but also various cell priming strategies, such as cytokine and mechano-transduction licensing; and 5) Better understanding of the mechanisms of action (MoA) of MSC products *in vitro* and particularly *in vivo* in respective patients and clinical cohorts with their very own specific requirements and covariates that may confound treatment safety and efficacy; and 6) Coordinated and relevant safety, efficacy, and potency Assessment with suitable approaches, e.g. the combinatorial assay-matrix-approach, and concomitant potency screening but also potency and safety improvements.

manufacturing process minimize product variations and accelerate effective wound healing in the animal model. This "decision-making approach" identified the preferable use of fresh MSCs over readily thawed MSCs and the significance of repeated delivery for future clinical wound healing studies. Accomplishment of sustained efficacy of MSCs is imminent in moving forward and thus inclusion of the "Freeze-Thawing" confounder in the cell manufacturing needs to be taken into consideration.

Potency metrics of MSCs

Potency analysis is now often mandatory for determining MSCs' release criteria as cellular therapeutics in advanced clinical trials and marketing approval depending on the regional regulatory requirements (32). Considering the complex MoA and the involvement of more than one single effector molecule/pathway associated with MSCs' functionality, a "combinatorial-potency-assay-matrix" approach to define MSC potency has recently been proposed by the International Society for Cell Therapy (ISCT) (22, 30). Robb et al. developed an innovative, sensitive and quantitative assay matrix strategy to define putative critical quality attributes of adipose tissue (AT)-derived AT-MSCs and to distinguish some critical processing parameters and the impact of donor heterogeneity. This strategy included combinatorial analysis of AT-MSCs' morphometrics, gene and protein multiplex, and functionality, such as macrophage polarization and angiogenic fitness. This multivariate assay-matrix-strategy identified panels of putative critical quality attributes for immunomodulatory and angiogenesis fitness (with minimum and maximum value ranges), which can be used to screen culture conditions and potential donors for optimal MSC potency. Wiese et al. deployed a robust and standardized potency assay to identify tissue specific effector molecules on MSCs. Umbilical cord (UC)- and BM-derived MSCs were compared with and without exogenous cytokine activation for the enumeration and quantification of effector genes and soluble analytes as a surrogate measure of potency, to correlate them in the future with functional clinical outcomes (positive/negative). This cytokine activation strategy attenuated heterogeneity of unstimulated MSC populations and thus can inform a more standardized potency assay.

Augmentation of MSC's potency

First generation clinical trials largely employed MSCs in their non-activated "resting stage", while preclinical studies provided pathway to inform on second generation clinical trials with augmented potency involving not only primed/activated/preconditioned MSCs (33), but also their products such as exosomes and extracellular vesicles (EVs) (34). Hackel et al. compared the immunoregulatory properties of unstimulated and cytokine-cocktail-licensed/primed MSCs and their EVs, to obtain more robust therapeutic responses *in vivo*. EVs derived from cytokine-cocktail-primed MSCs displayed enhanced therapeutic efficacy in the animal model of GvHD, which was abrogated with the blockade of PD1-PDL1/PDL2 pathway. This strategy provided insights that EVs from primed MSCs can be used therapeutically with augmented potency. In contrast to cytokine mediated priming, Skibber et al. deployed a mechano-transduction strategy with distinct biomechanical cue named Wall Shear Stress (WSS) to enhance MSC potency. The WSS-conditioning did not affect MSCs' viability and identity, but enhanced their immunomodulatory potency. This mechanotransduction mediated priming is an exciting step forward, since it can be easily translated to enhance MSCs' potency. Boland et al. reviewed the challenges of employing resting MSCs in patients with comorbidities, such as obesity, since obese microenvironment alters the immunomodulatory functions of MSCs (35). The authors propose that "one size fits all" strategy may not work when considering diverse comorbidities. Utilizing such an approach may not only mitigate the potency of MSCs, but also compromise patient safety due to the thromboembolic nature of obesity and its associated cardiovascular comorbidities (2, 4–6, 10, 14, 15, 19, 36, 37). Consistent with other studies, the authors propose that clinical studies should consider priming of MSCs and anti-thrombotic prophylaxis for patients with obesity and metabolic disorders, to lower any apparent risk of severe thromboembolic events (e.g. venous or pulmonary thromboembolism), which is a well-known potential side-effect of MSC infusion undertaken without the necessary precautions or awareness (2, 4–6, 10, 13–15, 19, 36, 37).

Reprogramming and genetic manipulation of MSCs

Although MSCs are considered more-than-minimally-manipulated cell therapy products by regulatory authorities, advances are necessary to reprogram and genetically manipulate MSCs for the management of certain illness. Balina-Sanchez et al. demonstrated the feasibility of reprogramming and generating induced pluripotent stem cell (iPSC)-derived MSCs from urine epithelial cells of pediatric patients with brain tumor. This study also showed that these reprogrammed MSC populations from brain tumor patients are equivalent to healthy controls in their immunomodulatory functions. This brings insights on the utility of non-invasive technology to manufacture MSCs for the investigational clinical use in pediatric patients. Ramamurthy et al. detailed challenges and drawbacks of gene editing/addition strategies to produce FVIII in placenta derived MSCs. Although reporter genes can be efficiently inserted to the specific locus utilizing CRISPR/CAS9 strategy, transgene of FVIII could not be knocked in due to the size limitation. Transgene or CRISPR/CAS9 introduction using plasmids upregulates several proinflammatory Toll Like Receptors and stress responses in endoplasmic reticulum which can intervene MSCs' functionality. These raise caution when utilizing gene addition strategies on human MSCs.

MSC therapy for COVID 19 and mechanism of action

MSC's beneficial lung homing, immunosuppressive and regenerative properties have attracted their use to mitigate acute respiratory distress syndrome (ARDS) resulting from coronavirus-induced disease-2019 (COVID-19) (6, 10, 38). Gregoire et al. tested the safety and efficacy of IV infusions of BM-MSCs in eight patients with severe COVID-19 who were admitted in intensive care unit. No adverse effect related to MSC infusion was observed in these patients. Retrospect comparison with the matched patient controls has demonstrated that survival is significantly higher for patients receiving MSC therapy. In contrast to Stenger et al., this clinical trial utilized immediately thawed MSCs, which is a feasible strategy in medical emergency management situations. However, preclinical data also has demonstrated that cytokine priming strategies and other cryopreservation optimization strategies can be deployed to attenuate the cellular injury associated with freeze thawing (11, 16, 27, 31, 39, 40). Adoption of these strategies in cell manufacturing and clinical utilization would further enhance the efficacy of MSCs for clinical emergency management. Nevertheless, the MoA of MSCs in executing anti-inflammation and immunoregulation in mitigating the severity of COVID-19 akin to ARDS is yet to be understood (2, 10, 41). Indeed, the MoA of MSCs upon infusion into patients is highly complex, and this knowledge is still developing (5, 10, 41), though at least three major MoAs has been proposed including differentiation into mesodermal tissues, modulation of immune cells, and in particular the polarization of macrophages with efferocytosis of apoptotic MSCs (23, 42, 43), although *in vivo* engraftment and differentiation of MSCs is only transient and very minimal at least in part due to triggering of the Instant Blood-Mediated Inflammatory Reaction (IBMIR) and the concomitant rapid destruction of the majority of the infused cells (4, 5, 12–16, 27, 39); Indeed, typically >80% of the therapeutic cells are lost within the first 24 hours post infusion. Zheng et al. provided key insights on the MoA of MSCs involving efferocytosis, a phenomenon in which apoptotic debris is cleared by phagocytes and maintain or restore homeostasis (8, 31, 43). They discussed the role of resident and migratory phagocytic cells of the secondary lymphoid organs in mediating MSCs' therapeutic effect. The role of efferocytosis and associated phagocytes in the secondary lymphoid organs in mediating MSCs' therapeutic effect in COVID needs further investigation.

Conclusion

The horizon for the use of next generation engineered MSCs appears bright with both genetic and non-genetic engineering strategies emerging. Together with quantitative approaches to fully and carefully characterize MSC potency attributes, the editors of this series are optimistic that the next generation MSCs will be more efficacious in clinical trial outcomes and bridge the gap to clinical and commercial success.

Author contributions

RC drafted the first version. GM drafted the figure. RC, SV and GM have made a substantial, direct, and intellectual contribution to the writing and approved it for publication. All authors listed have made a substantial, direct, and intellectual contribution to the work and approved it for publication.

Funding

GM's contributions were made possible by the German Research Foundation/Deutsche Forschungsgemeinschaft (DFG; EX-PAND-PD CA2816/1-1) and the German Federal Ministry of Education and Research (BMBF) funding through the BSRT (GSC203) and BCRT, and in part by funding from the European Union's Horizon 2020 research and innovation program under grant agreements No. 733006 (PACE) and No. 779293 (HIPGEN).

Acknowledgments

We would like to thank all authors who contributed submitting manuscripts to this Research Topic and all reviewers who provided insightful feedback and helpful comments.

Conflict of interest

SV has 60% ownership in Regulatory Cell Therapy Consultants Inc. which does not pose real or perceived conflict of interest.

The remaining authors declare that the research was conducted in the absence of any commercial or financial relationships that could be construed as a potential conflict of interest.

Publisher's note

References

1. Viswanathan S, Shi Y, Galipeau J, Krampera M, Leblanc K, Martin I, et al. Mesenchymal stem versus stromal cells: international society for cell & gene therapy (ISCT®) mesenchymal stromal cell committee position statement on nomenclature. *Cytotherapy* (2019) 21:1019–24. doi: 10.1016/j.jcyt.2019.08.002

2. Moll G, Hoogduijn MJ, Ankrum JA. Editorial: Safety, efficacy and mechanisms of action of mesenchymal stem cell therapies. *Front Immunol* (2020) 11:243. doi: 10.3389/fimmu.2020.00243

3. Capilla-González V, Herranz-Pérez V, Sarabia-Estrada R, Kadri N, Moll G. Editorial: mesenchymal stromal cell therapy for regenerative medicine. *Front Cell Neurosci* (2022) 16.

4. Moll G, Ankrum JA, Kamhieh-Milz J, Bieback K, Ringdén O, Volk HD, et al. Intravascular mesenchymal Stromal/Stem cell therapy product diversification: time for new clinical guidelines. *Trends Mol Med* (2019). doi: 10.1016/j.molmed.2018.12.006

5. Moll G, Ankrum JA, Olson SD, Nolta JA. Improved MSC minimal criteria to maximize patient safety: a call to embrace tissue factor and hemocompatibility assessment of MSC products. *Stem Cells Trans Med* (2022) 11:2–13. doi: 10.1093/stcltm/szab005

6. Ringdén O, Moll G, Gustafsson B, Sadeghi B. Mesenchymal stromal cells for enhancing hematopoietic engraftment and treatment of graft-versus-Host disease, hemorrhages and acute respiratory distress syndrome. *Front Immunol* (2022). doi: 10.3389/fimmu.2022.839844

7. Levy O, Kuai R, Siren EMJ, Bhere D, Milton Y, Nissar N, et al. Shattering barriers toward clinically meaningful MSC therapies. *Sci Adv* (2020) 6:eaba6884. doi: 10.1126/sciadv.aba6884

8. Galipeau J, Sensebe L. Mesenchymal stromal cells: clinical challenges and therapeutic opportunities. *Cell Stem Cell* (2018) 22:824–33. doi: 10.1016/j.stem.2018.05.004

9. Robb KP, Fitzgerald JC, Barry F, Viswanathan S. Mesenchymal stromal cell therapy: progress in manufacturing and assessments of potency. *Cytotherapy* (2019) 21:289–306. doi: 10.1016/j.jcyt.2018.10.014

10. Moll G, Drzeniek N, Kamhieh-Milz J, Geissler S, Volk H-D, Reinke P, et al. MSC therapies for COVID-19: Importance of patient coagulopathy, thromboprophylaxis, cell product quality and mode of delivery for treatment safety and efficacy. *Front Immunol* (2020) 11:1091. doi: 10.3389/ fimmu.2020.01091

11. Cottle C, Porter AP, Lipat A, Turner-Lyles C, Nguyen J, Moll G, et al. Impact of cryopreservation and freeze-thawing on therapeutic properties of mesenchymal Stromal/Stem cells and other common cellular therapeutics. *Curr Stem Cell Rep* (2022) 8:72–92. doi: 10.1007/s40778-022-00212-1

12. Moll G, Jitschin R, von Bahr L, Rasmusson-Duprez I, Sundberg B, Lonnies L, et al. Mesenchymal stromal cells engage complement and complement receptor bearing innate effector cells to modulate immune responses. *PLoS One* (2011) 6:e21703. doi: 10.1371/journal.pone.0021703

13. Von Bahr L, Batsis I, Moll G, Hägg M, Szakos A, Sundberg B, et al. Analysis of tissues following mesenchymal stromal cell therapy in humans indicates limited long-term engraftment and no ectopic tissue formation. *Stem Cells* (2012) 30:1575–8. doi: 10.1002/stem.1118

14. Moll G, Rasmusson-Duprez I, von Bahr L, Connolly-Andersen AM, Elgue G, Funke L, et al. Are therapeutic human mesenchymal stromal cells compatible with human blood? *Stem Cells* (2012) 30:1565–74. doi: 10.1002/stem.1111

15. Moll G, Ignatowicz L, Catar R, Luecht C, Sadeghi B, Hamad O, et al. Different procoagulant activity of therapeutic mesenchymal stromal cells derived from bone marrow and placental decidua. *Stem Cells Dev* (2015) 24:2269–79. doi: 10.1089/scd.2015.0120

16. Moll G, Le Blanc K. Engineering more efficient multipotent mesenchymal stromal (stem) cells for systemic delivery as cellular therapy. *ISBT Sci Ser* (2015) 10:357–65. doi: 10.1111/voxs.12133

17. Nolta JA, Galipeau J, Phinney DG. Improving mesenchymal stem/stromal cell potency and survival: proceedings from the international society of cell therapy (ISCT) MSC preconference held in may 2018, palais des congres de Montreal, organized by the ISCT MSC scientific committee. *Cytotherapy* (2020) 22:123–6. doi: 10.1016/j.jcyt.2020.01.004

18. Galipeau J, Krampera M, Leblanc K, Nolta JA, Phinney DG, Shi Y, et al. Mesenchymal stromal cell variables influencing clinical potency: the impact of viability, fitness, route of administration and host predisposition. *Cytotherapy* (2021). doi: 10.1016/j.jcyt.2020.11.007

19. Caplan H, Olson SD, Kumar A, George M, Prabhakara KS, Wenzel P, et al. Mesenchymal stromal cell therapeutic delivery: Translational challenges to clinical application. *Front Immunol* (2019) 10:1645. doi: 10.3389/fimmu.2019.01645

20. Garcia-Bernal D, Garcia-Arranz M, Yanez RM, Hervas-Salcedo R, Cortes A, Fernandez-Garcia M, et al. The current status of mesenchymal stromal cells: controversies, unresolved issues and some promising solutions to improve their therapeutic efficacy. *Front Cell Dev Biol* (2021) 9:650664. doi: 10.3389/fcell.2021.650664

21. Chinnadurai R, Rajakumar A, Schneider AJ, Bushman WA, Hematti P, Galipeau J. Potency analysis of mesenchymal stromal cells using a phospho-STAT matrix loop analytical approach. *Stem Cells* (2019) 37:1119–25. doi: 10.1002/stem.3035

22. Galipeau J, Krampera M, Barrett J, Dazzi F, Deans RJ, Debruijn J, et al. International society for cellular therapy perspective on immune functional assays for mesenchymal stromal cells as potency release criterion for advanced phase clinical trials. *Cytotherapy* (2016) 18:151–9. doi: 10.1016/j.jcyt.2015.11.008

23. Krampera M, Le Blanc K. Mesenchymal stromal cells: putative microenvironmental modulators become cell therapy. *Cell Stem Cell* (2021) 28:1708–25. doi: 10.1016/j.stem.2021.09.006

24. Galipeau J. The mesenchymal stromal cells dilemma–does a negative phase III trial of random donor mesenchymal stromal cells in steroid-resistant graft-versus-host disease represent a death knell or a bump in the road? *Cytotherapy* (2013) 15:2–8. doi: 10.1016/j.jcyt.2012.10.002

25. Galipeau J. Concerns arising from MSC retrieval from cryostorage and effect on immune suppressive function and pharmaceutical usage in clinical trials. *ISBT Sci Ser* (2013) 8:100–1. doi: 10.1111/voxs.12022

26. Francois M, Copland IB, Yuan S, Romieu-Mourez R, Waller EK, Galipeau J. Cryopreserved mesenchymal stromal cells display impaired immunosuppressive properties as a result of heat-shock response and impaired interferon-gamma licensing. *Cytotherapy* (2012) 14:147–52. doi: 10.3109/14653249.2011.623691

27. Moll G, Alm JJ, Davies LC, von Bahr L, Heldring N, Stenbeck-Funke L, et al. Do cryopreserved mesenchymal stromal cells display impaired immunomodulatory and therapeutic properties? *Stem Cells* (2014) 32:2430–42. doi: 10.1002/stem.1729

28. Chinnadurai R, Garcia MA, Sakurai Y, Lam WA, Kirk AD, Galipeau J, et al. Actin cytoskeletal disruption following cryopreservation alters the biodistribution of human mesenchymal stromal cells. *vivo Stem Cell Rep* (2014) 3:60–72. doi: 10.1016/j.stemcr.2014.05.003

29. Chinnadurai R, Copland IB, Garcia MA, Petersen CT, Lewis CN, Waller EK, et al. Cryopreserved mesenchymal stromal cells are susceptible to T-cell mediated apoptosis which is partly rescued by IFNgamma licensing. *Stem Cells* (2016) 34:2429–42. doi: 10.1002/stem.2415

30. Chinnadurai R, Rajan D, Qayed M, Arafat D, Garcia M, Liu YF, et al. Potency analysis of mesenchymal stromal cells using a combinatorial assay matrix approach. *Cell Rep* (2018) 22:2504–17. doi: 10.1016/j.celrep.2018.02.013

31. Moll G, Geissler S, Catar R, Ignatowicz L, Hoogduijn MJ, Strunk D, et al. Cryopreserved or fresh mesenchymal stromal cells: only a matter of taste or key to unleash the full clinical potential of MSC therapy? *Adv Exp Med Biol* (2016) 951:77–98. doi: 10.1007/978-3-319-45457-3_7

32. Goldsobel G, von Herrath C, Schlickeiser S, Brindle N, Stähler F, Reinke P, et al. RESTORE survey on the public perception of advanced therapies and ATMPs in Europe-why the European union should invest more! *Front Med (Lausanne)* (2021) 8:739987. doi: 10.3389/fmed.2021.739987

33. Doorn J, Moll G, Le Blanc K, van Blitterswijk C, de Boer J. Therapeutic applications of mesenchymal stromal cells: paracrine effects and potential improvements. *Tissue engineering Part B Rev* (2012) 18:101–15. doi: 10.1089/ten.TEB.2011.0488

34. Lener T, Gimona M, Aigner L, Borger V, Buzas E, Camussi G, et al. Applying extracellular vesicles based therapeutics in clinical trials - an ISEV position paper. *J Extracell Vesicles* (2015) 4:30087. doi: 10.3402/jev.v4.30087

35. Soria-Juan B, Escacena N, Capilla-González V, Aguilera Y, Llanos L, Tejedo JR, et al. Cost-effective, safe, and personalized cell therapy for critical limb ischemia in type 2 diabetes mellitus. *Olson SD, Kumar A, George M, Prabhakara KS, Wenzel P,* (2019) 10:1151. doi: 10.3389/fimmu.2019.01151

36. Giri J, Moll G. MSCs in space: mesenchymal stromal cell therapeutics as enabling technology for long-distance manned space travel. *Curr Stem Cell Rep* (2022) 8:1–13.

37. Wu Z, Zhang S, Zhou L, Cai J, Tan J, Gao X, et al. Thromboembolism induced by umbilical cord mesenchymal stem cell infusion: a report of two cases and literature review. *Transplant Proc* (2017) 49:1656–8. doi: 10.1016/j.transproceed.2017.03.078

38. Kirkham AM, Bailey AJM, Shorr R, Lalu MM, Fergusson DA, Allan DS. Systematic review and meta-analysis of randomized controlled trials of mesenchymal stromal cells to treat coronavirus disease 2019: is it too late? *Cytotherapy* (2023) 25:341–52. doi: 10.1016/j.jcyt.2022.10.00

39. Moll G, Hult A, von Bahr L, Alm JJ, Heldring N, Hamad OA, et al. Do ABO blood group antigens hamper the therapeutic efficacy of mesenchymal stromal cells? *PLoS One* (2014) 9:e85040. doi: 10.1371/journal.pone.0085040

40. Hoogduijn MJ, de Witte SF, Luk F, van den Hout-van Vroonhoven MC, Ignatowicz L, Catar R, et al. Effects of freeze-thawing and intravenous infusion on mesenchymal stromal cell gene expression. *Stem Cells Dev* (2016) 25:586–97. doi: 10.1089/scd.2015.032

41. Weiss DJ, Filiano A, Galipeau J, Khoury M, Krampera M, Lalu M, et al. An international society for cell and gene therapy mesenchymal stromal cells committee editorial on overcoming limitations in clinical trials of mesenchymal stromal cell therapy for coronavirus disease-19: time for a global registry. *Cytotherapy* (2022) 24:1071–3. doi: 10.1016/j.jcyt.2022.07.010

42. Galleu A, Riffo-Vasquez Y, Trento C, Lomas C, Dolcetti L, Cheung TS, et al. Apoptosis in mesenchymal stromal cells induces *in vivo* recipient-mediated immunomodulation. *Sci Trans Med* (2017) 9. doi: 10.1126/scitranslmed.aam7828

43. Galipeau J. Macrophages at the nexus of mesenchymal stromal cell potency: the emerging role of chemokine cooperativity. *Stem Cells* (2021). doi: 10.1002/stem.3380

frontiers | Frontiers in Immunology

REVIEW
published: 09 June 2022
doi: 10.3389/fimmu.2022.918565

Optimization of Mesenchymal Stromal Cell (MSC) Manufacturing Processes for a Better Therapeutic Outcome

Maria Eugenia Fernández-Santos[1,2†], Mariano Garcia-Arranz[3,2†], Enrique J. Andreu[4,2], Ana Maria García-Hernández[5,2], Miriam López-Parra[6,2], Eva Villarón[6,2], Pilar Sepúlveda[7,2], Francisco Fernández-Avilés[1,2], Damian García-Olmo[3,2], Felipe Prosper[4,2], Fermin Sánchez-Guijo[6,2], Jose M. Moraleda[5,2] and Agustin G. Zapata[8,2*]*

[1] Cardiology Department, HGU Gregorio Marañón. GMP-ATMPs Production Unit, Instituto de Investigación Sanitaria Gregorio Marañón (IiSGM). Complutense University, CIBER Cardiovascular (CIBERCV), ISCIII, Madrid, Spain, [2] Platform GMP Units from TerCel and TERAV Networks. RETIC TerCel & RICORS TERAV, ISCIII, Madrid, Spain, [3] New Therapies Laboratory, Health Research Institute-Fundación Jiménez Díaz University Hospital (IIS-FJD). Surgery Department, Autonoma University of Madrid, Madrid, Spain, [4] Hematology Department and Cell Therapy Area, Clínica Universidad de Navarra. CIBEROC and IDISNA, Pamplona, Spain, [5] Hematopoietic Transplant and Cellular Therapy Unit, Instituto Murciano de Investigación Biosanitaria IMIB-Arrixaca, Virgen de la Arrixaca University Hospital, University of Murcia, Murcia, Spain, [6] Cell Therapy Area and Hematology Department, IBSAL-University Hospital of Salamanca, University of Salamanca, Salamanca, Spain, [7] Regenerative Medicine and Heart Transplantation Unit, Instituto de Investigación Sanitaria La Fe, Valencia, Spain, [8] Department of Cell Biology, Complutense University, Madrid, Spain

MSCs products as well as their derived extracellular vesicles, are currently being explored as advanced biologics in cell-based therapies with high expectations for their clinical use in the next few years. In recent years, various strategies designed for improving the therapeutic potential of mesenchymal stromal cells (MSCs), including pre-conditioning for enhanced cytokine production, improved cell homing and strengthening of immunomodulatory properties, have been developed but the manufacture and handling of these cells for their use as advanced therapy medicinal products (ATMPs) remains insufficiently studied, and available data are mainly related to non-industrial processes. In the present article, we will review this topic, analyzing current information on the specific regulations, the selection of living donors as well as MSCs from different sources (bone marrow, adipose tissue, umbilical cord, etc.), in-process quality controls for ensuring cell efficiency and safety during all stages of the manual and automatic (bioreactors) manufacturing process, including cryopreservation, the use of cell banks, handling medicines, transport systems of ATMPs, among other related aspects, according to European and US legislation. Our aim is to provide a guide for a better, homogeneous manufacturing of therapeutic cellular products with special reference to MSCs.

Keywords: MSCs, ATMPs, legal requirements, GMP manufacturing, extracellular vesicles

OPEN ACCESS

Edited by:
Guido Moll, Charité Universitätsmedizin Berlin, Germany

Reviewed by:
Takeo Mukai, The University of Tokyo, Japan
Clara Sanz-Nogues, National University of Ireland Galway, Ireland

***Correspondence:**
Maria Eugenia Fernández-Santos
mariuge@fibhgm.org
Agustin G. Zapata
zapata@bio.ucm.es

†These authors have contributed equally to this work and share first authorship

Specialty section:
This article was submitted to Alloimmunity and Transplantation, a section of the journal Frontiers in Immunology

Received: *12 April 2022*
Accepted: *10 May 2022*
Published: *09 June 2022*

Citation:
Fernández-Santos ME, Garcia-Arranz M, Andreu EJ, García-Hernández AM, López-Parra M, Villarón E, Sepúlveda P, Fernández-Avilés F, García-Olmo D, Prosper F, Sánchez-Guijo F, Moraleda JM and Zapata AG (2022) Optimization of Mesenchymal Stromal Cell (MSC) Manufacturing Processes for a Better Therapeutic Outcome. Front. Immunol. 13:918565. doi: 10.3389/fimmu.2022.918565

INTRODUCTION

Mesenchymal stromal cells (MSCs) are among the cell types most frequently used as therapeutic agents. Despite diverse approaches for improving their clinical efficiency, this remains low and is restricted to few diseases, including skeletal disorders, graft-versus-host disease and intestinal inflammation (1). Remarkably, protocols devoted to the clinical applications of MSCs are extremely variable, exhibiting differences in cell sources, banking processes, cell preservation, ways of administration, among others, and producing heterogeneous functionality of MSC products. In the present article, we review these issues, which have been significantly less investigated than the biology of MSCs used as therapeutic tools but, undoubtedly, important for the success of clinical trials. We also address the rules and legislations that govern these products of cell therapy. All steps from potential donor selection and manufacturing to cell transportation and administration to patients are reviewed. A section is devoted to MSC-derived extracellular vesicles (ECV) that are becoming an interesting therapeutic product whose generation, maintenance and administration have specific challenges. Our goal is to provide a general guide for a better and more homogeneous manufacturing of MSCs for use in cell therapy.

RULES AND LEGISLATION FOR THE USE OF MSCs AS ADVANCED THERAPY MEDICINAL PRODUCTS

Although cell therapy products have been produced for years for the treatment of different diseases, only in the first decade of the twenty-first century has the process of legally regulating their production and therapeutic use as medicines begun. In both the European Union (EU) and the United States (US), specific legislation has been established to approve the commercialization of cell and gene therapy products to ensure their quality, safety and efficacy (**Table 1**). The possibility of these products becoming medicines was initially addressed in the European Union (EU) by the first

TABLE 1 | European Union and United States Legislation related with ATMPs.

ABBREVIATION	LEGISLATION	DESCRIPTION
EUROPEAN UNION LEGISLATION		
Directive 2003/63/EC	Commission Directive 2003/63/EC of 25 June 2003 amending Directive 2001/83/EC of the European Parliament and of the Council on the Community code relating to medicinal products for human use.	First Regulation on gene and cell therapy as medicines
Directive 2004/23/EC	Commission Directive 2004/23/EC of the European Parliament and of the Council of 31 March 2004 on setting standards of quality and safety for the donation, procurement, testing, processing, preservation, storage and distribution of human tissues and cells.	Regulation on donors and cells and tissues as starting materials
Directive 2015/566/EU	Commission Directive (EU) 2015/566 of 8 April 2015 implementing Directive 2004/23/EC as regards the procedures for verifying the equivalent standards of quality and safety of imported tissues and cells.	Selection leaving donors
2006/17/EC	Commission Directive 2006/17/EC of 8 February 2006 implementing Directive 2004/23/EC of the European Parliament and of the Council as regards certain technical requirements for the donation, procurement and testing of human tissues and cells.	Regulation on donors and cells and tissues as starting materials
Directive 2009/120/EC	Commission Directive 2009/120/EC of 14 September 2009 amending Directive 2001/83/EC of the European Parliament and of the Council on the Community code relating to medicinal products for human use as regards advanced therapy medicinal products.	Regulation on the scientific and technical requirements of ATMPs
Regulation (EC) No 726/2004	Regulation (EC) No 726/2004 of the European Parliament and of the Council of 31 March 2004 laying down Community procedures for the authorisation and supervision of medicinal products for human and veterinary use and establishing a European Medicines Agency.	First mention of ATMP as medicines
Regulation (EC) No 1394/2007	Regulation (EC) No 1394/2007 of the European Parliament and of the Council of 13 November 2007 on advanced therapy medicinal products.	Developed Regulation on ATMP
Regulation (EU) 2017/745	Regulation (EU) 2017/745 of the European Parliament and of the Council of 5 April 2017 on medical devices, amending Directive 2001/83/EC, Regulation (EC) No 178/2002 and Regulation (EC) No 1223/2009 and repealing Council Directives 90/385/EEC and 93/42/EEC.	Regulation on the combined use of Cell Therapy Products and Medical Devices
Regulation (EU) 2017/746	Regulation (EU) 2017/746 of the European Parliament and of the Council of 5 April 2017 on *in vitro* diagnostic medical devices and repealing Directive 98/79/EC and Commission Decision 2010/227/EU (Text with EEA relevance)	
UNITED STATES LEGISLATION		
21 CFR 1271	Code of Federal Regulations. Title 21 - Food and Drugs. Chapter I - Food and Drug administration. Department of Health and Human Services. Subchapter I - Regulations under certain other acts administered by the Food and Drug Administration. Part 1271 - Human cells, tissues, and cellular and tissue-based products.	Regulation on Human Cells, Tissues, and Cellular and Tissue-Based Products
21 CFR 211	Code of Federal Regulations. Title 21- Food and Drugs. Chapter I - Food and Drug Administration Department of Health and human services. Subchapter C - Drugs: General. Part 211: Current Good Manufacturing Practice for finished pharmaceuticals.	Current Good Manufacturing Practices (cGMP)
21 CFR 312	Code of Federal Regulations. Title 21- Food and Drugs. Chapter I - Food and Drug Administration Department of Health and human services. Subchapter D – Drugs for human use. Part 312: Investigational New Drug application.	Investigational New Drug Requirements
21 CFR 600.	Code of Federal Regulations. Title 21- Food and Drugs. Chapter I - Food and Drug Administration Department of Health and human services. Subchapter F - Biologics. Part 600: Biological products: General	Biologics License Application Requirements
42 USC 262.	United States Code. Title 42 - The Public Health and Welfare. Chapter 6A - Public Health Service. Subchapter II - General powers and duties. Part F - Licensing of Biological Products and Clinical Laboratories. Subpart 1 - biological products. Sec. 262 - Regulation of biological products.	Regulation of biological products

European directives on medicines (Directive 2003/63/EC and Regulation 726/2004/EC), but it was not until 2007 when a specific regulatory framework for so-called Advanced Therapies Medicinal Products (ATMPs) was introduced (Regulation 1394/2007/EC). Subsequently, the scientific and technical requirements for these ATMPs have been supplemented with successive directives (Directive 2009/120/EC, EU GMP-ATMPs).

Gene Therapy products, Somatic Cell Therapy products, Tissue Engineering products and their combinations are considered ATMPs if they contain genes, cells or tissues that have undergone substantial manipulation (Regulation 1394/2007/EC, Annex I) that affects biological characteristics, physiological functions, or structural properties relevant for their clinical use. They also include cells or tissues that are used for different functions than their original ones, or in different locations in the recipient than in the donor. It is important to remark that products of cell therapy are considered as different from tissues or organs used for transplantation at a regulatory level, in that cell therapy products are considered to be medicines (ATMPs). Cell therapy products are also regulated by the guidelines of medical devices, Regulation (EU) 2017/745 and Regulation (EU) 2017/746 when these are used in combination with medical devices (**Table 1**).

MSCs meet the requirements to be ATMPs. They undergo substantial manipulations such as cell culturing or, sometimes, chemical (i.e. Fucosylation) or gene modifications (1). Moreover, they are obtained from different sources and can be used for a wide variety of applications. Besides, the European Medicine Agency (EMA) responsible for evaluating marketing commercialization of ATMPs through the Committee on Advanced Therapies-CAT (2) considers these products to be special medicines and their production to follow its own quality standards (see the Guidelines on Good Manufacturing Practice specific to Advanced Therapy Medicinal Products - EU ATMPs-GMP **Table 2**).

TABLE 2 | Guidelines, ISOs (International Organization for Standardization) and rules related with ATMPs.

GUIDELINES and RULES

ABBREVIATION	TITLE	DESCRIPTION	APPLY TO
EU GMP-ATMP	EudraLex-The Rules Governing Medicinal Products in the European Union. Volume 4: Good Manufacturing Practice. Guidelines on Good Manufacturing Practice specific to Advanced Therapy Medicinal Products. 22 November 2017.	Good Manufacturing Practice specific ATMPs	EU
CMCa	Guidance for FDA Reviewers and Sponsors: Content and Review of Chemistry, Manufacturing, and Control (CMC) Information for Human Gene Therapy Investigational New Drug Applications (INDs) (2008).	FDA guidance on Chemistry, Manufacturing, and Control of Gene Therapy products	US
CMCb.	Guidance for FDA Reviewers and Sponsors: Content and Review of Chemistry, Manufacturing, and Control (CMC) Information for Human Somatic Cell Therapy Investigational New Drug Applications (INDs) (2008).	FDA guidance on Chemistry, Manufacturing, and Control of Somatic Cell Therapy products	US
(WHO) EB123/5	Executive Board, 123. (2008). Human organ and tissue transplantation: report by the Secretariat. World Health Organization. https://apps.who.int/iris/handle/10665/23650.	WHO guiding principles on human cell, tissue and organ transplantation	BOTH
WHA57.18	Resolution of 2009: Human organ and tissue transplantation (https://apps.who.int/gb/ebwha/pdf_files/WHA57/A57_R18-en.pdf)	Resolution on organ procurement and Allogenic/Xenogeneic transplantation	BOTH
EMEA/CHMP/410869/2006	Guideline on human cell-based medicinal products	Development, manufacturing and quality control, and non-clinical and clinical development of cell-based medicinal products. It covers somatic cell therapy medicinal products and tissue engineered products.	EU
FDA-2008-D-0520	Guidance for Industry: Potency Tests for Cellular and Gene Therapy Products (01/2011)	Recommendations for Potency Assay design in cellular and gene therapy products.	US
ICHQ5D	Quality of Biotechnological Products: Derivation and Characterization of Cell Substrates Used for Production of Biotechnological/Biological Products. CPMP/ICH/294/95. 1998.	Standards for the derivation of human and animal cell lines and microbial cells to be used in biotechnological/biological products	BOTH
CPMP/ICH/138/95	Note for guidance on quality of biotechnological products: stability testing of biotechnological/biological products	Generation and submission of stability data for well-characterized different products.	BOTH
CPMP/ICH/365/96	Note for guidance on Specifications: test procedures and acceptance criteria for biotechnological/biological products (ICHQ6B)	International specifications for biotechnological and biological products to support new marketing applications	BOTH
EMA/CHMP/BWP/534898/2008 (Rev. 2)	Guideline on the requirements for quality documentation concerning biological investigational medicinal products in clinical trials (27 January 2022)	Quality requirements of an investigational medicinal product for a clinical trial	US
GDP	Good distribution practice (https://www.ema.europa.eu/en/human-regulatory/post-authorisation/compliance/good-distribution-practice)	The minimum standards that a wholesale distributor must meet to ensure that the quality and integrity of medicines is maintained throughout the supply chain	EU
ISO 21973	Biotechnology-General requirements for transportation of cells for therapeutic use. (https://www.iso.org/obp/ui/es/#iso:std:iso:21973:ed-1:v1:en)	General requirements and reviews the points to consider for the transportation of cells for therapeutic use, including storage during transportation.	BOTH

US regulations also classify gene therapy and cell therapy products as biological products (42 USC 262), distinguishing them from conventional drugs. Traditional transplantation of cell or tissue products (Human Cell, Tissue and Cellular and Tissue-based product - HCT/P) is also different from that of biologicals (21 CFR 1271). As in the European legislation, HCT/P are characterized by their minimal manipulation and homologous use. Besides, they cannot produce systemic effects and their potential effects do not depend on the metabolic activity of living cells (3, 4). HCT/P intended for non-homologous use, or substantially modified, are regulated as biological products and will be included within the regulations for new investigational drugs (21 CFR 312), biologics (21 CFR 600) and cGMP (21 CFR 211). In the US, all these products are regulated by the Center of Biologics Evaluation and Research (CBER) within the Food and Drug Administration (FDA) (5).

Legal Requirements for Donor Selection

Both American and European legislation requires an adequate selection of the donor, a guarantee of the traceability of the donated cells and tissues, and their processing under quality conditions that ensure their safety. According to European Directive 2004/23/EC, the donations must be voluntary, and the donors should have appropriate information about the obtaining procedure and the future use of their donated cells or tissues. The confidentiality of donated cells and tissues must also be assured. Donor evaluation and testing procedures must be documented, and any major anomalies reported. Selection criteria are described in section 2. Procedures for donor selection are similar in the US (see American 21 CFR 1271).

In Europe, the authorization of Tissue establishments is granted according to the provisions of Directive 2004/23/EC of 31 March 2004 on setting standards of quality and safety for the donation, procurement, testing, processing, preservation, storage and distribution of human tissues and cells. These authorizations are usually specific to each type of tissue or cell obtained and are valid for a specified period of time, at the end of which they can be renewed upon verification that the conditions and requirements that gave rise to their concession persist. When the collection of tissues and/or cells have to be obtained in a non-authorized health center, the procedure must always be carried out by professionals integrated in a collection team from a properly authorized center and under the conditions set by this center. The collection team must also have the proper authorization for this specific practice.

The obtained tissues must be packed and labeled according to Directive 2004/23/EC and 2006/17/EC and delivery to the manufacturing centers must be done with temperature traceability and by a qualified transportation company (6).

GMP Manufacturing

ATMPs manufacturing is very similar to conventional sterile medicines production with some particularities. In fact, both in the EU and in the US, this is conducted in accordance with the Good Manufacturing Practice of Medicines (EU GMP-ATMPs and 21 CFR 211, respectively) (**Tables 1**, **2**).

The EU Part IV of Volume 4 of the Good Manufacturing Practice (see EU GMP-ATMPs guide) includes the guidelines that develop GMP requirements in accordance with EU Regulation 1394/2007/EC and Directive 2009/120/EC. Essentially, the protocol for obtaining starting materials (Bone Marrow, Adipose Tissue, Umbilical Cord, etc.) must be well-defined, materials used for collection and shipment must be controlled, and the shipment protocol must be validated to guarantee stability (at least composition, viability and microbiological safety). Complementary legislation would be applied to the manufacturing of ATMPs that have been granted a marketing authorization and ATMPs used in a clinical trial setting. In the US, the FDA has provided two guidance documents of regulations for the Chemistry, Manufacturing and Controls (CMC) for gene (see CMCa) and cell therapy (see CMCb) products under the term of new drug procedure (**Table 2**) (3). Therefore, the EU and US regulations reflect the differences between GMP that apply to conventional medicines and those that apply to ATMPs (2). The GMP-specific regulation for ATMPs summarizes all the main issues of nonconventional drug manufacturing supported on the risk-based approach. ATMPs-specific GMPs highlight the personnel qualification, as well as the qualification and validation of facilities, equipment, documentation, starting and raw materials and excipients, aseptic production, test methods and quality control, batch release and distribution.

The Impact of the ATMPs Regulatory Framework on the Development of MSC-Based Therapies

The development of ATMPs has traditionally been associated with GMP facilities. On the one hand, they must comply with GMP to ensure the safety, quality and efficacy of the ATMPs produced, but there may be impediments in the EU to the implementation of all the requirements. For instance, it is necessary to provide pre-clinical data on the proposed medicine product and a qualified person (QP) for formal release of the ATMPs. In addition, the lack of standard procedures for the application of EU directives among EU member states makes it difficult to regulate certain cellular products (7).

Although regulations are similar, some aspects of US legislation make it easier to conduct the early stages of ATMPs development there. Unlike the EU, US GMP facilities for manufacturing phase I/II and phase II trials are not subjected to regulatory inspection, so the burden of compliance is lower. In the US, there is no requirement for QP the formal release of investigational medicines (8). On the other hand, the lack of advanced phase III trials explains why only a few MSC-based cell therapy products have been approved today for market commercialization world-wide. The first products approved corresponded to Queencell (autologous adipose tissue-derived MSCs (AT-MSCs) for subcutaneous tissue defect, 2010), HeartiCell gram (autologous bone marrow-derived MSC (BM-MSC) for myocardial infarction, 2011), Cartistem (allogenic umbilical-cord blood (UC-MSC) derived MSC for

osteoarthritis, 2012) or Prochymal (allogenic BM-MSC for acute graft vs host disease, 2012), but nowadays all of them remain in the market. Since then, as of 2021, only ten MSC-based products have been approved worldwide (9). However, in the EU only one product has been developed (Alofisel, allogenic adipose tissue derived MSCs (ADSCs) for perianal fistula) and, to date, there is no FDA-approved MSC therapy on the market[1]. This situation is particularly evident in EU academic institutions, which have limited experience in the regulatory protocols. Therefore, to develop guidelines, interactive initiatives or platforms, some previously mentioned, would be particularly useful. In the EU, EMA offers personalized scientific advice about any stage of MSC product development (10).

In the EU, MSC-based products are also authorized under the hospital exception clause. Centralized marketing authorization is not required in the EU if the ATMPs are prepared on a non-routine basis, according to GMP, in a specific hospital under responsibility of a medical specialist to cover an individual medical prescription for a custom-made product for an individual patient (7).

SELECTION OF LIVING DONORS

Manufacturing of cells for clinical applications begins with an accurate selection of living donors according to the legal/ethical rules. This selection includes both the tissue of origin and the donor person. Regarding the donor tissue, much has been written emphasizing that MSCs from different origins (adipose tissue, bone marrow, Wharton's jelly, etc.) have some specific properties. However, little is known about the influence of the donor on the capabilities of MSCs. Accordingly, here we briefly summarize some minimal requirements for MSC donation. Before addressing this point, it seems interesting to board a crucial question: Are autologous or allogeneic MSCs the best for therapeutic application? In fact, autologous MSCs would potentially be the best product because immunological rejection is avoided, but they do have a high production cost, requiring two procedures for the patient: one for obtaining the cell product and a second for the cell implantation, and the time of availability of the cellular product is also increased. Allogeneic MSCs from selected donors have three fundamental advantages and have become the most frequently used MSCs for cellular treatments: they have lower production costs, provide shorter treatment times and, most importantly, are barely immunogenic, evading the host immune system (Immunoevasive) (11–13), although data in this respect are controversial (1). In terms of safety, allogenic MSCs are considered to have the same properties as autologous ones. Regarding the effectiveness, to our knowledge, the ALOFISEL trial was the first Phase III clinical assay performed with allogeneic ADSCs with significant efficacy (14, 15). On the other hand, the use of allogeneic cells allows the generation of cell banks derived from optimal donors, i.e. those that have MSCs with the highest anti-inflammatory and immunosuppressive potential.

In this respect, a fundamental requirement in an optimal donor would be the absence of pathogens, for which the following must be ruled out: HIV, HBV, HCV, *Treponema pallidum*, Toxoplasmosis, Parvovirus, Epstein-Barr virus, Cytomegalovirus, Nile Virus and prions, and donors must have two negative PCRs and a negative IgM antibody test for COVID-19. They would also be required to have normal routine test results (hematology, biochemistry), and an absence of the following: fever, signs or symptoms of concurrent bacterial, fungal or viral infections, neoplastic antecedents, blood transfusions and tattoos or piercing during 4-6 months. Finally, it is advisable that they have not travelled to areas at risk of infectious diseases in the previous three months (Official WHO Guiding Principles (EB123/5) and resolution WHA57.18 of 2009, **Table 2**).

Individuals who meet the requirements set out above can be MSC donors but, how to select those whose MSCs maintain their regenerative/reparative properties intact? In the case of ADSCs, some studies have been conducted to answer this question in relation to gender, age/microsatellite length, lifestyle habits (Tobacco/Alcohol, Sport), type of fat (white or brown) and body mass index (BMI) (16).

This research found that women yielded a higher number of ADSCs with better immunomodulatory potential (17). Also, distinct anatomical sites provided different MSC yields, with variations in their immunomodulatory and differentiation potential (18, 19). Studies evaluating senescence showed a significant decrease in the overall cellular yield with increasing age and, more importantly, a significant fall in the proliferation and differentiation capacities of the obtained MSCs (20–25). On the other hand, numerous reports have related lifestyle habits with MSC "quality": various by-products of tobacco inhalation/consumption, especially nicotine, have a detrimental effect on the number and capacities of MSCs (26–29). It has also been shown that regular alcohol consumption leads to a lower potential of MSCs as well as to decreased MSC numbers, especially those originated in the bone marrow (30–32). In the case of ADSCs, it is unclear whether subcutaneous fat and omentum fat have similar capacities, although the initial yield at isolation is higher in the omentum per gram (33, 34); and finally, different studies have shown that the highest cell yield is obtained from donors with a BMI between 17.5 and 26.8 (16, 20, 35–41). In summary, the "ideal" donor to obtain ADSCs is a young woman (<40 years) with healthy lifestyle habits (no tobacco, alcohol or drugs), no excessive fibrous tissue (such as athletes), and a BMI lower than 26.8.

In the case of BM-MSCs, any person in good health and aged between 18 and 40 years may be a good candidate (Directive 2015/566/EU). Nevertheless, some studies do not recommend donors suffering from uncontrolled high blood pressure, insulin-dependent diabetes mellitus, any severe cardiovascular, neurological, pulmonary, renal, hepatic disease, etc. Other risk factors include intravenous drug abuse, sexual risk practices,

[1] https://www.fda.gov/vaccines-blood-biologics/cellular-gene-therapy-products/approvedcellular-and-gene-therapy-products. (Accessed March 31, 2022).

hemophilia, etc.; history of ocular inflammatory diseases (iritis, episcleritis) or fibromyalgia, donors receiving lithium treatment platelet counts below 120,000 ml. or those weighing less than 50 kg or more than 130 kg (42–44).

With regards to the donations of UC-MSC, the requirements established by world legislation for the donors are: the mother's clinical history particularly in relation to possible infectious, hematological or any other type of illnesses that might contraindicate the use of cord blood; analysis of the mother's blood at the time of birth to rule out any infectious process that could be transmissible to the cord blood; and clinical examination of the baby at birth and advisable 3 months after the sample collection. To our knowledge there are no studies that have evaluated the best umbilical cord donor, either in relation to the age of the mother or race. Therefore, with the exception of safety data, it is not possible to propose criteria for selecting donors for this type of MSCs.

ISOLATION AND EXPANSION OF MSCs DERIVED FROM DIFFERENT SOURCES

MSCs have been isolated from numerous adult and perinatal tissues, more frequently adipose tissue, bone marrow and umbilical cord, but also from dental pulp, menstrual blood, amniotic fluid or others (45). Regardless of their origin, all these MSCs can satisfy the minimal criteria of the International Society for Cellular Therapy (ISCT) in terms of phenotype, differentiation and immunoregulatory capabilities (46), but the cell yield, growth kinetics and potency may be affected by the tissue of origin or the protocol followed to obtain the starting material for cultures (47–49). So, with the available knowledge to date, the selection of the starting material as well as the methods of cell isolation and expansion are based on a mixture of logistical, intellectual and center experience or industry arguments.

Given that *in vitro* expansion is always necessary for clinical escalation, we would select an MSC source that ensures large amounts of cells with high proliferation potential and capable of withstanding long periods in culture before acquiring genetic instability or a senescent profile (50). The most common sources of MSCs assessed in clinical trials have been umbilical cord, bone marrow, and adipose tissue (51), and although MSCs isolated from other sources have also being used, there is less experience with them (**Figure 1A**).

Collection of Starting Material and MSCs Isolation

Friedenstein et al. first described BM-MSCs in 1968 as a population of adherent fibroblast-like cells present in the bone marrow and they are now the most studied source globally (52). Bone marrow harvesting is an invasive procedure that requires local anesthesia with or without superficial sedation, with the iliac crest being the preferred site to obtain larger volumes of BM for clinical applications. The procedure can be performed by multiple punctures and marrow aspirations of small volumes of 1-4 ml with 10-ml syringes prefilled with heparin, or by few or single-site large BM aspiration with needle redirection. Although

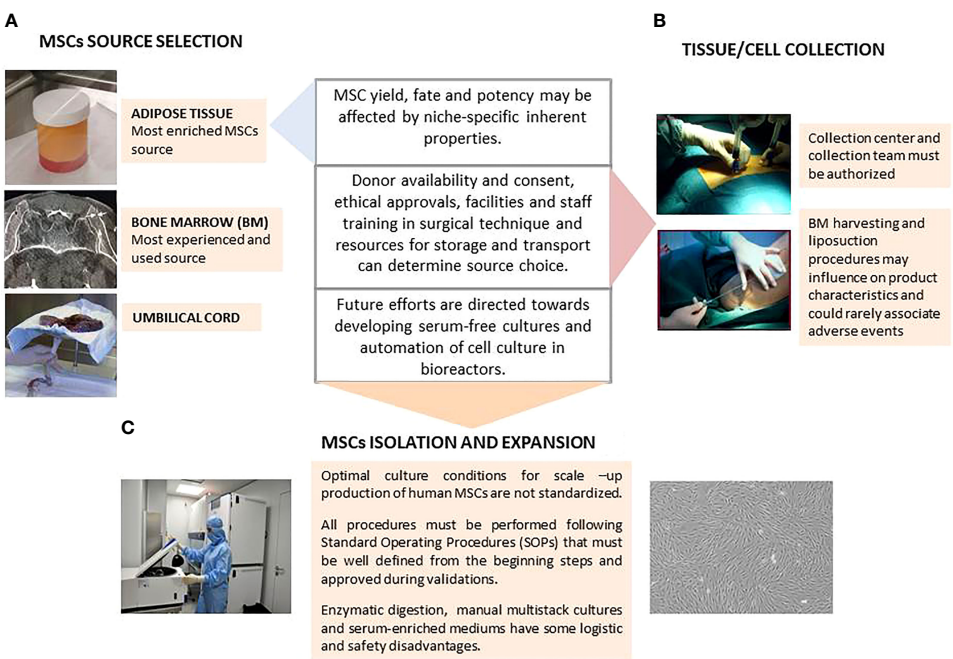

FIGURE 1 | Schematic representation of key aspects on Mesenchymal Stromal Cells (MSCs) isolation and expansion. **(A)** MSC Source Selection; **(B)** Tissue/Cell Collection; **(C)** MSCs Isolation and Expansion.

small repeated aspirations need a longer operation time, in combination with 10-ml syringes they obtain larger MSC yields than BM harvest through single-site puncture aspirated with 50-ml syringes, probably because of blood dilution in the latter (53). Other authors found that the single-stick aspiration method is sufficient to obtain quality marrow aspirates (54). Once obtained, the optimum temperature for maintaining the BM is 2-8°C degrees if overnight storage or shipping is needed (**Figure 1B**).

BM must be processed within 24 hours of collection, although some studies have shown that MSCs derived from cryopreserved marrow have the same growth kinetics and fulfill ISCT criteria as well as fresh marrow–derived MSCs, but further investigation about the effects of cryopreservation on their therapeutic potential is required (55). BM aspirates can be directly cultured, but are more often submitted to a density gradient centrifugation process to isolate BM nucleated cells (BM-NC). Interestingly, both hematocrit and red blood cell release can induce necrosis and apoptosis of MSC (56). In this first step of BM-NC isolation, the yield of cells can vary between different density gradient separation protocols (whether manual or automated). Once obtained, BM-NC must be seeded in a low plating density, about 1-2 x 10^5 cells/cm^2, to enhance the proliferation of adherent cell populations at P0. In some cases, positive immunoselection strategies allow the culture of smaller subpopulations of MSCs (**Figure 1C**) (50).

In recent years, both umbilical cord and adipose tissue have gained more ground than BM as MSC sources because of some logistic and functional advantages. UC-MSCs have a higher proliferative and differentiation potential than MSCs obtained from adult tissues and express pluripotency markers that are not present in adult cells (57). UC samples can be stored at 2-8°C and then MSCs can be isolated by explant or enzymatic digestion methods. In the explant method after arteries and vein removal, the remaining tissue and the Wharton's jelly is cut into small fragments and suspended in culture medium for 7 days in a 37°C humidified incubator with 5% CO_2. The tissue must be left undisturbed to allow cell migration from the explants while the culture medium must be replaced periodically. For enzymatic digestion, the cord is cut into small fragments and incubated with 500 U/mL collagenase at 37°C in a tissue dissociator. Then, the obtained cells are seeded in culture flasks (58) (**Figures 1B, C**).

Subcutaneous adipose tissue can be easily obtained from donors by in bloc resection (usually discarded as waste in many surgeries) or with a cannula connected to a suction system. In any condition, a 100–500 fold higher number of stem cells compared to BM are yielded (59). Fat removal by liposuction is the preferred harvesting technique for healthy donors and can be combined with ultrasound energy to breakdown adipose tissue facilitate its removal and decrease bleeding and operation time (60, 61). Lipoaspirate must be stored for no longer than 24 h at 2-8°C to maintain the optimal quality of ADSCs (62).

Enzymatic digestion with GMP degree recombinant collagenase followed by centrifugation and washing is the most widespread isolation method for adipose tissue, with a concentration of lyophilized enzyme ranging from 0.075% (w/v) to 0.3% (w/v). This step can be followed by an erythrocyte lysis phase to get rid of erythrocyte contamination. Some protocols improve ADSC isolation and facilitate enzymatic digestion by using mechanical disruption (63), or by replacing enzymatic digestion by mechanical procedures, such as centrifugation, filtration, and micro-fragmentation to minimize costs and to avoid safety issues associated with the use of collagenase (64). ADSCs show more genetic and morphologic stability in long-term cultures and faster proliferation than BM-MSC, even when harvested from the same donor. This is a clear advantage for large scale culture over BM-MSCs in which cultures beyond 20 days and passages beyond 6-7 are associated with senescence (51) (**Figure 1C**).

These tissues and cells used as starting materials for ATMPs may only be obtained in centers authorized by the competent health authority such as collection centers, according to the rules described in section 1.2. All these variables are critical from the beginning of the manufacturing process and each modification must be considered and approved during validations (65) (**Figure 1B**).

MSC Expansion

The optimal culture conditions for clinical scale production of human MSCs are not standardized across laboratories although it is well known that plate density, culture time and medium composition have a critical influence on the final MSC properties (66), which complicates product comparability among manufacturing centers and extrapolation of results in terms of MSC safety and efficiency across different clinical studies.

Before each culture, the MSCs must have adhered to the culture surface and proliferated, but should not reach over 80% confluence to prevent inhibition by cell-to–cell contact. Accordingly, MSCs have to be plated at a cell density that allows for optimal cellular expansion avoiding continuous premature passages if we plate at high seeding density, or excessively long-term cultures if we plate cell at too low a seeding density. These two situations affect cell proliferation and could lead to senescence or genetic instability (67). Automation of cell cultures for growing large numbers of adherent cells can provide savings in labor costs and improvements in cell quality, a key issue when scaling-up the processes. Bioreactors can enable frequent feeding of the culture, maintaining the levels of metabolites critical for cell expansion under control and allowing a faster and healthier expansion of MSCs than conventional cultures (68–70).

Oxygen concentration is also an important parameter to control. In recent years, hypoxia (3-5%) has been claimed as more physiological environment for cells than normoxia (21%). However, to date, MSCs are mainly cultured under normoxic conditions and reasons to justify the change require validation (71). Alpha- minimum essential medium (α-MEM) or Dulbecco's modified Eagle's medium (DMEM) supplemented with fetal bovine serum (FBS) are the gold standard culture mediums for MSC used in most clinical trials. However, xenogenic FBS have some immunological disadvantages and infectious concerns that require controls and validation of each batch. Accordingly, there is interest in the development of

serum-substitutes and serum-free media for large scale expansion but taking care to retain MSC characteristics. Cultures of UC-MSCs supplied with 7.5%-10% of activated platelet rich plasma obtained from donor cord blood showed better results than those cultured with standard FBS-containing media. Furthermore, ADSC have been successfully cultured with allogenic platelet lysate generated by freeze-thawing of human platelet concentrates (76–79). However, as the use of hPL has also economic and regulatory concerns, future efforts are directed towards developing standardized GMP-grade formulation with recombinant bioactive molecules to "compensate" for the reduction or lack of serum (76, 77).

QUALITY METHODS THAT ENSURE EFFICIENCY AND SAFETY

Quality controls ensure the quality of drug products under the rules of the International Council for Harmonization of Technical Requirements for Pharmaceuticals for Human Use (ICH)[2]. Mandatory guidelines for the producers of ATMPs contain important consensuses on the performance of stability studies, the definition of thresholds for impurities testing, and on quality based on Good Manufacturing Practice (GMP) risk management. The quality controls carried out on the ATMPs would be based on the aforementioned guidelines, as well as those dictated by the Pharmacopoeia (78) for performance in a range of tests.

The quality of MSC products is broadly ensured at three different levels: selection of the starting material and raw and packaging materials, control of the manufacturing process (GMP and in-process testing) and the final release testing of the product to ensure patient safety. Selection of the starting material that implies the donation, attainment and testing of human tissues and cells used as starting materials, would be in accordance with the Directive 2004/23/EC (**Table 1**). The ATMPs manufacturer together with the supplier will establish the specifications which in-process controls include: tests performed during the manufacturing process to monitor and, if necessary, adjust the process to ensure that the intermediate/finished product meets its specification. Before the release of MSCs to be administered to patients, quality controls must also be performed to ensure the quality of the final products. Likewise, the excipients used in the manufacturing would be of suitable quality and manufactured under adequate conditions.

MSCs are ATMPs with specific attributes. The first condition to generate a reliable stem cell (MSC) product for clinical trials and routine patient care is to ensure their identity by isolating homogeneous cell populations, following the ISCT recommendations (46). As a living cell product, viability of the MSCs must be ensured in all steps of the manufacturing process and before their administration. The most used test, due to its speed and simplicity of elaboration, is the trypan blue exclusion. Purity is necessary to demonstrate that the cellular population of the drug product does not contain cells other than MSCs (EMEA/CHMP/410869/2006, **Table 2**). Immunophenotyping of the MSCs by flow cytometry according to the ISCT criteria is the most widely used technique.

Potency is a quantitative measure of the biological activity of the product to be tested, which is linked to its biological properties (FDA-2008-D-0520; CPMP/ICH/365/96, **Table 2**). Assessment of these biological properties constitutes another essential step to establish a complete characterization profile of the medicinal product. The biological activity is the capacity of a product to achieve a specific biological effect. Furthermore, the potency test is also the only property that is linked directly to efficacy, shows a correlation with the intended use or predicts the desired therapeutic effect (79). This could be based on *in vitro* co-culture assays to demonstrate the status of MSC activation, and MSC-mediated inhibition of T cell activation or proliferation (80). Unfortunately, it is not clear which is the best potency assay to demonstrate immunomodulatory and regenerative capacities of the MSCs, but this would undoubtedly include tests of safety and stability and, in addition, potency also correlates with the desired effect (FDA-2008-D-050, **Table 2**).

Safety concerns can be derived from the intrinsic characteristics of the ATMPs, the manufacturing process, or the risk of transmitting pathogens to the product.

However, conventional safety studies may not be suitable due to the unpredictable evolution of the cells and/or the *in vivo* behavior of the product; accordingly, both *in vitro* and *in vivo* studies may be required for a safety profile characterization.

On the other hand, the tumorigenic potential of MSCs does not appear to constitute a substantial problem, because short- rather than long-term MSC cultures are used for therapeutic proposes to reduce the duration of *in vitro* MSC expansions (81). In this regard, because most cells can acquire chromosomal aberrations during extensive culture, it would be pertinent to perform a genetic analysis prior to MSC administration. There is a legal requirement to demonstrate the genetic stability of the final cell product. Karyotyping is used to detect abnormal chromosome structure or number. Array-CGH allows a higher resolution in the detection of alterations or copy number changes (82). Indeed, both tests are complementary, because CGH-arrays have a high sensitivity but do not detect polyploidy or balanced translocations, whereas karyotyping detects them but has a lower sensitivity.

Also, safety studies involving microbiological testing (83) must be carried out immediately before packaging or as late as possible during the manufacturing process. In-process testing would also be performed at appropriate steps of the production process such as when changing the storage medium. Microbiological testing includes: testing for aerobic and anaerobic bacteria and fungi (see the *European Pharmacopoeia (Ph. Eur.)*, in particular chapters 2.6.1, 2.6.12, 2.6.13 and 2.6.27); mycoplasma (*Ph. Eur*. chapter 2.6.7) and bacterial endotoxins (according *Ph. Eur*. chapters 2.6.14 and 5.1.10) (78). Although, most of the MSC manufacturing process is open processing, there are also closed manufacturing systems. In all cases without a terminal sterilization process, the environmental microbiological monitoring of cleanrooms is mandatory (EU-GMP-ATMPs, **Table 2**) to minimize risks of

[2]https://www.ich.org/page/quality-guidelines (Accessed March 31, 2022).

microbiological contamination of the product. These monitoring tests include:

-*Volumetric sampling*: Quantifies bacteria and fungi suspended in the air surrounding the open product.
-*Settle plates*: Qualitative evaluation of bacteria and fungi in the air over the plate. At rest and in process conditions.
- *Contact plates*: Qualitative test to detect contamination on the surface of the work area, conducted under uniform pressure for 10 seconds.
- *Swabs*: Qualitative test of the bacteria and fungi on the surface. In this case, the settling plates can be exposed for less than 4 hours during critical operations.
-*Glove prints:* Assessment of the bacteria and fungi contamination of the glove prints (all five fingers) of the operator, after processing or before changing gloves.

Stability testing is required to generate data as well as for establishment of the shelf-life of all the intermediate products subjected to storage and of the finished product. The stability would be demonstrated for the conditions and maximum storage period specified for the MSC product, providing assurance that changes in the identity, purity and potency of the product will be detected (CPMP7ICH7138/95, **Table 2**). Therefore, we use the same test to assess the conditions described above. The intermediate products and cell banks would be tested in a similar way as the finished product. In addition, these quality controls allow for the evaluation of the consistency of batch-to-batch manufacturing.

Manufacturing processes are continuously being improved, especially in the first phases of development of the ATMPs. Depending on the consequences of the changes introduced and the stage of development, comparability studies may be needed to ensure that the changes do not have a negative impact on the product (EMA8CHMP7BWP7534898/2009, **Table 2**). The challenge of these studies is to ensure that the quality, safety and efficacy of the product are not altered by changes in the manufacturing process. The protocol would include molecular characterization, purity, potency and stability assays. A demonstration of comparability does not imply that the quality attributes are identical, but that they are highly similar and any difference between them has no negative impact on the drug product (80). The definition of the strategy for comparability testing must be documented and an experimental plan would be available with written procedures and specifications for each test.

Assessment of the quality of the finished product is mandatory to ensure patient safety. The finished product will not be released for administration until it conforms to the specifications and its quality has been considered satisfactory in accordance with pre-specified requirements. Homogenizing the quality controls carried out on MSCs is critical in order to evaluate their therapeutic efficacy.

CELL BANKS FOR MSCs

One of the most relevant objectives of cell production units for clinical application is the optimization and improvement of cell culture production yields. Culture conditions can be improved by using different culture media and growth factors, but cell banks can greatly increase the final cell yield (84).

Cell banks allow the storage of intermediate production products that occupy a reduced storage space and that, once thawed, allow a large number of cells to be expanded without the need to resort to primary culture originated from the initial tissue. In addition, if a sequential, or two-tiered, system of cell banks is established, large numbers of cells can be obtained from a small amount of starting material.

In general terms, a Cellular Bank is a collection of approved cell containers, with a uniform composition, which are stored under defined conditions. Each container represents an aliquot of one cell type pool (ICHQ5D, **Table 2**).

According to the EU ATMPs-GMP, cell banks can be classified into:

a. *Master Cell Bank* (MCB): a culture of fully characterized cells, which have been obtained from a selected cell population under defined conditions, distributed in containers in a single operation, treated in a way that guarantees uniformity and stored in a way that stability is guaranteed.
b. *Working Cell Bank* (WCB): a culture of cells derived from the Master Cell Bank, distributed in containers in a single operation, treated in a way that guarantees uniformity, and stored guaranteeing its stability. Intended for use in the preparation of cell cultures within production processes for clinical and commercial phases.

A good example of the two-tiered system of a *Master Cell Bank* (MCB) and *Working Cell Bank* (WCB) with MSCs is found in Oliver-Vila et al. (85), where the obtained primary culture of 5 x10^6 Wharton jelly cells derived from one single umbilical cord is described. From this primary culture they could obtain a MCB with 20 aliquots of 2.5 x10^6 MSCs. One of these aliquots of MCB could be expanded to obtain a WCB with 8 aliquots of 3 x10^6 cells. Finally, one of the aliquots of WCB could be expanded to obtain 12 doses of 50 x10^6 cells of final medicine product. With this two-tiered system of cell banks, the authors report a potential culture yield of 96,000 x10^6 cells from an initial population of 5 x10^6 Wharton jelly MSCs from one single umbilical cord. Obviously, the success of this bank system is based on the high growth rate of this type of primary culture. Therefore, this approach is the most recommended when MSCs are used in an allogeneic setting and primary cultures have a good growth rate.

Nevertheless, depending on the donor characteristics and the tissue of origin of the primary culture, it may be difficult to obtain such high yields. On the other hand, if the cells are intended for autologous use, it is usually not necessary to obtain large amounts of final product, although if the treatment implies the administration of several doses over time, it may be convenient to generate small cell banks that allow the rapid production of final products without the need to perform new biopsies and primary cultures (86).

For these cases, the EU ATMPs-GMP (**Table 2**) defines the possibility of creating these small cell banks, calling them *Cellular Stocks* (CS). Therefore, CS are those performed by primary cells expanded to a given number of cells to be aliquoted and used as starting material for production of a limited number of batches of a cell-based ATMPs.

MSCs Cryopreservation, Storage and Traceability

In recent years, considerable experience has been generated worldwide on MSC cryopreservation procedures. Different methods, rates of cooling and compositions of cryoprotectants have been developed (84, 85, 87). The most widely-used cryoprotectant to date is dimethyl sulfoxide (DMSO), although there are different excipient formulations that can give better performances in post-thaw viability (88). 10% DMSO could be supplemented with a buffer containing reagents ranging from 5% Human Albumin, Human Serum or Human Plasma A/B to more complex formulations involving Dextran-40, Lactobionate, Sucrose, Mannitol, Glucose, Adenosine or Glutathione (89). Freezing procedures usually involve controlled rate freezing for optimal cryopreservation.

Another variable to take into account is the container where the cells are cryogenized. The best ones are cryogenization cell bags, but if small volumes must be frozen the standard screw cap cryotube is more common. However, this system is not the most suitable for procedures under GMP, since its closing systems are not safe and can favor pollutant entry (84). Small volume cryopreservation systems are currently being developed in a completely closed system to prevent this from occurring.

The labeling system must ensure traceability of the cryopreserved batch, including the main data that clearly identifies the sample it contains. Labels must be suitable to withstand cryogenic temperatures and must resist erasure due to chemical agents or organic solvents.

Storage for long periods of time requires temperatures below -120°C, usually in the gaseous phase of liquid nitrogen, as the liquid phase can transmit contamination from one cryobag or cryotube to another (84). Nitrogen tanks must be suitable for their function and have clearly differentiated compartments (i.e. racks) to store the different batches without loss or cross-contamination. In addition, a record form must be kept in order to ensure the traceability of the cells, employing a storage inventory system that indicates the exact place where the different aliquots are stored. There must be a qualified storage temperature recording system that activates an alarm when there is a problem with the storage temperature. The cryopreservation unit must have limited access to authorized personnel only.

Once the MSC has been thawed, the final characterization and delivery to the patient must be performed. Post-thawing release criteria should include parameters such as viability, recovery, phenotyping and potency assay (87, 88). In our experience, thawing of cryopreserved cells is a critical step, it must be done quickly. Before their clinical application, cells should be cultured for a passage, although other available protocols also provide optimal therapeutic potential. On the other hand, although some assays have been developed on the basis of the immunomodulatory and anti-inflammatory activity of the secretome generated by apoptotic cells infusing them after thawing (90), in our experience the medium and long-term results are less promising, as the potential generated is limited.

SMALL EXTRACELLULAR VESICLES DERIVED FROM MSCs AS CELL-FREE THERAPY

In recent years, the secretome of MSCs, in particular its non-protein fraction consisting of vesicles of different sizes, has attracted attention as a mediator of the paracrine actions of MSCs. Among them, exosomes, also known as small extracellular vesicles (EVs), are nanosized vesicles released by almost all cell types across species (91). MSC-derived EVs (MSC-EVs) are currently being explored as advanced medical products in cell-free therapies for the treatment of acute kidney injury (92), myocardial ischemia (93–95), spinal cord injury (96), hearing loss after noise trauma (97) among other diseases, although few clinical trials are ongoing. MSC-EVs have several advantages over MSCs. For example: i) their smaller size can prevent microvasculature obstruction inherent to the use of MSCs, especially in solid organs. ii) MSC-EVs can cross the blood brain barrier (BBB) extending their use to neurological disorders (98) while MSC cannot (99), iii) although still complex and with a bioactive cargo dependent on the parental sources, they have a significantly simpler composition than MSCs, iv) as non-living biological products, MSC-EVs are more resistant to manipulation than living cells, v) modification of the MSC-EV cargo through the genetic modification of parental cells with associated adeno- or lentivirus vectors exert reduced risk of tumorigenicity after grafting than transplantation of genetically modified cells (100), vi) MSC-EVs can evade phagocytes (101), so reduced doses can be used *in vivo* to achieve a therapeutic response.

Definition of EVs

The generation of EVs in a reproducible way is not an easy task since multiple parameters ranging from passage number and cell culture conditions to environmental stimuli can induce modifications of their cargo. They also remarked on the relevance of quantitation and single-particle characterization (size, shape and density) by electron microscopy (102) nanoparticle tracking analysis, dynamic light scattering, Z potential quantification (103) and flow cytometry (104), as well as the functional analysis of EVs.

Large Scale Production of EVs and Control of Heterogeneity

The use of EVs in clinical practice requires the production of large quantities of these biological products, which cannot be achieved with a single donor of parental cells. One strategy can

be to use different donors to generate a large batch or to develop strategies to increase EV production. In this context, two different strategies can be adopted. The first one consists of the immortalization of parental cells using hTERT, c-MYC (105) or others. The second approach is based on the modification of parental cells to increase the EV biogenesis and/or potency. There is growing consensus about the need for parental cell modifications to boost EV therapeutic potential. This can be achieved either by modification of the biosynthetic pathway (106) or by stress signals like radiation, oxidative stress or hypoxia, with the latter being the most commonly used (94, 107, 108). Indeed, many investigations have tried to mimic the pathologic environment by conditioning MSCs with pro-inflammatory cocktails (109), low oxygen concentration (110), or HIF1-α overexpression (111, 112). Other strategies, such as the overexpression of miRNAs in parental cells, have also resulted effective (113). Nonetheless, to date, the vast majority of clinical trials used EVs isolated from non-modified MSC primary cultures on a small number of enrolled patients.

With regards to EV isolation, ultracentrifugation is not feasible in a clinical setting, not only because of the difficulty to ultracentrifuge large amounts of EV containing culture media but also because the process induces deposits of soluble proteins that reduce the purity of EV preparations. Size exclusion chromatography or tangential flow filtration techniques can bypass this problem and they are becoming a widely adopted method for EVs isolation in the clinical setting (114, 115).

MSC-EVs Manufacturing for Clinical Use

As in the case of clinical applications of MSCs, there are still important challenges to be addressed before implementing the use of EVs in a clinical scenario. The main major issues to be solved include: the scale-up of parental cells in sufficient amounts for clinical use, the costs associated with cell culture in GMP conditions, the use of xeno-free culture media and a minimal characterization of these biological products. MISEV14 and updated MISEV18 recommended, as mentioned above, specific criteria for the definition and classification of MSC-EVs. However, they did not provide guidance on the functional testing of their biological activities. In this context, Dr. Gimona's group provided an extensive list of *in vitro* and *in vivo* potency assays that should be considered before developing clinical trials with a given biological product based on EVs (116). Several factors must be considered during the manufacturing process such as the: i) tissue source, ii) age of donor, iii) passages of parental cells, or if they are primary cultures or have been immortalized, iv) genetic modifications of parental cells, v) priming of parental cell growth factors or culture under hypoxia and vi) isolation procedures of EVs (117). Comparative studies of clinical grade EVs are scarce and the best players together with appropriate strategies to boost MSC-EV therapeutic potential in a clinical setting remain to be elucidated. Therefore, the use of MSC-EVs offers several advantages to MSC administration but, before these biological products can enter into the clinical arena, important obstacles must be resolved from a medicinal product point of view. These include:

1. Control of heterogeneity in EV production by a given parental cell source by defining an optimal range for EV size and composition. This can be achieved by using immortalized parental cell cultures seeded at a given cell concentration with a controlled number of passages and other culture parameters that can influence EV biogenesis.
2. Isolation of MSC-EVs with procedures that minimize protein contaminants including growth factors or lipoproteins that could be co-purified.
3. Preservation of MSC-EV integrity upon scale-up procedures by measuring the degree of aggregation and agglomeration, given that storage conditions including concentration, pH and temperature can induce the fusion of EVs or damage of the lipid bilayer resulting in leakage of the EV cargo.
4. Implementation of GMP procedures to ensure pathogen-free biological products that can be safely used in humans.

In view of the extensive challenges that native or genetically modified EVs need to overcome, novel strategies to design artificial EVs inspired by native biological products are being designed (118). By combining novel drug delivery systems with recombinant surface molecules or synthetic miRNAs, new biological products could be designed. Ideally, artificial nanotechnologies would emulate EVs thus allowing the functional delivery of RNA and other molecules to site-specific targets, since they could be also loaded by integrins and other surface molecules that could guide internalization in host cells and tissues for target-drug delivery (119). These nanotechnologies would recapitulate the favorable characteristics of EVs while reducing heterogeneity and complexity, enabling them to become realistic medical products. Nonetheless, whatever the use of native or synthetic EVs, it is essential to unravel EV structure and composition and to identify relevant molecules for cell-to-cell communication, intracellular uptake and tissue repair and regeneration in order to define the therapeutic product. This will permit the manufacturing processes to be standardized in a move towards the clinical application of these products.

TRANSPORT SYSTEMS OF ATMPs

Control of the distribution and transport of ATMPs, and specifically of MSCs, is a critical part of the production process for this type of medicament; the process must guarantee the product quality and ensure the conditions are ideal until administration. The main hurdle with these medical products is their condition of being living organisms, which must maintain sterility, viability, proliferation capacity and potential at the moment of patient infusion (83). Thus, not only does the production of these cells imply, as explained previously, the challenge of obtaining a safe and effective product, but possible deficiencies in their transport may also contribute thus generating doubts about the real efficacy of the medicament.

MSC production as an advanced therapy medicament for application in patients must therefore be understood as the whole process from dispatch and reception of the cell source

(BM, Adipose tissue, etc.), processing to obtain the active substance and the final product, to the dispatch and reception of the medicament in a hospital setting. All these form part of a larger puzzle and any, even minor, error at any stage could lead to rejection of the medicament batch. In addition, in the case of autologous use, this batch would be unique. Accordingly, the maintenance of transport conditions ensuring medicament quality and safety is a fundamental and necessary step for obtaining good results in the use of these types of medicaments.

It is the producer's responsibility to define the best conditions for cell stability, including excipient choice and medium, storage temperature and the time these cells are kept in the cited conditions until implantation without losing properties. Distribution of these products is usually carried out by the producer or an outsourced company. In both cases, they must fulfill GDP (GDP, Good Distribution Practices) defined by European Directives, and ISO-21973, specific certification on logistics used in Stem Cell Therapy (**Table 2**). The chosen conditions: excipient, temperature, container type etc., according to GMP rules, are mandatorily in writing, approved and validated.

Search for the Best Excipients for Conservation and Distribution of MSCs

One of the more critical problems for MSC producers is cell conservation in a suitable medium/excipient from the end of culture to its application in patients. Not only should the medium keep the cells viable with their properties intact, but the form of administration must also be taken into account, since this affects the choice of excipient if a direct infusion is to be performed, which does not require unnecessary manipulation, which could affect sterility. In systemic infusions, the excipient must have very low density, and would ideally be a liquid to avoid complications such as clots. In the case of local cell implantation, the problem is not the density of the excipient but the method of application, namely the caliber or lumen size of the different tools used: catheters/sheaths (measured in French, the equivalent of diameter in mm multiplied by three) or needles (measured in G, size or diameter of the needle). This caliber would be large enough so as not to offer resistance to the product and break the cells by pressure, which would mean the patient receiving only the excipient with dead cells.

In the majority of studies, the most widely used excipients are isotonic solutions included among intravenous solutions administered to maintain electrolyte balance, such as physiological saline, Ringer's lactate, etc. (14, 15). These media allow the cells to remain stable, sterile, viable, with proliferation capacity and potential until their application; furthermore, they offer easy systemic and local application. As clinical studies with MSCs are moving from a single center to multicenter settings, and even in cases of MSC production with authorization for commercialization, the administration is often performed in clinical centers different to the production centers and, therefore, at some distance away. In these cases, it is essential to maintain optimum product conditions over longer time periods and recently great advances have been made in this area. Currently, some commercial solutions use biopreservative mediums, optimized for conservation and distribution of these products at low temperatures, either in cold (2-8°C) or cryopreserved conditions (-70°C to -196°C). These mediums, which eliminate the need for serums, proteins and cytotoxic products, reduce the product pH at low temperatures, as well as in other conditions, permitting the recovery of ATMPs post-preservation in safe and good quality conditions for their application to patients (120, 121).

Primary Packaging

As mentioned previously, one of the main properties of MSCs is their capacity to adhere to plastic, which is maintained beyond the production process and represents an important limitation to be considered when choosing the packaging container. Therefore, the chosen containers must be composed of materials with low adherence, certain types of plastic, resin or glass, with a design that allows total and simple recovery of the product, as well as reducing risks of contamination by manipulation. Products have been designed that meet these requirements and also cryopreserve the cells. Some of the most commonly used are: plastic syringes with Luer-Look, specific polymer and resin vials, ethylene vinyl acetate bags (EVA) for lower volumes, etc (120, 122).

Secondary Packaging

The choice of secondary packaging, must take into account whether the cells are refrigerated or cryopreserved for transportation, and whether the required packaging is multi-use or single use, as the packaging must protect the product but at the same time insulate and be able to maintain the temperature defined as optimal for transport by the cell producer. These types of packaging are usually composed of expanded foam with low thermal conductivity and high resistance to compression, and must be validated either by the cell producer or the distribution company.

Furthermore, the packaging would include a continuous temperature monitoring system during the complete duration of medicament transport, from leaving the Production Unit to its reception by clinical staff responsible for application of the product to patients. For this reason, the delivery must include dataloggers or continuous registries providing essential information on temperature during the delivery, which will be included in the accompanying documentation. This monitoring allows detection of possible variations in temperature, which if serious could affect the product quality.

Distribution or Transport Flow

GDPs for MSCs in particular and all ATMPs in general, establish mandatory compliance directives aimed at maintaining product quality and safety, so as to implement a rigorous system of quality management by all those involved in cell distribution, thus guaranteeing the quality and integrity of the product (GDPs, **Table 2**).

In the case of obtaining MSCs from different tissues, it is important to clearly establish the distribution flow. In these types of medicaments, a first shipment must be made with an initial container of transport solution for collection of the source tissue

(bone marrow, adipose tissue, periodontal ligament, etc.) from the clinical center to the Production Unit. This is followed by a second shipment of the final product (FP) from the Production Unit to the hospital for patient application.

In both cases, the refrigeration units or packaging must be accompanied by the required documentation from the producer. This must include at least one shipment record including the description of the shipment as well as its state, finalized with the reception record by the clinician. It must also include the shipment label with data required by regulators, including the product name, pharmaceutical form, administration method and unit doses; and, finally, a third document with drug release certification and forms for the communication of adverse reactions.

The packaging will also display exterior labels informing on correct positioning of the shipment (upwards arrows); existence (if any) of infectious agents (three half-moons above a circle); if a genetically modified organism (GMO) is shipped it must be accompanied by mandatory, specific labelling, if it is noninfectious biological material (UN3373), as well as including a number indicating that the medicament presents the lowest degree of hazard; labels indicating whether the shipment includes dry ice (UN1845), or a label indicating maximum and minimum temperatures to which the packaging may be exposed in order to maintain adequate conditions in transit and during delays.

HANDLING AND DELIVERY OF ATMPs FOR THERAPEUTIC USE

As described in previous sections, since the beginnings of the 21st century a new type of medicine has emerged in which the used products are living cells, a paradigm that has substantially changed both the pharmaceutical industry and clinical practice. On the one hand, the effects of these living medicines occur in the medium to long-term and, on the other hand, their manipulation and application needs important training. In addition, their efficiency is closely linked to the survival of the medical product and, therefore, to their accurate manipulation. For example, the FATT-1 clinical trial for the treatment of complex perianal fistulas with ADSCs failed to obtain statistically significant results owing to incorrect handling and erroneous application of the cells (i.e., use of hydrogen peroxide, vial shaking for cell resuspending, high speed of cell infusion, etc.) by the professionals; errors that do not occur when non-living drugs are tested (123). Remarkably, despite these mistakes, the low percentage of inoculated living cells that survived continued working for at least one year (86).

In this respect, as remarked above, the clinical use of stem cells, mainly MSCs in advanced phases (Phase III, multicenter) of clinical trials, have provided results that do not meet the expectations generated (121, 124). These disappointing results have raised doubts in society about the real capabilities of stem cells. However, further analysis has shown that there are numerous aspects involved, not just the cell product. It is noteworthy that in this type of medicine, a good experimental design is as important as good training in the handling and application of the medicine to fulfill the expectations of success generated by the research laboratories. There are numerous differences between a conventional clinical trial and those using live drugs. Our experience has shown us the enormous difficulty of working with a short life-span product, highly sensitive to external physical factors such as temperature, or to mishandling.

There are many routes to deliver MSCs to patients, but all can be summarized in two general approaches: systemic injection and local injection. Systemic intravenous (IV) injection delivery is the most widely used method because of its few complications. Patients usually receive premedication with intravenous steroids and chlorphenamine, complying with local protocols for the prevention of allergic and nonhemolytic transfusion reactions. If the cells are cryopreserved with DMSO they would be refrigerated and infused as soon as possible after thawing to avoid DMSO toxicity at room temperature, so premedication must be administered and venous access must be ready before thawing. MSCs can be infused through a peripheral vein or a central venous line at a slow infusion rate of around 2-5 ml/min; nevertheless, detailed information on cell handling during intravascular (iv) infusion in published clinical trials is frequently lacking. It is preferred not to use filters or anti-reflux caps in the case of BM-MSCs whereas for IV deliver of ADSCs, 200 micron infusion filters are usually used to retain any clump that might form. Another matter of discussion is the use of subcutaneous reservoirs or long-running plastic based catheters that could lead to some cell retention in the device itself. In this respect, a subsequent flushing with saline solution of the cell bag and the intravascular device is always recommended after cell infusion.

In our experience, the main clinical mistakes detected in the handling of living stem cell products include (i) vigorous shaking of cell vials resulting in cell death by friction, (ii) breach of storage temperature leading to cell senescence or apoptosis, (iii) fast resuspension of the cell pellets resulting in disruption of plasma membranes and cell clumping, (iv) fast injection of cells that also results in cell death due to needle friction, (v) local injection of cells in a hostile environment (i.e., use of hydrogen peroxide as a disinfectant), and (vi) poor location of the cell implant after local delivery that needs critically precise injection. In this respect, the cells must be deposited with precision controlling infusion rate and exact site of delivery, neither too superficial nor too deep. When this step depends on the skill of the surgeon alone, variations occur between centers and clinical trials making standardization and eventually automation of this process essential. In this regard, effective delivery techniques must be considered. It is important to ensure that cell survival after local injection is sufficient to have a therapeutic effect at the site of injury. Therefore, experimental pre-studies for each application are essential (125, 126). Particularly relevant is the culture prior to local injection of MSC cryopreserved with DMSO because the resuspension volume of the cell product in the local injection is insufficient to dilute the toxicity of the cryopreservative; so, it is essential "to refresh" the cells after thawing for safe

application. In order to resolve these problems and improve MSC handling we propose the following solutions:

- To have a team of doctors, nurses and supporting staff in charge of cell therapies with training and experience in the handling of live medicines. It is important that the auxiliary staff have been specifically trained in the handling of cells for therapeutic use and are involved in the design and implementation of the logistics for the intervention and administration of the cells.
- Likewise, involvement of the Hospital Pharmacy or the Cell Therapy Area is also important. This department is in charge of receiving the treatment and transporting it to the department where the cells will be administered. These facilities must store the cells properly and dispense them in a timely manner for their correct implantation, including controlled transport.
- The presence of an expert during the first treatments in a center guarantees the proper handling of the cells and their correct administration in each disease and ensures that the process is homogeneously performed from one center to another.
- A subsequent flushing of the intravascular device is recommended after cell infusion. Other requirements include the use of systems with a treated plastic that prevents MSC adherence, as well as glass bottles instead of plastic bags during cell manipulation

CONCLUSIONS AND FUTURE DIRECTION

In the present review, we focus on the protocols that allow an adequate manufacturing of MSCs for their application as ATMPs. The flow diagram of **Figure 2** summarizes the main steps of MSC manufacturing. Firstly, we reviewed the regulation for controlling the production, commercialization and application of cellular and gene therapy products, a critical point for ensuring the quality, safety and efficacy of ATMPs. It was particularly important: the definition of ATMPs, the role for donor selection, and the determination of cellular manufacturing under GMP conditions. ATMPs are those containing genes, cells or tissues suffering manipulation and/or cells that may be used in different ways than in the tissues of origin. The aim of donor selection is to guarantee the traceability of donated ATMPs to ensure information is available on the future of the donation. The regulation of cell products generated under GMP conditions is important because they emphasize the significance of a good definition of the products used, from the starting materials, to the collection and shipping of ATMPs. Under the legal and ethical rules dictated by the authorities, we highlight the parameters to define an "optimal donor", highly dependent on the source of MSCs. For instance, the best adipose tissue-derived MSCs would be isolated from the subcutaneous fat of women under 40 years old, with healthy habits and a BMI lower than 26.8. However, further studies are required to determine the influence of severe and/or chronic diseases on the therapeutic properties of the isolated MSCs, or the age or race of mothers on the quality of UC-derived MSCs. Currently, the MSCs used as starting material to obtain ATMPs can only be isolated in authorized centers, and the processes involved are standardized around the world. On the contrary, the optimal conditions for culturing isolated MSCs are not standardized, constituting a major challenge to improve their therapeutic properties. Cell density in the culture, time of culture and the composition of culture medium are bottlenecks that need critical controls. When many cells are required, this can be controlled by the automation of culture that control metabolites and O_2 concentration essential for cell expansion. Nevertheless, further studies are required to conclusively determine whether normoxic or hypoxic conditions are the best for MSC cultures, and the culture supplements must be carefully selected, considering that MSC from different sources presumably have distinct needs. In summary, it is important a

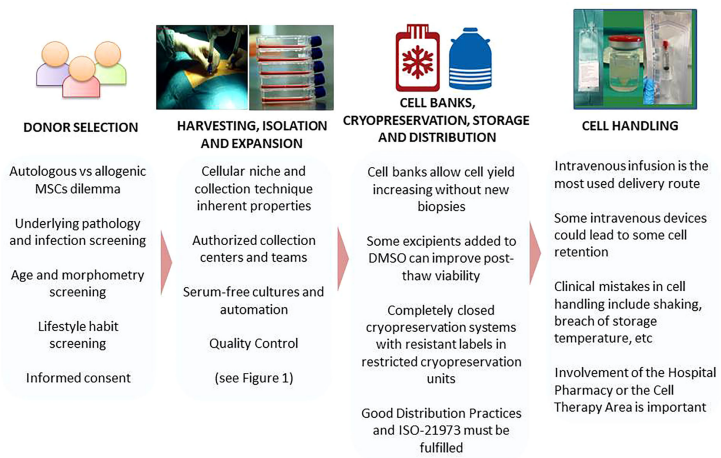

FIGURE 2 | Critical Steps in MSC Manifacturing. (MSCs, Mesenchymal Stromal Cells; DMSO, Dimethyl sulfoxide).

better definition of the critical quality attributes that reflect in part the known heterogeneity of cultured MSCs. Thus, specific surface markers (i.e., CD200, CD106, CD146, Stro1, CD271), biophysical attributes and genomic markers have been proposed for this evaluation (127).

After MSC production, the quality of ATMPs must be tested according to the available guidelines based on GMPs. The quality of MSC products involves the selection of starting and packaging materials, control of the manufacturing process and testing the quality of the final products. MSC quality is evaluated by measuring purity, potency and safety and is key to the success of the subsequent therapeutic administration. The procedures for achieving these tests are extensively standardized but, especially when cells are long-term cultures, a combination of karyotyping and array-CGH is recommended. In addition, microbiological tests must be performed before packaging and as late as possible during the manufacturing procedure.

Cell banks (i.e., Master Cell Banks, Working Cell Banks and Cellular Stocks) are also necessary for storage of the medicinal products, particularly those to be used in allogeneic conditions. Related to cell banking, numerous procedures have been developed for MSC cryopreservation. Distinct compositions of DMSO supplied with diverse molecules are the most used cryopreservatives. Special containers are used for cryogenization and cell volumes for freezing are a critical feature. In addition, after thawing new challenges arise concerning cell recovery, viability, phenotype and potency. Once again, only authorized personal can manipulate the cryopreserved materials.

Although MSC-EVs have some advantages as therapeutic products over MSCs, their production, maintenance and administration have unresolved challenges. Indeed, a reproducible, standardized generation of MSC-EVs is lacking for several reasons: multiple parameters affect the nature of cargos; MSCs from different donors produce many vesicles and aggregation and fusion of MSC-EVs in large particles is frequent. Moreover, EVs must be produced in large amounts to be used in clinical trials, requiring several donors that result in heterogeneous EVs. Indeed, numerous factors, including MSC source, age of donor, culture conditions and modifications undergone by parental cells can affect the nature of the isolated MSC-EVs. Accordingly, new strategies are required to avoid these problems, by generating "artificial" EVs that maintain the most relevant characteristics of MSC-EVs but reduce their heterogeneity and complexity. The identification of key molecules in MSC-EVs will contribute to define minimal features for improving their therapeutic applications.

In a next future, cell therapy, particularly by the routine administration of MSCs or CAR (chimeric antigen receptor) cells, might become predominant in medicine, but only some centers would be able to produce and supply cells, development procedures to control these shipments critical. Any mistake in this process could result in alterations of the product making its therapeutic application inviable. The selection of excipients, storage and shipping temperature and the container conditions are particularly important. On arrival at hospitals, correct handling of the cells is critical for the success of cellular therapies. Here, we emphasize once again that in this area of medicine the drugs are actually living cells, whose manipulation and administration require special care and training. It is particularly important that the personnel, including auxiliary staff, in charge of the cell therapy and those present during the cell infusion receive special training. As discussed in the text, gentle handling of live products is essential. Emphasis should be placed on the absence of vigorous movements, low infusion rate and, in the case of local injection, optimal choice of injection site based on previous studies. All of this must be achieved with trained personnel in the handling of live medicines. Therefore, it is an unmet need to publish recommendations that standardize a basic protocol for MSC handling worldwide.

AUTHOR CONTRIBUTIONS

MF-S, MG-A and AZ made contributions to the coordination and writing of this manuscript. EA, AG-H, ML-P, EV, and PS: manuscript writing. FF-A, DG-O, FP, FS-G, JM and AZ: manuscript review and funding acquisition. All authors accept the published version of the manuscript. All authors contributed to the article and approved the submitted version.

FUNDING

This manuscript has been supported by the Instituto de Salud Carlos III (ISCIII) through the project "RD16/0011: Red de Terapia Celular" (Groups: 0001, 0002, 0004, 0005, 0013, 0015, and 0029), from the sub-programme RETICS, integrated in the "Plan Estatal de I+D+I 2013-2016" and co-financed by the European Regional Development Fund (ERDF) "A way to make Europe", and also by the ISCIII through the project RICORS "RD21/0017;TERAV" (Groups: 001, 002, 003, 006, 009 and 010) that is supported by the Next Generation EU program (Plan de Recuperación, Transformación y Resiliencia); and the Regional Government of Madrid (S2017/BMD-3962, Avancell-CM).

ACKNOWLEDGMENTS

We are indebted to the researchers of the TerCel and TeraV cell production rooms platform of the Institute of Health Carlos III.

REFERENCES

1. García-Bernal D, García-Arranz M, Yáñez RM, Hervás-Salcedo R, Cortés A, Fernández-García M, et al. The Current Status of Mesenchymal Stromal Cells: Controversies, Unresolved Issues and Some Promising Solutions to Improve Their Therapeutic Efficacy. *Front Cell Dev Biol* (2021) 9:650664. doi: 10.3389/fcell.2021.650664
2. Salmikangas P, Schuessler-Lenz M, Ruiz S, Celis P, Reischl I, Menezes-Ferreira M, et al. Marketing Regulatory Oversight of Advanced Therapy Medicinal Products (ATMPs) in Europe: The EMA/CAT Perspective.

Adv Exp Med Biol (2015) 871:103–30. doi: 10.1007/978-3-319-18618-4_6
3. Bailey AM, Arcidiacono J, Benton KA, Taraporewala Z, Winitsky S. United States Food and Drug Administration Regulation of Gene and Cell Therapies. *Adv Exp Med Biol* (2015) 871:1–29. doi: 10.1007/978-3-319-18618-4_1
4. Iglesias-López C, Agustí A, Obach M, Vallano A. Regulatory Framework for Advanced Therapy Medicinal Products in Europe and United States. *Front Pharmacol* (2019) 10:921. doi: 10.3389/fphar.2019.00921
5. Yen-Shun C, Yi-An C, Pei-Hsun T, Chih-Ping C, Sheng-Wen S, Yogi H. Mesenchymal Stem Cell: Considerations for Manufacturing and Clinical Trials on Cell Therapy Product. *Int J Stem Cell Res Ther* (2016) 3:29. doi: 10.23937/2469-570X/1410029
6. Rojewski MT, Lotfi R, Gjerde C, Mustafa K, Veronesi E, Ahmed AB, et al. Translation of a Standardized Manufacturing Protocol for Mesenchymal Stromal Cells: A Systematic Comparison of Validation and Manufacturing Data. *Cytotherapy* (2019) 21(4):468–82. doi: 10.1016/j.jcyt.2019.03.001
7. Ivaskiene T, Mauricas M, Ivaska J. Hospital Exemption for Advanced Therapy Medicinal Products: Issue in Application in the European Union Member States. *Curr Stem Cell Res Ther* (2016) 12(1):45–51. doi: 10.2174/1574888X11666160714114854
8. Pearce KF, Hildebrandt M, Greinix H, Scheding S, Koehl U, Worel N, et al. Regulation of Advanced Therapy Medicinal Products in Europe and the Role of Academia. *Cytotherapy* (2014) 16(3):289–97. doi: 10.1016/j.jcyt.2013.08.003
9. Wright A, Arthaud-Day ML, Weiss ML. Therapeutic Use of Mesenchymal Stromal Cells: The Need for Inclusive Characterization Guidelines to Accommodate All Tissue Sources and Species. *Front Cell Dev Biol* (2021) 9:632717. doi: 10.3389/fcell.2021.632717
10. Ancans J. Cell Therapy Medicinal Product Regulatory Framework in Europe and its Application for MSC-Based Therapy Development. *Front Immunol* (2012) 3:253. doi: 10.3389/fimmu.2012.00253
11. Avivar-Valderas A, Martín-Martín C, Ramírez C, Del Río B, Menta R, Mancheño-Corvo P, et al. Dissecting Allo-Sensitization After Local Administration of Human Allogeneic Adipose Mesenchymal Stem Cells in Perianal Fistulas of Crohn's Disease Patients. *Front Immunol* (2019) 10:1244. doi: 10.3389/fimmu.2019.01244
12. DelaRosa O, Sánchez-Correa B, Morgado S, Ramírez C, del Río B, Menta R, et al. Human Adipose-Derived Stem Cells Impair Natural Killer Cell Function and Exhibit Low Susceptibility to Natural Killer-Mediated Lysis. *Stem Cells Dev* (2012) 21(8):1333–43. doi: 10.1089/scd.2011.0139
13. Hoogduijn MJ, Lombardo E. Mesenchymal Stromal Cells Anno 2019: Dawn of the Therapeutic Era? Concise Review. *Stem Cells Transl Med* (2019) 8 (11):1126–34. doi: 10.1002/sctm.19-0073
14. Panés J, García-Olmo D, Van Assche G, Colombel JF, Reinisch W, Baumgart DC, et al. Expanded Allogeneic Adipose-Derived Mesenchymal Stem Cells (Cx601) for Complex Perianal Fistulas in Crohn's Disease: A Phase 3 Randomised, Double-Blind Controlled Trial. *Lancet (London England)* (2016) 388(10051):1281–90. doi: 10.1016/S0140-6736(16)31203-X
15. European Medicines Agency. *Alofisel*. Available at: https://www.ema.europa.eu/en/documents/assessment-report/alofisel-epar-public-assessment-report_en.pdf.
16. Geissler PJ, Davis K, Roostaeian J, Unger J, Huang J, Rohrich RJ. Improving Fat Transfer Viability: The Role of Aging, Body Mass Index, and Harvest Site. *Plast Reconstr Surg* (2014) 134(2):227–32. doi: 10.1097/PRS.0000000000000398
17. Ogawa R, Mizuno H, Hyakusoku H, Watanabe A, Migita M, Shimada T. Chondrogenic and Osteogenic Differentiation of Adipose-Derived Stem Cells Isolated From GFP Transgenic Mice. *J Nippon Med Sch* (2004) 71 (4):240–1. doi: 10.1272/jnms.71.240
18. Van Harmelen V, Röhrig K, Hauner H. Comparison of Proliferation and Differentiation Capacity of Human Adipocyte Precursor Cells From the Omental and Subcutaneous Adipose Tissue Depot of Obese Subjects. *Metabolism* (2004) 53(5):632–7. doi: 10.1016/j.metabol.2003.11.012
19. Aksu AE, Rubin JP, Dudas JR, Marra KG. Role of Gender and Anatomical Region on Induction of Osteogenic Differentiation of Human Adipose-Derived Stem Cells. *Ann Plast Surg* (2008) 60(3):306–22. doi: 10.1097/SAP.0b013e3180621ff0
20. Yoshimura K, Shigeura T, Matsumoto D, Sato T, Takaki Y, Aiba-Kojima E, et al. Characterization of Freshly Isolated and Cultured Cells Derived From the Fatty and Fluid Portions of Liposuction Aspirates. *J Cell Physiol* (2006) 208(1):64–76. doi: 10.1002/jcp.20636
21. Yu G, Wu X, Dietrich MA, Polk P, Scott LK, Ptitsyn AA, et al. Yield and Characterization of Subcutaneous Human Adipose-Derived Stem Cells by Flow Cytometric and Adipogenic mRNA Analyzes. *Cytotherapy* (2010) 12 (4):538–46. doi: 10.3109/14653241003649528
22. Choudhery MS, Badowski M, Muise A, Pierce J, Harris DT. Donor Age Negatively Impacts Adipose Tissue-Derived Mesenchymal Stem Cell Expansion and Differentiation. *J Transl Med* (2014) 12(1):8. doi: 10.1186/1479-5876-12-8
23. Alt EU, Senst C, Murthy SN, Slakey DP, Dupin CL, Chaffin AE, et al. Aging Alters Tissue Resident Mesenchymal Stem Cell Properties. *Stem Cell Res* (2012) 8(2):215–25. doi: 10.1016/j.scr.2011.11.002
24. Wang B, Liu Z, Chen VP, Wang L, Inman CL, Zhou Y, et al. Transplanting Cells From Old But Not Young Donors Causes Physical Dysfunction in Older Recipients. *Aging Cell* (2020) 19(3):e13106. doi: 10.1111/acel.13106
25. Wu W, Niklason L, Steinbacher DM. The Effect of Age on Human Adipose-Derived Stem Cells. *Plast Reconstr Surg* (2013) 131(1):27–37. doi: 10.1097/PRS.0b013e3182729cfc
26. Aspera-Werz RH, Chen T, Ehnert S, Zhu S, Fröhlich T, Nussler AK. Cigarette Smoke Induces the Risk of Metabolic Bone Diseases: Transforming Growth Factor Beta Signaling Impairment *via* Dysfunctional Primary Cilia Affects Migration, Proliferation, and Differentiation of Human Mesenchymal Stem Cells. *Int J Mol Sci* (2019) 20(12):2915. doi: 10.3390/ijms20122915
27. Aspera-Werz RH, Ehnert S, Müller M, Zhu S, Chen T, Weng W, et al. Assessment of Tobacco Heating System 2.4 on Osteogenic Differentiation of Mesenchymal Stem Cells and Primary Human Osteoblasts Compared to Conventional Cigarettes. *World J Stem Cells* (2020) 12(8):841–56. doi: 10.4252/wjsc.v12.i8.841
28. Nguyen B, Alpagot T, Oh H, Ojcius D, Xiao N. Comparison of the Effect of Cigarette Smoke on Mesenchymal Stem Cells and Dental Stem Cells. *Am J Physiol Cell Physiol* (2021) 320(2):C175–81. doi: 10.1152/ajpcell.00217.2020
29. Shaito A, Saliba J, Husari A, El-Harakeh M, Chhouri H, Hashem Y, et al. Electronic Cigarette Smoke Impairs Normal Mesenchymal Stem Cell Differentiation. *Sci Rep* (2017) 7(1):14281. doi: 10.1038/s41598-017-14634-z
30. Di Rocco G, Baldari S, Pani G, Toietta G. Stem Cells Under the Influence of Alcohol: Effects of Ethanol Consumption on Stem/Progenitor Cells. *Cell Mol Life Sci* (2019) 76(2):231–44. doi: 10.1007/s00018-018-2931-8
31. Varlamov O, Bucher M, Myatt L, Newman N, Grant KA. Daily Ethanol Drinking Followed by an Abstinence Period Impairs Bone Marrow Niche and Mitochondrial Function of Hematopoietic Stem/Progenitor Cells in Rhesus Macaques. *Alcohol Clin Exp Res* (2020) 44(5):1088–98. doi: 10.1111/acer.14328
32. Li J, Wang Y, Li Y, Sun J, Zhao G. The Effect of Combined Regulation of the Expression of Peroxisome Proliferator-Activated Receptor-γ and Calcitonin Gene-Related Peptide on Alcohol-Induced Adipogenic Differentiation of Bone Marrow Mesenchymal Stem Cells. *Mol Cell Biochem* (2014) 392(1–2):39–48. doi: 10.1007/s11010-014-2016-4
33. Schweizer R, Waldner M, Oksuz S, Zhang W, Komatsu C, Plock JA, et al. Evaluation of Porcine Versus Human Mesenchymal Stromal Cells From Three Distinct Donor Locations for Cytotherapy. *Front Immunol* (2020) 11:826. doi: 10.3389/fimmu.2020.00826
34. Ferng AS, Marsh KM, Fleming JM, Conway RF, Schipper D, Bajaj N, et al. Adipose-Derived Human Stem/Stromal Cells: Comparative Organ Specific Mitochondrial Bioenergy Profiles. *Springerplus* (2016) 5(1):2057. doi: 10.1186/s40064-016-3712-1
35. Aust L, Devlin B, Foster SJ, Halvorsen YDC, Hicok K, du Laney T, et al. Yield of Human Adipose-Derived Adult Stem Cells From Liposuction Aspirates. *Cytotherapy* (2004) 6(1):7–14. doi: 10.1080/14653240310004539
36. Faustini M, Bucco M, Chlapanidas T, Lucconi G, Marazzi M, Tosca MC, et al. Nonexpanded Mesenchymal Stem Cells for Regenerative Medicine: Yield in Stromal Vascular Fraction From Adipose Tissues. *Tissue Eng Part C Methods* (2010) 16(6):1515–21. doi: 10.1089/ten.TEC.2010.0214
37. Harris LJ, Zhang P, Abdollahi H, Tarola NA, DiMatteo C, McIlhenny SE, et al. Availability of Adipose-Derived Stem Cells in Patients Undergoing

Vascular Surgical Procedures. *J Surg Res* (2010) 163(2):e105–12. doi: 10.1016/j.jss.2010.04.025
38. Mojallal A, Lequeux C, Shipkov C, Duclos A, Braye F, Rohrich R, et al. Influence of Age and Body Mass Index on the Yield and Proliferation Capacity of Adipose-Derived Stem Cells. *Aesthetic Plast Surg* (2011) 35 (6):1097–105. doi: 10.1007/s00266-011-9743-7
39. Padoin AV, Braga-Silva J, Martins P, Rezende K, Rezende AR da R, Grechi B, et al. Sources of Processed Lipoaspirate Cells: Influence of Donor Site on Cell Concentration. *Plast Reconstr Surg* (2008) 122(2):614–8. doi: 10.1097/PRS.0b013e31817d5476
40. Schipper BM, Marra KG, Zhang W, Donnenberg AD, Rubin JP. Regional Anatomic and Age Effects on Cell Function of Human Adipose-Derived Stem Cells. *Ann Plast Surg* (2008) 60(5):538–44. doi: 10.1097/SAP.0b013e3181723bbe
41. van Harmelen V, Skurk T, Röhrig K, Lee Y-M, Halbleib M, Aprath-Husmann I, et al. Effect of BMI and Age on Adipose Tissue Cellularity and Differentiation Capacity in Women. *Int J Obes Relat Metab Disord* (2003) 27(8):889–95. doi: 10.1038/sj.ijo.0802314
42. Russell AL, Lefavor R, Durand N, Glover L, Zubair AC. Modifiers of Mesenchymal Stem Cell Quantity and Quality. *Transfusion* (2018) 58 (6):1434–40. doi: 10.1111/trf.14597
43. Katsara O, Mahaira LG, Iliopoulou EG, Moustaki A, Antsaklis A, Loutradis D, et al. Effects of Donor Age, Gender, and *In Vitro* Cellular Aging on the Phenotypic, Functional, and Molecular Characteristics of Mouse Bone Marrow-Derived Mesenchymal Stem Cells. *Stem Cells Dev* (2011) 20 (9):1549–61. doi: 10.1089/scd.2010.0280
44. Ulum B, Teker HT, Sarikaya A, Balta G, Kuskonmaz B, Uckan-Cetinkaya D, et al. Bone Marrow Mesenchymal Stem Cell Donors With a High Body Mass Index Display Elevated Endoplasmic Reticulum Stress and are Functionally Impaired. *J Cell Physiol* (2018) 233(11):8429–36. doi: 10.1002/jcp.26804
45. Gronthos S, Brahim J, Li W, Fisher LW, Cherman N, Boyde A, et al. Stem Cell Properties of Human Dental Pulp Stem Cells. *J Dent Res* (2002) 81 (8):531–5. doi: 10.1177/154405910208100806
46. Dominici M, Le Blanc K, Mueller I, Slaper-Cortenbach I, Marini F, Krause D, et al. Minimal Criteria for Defining Multipotent Mesenchymal Stromal Cells. The International Society for Cellular Therapy position statement. *Cytotherapy* (2006) 8(4):315–7. doi: 10.1080/14653240600855905
47. Di Taranto G, Cicione C, Visconti G, Isgrò MA, Barba M, Di Stasio E, et al. Qualitative and Quantitative Differences of Adipose-Derived Stromal Cells From Superficial and Deep Subcutaneous Lipoaspirates: A Matter of Fat. *Cytotherapy* (2015) 17(8):1076–89. doi: 10.1016/j.jcyt.2015.04.004
48. Xu L, Liu Y, Sun Y, Wang B, Xiong Y, Lin W, et al. Tissue Source Determines the Differentiation Potentials of Mesenchymal Stem Cells: A Comparative Study of Human Mesenchymal Stem Cells From Bone Marrow and Adipose Tissue. *Stem Cell Res Ther* (2017) 8(1):275. doi: 10.1186/s13287-017-0716-x
49. Posada-González M, Villagrasa A, García-Arranz M, Vorwald P, Olivera R, Olmedillas-López S, et al. Comparative Analysis Between Mesenchymal Stem Cells From Subcutaneous Adipose Tissue and Omentum in Three Types of Patients: Cancer, Morbid Obese and Healthy Control. *Surg Innov* (2022) 29(1):9–21. doi: 10.1177/15533506211013142
50. Calcat-I-Cervera S, Sanz-Nogués C, O'Brien T. When Origin Matters: Properties of Mesenchymal Stromal Cells From Different Sources for Clinical Translation in Kidney Disease. *Front Med* (2021) 8:728496. doi: 10.3389/fmed.2021.728496
51. Kouchakian MR, Baghban N, Moniri SF, Baghban M, Bakhshalizadeh S, Najafzadeh V, et al. The Clinical Trials of Mesenchymal Stromal Cells Therapy. *Stem Cells Int* (2021) 2021:1634782. doi: 10.1155/2021/1634782
52. Friedenstein AJ, Chailakhjan RK, Lalykina KS. The Development of Fibroblast Colonies in Monolayer Cultures of Guinea-Pig Bone Marrow and Spleen Cells. *Cell Tissue Kinet* (1970) 3(4):393–403. doi: 10.1111/j.1365-2184.1970.tb00347.x
53. Hernigou P, Homma Y, Flouzat Lachaniette CH, Poignard A, Allain J, Chevallier N, et al. Benefits of Small Volume and Small Syringe for Bone Marrow Aspirations of Mesenchymal Stem Cells. *Int Orthop* (2013) 37 (11):2279–87. doi: 10.1007/s00264-013-2017-z
54. Oliver K, Awan T, Bayes M. Single- Versus Multiple-Site Harvesting Techniques for Bone Marrow Concentrate: Evaluation of Aspirate Quality and Pain. *Orthop J Sport Med* (2017) 5(8):2325967117724398. doi: 10.1177/2325967117724398
55. Kaplan A, Sackett K, Sumstad D, Kadidlo D, McKenna DH. Impact of Starting Material (Fresh Versus Cryopreserved Marrow) on Mesenchymal Stem Cell Culture. *Transfusion* (2017) 57(9):2216–9. doi: 10.1111/trf.14192
56. Dregalla RC, Herrera JA, Donner EJ. Red Blood Cells and Their Releasates Compromise Bone Marrow-Derived Human Mesenchymal Stem/Stromal Cell Survival *In Vitro*. *Stem Cell Res Ther* (2021) 12(1):547. doi: 10.1186/s13287-021-02610-4
57. Kern S, Eichler H, Stoeve J, Klüter H, Bieback K. Comparative Analysis of Mesenchymal Stem Cells From Bone Marrow, Umbilical Cord Blood, or Adipose Tissue. *Stem Cells* (2006) 24(5):1294–301. doi: 10.1634/stemcells.2005-0342
58. Hoang VT, Trinh Q-M, Phuong DTM, Bui HTH, Hang LM, Ngan NTH, et al. Standardized Xeno- and Serum-Free Culture Platform Enables Large-Scale Expansion of High-Quality Mesenchymal Stem/Stromal Cells From Perinatal and Adult Tissue Sources. *Cytotherapy* (2021) 23(1):88–99. doi: 10.1016/j.jcyt.2020.09.004
59. Chu D-T, Nguyen Thi Phuong T, Tien NLB, Tran DK, Minh LB, Van Thanh V, et al. Adipose Tissue Stem Cells for Therapy: An Update on the Progress of Isolation, Culture, Storage, and Clinical Application. *J Clin Med* (2019) 8 (7):917. doi: 10.3390/jcm8070917
60. Duscher D, Maan ZN, Luan A, Aitzetmüller MM, Brett EA, Atashroo D, et al. Ultrasound-Assisted Liposuction Provides a Source for Functional Adipose-Derived Stromal Cells. *Cytotherapy* (2017) 19(12):1491–500. doi: 10.1016/j.jcyt.2017.07.013
61. Dubey NK, Mishra VK, Dubey R, Deng Y-H, Tsai F-C, Deng W-P. Revisiting the Advances in Isolation, Characterization and Secretome of Adipose-Derived Stromal/Stem Cells. *Int J Mol Sci* (2018) 19(8):2200. doi: 10.3390/ijms19082200
62. Svalgaard JD, Juul S, Vester-Glovinski PV, Haastrup EK, Ballesteros OR, Lynggaard CD, et al. Lipoaspirate Storage Time and Temperature: Effects on Stromal Vascular Fraction Quality and Cell Composition. *Cells Tissues Org* (2020) 209(1):54–63. doi: 10.1159/000507825
63. Alstrup T, Eijken M, Bohn AB, Møller B, Damsgaard TE. Isolation of Adipose Tissue-Derived Stem Cells: Enzymatic Digestion in Combination With Mechanical Distortion to Increase Adipose Tissue-Derived Stem Cell Yield From Human Aspirated Fat. *Curr Protoc Stem Cell Biol* (2019) 48(1): e68. doi: 10.1002/cpsc.68
64. Gentile P, Calabrese C, De Angelis B, Pizzicannella J, Kothari A, Garcovich S. Impact of the Different Preparation Methods to Obtain Human Adipose-Derived Stromal Vascular Fraction Cells (AD-SVFs) and Human Adipose-Derived Mesenchymal Stem Cells (AD-MSCs): Enzymatic Digestion Versus Mechanical Centrifugation. *Int J Mol Sci* (2019) 20(21):5471. doi: 10.3390/ijms20215471
65. Jayaraman P, Lim R, Ng J, Vemuri MC. Acceleration of Translational Mesenchymal Stromal Cell Therapy Through Consistent Quality GMP Manufacturing. *Front Cell Dev Biol* (2021) 9:648472. doi: 10.3389/fcell.2021.648472
66. Stroncek DF, Jin P, McKenna DH, Takanashi M, Fontaine MJ, Pati S, et al. Human Mesenchymal Stromal Cell (MSC) Characteristics Vary Among Laboratories When Manufactured From the Same Source Material: A Report by the Cellular Therapy Team of the Biomedical Excellence for Safer Transfusion (BEST) Collaborative. *Front Cell Dev Biol* (2020) 8:458. doi: 10.3389/fcell.2020.00458
67. Kim DS, Lee MW, Lee T-H, Sung KW, Koo HH, Yoo KH. Cell Culture Density Affects the Stemness Gene Expression of Adipose Tissue-Derived Mesenchymal Stem Cells. *BioMed Rep* (2017) 6(3):300–6. doi: 10.3892/br.2017.845
68. Gadelorge M, Bourdens M, Espagnolle N, Bardiaux C, Murrell J, Savary L, et al. Clinical-Scale Expansion of Adipose-Derived Stromal Cells Starting From Stromal Vascular Fraction in a Single-Use Bioreactor: Proof of Concept for Autologous Applications. *J Tissue Eng Regener Med* (2018) 12 (1):129–41. doi: 10.1002/term.2377
69. Silva Couto P, Rotondi MC, Bersenev A, Hewitt CJ, Nienow AW, Verter F, et al. Expansion of Human Mesenchymal Stem/Stromal Cells (hMSCs) in Bioreactors Using Microcarriers: Lessons Learnt and What

the Future Holds. *Biotechnol Adv* (2020) 45:107636. doi: 10.1016/j.biotechadv.2020.107636
70. Barckhausen C, Rice B, Baila S, Sensebé L, Schrezenmeier H, Nold P, et al. GMP-Compliant Expansion of Clinical-Grade Human Mesenchymal Stromal/Stem Cells Using a Closed Hollow Fiber Bioreactor. *Methods Mol Biol* (2016) 1416:389–412. doi: 10.1007/978-1-4939-3584-0_23
71. Zhao AG, Shah K, Freitag J, Cromer B, Sumer H. Differentiation Potential of Early- and Late-Passage Adipose-Derived Mesenchymal Stem Cells Cultured Under Hypoxia and Normoxia. *Stem Cells Int* (2020) 2020:8898221. doi: 10.1155/2020/8898221
72. Van Pham P, Truong NC, Le PT-B, Tran TD-X, Vu NB, Bui KH-T, et al. Isolation and Proliferation of Umbilical Cord Tissue Derived Mesenchymal Stem Cells for Clinical Applications. *Cell Tissue Bank* (2016) 17(2):289–302. doi: 10.1007/s10561-015-9541-6
73. Liu S, de Castro LF, Jin P, Civini S, Ren J, Reems J-A, et al. Manufacturing Differences Affect Human Bone Marrow Stromal Cell Characteristics and Function: Comparison of Production Methods and Products From Multiple Centers. *Sci Rep* (2017) 7:46731. doi: 10.1038/srep46731
74. Czapla J, Matuszczak S, Kulik K, Wiśniewska E, Pilny E, Jarosz-Biej M, et al. The Effect of Culture Media on Large-Scale Expansion and Characteristic of Adipose Tissue-Derived Mesenchymal Stromal Cells. *Stem Cell Res Ther* (2019) 10(1):235. doi: 10.1186/s13287-019-1331-9
75. Karnieli O, Friedner OM, Allickson JG, Zhang N, Jung S, Fiorentini D, et al. A Consensus Introduction to Serum Replacements and Serum-Free Media for Cellular Therapies. *Cytotherapy* (2017) 19(2):155–69. doi: 10.1016/j.jcyt.2016.11.011
76. Kouroupis D, Bowles AC, Greif DN, Leñero C, Best TM, Kaplan LD, et al. Regulatory-Compliant Conditions During Cell Product Manufacturing Enhance *In Vitro* Immunomodulatory Properties of Infrapatellar Fat Pad-Derived Mesenchymal Stem/Stromal Cells. *Cytotherapy* (2020) 22(11):677–89. doi: 10.1016/j.jcyt.2020.06.007
77. Bui HTH, Nguyen LT, Than UTT. Influences of Xeno-Free Media on Mesenchymal Stem Cell Expansion for Clinical Application. *Tissue Eng Regener Med* (2021) 18(1):15–23. doi: 10.1007/s13770-020-00306-z
78. Council of Europe and European Pharmacopoeia (Ph. Eur.). *10th Ed. European Directorate for the Quality of Medicines & HealthCare of the Council of Europe (EDQM), 10th*. Strasbourg (France): Council of Europe (2020).
79. Detela G, Lodge A. Manufacturing Process Development of ATMPs Within a Regulatory Framework for EU Clinical Trial & Marketing Authorisation Applications. *Cell Gene Ther Insights* (2016) 2(4):425–52. doi: 10.18609/cgti.2016.056
80. de Wolf C, van de Bovenkamp M, Hoefnagel M. Regulatory Perspective on *In Vitro* Potency Assays for Human Mesenchymal Stromal Cells Used in Immunotherapy. *Cytotherapy* (2017) 19(7):784–97. doi: 10.1016/j.jcyt.2017.03.076
81. Wuchter P, Bieback K, Schrezenmeier H, Bornhäuser M, Müller LP, Bönig H, et al. Standardization of Good Manufacturing Practice–compliant Production of Bone Marrow–Derived Human Mesenchymal Stromal Cells for Immunotherapeutic Applications. *Cytotherapy* (2015) 17(2):128–39. doi: 10.1016/j.jcyt.2014.04.002
82. Saito S, Morita K, Kohara A, Masui T, Sasao M, Ohgushi H, et al. Use of BAC Array CGH for Evaluation of Chromosomal Stability of Clinically Used Human Mesenchymal Stem Cells and of Cancer Cell Lines. *Hum Cell* (2011) 24(1):2–8. doi: 10.1007/s13577-010-0006-8
83. Council of Europe. *Guide to the Quality and Safety of Tissues and Cells for Human Application. 4th*. Strasbourg Cedex, France: Council of Europe (2019).
84. Thirumala S, Goebel WS, Woods EJ. Clinical Grade Adult Stem Cell Banking. *Organogenesis* (2009) 5(3):143–54. doi: 10.4161/org.5.3.9811
85. Oliver-Vila I, Coca MI, Grau-Vorster M, Pujals-Fonts N, Caminal M, Casamayor-Genescà A, et al. Evaluation of a Cell-Banking Strategy for the Production of Clinical Grade Mesenchymal Stromal Cells From Wharton's Jelly. *Cytotherapy* (2016) 18(1):25–35. doi: 10.1016/j.jcyt.2015.10.001
86. Garcia-Arranz M, Garcia-Olmo D, Herreros MD, Gracia-Solana J, Guadalajara H, de la Portilla F, et al. Autologous Adipose-Derived Stem Cells for the Treatment of Complex Cryptoglandular Perianal Fistula: A Randomized Clinical Trial With Long-Term Follow-Up. *Stem Cells Transl Med* (2020) 9(3):295–301. doi: 10.1002/sctm.19-0271
87. Harel A. Cryopreservation and Cell Banking for Autologous Mesenchymal Stem Cell-Based Therapies. *Cell Tissue Transplant Ther* (2013) 5:1. doi: 10.4137/CTTT.S11249
88. Semenova E, Grudniak MP, Bocian K, Chroscinska-Krawczyk M, Trochonowicz M, Stepaniec IM, et al. Banking of AT-MSC and its Influence on Their Application to Clinical Procedures. *Front Bioeng Biotechnol* (2021) 9:773123. doi: 10.3389/fbioe.2021.773123
89. Jitraruch S, Dhawan A, Hughes RD, Filippi C, Lehec SC, Glover L, et al. Cryopreservation of Hepatocyte Microbeads for Clinical Transplantation. *Cell Transpl* (2017) 26(8):1341–54. doi: 10.1177/0963689717720050
90. Giri J, Galipeau J. Mesenchymal Stromal Cell Therapeutic Potency Is Dependent Upon Viability, Route of Delivery, and Immune Match. *Blood Adv* (2020) 4(9):1987–97. doi: 10.1182/bloodadvances.2020001711
91. Raposo G, Stoorvogel W. Extracellular Vesicles: Exosomes, Microvesicles, and Friends. *J Cell Biol* (2013) 200(4):373–83. doi: 10.1083/jcb.201211138
92. Bruno S, Grange C, Deregibus MC, Calogero RA, Saviozzi S, Collino F, et al. Mesenchymal Stem Cell-Derived Microvesicles Protect Against Acute Tubular Injury. *J Am Soc Nephrol* (2009) 20(5):1053–67. doi: 10.1681/ASN.2008070798
93. Ma J, Zhao Y, Sun L, Sun X, Zhao X, Sun X, et al. Exosomes Derived From *Akt* -Modified Human Umbilical Cord Mesenchymal Stem Cells Improve Cardiac Regeneration and Promote Angiogenesis *via* Activating Platelet-Derived Growth Factor D. *Stem Cells Transl Med* (2017) 6(1):51–9. doi: 10.5966/sctm.2016-0038
94. Zhu L-P, Tian T, Wang J-Y, He J-N, Chen T, Pan M, et al. Hypoxia-Elicited Mesenchymal Stem Cell-Derived Exosomes Facilitates Cardiac Repair Through miR-125b-Mediated Prevention of Cell Death in Myocardial Infarction. *Theranostics* (2018) 8(22):6163–77. doi: 10.7150/thno.28021
95. Charles CJ, Li RR, Yeung T, Mazlan SMI, Lai RC, de Kleijn DPV, et al. Systemic Mesenchymal Stem Cell-Derived Exosomes Reduce Myocardial Infarct Size: Characterization With MRI in a Porcine Model. *Front Cardiovasc Med* (2020) 7:601990. doi: 10.3389/fcvm.2020.601990
96. Wang Y, Lai X, Wu D, Liu B, Wang N, Rong L. Umbilical Mesenchymal Stem Cell-Derived Exosomes Facilitate Spinal Cord Functional Recovery Through the miR-199a-3p/145-5p-Mediated NGF/TrkA Signaling Pathway in Rats. *Stem Cell Res Ther* (2021) 12(1):117. doi: 10.1186/s13287-021-02148-5
97. Warnecke A, Harre J, Staecker H, Prenzler N, Strunk D, Couillard-Despres S, et al. Extracellular Vesicles From Human Multipotent Stromal Cells Protect Against Hearing Loss After Noise Trauma *In Vivo*. *Clin Transl Med* (2020) 10(8):e262. doi: 10.1002/ctm2.262
98. Moon GJ, Sung JH, Kim DH, Kim EH, Cho YH, Son JP, et al. Application of Mesenchymal Stem Cell-Derived Extracellular Vesicles for Stroke: Biodistribution and MicroRNA Study. *Transl Stroke Res* (2019) 10(5):509–21. doi: 10.1007/s12975-018-0668-1
99. Cerri S, Greco R, Levandis G, Ghezzi C, Mangione AS, Fuzzati-Armentero M-T, et al. Intracarotid Infusion of Mesenchymal Stem Cells in an Animal Model of Parkinson's Disease, Focusing on Cell Distribution and Neuroprotective and Behavioral Effects. *Stem Cells Transl Med* (2015) 4(9):1073–85. doi: 10.5966/sctm.2015-0023
100. Lai CP-K, Breakefield XO. Role of Exosomes/Microvesicles in the Nervous System and Use in Emerging Therapies. *Front Physiol* (2012) 3:228. doi: 10.3389/fphys.2012.00228
101. Baglio SR, Rooijers K, Koppers-Lalic D, Verweij FJ, Pérez Lanzón M, Zini N, et al. Human Bone Marrow- and Adipose-Mesenchymal Stem Cells Secrete Exosomes Enriched in Distinctive miRNA and tRNA Species. *Stem Cell Res Ther* (2015) 6(1):127. doi: 10.1186/s13287-015-0116-z
102. Zabeo D, Cvjetkovic A, Lässer C, Schorb M, Lötvall J, Höög JL. Exosomes Purified From a Single Cell Type Have Diverse Morphology. *J Extracell Vesicles* (2017) 6(1):1329476. doi: 10.1080/20013078.2017.1329476
103. Midekessa G, Godakumara K, Ord J, Viil J, Lättekivi F, Dissanayake K, et al. Zeta Potential of Extracellular Vesicles: Toward Understanding the Attributes That Determine Colloidal Stability. *ACS Omega* (2020) 5(27):16701–10. doi: 10.1021/acsomega.0c01582
104. van der Vlist EJ, Nolte-'t Hoen ENM, Stoorvogel W, Arkesteijn GJA, Wauben MHM. Fluorescent Labeling of Nano-Sized Vesicles Released by Cells and

Subsequent Quantitative and Qualitative Analysis by High-Resolution Flow Cytometry. *Nat Protoc* (2012) 7(7):1311–26. doi: 10.1038/nprot.2012.065
105. Chen TS, Arslan F, Yin Y, Tan SS, Lai RC, Choo ABH, et al. Enabling a Robust Scalable Manufacturing Process for Therapeutic Exosomes Through Oncogenic Immortalization of Human ESC-Derived MSCs. *J Transl Med* (2011) 9(1):47. doi: 10.1186/1479-5876-9-47
106. Kojima R, Bojar D, Rizzi G, Hamri GC-E, El-Baba MD, Saxena P, et al. Designer Exosomes Produced by Implanted Cells Intracerebrally Deliver Therapeutic Cargo for Parkinson's Disease Treatment. *Nat Commun* (2018) 9(1):1305. doi: 10.1038/s41467-018-03733-8
107. Bister N, Pistono C, Huremagic B, Jolkkonen J, Giugno R, Malm T. Hypoxia and Extracellular Vesicles: A Review on Methods, Vesicular Cargo and Functions. *J Extracell Vesicles* (2020) 10(1):e12002. doi: 10.1002/jev2.12002
108. Gregorius J, Wang C, Stambouli O, Hussner T, Qi Y, Tertel T, et al. Small Extracellular Vesicles Obtained From Hypoxic Mesenchymal Stromal Cells Have Unique Characteristics That Promote Cerebral Angiogenesis, Brain Remodeling and Neurological Recovery After Focal Cerebral Ischemia in Mice. *Basic Res Cardiol* (2021) 116(1):40. doi: 10.1007/s00395-021-00881-9
109. Gorgun C, Ceresa D, Lesage R, Villa F, Reverberi D, Balbi C, et al. Dissecting the Effects of Preconditioning With Inflammatory Cytokines and Hypoxia on the Angiogenic Potential of Mesenchymal Stromal Cell (MSC)-Derived Soluble Proteins and Extracellular Vesicles (EVs). *Biomaterials* (2021) 269:120633. doi: 10.1016/j.biomaterials.2020.120633
110. Han Y, Ren J, Bai Y, Pei X, Han Y. Exosomes From Hypoxia-Treated Human Adipose-Derived Mesenchymal Stem Cells Enhance Angiogenesis Through VEGF/VEGF-R. *Int J Biochem Cell Biol* (2019) 109:59–68. doi: 10.1016/j.biocel.2019.01.017
111. Gonzalez-King H, García NA, Ontoria-Oviedo I, Ciria M, Montero JA, Sepúlveda P. Hypoxia Inducible Factor-1α Potentiates Jagged 1-Mediated Angiogenesis by Mesenchymal Stem Cell-Derived Exosomes. *Stem Cells* (2017) 35(7):1747–59. doi: 10.1002/stem.2618
112. Sun J, Shen H, Shao L, Teng X, Chen Y, Liu X, et al. HIF-1α Overexpression in Mesenchymal Stem Cell-Derived Exosomes Mediates Cardioprotection in Myocardial Infarction by Enhanced Angiogenesis. *Stem Cell Res Ther* (2020) 11(1):373. doi: 10.1186/s13287-020-01881-7
113. Qu Y, Zhang Q, Cai X, Li F, Ma Z, Xu M, et al. Exosomes Derived From miR-181-5p-Modified Adipose-Derived Mesenchymal Stem Cells Prevent Liver Fibrosis *via* Autophagy Activation. *J Cell Mol Med* (2017) 21(10):2491–502. doi: 10.1111/jcmm.13170
114. Monguió-Tortajada M, Gálvez-Montón C, Bayes-Genis A, Roura S, Borràs FE. Extracellular Vesicle Isolation Methods: Rising Impact of Size-Exclusion Chromatography. *Cell Mol Life Sci* (2019) 76(12):2369–82. doi: 10.1007/s00018-019-03071-y
115. Guo J, Wu C, Lin X, Zhou J, Zhang J, Zheng W, et al. Establishment of a Simplified Dichotomic Size-Exclusion Chromatography for Isolating Extracellular Vesicles Toward Clinical Applications. *J Extracell Vesicles* (2021) 10(11):e12145. doi: 10.1002/jev2.12145
116. Gimona M, Pachler K, Laner-Plamberger S, Schallmoser K, Rohde E. Manufacturing of Human Extracellular Vesicle-Based Therapeutics for Clinical Use. *Int J Mol Sci* (2017) 18(6):1190. doi: 10.3390/ijms18061190
117. Witwer KW, Van Balkom BWM, Bruno S, Choo A, Dominici M, Gimona M, et al. Defining Mesenchymal Stromal Cell (MSC)-Derived Small Extracellular Vesicles for Therapeutic Applications. *J Extracell Vesicles* (2019) 8(1):1609206. doi: 10.1080/20013078.2019.1609206
118. de Jong OG, Kooijmans SAA, Murphy DE, Jiang L, Evers MJW, Sluijter JPG, et al. Drug Delivery With Extracellular Vesicles: From Imagination to Innovation. *Acc Chem Res* (2019) 52(7):1761–70. doi: 10.1021/acs.accounts.9b00109
119. Kanasty R, Dorkin JR, Vegas A, Anderson D. Delivery Materials for siRNA Therapeutics. *Nat Mater* (2013) 12(11):967–77. doi: 10.1038/nmat3765
120. Sinden JD, Hicks C, Stroemer P, Vishnubhatla I, Corteling R. Human Neural Stem Cell Therapy for Chronic Ischemic Stroke: Charting Progress From Laboratory to Patients. *Stem Cells Dev* (2017) 26(13):933–47. doi: 10.1089/scd.2017.0009
121. Mathur A, Fernández-Avilés F, Bartunek J, Belmans A, Crea F, Dowlut S, et al. The Effect of Intracoronary Infusion of Bone Marrow-Derived Mononuclear Cells on All-Cause Mortality in Acute Myocardial Infarction: The BAMI Trial. *Eur Heart J* (2020) 41(38):3702–10. doi: 10.1093/eurheartj/ehaa651
122. Vaquero J, Zurita M, Rico MA, Aguayo C, Bonilla C, Marin E, et al. Intrathecal Administration of Autologous Mesenchymal Stromal Cells for Spinal Cord Injury: Safety and Efficacy of the 100/3 Guideline. *Cytother* (2018) 20(6):806–19. doi: 10.1016/j.jcyt.2018.03.032
123. Herreros MD, Garcia-Arranz M, Guadalajara H, De-La-Quintana P, Garcia-Olmo DFATT Collaborative Group. Autologous Expanded Adipose-Derived Stem Cells for the Treatment of Complex Cryptoglandular Perianal Fistulas: A Phase III Randomized Clinical Trial (FATT 1: Fistula Advanced Therapy Trial 1) and Long-Term Evaluation. *Dis Colon Rectum* (2012) 55(7):762–72. doi: 10.1097/DCR.0b013e318255364a
124. Galipeau J. The Mesenchymal Stromal Cells Dilemma–Does a Negative Phase III Trial of Random Donor Mesenchymal Stromal Cells in Steroid-Resistant Graft-Versus-Host Disease Represent a Death Knell or a Bump in the Road? *Cytotherapy* (2013) 15(1):2–8. doi: 10.1016/j.jcyt.2012.10.002
125. Figiel-Dabrowska A, Krześniak NE, Noszczyk BH, Domańska-Janik K, Sarnowska A. Efficiency Assessment of Irrigation as an Alternative Method for Improving the Regenerative Potential of Nonhealing Wounds. *Wound Repair Regen* (2022) 30:303–16. doi: 10.1111/wrr.13013
126. Alagesan S, Brady J, Byrnes D, Fandiño J, Masterson C, McCarthy S, et al. Enhancement Strategies for Mesenchymal Stem Cells and Related Therapies. *Stem Cell Res Ther* (2022) 13(1):75. doi: 10.1186/s13287-022-02747-w
127. Srinivasan A, Sathiyanathan P, Yin L, Liu TM, Lam A, Ravikumar M, et al. Strategies to Enhance Immunomodulatory Properties and Reduce Heterogeneity in Mesenchymal Stromal Cells During Ex Vivo Expansion. *Cytotherapy* (2022) 24(5):456–72. doi: 10.1016/j.jcyt.2021.11.009

Conflict of Interest: FS-G has received honoraria and/or research support from Novartis, Kite/Gilead, Celgene/BMS, Pfizer, Takeda and Roche. DG-O is a member of the Advisory Board of Tigenix SAU and received fees from Takeda. ML-P has received honoraria from Novartis, Kite/Gilead and Celgene/BMS. JM has received research support from Roche, Pfizer, Jazz Pharma, Sandoz-Novartis, Gilead, Celgene, and Takeda not related to this manuscript.

The remaining authors declare that the research was conducted in the absence of any commercial or financial relationships that could be construed as a potential conflict of interest.

Publisher's Note: All claims expressed in this article are solely those of the authors and do not necessarily represent those of their affiliated organizations, or those of the publisher, the editors and the reviewers. Any product that may be evaluated in this article, or claim that may be made by its manufacturer, is not guaranteed or endorsed by the publisher.

frontiers | Frontiers in Immunology

REVIEW
published: 16 June 2022
doi: 10.3389/fimmu.2022.892443

Secondary Lymphoid Organs in Mesenchymal Stromal Cell Therapy: More Than Just a Filter

Di Zheng[1], *Tejasvini Bhuvan*[1], *Natalie L. Payne*[1,2] *and Tracy S. P. Heng*[1,3]*

[1] Department of Anatomy and Developmental Biology, Biomedicine Discovery Institute, Monash University, Clayton, VIC, Australia, [2] Australian Regenerative Medicine Institute, Monash University, Clayton, VIC, Australia, [3] ARC Training Centre for Cell and Tissue Engineering Technologies, Monash University, Clayton, VIC, Australia

Mesenchymal stromal cells (MSCs) have demonstrated therapeutic potential in inflammatory models of human disease. However, clinical translation has fallen short of expectations, with many trials failing to meet primary endpoints. Failure to fully understand their mechanisms of action is a key factor contributing to the lack of successful commercialisation. Indeed, it remains unclear how the long-ranging immunomodulatory effects of MSCs can be attributed to their secretome, when MSCs undergo apoptosis in the lung shortly after intravenous infusion. Their apoptotic fate suggests that efficacy is not based solely on their viable properties, but also on the immune response to dying MSCs. The secondary lymphoid organs (SLOs) orchestrate immune responses and play a key role in immune regulation. In this review, we will discuss how apoptotic cells can modify immune responses and highlight the importance of MSC-immune cell interactions in SLOs for therapeutic outcomes.

Keywords: mesenchymal stromal cells, cell therapy, immune responses, apoptosis, secondary lymphoid organs, spleen, lymph nodes, efferocytosis

OPEN ACCESS

Edited by:
Guido Moll,
Charité Universitätsmedizin Berlin, Germany

Reviewed by:
Lorena Braid,
Simon Fraser University, Canada
Cees Van Kooten,
Leiden University, Netherlands

***Correspondence:**
Tracy S. P. Heng
Tracy.Heng@monash.edu

Specialty section:
This article was submitted to Alloimmunity and Transplantation, a section of the journal Frontiers in Immunology

Received: *09 March 2022*
Accepted: *19 May 2022*
Published: *16 June 2022*

Citation:
Zheng D, Bhuvan T, Payne NL and Heng TSP (2022) Secondary Lymphoid Organs in Mesenchymal Stromal Cell Therapy: More Than Just a Filter. Front. Immunol. 13:892443. doi: 10.3389/fimmu.2022.892443

INTRODUCTION

Mesenchymal stem cells, more accurately known as mesenchymal stromal cells (MSCs), are one of the most widely investigated therapeutic cell types, owing to their ease of accessibility and expansion from tissues free of ethical concerns, as well as their immunomodulatory capacity in various preclinical disease models (1–3) . MSCs can be sourced from the stroma of almost all tissues, but most commonly from bone marrow (BM), adipose tissue (AD) and umbilical cord (UC) (4, 5). MSCs are contained within a heterogeneous population expressing CD105, CD73 and CD90 while lacking CD45, CD11b, CD19 and HLA-DR. They are characterized by their adherence to plastic and ability to differentiate into osteoblasts, adipocytes and chondrocytes *in vitro* (6).

With increasing clinical translation, however, this minimal set of criteria is now recognized as inadequate for defining MSCs. It does not reflect MSC potency, which is largely based on broad immunomodulatory properties (7), rather than their self-renewal or multipotential capacity (8, 9). It does not address changes in marker expression levels or biological properties due to culture expansion and cell manufacturing processes (10), including cryopreservation and freeze-thawing (11). Additionally, it does not identify the risk profile of the MSC product, particularly with regard to hemocompatibility of intravenously (IV) delivered cells and their potential to trigger adverse thromboembolic events (12). Thus, proposed amendments to the criteria have included functional

potency assays based on the immunomodulatory activity of MSCs (13), and profiling of the hemocompatibility of the diverse array of MSC products now in clinical use (14).

The preclinical efficacy of MSCs in various unrelated conditions such as graft-versus-host disease (GvHD), Crohn's disease, kidney transplantation, myocardial infarction, stroke, diabetes, acute respiratory distress syndrome (ARDS), multiple sclerosis, and brain and spinal cord injury, mainly relates to immune regulation (15–20). *In vitro* studies have shown that MSCs can modulate adaptive and innate immune responses. MSCs suppress T cell proliferation, cytokine response (e.g. IFN-γ production) and cytotoxic activity in response to antigen-specific stimuli (21–23) whist promoting regulatory T cells (Tregs), *via* their production of soluble factors (**Figure 1**) such as nitric oxide (NO), indolamine 2,3 dioxygenase (IDO) and transforming growth factor-beta (TGF-β) (24, 30–32). MSCs can also downregulate the cytokine responses of innate immune cells, including dendritic cells (DCs) and monocytes, *via* the expression of prostaglandin E2 (PGE_2) (33). How these *in vitro* findings relate to their mode of action remains to be clarified, given the complexity of immune responses *in vivo* and the short persistence of MSCs following infusion.

MSC SURVIVAL AND BIODISTRIBUTION

To date, studies have investigated different routes of MSC administration in order to maximise therapeutic efficacy. The different administration routes result in variations in MSC survival. IV infusion has been the most commonly used and studied method for MSC delivery because it is convenient, minimally invasive and reproducible (4). However, MSCs administered *via* the IV route are entrapped in the lung and rapidly cleared, with few traces detected in other tissues (34, 35). Studies using various MSC detection techniques, including MSCs constitutively expressing fluorescent proteins or luciferase, or labelled with fluorescent dyes or radioactive tracers, showed that viable MSCs are detected in the lung within 24 hours of IV administration but not at 72 hours (35–37). The decrease in detectable viable cells is directly proportional to the increase in dead cells in the lungs, indicating that IV-infused MSCs undergo cell death (37). Activation of caspase 3, a hallmark of apoptosis, in MSCs further indicates that MSCs undergo programmed cell death following their entrapment in the lung (38, 39).

The survival of IV-delivered MSCs can also be compromised if cells trigger the instant blood-mediated inflammatory reaction (IBMIR) due to incompatibility with blood (40). Expression of secreted and cell surface immunogenic factors (e.g. tissue factor (TF)/CD142) vary across MSC tissue sources and cell manufacturing conditions, including freeze-thawing and culture passaging (12, 14). These factors can activate the innate immune system and trigger the coagulation and complement cascades, which limit MSC engraftment and efficacy, but also increase the potential for adverse thromboembolic events (41).

Other injection routes, including intraperitoneal (IP), subcutaneous (SC), and intramuscular (IM), which bypass the lung, have also been examined. Prolonged detection of MSCs has been observed following IP and SC injection (42, 43). Following IM injection, a dwell time of up to 5-month was observed (44). Other studies have administered MSCs directly into the diseased tissue, for example, intratracheal administration in models of lung inflammation or intrathecal administration in models of spinal cord injury or neuroinflammatory disease (45–48). In these studies, MSCs are directly exposed to an inflammatory

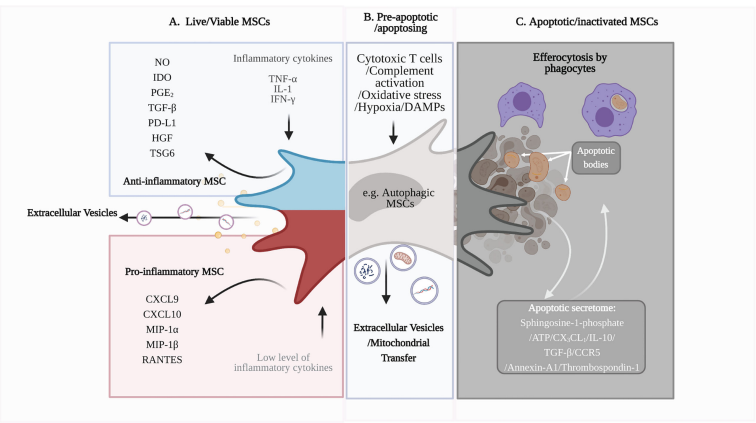

FIGURE 1 | Immunomodulatory capacity of viable and apoptotic MSCs. **(A)** Live or viable MSCs can sense the microenvironment and respond to cytokine signals by polarizing into 'pro-inflammatory' or 'anti-inflammatory' phenotypes (24). 'Anti-inflammatory' MSCs produce anti-inflammatory soluble factors, including IDO and TGF-β, to modulate immune cell function and dampen inflammation. MSCs also produce extracellular vesicles (EV), such as exosomes, that can be immunomodulatory, depending on their cargo (19, 25). **(B)** Excessive inflammatory stress or the presence of cytotoxic immune cells will induce apoptosis of MSCs (26). MSCs can undergo a pre-apoptotic stage, known as autophagy. Autophagic MSCs, as well as the EVs produced during this stage, may have roles in immunosuppression (27). **(C)** As MSCs undergo apoptosis, their apoptotic secretome can promote an anti-inflammatory microenvironment and attract phagocytes for efferocytosis (28). Phagocytes that have engulfed the apoptotic MSCs become immunomodulatory and have downstream regulatory effects on adaptive immune cells, such as T cells (29). Figure was created with BioRender.com.

environment, which can influence MSCs survival and therapeutic efficacy (26, 49). Pre-conditioning of MSCs *via* hypoxia or serum deprivation for instance, can promote cell survival when subsequently exposed to an ischemic environment (50–52). Although the quantity, duration and the type of stress insult matter, overall, excessive stress will likely predispose MSCs to cell death (26).

In some disease settings, dead or dying MSCs and their associated 'by-products' can contribute to therapeutic efficacy (38, 39, 53–55) raising additional questions about their mode of action. How are MSCs killed in different microenvironments? How does the dying process contribute to therapeutic efficacy in different disease settings? Importantly, how do IV administered MSCs dying in the lung exert anti-inflammatory effects in distal organs in disease settings that seemingly do not involve the lung?

MSC APOPTOSIS AND THEIR IMMUNOSUPPRESSIVE 'BY-PRODUCTS'

The molecular pathway that induces the death of MSCs *in vivo* is unclear and complicated by pre-existing disease, inflammatory cell infiltrate and the presence of different pathogens (26). The stress signals from the inflammatory microenvironment can trigger the apoptosis of MSCs. In a mouse model of GvHD, the presence of elevated numbers of cytotoxic $CD8^+$ T cells and $CD56^+$ natural killer (NK) cells in the lung caused MSC apoptosis (38). Settings that do not involve cytotoxic cell infiltrate likely involve other mechanisms. We recently showed that disabling the intrinsic (mitochondrial) pathway of apoptosis in MSCs prevented caspase 3 activation in the lung shortly after IV injection, indicating that MSCs were predominantly killed *via* the intrinsic pathway in non-GvHD settings (39). Activation of coagulation and complement by infused MSCs has also been shown to damage and reduce viability of MSCs (40, 56). Stronger activation of these proteolytic cascades is demonstrated by freeze-thawed (without culture recovery) and high-passage MSCs compared with fresh culture-derived, minimally expanded cells. This is due to variations in expression of immunogenic triggers, which may subsequently impact their *in vivo* therapeutic function (11).

In general, apoptosis is an ordered event that creates a transient immunosuppressive microenvironment *via* the release of anti-inflammatory mediators, including IL-10, TGF-β, CCR5, annexin-A1 and thrombospondin-1 (**Figure 1**) (28). Besides these secreted factors, cells can undergo a pre-apoptotic stage known as autophagy when they sense danger or stress signals from the microenvironment (57). By culturing MSCs in a stressed environment, autophagic MSCs can be pre-engineered to secrete immunomodulatory factors, such as TGF-β, to regulate T cell proliferation (58). Interestingly, MSCs have been shown to communicate with damaged cells *via* bidirectional transfer of mitochondria to increase mitochondrial biogenesis and rescue the cellular function of damaged cells (27). In preclinical models of myocardial infarction and respiratory disorders, mitochondrial transfer has been shown to contribute to the therapeutic effects of MSCs (**Figure 1**) (27, 59–61). MSCs can transfer mitochondria to macrophages *via* tunnelling nanotubules, cell fusion or extracellular vesicles (EV), which influence the macrophage function to modulate inflammation (59, 62). Whilst mitochondrial transfer has yet to be demonstrated in apoptotic MSCs, apoptotic bodies, which are a distinct type of extracellular vesicles formed when apoptotic cells disassemble into fragments (63), may also contribute to therapeutic efficacy upon engulfment by macrophages (64). Thus, MSCs are susceptible to cell death post-administration, which contributes to the anti-inflammatory effects of MSC therapy (10, 39).

EFFEROCYTOSIS OF MSCs

Rapid clearance of apoptotic debris by phagocytes is essential in maintaining body homeostasis. Known as efferocytosis, this physiological process 'silently' removes apoptotic cells, inducing peripheral tolerance and avoiding inflammation. Phagocytic cells, including macrophages and monocytes, play a critical role in MSC therapy, as demonstrated in disease models where depletion of macrophages with clodronate liposomes renders MSC therapy ineffective (33, 36, 38). Phagocytes that have engulfed apoptotic cells, including MSCs, display a regulatory phenotype characterized by upregulation of PD-L1, IDO, COX2 and CD206, increased production of IL-6, IL-10, TGF-β and PGE_2, and decreased production of pro-inflammatory cytokines such as TNF-α and IL-12 (29, 37, 65). Phagocytes that have engulfed apoptotic MSCs can suppress T cell proliferation, downregulate $CD4^+$ T cell activation and promote $Foxp3^+$ Treg generation (29, 37). The inhibition of COX2 abrogated the immunosuppressive capacity of efferocytic monocytes that had engulfed apoptotic MSCs, highlighting the importance of the PGE_2/COX2 axis in this immunosuppressive function (29).

Since MSC apoptosis and the subsequent response of immune cells to this process contributes to their immunomodulatory effects, an outstanding question is whether viable MSCs are still required for MSC therapy, or can pre-inactivated MSCs be used as an alternative?

APOPTOTIC OR DEAD MSCs AS A THERAPEUTIC CELL OPTION

Several studies have investigated the efficacy of *in vitro* induced apoptotic, dead or inactivated MSCs. Treatment outcomes can be influenced by the type and duration of stimulation used to inactivate the cells, and also the disease setting (26). Apoptotic MSCs (39, 53, 54), but not dead MSCs (36, 66) could inhibit lung inflammation. In certain disease settings, such as LPS-induced sepsis, inactivated or dead MSCs could replicate the immunomodulatory effects, as pre-inactivation enhanced the phagocytosis of MSCs (55, 67). In other settings, non-viable MSCs were ineffective or did not fully replicate the effects of

viable MSCs (33, 42, 67). For instance, in GvHD, apoptotic MSCs had to be administered at a much higher dose than viable MSCs to achieve comparable therapeutic benefits (38). It is plausible that inflammatory diseases driven by innate immune or phagocytic cells are more likely to benefit from treatment with inactivated MSCs, while suppression of T cell responses require MSCs with an active secretome (67). Importantly, the type and stage of cell death at the time of MSC administration are key considerations, as apoptosis, but not necrosis or lytic cell death, induces anti-inflammatory responses (68).

Although MSC apoptosis and the subsequent host phagocytic response contribute to immunomodulation, there remains much to learn about the full mechanisms of MSC therapy. As MSC apoptosis and efferocytosis occurs in the lung post-infusion, how does this dampen inflammation in other organs or tissues? *In vitro* studies have shown that MSCs can regulate immune cell function *via* their paracrine activity, but such molecules must have a relatively long half-life and broad biodistribution for this to be a plausible mechanism *in vivo*. Immune responses are initiated and maintained in the SLOs, which play a key role in immune regulation during health and disease. Thus, our knowledge of how MSC therapy modulates immune responses would be improved by considering the known function of SLOs, their role in clearance of apoptotic cells and gaining a better understanding of the effects of MSCs in these organs.

ORGANIZATION AND FUNCTION OF SECONDARY LYMPHOID ORGANS

Primary lymphoid organs, also known as central lymphoid organs, are the sites for the development and maturation of leukocytes. Primary lymphoid organs include the bone marrow and thymus (69–71). Lymphocytes (a class of leukocytes, e.g. T and B cells) generated in primary lymphoid organs then seed the SLOs where they initiate adaptive immune responses. SLOs include lymph nodes (LNs), spleen, tonsils, adenoids, Peyer's patches, and mucosal-associated lymphoid tissues (MALT) (71). The localisation of lymphocytes in SLOs maximizes their interaction with foreign antigens that drain to the SLOs *via* blood or lymphatics. Antigen presenting cells, such as DCs, can also transport antigens to SLOs and activate lymphocytes there. Once activated, these lymphocytes undergo expansion and differentiate into effector or memory cells to provide antigen-specific responses. This review will focus on the spleen and LNs as the major SLOs.

Structure and Function of the Spleen

The spleen is a network of branching arterial vessels that functions to filter blood, allowing for the capture of blood-borne pathogens and antigens, and is a key organ for iron metabolism and erythrocyte homeostasis (72, 73). Although early research suggested that excision of the spleen does not largely impact the human immune system, its functional significance has been demonstrated through various studies over the years. While the human and mouse spleen is similar in terms of gross structure and immune cell function, some key differences are known to exist and have been reported elsewhere (73–75). This section will focus on the mouse spleen.

The spleen is composed of the white pulp (WP) and red pulp (RP), with the marginal zone (MZ) situated in between (76, 77), (**Figure 2**). Arterial blood arrives at the MZ and runs through the cords in the RP, where the F4/80$^+$ RP macrophages (RPMs) monitor and phagocytose incoming aged erythrocytes (85, 86). In addition, RPMs also extract any dead or opsonized cells from the circulation, while simultaneously surveying for pathogens and tissue damage (78). Other leukocyte populations located in the RP, including neutrophils, monocytes and γδ T cells, exert immune effector functions upon encountering an inflammatory insult (72, 76, 77). Blood is recollected in sinuses to form the venous sinusoidal system and ultimately enters the efferent vein for return to the systemic circulation (77, 79, 80).

The white pulp is the site of lymphocyte differentiation and initiation of immune responses to blood borne antigens. Correct organization and maintenance of the WP is regulated by specific chemokines that attract T cells and B cells and establish their respective zones within the WP (81, 82). The continuous traffic of haematopoietic cells in and out of the spleen is an efficient way for these cells to survey the blood for pathogens and antigens.

The MZ is an important transit area for cells that are leaving the bloodstream and entering the WP. It contains a number of resident cells that have unique properties, including a subset of DCs and innate-like B cells called MZB cells (73, 84). Two specific subsets of macrophages are also found here: MZ macrophages (MZMs) and marginal metallophilic macrophages (MMMs) (76, 87). The MZMs line the outer ring of the WP and are characterized by expression of C-type lectin SIGNR1 and type I scavenger receptor MARCO (85, 88). The MMMs form the inner ring, located closer to the WP (89, 90). These macrophages are characterized by expression of the adhesion molecule SIGLEC1 (CD169) (82, 91–93).

Structure and Function of the Lymph Node

While the spleen filters the blood and protects the host against blood-borne pathogens, LNs bring antigens draining from tissues together with lymphocytes circulating in the blood. There are more than 20 identified lymph nodes in mice and over 500 in humans, located at multiple sites throughout the lymphatic circulatory system (94, 95). Current understanding of LN structure and function is mainly gained from animal studies.

The parenchyma of the LN is compartmentalized by stromal cells and organized into the cortex at the outermost region containing B cell follicles, the paracortex in the inner region containing the T cell zone, and the medulla proximal to the efferent lymphatic vessels containing the medullary sinuses (95, 96), (**Figure 3**). Lymphocytes in the blood enter the LNs *via* high endothelial venules (HEVs) directly into the paracortex area. Lymph, containing soluble and cell-associated antigens, enters the LNs *via* afferent lymphatic vessels and is filtered through the lymphatic sinus (71, 95). Subcapsular sinus macrophages (SSMs) survey and capture lymph-borne antigens before they enter the

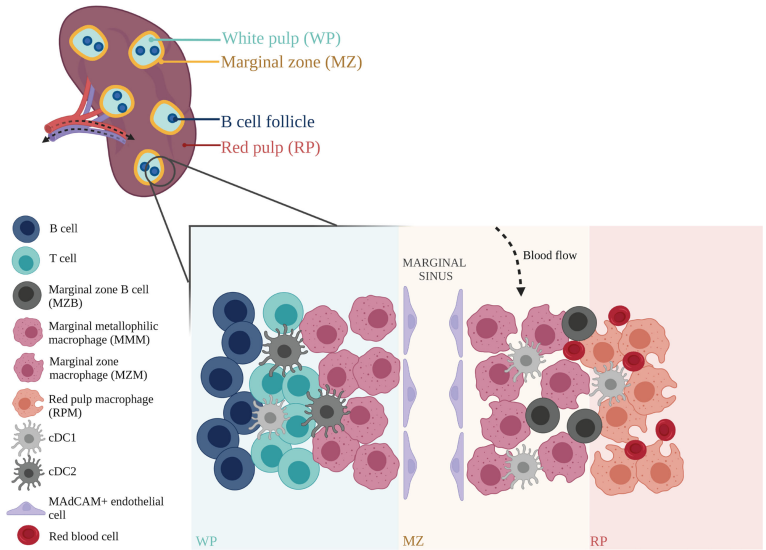

FIGURE 2 | Anatomical structure and organization of mouse spleen. The splenic arterial network functions to filter blood and maintain erythrocyte homeostasis. Arterial blood, arriving at the marginal zone (MZ), passes through the red pulp (RP) cords, and is monitored by red pulp macrophages (RPMs) that survey for blood-borne antigens (78). Blood is recollected in sinuses before exiting the spleen through the efferent vein for return to the systemic circulation (79, 80). Within the spleen, adaptive immune responses to incoming systemic antigens are initiated in the white pulp (WP) which are largely driven by T and B cells (81, 82). Circulating lymphocytes arriving at the spleen may exit the bloodstream and enter the WP *via* the MZ (77). Marginal zone macrophages (MZMs) and marginal metallophilic macrophages (MMMs) are involved in the clearance of apoptotic cells, and maintenance of immune tolerance (83). Their functions are mediated by dendritic cell subsets, cDC1 and cDC2, which present antigens to T cells, and marginal zone B cells (MZBs) that help synchronize immune responses between the adaptive and innate arms (73, 84). This immune network is closely supported by stromal cells such as MAdCAM$^+$ endothelial cells that line the marginal sinus, and help mediate tissue homeostasis (77). Figure was created with BioRender.com.

cortex and paracortex, acting as gatekeepers that protect the host from aberrant immune responses and preventing the systemic spread of antigens (97–99, 102, 103). SSMs initiate innate immune responses by producing pro-inflammatory cytokines to recruit innate immune cells, and can also activate adaptive immunity by extending across the subcapsular sinus floor to present antigen to B cells in the follicles (99, 104).

Lymph passing by the subcapsular sinus will encounter another type of sinus macrophage, known as medullary sinus macrophages (MSMs). MSMs are located along the sinus of the medulla region, interacting with the lymph and also lymphocytes that are egressing the LN (97). Functionally, MSMs can actively phagocytose antigens, as well as apoptotic immune cells in the lymph (105–107). As the lymph passes through the medullary sinus, it then exits the LNs *via* the efferent lymphatic vessel and eventually return to the blood circulation.

The LN contains other macrophages that are also important in maintaining tissue homeostasis and clearing apoptotic debris. Medullary cord macrophages (MCMs) support plasma cell survival and efferocytose apoptotic debris, while tingible body macrophages (TBMs) are involved in the clearance of apoptotic B cells in the germinal centre (97). A recent study has identified a resident macrophage population in the T cell zone, known as T cell zone macrophages (TZMs), that efferocytose apoptotic DCs draining from the periphery (100). As efferocytosis induces an immunomodulatory phenotype in phagocytes, these LN resident macrophages play an important role in immune regulation.

APOPTOTIC CELL CLEARANCE AND TOLERANCE IN SLOs

Essentially all tissues undergo programmed cell death, known as apoptosis, evident through the constant turnover of cells. Under homeostatic conditions, apoptotic cells rarely accumulate in tissues due to the efficient efferocytosis by tissue phagocytes. The clearance of apoptotic cells is linked to an anti-inflammatory response that also induces immunological tolerance (108, 109). The precise apoptotic cell machinery and phagocytic components involved in apoptotic cell-induced immunosuppression are reviewed extensively elsewhere (109–112). However, it is clear that the efficient clearance of apoptotic cells can be attributed to the redundancy in the mechanisms of apoptotic cell recognition.

Splenic and LN macrophages are known to participate in the efferocytosis of apoptotic cells and maintenance of immune tolerance. TZMs and TBMs in the LN are known to engulf apoptotic debris silently without stimulating T cells, in order to maintain local immune homeostasis (100). The splenic MZ is also involved in the clearance of apoptotic cells from the circulation. IV-injected apoptotic cells drain to the splenic MZ, where they are rapidly engulfed by macrophages in the marginal zone (83). MZMs are known to be critical for particulate trapping in the spleen (72). Depletion studies (in which both MZMs and MMMs are depleted) have also indicated a crucial role for MZ macrophages in apoptotic cell-driven immunomodulation. The initial engulfment of apoptotic cells by macrophages in the MZ is

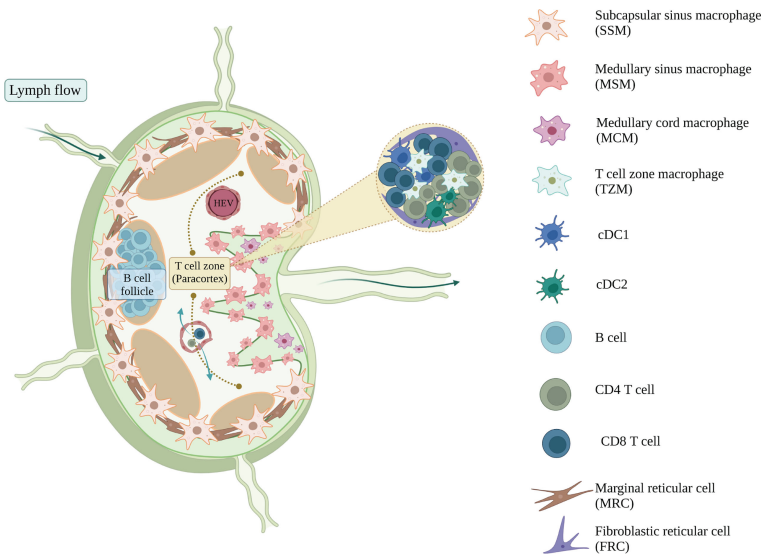

FIGURE 3 | The immune and stromal cell composition of mouse lymph node. Lymph nodes filter the lymph and respond to the lymph-borne antigens, from which T and B cells will get activated, proliferate, and provide adaptive immune responses. Myeloid populations of lymph nodes support and regulate this adaptive response and maintain the homeostasis of lymph nodes (97). Subcapsular sinus macrophages (SSM) survey the infiltrating lymph before they transduce the activation signals towards the B cells sitting in the B cell follicles (98, 99), whereas cDC1 and cDC2 present the antigens that activate the $CD4^+$ and $CD8^+$ T cells inside the T cell zone, respectively (95). Subsets of lymph node macrophages, including medullary cord macrophages (MCM), T cell zone macrophages (TZM) and tingible body macrophages (TBM), are known for their efferocytotic ability (97, 100). They clear the apoptotic cell debris and maintain the homeostasis of lymph nodes. Lymph node stromal cells also help in regulating tissue homeostasis. Marginal reticular cells (MRC) organize and regulate the B cell follicles, whereas fibroblastic reticular cells (FRC) maintain the T cell homeostasis within the paracortex (101). Figure was created with BioRender.com.

vital in the generation of tolerance to self, whereby delayed clearance of apoptotic cells results in reduced immune tolerance to apoptotic cell-associated antigens (113). For example, depletion of MZ macrophages led to development of systemic tolerance breakdown in mouse models of systemic lupus erythematosus (SLE) and induced inflammatory responses towards apoptotic cell antigens (113).

The infusion of apoptotic cells has been reported to induce immunosuppression in experimental inflammatory diseases, autoimmunity and transplantation. In animal models of autoimmune arthritis, when apoptotic cells were infused not at the joint, but *via* the IV (114–116) or IP route (114, 117), the resolution of arthritic inflammation was conserved at the joint. In mouse models of transplantation, IV infusion of donor apoptotic splenocytes was shown to promote donor-specific immunosuppression, prolonging the survival of heart allografts (118, 119). Clinical studies have also shown that infusion of leukocytes rendered non-viable, either *via* a chemical cross-linker, 1-ethyl-3-(3-dimethylaminopropyl)-carbodiimide (ECDI) or extracorporeal photochemotherapy, is safe and potentially beneficial in multiple sclerosis (120) and cutaneous T cell lymphoma (121). In apoptotic cell-based therapies, the spleen plays a pivotal role as splenic macrophages and DCs are involved in the phagocytosis of apoptotic leukocytes administrated *via* the IV route (122, 123). Together, these findings point to a critical role for the SLOs in the clearance of apoptotic cells and establishment of a tolerogenic state.

SLOs IN DISEASE

SLOs have a crucial role in host immune defense. In SLOs, antigen priming and immune cell activation occurs, followed by clonal expansion of antigen-specific effector lymphocytes, and the formation of immunological memory and tolerance. The importance of the spleen in host immunity has been demonstrated in various disease settings. In a long-term follow-up study, patients whose spleen had been surgically removed had an increased risk of developing bacterial infections (124). In malaria, the spleen is important in controlling the blood stage infection, clearance of parasitized red blood cells, induction of memory lymphocytes and replenishment of healthy red blood cells (125, 126). Splenectomized patients infected with malaria experienced enhanced parasitic burden, severe disease symptoms, and higher mortality rate (126).

Although SLOs are protective during infection, they may also promote the establishment and progression of some inflammatory diseases. LNs are the key sites for the initiation of GvHD and acute colitis (127, 128). In GvHD, donor cells migrate to the recipient LNs *via* their expression of lymphoid homing molecules, CD62L (L-selectin) and CCR7 (C-C chemokine receptor 7) (129). Upon recognition of alloantigen on the donor cells, T cells in the recipient LNs are activated and migrate to tissues where they cause damage (commonly in skin, gut and liver) (127). In acute colitis, intestinal migratory DCs

drain to the mesenteric LNs where they present antigen and induce Th1 or Th17 responses (128, 130, 131). Pathogenic Th17 cells can also migrate from the mesenteric LNs to the gut and cause inflammatory bowel disease (131). Some studies have shown that lymphadenectomy (surgical removal of a group of lymph nodes and surrounding lymphatic tissues) protected rats from GvHD (132, 133). Lymphadenectomy is rarely investigated in clinical studies for the purpose of reducing inflammation, although it is performed on cancer patients to stop the spread of tumor metastases *via* the lymphatic system, or to remove the tumor cells in the lymphatic tissues (134, 135).

The spleen can also promote inflammatory responses in some disease settings. For example, splenectomy showed protective effects (e.g. reduced infarct volume) in rat models of brain, liver, kidney and intestine ischemic injury (136–140). In animal models of ischemic brain injury and also in patients with stroke, spleen atrophy (reduction in splenic weight and size) is commonly observed and thought to be a result of splenic leukocytes egressing *via* the blood circulation and into the injured brain (141). These circulating leukocytes are composed of monocytes, macrophages, neutrophils and lymphocytes, and their migration to the brain exacerbates inflammation and neurodegeneration (142, 143). Splenectomy performed on a rat stroke model (middle cerebral artery occlusion, MCAO), prior to injury, showed neuroprotective effects, with a reduction in brain infarct volume, peripheral immune cells and activated microglia in the brain infarct tissue (140, 142). Apart from the infiltration of splenic immune cells into the brain injury sites, the spleen also contributes to brain inflammation by producing pro-inflammatory signals, such as IFN-γ (140).

The involvement of SLOs and peripheral immune cells in the progression of central nervous system (CNS) inflammation has also been highlighted in other disease models, including spinal cord injury and experimental autoimmune encephalomyelitis (EAE, mouse model of multiple sclerosis) (144–146). In these disease settings, peripheral T cells and myeloid cells are recruited to the CNS and promote disease symptoms by enhancing inflammation. The crucial contribution of splenic T cells in promoting neuroinflammation is further demonstrated in neuropathic pain studies, in which the adoptive transfer of splenic T cells elevated neuropathic pain symptoms in the recipient (144).

Understanding how SLOs regulate the inflammatory response in such disease settings is important in defining the role of these SLOs in mediating the immunomodulatory effects of cell therapy.

SLOs IN CELL THERAPY

Given the importance of SLOs in disease progression and tolerance induction, there is emerging evidence for their involvement in cell therapy in experimental disease models. A notable example is stroke, where IV administration of different therapeutic cell types, such as umbilical cord blood cells, haematopoietic stem cells, amnion epithelial cells, bone marrow stromal cells and multipotent adult progenitor cells, were shown to induce neuroprotective effects (147–150). IV-injected therapeutic cells were detected in the spleen and induced an anti-inflammatory environment that promoted repair in the CNS (e.g. infarct size, peripheral immune cell infiltration) (149–151). Of note, a study using neural stem cells to treat stroke showed that the direct interaction between IV-administered stem cells with splenocytes, particularly $CD11b^+$ cells, was necessary for the treatment to be neuroprotective, with splenectomy abolishing the beneficial effect (152). In line with this, the improvement in functional recovery from stroke in MAPC-treated animals was also not evident in the absence of a spleen, supporting a critical role for the spleen (153).

MSC Biodistribution in SLOs

Despite the central role of the spleen and lymph nodes in the blood and lymph network respectively, MSCs are rarely detected in the SLOs. When reported, the presence of MSCs in the SLOs is usually minimal and requires sensitive detection techniques (**Figure 4**). Small numbers of MSCs were detected in spleen and lymph nodes 24 hours post-IV infusion in naïve mice (154), and for up to 5 weeks in a mouse model of sclerodermatous GvHD (155). Similarly, localization within the spleen and LNs may also occur in the days after IP, but not SC or IM, infusion (44), although MSC biodistribution was variable following this delivery route and attachment of MSC aggregates to the peritoneal walls has been reported (157).

It is thought that the presence of MSCs in SLOs is a result of their active migration, since they express higher levels of homing molecules, including CCR7, CD62L and intercellular adhesion molecule-1 (ICAM-1), compared to other fibroblastic cells (154, 158, 159). MSCs engineered to overexpress CCR7 or ICAM-1 showed improved MSC migration to the spleen and LNs post-IV injection in a GvHD model (158, 159). The increased distribution of MSCs within SLOs correlated with an improvement in their immunomodulatory effects and clinical outcomes in these disease models (158, 159).

The presence of inflammation can influence the biodistribution of MSCs in SLOs. In a myocardial infarction (MI) model, the presence of inflammation increased the recruitment of IV-infused MSCs to the spleen compared to controls without MI (160). In contrast, inflammation can reduce the presence of MSCs in the LNs. In experimental models of colitis and delayed-type hypersensitivity (DTH) (154, 161), accumulation of MSCs was reduced in the LNs and redistributed towards the inflamed tissues.

However, it is important to note the caveats of the labelling approaches used in such studies. For example, membrane dyes are retained when cells lose membrane integrity upon cell death, making it hard to discriminate signals from viable cells, cellular debris, or redistribution by phagocytes that had engulfed apoptotic cells (162). Moreover, studies have repeatedly shown that the small numbers of detectable MSCs eventually get cleared (35, 39, 163), yet their interaction with the host immune system within minutes to hours post-IV infusion is likely critical to therapeutic outcomes. For instance, complement activation by MSCs can adversely trigger IBMIR, but has also been found to

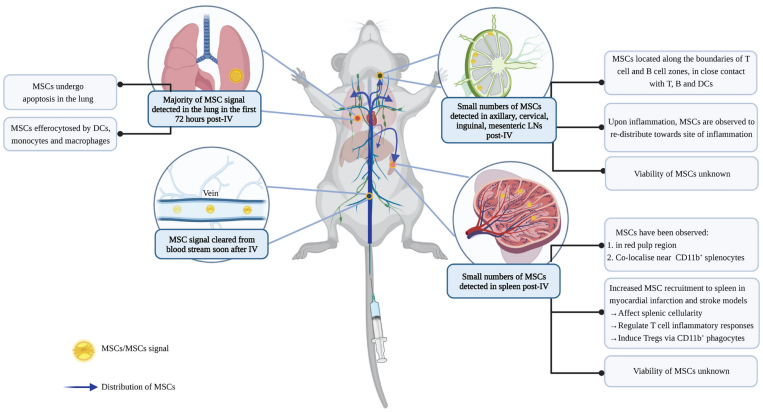

FIGURE 4 | Biodistribution of MSCs post-IV infusion. IV administration is the most commonly used method for MSC delivery. To study the biodistribution of MSCs following IV infusion, studies have used different labelling approaches to track cell signals. Depending on the sensitivity of the techniques, MSCs (or signals of labels) have been found in lung, liver, and SLOs following IV infusion (37, 154). MSCs are cleared rapidly from the blood, and the majority of them are then detected in the lung where they undergo cell death (35). Some signals can also be found in the liver, although these are mostly dead MSCs (37, 154). Dead MSCs in the lung are cleared by lung phagocytes to avoid inflammation (37). Recent studies identified small numbers of MSCs in the SLOs, however, it is unclear whether they remain viable inside the SLOs (154–156). In LNs, MSCs are observed to localize along the boundaries of the germinal center and paracortical area; while in the spleen, MSC signals are detected in the red pulp region, co-localizing with $CD11b^+$cells (155, 156). MSCs in the SLOs can regulate T cell response and induce Tregs, and their recruitment is influenced by inflammation. However, the extent by which these immunomodulatory effects in the SLOs are induced by efferocytosis of dying MSCs, or direct contact with viable MSCs or their secretome, remains unknown. Figure was created with BioRender.com.

upregulate the expression of CD11b on blood myeloid cells, which mediate the immunosuppressive effects of MSCs (164). Clarification of whether the detection of MSC signals in SLOs indicates the presence of viable MSCs or apoptotic cell clearance therefore has important implications for our understanding of the mechanisms of MSC therapy.

MSCs Regulate the T Cell Profile in SLOs

In several disease settings, the cellular composition of SLOs and function of their immune cells are changed upon cell therapy. The presence of MSCs is also found to associate with a change in the total cellularity of the SLO (154, 158, 160, 165), (**Figure 4**). In a model of myocardial infarction, MSC recruitment to the spleen was shown to decrease splenic natural killer cells and neutrophils (160). In a stroke model, the infusion of human umbilical cord blood cells altered the T cell and monocyte/macrophage composition in the spleen (165). In GvHD and DTH models, MSC recruitment to the LNs was also observed to regulate the survival and activation of lymphocytes, in particular, T cells (154, 158).

The splenic T cell profile is further modulated following cell therapy. Splenic T cells from animals that had received cell therapy were composed of a less pro-inflammatory population (with reduced IFN-γ^+ and IL-17^+ $CD4^+$ T cells), which exhibited a reduced pro-inflammatory response when restimulated *in vitro* (165, 166). In an autoimmune uveitis model (166), T cells from MSC-treated groups showed reduced proliferative response and produced less pro-inflammatory Th1 and Th17 cytokines, but more anti-inflammatory IL-10, upon antigen restimulation.

Apart from modulating the T cell profile and inflammatory responses, MSC treatment can also induce Tregs in SLOs. In studies of autoimmune disease and allograft transplantation, MSCs inhibited inflammation by inducing an increase in $FoxP3^+$ Tregs in the draining LNs and the spleen (156, 166–169). Similarly, an increase in splenic Tregs after MSC treatment was observed in ischemic kidney injury models. The importance of Treg induction in this model was highlighted when the therapeutic effects of MSCs were abrogated following the depletion of Tregs or the complete excision of the spleen (170).

Myeloid Cells in SLOs Are a Critical Mediator of MSC Effects

Studies have established that co-culturing different myeloid cell populations with MSCs induces regulatory phenotypes, which can modulate immune responses. For example, DCs co-cultured with MSCs downregulated their expression of co-stimulatory molecules and were found to be less stimulatory in activating T cell responses *in vitro* (171–173). Monocytes and macrophages exposed to MSCs were less pro-inflammatory (produced less TNF and IL-12, and more IL-10 and IL-6) (174), more phagocytic and had increased bacterial killing capacity (33, 174–176). Macrophages with an immunoregulatory profile could further maintain an anti-inflammatory microenvironment and influence Treg generation (174, 177). Induction of amphiregulin in MSC-primed macrophages was recently identified as one pathway leading to induction of Tregs and decreased Th1 responses (178). The phenotype and morphology of macrophages 're-educated' by MSCs share some similarities with myeloid-derived suppressor cells (MDSCs), which are differentiated from immature myeloid cells *via* PGE_2 and IL-10-dependent mechanisms, and have immunosuppressive function (177). However, these *in vitro* findings need to be contextualized within the complex structural organization and cellular composition of the SLOs.

Studies examining immune cell changes in SLOs following MSC therapy support a role for myeloid cells in mediating the immunomodulatory effects of MSCs. When infused in a GvHD model, MSCs overexpressing the homing molecule, ICAM-1, were found in greater numbers in the SLOs (compared to control MSCs) and were found to inhibit splenic DC activation and maturation, suppress $CD4^+$ T cell differentiation, and increase the splenic Treg/effector T cell ratio (159). Whilst it remains to be established that the change in regulatory/effector T cell balance is a direct consequence of DC function altered by MSCs in the spleen, studies have linked the induction of Tregs to $CD11b^+$ phagocytic cells. Co-culture of splenocytes with MSCs induced Tregs, but not in the absence of $CD11b^+$ cells (156). In a model of enterocolitis, the increase in Tregs in the SLOs underlies MSC therapeutic efficacy, which is abrogated upon the depletion of $CD11b^+$ cells by clodronate-filled liposomes (156). Importantly, adoptive transfer of $CD11b^+$ cells that had been co-cultured with MSCs was sufficient to increase Tregs in the SLOs and protect against disease (156). In another study using an osteosarcoma xenograft model in mice lacking T cells, clodronate depletion of $CD11b^+$ splenic macrophages increased the amount of bioluminescence signal of luciferase-expressing MSCs found in the spleen after IV injection, and subsequently facilitated MSC delivery to the tumor (179). The data suggest that MSCs are phagocytosed by macrophages in the spleen, and overcoming this barrier promotes tissue-targeted delivery of MSCs. Thus, while the tolerogenic outcome of efferocytosis can contribute to the anti-inflammatory effects of MSC therapy, settings that require efficient delivery of MSCs to tissues may need to employ strategies that avoid splenic macrophage clearance.

CONCLUSION AND FUTURE DIRECTIONS

MSCs exhibit broad spectrum immunomodulatory effects in various inflammatory diseases, but do not persist for significant periods in any part of the body following IV infusion. Instead, their lung entrapment and rapid clearance has shifted the focus to lung phagocytic cells as mediators of their therapeutic effects. Although traces of MSCs have been found in SLOs, along with changes in immune cell composition and function, limitations in labelling and imaging techniques make it difficult to establish with certainty that the small numbers detected are viable MSCs, cell debris or label redistribution following phagocytic uptake. There are several cell types with phagocytic capacity in the SLOs, including migratory cells from the circulation. Cells found in different compartments of the spleen and LNs perform different function, which depends crucially upon their spatial interactions with other cells and chemical cues. Furthermore, SLOs comprise not just immune cells, but also a variety of stromal populations that have functional roles in health and disease (180, 181), including the capacity to efferocytose apoptotic cells (182). Whether these stromal populations have a role in MSC therapy is an open area to explore.

AUTHOR CONTRIBUTIONS

DZ, TB, NP, and TH contributed conception and design of the manuscript. DZ wrote the first draft of the manuscript and made the figures. TB, NP, and TH wrote sections of the manuscript. All authors contributed to manuscript revision, read and approved the submitted version.

FUNDING

DZ and TB are recipients of the Australian Government Research Training Program (RTP) Scholarship. TH is supported by funding from the National Health and Medical Research Council of Australia (GNT1107188, GNT1162499, GNT2012290) and the Australian Research Council (IC190100026). The Australian Regenerative Medicine Institute is supported by grants from the State Government of Victoria and the Australian Government.

ACKNOWLEDGMENTS

The authors thank Ivan Poon and Scott Mueller for helpful discussion.

REFERENCES

1. Rendra E, Scaccia E, Bieback K. Recent Advances in Understanding Mesenchymal Stromal Cells. *F1000Res* (2020) 9:156. doi: 10.12688/f1000research.21862.1
2. Jossen V, van den Bos C, Eibl R, Eibl D. Manufacturing Human Mesenchymal Stem Cells at Clinical Scale: Process and Regulatory Challenges. *Appl Microbiol Biotechnol* (2018) 102:3981–94. doi: 10.1007/s00253-018-8912-x
3. Martin I, Galipeau J, Kessler C, Le Blanc K, Dazzi F. Challenges for Mesenchymal Stromal Cell Therapies. *Sci Transl Med* (2019) 11(480): eaat2189. doi: 10.1126/scitranslmed.aat2189
4. Kabat M, Bobkov I, Kumar S, Grumet M. Trends in Mesenchymal Stem Cell Clinical Trials 2004-2018: Is Efficacy Optimal in a Narrow Dose Range? *Stem Cells Transl Med* (2020) 9:17–27. doi: 10.1002/sctm.19-0202
5. Mendicino M, Bailey AM, Wonnacott K, Puri RK, Bauer SR. MSC-Based Product Characterization for Clinical Trials: An FDA Perspective. *Cell Stem Cell* (2014) 14:141–5. doi: 10.1016/j.stem.2014.01.013
6. Dominici M, Le Blanc K, Mueller I, Slaper-Cortenbach I, Marini F, Krause D, et al. Minimal Criteria for Defining Multipotent Mesenchymal Stromal Cells. The International Society for Cellular Therapy Position Statement. *Cytotherapy* (2006) 8:315–7. doi: 10.1080/14653240600855905
7. Krampera M, Galipeau J, Shi Y, Tarte K, Sensebe L. Therapy MSCCotISfC. Immunological Characterization of Multipotent Mesenchymal Stromal Cells–The International Society for Cellular Therapy (ISCT) Working Proposal. *Cytotherapy* (2013) 15:1054–61. doi: 10.1016/j.jcyt.2013.02.010
8. Bianco P, Cao X, Frenette PS, Mao JJ, Robey PG, Simmons PJ, et al. The Meaning, the Sense and the Significance: Translating the Science of Mesenchymal Stem Cells Into Medicine. *Nat Med* (2013) 19:35–42. doi: 10.1038/nm.3028

9. Robey P. "Mesenchymal Stem Cells": Fact or Fiction, and Implications in Their Therapeutic Use. *F1000Res* (2017) 6:524. doi: 10.12688/f1000research.10955.1
10. Cherian DS, Bhuvan T, Meagher L, Heng TSP. Biological Considerations in Scaling Up Therapeutic Cell Manufacturing. *Front Pharmacol* (2020) 11:654. doi: 10.3389/fphar.2020.00654
11. Cottle C, Porter AP, Lipat A, Turner-Lyles C, Nguyen J, Moll G, et al. Impact of Cryopreservation and Freeze-Thawing on Therapeutic Properties of Mesenchymal Stromal/Stem Cells and Other Common Cellular Therapeutics. *Curr Stem Cell Rep* (2022) 8:72-92. doi: 10.1007/s40778-022-00212-1
12. Moll G, Ankrum JA, Olson SD, Nolta JA. Improved MSC Minimal Criteria to Maximize Patient Safety: A Call to Embrace Tissue Factor and Hemocompatibility Assessment of MSC Products. *Stem Cells Trans Med* (2022) 11:2–13. doi: 10.1093/stcltm/szab005
13. Galipeau J, Krampera M, Barrett J, Dazzi F, Deans RJ, DeBruijn J, et al. International Society for Cellular Therapy Perspective on Immune Functional Assays for Mesenchymal Stromal Cells as Potency Release Criterion for Advanced Phase Clinical Trials. *Cytotherapy* (2016) 18:151–9. doi: 10.1016/j.jcyt.2015.11.008
14. Moll G, Ankrum JA, Kamhieh-Milz J, Bieback K, Ringdén O, Volk HD, et al. Intravascular Mesenchymal Stromal/Stem Cell Therapy Product Diversification: Time for New Clinical Guidelines. *Trends Mol Med* (2019) 25:149–63. doi: 10.1016/j.molmed.2018.12.006
15. Hoogduijn MJ, Roemeling-van Rhijn M, Engela AU, Korevaar SS, Mensah FK, Franquesa M, et al. Mesenchymal Stem Cells Induce an Inflammatory Response After Intravenous Infusion. *Stem Cells Dev* (2013) 22:2825–35. doi: 10.1089/scd.2013.0193
16. Moll G, Geissler S, Catar R, Ignatowicz L, Hoogduijn MJ, Strunk D, et al. Cryopreserved or Fresh Mesenchymal Stromal Cells: Only a Matter of Taste or Key to Unleash the Full Clinical Potential of MSC Therapy? *Adv Exp Med Biol* (2016) 951:77–98. doi: 10.1007/978-3-319-45457-3_7
17. Ankrum JA, Ong JF, Karp JM. Mesenchymal Stem Cells: Immune Evasive, Not Immune Privileged. *Nat Biotechnol* (2014) 32:252–60. doi: 10.1038/nbt.2816
18. Thomi G, Surbek D, Haesler V, Joerger-Messerli M, Schoeberlein A. Exosomes Derived From Umbilical Cord Mesenchymal Stem Cells Reduce Microglia-Mediated Neuroinflammation in Perinatal Brain Injury. *Stem Cell Res Ther* (2019) 10:105. doi: 10.1186/s13287-019-1207-z
19. Lu Y, Zhou Y, Zhang R, Wen L, Wu K, Li Y, et al. Bone Mesenchymal Stem Cell-Derived Extracellular Vesicles Promote Recovery Following Spinal Cord Injury *via* Improvement of the Integrity of the Blood-Spinal Cord Barrier. *Front Neurosci* (2019) 13:209. doi: 10.3389/fnins.2019.00209
20. Gama KB, Santos DS, Evangelista AF, Silva DN, de Alcantara AC, Dos Santos RR, et al. Conditioned Medium of Bone Marrow-Derived Mesenchymal Stromal Cells as a Therapeutic Approach to Neuropathic Pain: A Preclinical Evaluation. *Stem Cells Int* (2018) 2018:8179013–8179013. doi: 10.1155/2018/8179013
21. Di Nicola M, Carlo-Stella C, Magni M, Milanesi M, Longoni PD, Matteucci P, et al. Human Bone Marrow Stromal Cells Suppress T-Lymphocyte Proliferation Induced by Cellular or Nonspecific Mitogenic Stimuli. *Blood* (2002) 99:3838–43. doi: 10.1182/blood.V99.10.3838
22. Bartholomew A, Sturgeon C, Siatskas M, Ferrer K, McIntosh K, Patil S, et al. Mesenchymal Stem Cells Suppress Lymphocyte Proliferation *In Vitro* and Prolong Skin Graft Survival *In Vivo*. *Exp Hematol* (2002) 30:42–8. doi: 10.1016/S0301-472X(01)00769-X
23. Krampera M. Mesenchymal Stromal Cell 'Licensing': A Multistep Process. *Leukemia* (2011) 25:1408–14. doi: 10.1038/leu.2011.108
24. Bernardo ME, Fibbe WE. Mesenchymal Stromal Cells: Sensors and Switchers of Inflammation. *Cell Stem Cell* (2013) 13:392–402. doi: 10.1016/j.stem.2013.09.006
25. Del Fattore A, Luciano R, Pascucci L, Goffredo BM, Giorda E, Scapaticci M, et al. Immunoregulatory Effects of Mesenchymal Stem Cell-Derived Extracellular Vesicles on T Lymphocytes. *Cell Transplant* (2015) 24:2615–27. doi: 10.3727/096368915X687543
26. Weiss DJ, English K, Krasnodembskaya A, Isaza-Correa JM, Hawthorne IJ, Mahon BP. The Necrobiology of Mesenchymal Stromal Cells Affects Therapeutic Efficacy. *Front Immunol* (2019) 10:1228. doi: 10.3389/fimmu.2019.01228
27. Mahrouf-Yorgov M, Augeul L, Da Silva CC, Jourdan M, Rigolet M, Manin S, et al. Mesenchymal Stem Cells Sense Mitochondria Released From Damaged Cells as Danger Signals to Activate Their Rescue Properties. *Cell Death Differ* (2017) 24:1224–38. doi: 10.1038/cdd.2017.51
28. Saas P, Daguindau E, Perruche S. Concise Review: Apoptotic Cell-Based Therapies-Rationale, Preclinical Results and Future Clinical Developments. *Stem Cells* (2016) 34:1464–73. doi: 10.1002/stem.2361
29. Cheung TS, Galleu A, von Bonin M, Bornhauser M, Dazzi F. Apoptotic Mesenchymal Stromal Cells Induce Prostaglandin E2 in Monocytes: Implications for the Monitoring of Mesenchymal Stromal Cell Activity. *Haematologica* (2019) 104:e438–41. doi: 10.3324/haematol.2018.214767
30. Uccelli A, Moretta L, Pistoia V. Mesenchymal Stem Cells in Health and Disease. *Nat Rev Immunol* (2008) 8:726–36. doi: 10.1038/nri2395
31. Sato K, Ozaki K, Oh I, Meguro A, Hatanaka K, Nagai T, et al. Nitric Oxide Plays a Critical Role in Suppression of T-Cell Proliferation by Mesenchymal Stem Cells. *Blood* (2007) 109:228–34. doi: 10.1182/blood-2006-02-002246
32. Ren G, Zhang L, Zhao X, Xu G, Zhang Y, Roberts AI, et al. Mesenchymal Stem Cell-Mediated Immunosuppression Occurs *via* Concerted Action of Chemokines and Nitric Oxide. *Cell Stem Cell* (2008) 2:141–50. doi: 10.1016/j.stem.2007.11.014
33. Nemeth K, Leelahavanichkul A, Yuen PS, Mayer B, Parmelee A, Doi K, et al. Bone Marrow Stromal Cells Attenuate Sepsis *via* Prostaglandin E(2)-Dependent Reprogramming of Host Macrophages to Increase Their Interleukin-10 Production. *Nat Med* (2009) 15:42–9. doi: 10.1038/nm.1905
34. Lee RH, Pulin AA, Seo MJ, Kota DJ, Ylostalo J, Larson BL, et al. Intravenous hMSCs Improve Myocardial Infarction in Mice Because Cells Embolized in Lung are Activated to Secrete the Anti-Inflammatory Protein TSG-6. *Cell Stem Cell* (2009) 5:54–63. doi: 10.1016/j.stem.2009.05.003
35. Eggenhofer E, Benseler V, Kroemer A, Popp FC, Geissler EK, Schlitt HJ, et al. Mesenchymal Stem Cells are Short-Lived and do Not Migrate Beyond the Lungs After Intravenous Infusion. *Front Immunol* (2012) 3:297. doi: 10.3389/fimmu.2012.00297
36. Mathias LJ, Khong SM, Spyroglou L, Payne NL, Siatskas C, Thorburn AN, et al. Alveolar Macrophages are Critical for the Inhibition of Allergic Asthma by Mesenchymal Stromal Cells. *J Immunol* (2013) 191:5914–24. doi: 10.4049/jimmunol.1300667
37. de Witte SFH, Luk F, Sierra Parraga JM, Gargesha M, Merino A, Korevaar SS, et al. Immunomodulation By Therapeutic Mesenchymal Stromal Cells (MSC) Is Triggered Through Phagocytosis of MSC By Monocytic Cells. *Stem Cells* (2018) 36:602–15. doi: 10.1002/stem.2779
38. Galleu A, Riffo-Vasquez Y, Trento C, Lomas C, Dolcetti L, Cheung TS, et al. Apoptosis in Mesenchymal Stromal Cells Induces *In Vivo* Recipient-Mediated Immunomodulation. *Sci Transl Med* (2017) 9(416):eaam7828. doi: 10.1126/scitranslmed.aam7828
39. Pang SHM, D'Rozario J, Mendonca S, Bhuvan T, Payne NL, Zheng D, et al. Mesenchymal Stromal Cell Apoptosis is Required for Their Therapeutic Function. *Nat Commun* (2021) 12:6495. doi: 10.1038/s41467-021-26834-3
40. Moll G, Rasmusson-Duprez I, von Bahr L, Connolly-Andersen AM, Elgue G, Funke L, et al. Are Therapeutic Human Mesenchymal Stromal Cells Compatible With Human Blood? *Stem Cells* (2012) 30:1565–74. doi: 10.1002/stem.1111
41. Caplan H, Olson SD, Kumar A, George M, Prabhakara KS, Wenzel P, et al. Mesenchymal Stromal Cell Therapeutic Delivery: Translational Challenges to Clinical Application. *Front Immunol* (2019) 10. doi: 10.3389/fimmu.2019.01645
42. Giri J, Galipeau J. Mesenchymal Stromal Cell Therapeutic Potency is Dependent Upon Viability, Route of Delivery, and Immune Match. *Blood Adv* (2020) 4:1987–97. doi: 10.1182/bloodadvances.2020001711
43. Kallmeyer K, Andre-Levigne D, Baquie M, Krause KH, Pepper MS, Pittet-Cuenod B, et al. Fate of Systemically and Locally Administered Adipose-Derived Mesenchymal Stromal Cells and Their Effect on Wound Healing. *Stem Cells Transl Med* (2020) 9:131–44. doi: 10.1002/sctm.19-0091
44. Braid LR, Wood CA, Wiese DM, Ford BN. Intramuscular Administration Potentiates Extended Dwell Time of Mesenchymal Stromal Cells Compared to Other Routes. *Cytotherapy* (2018) 20:232–44. doi: 10.1016/j.jcyt.2017.09.013
45. Chen G, Park CK, Xie RG, Ji RR. Intrathecal Bone Marrow Stromal Cells Inhibit Neuropathic Pain *via* TGF-Beta Secretion. *J Clin Invest* (2015) 125:3226–40. doi: 10.1172/JCI80883

46. Schafer S, Berger JV, Deumens R, Goursaud S, Hanisch UK, Hermans E. Influence of Intrathecal Delivery of Bone Marrow-Derived Mesenchymal Stem Cells on Spinal Inflammation and Pain Hypersensitivity in a Rat Model of Peripheral Nerve Injury. *J Neuroinflamm* (2014) 11:157. doi: 10.1186/s12974-014-0157-8
47. Sun J, Han ZB, Liao W, Yang SG, Yang Z, Yu J, et al. Intrapulmonary Delivery of Human Umbilical Cord Mesenchymal Stem Cells Attenuates Acute Lung Injury by Expanding CD4+CD25+ Forkhead Boxp3 (FOXP3)+ Regulatory T Cells and Balancing Anti- and Pro-Inflammatory Factors. *Cell Physiol Biochem* (2011) 27:587–96. doi: 10.1159/000329980
48. Gupta N, Su X, Popov B, Lee JW, Serikov V, Matthay MA. Intrapulmonary Delivery of Bone Marrow-Derived Mesenchymal Stem Cells Improves Survival and Attenuates Endotoxin-Induced Acute Lung Injury in Mice. *J Immunol* (2007) 179:1855–63. doi: 10.4049/jimmunol.179.3.1855
49. Abreu SC, Hampton TH, Hoffman E, Dearborn J, Ashare A, Singh Sidhu K, et al. Differential Effects of the Cystic Fibrosis Lung Inflammatory Environment on Mesenchymal Stromal Cells. *Am J Physiol Lung Cell Mol Physiol* (2020) 319:L908–25. doi: 10.1152/ajplung.00218.2020
50. Moya A, Larochette N, Paquet J, Deschepper M, Bensidhoum M, Izzo V, et al. Quiescence Preconditioned Human Multipotent Stromal Cells Adopt a Metabolic Profile Favorable for Enhanced Survival Under Ischemia. *Stem Cells* (2017) 35:181–96. doi: 10.1002/stem.2493
51. Liu J, Hao H, Huang H, Tong C, Ti D, Dong L, et al. Hypoxia Regulates the Therapeutic Potential of Mesenchymal Stem Cells Through Enhanced Autophagy. *Int J Low Extrem Wounds* (2015) 14:63–72. doi: 10.1177/1534734615573660
52. Lv B, Hua T, Li F, Han J, Fang J, Xu L, et al. Hypoxia-Inducible Factor 1 Alpha Protects Mesenchymal Stem Cells Against Oxygen-Glucose Deprivation-Induced Injury *via* Autophagy Induction and PI3K/AKT/mTOR Signaling Pathway. *Am J Transl Res* (2017) 9:2492–9.
53. Liu FB, Lin Q, Liu ZW. A Study on the Role of Apoptotic Human Umbilical Cord Mesenchymal Stem Cells in Bleomycin-Induced Acute Lung Injury in Rat Models. *Eur Rev Med Pharmacol Sci* (2016) 20:969–82.
54. Sung PH, Chang CL, Tsai TH, Chang LT, Leu S, Chen YL, et al. Apoptotic Adipose-Derived Mesenchymal Stem Cell Therapy Protects Against Lung and Kidney Injury in Sepsis Syndrome Caused by Cecal Ligation Puncture in Rats. *Stem Cell Res Ther* (2013) 4:155. doi: 10.1186/scrt385
55. Luk F, de Witte SF, Korevaar SS, Roemeling-van Rhijn M, Franquesa M, Strini T, et al. Inactivated Mesenchymal Stem Cells Maintain Immunomodulatory Capacity. *Stem Cells Dev* (2016) 25:1342–54. doi: 10.1089/scd.2016.0068
56. Li Y, Lin F. Mesenchymal Stem Cells are Injured by Complement After Their Contact With Serum. *Blood* (2012) 120:3436–43. doi: 10.1182/blood-2012-03-420612
57. Ghanta S, Tsoyi K, Liu X, Nakahira K, Ith B, Coronata AA, et al. Mesenchymal Stromal Cells Deficient in Autophagy Proteins Are Susceptible to Oxidative Injury and Mitochondrial Dysfunction. *Am J Respir Cell Mol Biol* (2017) 56:300–9. doi: 10.1165/rcmb.2016-0061OC
58. Gao L, Cen S, Wang P, Xie Z, Liu Z, Deng W, et al. Autophagy Improves the Immunosuppression of CD4+ T Cells by Mesenchymal Stem Cells Through Transforming Growth Factor-Beta1. *Stem Cells Transl Med* (2016) 5:1496–505. doi: 10.5966/sctm.2015-0420
59. Jackson MV, Morrison TJ, Doherty DF, McAuley DF, Matthay MA, Kissenpfennig A, et al. Mitochondrial Transfer *via* Tunneling Nanotubes is an Important Mechanism by Which Mesenchymal Stem Cells Enhance Macrophage Phagocytosis in the *In Vitro* and *In Vivo* Models of ARDS. *Stem Cells* (2016) 34:2210–23. doi: 10.1002/stem.2372
60. Tseng N, Lambie SC, Huynh CQ, Sanford B, Patel M, Herson PS, et al. Mitochondrial Transfer From Mesenchymal Stem Cells Improves Neuronal Metabolism After Oxidant Injury *In Vitro*: The Role of Miro1. *J Cereb Blood Flow Metab* (2021) 41:761–70. doi: 10.1177/0271678X20928147
61. Islam MN, Das SR, Emin MT, Wei M, Sun L, Westphalen K, et al. Mitochondrial Transfer From Bone-Marrow-Derived Stromal Cells to Pulmonary Alveoli Protects Against Acute Lung Injury. *Nat Med* (2012) 18:759–65. doi: 10.1038/nm.2736
62. Phinney DG, Di Giuseppe M, Njah J, Sala E, Shiva S, St Croix CM, et al. Mesenchymal Stem Cells Use Extracellular Vesicles to Outsource Mitophagy and Shuttle microRNAs. *Nat Commun* (2015) 6:8472. doi: 10.1038/ncomms9472
63. Phan TK, Ozkocak DC, Poon IKH. Unleashing the Therapeutic Potential of Apoptotic Bodies. *Biochem Soc Trans* (2020) 48:2079–88. doi: 10.1042/BST20200225
64. Liu J, Qiu X, Lv Y, Zheng C, Dong Y, Dou G, et al. Apoptotic Bodies Derived From Mesenchymal Stem Cells Promote Cutaneous Wound Healing *via* Regulating the Functions of Macrophages. *Stem Cell Res Ther* (2020) 11:507. doi: 10.1186/s13287-020-02014-w
65. Fadok VA, Bratton DL, Konowal A, Freed PW, Westcott JY, Henson PM. Macrophages That Have Ingested Apoptotic Cells *In Vitro* Inhibit Proinflammatory Cytokine Production Through Autocrine/Paracrine Mechanisms Involving TGF-Beta, PGE2, and PAF. *J Clin Invest* (1998) 101:890–8. doi: 10.1172/JCI1112
66. Kavanagh H, Mahon BP. Allogeneic Mesenchymal Stem Cells Prevent Allergic Airway Inflammation by Inducing Murine Regulatory T Cells. *Allergy* (2011) 66:523–31. doi: 10.1111/j.1398-9995.2010.02509.x
67. Weiss ARR, Lee O, Eggenhofer E, Geissler E, Korevaar SS, Soeder Y, et al. Differential Effects of Heat-Inactivated, Secretome-Deficient MSC and Metabolically Active MSC in Sepsis and Allogenic Heart Transplantation. *Stem Cells* (2020) 38:797–807. doi: 10.1002/stem.3165
68. Kim EH, Wong SW, Martinez J. Programmed Necrosis and Disease:We Interrupt Your Regular Programming to Bring You Necroinflammation. *Cell Death Differ* (2019) 26:25–40. doi: 10.1038/s41418-018-0179-3
69. Burrell BE, Ding Y, Nakayama Y, Park KS, Xu J, Yin N, et al. Tolerance and Lymphoid Organ Structure and Function. *Front Immunol* (2011) 2:64. doi: 10.3389/fimmu.2011.00064
70. Boehm T, Hess I, Swann JB. Evolution of Lymphoid Tissues. *Trends Immunol* (2012) 33:315–21. doi: 10.1016/j.it.2012.02.005
71. Ruddle NH, Akirav EM. Secondary Lymphoid Organs: Responding to Genetic and Environmental Cues in Ontogeny and the Immune Response. *J Immunol* (2009) 183:2205–12. doi: 10.4049/jimmunol.0804324
72. Borges da Silva H, Fonseca R, Pereira RM, Cassado Ados A, Alvarez JM, D'Imperio Lima MR. Splenic Macrophage Subsets and Their Function During Blood-Borne Infections. *Front Immunol* (2015) 6:480. doi: 10.3389/fimmu.2015.00480
73. Lewis SM, Williams A, Eisenbarth SC. Structure and Function of the Immune System in the Spleen. *Sci Immunol* (2019) 4:eaau6085. doi: 10.1126/sciimmunol.aau6085
74. Steiniger BS. Human Spleen Microanatomy: Why Mice do Not Suffice. *Immunology* (2015) 145:334–46. doi: 10.1111/imm.12469
75. Garraud O, Borhis G, Badr G, Degrelle S, Pozzetto B, Cognasse F, et al. Revisiting the B-Cell Compartment in Mouse and Humans: More Than One B-Cell Subset Exists in the Marginal Zone and Beyond. *BMC Immunol* (2012) 13:63. doi: 10.1186/1471-2172-13-63
76. Bronte V, Pittet MJ. The Spleen in Local and Systemic Regulation of Immunity. *Immunity* (2013) 39:806–18. doi: 10.1016/j.immuni.2013.10.010
77. Mebius RE, Kraal G. Structure and Function of the Spleen. *Nat Rev Immunol* (2005) 5:606–16. doi: 10.1038/nri1669
78. Kurotaki D, Uede T, Tamura T. Functions and Development of Red Pulp Macrophages. *Microbiol Immunol* (2015) 59:55–62. doi: 10.1111/1348-0421.12228
79. Satodate R, Tanaka H, Sasou S, Sakuma T, Kaizuka H. Scanning Electron Microscopical Studies of the Arterial Terminals in the Red Pulp of the Rat Spleen. *Anat Rec* (1986) 215:214–6. doi: 10.1002/ar.1092150304
80. Cesta MF. Normal Structure, Function, and Histology of the Spleen. *Toxicol Pathol* (2006) 34:455–65. doi: 10.1080/01926230600867743
81. Nolte MA, Belien JA, Schadee-Eestermans I, Jansen W, Unger WW, van Rooijen N, et al. A Conduit System Distributes Chemokines and Small Blood-Borne Molecules Through the Splenic White Pulp. *J Exp Med* (2003) 198:505–12. doi: 10.1084/jem.20021801
82. Nolte MA, Arens R, Kraus M, van Oers MH, Kraal G, van Lier RA, et al. B Cells are Crucial for Both Development and Maintenance of the Splenic Marginal Zone. *J Immunol* (2004) 172:3620–7. doi: 10.4049/jimmunol.172.6.3620
83. McGaha TL, Chen Y, Ravishankar B, van Rooijen N, Karlsson MC. Marginal Zone Macrophages Suppress Innate and Adaptive Immunity to Apoptotic

Cells in the Spleen. *Blood* (2011) 117:5403–12. doi: 10.1182/blood-2010-11-320028
84. You Y, Myers RC, Freeberg L, Foote J, Kearney JF, Justement LB, et al. Marginal Zone B Cells Regulate Antigen Capture by Marginal Zone Macrophages. *J Immunol* (2011) 186:2172–81. doi: 10.4049/jimmunol.1002106
85. den Haan JM, Mebius RE, Kraal G. Stromal Cells of the Mouse Spleen. *Front Immunol* (2012) 3:201. doi: 10.3389/fimmu.2012.00201
86. Schmidt EE, MacDonald IC, Groom AC. Microcirculation in Mouse Spleen (Nonsinusal) Studied by Means of Corrosion Casts. *J Morphol* (1985) 186:17–29. doi: 10.1002/jmor.1051860103
87. van Vliet E, Melis M, van Ewijk W. Marginal Zone Macrophages in the Mouse Spleen Identified by a Monoclonal Antibody. Anatomical Correlation With a B Cell Subpopulation. *J Histochem Cytochem* (1985) 33:40–4. doi: 10.1177/33.1.3880783
88. Geijtenbeek TB, Groot PC, Nolte MA, van Vliet SJ, Gangaram-Panday ST, van Duijnhoven GC, et al. Marginal Zone Macrophages Express a Murine Homologue of DC-SIGN That Captures Blood-Borne Antigens. *vivo. Blood* (2002) 100:2908–16. doi: 10.1182/blood-2002-04-1044
89. Crocker PR, Gordon S. Mouse Macrophage Hemagglutinin (Sheep Erythrocyte Receptor) With Specificity for Sialylated Glycoconjugates Characterized by a Monoclonal Antibody. *J Exp Med* (1989) 169:1333–46. doi: 10.1084/jem.169.4.1333
90. Kraal G, Janse M. Marginal Metallophilic Cells of the Mouse Spleen Identified by a Monoclonal Antibody. *Immunology* (1986) 58:665–9.
91. Fujiyama S, Nakahashi-Oda C, Abe F, Wang Y, Sato K, Shibuya A. Identification and Isolation of Splenic Tissue-Resident Macrophage Sub-Populations by Flow Cytometry. *Int Immunol* (2019) 31:51–6. doi: 10.1093/intimm/dxy064
92. Kleinclauss F, Perruche S, Masson E, de CarvalhoBittencourt M, Biichle S, Remy-Martin JP, et al. Intravenous Apoptotic Spleen Cell Infusion Induces a TGF-Beta-Dependent Regulatory T-Cell Expansion. *Cell Death Differ* (2006) 13:41–52. doi: 10.1038/sj.cdd.4401699
93. Khanna KM, Lefrancois L. Geography and Plumbing Control the T Cell Response to Infection. *Immunol Cell Biol* (2008) 86:416–22. doi: 10.1038/icb.2008.22
94. Willard-Mack CL. Normal Structure, Function, and Histology of Lymph Nodes. *Toxicol Pathol* (2006) 34:409–24. doi: 10.1080/01926230600867727
95. Grant SM, Lou M, Yao L, Germain RN, Radtke AJ. The Lymph Node at a Glance - How Spatial Organization Optimizes the Immune Response. *J Cell Sci* (2020) 133:jcs241828. doi: 10.1242/jcs.241828
96. Camara A, Cordeiro OG, Alloush F, Sponsel J, Chypre M, Onder L, et al. Lymph Node Mesenchymal and Endothelial Stromal Cells Cooperate *via* the RANK-RANKL Cytokine Axis to Shape the Sinusoidal Macrophage Niche. *Immunity* (2019) 50:1467–1481e6. doi: 10.1016/j.immuni.2019.05.008
97. Gray EE, Cyster JG. Lymph Node Macrophages. *J Innate Immun* (2012) 4:424–36. doi: 10.1159/000337007
98. Asano K, Kikuchi K, Tanaka M. CD169 Macrophages Regulate Immune Responses Toward Particulate Materials in the Circulating Fluid. *J Biochem* (2018) 164:77–85. doi: 10.1093/jb/mvy050
99. Louie DAP, Liao S. Lymph Node Subcapsular Sinus Macrophages as the Frontline of Lymphatic Immune Defense. *Front Immunol* (2019) 10:347. doi: 10.3389/fimmu.2019.00347
100. Baratin M, Simon L, Jorquera A, Ghigo C, Dembele D, Nowak J, et al. T Cell Zone Resident Macrophages Silently Dispose of Apoptotic Cells in the Lymph Node. *Immunity* (2017) 47:349–362 e345. doi: 10.1016/j.immuni.2017.07.019
101. Alexandre YO, Mueller SN. Stromal Cell Networks Coordinate Immune Response Generation and Maintenance. *Immunol Rev* (2018) 283:77–85. doi: 10.1111/imr.12641
102. Grabowska J, Lopez-Venegas MA, Affandi AJ, den Haan JMM. CD169(+) Macrophages Capture and Dendritic Cells Instruct: The Interplay of the Gatekeeper and the General of the Immune System. *Front Immunol* (2018) 9:2472. doi: 10.3389/fimmu.2018.02472
103. Kuka M, Iannacone M. The Role of Lymph Node Sinus Macrophages in Host Defense. *Ann N Y Acad Sci* (2014) 1319:38–46. doi: 10.1111/nyas.12387
104. Junt T, Moseman EA, Iannacone M, Massberg S, Lang PA, Boes M, et al. Subcapsular Sinus Macrophages in Lymph Nodes Clear Lymph-Borne Viruses and Present Them to Antiviral B Cells. *Nature* (2007) 450:110–4. doi: 10.1038/nature06287
105. Steer HW, Foot RA. Changes in the Medulla of the Parathymic Lymph Nodes of the Rat During Acute Gastro-Intestinal Inflammation. *J Anat* (1987) 152:23–36.
106. Fossum S. The Architecture of Rat Lymph Nodes. IV. Distribution of Ferritin and Colloidal Carbon in the Draining Lymph Nodes After Foot-Pad Injection. *Scand J Immunol* (1980) 12:433–41. doi: 10.1111/j.1365-3083.1980.tb00087.x
107. Nossal GJ, Abbot A, Mitchell J. Antigens in Immunity. XIV. Electron Microscopic Radioautographic Studies of Antigen Capture in the Lymph Node Medulla. *J Exp Med* (1968) 127:263–76. doi: 10.1084/jem.127.2.263
108. Kuang R, Perruche S, Chen W. Apoptotic Cell-Linked Immunoregulation: Implications for Promoting Immune Tolerance in Transplantation. *Cell Biosci* (2015) 5:27. doi: 10.1186/s13578-015-0019-9
109. Morelli AE, Larregina AT. Concise Review: Mechanisms Behind Apoptotic Cell-Based Therapies Against Transplant Rejection and Graft Versus Host Disease. *Stem Cells* (2016) 34:1142–50. doi: 10.1002/stem.2326
110. Poon IK, Lucas CD, Rossi AG, Ravichandran KS. Apoptotic Cell Clearance: Basic Biology and Therapeutic Potential. *Nat Rev Immunol* (2014) 14:166–80. doi: 10.1038/nri3607
111. Elliott MR, Ravichandran KS. The Dynamics of Apoptotic Cell Clearance. *Dev Cell* (2016) 38:147–60. doi: 10.1016/j.devcel.2016.06.029
112. Green DR, Oguin TH, Martinez J. The Clearance of Dying Cells: Table for Two. *Cell Death Differ* (2016) 23:915–26. doi: 10.1038/cdd.2015.172
113. Miyake Y, Asano K, Kaise H, Uemura M, Nakayama M, Tanaka M. Critical Role of Macrophages in the Marginal Zone in the Suppression of Immune Responses to Apoptotic Cell-Associated Antigens. *J Clin Invest* (2007) 117:2268–78. doi: 10.1172/JCI31990
114. Gray M, Miles K, Salter D, Gray D, Savill J. Apoptotic Cells Protect Mice From Autoimmune Inflammation by the Induction of Regulatory B Cells. *Proc Natl Acad Sci U.S.A.* (2007) 104:14080–5. doi: 10.1073/pnas.0700326104
115. Notley CA, Brown MA, Wright GP, Ehrenstein MR. Natural IgM is Required for Suppression of Inflammatory Arthritis by Apoptotic Cells. *J Immunol* (2011) 186:4967–72. doi: 10.4049/jimmunol.1003021
116. Bonnefoy F, Daoui A, Valmary-Degano S, Toussirot E, Saas P, Perruche S. Apoptotic Cell Infusion Treats Ongoing Collagen-Induced Arthritis, Even in the Presence of Methotrexate, and is Synergic With Anti-TNF Therapy. *Arthritis Res Ther* (2016) 18:184. doi: 10.1186/s13075-016-1084-0
117. Perruche S, Saas P, Chen W. Apoptotic Cell-Mediated Suppression of Streptococcal Cell Wall-Induced Arthritis Is Associated With Alteration of Macrophage Function and Local Regulatory T-Cell Increase: A Potential Cell-Based Therapy? *Arthritis Res Ther* (2009) 11:R104. doi: 10.1186/ar2750
118. Sun E, Gao Y, Chen J, Roberts AI, Wang X, Chen Z, et al. Allograft Tolerance Induced by Donor Apoptotic Lymphocytes Requires Phagocytosis in the Recipient. *Cell Death Differ* (2004) 11:1258–64. doi: 10.1038/sj.cdd.4401500
119. Wang Z, Larregina AT, Shufesky WJ, Perone MJ, Montecalvo A, Zahorchak AF, et al. Use of the Inhibitory Effect of Apoptotic Cells on Dendritic Cells for Graft Survival *via* T-Cell Deletion and Regulatory T Cells. *Am J Transplant* (2006) 6:1297–311. doi: 10.1111/j.1600-6143.2006.01308.x
120. Lutterotti A, Yousef S, Sputtek A, Sturner KH, Stellmann JP, Breiden P, et al. Antigen-Specific Tolerance by Autologous Myelin Peptide-Coupled Cells: A Phase 1 Trial in Multiple Sclerosis. *Sci Transl Med* (2013) 5:188ra175. doi: 10.1126/scitranslmed.3006168
121. Edelson R, Berger C, Gasparro F, Jegasothy B, Heald P, Wintroub B, et al. Treatment of Cutaneous T-Cell Lymphoma by Extracorporeal Photochemotherapy. Preliminary Results. *N Engl J Med* (1987) 316:297–303. doi: 10.1056/NEJM198702053160603
122. Morelli AE, Larregina AT, Shufesky WJ, Zahorchak AF, Logar AJ, Papworth GD, et al. Internalization of Circulating Apoptotic Cells by Splenic Marginal Zone Dendritic Cells: Dependence on Complement Receptors and Effect on Cytokine Production. *Blood* (2003) 101:611–20. doi: 10.1182/blood-2002-06-1769
123. Wang Z, Shufesky WJ, Montecalvo A, Divito SJ, Larregina AT, Morelli AE. In Situ-Targeting of Dendritic Cells With Donor-Derived Apoptotic Cells Restrains Indirect Allorecognition and Ameliorates Allograft Vasculopathy. *PloS One* (2009) 4:e4940. doi: 10.1371/journal.pone.0004940

124. Robinette CD, Fraumeni JF Jr. Splenectomy and Subsequent Mortality in Veterans of the 1939-45 War. *Lancet* (1977) 2:127–9. doi: 10.1016/S0140-6736(77)90132-5
125. Chotivanich K, Udomsangpetch R, McGready R, Proux S, Newton P, Pukrittayakamee S, et al. Central Role of the Spleen in Malaria Parasite Clearance. *J Infect Dis* (2002) 185:1538–41. doi: 10.1086/340213
126. Ghosh D, Stumhofer JS. The Spleen: "Epicenter" in Malaria Infection and Immunity. *J Leukoc Biol* (2021) 110:753–69. doi: 10.1002/JLB.4RI1020-713R
127. Portero-Sainz I, Gomez-Garcia deSoria V, Cuesta-Mateos C, Fernandez-Arandojo C, Vega-Piris L, Royg M, et al. A High Migratory Capacity of Donor T-Cells in Response to the Lymph Node Homing Receptor CCR7 Increases the Incidence and Severity of GvHD. *Bone Marrow Transplant* (2017) 52:745–52. doi: 10.1038/bmt.2016.342
128. Acedo SC, Gotardo EM, Lacerda JM, de Oliveira CC, de Oliveira Carvalho P, Gambero A. Perinodal Adipose Tissue and Mesenteric Lymph Node Activation During Reactivated TNBS-Colitis in Rats. *Dig Dis Sci* (2011) 56:2545–52. doi: 10.1007/s10620-011-1644-8
129. Yakoub-Agha I, Saule P, Depil S, Micol JB, Grutzmacher C, Boulanger-Villard F, et al. A High Proportion of Donor CD4+ T Cells Expressing the Lymph Node-Homing Chemokine Receptor CCR7 Increases Incidence and Severity of Acute Graft-Versus-Host Disease in Patients Undergoing Allogeneic Stem Cell Transplantation for Hematological Malignancy. *Leukemia* (2006) 20:1557–65. doi: 10.1038/sj.leu.2404308
130. Tamoutounour S, Henri S, Lelouard H, de Bovis B, de Haar C, van derWoude CJ, et al. CD64 Distinguishes Macrophages From Dendritic Cells in the Gut and Reveals the Th1-Inducing Role of Mesenteric Lymph Node Macrophages During Colitis. *Eur J Immunol* (2012) 42:3150–66. doi: 10.1002/eji.201242847
131. Bsat M, Chapuy L, Rubio M, Wassef R, Richard C, Schwenter F, et al. Differential Pathogenic Th17 Profile in Mesenteric Lymph Nodes of Crohn's Disease and Ulcerative Colitis Patients. *Front Immunol* (2019) 10:1177. doi: 10.3389/fimmu.2019.01177
132. Clark CL, Price BA, Malcolm P, Lear PA, Wood RF. Graft Versus Host Disease in Small Bowel Transplantation. *Br J Surg* (1991) 78:1077–9. doi: 10.1002/bjs.1800780915
133. Brouha PC, Perez-Abadia G, Francois CG, Laurentin-Perez LA, Gorantla V, Vossen M, et al. Lymphadenectomy Prior to Rat Hind Limb Allotransplantation Prevents Graft-Versus-Host Disease in Chimeric Hosts. *Transpl Int* (2004) 17:341–50. doi: 10.1111/j.1432-2277.2004.tb00453.x
134. Neubauer NL, Lurain JR. The Role of Lymphadenectomy in Surgical Staging of Endometrial Cancer. *Int J Surg Oncol* (2011) 2011:814649. doi: 10.1155/2011/814649
135. Giuliano AE, Jones RC, Brennan M, Statman R. Sentinel Lymphadenectomy in Breast Cancer. *J Clin Oncol* (1997) 15:2345–50. doi: 10.1200/JCO.1997.15.6.2345
136. Li M, Li F, Luo C, Shan Y, Zhang L, Qian Z, et al. Immediate Splenectomy Decreases Mortality and Improves Cognitive Function of Rats After Severe Traumatic Brain Injury. *J Trauma* (2011) 71:141–7. doi: 10.1097/TA.0b013e3181f30fc9
137. Das M, Leonardo CC, Rangooni S, Pennypacker KR, Mohapatra S, Mohapatra SS. Lateral Fluid Percussion Injury of the Brain Induces CCL20 Inflammatory Chemokine Expression in Rats. *J Neuroinflamm* (2011) 8:148. doi: 10.1186/1742-2094-8-148
138. Savas MC, Ozguner M, Ozguner IF, Delibas N. Splenectomy Attenuates Intestinal Ischemia-Reperfusion-Induced Acute Lung Injury. *J Pediatr Surg* (2003) 38:1465–70. doi: 10.1016/S0022-3468(03)00497-4
139. Okuaki Y, Miyazaki H, Zeniya M, Ishikawa T, Ohkawa Y, Tsuno S, et al. Splenectomy-Reduced Hepatic Injury Induced by Ischemia/Reperfusion in the Rat. *Liver* (1996) 16:188–94. doi: 10.1111/j.1600-0676.1996.tb00726.x
140. Seifert HA, Leonardo CC, Hall AA, Rowe DD, Collier LA, Benkovic SA, et al. The Spleen Contributes to Stroke Induced Neurodegeneration Through Interferon Gamma Signaling. *Metab Brain Dis* (2012) 27:131–41. doi: 10.1007/s11011-012-9283-0
141. Chiu NL, Kaiser B, Nguyen YV, Welbourne S, Lall C, Cramer SC. The Volume of the Spleen and Its Correlates After Acute Stroke. *J Stroke Cerebrovasc Dis* (2016) 25:2958–61. doi: 10.1016/j.jstrokecerebrovasdis.2016.08.012
142. Ajmo CTJr., Vernon DO, Collier L, Hall AA, Garbuzova-Davis S, Willing A, et al. The Spleen Contributes to Stroke-Induced Neurodegeneration. *J Neurosci Res* (2008) 86:2227–34. doi: 10.1002/jnr.21661
143. Pennypacker KR, Offner H. The Role of the Spleen in Ischemic Stroke. *J Cereb Blood Flow Metab* (2015) 35:186–7. doi: 10.1038/jcbfm.2014.212
144. Grace PM, Hutchinson MR, Bishop A, Somogyi AA, Mayrhofer G, Rolan PE. Adoptive Transfer of Peripheral Immune Cells Potentiates Allodynia in a Graded Chronic Constriction Injury Model of Neuropathic Pain. *Brain Behav Immun* (2011) 25:503–13. doi: 10.1016/j.bbi.2010.11.018
145. Barthelmes J, Tafferner N, Kurz J, de Bruin N, Parnham MJ, Geisslinger G, et al. Induction of Experimental Autoimmune Encephalomyelitis in Mice and Evaluation of the Disease-Dependent Distribution of Immune Cells in Various Tissues. *J Vis Exp* (2016) 8(111):53933. doi: 10.3791/53933
146. Zheng P, Fu H, Wei G, Wei Z, Zhang J, Ma X, et al. Antigen-Oriented T Cell Migration Contributes to Myelin Peptide Induced-EAE and Immune Tolerance. *Clin Immunol* (2016) 169:36–46. doi: 10.1016/j.clim.2016.06.004
147. Vendrame M, Cassady J, Newcomb J, Butler T, Pennypacker KR, Zigova T, et al. Infusion of Human Umbilical Cord Blood Cells in a Rat Model of Stroke Dose-Dependently Rescues Behavioral Deficits and Reduces Infarct Volume. *Stroke* (2004) 35:2390–5. doi: 10.1161/01.STR.0000141681.06735.9b
148. Vendrame M, Gemma C, Pennypacker KR, Bickford PC, Davis Sanberg C, Sanberg PR, et al. Cord Blood Rescues Stroke-Induced Changes in Splenocyte Phenotype and Function. *Exp Neurol* (2006) 199:191–200. doi: 10.1016/j.expneurol.2006.03.017
149. Schwarting S, Litwak S, Hao W, Bahr M, Weise J, Neumann H. Hematopoietic Stem Cells Reduce Postischemic Inflammation and Ameliorate Ischemic Brain Injury. *Stroke* (2008) 39:2867–75. doi: 10.1161/STROKEAHA.108.513978
150. Evans MA, Lim R, Kim HA, Chu HX, Gardiner-Mann CV, Taylor KWE, et al. Acute or Delayed Systemic Administration of Human Amnion Epithelial Cells Improves Outcomes in Experimental Stroke. *Stroke* (2018) 49:700–9. doi: 10.1161/STROKEAHA.117.019136
151. Acosta SA, Tajiri N, Hoover J, Kaneko Y, Borlongan CV. Intravenous Bone Marrow Stem Cell Grafts Preferentially Migrate to Spleen and Abrogate Chronic Inflammation in Stroke. *Stroke* (2015) 46:2616–27. doi: 10.1161/STROKEAHA.115.009854
152. Lee ST, Hamilton JA, Valenzuela KS, Bogaerts A, Xi X, Aronowski J, et al. Anti-Inflammatory Mechanism of Intravascular Neural Stem Cell Transplantation in Haemorrhagic Stroke. *Brain* (2008) 131:616–29. doi: 10.1093/brain/awm306
153. Yang B, Hamilton JA, Valenzuela KS, Bogaerts A, Xi X, Aronowski J, et al. Multipotent Adult Progenitor Cells Enhance Recovery After Stroke by Modulating the Immune Response From the Spleen. *Stem Cells* (2017) 35:1290–302. doi: 10.1002/stem.2600
154. Lim JH, Kim JS, Yoon IH, Shin JS, Nam HY, Yang SH, et al. Immunomodulation of Delayed-Type Hypersensitivity Responses by Mesenchymal Stem Cells Is Associated With Bystander T Cell Apoptosis in the Draining Lymph Node. *J Immunol* (2010) 185:4022–9. doi: 10.4049/jimmunol.0902723
155. Lim JY, Ryu DB, Lee SE, Park G, Min CK. Mesenchymal Stem Cells (MSCs) Attenuate Cutaneous Sclerodermatous Graft-Versus-Host Disease (Scl-GVHD) Through Inhibition of Immune Cell Infiltration in a Mouse Model. *J Invest Dermatol* (2017) 137:1895–904. doi: 10.1016/j.jid.2017.02.986
156. Parekkadan B, Upadhyay R, Dunham J, Iwamoto Y, Mizoguchi E, Mizoguchi A, et al. Bone Marrow Stromal Cell Transplants Prevent Experimental Enterocolitis and Require Host CD11b+ Splenocytes. *Gastroenterology* (2011) 140:966–75. doi: 10.1053/j.gastro.2010.10.013
157. Bazhanov N, Ylostalo JH, Bartosh TJ, Tiblow A, Mohammadipoor A, Foskett A, et al. Intraperitoneally Infused Human Mesenchymal Stem Cells Form Aggregates With Mouse Immune Cells and Attach to Peritoneal Organs. *Stem Cell Res Ther* (2016) 7:27. doi: 10.1186/s13287-016-0284-5
158. Li H, Jiang Y, Jiang X, Guo X, Ning H, Li Y, et al. CCR7 Guides Migration of Mesenchymal Stem Cell to Secondary Lymphoid Organs: A Novel Approach to Separate GvHD From GvL Effect. *Stem Cells* (2014) 32:1890–903. doi: 10.1002/stem.1656
159. Tang B, Li X, Liu Y, Chen X, Li X, Chu Y, et al. The Therapeutic Effect of ICAM-1-Overexpressing Mesenchymal Stem Cells on Acute Graft-Versus-Host Disease. *Cell Physiol Biochem* (2018) 46:2624–35. doi: 10.1159/000489689
160. Luger D, Lipinski MJ, Westman PC, Glover DK, Dimastromatteo J, Frias JC, et al. Intravenously Delivered Mesenchymal Stem Cells: Systemic Anti-

Inflammatory Effects Improve Left Ventricular Dysfunction in Acute Myocardial Infarction and Ischemic Cardiomyopathy. *Circ Res* (2017) 120:1598–613. doi: 10.1161/CIRCRESAHA.117.310599
161. Lopez-Santalla M, Mancheno-Corvo P, Escolano A, Menta R, DelaRosa O, Abad JL, et al. Biodistribution and Efficacy of Human Adipose-Derived Mesenchymal Stem Cells Following Intranodal Administration in Experimental Colitis. *Front Immunol* (2017) 8:638. doi: 10.3389/fimmu.2017.00638
162. Krueger TEG, Thorek DLJ, Denmeade SR, Isaacs JT, Brennen WN. Concise Review: Mesenchymal Stem Cell-Based Drug Delivery: The Good, the Bad, the Ugly, and the Promise. *Stem Cells Transl Med* (2018) 7:651–63. doi: 10.1002/sctm.18-0024
163. von Bahr L, Batsis I, Moll G, Hagg M, Szakos A, Sundberg B, et al. Analysis of Tissues Following Mesenchymal Stromal Cell Therapy in Humans Indicates Limited Long-Term Engraftment and No Ectopic Tissue Formation. *Stem Cells* (2012) 30:1575–8. doi: 10.1002/stem.1118
164. Moll G, Jitschin R, von Bahr L, Rasmusson-Duprez I, Sundberg B, Lönnies L, et al. Mesenchymal Stromal Cells Engage Complement and Complement Receptor Bearing Innate Effector Cells to Modulate Immune Responses. *PloS One* (2011) 6:e21703. doi: 10.1371/journal.pone.0021703
165. Golden JE, Shahaduzzaman M, Wabnitz A, Green S, Womble TA, Sanberg PR, et al. Human Umbilical Cord Blood Cells Alter Blood and Spleen Cell Populations After Stroke. *Transl Stroke Res* (2012) 3:491–9. doi: 10.1007/s12975-012-0208-3
166. Zhang L, Zheng H, Shao H, Nian H, Zhang Y, Bai L, et al. Long-Term Therapeutic Effects of Mesenchymal Stem Cells Compared to Dexamethasone on Recurrent Experimental Autoimmune Uveitis of Rats. *Invest Ophthalmol Vis Sci* (2014) 55:5561–71. doi: 10.1167/iovs.14-14788
167. Ko JH, Lee HJ, Jeong HJ, Kim MK, Wee WR, Yoon SO, et al. Mesenchymal Stem/Stromal Cells Precondition Lung Monocytes/Macrophages to Produce Tolerance Against Allo- and Autoimmunity in the Eye. *Proc Natl Acad Sci U.S.A.* (2016) 113:158–63. doi: 10.1073/pnas.1522905113
168. Mancheno-Corvo P, Lopez-Santalla M, Menta R, DelaRosa O, Mulero F, Del Rio B, et al. Intralymphatic Administration of Adipose Mesenchymal Stem Cells Reduces the Severity of Collagen-Induced Experimental Arthritis. *Front Immunol* (2017) 8:462. doi: 10.3389/fimmu.2017.00462
169. Murphy N, Treacy O, Lynch K, Morcos M, Lohan P, Howard L, et al. TNF-α/IL-1β-Licensed Mesenchymal Stromal Cells Promote Corneal Allograft Survival *via* Myeloid Cell-Mediated Induction of Foxp3(+) Regulatory T Cells in the Lung. *FASEB J* (2019) 33:9404–21. doi: 10.1096/fj.201900047R
170. Hu J, Zhang L, Wang N, Ding R, Cui S, Zhu F, et al. Mesenchymal Stem Cells Attenuate Ischemic Acute Kidney Injury by Inducing Regulatory T Cells Through Splenocyte Interactions. *Kidney Int* (2013) 84:521–31. doi: 10.1038/ki.2013.114
171. Zhang Y, Ge XH, Guo XJ, Guan SB, Li XM, Gu Wc , et al. Bone Marrow Mesenchymal Stem Cells Inhibit the Function of Dendritic Cells by Secreting Galectin-1. *BioMed Res Int* (2017) 2017:3248605. doi: 10.1155/2017/3248605
172. Jiang XX, Zhang Y, Liu B, Zhang SX, Wu Y, Yu XD, et al. Human Mesenchymal Stem Cells Inhibit Differentiation and Function of Monocyte-Derived Dendritic Cells. *Blood* (2005) 105:4120–6. doi: 10.1182/blood-2004-02-0586
173. Aldinucci A, Rizzetto L, Pieri L, Nosi D, Romagnoli P, Biagioli T, et al. Inhibition of Immune Synapse by Altered Dendritic Cell Actin Distribution: A New Pathway of Mesenchymal Stem Cell Immune Regulation. *J Immunol* (2010) 185:5102–10. doi: 10.4049/jimmunol.1001332
174. Kim J, Hematti P. Mesenchymal Stem Cell-Educated Macrophages: A Novel Type of Alternatively Activated Macrophages. *Exp Hematol* (2009) 37:1445–53. doi: 10.1016/j.exphem.2009.09.004
175. Rabani R, Volchuk A, Jerkic M, Ormesher L, Garces-Ramirez L, Canton J, et al. Mesenchymal Stem Cells Enhance NOX2-Dependent Reactive Oxygen Species Production and Bacterial Killing in Macrophages During Sepsis. *Eur Respir J* (2018) 51(4):1702021. doi: 10.1183/13993003.02021-2017
176. Maggini J, Mirkin G, Bognanni I, Holmberg J, Piazzon IM, Nepomnaschy I, et al. Mouse Bone Marrow-Derived Mesenchymal Stromal Cells Turn Activated Macrophages Into a Regulatory-Like Profile. *PloS One* (2010) 5: e9252. doi: 10.1371/journal.pone.0009252
177. Eggenhofer E, Hoogduijn MJ. Mesenchymal Stem Cell-Educated Macrophages. *Transplant Res* (2012) 1:12. doi: 10.1186/2047-1440-1-12
178. Ko JH, Kim HJ, Jeong HJ, Lee HJ, Oh JY. Mesenchymal Stem and Stromal Cells Harness Macrophage-Derived Amphiregulin to Maintain Tissue Homeostasis. *Cell Rep* (2020) 30(11):3806-20.e6. doi: 10.1016/j.celrep.2020.02.062
179. Hasgur S, Desbourdes L, Relation T, Overholt KM, Stanek JR, Guess AJ, et al. Splenic Macrophage Phagocytosis of Intravenously Infused Mesenchymal Stromal Cells Attenuates Tumor Localization. *Cytotherapy* (2021) 23:411–22. doi: 10.1016/j.jcyt.2020.04.102
180. Fletcher AL, Heng TS. Lymph Node Stroma Join the Cancer Support Network. *Cell Death Differ* (2016) 23:1899–901. doi: 10.1038/cdd.2016.103
181. Fletcher AL, Elman JS, Astarita J, Murray R, Saeidi N, D'Rozario J. Lymph Node Fibroblastic Reticular Cell Transplants Show Robust Therapeutic Efficacy in High-Mortality Murine Sepsis. *Sci Transl Med* (2014) 6:249ra109. doi: 10.1126/scitranslmed.3009377
182. Sato K, Honda SI, Shibuya A, Shibuya K. Cutting Edge: Identification of Marginal Reticular Cells as Phagocytes of Apoptotic B Cells in Germinal Centers. *J Immunol* (2018) 200:3691–6. doi: 10.4049/jimmunol.1701293

Conflict of Interest: TSPH received funding from Regeneus Ltd outside of this work. The remaining authors declare that the research was conducted in the absence of any commercial or financial relationships that could be construed as a potential conflict of interest.

frontiers | Frontiers in Immunology

REVIEW
published: 04 July 2022
doi: 10.3389/fimmu.2022.943333

Translating MSC Therapy in the Age of Obesity

Lauren Boland[1,2†], *Laura Melanie Bitterlich*[3,4†], *Andrew E. Hogan*[3,4], *James A. Ankrum*[1,2*] and *Karen English*[3,4*]

[1] Roy J. Carver Department of Biomedical Engineering, University of Iowa, Iowa City, IA, United States, [2] Fraternal Order of Eagles Diabetes Research Center, University of Iowa, Iowa City, IA, United States, [3] Biology Department, Maynooth University, Maynooth, Ireland, [4] Kathleen Lonsdale Institute for Human Health Research, Maynooth, Ireland

Mesenchymal stromal cell (MSC) therapy has seen increased attention as a possible option to treat a number of inflammatory conditions including COVID-19 acute respiratory distress syndrome (ARDS). As rates of obesity and metabolic disease continue to rise worldwide, increasing proportions of patients treated with MSC therapy will be living with obesity. The obese environment poses critical challenges for immunomodulatory therapies that should be accounted for during development and testing of MSCs. In this review, we look to cancer immunotherapy as a model for the challenges MSCs may face in obese environments. We then outline current evidence that obesity alters MSC immunomodulatory function, drastically modifies the host immune system, and therefore reshapes interactions between MSCs and immune cells. Finally, we argue that obese environments may alter essential features of allogeneic MSCs and offer potential strategies for licensing of MSCs to enhance their efficacy in the obese microenvironment. Our aim is to combine insights from basic research in MSC biology and clinical trials to inform new strategies to ensure MSC therapy is effective for a broad range of patients.

Keywords: mesenchymal stromal cells (MSCs), disease microenvironment, obesity, immunomodulation, metabolic disease

OPEN ACCESS

Edited by:
Guido Moll,
Charité Universitätsmedizin Berlin, Germany

Reviewed by:
Vivian Capilla-González,
Andalusian Center of Molecular Biology and Regenerative Medicine (CSIC), Spain
Celine Gregoire,
University of Liege, Belgium

***Correspondence:**
James A. Ankrum
james-ankrum@uiowa.edu
Karen English
karen.english@mu.ie

†*These authors share first authorship*

Specialty section:
This article was submitted to Alloimmunity and Transplantation, a section of the journal Frontiers in Immunology

Received: *13 May 2022*
Accepted: *10 June 2022*
Published: *04 July 2022*

Citation:
Boland L, Bitterlich LM, Hogan AE, Ankrum JA and English K (2022) Translating MSC Therapy in the Age of Obesity. Front. Immunol. 13:943333. doi: 10.3389/fimmu.2022.943333

INTRODUCTION

The recent SARS-CoV-2 pandemic has prompted an increased interest in mesenchymal stromal cells (MSCs) as a therapeutic to treat acute respiratory distress syndrome (ARDS) (1–6). In contrast to unregulated and often predatory "stem cell clinics" that have cast MSC therapy in a bad light, academic labs, regulatory bodies, professional societies and industry continue to advocate for and adopt rigorous standards, thoughtfully designed clinical trials, and diligent scientific studies to develop high-quality cellular products for patients with life-threatening disease (7). Ten MSC cell therapy products have been approved for use in major indications including graft versus host disease (GvHD), Crohn's disease, and myocardial infarction (8). As more MSC based therapies gain approval, it is prudent to look to the challenges that exist on the horizon as these therapies are applied to a broad, complex, and heterogeneous patient population. An increasingly common challenge to the translation of other immunotherapies has been the influence of metabolic disease on a patient's clinical response (9, 10). Obesity and other metabolic syndromes alter the immune system and have proven consequential to

patient responses to immunotherapies, begging the question: how will MSC therapy perform as an immunomodulatory therapy when placed within metabolically diseased environments?

With the rising incidence of obesity throughout the world, the average patient being treated with cellular therapies, including MSC therapy, will increasingly have comorbid obesity (11–13). As of 2018, over 40% of Americans are living with obesity and about 1 in 10 American women are classified in the severe obesity category (BMI≥40 kg/m^2) (14). In Europe, 36% of the population are considered pre-obese and 17% obese, based on a study in 2019 (15). Obesity is associated with a substantially increased risk for a number of comorbid diseases, including type 2 diabetes mellitus (T2DM), hypertension, and coronary artery disease (16–18). In the clinic, these epidemiological shifts translate to a rise in complex patients presenting with metabolic comorbidities in addition to their primary diagnosis, as well as to 42% higher total healthcare expenditures in patients living with obesity (19). Unfortunately, the ubiquity and chronicity of obesity often lulls us into a belief that it is innocuous; however, the pathological effects of obesity cannot be understated. Patients living with class 2 or 3 obesity have a ~30% higher risk for all-cause mortality than their non-obese age- and sex-matched counterparts (13, 20). Additionally, an umbrella review from 2017 concluded that 11 out of 36 cancer types are positively associated with obesity (21). As we aim to translate MSC therapies in the era of obesity, we must take the time to understand the consequences metabolic disease has on specific applications of MSC therapy.

Obesity is clinically defined as a body mass index (BMI) greater than 30 kg/m^2 (11). However, underlying cellular and molecular changes reveal a much more complex story of obesity than BMI can capture (22–26). Key pathologic features of overt obesity include ectopic lipid deposition, broad hormonal disturbances, and a substantially elevated risk of developing metabolic syndrome (27–29). While a significant focus of obesity research has been on the function of the liver and adipose tissue in obesity, systemic ramifications should not be overlooked (30, 31). Early observations in the 1990s of obesity-induced increases in systemic pro-inflammatory cytokines were integral in recontextualizing obesity not solely as a disturbance of metabolism, but of the immune system, as well (32–34). Since that time, insight into the degree and specificity of obesity's effects on particular immune populations has grown rapidly. Obesity-induced alterations in the composition, activity, metabolism, and effector response of the immune system have lent much needed insight into the potential mechanisms by which obesity alters disease severity, progression, and response to therapies for immune-mediated pathologies (35–40). Because MSC therapy relies on paracrine activity and cell-to-cell interactions (41, 42), significant questions remain regarding whether MSCs can appropriately function within this environment. It remains unknown if patient BMI may affect responsiveness to MSC therapy. Since the immune system is grossly altered in patients with comorbid obesity it remains to be seen whether the recipient immune populations are present, functional, and responsive to MSC mechanisms of action. Additionally, critical features that make allogeneic MSC therapy possible (43, 44), notably the high hemocompatibility and low immunogenicity profile of MSCs, may be modified by exposure to obese environments, thus potentiating the risk for adverse events (45–49).

There are still notable outstanding questions that remain to be answered to determine how and if MSC therapy can optimally function within an obese environment. Questions that remain unanswered include: do biomarkers within patients with obesity help predict responsiveness to MSC therapy? and does treating obesity or T2DM improve MSC immunosuppression? In this review, we examine emerging data from cancer immunotherapy as a model for the challenges MSC immunotherapies may face in obese environments. We then summarize the current evidence that obesity alters critical features intrinsic to the health and function of autologous MSCs, drastically modifies the host immune system, and reshapes crosstalk between MSCs and immune cells. We challenge the assumption that essential features of allogeneic MSC therapy (high hemocompatibility and low immunogenicity) will inherently be maintained in obese environments. Finally, we suggest ways to re-train MSCs from individuals living with obesity, to restore their therapeutic efficacy. Our goal is to draw critically needed attention to the influence of metabolic environments on MSC therapies in order to guide new clinical and basic research questions that will ensure that emerging therapeutics are available to all patients regardless of metabolic health.

LESSONS FROM CANCER IMMUNOTHERAPY

Cancer immunotherapy has served as a forewarning for the potent modifying effect of obesity on immunotherapies and provides insight as to the potential effects that obesity may have on MSC therapeutic functions that are necessary for other indications. For some varieties of cancer, immunotherapies have replaced classic cytoreductive therapies as primary treatment modalities due in part to lower rates of adverse events and decreases in systemic off-target effects (50). Cancer immunotherapies harness the immune system to precipitate an anti-tumour response (51, 52). However, obesity has been shown to alter the efficacy, tolerance, and toxicity profiles for multiple cancer immunotherapies (10, 53–56). As a therapeutic regimen that relies on modulation of the patient's immune response, cancer immunotherapy can be used as a proof-of-concept model for MSC therapy, which relies on interactions with many of the same players in the adaptive and innate immune system (57–59).

Obesity has emerged as a potent modifier of the efficacy and toxicity of a variety of cancer immunotherapies. In three distinct preclinical murine models of obesity (high-fat diet, aged-related *ad libitum* fed, and leptin-receptor deficient *db/db* mice), immunostimulatory therapy with anti-CD40 antibodies and IL-2 resulted in complete lethality in obese mice, while non-obese mice and calorie-restricted aged mice survived and showed a positive anti-tumour response (55, 60). Lethality in obese

animals was driven by elevated levels of serum inflammatory cytokines, which is a common driver of immune-related adverse events in patients treated with immunotherapy. Blocking macrophage responses with TNFα neutralizing antibodies or depletion by clodronate liposomes abrogated the toxic effects of immunostimulatory therapy in obese animals. Therefore, obesity-induced alterations to specific immune cell populations can alter the risk of adverse events during treatment with immunomodulatory therapies.

Intriguingly, immune checkpoint blockade with an anti-CTLA-4 antibody shows a differential response between obese mice cohorts (61, 62). In an orthotopic model of renal cell carcinoma, diet-induced obese (DIO) mice showed no therapeutic anti-tumour response to anti-CTLA-4 therapy. However, obese *ob/ob* mice, which have a genetic deletion of the satiety hormone leptin, showed effective anti-tumour responses. DIO mice had serum leptin levels 40-times higher than *ob/ob* animals, more closely reflecting obesity in humans. To determine if leptin contributed to the differential response to immunotherapy, the researchers neutralized leptin prior to anti-CTLA-4 therapy, which restored anti-tumour effects in DIO mice. This work specifically implicated elevated leptin levels as a modifier of immunotherapy response. Therefore, in addition to changes in host immune populations, obesity-induced hormonal changes can modify responsiveness to immunomodulatory therapies. With a hormone-centric focus, actual fat mass itself may be a poor predictor of therapeutic responsiveness, while serum hormone levels may serve as better response predictors (63–65). Similarly, immunotherapies targeting programmed cell death protein 1 (PD-1) show decreased success in obese mice (66), which a different study links to a leptin-dependant increase in PD-1 expression on $CD8^+$ T cells in humans (10). In the case of cancer immunotherapy, obesity can alter efficacy and toxicity, highlighting the need to understand both parameters when applying these lessons to MSC therapy.

Although obese murine models predicted that obesity in human patients would result in poorer overall response rates, emerging clinical data has demonstrated the opposite. In one retrospective study in patients with metastatic melanoma treated with anti-PD-L1, men living with obesity were found to have a significant survival advantage compared to normal-overweight men (67). An analysis of patients treated with anti-PD-L1 therapies showed a notable beneficial effect of elevated BMI regardless of sex, with patients living with obesity showing greater overall survival (10). In this study, obese, otherwise healthy, patients had increased circulating $PD1^+$ T cells with low proliferative capacity, suggestive of T cell exhaustion. Interestingly, obesity was associated with T cell exhaustion across several species and models and drove faster tumour growth in murine models; however, immunotherapy in obese human patients provided a significant survival benefit. A potential explanation for this surprising finding provided by the authors was that immune checkpoint blockade may revive an immune system otherwise exhausted by the chronic inflammation of obesity, thus potentiating a stronger immunologic anti-tumour response in patients living with obesity. In opposition to these findings, a more recent study reported obesity-induced lower PD1 levels in T cells, which correlated with lower PD-L1 levels in tumour cells of both mice and humans. However, immunotherapy was still effective in a mouse model, and human patients who underwent weight loss experienced tumour regression, suggesting that obesity-induced defects of T cells are reversible (68). It is important to note that immune checkpoint blockade, including anti-PD-L1 therapy, is an immunostimulatory therapy, in which a critical brake on the immune system is released to precipitate an anti-tumour response (69). In contrast, the main therapeutic aim of MSC therapy in diseases like GvHD is to dampen hyperactive immune responses (70). Therefore, it is unclear if MSC therapy in a similar patient base would show an equivalent benefit or be at a significant disadvantage in a more inflammatory and exhausted environment.

IMPACT OF DISEASE MICROENVIRONMENT ON MSC EFFICACY

The patient's microenvironment is a major factor in the efficacy of MSC therapy in GvHD. If MSCs are administered too early in pre-clinical models of acute GvHD, they fail to dampen the GvHD response as levels of the pro-inflammatory cytokine IFN-γ, which is known to activate MSC immunomodulatory function, are too low (71, 72). Furthermore, interactions between MSCs and immune cells are of utmost importance in dictating response to MSC therapy. A small study investigating differences between responders and non-responders to MSC therapy for GvHD found that patients with high peripheral blood lymphocyte counts ($CD3^+$ T cells and $CD56^+$ NK cells) before MSC therapy responded better (73). In addition strong cytotoxicity towards MSCs by peripheral blood mononuclear cells (PBMCs) from GvHD patients (74) was associated with a better response to MSC therapy. The gut is a key organ in the pathophysiology of aGvHD and retrospective assessment of gut mucosa biopsies from a small number of patients (n=16) pre and post MSC therapy for GvHD has shown that the tissue immune profile of the gut is distinct in non-responders to MSC therapy (75). Importantly, obesity can promote (76) and even worsen aGvHD, leading to decreased survival in both mice and humans (77). These effects have been partially ascribed to diet-induced changes in the host gut microbiota (77, 78). Surprisingly, no study has investigated the impact of the obese microenvironment on MSCs in GvHD and equally little is understood about how the host gut microbiota might influence MSC therapeutic efficacy.

Conversely, obesity seems to reduce mortality in ARDS. While obesity generally increases the risk for the development of ARDS (79–81) and can even lead to additional acute kidney injury (82), patients with moderate obesity experience a lower mortality from ARDS than lean patients (79–81, 83). This

"obesity paradox" makes it difficult to predict the efficacy of MSC therapy in ARDS patients living with obesity, as the inflammatory response is already impaired due to exhaustion from the chronic low-grade inflammation of the obese microenvironment (80), potentially making the patient unresponsive to further immunosuppression by MSCs.

Determining the effect of comorbid obesity on MSC efficacy and toxicity is currently difficult to do for two essential reasons. First, much of the clinical trial data testing MSC therapies remains unpublished (7, 84) and, second, metabolic parameters are either not captured or not reported in published MSC clinical trial data. A search on March 9, 2022 of ClinicalTrials.gov for "mesenchymal stem cells", "mesenchymal stromal cells" OR "mesenchymal precursor cells" returned 1487 clinical trials. However, pairing "BMI", "body mass index", "obesity" OR "obese" with this search returned only 14 trials. In the primary literature, however, some insight into the interactions of metabolic disease and MSCs is beginning to unfold. In two Mesoblast trials for the treatment of diabetic nephropathy and T2DM, the average patient's BMI was obese (85, 86). In another trial using autologous MSCs to treat diabetes-associated critical limb ischemia, severe obesity was part of the exclusion criteria (87). Thus, not only are patients living with comorbid obesity actively being treated with MSC therapy, but BMI is currently being used to decide patient "fitness" for treatment. The ultimate lesson to be learned from the results of cancer immunotherapy is that the metabolic status of patients can influence therapeutic efficacy and toxicity and, as such, should not be overlooked in the design of MSC products and trials.

THE EFFECT OF OBESITY ON MESENCHYMAL STROMAL CELLS

Efficacy of Therapy With Lean MSC in Obese Subjects

Nearly all studies investigating the therapeutic efficacy of healthy MSCs in subjects with obesity are pre-clinical models using high-fat diet (HFD). Application methods, treatment regimens, and tissue sources vary, but lead to similar outcomes (**Table 1**). Mice with diet-induced obesity that were given human adipose tissue MSCs (atMSCs) *via* intraperitoneal (i.p.) injections twice two weeks apart showed a decrease in fat mass and, more interestingly, a decrease of atherogenic index of plasma (AIP) levels (88). The AIP is a logarithmically transformed ratio of molar concentrations of triglycerides to HDL-cholesterol and serves as a marker of cardiovascular disease (96).

This suggests that therapy with lean MSCs has a positive effect on heart health, which is corroborated by a study in which HFD-fed mice with cardiac arrhythmias were given murine bmMSC, murine bmMSC conditioned medium (CM), or unconditioned cell culture medium intravenously multiple times over the course of a month. At the end of the treatment, the cardiac arrhythmias were reversed, adiponectin levels were restored to those observed in lean mice, and TGF-β1 levels were decreased. HFD-fed mice treated with cell culture medium as a control showed high levels of heart fibrosis which were much lower in their murine bmMSC or bmMSC-CM treated counterparts (95). As the AIP is associated with the concentration of triglycerides which are in turn correlated with the severity of non-alcoholic fatty liver disease (97) it would stand to reason that MSC should also be able to alleviate the symptoms of HFD-induced liver damage. Indeed, this seems to be the case (98–102). Intraperitoneal injection of human atMSC every 2 weeks for 10 weeks decreased both lipotoxicity and fat accumulation in the liver of HFD mice (89). A single dose of human atMSC that had been genetically modified with adenovirus constructs to overexpress one of two antioxidants, either superoxide dismutase 2 (Sod2) or catalase (Cat), improved hepatic steatosis and systemic inflammation significantly after just 4 weeks. Fewer fat cells were found in the liver of both treatment groups compared to the control, and plasma TNF-α levels were lower (91).

Additional positive effects on the systemic manifestations of metabolic syndrome have been described. Intramuscular injection of human atMSCs (90), injection of murine atMSCs into visceral epididymal adipose tissue (94), and intraperitoneal

TABLE 1 | Therapeutic effect of lean MSCs in obesity.

MSC type	Model	Therapeutic effect	Reference
human atMSCs	mice with diet-induced obesity	decreased fat mass, decreased AIP levels	88
human atMSCs	HFD-fed mice with liver damage	decreased lipotoxicity and fat accumulation in liver	89
human atMSCs	mice with metabolic syndrome	decreased blood glucose, improved insulin sensitivity, decreased triglyceride levels	90
human atMSCs (overexpressing Sod2 or Cat)	HFD-fed mice with hepatic steatosis	improved hepatic steatosis and systemic inflammation	91
human amniotic MSC CM	mice with metabolic syndrome	decreased blood glucose, improved insulin sensitivity, decreased weight gain	92
human umbilical cord MSCs	humans with osteoarthritis	improvement of osteoarthritis in both lean patients and patients with obesity	93
murine atMSCs	mice with metabolic syndrome	decreased blood glucose, improved insulin sensitivity, decreased triglyceride levels	94
murine bmMSCs	HFD-fed mice with cardiac arrhythmias	reversal of cardiac arrhythmias, restoration of adiponectin levels	95

HFD, high fat diet; AIP, atherogenic index of plasma; Sod2, superoxide dismutase 2 (Sod2); Cat, catalase.

injection of human amniotic MSC CM (92) all significantly decreased blood glucose levels and improved insulin sensitivity. The human and murine atMSCs further caused a significant drop in serum triglyceride levels (90, 94) which has the potential of being cardioprotective (96). Human amniotic atMSC CM led to increased energy expenditure, elevated thermogenesis, and inhibited adipogenesis by suppressing the expression of genes required for the differentiation of pre-adipocytes. As a result, these mice experienced lower weight gain than the control group (92).

A small human study showed that the administration of human umbilical cord blood-derived MSCs improves osteoarthritis of the knee in both lean patients and patients living with obesity, with patient age being a much more relevant factor in treatment outcome than body weight (93). In summary, lean MSCs administered into an obese microenvironment maintain their therapeutic value and can reduce the negative effects associated with metabolic syndrome, however, the therapeutic efficacy of MSCs in pro-inflammatory conditions such as GvHD and ARDS in the setting of an obese microenvironment remain to be investigated.

Therapeutic Efficacy of Obese MSCs

Although MSCs isolated from patients with sickle cell disease (103), GvHD (104), and Crohn's disease (105) show functional equivalence to MSCs from healthy donors, a growing body of evidence demonstrates that MSCs isolated from patients with metabolic disease are fundamentally altered (106–110) (**Tables 2**, **3**). Under the influence of the obese microenvironment, immune cells become dysregulated in their function and undergo phenotypic changes (116). Similar effects seem to apply to obese human atMSCs, as early studies from Kizilay-Mancini and colleagues demonstrated that atMSCs isolated from patients with obesity-related comorbidities had a significantly lower suppressive effect on activated T cells (108), and bmMSCs isolated from patients with >10 years history of T2D exhibit a compromised metabolism (117). Notably, while the study by Kizilay-Mancini et al. showed a drop in immunosuppressive ability, other studies have actually shown an increase in T-cell stimulation when using atMSCs from patients with obesity. Serena et al. found that conditioned media from obese-T2D atMSCs led to more T cell proliferation in mixed lymphocyte reactions secondary to NLRP3 inflammasome activation (109). Additionally, in a study by Ritter et al., obese atMSCs actively secreted higher levels of IL-6 and TNFα and lower levels of adiponectin compared to lean controls (113). Moreover, obese atMSCs can secrete harmful proteins like osteoclast stimulation factor 1 (Ostf1), which can promote osteoporosis (118), polarise murine macrophages towards a pro-inflammatory M1 instead of an anti-inflammatory M2 phenotype (111), and suffer from increased early senescence (112). This shift between pro- and anti-inflammatory cytokines could potentially explain the pro-inflammatory effect of obese atMSCs. It is critical to note that these findings suggest that obese atMSCs may not simply fail to appropriately suppress inflammation but may amplify existing inflammatory processes.

While the previous studies were conducted using *in vitro* potency assays, only a few studies have validated the effect of

TABLE 2 | Differences in therapeutic action of lean and obese MSCs *in vitro*.

MSC Source	Modulated cells	Lean MSCs	Obese MSCs	Cause of difference in therapeutic action	Reference
Human atMSC CM	Human PBMCs	suppression of proliferation	weak suppression of proliferation	inflammasome activation (T2DM > Obese)	109
Human atMSC CM	Mouse T cells (MOG)	suppression of proliferation	increased proliferation	not clear	110
Human atMSC CM	Human THP1 Macrophages	polarisation towards M2 phenotype	weak polarisation towards M2 phenotype	inflammasome activation	109
Human atMSC	Macrophages (RAW264.7	no effect on phenotype	strong polarisation towards M1 phenotype	not clear	111
Transwell	and SIM-A9 (microglia)	increased migration no effect on phagocytosis	no effect on migration decreased phagocytosis	not clear not clear	111 111
Human atMSC	HUVEC	promotion of angiogenesis: tube formation and enhanced production of VEGF in injured HUVEC cells	no promotion of angiogenesis: tube formation, no production of VEGF in injured HUVEC cells	not clear, but may be associated with senescence phenotype in obese human atMSC	112
Human atMSC	None tested	normal cilia and cilia associated functions in lean atMSC. Normal differentiation, motility and secretion.	shortened and deficient cilia. increased production of IL-6 and TNF-α and decreased adiponectin. Impaired differentiation, motility and secretion.	Obesity (hypoxia, TNF-α, IL6) induced expression of Aurora A and its downstream target HDAC6. Inhibition of Aurora A or HDAC6 rescues cilium length and function of obese atMSC	113
Human atMSC	Human CD4+ T cells	suppression of proliferation	weak suppression of proliferation	oxidative stress due to mitochondrial dysfunction	106, 108

T2DM, type II diabetes mellitus; MOG, myelin oligodendrocyte glycoprotein; HUVEC, human umbilical vein endothelial cells; VEGF, vascular endothelial growth factor; IL-6, interleukin-6; TNF-α, tumour necrosis factor-alpha; HDAC6, histone deacetylase 6.

obese atMSCs in *in vivo* model systems. In one study of experimental autoimmune encephalitis, only lean atMSCs could effectively lower clinical score (110). When obese MSCs were administered at the onset of disease there was a higher total lesion area in the spinal cord compared to vehicle treated controls. In addition, lean MSCs but not obese MSCs protected against ischemic injury, reducing renal atrophy and alleviating renovascular hypertension in mouse models of renal artery stenosis (94, 114, 115). Therefore, both *in vitro* and *in vivo* analyses of immunomodulatory behaviour in MSCs isolated from patients with metabolic disease support a compromised immunomodulatory phenotype (**Tables 2**, **3**). However, it remains to be determined which factors present in obesity alter MSC immunomodulation.

One possible reason for this dysfunction of obese MSCs is metabolic reprogramming, which leads to changes in the cellular metabolism resulting in altered functions. Obesity can lead to metabolic reprogramming in immune cells including natural killer (NK) cells, which become blunted in their ability to reduce tumour growth (37) and experience exhaustion when challenged with the pro-inflammatory cytokines IL-15 and IL-2 (119). A switch to glycolysis is required for NK cells to produce cytokines and exhibit cytotoxic effects on tumour cells, but is impaired in obese NK cells (37).

In MSCs, glycolysis is of similar importance for immunomodulation. When glycolysis of MSCs is impaired through silencing of hypoxia-inducible factor 1-alpha (HIF-1α), expression of ICAM, IL-6, and NO_2 is reduced, resulting in a decreased ability to suppress T cell proliferation (120). Correspondingly, boosted glycolysis promotes stronger T cell suppression (121, 122) and an overexpression of HIF-1α is associated with the recruitment of anti-inflammatory monocytes and a higher resistance of MSCs against lysis by NK cells (123).

Current gaps in knowledge regarding how components of the obese environment individually and collectively affect MSC phenotype will need to be addressed if we are to understand how best to use MSCs to treat patients with comorbid metabolic disease.

CONSEQUENCES OF OBESITY-INDUCED ALTERATIONS TO THE IMMUNE SYSTEM FOR MSC THERAPY

The breadth of alterations to immune cell populations in obesity is staggering (31, 39, 40). In the treatment of immune-mediated pathologies, MSCs directly or indirectly interact with immune cells to promote an immunosuppressive state (41, 42). Therefore, alterations in the basal immune system in the setting of obesity, may have critical consequences for MSC therapeutic efficacy. In this review, we focus on how obesity affects three immune cell populations; T cells, monocytes/macrophages, and NK cells, because of the extensive interactions of MSCs with these cells (**Figure 1**).

T Lymphocytes

T lymphocytes are essential players in the adaptive immune system that can initiate, maintain, suppress, and/or amplify inflammation and tissue damage in autoimmunity and hyperactive immune responses (124). As such, the ability of MSCs to modify T cell response has been a major focus in understanding MSC immunomodulation within diseases like GvHD and multiple sclerosis, wherein T cells drive pathology (72, 125, 126). Early work identifying the immunosuppressive mechanism of MSCs showed that MSC infusion correlated with increased numbers of T regulatory cells (T_{REG}), a potent regulatory population that aids in the maintenance of peripheral tolerance (125). This finding has subsequently been corroborated by several groups in both *in vitro* and *in vivo* analyses (127–129). The production of indoleamine-2,3-dioxygenase (IDO) appears to be critical for MSC induction of T_{REG} (130–133). In patients with multiple sclerosis, the total number of circulating T_{REG} is decreased, which has been suggested to play a role in the breakdown of self-tolerance (134). Additionally, during allogeneic hematopoietic stem cell transplant, increasing T_{REG} has been shown to decrease GvHD severity (135). Therefore, the MSC-T_{REG} axis is of crucial importance in the treatment of autoimmune disease and post-transplant tolerance (136–139).

TABLE 3 | Studies comparing lean versus obese MSC therapeutic efficacy in disease models.

MSC Source	Disease Model	Lean MSC	Obese MSC	Cause of difference in therapeutic action	Reference
Human atMSC (1x10^6 i.p.)	Mouse Experimental autoimmune encephalitis	improved clinical score (inflammation, lesion size, preserved myelin) in mice with experimental autoimmune encephalitis	no improvement in mice with experimental autoimmune encephalitis	increased expression of pro-inflammatory cytokines	110
Human atMSC (5x10^5 intra-aorta)	Mouse Renal stenosis	normalisation of ischemic kidney cortical perfusion in stenotic mouse kidneys	no effect on ischemic kidney cortical perfusion in stenotic mouse kidneys	increased cellular senescence	114
Human atMSC (5x10^5 intra-aorta)	Mouse model of renal artery stenosis	normalisation of renovascular hypertension	partial alleviation of renovascular hypertension	not clear	115
Human atMSC (5x10^5 intra-aorta)	Mouse model of renal artery stenosis (RAS)	small improvement in renal atrophy. decreased M1 macrophages, M1/M2 ratio and inflammation in RAS kidneys	no improvement in renal atrophy. M1 macrophages remained high	obese MSC had a pro-inflammatory phenotype releasing more TNF-α	94

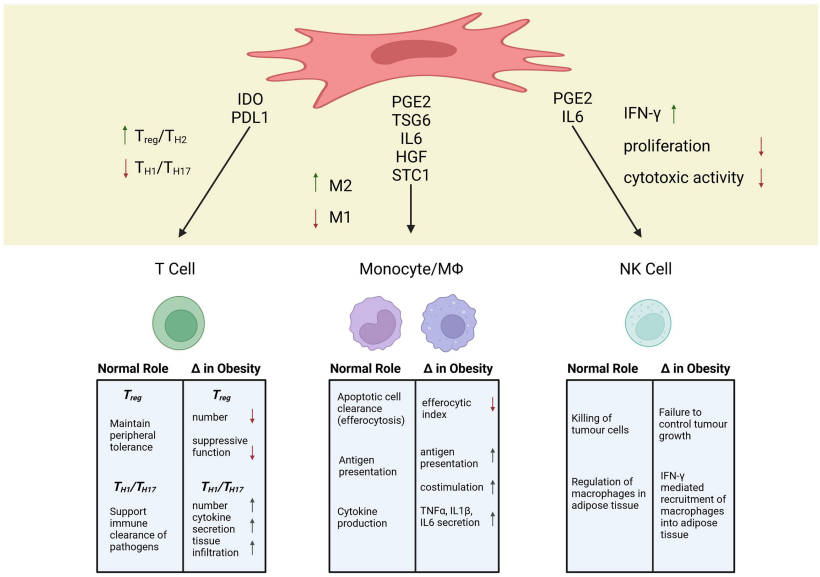

FIGURE 1 | Mechanisms of MSC Immunosuppression and Alterations to Immune Populations in Obesity. Created with BioRender.com.

In the setting of metabolic disease, T_{REG} show a number of alterations that could impact interactions with MSCs. In human visceral adipose tissue, there is a negative correlation between *FOXP3* transcripts (a marker of T_{REG}) and BMI, indicating a lower regulatory profile in patients living with obesity (140). In addition, human studies have found a negative correlation between circulating T_{REG} numbers and BMI, as well as, markers of systemic inflammation (141, 142). Although correlations have been identified, the mechanistic underpinning as to why T_{REG} are altered in metabolic disease is still an evolving research area (124). To date, specific components elevated in the obese serum environment have been shown to modify T_{REG} behaviour. Leptin, which tends to be elevated in the serum of patients with obesity (143), has been shown to suppress T_{REG} proliferation, while leptin deficiency is associated with a higher frequency of T_{REG} (144, 145). When exposed to high insulin levels, IL10 secretion by murine T_{REG} is attenuated, thereby reducing their ability to block TNFα production from LPS-stimulated macrophages (146). Hyperinsulinemia appears, therefore, to compromise the immunosuppressive potential of T_{REG}. If MSCs rely on T_{REG} to facilitate long-term immunosuppression, this finding could indicate that hyperinsulinemic environments may compromise MSC mediated immunosuppression. Notably, in patients with multiple sclerosis and metabolic syndrome, treatment with metformin, a commonly prescribed first-line treatment for T2DM, significantly enhanced the number and potency of circulating T_{REG} (147). Therefore, treating underlying metabolic disease can positively affect comorbid immune-mediated pathologies through modulation of T_{REG} function.

While the MSC-T_{REG} axis is clearly a major player in the setting of autoimmune disease, the ability of MSCs to dampen pro-inflammatory Th1/Th17 populations is also essential (70). *In vitro* studies of MSC immunomodulatory potency have routinely demonstrated that MSCs suppress the proliferation and activity of allogeneic Th1 cells (41). In a humanized mouse model of GvHD, the ability of MSCs to decrease mortality was independent of T_{REG} induction, but was, rather, due to suppression of $CD4^+$ T effector cell expansion and TNFα production (72, 148). An essential pathway by which MSCs control Th1 responses is through expression and secretion of PD-L1, a ligand for PD1 (57, 58). A less comprehensive picture exists for MSCs ability to modulate Th17 responses. Several early studies showed that MSCs could inhibit Th17 differentiation and cytokine production. However, nearly all of these studies were conducted with murine MSCs, which have distinct immunomodulatory programs compared to human (149, 150). Conversely, in a study of human bone marrow MSCs, *in vitro* incubation with MSCs resulted in higher Th17 cytokine secretion from activated PBMCs, due to MSC production of PGE2 (151). However, patients treated with MSC infusion for acute GvHD show either a modest suppression of or no difference in Th17 numbers (125, 152). Th17 and T_{REG} both differentiate from naïve T cells *via* TGFβ signalling (153). Therefore, one mechanism by which MSCs modulate Th17 cells may be through preferential induction of T_{REG}. However, further analysis of human MSCs and Th17 cells is critically needed to better understand their potential interaction *in vivo*.

Patients with metabolic disease have significant changes in Th1/Th17 immune cell populations. Within the visceral adipose of patients with metabolic disease, Th1 numbers and function are increased, which is integral to initiation and maintenance of meta-inflammation (31, 154). Additionally, both adults and children with obesity have elevations in Th17 cytokines, which is associated with T2DM and an IL-17 mediated disturbance of insulin signalling (35, 38, 155, 156). This increased Th17 cytokine production appears to be linked to obesity-associated

mitochondrial dysfunction in T cells (157). Given the poorly understood interaction between MSCs and Th17 cells, the dominance of this Th17 profile within patients living with obesity and T2DM is concerning. Interestingly, in a study of patients living with obesity but no metabolic disease, higher numbers of circulating T lymphocytes, but fewer naïve T cells were reported (158). Additionally, the percentage of $CD4^+$ effector memory T cells was higher in patients living with obesity. A murine model of high fat diet recapitulated this elevation in $CD4^+$ effector memory cells and showed that these cells infiltrated non-lymphoid tissues at higher rates compared to animals fed standard diet. Interestingly, this finding indicates that high-fat conditioning alone can influence the migration and activation state of $CD4^+$ T cells. Furthermore, Wang et al. showed higher rates of circulating T cells with an exhausted profile ($PD1^+$ with low proliferative rate) in obese, otherwise healthy patients (10). While intratumoural $CD8^+$ T cells from patients living with obesity have impaired function, expression of PD1 remains unchanged. This functional impairment is associated with alterations in $CD8^+$ T cell metabolism with decreased glutamine production which is required for normal cell function (68). Additionally, increased consumption of free fatty acids by tumour cells deprives $CD8^+$ T cells of this metabolite further impairing their activity (159).

While immunostimulatory therapies are effective at bolstering anti-tumour effects in the setting of obesity (10, 67), it is unclear how an immunosuppressive mechanism, like PD-L1 expression by MSCs, might behave in the same environment. It remains to be determined if MSCs are able to suppress activation of obese or T2DM T cells. What is clear is that particular T effector cell populations are sensitive to obese environments, supporting the idea that the obese "basal" immune system is unique and should be considered as such when designing and evaluating MSC therapies.

Monocytes/Macrophages

Given their broad and encompassing participation in many autoimmune and inflammatory disorders, monocytes and macrophages have been of keen interest in defining MSC immunomodulation (160–162). Monocytes and macrophages exist on a phenotypic spectrum that can broadly be defined as inflammatory (M1) or anti-inflammatory (M2) (163). However, the phenotype of monocytes and macrophages is highly plastic and, as such, can display a spectrum of intermediate and complex phenotypes (164). With that caveat in mind, incubation with MSCs or MSC conditioned media tends to cause a decreased inflammatory and increased anti-inflammatory profile in monocytes/macrophages (59, 165–168).

The ability of MSCs to modulate the balance between inflammatory and anti-inflammatory phenotypes in monocytes and macrophages has been linked to their production of PGE2 (169, 170, p. 14), TSG6 (171), IL6 (172), and HGF (173). PGE2 from MSCs modifies monocyte costimulatory ability and inhibits the maturation of monocyte subtypes (170, 174, 175). For bmMSCs, secretion of PGE2 is necessary to reprogram host macrophages toward an anti-inflammatory IL10-secreting profile (176). Additionally, Rozenberg et al. found that when $CD14^+$ cells were depleted from mixed PBMC cultures, MSC conditioned media could no longer dampen IFNγ production, indicating that MSCs effects on monocytes can influence subsequent T cell cytokine production (151). *In vivo*, a number of independent research groups have confirmed that secretome-based crosstalk between macrophages and MSC is essential in models of inflammatory and autoimmune diseases, including sepsis (176–178), allergic asthma (179, 180), peritonitis (181), colitis (182, 183), GvHD (184), and rheumatoid arthritis (185, 186). Although a unidirectional focus of MSC secreted factors to monocytes has been documented, a bidirectional crosstalk whereby secreted factors from either cell population can influence the other is likely more accurate. To this point, studies have shown that secretion of IL1β from $CD14^+$ cells was integral to initiating MSCs and MSC like cells -multipotent adult progenitor cells (MAPCs) immunosuppressive potency toward T cells (187, 188). Therefore, a bidirectional crosstalk of secreted factors both from and between monocytes and MSCs influences downstream immunosuppressive effects.

Interestingly, several secretome independent modes of MSC-myeloid cell interactions have recently been described. These emerging mechanisms include direct cytoplasmic communication through processing bodies (189), tunnelling nanotubules (190–192), transfer of extracellular vesicles and miRNAs (193, 194), and the uptake of apoptotic MSCs by host phagocytes (i.e. efferocytosis) (74, 195, 196). In a model of acute respiratory distress, Jackson et al. demonstrated that MSCs pass healthy mitochondria to stressed alveolar macrophages *via* tunnelling nanotubules (191). In addition, MSCs can release extracellular vesicles ranging in size and cargo. After uptake of MSC vesicles, macrophages show decreased sensitivity to mitochondrial damage by silica particles and attenuated inflammatory cytokine production (197). Finally, efferocytosis has emerged as an intriguing pathway by which MSCs leave a lasting impression on the host immune system. De Witte et al. found that by 24-72 hours after infusion the vast majority of MSCs were within circulating blood monocytes or resident macrophage populations (59). Additionally, Galleu et al. demonstrated that killing of MSCs by host cytotoxic T cells was predictive of the therapeutic response of patients treated with MSCs for acute GvHD (74). In a follow-up study, this group demonstrated that incubation with apoptotic MSCs increased immunosuppressive gene expression in macrophages, as well as secretion of IL10 and PGE2 (195). Overall, the unique feature of macrophages as professional phagocytes enables a broad range of MSC mechanisms of action that are still actively being uncovered. To date, no study has investigated if MSC efferocytosis is a functioning mechanism of obese monocytes/macrophages.

In obesity and metabolic disease, monocytes and macrophages are integral players in the initiation and sustained inflammation that drives systemic and adipose-specific physiological alterations (32, 33, 38–40, 198). A number of intrinsic features of monocytes and macrophages are compromised in patients living with obesity. Crown-like structures of macrophages within the adipose tissue are thought

to form to clear apoptotic adipocytes that die due to hypoxic, hypertrophic growth (28, 199). In murine models of diet induced obesity, clearance of apoptotic adipocytes was decreased in the absence of mannose-binding lectin, a protein that facilitates macrophage phagocytosis (200). As antigen-presenting cells within adipose, macrophages show higher levels of MHC class I and II expression and increased antigen-presentation to T cells in obesity (201). Adipose-tissue macrophages in HFD-fed animals also show increased costimulatory profiles, leading to higher overall T cell activation (202). In addition, in patients with asthma and comorbid obesity, airway macrophages and peripheral blood monocytes show a significant reduction in efferocytic index (40% and 36% decrease compared to non-obese asthmatic patients, respectively), suggesting that obesity dampens the efferocytic response of critical macrophage populations (203). If efferocytosis is a major mechanism by which MSCs exert long-term immunosuppressive effects (84), alterations in the basal efferocytic capacity of host phagocytes could lead to lower MSC therapeutic efficacy.

NK Cells

The primary role of NK cells is the killing of tumour cells or cells infected by a virus (204). A blunted NK cell function is associated with a worsened outcome of Covid19 (205), and a higher percentage of NK cells is associated with a longer survival of sepsis patients (206). However, the role of NK cells in autoimmune diseases like multiple sclerosis, lupus erythematosus, and arthritis is debated. There are indications for NK cells being both protective from and promoting the effects of autoimmune diseases (207–209).

Interactions between MSCs and NK cells happen in both directions. Activated NK cells lyse allogeneic MSCs, reducing the time during which they can exhibit their therapeutic efficacy (210, 211). At the same time, IFN-γ produced by NK cells promotes the production of monocyte chemoattractant protein 1 (MCP-1) in MSCs (212), which is associated with an anti-inflammatory polarisation of macrophages (213). Interestingly, IFN-γ- stimulated MSCs have been reported to reduce IFN-γ production by NK cells (214) and NK cell proliferation, at least partially through the production of PGE2 (215). Conversely, MSCs have also been shown to promote NK cell expansion (216) and increasing their IFN-γ production through both soluble factors and cell-cell interaction, at least partially by triggering the IL-12/STAT4 pathway of the NK cells (212, 217). These conflicting results likely arise due to several factors. Ratios of MSCs to NK cells range from 1:1 (216) to 1:8 (211), experiments were carried out *in vivo* (215) and *in vitro* (217), and MSCs were either pre-stimulated (214) or naïve MSCs (212). Additionally, while MSCs are able to successfully suppress IL-2 induced proliferation of resting NK cells, already proliferating NK cells are not as effectively suppressed (211). Some of the effects of MSCs on NK cells seem to also be time-dependant, as poly(I:C) activated MSCs initially promote NK cell function, followed by TGF-β and IL-6 induced cell death (218). Considering this delicate balance of interaction, a disturbance of NK cell function due to obesity could lead to impaired MSC therapeutic efficacy.

In the setting of metabolic disease numerous studies have detailed defective NK cells, with reduced peripheral frequencies and a loss of effector functions (119, 219–224) such as cytokine production and tumour cytotoxicity. Using murine models of cancer, Michelet and colleagues demonstrated that NK cells with an obese phenotype fail to control tumour growth highlighting the potential consequences of defective NK cell responses in people with obesity (37). The same study identified increased expression of PPAR controlled lipid uptake as the underlying mechanism of defect. Increased lipid uptake limited NK cell metabolic activity, which is critical for their effector functions (225). Leptin has also been identified as an important NK cell regulator, with reduced NK cell frequencies (peripheral, liver and spleen) and activity in leptin receptor deficient mice (db/db) (226, 227). Collectively these studies suggest the obese microenvironment underpins the dysregulation of NK cells in obesity. Further evidence for this comes from the reversibility of NK cell defects with weight loss, either *via* exercise or metabolic surgery (228–230). The unanswered question is whether or not obese NK cells are equally affected by MSC co-cultures as non-obese NK cells.

Another facet of NK cell biology impacted by obesity is their regulation of macrophages in adipose tissue. In 2014, O'Rourke and colleagues demonstrated that NK cells could regulate adipose tissue macrophage infiltration, with systemic ablation of NK cells reducing macrophage numbers in obese adipose tissue (231). In a subsequent study, Wensveen and colleagues provided detailed evidence for NK cell regulation of macrophages. The authors demonstrated that NK cells are activated by obesity induced adipose tissue stress, which leads to the rapid production of IFN-γ, which promoted the recruitment of macrophages into adipose tissue (232). In 2016, Boulenouar and colleagues showed that NK cells could regulate adipose tissue macrophages *via* their ability to kill inflammatory macrophages, but with the onset of obesity, NK cells lost their ability to kill macrophages and increased their production of IFN-γ which promoted the recruitment of inflammatory macrophages, promoting obesity related metabolic defects (233). Based on these findings, the ratio of MSCs to NK cells, or insufficient priming of MSCs, may exacerbate IFN-γ production by obese NK cells, and result in a pro-inflammatory effect.

IMMUNOGENICITY AND HEMOCOMPATIBILITY OF MSC IN OBESE ENVIRONMENTS

While alterations in the immune system critically shape the *in vivo* environment of patients with obesity, changes within the composition of the serum environment are also evident (27, 234). Obesity presents a unique challenge to MSC therapy due to increased immunogenic and prothrombotic risks. Increased immunogenicity within obesity has been well-documented within the organ transplant field. Molinero et al. demonstrated that in murine cardiac allograft, allo-sensitization and subsequent rejection were higher in HFD-fed animals due to increased frequency and co-stimulatory profile in host antigen-presenting cells (235).

Additionally, Okamoto et al. found that adiponectin ablation led to higher rates of cardiac allograft rejection (236). Adiponectin, therefore, appears to be protective against allo-sensitization and is, notably, decreased in patients with obesity (237). Leptin, on the other hand, tends to positively correlate with BMI (143) and is associated with a higher risk of allograft rejection (238, 239). In murine skin allograft, an increased rate of rejection in HFD-fed mice was due to the direct effect of $CD4^+$ T cell exposure to elevated palmitate (158). Obesity also appears to be associated with increased graft failure in solid organ transplants in humans. In a study of patients receiving kidney allograft, all obesity classes were associated with an elevated risk of graft failure (240). In an additional study, patients with obesity and comorbid diabetes had a significantly higher number of donor-reactive T cells, poorer graft function, and the highest rates of graft-failure (241). Therefore, the absence and excess of specific molecules within the obese environment can have crucial consequences for immunogenicity within allogeneic transplant scenarios. This highlights the need to investigate the impact of the obese environment on relative immunogenicity of MSC products.

In addition to increased risk of immunogenicity, obesity is a pro-thrombotic state (45). Due to elevated coagulability, patients with obesity are at increased risk of life-threatening thrombotic events including myocardial infarction, stroke, and pulmonary embolism (46). This raises the question: is hemocompatibility of MSCs affected by exposure to obese environments? Intravascular delivery of MSCs into a hypercoagulable obese environment could have severe consequences for adverse thrombotic and/or ischemic events (46, 47). In addition, both infection and inflammation can increase coagulability through direct effects on coagulation factors, platelet activation state, and vascular endothelium (48, 49); therefore, many patients treated with MSC therapy for immune-based pathologies may be pro-coagulant at time of infusion. The additive nature of these pro-coagulant risks, obesity and disease-specific inflammation, could have a detrimental impact not solely on MSC therapeutic efficacy, but safety, as well. As a more diverse and increasingly obese patient base is treated with MSC therapy, the need to understand how to maintain efficacy and decrease adverse thrombotic events within this environment will be critical to the broad scalability and generalizability of MSC therapy (242).

As the breadth of MSC products has expanded, transitive application of properties between tissue sources cannot be assumed to hold true (44). While bmMSCs show low levels of pro-coagulant tissue factor, both adipose and perinatal sources have relatively high levels of tissue factor expression (44, 243). In a clinical trial for critical limb ischemia using autologous atMSCs, adverse thrombi occurred only in diabetic patients, suggesting an intrinsic decline in the hemocompatibility of diabetic atMSCs (87). Diabetic atMSCs had decreased secretion of antithrombotic tPA and increased secretion of the pro-coagulant factor, PAI1, leading to less overall fibrinolytic activity. Interestingly, in the same study, healthy atMSCs appeared to have a differential response to being grown in either healthy or diabetic serum; however, this comparison was not the major focus of the study and therefore explicit quantification and statistical comparisons were not expressly reported. Follow-up studies showed that the atMSCs from diabetic patients who developed distal microthrombi exhibited high levels of tissue factor, linking changes in tissue factor expression with increased incidence of adverse thrombotic events (244). A better understanding of how the balance between pro- and anti-thrombotic factors is altered by intrinsic donor characteristics like comorbid metabolic disease will be critical to ensuring safety and efficacy for patients treated with MSC therapy.

RETRAINING OBESE MSCS TO RESTORE THERAPEUTIC EFFICACY

Due to the strong correlation of metabolic phenotype and immunomodulatory capacity in MSC (120), targeting the metabolism of obese MSC could lead to a restoration of their therapeutic efficacy. It is already known that culture conditions during *in vitro* expansion of MSC can considerably affect their therapeutic potential (245, 246). The metabolism of healthy MSC in early passages after isolation is typically highly glycolytic, but switches to OXPHOS over time due to a greater availability of oxygen compared to their niche in the body (247, 248). Expanding MSC in a hypoxic environment could counteract this switch. Similar to NK cells, which experience an impairment of their glycolytic function under obese conditions (37, 119), obese MSCs may suffer metabolic impairments. Human umbilical cord MSCs (ucMSCs) from mothers with obesity exhibit significant lower glycolytic capacity than ucMSCs from lean mothers (249). Pre-licensing obese MSCs to rescue or even amplify a glycolytic phenotype might rescue their immunosuppressive potential, however, this remains to be determined.

Pre-licensing human bmMSC with interferon γ (IFN-γ) has been shown to activate the protein kinase B (Akt)/mTor pathway, leading to increased glycolysis and increased expression of hexokinase isoform 2 (HK2), a key gene for glycolysis (250). Given that mTOR activation induces expression of HIF-1α (251), the involvement for the IFN-γ/Akt/mTOR/HIF-1α pathway can be theorised in this case. IFN-γ licensing also increases indolamine-2,3-dioxygenase (IDO) and prostaglandin E2 (PGE2) production which are both important for MSC immunomodulation (250, 252).

TNF-α has also been shown to activate HIF-1α. Human fibroblasts, which share similarities with MSCs (253), experience an upregulation of reactive oxygen species (ROS) upon exposure to TNF-α, resulting in a hypoxia-independent expression of HIF-1α (254, 255). Similarly, exposing human fibroblasts to lactate also results in a HIF-1α mediated switch to glycolysis and an increase of c-Myc (256), a multifunctional transcription factor that regulates, among other things, cell proliferation and glycolysis (257, 258).

Confirming the beneficial effects of inflammatory pre-licensing on MSC metabolism, Mendt et al, showed that human ucMSC pre-licensed with a mix of IL-17, IL-1β, TNF-α, and IFN- γ resulted in an increase in glycolysis which promoted the production of

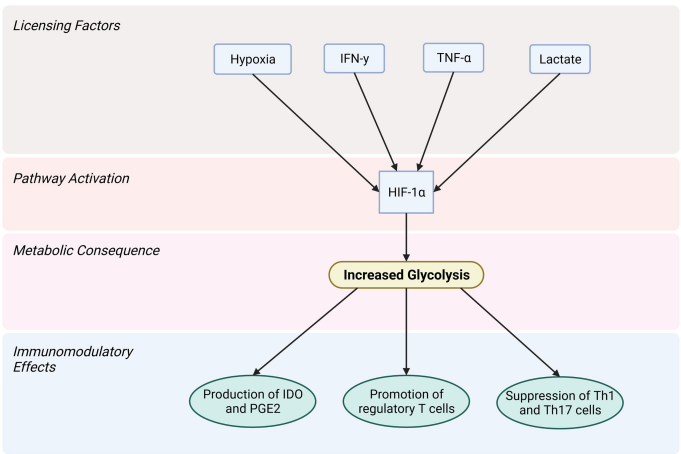

FIGURE 2 | Licensing factors that activate the HIF-1α pathway in MSCs lead to increased glycolysis and allow for the immunomodulatory actions carried out by MSCs. Created with BioRender.com.

immunomodulatory factors. *In vitro*, these pre-licensed human ucMSC were able to disrupt the glycolytic upregulation in T cells, causing those T cells to differentiate into a regulatory instead of an inflammatory phenotype improving the outcome of a murine graft versus host disease model (259).

Pre-licensing MSCs with both IFN- γ and TNF-α has been shown to prevent MSCs exposed to palmitate from taking on a pro-inflammatory phenotype, instead remaining strongly immunosuppressive toward activated PBMCs (260). Aside from shifting the MSC metabolism to a more hypoxic phenotype (**Figure 2**), simply culturing them in medium free from FFAs may also help to restore their immunosuppressive function. Following chronic exposure of human MSCs to palmitate, and subsequent loss of immunosuppressive potency, it is possible for the MSCs to recover upon removal of palmitate (260).

More research is needed to fully understand the role of altered metabolism in MSCs, the ways in which this might be best achieved and the functionality of licensed MSCs in inflammatory disease with an underlying obese environment.

FUTURE DIRECTIONS/CONCLUSION

For the use of immunomodulatory therapies, like MSCs, a careful and comprehensive understanding of how patient comorbidities affect the underlying immune system is pivotal to optimizing therapeutic performance. A one size fits all approach to MSC therapy is not scientifically justified and may compromise both patient safety and therapeutic efficacy (7, 84, 242). The expansion of patients treated with MSCs and the breadth of emerging MSC products warrants a more complete understanding of the interaction between characteristics of different *in vivo* transplant environments and intrinsic properties of the cell product. In patients living with obesity, the immune system and serum environment are fundamentally altered compared to metabolically healthy individuals (9, 10, 12). By not recognizing and identifying obesity as a unique transplant environment, we fail to tailor MSC therapies for the context in which they will perform. Moving forward, improved reporting of metabolic health in clinical trial data to the research community would allow for the evaluation of the function and health of MSCs within obese environments. Obesity and metabolic disease need not be exclusion criteria for the use of MSC therapy, as long as we understand how MSCs behave within these environments and the mechanisms of potential adverse events. In the future, both the patient and/or the cell therapy could be conditioned to reduce risk of adverse events, while maintaining therapeutic efficacy within obese environments. For example, given the pro-thrombotic nature of obesity, intravascular delivery of MSCs within patients with obesity could be paired with anti-thrombotic prophylaxis, thereby mitigating potential thromboembolic complications without excluding patients with obesity from vital therapeutic options. In addition, MSCs from donors with obesity could be licensed to regain their immunomodulatory potential. New immunomodulatory therapies should be available to all patients regardless of metabolic health, but for this to be true, critical gaps in our current knowledge regarding the interaction between MSC therapy and metabolic disease need to be filled.

AUTHOR CONTRIBUTIONS

LB performed a literature search, wrote the manuscript and approved the final manuscript. LMB performed a literature search, created the figures, wrote the manuscript and approved the final manuscript. AH, JA, and KE performed a literature search, wrote the manuscript and approved the final manuscript. All authors contributed to the article and approved the submitted version.

FUNDING

LB is supported in part by the University of Iowa MSTP Grant, NIH T32 GM139776. LMB is supported through the John & Pat Hume Doctoral Awards of Maynooth University. KE is supported by an Irish Research Council Laureate Award (IRCLA/2017/288) and by a Science Foundation Ireland Frontiers for the Future Award (20/FFP-A/8948). JA is supported by the Straub Foundation, Diabetes Action Research and Education Foundation, and NIH P42 ES013661.

REFERENCES

1. Dilogo IH, Aditianingsih D, Sugiarto A, Burhan E, Damayanti T, Sitompul PA, et al. Umbilical Cord Mesenchymal Stromal Cells as Critical COVID-19 Adjuvant Therapy: A Randomized Controlled Trial. *Stem Cells Transl Med* (2021) 10:1279–87. doi: 10.1002/sctm.21-0046
2. Golchin A. Cell-Based Therapy for Severe COVID-19 Patients: Clinical Trials and Cost-Utility. *Stem Cell Rev Rep* (2021) 17:56–62. doi: 10.1007/s12015-020-10046-1
3. Häberle H, Magunia H, Lang P, Gloeckner H, Körner A, Koeppen M, et al. Mesenchymal Stem Cell Therapy for Severe COVID-19 ARDS. *J Intensive Care Med* (2021) 36:681–8. doi: 10.1177/0885066621997365
4. Lanzoni G, Linetsky E, Correa D, Messinger Cayetano S, Alvarez RA, Kouroupis D, et al. Umbilical Cord Mesenchymal Stem Cells for COVID-19 Acute Respiratory Distress Syndrome: A Double-Blind, Phase 1/2a, Randomized Controlled Trial. *Stem Cells Transl Med* (2021) 10:660–73. doi: 10.1002/sctm.20-0472
5. Sengupta V, Sengupta S, Lazo A, Woods P, Nolan A, Bremer N. Exosomes Derived From Bone Marrow Mesenchymal Stem Cells as Treatment for Severe COVID-19. *Stem Cells Dev* (2020) 29:747–54. doi: 10.1089/scd.2020.0080
6. Xu Z, Huang Y, Zhou J, Deng X, He W, Liu X, et al. Current Status of Cell-Based Therapies for COVID-19: Evidence From Mesenchymal Stromal Cells in Sepsis and ARDS. *Front Immunol* (2021) 12. doi: 10.3389/fimmu.2021.738697
7. Martin I, Galipeau J, Kessler C, Le Blanc K, Dazzi F. Challenges for Mesenchymal Stromal Cell Therapies. *Sci Transl Med* (2019) 11:eaat2189. doi: 10.1126/scitranslmed.aat2189
8. Levy O, Kuai R, Siren EMJ, Bhere D, Milton Y, Nissar N, et al. Shattering Barriers Toward Clinically Meaningful MSC Therapies. *Sci Adv* (2020) 6:eaba6884. doi: 10.1126/sciadv.aba6884
9. Klevorn LE, Teague RM. Adapting Cancer Immunotherapy Models for the Real World. *Trends Immunol* (2016) 37:354–63. doi: 10.1016/j.it.2016.03.010
10. Wang Z, Aguilar EG, Luna JI, Dunai C, Khuat LT, Le CT, et al. Paradoxical Effects of Obesity on T Cell Function During Tumor Progression and PD-1 Checkpoint Blockade. *Nat Med* (2019) 25:141–51. doi: 10.1038/s41591-018-0221-5
11. Chooi YC, Ding C, Magkos F. The Epidemiology of Obesity. *Metabolism* (2019) 92:6–10. doi: 10.1016/j.metabol.2018.09.005
12. Flegal KM, Kruszon-Moran D, Carroll MD, Fryar CD, Ogden CL. Trends in Obesity Among Adults in the United States 2005 to 2014. *Jama* (2016) 315:2284–91. doi: 10.1001/jama.2016.6458
13. Global, B.M.I.M.CDi Angelantonio E, Bhupathiraju Sh N, Wormser D, Gao P, Kaptoge S, et al. Body-Mass Index and All-Cause Mortality: Individual-Participant-Data Meta-Analysis of 239 Prospective Studies in Four Continents. *Lancet* (2016) 388:776–86. doi: 10.1016/S0140-6736<(>16<)>30175-1
14. Hales CM, Carroll MD, Fryar CD, Ogden CL. Prevalence of Obesity and Severe Obesity Among Adults: United State-2018. *NCHS Data Brief* (2020) 1–8. https://www.cdc.gov/nchs/data/databriefs/db360-h.pdf
15. European Commission. *Over Half of Adults in the EU are Overweight* (2019). Available at: https://ec.europa.eu/eurostat/web/products-eurostat-news/-/ddn-20210721-2 (Accessed 3.21.22).
16. Guh DP, Zhang W, Bansback N, Amarsi Z, Birmingham CL, Anis AH. The Incidence of Co-Morbidities Related to Obesity and Overweight: A Systematic Review and Meta-Analysis. *BMC Public Health* (2009) 9:88. doi: 10.1186/1471-2458-9-88
17. Hruby A, Hu FB. The Epidemiology of Obesity: A Big Picture. *Pharmacoeconomics* (2015) 33:673–89. doi: 10.1007/s40273-014-0243-x
18. Tremmel M, Gerdtham UG, Nilsson PM, Saha S. Economic Burden of Obesity: A Systematic Literature Review. *Int J Environ Res Public Health* (2017) 14:435. doi: 10.3390/ijerph14040435
19. Finkelstein EA, Trogdon JG, Cohen JW, Dietz W. Annual Medical Spending Attributable to Obesity: Payer-and Service-Specific Estimates. *Health Aff (Millwood)* (2009) 28:w822–31. doi: 10.1377/hlthaff.28.5.w822
20. Flegal KM, Kit BK, Orpana H, Graubard BI. Association of All-Cause Mortality With Overweight and Obesity Using Standard Body Mass Index Categories: A Systematic Review and Meta-Analysis. *Jama* (2013) 309:71–82. doi: 10.1001/jama.2012.113905
21. Kyrgiou M, Kalliala I, Markozannes G, Gunter MJ, Paraskevaidis E, Gabra H, et al. Adiposity and Cancer at Major Anatomical Sites: Umbrella Review of the Literature. *BMJ* (2017) 356:j477. doi: 10.1136/bmj.j477
22. Boi SK, Buchta CM, Pearson NA, Francis MB, Meyerholz DK, Grobe JL, et al. Obesity Alters Immune and Metabolic Profiles: New Insight From Obese-Resistant Mice on High-Fat Diet. *Obes (Silver Spring)* (2016) 24:2140–9. doi: 10.1002/oby.21620
23. Cildir G, Akincilar SC, Tergaonkar V. Chronic Adipose Tissue Inflammation: All Immune Cells on the Stage. *Trends Mol Med* (2013) 19:487–500. doi: 10.1016/j.molmed.2013.05.001
24. Donohoe CL, Lysaght J, O'Sullivan J, Reynolds JV. Emerging Concepts Linking Obesity With the Hallmarks of Cancer. *Trends Endocrinol Metab* (2017) 28:46–62. doi: 10.1016/j.tem.2016.08.004
25. Dyck L, Lynch L. Cancer, Obesity and Immunometabolism - Connecting the Dots. *Cancer Lett* (2018) 417:11–20. doi: 10.1016/j.canlet.2017.12.019
26. Ertunc ME, Hotamisligil GS. Lipid Signaling and Lipotoxicity in Metaflammation: Indications for Metabolic Disease Pathogenesis and Treatment. *J Lipid Res* (2016) 57:2099–114. doi: 10.1194/jlr.R066514
27. Gonzalez-Muniesa P, Martinez-Gonzalez MA, Hu FB, Despres JP, Matsuzawa Y, Loos RJF, et al. Obesity. *Nat Rev Dis Primers* (2017) 3:17034. doi: 10.1038/nrdp.2017.34
28. Reilly SM, Saltiel AR. Adapting to Obesity With Adipose Tissue Inflammation. *Nat Rev Endocrinol* (2017) 13:633–43. doi: 10.1038/nrendo.2017.90
29. Saltiel AR, Olefsky JM. Inflammatory Mechanisms Linking Obesity and Metabolic Disease. *J Clin Invest* (2017) 127:1–4. doi: 10.1172/JCI92035
30. Dietrich P, Hellerbrand C. Non-Alcoholic Fatty Liver Disease, Obesity and the Metabolic Syndrome. *Best Pract Res Clin Gastroenterol* (2014) 28:637–53. doi: 10.1016/j.bpg.2014.07.008
31. Liu R, Nikolajczyk BS. Tissue Immune Cells Fuel Obesity-Associated Inflammation in Adipose Tissue and Beyond. *Front Immunol* (2019) 10. doi: 10.3389/fimmu.2019.01587
32. Hotamisligil GS, Arner P, Caro JF, Atkinson RL, Spiegelman BM. Increased Adipose Tissue Expression of Tumor Necrosis Factor-Alpha in Human Obesity and Insulin Resistance. *J Clin Invest* (1995) 95:2409–15. doi: 10.1172/JCI117936
33. Hotamisligil GS, Shargill NS, Spiegelman BM. Adipose Expression of Tumor Necrosis Factor-Alpha: Direct Role in Obesity-Linked Insulin Resistance. *Science* (1993) 259:87–91. doi: 10.1126/science.7678183
34. Hotamisligil GS, Spiegelman BM. Tumor Necrosis Factor Alpha: A Key Component of the Obesity-Diabetes Link. *Diabetes* (1994) 43:1271–8. doi: 10.2337/diab.43.11.1271
35. Bergin R, Kinlen D, Kedia-Mehta N, Hayes E, Cassidy FC, Cody D, et al. Mucosal-Associated Invariant T Cells are Associated With Insulin Resistance in Childhood Obesity, and Disrupt Insulin Signalling *via* IL-17. *Diabetologia* (2022) 65:1012–7. doi: 10.1007/s00125-022-05682-w

36. Kedia-Mehta N, Tobin L, Zaiatz-Bittencourt V, Pisarska MM, De Barra C, Choi C, et al. Cytokine-Induced Natural Killer Cell Training is Dependent on Cellular Metabolism and is Defective in Obesity. *Blood Adv* (2021) 5:4447–55. doi: 10.1182/bloodadvances.2021005047
37. Michelet X, Dyck L, Hogan A, Loftus RM, Duquette D, Wei K, et al. Metabolic Reprogramming of Natural Killer Cells in Obesity Limits Antitumor Responses. *Nat Immunol* (2018) 19:1330–40. doi: 10.1038/s41590-018-0251-7
38. Nicholas DA, Proctor EA, Agrawal M, Belkina AC, Van Nostrand SC, Panneerseelan-Bharath L, et al. Fatty Acid Metabolites Combine With Reduced Beta Oxidation to Activate Th17 Inflammation in Human Type 2 Diabetes. *Cell Metab* (2019) 30:447–461 e5. doi: 10.1016/j.cmet.2019.07.004
39. Nikolajczyk BS, Jagannathan-Bogdan M, Denis GV. The Outliers Become a Stampede as Immunometabolism Reaches a Tipping Point. *Immunol Rev* (2012) 249:253–75. doi: 10.1111/j.1600-065X.2012.01142.x
40. Nikolajczyk BS, Jagannathan-Bogdan M, Shin H, Gyurko R. State of the Union Between Metabolism and the Immune System in Type 2 Diabetes. *Genes Immun* (2011) 12:239–50. doi: 10.1038/gene.2011.14
41. Andreeva E, Bobyleva P, Gornostaeva A, Buravkova L. Interaction of Multipotent Mesenchymal Stromal and Immune Cells: Bidirectional Effects. *Cytotherapy* (2017) 19:1152–66. doi: 10.1016/j.jcyt.2017.07.001
42. Fontaine MJ, Shih H, Schafer R, Pittenger MF. Unraveling the Mesenchymal Stromal Cells' Paracrine Immunomodulatory Effects. *Transfus Med Rev* (2016) 30:37–43. doi: 10.1016/j.tmrv.2015.11.004
43. Ankrum JA, Ong JF, Karp JM. Mesenchymal Stem Cells: Immune Evasive, Not Immune Privileged. *Nat Biotechnol* (2014) 32:252–60. doi: 10.1038/nbt.2816
44. Moll G, Ankrum JA, Kamhieh-Milz J, Bieback K, Ringdén O, Volk H-D, et al. Intravascular Mesenchymal Stromal/Stem Cell Therapy Product Diversification: Time for New Clinical Guidelines. *Trends Mol Med* (2019) 25:149–63. doi: 10.1016/j.molmed.2018.12.006
45. Blokhin IO, Lentz SR. Mechanisms of Thrombosis in Obesity. *Curr Opin Hematol* (2013) 20:437–44. doi: 10.1097/MOH.0b013e3283634443
46. Campello E, Spiezia L, Zabeo E, Maggiolo S, Vettor R, Simioni P. Hypercoagulability Detected by Whole Blood Thromboelastometry (ROTEM(R)) and Impedance Aggregometry (MULTIPLATE(R)) in Obese Patients. *Thromb Res* (2015) 135:548–53. doi: 10.1016/j.thromres.2015.01.003
47. Kornblith LZ, Howard B, Kunitake R, Redick B, Nelson M, Cohen MJ, et al. Obesity and Clotting: Body Mass Index Independently Contributes to Hypercoagulability After Injury. *J Trauma Acute Care Surg* (2015) 78:30–6. doi: 10.1097/TA.0000000000000490
48. Lentz SR. Thrombosis in the Setting of Obesity or Inflammatory Bowel Disease. *Blood* (2016) 128:2388–94. doi: 10.1182/blood-2016-05-716720
49. Samad F, Ruf W. Inflammation, Obesity, and Thrombosis. *Blood* (2013) 122:3415–22. doi: 10.1182/blood-2013-05-427708
50. Farkona S, Diamandis EP, Blasutig IM. Cancer Immunotherapy: The Beginning of the End of Cancer? *BMC Med* (2016) 14:73. doi: 10.1186/s12916-016-0623-5
51. Liu M, Guo F. Recent Updates on Cancer Immunotherapy. *Precis Clin Med* (2018) 1:65–74. doi: 10.1093/pcmedi/pby011
52. Tang J, Pearce L, O'Donnell-Tormey J, Hubbard-Lucey VM. Trends in the Global Immuno-Oncology Landscape. *Nat Rev Drug Discovery* (2018) 17:783–4. doi: 10.1038/nrd.2018.167
53. Aguilar EG, Murphy WJ. Obesity Induced T Cell Dysfunction and Implications for Cancer Immunotherapy. *Curr Opin Immunol* (2018) 51:181–6. doi: 10.1016/j.coi.2018.03.012
54. Canter RJ, Le CT, Beerthuijzen JMT, Murphy WJ. Obesity as an Immune-Modifying Factor in Cancer Immunotherapy. *J Leukoc Biol* (2018) 104:487–97. doi: 10.1002/JLB.5RI1017-401RR
55. Mirsoian A, Bouchlaka MN, Sckisel GD, Chen M, Pai CC, Maverakis E, et al. Adiposity Induces Lethal Cytokine Storm After Systemic Administration of Stimulatory Immunotherapy Regimens in Aged Mice. *J Exp Med* (2014) 211:2373–83. doi: 10.1084/jem.20140116
56. Mirsoian A, Murphy WJ. Obesity and Cancer Immunotherapy Toxicity. *Immunotherapy* (2015) 7:319–22. doi: 10.2217/imt.15.12
57. Chinnadurai R, Copland IB, Patel SR, Galipeau J. IDO-Independent Suppression of T Cell Effector Function by IFN-Gamma-Licensed Human Mesenchymal Stromal Cells. *J Immunol* (2014) 192:1491–501. doi: 10.4049/jimmunol.1301828
58. Davies LC, Heldring N, Kadri N, Blanc KL. Mesenchymal Stromal Cell Secretion of Programmed Death-1 Ligands Regulates T Cell Mediated Immunosuppression. *Stem Cells* (2017) 35:766–76. doi: 10.1002/stem.2509
59. de Witte SFH, Luk F, Sierra Parraga JM, Gargesha M, Merino A, Korevaar SS, et al. Immunomodulation By Therapeutic Mesenchymal Stromal Cells (MSC) Is Triggered Through Phagocytosis of MSC By Monocytic Cells. *Stem Cells* (2018) 36:602–15. doi: 10.1002/stem.2779
60. Bouchlaka MN, Sckisel GD, Chen M, Mirsoian A, Zamora AE, Maverakis E, et al. Aging Predisposes to Acute Inflammatory Induced Pathology After Tumor Immunotherapy. *J Exp Med* (2013) 210:2223–37. doi: 10.1084/jem.20131219
61. Murphy KA, James BR, Sjaastad FV, Kucaba TA, Kim H, Brincks EL, et al. Cutting Edge: Elevated Leptin During Diet-Induced Obesity Reduces the Efficacy of Tumor Immunotherapy. *J Immunol* (2018) 201:1837–41. doi: 10.4049/jimmunol.1701738
62. Turbitt WJ, Boi SK, Gibson JT, Orlandella RM, Norian LA. Diet-Induced Obesity Impairs Outcomes and Induces Multi-Factorial Deficiencies in Effector T Cell Responses Following Anti-CTLA-4 Combinatorial Immunotherapy in Renal Tumor-Bearing Mice. *Cancers (Basel)* (2021) 13:2295. doi: 10.3390/cancers13102295
63. Francisco V, Pino J, Campos-Cabaleiro V, Ruiz-Fernandez C, Mera A, Gonzalez-Gay MA, et al. Obesity, Fat Mass and Immune System: Role for Leptin. *Front Physiol* (2018) 9. doi: 10.3389/fphys.2018.00640
64. Rahmouni K. Obesity, Sympathetic Overdrive, and Hypertension: The Leptin Connection. *Hypertension* (2010) 55:844–5. doi: 10.1161/HYPERTENSIONAHA.109.148932
65. Schwartz MW, Seeley RJ, Zeltser LM, Drewnowski A, Ravussin E, Redman LM, et al. Obesity Pathogenesis: An Endocrine Society Scientific Statement. *Endocr Rev* (2017) 38:267–96. doi: 10.1210/er.2017-00111
66. Boi SK, Orlandella RM, Gibson JT, Turbitt WJ, Wald G, Thomas L, et al. Obesity Diminishes Response to PD-1-Based Immunotherapies in Renal Cancer. *J Immunother Cancer* (2020) 8:e000725. doi: 10.1136/jitc-2020-000725
67. McQuade JL, Daniel CR, Hess KR, Mak C, Wang DY, Rai RR, et al. Association of Body-Mass Index and Outcomes in Patients With Metastatic Melanoma Treated With Targeted Therapy, Immunotherapy, or Chemotherapy: A Retrospective, Multicohort Analysis. *Lancet Oncol* (2018) 19:310–22. doi: 10.1016/S1470-2045<(>18<)>30078-0
68. Dyck L, Prendeville H, Raverdeau M, Wilk MM, Loftus RM, Douglas A, et al. Suppressive Effects of the Obese Tumor Microenvironment on CD8 T Cell Infiltration and Effector Function. *J Exp Med* (2022) 219:e20210042. doi: 10.1084/jem.20210042
69. Postow MA, Sidlow R, Hellmann MD. Immune-Related Adverse Events Associated With Immune Checkpoint Blockade. *N Engl J Med* (2018) 378:158–68. doi: 10.1056/NEJMra1703481
70. Gao F, Chiu SM, Motan DA, Zhang Z, Chen L, Ji HL, et al. Mesenchymal Stem Cells and Immunomodulation: Current Status and Future Prospects. *Cell Death Dis* (2016) 7:e2062. doi: 10.1038/cddis.2015.327
71. Carty F, Dunbar H, Hawthorne IJ, Ting AE, Stubblefield SR, Van't Hof W, et al. IFN-γ and Pparδ Influence the Efficacy and Retention of Multipotent Adult Progenitor Cells in Graft vs Host Disease. *Stem Cells Transl Med* (2021) 10:1561–74. doi: 10.1002/sctm.21-0008
72. Tobin LM, Healy ME, English K, Mahon BP. Human Mesenchymal Stem Cells Suppress Donor CD4(+) T Cell Proliferation and Reduce Pathology in a Humanized Mouse Model of Acute Graft-Versus-Host Disease. *Clin Exp Immunol* (2013) 172:333–48. doi: 10.1111/cei.12056
73. Hinden L, Avner M, Stepensky P, Or R, Almogi-Hazan O. Lymphocyte Counts may Predict a Good Response to Mesenchymal Stromal Cells Therapy in Graft Versus Host Disease Patients. *PloS One* (2019) 14:e0217572. doi: 10.1371/journal.pone.0217572
74. Galleu A, Riffo-Vasquez Y, Trento C, Lomas C, Dolcetti L, Cheung TS, et al. Apoptosis in Mesenchymal Stromal Cells Induces *In Vivo* Recipient-

Mediated Immunomodulation. *Sci Trans Med* (2017) 9:eaam7828. doi: 10.1126/scitranslmed.aam7828
75. Gavin C, Boberg E, Von Bahr L, Bottai M, Andrén AT, Wernerson A, et al. Tissue Immune Profiles Supporting Response to Mesenchymal Stromal Cell Therapy in Acute Graft-Versus-Host Disease—a Gut Feeling. *Stem Cell Res Ther* (2019) 10:334. doi: 10.1186/s13287-019-1449-9
76. Khuat LT, Vick LV, Choi E, Dunai C, Merleev AA, Maverakis E, et al. Mechanisms by Which Obesity Promotes Acute Graft-Versus-Host Disease in Mice. *Front Immunol* (2021) 12. doi: 10.3389/fimmu.2021.752484
77. Khuat LT, Le CT, Pai C-CS, Shields-Cutler RR, Holtan SG, Rashidi A, et al. Obesity Induces Gut Microbiota Alterations and Augments Acute Graft-Versus-Host Disease After Allogeneic Stem Cell Transplantation. *Sci Trans Med* (2020) 12:eaay7713. doi: 10.1126/scitranslmed.aay7713
78. Michonneau D, Latis E, Curis E, Dubouchet L, Ramamoorthy S, Ingram B, et al. Metabolomics Analysis of Human Acute Graft-Versus-Host Disease Reveals Changes in Host and Microbiota-Derived Metabolites. *Nat Commun* (2019) 10:5695. doi: 10.1038/s41467-019-13498-3
79. Maia L, Cruz FF, de Oliveira MV, Samary CS, Fernandes MVdeS, et al. Effects of Obesity on Pulmonary Inflammation and Remodeling in Experimental Moderate Acute Lung Injury. *Front Immunol* (2019) 10. doi: 10.3389/fimmu.2019.01215
80. Stapleton RD, Suratt BT. Obesity And Nutrition In Ards. *Clin Chest Med* (2014) 35:655–71. doi: 10.1016/j.ccm.2014.08.005
81. Zhi G, Xin W, Ying W, Guohong X, Shuying L. Obesity Paradox" in Acute Respiratory Distress Syndrome: Asystematic Review and Meta-Analysis. *PloS One* (2016) 11:e0163677. doi: 10.1371/journal.pone.0163677
82. Cruz-Lagunas A, Jiménez-Alvarez L, Ramírez G, Mendoza-Milla C, García-Sancho M, Avila-Moreno F, et al. Obesity and Pro-Inflammatory Mediators are Associated With Acute Kidney Injury in Patients With A/H1N1 Influenza and Acute Respiratory Distress Syndrome. *Exp Mol Pathol* (2014) 97:453–7. doi: 10.1016/j.yexmp.2014.10.006
83. Zhang W, Wang Y, Li W, Wang J. Association Between Obesity and Short- And Long-Term Mortality in Patients With Acute Respiratory Distress Syndrome Based on the Berlin Definition. *Front Endocrinol (Lausanne)* (2020) 11. doi: 10.3389/fendo.2020.611435
84. Galipeau J, Sensebe L. Mesenchymal Stromal Cells: Clinical Challenges and Therapeutic Opportunities. *Cell Stem Cell* (2018) 22:824–33. doi: 10.1016/j.stem.2018.05.004
85. Packham DK, Fraser IR, Kerr PG, Segal KR. Allogeneic Mesenchymal Precursor Cells (MPC) in Diabetic Nephropathy: A Randomized, Placebo-Controlled, Dose Escalation Study. *EBioMedicine* (2016) 12:263–9. doi: 10.1016/j.ebiom.2016.09.011
86. Skyler JS, Fonseca VA, Segal KR, Rosenstock JMsb-Dm Investigators. Allogeneic Mesenchymal Precursor Cells in Type 2 Diabetes: A Randomized, Placebo-Controlled, Dose-Escalation Safety and Tolerability Pilot Study. *Diabetes Care* (2015) 38:1742–9. doi: 10.2337/dc14-2830
87. Acosta L, Hmadcha A, Escacena N, Perez-Camacho I, de la Cuesta A, Ruiz-Salmeron R, et al. Adipose Mesenchymal Stromal Cells Isolated From Type 2 Diabetic Patients Display Reduced Fibrinolytic Activity. *Diabetes* (2013) 62:4266–9. doi: 10.2337/db13-0896
88. Jaber H, Issa K, Eid A, Saleh FA. The Therapeutic Effects of Adipose-Derived Mesenchymal Stem Cells on Obesity and its Associated Diseases in Diet-Induced Obese Mice. *Sci Rep* (2021) 11:6291. doi: 10.1038/s41598-021-85917-9
89. Lee C-W, Hsiao W-T, Lee OK-S. Mesenchymal Stromal Cell-Based Therapies Reduce Obesity and Metabolic Syndromes Induced by a High-Fat Diet. *Trans Res* (2017) 182:61–74.e8. doi: 10.1016/j.trsl.2016.11.003
90. Shree N, Venkategowda S, Venkatranganna MV, Datta I, Bhonde RR. Human Adipose Tissue Mesenchymal Stem Cells as a Novel Treatment Modality for Correcting Obesity Induced Metabolic Dysregulation. *Int J Obes* (2019) 43:2107–18. doi: 10.1038/s41366-019-0438-5
91. Domingues CC, Kundu N, Kropotova Y, Ahmadi N, Sen S. Antioxidant-Upregulated Mesenchymal Stem Cells Reduce Inflammation and Improve Fatty Liver Disease in Diet-Induced Obesity. *Stem Cell Res Ther* (2019) 10:280. doi: 10.1186/s13287-019-1393-8
92. Tan H-L, Guan X-H, Hu M, Wu J, Li R-Z, Wang L-F, et al. Human Amniotic Mesenchymal Stem Cells-Conditioned Medium Protects Mice From High-Fat Diet-Induced Obesity. *Stem Cell Res Ther* (2021) 12:364. doi: 10.1186/s13287-021-02437-z
93. Song J-S, Hong K-T, Kim N-M, Park H-S, Choi N-H. Human Umbilical Cord Blood-Derived Mesenchymal Stem Cell Implantation for Osteoarthritis of the Knee. *Arch Orthop Trauma Surg* (2020) 140:503–9. doi: 10.1007/s00402-020-03349-y
94. Zhu L, Feng Z, Shu X, Gao Q, Wu J, Du Z, et al. In Situ Transplantation of Adipose-Derived Stem Cells *via* Photoactivation Improves Glucose Metabolism in Obese Mice. *Stem Cell Res Ther* (2021) 12:408. doi: 10.1186/s13287-021-02494-4
95. Daltro PS, Barreto BC, Silva PG, Neto PC, Sousa Filho PHF, Santana Neta D, et al. Therapy With Mesenchymal Stromal Cells or Conditioned Medium Reverse Cardiac Alterations in a High-Fat Diet–Induced Obesity Model. *Cytotherapy* (2017) 19:1176–88. doi: 10.1016/j.jcyt.2017.07.002
96. Dobiásová M. AIP-Atherogenic Index of Plasma as a Significant Predictor of Cardiovascular Risk: From Research to Practice. *Vnitr Lek* (2006) 52:64–71.
97. Kashyap SR, Diab DL, Baker AR, Yerian L, Bajaj H, Gray-McGuire C, et al. Triglyceride Levels and Not Adipokine Concentrations Are Closely Related to Severity of Nonalcoholic Fatty Liver Disease in an Obesity Surgery Cohort. *Obesity* (2009) 17:1696–701. doi: 10.1038/oby.2009.89
98. Huang S, Rutkowsky JM, Snodgrass RG, Ono-Moore KD, Schneider DA, Newman JW, et al. Saturated Fatty Acids Activate TLR-Mediated Proinflammatory Signaling Pathways. *J Lipid Res* (2012) 53:2002–13. doi: 10.1194/jlr.D029546
99. Karasawa T, Kawashima A, Usui-Kawanishi F, Watanabe S, Kimura H, Kamata R, et al. Saturated Fatty Acids Undergo Intracellular Crystallization and Activate the NLRP3 Inflammasome in Macrophages. *Arterioscler Thromb Vasc Biol* (2018) 38:744–56. doi: 10.1161/ATVBAHA.117.310581
100. Lichtenstein L, Mattijssen F, de Wit NJ, Georgiadi A, Hooiveld GJ, van der Meer R, et al. Angptl4 Protects Against Severe Proinflammatory Effects of Saturated Fat by Inhibiting Fatty Acid Uptake Into Mesenteric Lymph Node Macrophages. *Cell Metab* (2010) 12:580–92. doi: 10.1016/j.cmet.2010.11.002
101. Rocha DM, Caldas AP, Oliveira LL, Bressan J, Hermsdorff HH. Saturated Fatty Acids Trigger TLR4-Mediated Inflammatory Response. *Atherosclerosis* (2016) 244:211–5. doi: 10.1016/j.atherosclerosis.2015.11.015
102. Zhou H, Urso C, Jadeja V. Saturated Fatty Acids in Obesity-Associated Inflammation. *J Inflammation Res* (2020) 13:1–14. doi: 10.2147/JIR.S229691
103. Stenger EO, Chinnadurai R, Yuan S, Garcia M, Arafat D, Gibson G, et al. Bone Marrow-Derived Mesenchymal Stromal Cells From Patients With Sickle Cell Disease Display Intact Functionality. *Biol Blood Marrow Transplant* (2017) 23:736–45. doi: 10.1016/j.bbmt.2017.01.081
104. Copland IB, Qayed M, Garcia MA, Galipeau J, Waller EK. Bone Marrow Mesenchymal Stromal Cells From Patients With Acute and Chronic Graft-Versus-Host Disease Deploy Normal Phenotype, Differentiation Plasticity, and Immune-Suppressive Activity. *Biol Blood Marrow Transplant* (2015) 21:934–40. doi: 10.1016/j.bbmt.2015.01.014
105. Chinnadurai R, Copland IB, Ng S, Garcia M, Prasad M, Arafat D, et al. Mesenchymal Stromal Cells Derived From Crohn's Patients Deploy Indoleamine 2,3-Dioxygenase-Mediated Immune Suppression, Independent of Autophagy. *Mol Ther* (2015) 23:1248–61. doi: 10.1038/mt.2015.67
106. Kizilay Mancini O, Lora M, Cuillerier A, Shum-Tim D, Hamdy R, Burelle Y, et al. Mitochondrial Oxidative Stress Reduces the Immunopotency of Mesenchymal Stromal Cells in Adults With Coronary Artery Disease. *Circ Res* (2018) 122:255–66. doi: 10.1161/CIRCRESAHA.117.311400
107. Kizilay Mancini O, Lora M, Shum-Tim D, Nadeau S, Rodier F, Colmegna I. A Proinflammatory Secretome Mediates the Impaired Immunopotency of Human Mesenchymal Stromal Cells in Elderly Patients With Atherosclerosis. *Stem Cells Transl Med* (2017) 6:1132–40. doi: 10.1002/sctm.16-0221
108. Kizilay Mancini O, Shum-Tim D, Stochaj U, Correa JA, Colmegna I. Age, Atherosclerosis and Type 2 Diabetes Reduce Human Mesenchymal Stromal Cell-Mediated T-Cell Suppression. *Stem Cell Res Ther* (2015) 6:140. doi: 10.1186/s13287-015-0127-9
109. Serena C, Keiran N, Ceperuelo-Mallafre V, Ejarque M, Fradera R, Roche K, et al. Obesity and Type 2 Diabetes Alters the Immune Properties of Human Adipose Derived Stem Cells. *Stem Cells* (2016) 34:2559–73. doi: 10.1002/stem.2429

110. Strong AL, Bowles AC, Wise RM, Morand JP, Dutreil MF, Gimble JM, et al. Human Adipose Stromal/Stem Cells From Obese Donors Show Reduced Efficacy in Halting Disease Progression in the Experimental Autoimmune Encephalomyelitis Model of Multiple Sclerosis. *Stem Cells* (2016) 34:614–26. doi: 10.1002/stem.2272
111. Harrison MAA, Wise RM, Benjamin BP, Hochreiner EM, Mohiuddin OA, Bunnell BA. Adipose-Derived Stem Cells From Obese Donors Polarize Macrophages and Microglia Toward a Pro-Inflammatory Phenotype. *Cells* (2020) 10:26. doi: 10.3390/cells10010026
112. Conley SM, Hickson LJ, Kellogg TA, McKenzie T, Heimbach JK, Taner T, et al. Human Obesity Induces Dysfunction and Early Senescence in Adipose Tissue-Derived Mesenchymal Stromal/Stem Cells. *Front Cell Dev Biol* (2020) 8. doi: 10.3389/fcell.2020.00197
113. Ritter A, Friemel A, Kreis N-N, Hoock SC, Roth S, Kielland-Kaisen U, et al. Primary Cilia Are Dysfunctional in Obese Adipose-Derived Mesenchymal Stem Cells. *Stem Cell Rep* (2018) 10:583–99. doi: 10.1016/j.stemcr.2017.12.022
114. Klomjit N, Conley SM, Zhu XY, Sadiq IM, Libai Y, Krier JD, et al. Effects of Obesity on Reparative Function of Human Adipose Tissue-Derived Mesenchymal Stem Cells on Ischemic Murine Kidneys. *Int J Obes* (2022) 46:1222–33. doi: 10.1038/s41366-022-01103-5
115. Yu S, Klomjit N, Jiang K, Zhu XY, Ferguson CM, Conley SM, et al. Human Obesity Attenuates Cardioprotection Conferred by Adipose Tissue–Derived Mesenchymal Stem/Stromal Cells. *J @ Cardiovasc Trans Res* (2022). doi: 10.1007/s12265-022-10279-0
116. O'Shea D, Hogan AE. Dysregulation of Natural Killer Cells in Obesity. *Cancers* (2019) 11:573. doi: 10.3390/cancers11040573
117. Nguyen LT, Hoang DM, Nguyen KT, Bui DM, Nguyen HT, Le HTA, et al. Type 2 Diabetes Mellitus Duration and Obesity Alter the Efficacy of Autologously Transplanted Bone Marrow-Derived Mesenchymal Stem/Stromal Cells. *Stem Cells Transl Med* (2021) 10:1266–78. doi: 10.1002/sctm.20-0506
118. Ayaz-Guner S, Alessio N, Acar MB, Aprile D, Özcan S, Di Bernardo G, et al. A Comparative Study on Normal and Obese Mice Indicates That the Secretome of Mesenchymal Stromal Cells Is Influenced by Tissue Environment and Physiopathological Conditions. *Cell Commun Signaling* (2020) 18:118. doi: 10.1186/s12964-020-00614-w
119. Tobin LM, Mavinkurve M, Carolan E, Kinlen D, O'Brien EC, Little MA, et al. NK Cells in Childhood Obesity are Activated, Metabolically Stressed, and Functionally Deficient. *JCI Insight* (2017) 2:e94939. doi: 10.1172/jci.insight.94939
120. Contreras-Lopez R, Elizondo-Vega R, Paredes MJ, Luque-Campos N, Torres MJ, Tejedor G, et al. Hif1α-Dependent Metabolic Reprogramming Governs Mesenchymal Stem/Stromal Cell Immunoregulatory Functions. *FASEB J* (2020) 34:8250–64. doi: 10.1096/fj.201902232R
121. Killer MC, Nold P, Henkenius K, Fritz L, Riedlinger T, Barckhausen C, et al. Immunosuppressive Capacity of Mesenchymal Stem Cells Correlates With Metabolic Activity and can be Enhanced by Valproic Acid. *Stem Cell Res Ther* (2017) 8:100. doi: 10.1186/s13287-017-0553-y
122. Vigo T, La Rocca C, Faicchia D, Procaccini C, Ruggieri M, Salvetti M, et al. Ifnβ Enhances Mesenchymal Stromal (Stem) Cells Immunomodulatory Function Through STAT1-3 Activation and mTOR-Associated Promotion of Glucose Metabolism. *Cell Death Dis* (2019) 10:1–8. doi: 10.1038/s41419-019-1336-4
123. Martinez VG, Ontoria-Oviedo I, Ricardo CP, Harding SE, Sacedon R, Varas A, et al. Overexpression of Hypoxia-Inducible Factor 1 Alpha Improves Immunomodulation by Dental Mesenchymal Stem Cells. *Stem Cell Res Ther* (2017) 8:208. doi: 10.1186/s13287-017-0659-2
124. Bantug GR, Galluzzi L, Kroemer G, Hess C. The Spectrum of T Cell Metabolism in Health and Disease. *Nat Rev Immunol* (2018) 18:19–34. doi: 10.1038/nri.2017.99
125. Jitschin R, Mougiakakos D, Von Bahr L, Volkl S, Moll G, Ringden O, et al. Alterations in the Cellular Immune Compartment of Patients Treated With Third-Party Mesenchymal Stromal Cells Following Allogeneic Hematopoietic Stem Cell Transplantation. *Stem Cells* (2013) 31:1715–25. doi: 10.1002/stem.1386
126. Popescu BF, Lucchinetti CF. Pathology of Demyelinating Diseases. *Annu Rev Pathol* (2012) 7:185–217. doi: 10.1146/annurev-pathol-011811-132443
127. Engela AU, Hoogduijn MJ, Boer K, Litjens NH, Betjes MG, Weimar W, et al. Human Adipose-Tissue Derived Mesenchymal Stem Cells Induce Functional De-Novo Regulatory T Cells With Methylated FOXP3 Gene DNA. *Clin Exp Immunol* (2013) 173:343–54. doi: 10.1111/cei.12120
128. Roux C, Saviane G, Pini J, Belaid N, Dhib G, Voha C, et al. Immunosuppressive Mesenchymal Stromal Cells Derived From Human-Induced Pluripotent Stem Cells Induce Human Regulatory T Cells *In Vitro* and *In Vivo*. *Front Immunol* (2017) 8. doi: 10.3389/fimmu.2017.01991
129. Vasilev G, Ivanova M, Ivanova-Todorova E, Tumangelova-Yuzeir K, Krasimirova E, Stoilov R, et al. Secretory Factors Produced by Adipose Mesenchymal Stem Cells Downregulate Th17 and Increase Treg Cells in Peripheral Blood Mononuclear Cells From Rheumatoid Arthritis Patients. *Rheumatol Int* (2019) 39:819–26. doi: 10.1007/s00296-019-04296-7
130. Cahill E, Tobin LM, Carthy F, Mahon BP, English K. Jagged-1 is Required for the Expansion of CD4+ CD25+ FoxP3+ Regulatory T Cells and Tolerogenic Dendritic Cells by Murine Mesenchymal Stromal Cells. *Stem Cell Res Ther* (2015) 6:19. doi: 10.1186/s13287-015-0021-5
131. English K, Ryan JM, Tobin L, Murphy MJ, Barry FP, Mahon BP. Cell Contact, Prostaglandin E2 and Transforming Growth Factor Beta 1 Play non-Redundant Roles in Human Mesenchymal Stem Cell Induction of CD4 +CD25Highforkhead Box P3+ Regulatory T Cells. *Clin Exp Immunol* (2009) 156:149–60. doi: 10.1111/j.1365-2249.2009.03874.x
132. Ge W, Jiang J, Arp J, Liu W, Garcia B, Wang H. Regulatory T-Cell Generation and Kidney Allograft Tolerance Induced by Mesenchymal Stem Cells Associated With Indoleamine 2,3-Dioxygenase Expression. *Transplantation* (2010) 90:1312–20. doi: 10.1097/TP.0b013e3181fed001
133. He Y, Zhou S, Liu H, Shen B, Zhao H, Peng K, et al. Indoleamine 2, 3-Dioxgenase Transfected Mesenchymal Stem Cells Induce Kidney Allograft Tolerance by Increasing the Production and Function of Regulatory T Cells. *Transplantation* (2015) 99:1829–38. doi: 10.1097/TP.0000000000000856
134. Li YF, Zhang SX, Ma XW, Xue YL, Gao C, Li XY, et al. The Proportion of Peripheral Regulatory T Cells in Patients With Multiple Sclerosis: A Meta-Analysis. *Mult Scler Relat Disord* (2019) 28:75–80. doi: 10.1016/j.msard.2018.12.019
135. Blazar BR, MacDonald KPA, Hill GR. Immune Regulatory Cell Infusion for Graft-Versus-Host Disease Prevention and Therapy. *Blood* (2018) 131:2651–60. doi: 10.1182/blood-2017-11-785865
136. Court AC, Le-Gatt A, Luz-Crawford P, Parra E, Aliaga-Tobar V, Bátiz LF, et al. Mitochondrial Transfer From MSCs to T Cells Induces Treg Differentiation and Restricts Inflammatory Response. *EMBO Rep* (2020) 21:e48052. doi: 10.15252/embr.201948052
137. Tang B, Li X, Liu Y, Chen X, Chu Y, Zhu H, et al. The Therapeutic Effect of ICAM-1-Overexpressing Mesenchymal Stem Cells on Acute Graft-Versus-Host Disease. *Cell Physiol Biochem* (2018) 46:2624–35. doi: 10.1159/000489689
138. Wu R, Liu C, Deng X, Chen L, Hao S, Ma L. Enhanced Alleviation of aGVHD by TGF-β1-Modified Mesenchymal Stem Cells in Mice Through Shifting MΦ Into M2 Phenotype and Promoting the Differentiation of Treg Cells. *J Cell Mol Med* (2020) 24:1684–99. doi: 10.1111/jcmm.14862
139. Zhang B, Yeo RWY, Lai RC, Sim EWK, Chin KC, Lim SK. Mesenchymal Stromal Cell Exosome-Enhanced Regulatory T-Cell Production Through an Antigen-Presenting Cell-Mediated Pathway. *Cytotherapy* (2018) 20:687–96. doi: 10.1016/j.jcyt.2018.02.372
140. Feuerer M, Herrero L, Cipolletta D, Naaz A, Wong J, Nayer A, et al. Lean, But Not Obese, Fat is Enriched for a Unique Population of Regulatory T Cells That Affect Metabolic Parameters. *Nat Med* (2009) 15:930–9. doi: 10.1038/nm.2002
141. Agabiti-Rosei C, Trapletti V, Piantoni S, Airo P, Tincani A, De Ciuceis C, et al. Decreased Circulating T Regulatory Lymphocytes in Obese Patients Undergoing Bariatric Surgery. *PloS One* (2018) 13:e0197178. doi: 10.1371/journal.pone.0197178
142. Wagner NM, Brandhorst G, Czepluch F, Lankeit M, Eberle C, Herzberg S, et al. Circulating Regulatory T Cells are Reduced in Obesity and may Identify Subjects at Increased Metabolic and Cardiovascular Risk. *Obes (Silver Spring)* (2013) 21:461–8. doi: 10.1002/oby.20087
143. Considine RV, Sinha MK, Heiman ML, Kriauciunas A, Stephens TW, Nyce MR, et al. Serum Immunoreactive-Leptin Concentrations in Normal-Weight

and Obese Humans. *New Engl J Med* (1996) 334:292–5. doi: 10.1056/NEJM199602013340503
144. De Rosa V, Procaccini C, Calì G, Pirozzi G, Fontana S, Zappacosta S, et al. A Key Role of Leptin in the Control of Regulatory T Cell Proliferation. *Immunity* (2007) 26:241–55. doi: 10.1016/j.immuni.2007.01.011
145. Matarese G, Procaccini C, De Rosa V, Horvath TL, La Cava A. Regulatory T Cells in Obesity: The Leptin Connection. *Trends Mol Med* (2010) 16:247–56. doi: 10.1016/j.molmed.2010.04.002
146. Han JM, Patterson SJ, Speck M, Ehses JA, Levings MK. Insulin Inhibits IL-10-Mediated Regulatory T Cell Function: Implications for Obesity. *J Immunol* (2014) 192:623–9. doi: 10.4049/jimmunol.1302181
147. Negrotto L, Farez MF, Correale J. Immunologic Effects of Metformin and Pioglitazone Treatment on Metabolic Syndrome and Multiple Sclerosis. *JAMA Neurol* (2016) 73:520–8. doi: 10.1001/jamaneurol.2015.4807
148. Auletta JJ, Eid SK, Wuttisarnwattana P, Silva I, Metheny L, Keller MD, et al. Human Mesenchymal Stromal Cells Attenuate Graft-Versus-Host Disease and Maintain Graft-Versus-Leukemia Activity Following Experimental Allogeneic Bone Marrow Transplantation. *Stem Cells* (2015) 33:601–14. doi: 10.1002/stem.1867
149. Duffy MM, Pindjakova J, Hanley SA, McCarthy C, Weidhofer GA, Sweeney EM, et al. Mesenchymal Stem Cell Inhibition of T-Helper 17 Cell-Differentiation is Triggered by Cell-Cell Contact and Mediated by Prostaglandin E2 *via* the EP4 Receptor. *Eur J Immunol* (2011) 41:2840–51. doi: 10.1002/eji.201141499
150. Luz-Crawford P, Kurte M, Bravo-Alegria J, Contreras R, Nova-Lamperti E, Tejedor G, et al. Mesenchymal Stem Cells Generate a CD4+CD25+Foxp3+ Regulatory T Cell Population During the Differentiation Process of Th1 and Th17 Cells. *Stem Cell Res Ther* (2013) 4:65. doi: 10.1186/scrt216
151. Rozenberg A, Rezk A, Boivin MN, Darlington PJ, Nyirenda M, Li R, et al. Human Mesenchymal Stem Cells Impact Th17 and Th1 Responses Through a Prostaglandin E2 and Myeloid-Dependent Mechanism. *Stem Cells Transl Med* (2016) 5:1506–14. doi: 10.5966/sctm.2015-0243
152. Te Boome LC, Mansilla C, van der Wagen LE, Lindemans CA, Petersen EJ, Spierings E, et al. Biomarker Profiling of Steroid-Resistant Acute GVHD in Patients After Infusion of Mesenchymal Stromal Cells. *Leukemia* (2015) 29:1839–46. doi: 10.1038/leu.2015.89
153. Bettelli E, Carrier Y, Gao W, Korn T, Strom TB, Oukka M, et al. Reciprocal Developmental Pathways for the Generation of Pathogenic Effector TH17 and Regulatory T Cells. *Nature* (2006) 441:235–8. doi: 10.1038/nature04753
154. McLaughlin T, Liu LF, Lamendola C, Shen L, Morton J, Rivas H, et al. T-Cell Profile in Adipose Tissue is Associated With Insulin Resistance and Systemic Inflammation in Humans. *Arterioscler Thromb Vasc Biol* (2014) 34:2637–43. doi: 10.1161/ATVBAHA.114.304636
155. Carolan E, Tobin LM, Mangan BA, Corrigan M, Gaoatswe G, Byrne G, et al. Altered Distribution and Increased IL-17 Production by Mucosal-Associated Invariant T Cells in Adult and Childhood Obesity. *J Immunol* (2015) 194:5775–80. doi: 10.4049/jimmunol.1402945
156. Ip B, Cilfone NA, Belkina AC, DeFuria J, Jagannathan-Bogdan M, Zhu M, et al. Th17 Cytokines Differentiate Obesity From Obesity-Associated Type 2 Diabetes and Promote TNFalpha Production. *Obes (Silver Spring)* (2016) 24:102–12. doi: 10.1002/oby.21243
157. Brien AO, Kedia-Mehta N, Tobin L, Veerapen N, Besra GS, Shea DO, et al. Targeting Mitochondrial Dysfunction in MAIT Cells Limits IL-17 Production in Obesity. *Cell Mol Immunol* (2020) 17:1193–5. doi: 10.1038/s41423-020-0375-1
158. Mauro C, Smith J, Cucchi D, Coe D, Fu H, Bonacina F, et al. Obesity-Induced Metabolic Stress Leads to Biased Effector Memory CD4(+) T Cell Differentiation *via* PI3K P110delta-Akt-Mediated Signals. *Cell Metab* (2017) 25:593–609. doi: 10.1016/j.cmet.2017.01.008
159. Ringel AE, Drijvers JM, Baker GJ, Catozzi A, García-Cañaveras JC, Gassaway BM, et al. Obesity Shapes Metabolism in the Tumor Microenvironment to Suppress Anti-Tumor Immunity. *Cell* (2020) 183:1848–1866.e26. doi: 10.1016/j.cell.2020.11.009
160. Abdolmaleki F, Farahani N, Gheibi Hayat SM, Pirro M, Bianconi V, Barreto GE, et al. The Role of Efferocytosis in Autoimmune Diseases. *Front Immunol* (2018) 9. doi: 10.3389/fimmu.2018.01645
161. Elliott MR, Koster KM, Murphy PS. Efferocytosis Signaling in the Regulation of Macrophage Inflammatory Responses. *J Immunol* (2017) 198:1387–94. doi: 10.4049/jimmunol.1601520
162. Wang D, Chen K, Du WT, Han ZB, Ren H, Chi Y, et al. CD14+ Monocytes Promote the Immunosuppressive Effect of Human Umbilical Cord Matrix Stem Cells. *Exp Cell Res* (2010) 316:2414–23. doi: 10.1016/j.yexcr.2010.04.018
163. Martinez FO, Gordon S. The M1 and M2 Paradigm of Macrophage Activation: Time for Reassessment. *F1000Prime Rep* (2014) 6:13. doi: 10.12703/P6-13
164. Xue J, Schmidt SV, Sander J, Draffehn A, Krebs W, Quester I, et al. Transcriptome-Based Network Analysis Reveals a Spectrum Model of Human Macrophage Activation. *Immunity* (2014) 40:274–88. doi: 10.1016/j.immuni.2014.01.006
165. Abumaree MH, Al Jumah MA, Kalionis B, Jawdat D, Al Khaldi A, Abomaray FM, et al. Human Placental Mesenchymal Stem Cells (pMSCs) Play a Role as Immune Suppressive Cells by Shifting Macrophage Differentiation From Inflammatory M1 to Anti-Inflammatory M2 Macrophages. *Stem Cell Rev Rep* (2013) 9:620–41. doi: 10.1007/s12015-013-9455-2
166. Blazquez R, Sanchez-Margallo FM, Alvarez V, Uson A, Casado JG. Surgical Meshes Coated With Mesenchymal Stem Cells Provide an Anti-Inflammatory Environment by a M2 Macrophage Polarization. *Acta Biomater* (2016) 31:221–30. doi: 10.1016/j.actbio.2015.11.057
167. Braza F, Dirou S, Forest V, Sauzeau V, Hassoun D, Chesné J, et al. Mesenchymal Stem Cells Induce Suppressive Macrophages Through Phagocytosis in a Mouse Model of Asthma. *Stem Cells* (2016) 34:1836–45. doi: 10.1002/stem.2344
168. Francois M, Romieu-Mourez R, Li M, Galipeau J. Human MSC Suppression Correlates With Cytokine Induction of Indoleamine 2,3-Dioxygenase and Bystander M2 Macrophage Differentiation. *Mol Ther* (2012) 20:187–95. doi: 10.1038/mt.2011.189
169. Park HJ, Kim J, Saima FT, Rhee KJ, Hwang S, Kim MY, et al. Adipose-Derived Stem Cells Ameliorate Colitis by Suppression of Inflammasome Formation and Regulation of M1-Macrophage Population Through Prostaglandin E2. *Biochem Biophys Res Commun* (2018) 498:988–95. doi: 10.1016/j.bbrc.2018.03.096
170. Qiu G, Zheng G, Ge M, Huang L, Tong H, Chen P, et al. Adipose-Derived Mesenchymal Stem Cells Modulate CD14(++)CD16(+) Expression on Monocytes From Sepsis Patients *In Vitro via* Prostaglandin E2. *Stem Cell Res Ther* (2017) 8:97. doi: 10.1186/s13287-017-0546-x
171. Song HB, Park SY, Ko JH, Park JW, Yoon CH, Kim DH, et al. Mesenchymal Stromal Cells Inhibit Inflammatory Lymphangiogenesis in the Cornea by Suppressing Macrophage in a TSG-6-Dependent Manner. *Mol Ther* (2018) 26:162–72. doi: 10.1016/j.ymthe.2017.09.026
172. Deng Y, Zhang Y, Ye L, Zhang T, Cheng J, Chen G, et al. Umbilical Cord-Derived Mesenchymal Stem Cells Instruct Monocytes Towards an IL10-Producing Phenotype by Secreting IL6 and HGF. *Sci Rep* (2016) 6:37566. doi: 10.1038/srep37566
173. Chen PM, Liu KJ, Hsu PJ, Wei CF, Bai CH, Ho LJ, et al. Induction of Immunomodulatory Monocytes by Human Mesenchymal Stem Cell-Derived Hepatocyte Growth Factor Through ERK1/2. *J Leukoc Biol* (2014) 96:295–303. doi: 10.1189/jlb.3A0513-242R
174. Cutler AJ, Limbani V, Girdlestone J, Navarrete CV. Umbilical Cord-Derived Mesenchymal Stromal Cells Modulate Monocyte Function to Suppress T Cell Proliferation. *J Immunol* (2010) 185:6617–23. doi: 10.4049/jimmunol.1002239
175. Spaggiari GM, Abdelrazik H, Becchetti F, Moretta L. MSCs Inhibit Monocyte-Derived DC Maturation and Function by Selectively Interfering With the Generation of Immature DCs: Central Role of MSC-Derived Prostaglandin E2. *Blood* (2009) 113:6576–83. doi: 10.1182/blood-2009-02-203943
176. Nemeth K, Leelahavanichkul A, Yuen PS, Mayer B, Parmelee A, Doi K, et al. Bone Marrow Stromal Cells Attenuate Sepsis *via* Prostaglandin E< (>2<)>-Dependent Reprogramming of Host Macrophages to Increase Their Interleukin-10 Production. *Nat Med* (2009) 15:42–9. doi: 10.1038/nm.1905

177. Krasnodembskaya A, Samarani G, Song Y, Zhuo H, Su X, Lee J-W, et al. Human Mesenchymal Stem Cells Reduce Mortality and Bacteremia in Gram-Negative Sepsis in Mice in Part by Enhancing the Phagocytic Activity of Blood Monocytes. *Am J Physiol Lung Cell Mol Physiol* (2012) 302:L1003–1013. doi: 10.1152/ajplung.00180.2011
178. Song Y, Dou H, Li X, Zhao X, Li Y, Liu D, et al. Exosomal miR-146a Contributes to the Enhanced Therapeutic Efficacy of Interleukin-1beta-Primed Mesenchymal Stem Cells Against Sepsis. *Stem Cells* (2017) 35:1208–21. doi: 10.1002/stem.2564
179. Mathias LJ, Khong SM, Spyroglou L, Payne NL, Siatskas C, Thorburn AN, et al. Alveolar Macrophages are Critical for the Inhibition of Allergic Asthma by Mesenchymal Stromal Cells. *J Immunol* (2013) 191:5914–24. doi: 10.4049/jimmunol.1300667
180. Song X, Xie S, Lu K, Wang C. Mesenchymal Stem Cells Alleviate Experimental Asthma by Inducing Polarization of Alveolar Macrophages. *Inflammation* (2015) 38:485–92. doi: 10.1007/s10753-014-9954-6
181. Choi H, Lee RH, Bazhanov N, Oh JY, Prockop DJ. Anti-Inflammatory Protein TSG-6 Secreted by Activated MSCs Attenuates Zymosan-Induced Mouse Peritonitis by Decreasing TLR2/NF-kappaB Signaling in Resident Macrophages. *Blood* (2011) 118:330–8. doi: 10.1182/blood-2010-12-327353
182. Song JY, Kang HJ, Hong JS, Kim CJ, Shim JY, Lee CW, et al. Umbilical Cord-Derived Mesenchymal Stem Cell Extracts Reduce Colitis in Mice by Re-Polarizing Intestinal Macrophages. *Sci Rep* (2017) 7:9412. doi: 10.1038/s41598-017-09827-5
183. Song WJ, Li Q, Ryu MO, Ahn JO, Ha Bhang D, Chan Jung Y, et al. TSG-6 Secreted by Human Adipose Tissue-Derived Mesenchymal Stem Cells Ameliorates DSS-Induced Colitis by Inducing M2 Macrophage Polarization in Mice. *Sci Rep* (2017) 7:5187. doi: 10.1038/s41598-017-04766-7
184. Bouchlaka MN, Moffitt AB, Kim J, Kink JA, Bloom DD, Love C, et al. Human Mesenchymal Stem Cell-Educated Macrophages Are a Distinct High IL-6-Producing Subset That Confer Protection in Graft-Versus-Host-Disease and Radiation Injury Models. *Biol Blood Marrow Transplant* (2017) 23:897–905. doi: 10.1016/j.bbmt.2017.02.018
185. Gonzalo-Gil E, Perez-Lorenzo MJ, Galindo M, Lopez-Millan B, Bueno C, Menendez P, et al. Human Embryonic Stem Cell-Derived Mesenchymal Stromal Cells Ameliorate Collagen-Induced Arthritis by Inducing Host-Derived Indoleamine 2,3 Dioxygenase. *Arthritis Res Ther* (2016) 18:77. doi: 10.1186/s13075-016-0979-0
186. Shin TH, Kim HS, Kang TW, Lee BC, Lee HY, Kim YJ, et al. Human Umbilical Cord Blood-Stem Cells Direct Macrophage Polarization and Block Inflammasome Activation to Alleviate Rheumatoid Arthritis. *Cell Death Dis* (2016) 7:e2524. doi: 10.1038/cddis.2016.442
187. Groh ME, Maitra B, Szekely E, Koc ON. Human Mesenchymal Stem Cells Require Monocyte-Mediated Activation to Suppress Alloreactive T Cells. *Exp Hematol* (2005) 33:928–34. doi: 10.1016/j.exphem.2005.05.002
188. Reading JL, Vaes B, Hull C, Sabbah S, Hayday T, Wang NS, et al. Suppression of IL-7-Dependent Effector T-Cell Expansion by Multipotent Adult Progenitor Cells and PGE2. *Mol Ther* (2015) 23:1783–93. doi: 10.1038/mt.2015.131
189. Min H, Xu L, Parrott R, Overall CC, Lillich M, Rabjohns EM, et al. Mesenchymal Stromal Cells Reprogram Monocytes and Macrophages With Processing Bodies. *Stem Cells* (2021) 39:115–28. doi: 10.1002/stem.3292
190. Carty F, Mahon BP, English K. The Influence of Macrophages on Mesenchymal Stromal Cell Therapy: Passive or Aggressive Agents? *Clin Exp Immunol* (2017) 188:1–11. doi: 10.1111/cei.12929
191. Jackson MV, Morrison TJ, Doherty DF, McAuley DF, Matthay MA, Kissenpfennig A, et al. Mitochondrial Transfer *via* Tunneling Nanotubes is an Important Mechanism by Which Mesenchymal Stem Cells Enhance Macrophage Phagocytosis in the *In Vitro* and *In Vivo* Models of ARDS. *Stem Cells* (2016) 34:2210–23. doi: 10.1002/stem.2372
192. Jiang D, Gao F, Zhang Y, Wong DS, Li Q, Tse HF, et al. Mitochondrial Transfer of Mesenchymal Stem Cells Effectively Protects Corneal Epithelial Cells From Mitochondrial Damage. *Cell Death Dis* (2016) 7:e2467. doi: 10.1038/cddis.2016.358
193. Hyvarinen K, Holopainen M, Skirdenko V, Ruhanen H, Lehenkari P, Korhonen M, et al. Mesenchymal Stromal Cells and Their Extracellular Vesicles Enhance the Anti-Inflammatory Phenotype of Regulatory Macrophages by Downregulating the Production of Interleukin (IL)-23 and IL-22. *Front Immunol* (2018) 9. doi: 10.3389/fimmu.2018.00771
194. Phinney DG, Di Giuseppe M, Njah J, Sala E, Shiva S, St Croix CM, et al. Mesenchymal Stem Cells Use Extracellular Vesicles to Outsource Mitophagy and Shuttle microRNAs. *Nat Commun* (2015) 6:8472. doi: 10.1038/ncomms9472
195. Cheung TS, Galleu A, von Bonin M, Bornhauser M, Dazzi F. Apoptotic Mesenchymal Stromal Cells Induce Prostaglandin E2 in Monocytes: Implications for the Monitoring of Mesenchymal Stromal Cell Activity. *Haematologica* (2019) 104:e438–41. doi: 10.3324/haematol.2018.214767
196. Weiss DJ, English K, Krasnodembskaya A, Isaza-Correa JM, Hawthorne IJ, Mahon BP. The Necrobiology of Mesenchymal Stromal Cells Affects Therapeutic Efficacy. *Front Immunol* (2019) 10. doi: 10.3389/fimmu.2019.01228
197. Morrison TJ, Jackson MV, Cunningham EK, Kissenpfennig A, McAuley DF, O'Kane CM, et al. Mesenchymal Stromal Cells Modulate Macrophages in Clinically Relevant Lung Injury Models by Extracellular Vesicle Mitochondrial Transfer. *Am J Respir Crit Care Med* (2017) 196:1275–86. doi: 10.1164/rccm.201701-0170OC
198. Weisberg SP, McCann D, Desai M, Rosenbaum M, Leibel RL, Ferrante AW. Obesity is Associated With Macrophage Accumulation in Adipose Tissue. *J Clin Invest* (2003) 112:1796–808. doi: 10.1172/JCI19246
199. Howe LR, Subbaramaiah K, Hudis CA, Dannenberg AJ. Molecular Pathways: Adipose Inflammation as a Mediator of Obesity-Associated Cancer. *Clin Cancer Res* (2013) 19:6074–83. doi: 10.1158/1078-0432.CCR-12-2603
200. Stienstra R, Dijk W, van Beek L, Jansen H, Heemskerk M, Houtkooper RH, et al. Mannose-Binding Lectin is Required for the Effective Clearance of Apoptotic Cells by Adipose Tissue Macrophages During Obesity. *Diabetes* (2014) 63:4143–53. doi: 10.2337/db14-0256
201. Morris DL, Cho KW, Delproposto JL, Oatmen KE, Geletka LM, Martinez-Santibanez G, et al. Adipose Tissue Macrophages Function as Antigen-Presenting Cells and Regulate Adipose Tissue CD4+ T Cells in Mice. *Diabetes* (2013) 62:2762–72. doi: 10.2337/db12-1404
202. Cho KW, Morris DL, DelProposto JL, Geletka L, Zamarron B, Martinez-Santibanez G, et al. An MHC II-Dependent Activation Loop Between Adipose Tissue Macrophages and CD4+ T Cells Controls Obesity-Induced Inflammation. *Cell Rep* (2014) 9:605–17. doi: 10.1016/j.celrep.2014.09.004
203. Fernandez-Boyanapalli R, Goleva E, Kolakowski C, Min E, Day B, Leung DY, et al. Obesity Impairs Apoptotic Cell Clearance in Asthma. *J Allergy Clin Immunol* (2013) 131:1047 e1–3. doi: 10.1016/j.jaci.2012.09.028
204. Myers JA, Miller JS. Exploring the NK Cell Platform for Cancer Immunotherapy. *Nat Rev Clin Oncol* (2021) 18:85–100. doi: 10.1038/s41571-020-0426-7
205. van Eeden C, Khan L, Osman MS, Cohen Tervaert JW. Natural Killer Cell Dysfunction and Its Role in COVID-19. *Int J Mol Sci* (2020) 21:6351. doi: 10.3390/ijms21176351
206. Giamarellos-Bourboulis EJ, Tsaganos T, Spyridaki E, Mouktaroudi M, Plachouras D, Vaki I, et al. Early Changes of CD4-Positive Lymphocytes and NK Cells in Patients With Severe Gram-Negative Sepsis. *Crit Care* (2006) 10:R166. doi: 10.1186/cc5111
207. Gianchecchi E, Delfino DV, Fierabracci A. NK Cells in Autoimmune Diseases: Linking Innate and Adaptive Immune Responses. *Autoimmun Rev* (2018) 17:142–54. doi: 10.1016/j.autrev.2017.11.018
208. Kucuksezer UC, Aktas Cetin E, Esen F, Tahrali I, Akdeniz N, Gelmez MY, et al. The Role of Natural Killer Cells in Autoimmune Diseases. *Front Immunol* (2021) 12. doi: 10.3389/fimmu.2021.622306
209. Liu M, Liang S, Zhang C. NK Cells in Autoimmune Diseases: Protective or Pathogenic? *Front Immunol* (2021) 12. doi: 10.3389/fimmu.2021.624687
210. Crop MJ, Korevaar SS, de Kuiper R, IJzermans JNM, van Besouw NM, Baan CC, et al. Human Mesenchymal Stem Cells are Susceptible to Lysis by CD8 (+) T Cells and NK Cells. *Cell Transplant* (2011) 20:1547–59. doi: 10.3727/096368910X564076
211. Spaggiari GM, Capobianco A, Becchetti S, Mingari MC, Moretta L. Mesenchymal Stem Cell-Natural Killer Cell Interactions: Evidence That Activated NK Cells are Capable of Killing MSCs, Whereas MSCs can Inhibit

IL-2-Induced NK-Cell Proliferation. *Blood* (2006) 107:1484–90. doi: 10.1182/blood-2005-07-2775
212. Cui R, Rekasi H, Hepner-Schefczyk M, Fessmann K, Petri RM, Bruderek K, et al. Human Mesenchymal Stromal/Stem Cells Acquire Immunostimulatory Capacity Upon Cross-Talk With Natural Killer Cells and Might Improve the NK Cell Function of Immunocompromised Patients. *Stem Cell Res Ther* (2016) 7:88. doi: 10.1186/s13287-016-0353-9
213. Giri J, Das R, Nylen E, Chinnadurai R, Galipeau J. CCL2 and CXCL12 Derived From Mesenchymal Stromal Cells Cooperatively Polarize IL-10+ Tissue Macrophages to Mitigate Gut Injury. *Cell Rep* (2020) 30:1923–1934.e4. doi: 10.1016/j.celrep.2020.01.047
214. Noone C, Kihm A, English K, O'Dea S, Mahon BP. IFN-γ Stimulated Human Umbilical-Tissue-Derived Cells Potently Suppress NK Activation and Resist NK-Mediated Cytotoxicity *In Vitro*. *Stem Cells Dev* (2013) 22:3003–14. doi: 10.1089/scd.2013.0028
215. Ishida N, Ishiyama K, Saeki Y, Tanaka Y, Ohdan H. Cotransplantation of Preactivated Mesenchymal Stem Cells Improves Intraportal Engraftment of Islets by Inhibiting Liver Natural Killer Cells in Mice. *Am J Transplant* (2019) 19:2732–45. doi: 10.1111/ajt.15347
216. Boissel L, Tuncer HH, Betancur M, Wolfberg A, Klingemann H. Umbilical Cord Mesenchymal Stem Cells Increase Expansion of Cord Blood Natural Killer Cells. *Biol Blood Marrow Transplant* (2008) 14:1031–8. doi: 10.1016/j.bbmt.2008.06.016
217. Thomas H, Jäger M, Mauel K, Brandau S, Lask S, Flohé SB. Interaction With Mesenchymal Stem Cells Provokes Natural Killer Cells for Enhanced IL-12/IL-18-Induced Interferon-Gamma Secretion. *Mediators Inflammation* (2014) 2014:143463. doi: 10.1155/2014/143463
218. Petri RM, Hackel A, Hahnel K, Dumitru CA, Bruderek K, Flohe SB, et al. Activated Tissue-Resident Mesenchymal Stromal Cells Regulate Natural Killer Cell Immune and Tissue-Regenerative Function. *Stem Cell Rep* (2017) 9:985–98. doi: 10.1016/j.stemcr.2017.06.020
219. Bähr I, Goritz V, Doberstein H, Hiller GGR, Rosenstock P, Jahn J, et al. Diet-Induced Obesity Is Associated With an Impaired NK Cell Function and an Increased Colon Cancer Incidence. *J Nutr Metab* (2017) 2017:e4297025. doi: 10.1155/2017/4297025
220. Lynch LA, O'Connell JM, Kwasnik AK, Cawood TJ, O'Farrelly C, O'Shea DB. Are Natural Killer Cells Protecting the Metabolically Healthy Obese Patient? *Obes (Silver Spring)* (2009) 17:601–5. doi: 10.1038/oby.2008.565
221. O'Shea D, Cawood TJ, O'Farrelly C, Lynch L. Natural Killer Cells in Obesity: Impaired Function and Increased Susceptibility to the Effects of Cigarette Smoke. *PloS One* (2010) 5:e8660. doi: 10.1371/journal.pone.0008660
222. Perdu S, Castellana B, Kim Y, Chan K, DeLuca L, Beristain AG. Maternal Obesity Drives Functional Alterations in Uterine NK Cells. *JCI Insight* (2016) 1:e85560. doi: 10.1172/jci.insight.85560
223. Theurich S, Tsaousidou E, Hanssen R, Lempradl AM, Mauer J, Timper K, et al. IL-6/Stat3-Dependent Induction of a Distinct, Obesity-Associated NK Cell Subpopulation Deteriorates Energy and Glucose Homeostasis. *Cell Metab* (2017) 26:171–184.e6. doi: 10.1016/j.cmet.2017.05.018
224. Viel S, Besson L, Charrier E, Marçais A, Disse E, Bienvenu J, et al. Alteration of Natural Killer Cell Phenotype and Function in Obese Individuals. *Clin Immunol* (2017) 177:12–7. doi: 10.1016/j.clim.2016.01.007
225. O'Brien KL, Finlay DK. Immunometabolism and Natural Killer Cell Responses. *Nat Rev Immunol* (2019) 19:282–90. doi: 10.1038/s41577-019-0139-2
226. Nave H, Mueller G, Siegmund B, Jacobs R, Stroh T, Schueler U, et al. Resistance of Janus Kinase-2 Dependent Leptin Signaling in Natural Killer (NK) Cells: A Novel Mechanism of NK Cell Dysfunction in Diet-Induced Obesity. *Endocrinology* (2008) 149:3370–8. doi: 10.1210/en.2007-1516
227. Tian Z, Sun R, Wei H, Gao B. Impaired Natural Killer (NK) Cell Activity in Leptin Receptor Deficient Mice: Leptin as a Critical Regulator in NK Cell Development and Activation. *Biochem Biophys Res Commun* (2002) 298:297–302. doi: 10.1016/s0006-291x<(>02<)>02462-2
228. Barra NG, Fan IY, Gillen JB, Chew M, Marcinko K, Steinberg GR, et al. High Intensity Interval Training Increases Natural Killer Cell Number and Function in Obese Breast Cancer-Challenged Mice and Obese Women. *J Cancer Prev* (2017) 22:260–6. doi: 10.15430/JCP.2017.22.4.260
229. Jahn J, Spielau M, Brandsch C, Stangl GI, Delank K-S, Bähr I, et al. Decreased NK Cell Functions in Obesity can be Reactivated by Fat Mass Reduction. *Obes (Silver Spring)* (2015) 23:2233–41. doi: 10.1002/oby.21229
230. Moulin CM, Marguti I, Peron JPS, Halpern A, Rizzo LV. Bariatric Surgery Reverses Natural Killer (NK) Cell Activity and NK-Related Cytokine Synthesis Impairment Induced by Morbid Obesity. *Obes Surg* (2011) 21:112–8. doi: 10.1007/s11695-010-0250-8
231. O'Rourke RW, White AE, Metcalf MD, Winters BR, Diggs BS, Zhu X, et al. Systemic Inflammation and Insulin Sensitivity in Obese IFN-γ Knockout Mice. *Metab Clin Exp* (2012) 61:1152–61. doi: 10.1016/j.metabol.2012.01.018
232. Wensveen FM, Jelenčić V, Valentić S, Šestan M, Wensveen TT, Theurich S, et al. NK Cells Link Obesity-Induced Adipose Stress to Inflammation and Insulin Resistance. *Nat Immunol* (2015) 16:376–85. doi: 10.1038/ni.3120
233. Boulenouar S, Michelet X, Duquette D, Alvarez D, Hogan AE, Dold C, et al. Adipose Type One Innate Lymphoid Cells Regulate Macrophage Homeostasis Through Targeted Cytotoxicity. *Immunity* (2017) 46:273–86. doi: 10.1016/j.immuni.2017.01.008
234. Gao X, Zhang W, Wang Y, Pedram P, Cahill F, Zhai G, et al. Serum Metabolic Biomarkers Distinguish Metabolically Healthy Peripherally Obese From Unhealthy Centrally Obese Individuals. *Nutr Metab (Lond)* (2016) 13:33. doi: 10.1186/s12986-016-0095-9
235. Molinero LL, Yin D, Lei YM, Chen L, Wang Y, Chong AS, et al. High-Fat Diet-Induced Obesity Enhances Allograft Rejection. *Transplantation* (2016) 100:1015–21. doi: 10.1097/TP.0000000000001141
236. Okamoto Y, Christen T, Shimizu K, Asano K, Kihara S, Mitchell RN, et al. Adiponectin Inhibits Allograft Rejection in Murine Cardiac Transplantation. *Transplantation* (2009) 88:879–83. doi: 10.1097/TP.0b013e3181b6efbf
237. Ouchi N, Walsh K. Adiponectin as an Anti-Inflammatory Factor. *Clin Chim Acta* (2007) 380:24–30. doi: 10.1016/j.cca.2007.01.026
238. Bielorai B, Weintraub Y, Hutt D, Hemi R, Kanety H, Modan-Moses D, et al. The Metabolic Syndrome and its Components in Pediatric Survivors of Allogeneic Hematopoietic Stem Cell Transplantation. *Clin Transplant* (2017) 31:e12903. doi: 10.1111/ctr.12903
239. Moraes-Vieira PMM, Bassi EJ, Larocca RA, Castoldi A, Burghos M, Lepique AP, et al. Leptin Modulates Allograft Survival by Favoring a Th2 and a Regulatory Immune Profile. *Am J Transplant* (2013) 13:36–44. doi: 10.1111/j.1600-6143.2012.04283.x
240. Naik AS, Sakhuja A, Cibrik DM, Ojo AO, Samaniego-Picota MD, Lentine KL. The Impact of Obesity on Allograft Failure After Kidney Transplantation: A Competing Risks Analysis. *Transplantation* (2016) 100:1963–9. doi: 10.1097/TP.0000000000000983
241. Schachtner T, Stein M, Reinke P. Increased Alloreactivity and Adverse Outcomes in Obese Kidney Transplant Recipients are Limited to Those With Diabetes Mellitus. *Transpl Immunol* (2017) 40:8–16. doi: 10.1016/j.trim.2016.11.005
242. Moll G, Ankrum JA, Olson SD, Nolta JA. Improved MSC Minimal Criteria to Maximize Patient Safety: A Call to Embrace Tissue Factor and Hemocompatibility Assessment of MSC Products. *Stem Cells Trans Med* (2022) 11:2–13. doi: 10.1093/stcltm/szab005
243. Moll G, Rasmusson-Duprez I, von Bahr L, Connolly-Andersen AM, Elgue G, Funke L, et al. Are Therapeutic Human Mesenchymal Stromal Cells Compatible With Human Blood? *Stem Cells* (2012) 30:1565–74. doi: 10.1002/stem.1111
244. Capilla-Gonzalez V, Lopez-Beas J, Escacena N, Aguilera Y, de la Cuesta A, Ruiz-Salmeron R, et al. PDGF Restores the Defective Phenotype of Adipose-Derived Mesenchymal Stromal Cells From Diabetic Patients. *Mol Ther* (2018) 26:2696–709. doi: 10.1016/j.ymthe.2018.08.011
245. Kouroupis D, Correa D. Increased Mesenchymal Stem Cell Functionalization in Three-Dimensional Manufacturing Settings for Enhanced Therapeutic Applications. *Front Bioeng Biotechnol* (2021) 9. doi: 10.3389/fbioe.2021.621748
246. Yang Y-HK, Ogando CR, Wang See C, Chang T-Y, Barabino GA. Changes in Phenotype and Differentiation Potential of Human Mesenchymal Stem Cells Aging *In Vitro*. *Stem Cell Res Ther* (2018) 9:131. doi: 10.1186/s13287-018-0876-3
247. Liu Y, Ma T. Metabolic Regulation of Mesenchymal Stem Cell in Expansion and Therapeutic Application. *Biotechnol Prog* (2015) 31:468–81. doi: 10.1002/btpr.2034
248. Yuan X, Logan TM, Ma T. Metabolism in Human Mesenchymal Stromal Cells: A Missing Link Between hMSC Biomanufacturing and Therapy? *Front Immunol* (2019) 10. doi: 10.3389/fimmu.2019.00977

249. Iaffaldano L, Nardelli C, D'Alessio F, D'Argenio V, Nunziato M, Mauriello L, et al. Altered Bioenergetic Profile in Umbilical Cord and Amniotic Mesenchymal Stem Cells From Newborns of Obese Women. *Stem Cells Dev* (2018) 27:199–206. doi: 10.1089/scd.2017.0198
250. Liu Y, Yuan X, Muñoz N, Logan TM, Ma T. Commitment to Aerobic Glycolysis Sustains Immunosuppression of Human Mesenchymal Stem Cells. *Stem Cells Transl Med* (2018) 8:93–106. doi: 10.1002/sctm.18-0070
251. Düvel K, Yecies JL, Menon S, Raman P, Lipovsky AI, Souza AL, et al. Activation of a Metabolic Gene Regulatory Network Downstream of mTOR Complex 1. *Mol Cell* (2010) 39:171–83. doi: 10.1016/j.molcel.2010.06.022
252. Burand AJ, Di L, Boland LK, Boyt DT, Schrodt MV, Santillan DA, et al. Aggregation of Human Mesenchymal Stromal Cells Eliminates Their Ability to Suppress Human T Cells. *Front Immunol* (2020) 11. doi: 10.3389/fimmu.2020.00143
253. Soundararajan M, Kannan S. Fibroblasts and Mesenchymal Stem Cells: Two Sides of the Same Coin? *J Cell Physiol* (2018) 233:9099–109. doi: 10.1002/jcp.26860
254. Haddad JJ, Land SC. A non-Hypoxic, ROS-Sensitive Pathway Mediates TNF-α-Dependent Regulation of HIF-1α. *FEBS Lett* (2001) 505:269–74. doi: 10.1016/S0014-5793<(>01<)>02833-2
255. Kim KW, Lee SJ, Kim JC. TNF-α Upregulates HIF-1α Expression in Pterygium Fibroblasts and Enhances Their Susceptibility to VEGF Independent of Hypoxia. *Exp Eye Res* (2017) 164:74–81. doi: 10.1016/j.exer.2017.08.008
256. Kozlov AM, Lone A, Betts DH, Cumming RC. Lactate Preconditioning Promotes a HIF-1α-Mediated Metabolic Shift From OXPHOS to Glycolysis in Normal Human Diploid Fibroblasts. *Sci Rep* (2020) 10:8388. doi: 10.1038/s41598-020-65193-9
257. Haikala HM, Anttila JM, Klefström J. MYC and AMPK–Save Energy or Die! *Front Cell Dev Biol* (2017) 5. doi: 10.3389/fcell.2017.00038
258. Sato Y, Mabuchi Y, Miyamoto K, Araki D, Niibe K, Houlihan DD, et al. Notch2 Signaling Regulates the Proliferation of Murine Bone Marrow-Derived Mesenchymal Stem/Stromal Cells *via* C-Myc Expression. *PloS One* (2016) 11:e0165946. doi: 10.1371/journal.pone.0165946
259. Mendt M, Daher M, Basar R, Shanley M, Kumar B, Wei Inng FL, et al. Metabolic Reprogramming of GMP Grade Cord Tissue Derived Mesenchymal Stem Cells Enhances Their Suppressive Potential in GVHD. *Front Immunol* (2021) 12. doi: 10.3389/fimmu.2021.631353
260. Boland L, Burand AJ, Brown AJ, Boyt D, Lira VA, Ankrum JA. IFN-γ and TNF-α Pre-Licensing Protects Mesenchymal Stromal Cells From the Pro-Inflammatory Effects of Palmitate. *Mol Ther* (2018) 26:860–73. doi: 10.1016/j.ymthe.2017.12.013

Conflict of Interest: The authors declare that the research was conducted in the absence of any commercial or financial relationships that could be construed as a potential conflict of interest.

Publisher's Note: All claims expressed in this article are solely those of the authors and do not necessarily represent those of their affiliated organizations, or those of the publisher, the editors and the reviewers. Any product that may be evaluated in this article, or claim that may be made by its manufacturer, is not guaranteed or endorsed by the publisher.

frontiers | Frontiers in Immunology

CLINICAL TRIAL
published: 04 July 2022
doi: 10.3389/fimmu.2022.932360

Bone Marrow-Derived Mesenchymal Stromal Cell Therapy in Severe COVID-19: Preliminary Results of a Phase I/II Clinical Trial

Céline Grégoire[1,2†], Nathalie Layios[3,4†], Bernard Lambermont[3,5], Chantal Lechanteur[6], Alexandra Briquet[6], Virginie Bettonville[6], Etienne Baudoux[6], Marie Thys[7], Nadia Dardenne[8], Benoît Misset[3‡] and Yves Beguin[1,2,6*‡]*

[1] Department of Clinical Hematology, University Hospital Center of Liège, Liège, Belgium, [2] Hematology Research Unit, Groupe Interdisciplinaire de Génoprotéomique Appliquée - Infection, Immunité & Inflammation (GIGA-I3), Groupe Interdisciplinaire de Génoprotéomique Appliquée (GIGA) Institute, University of Liège, Liège, Belgium, [3] Department of Intensive Care, University Hospital Center of Liège, Liège, Belgium, [4] Laboratory of Cardiology, Groupe Interdisciplinaire de Génoprotéomique Appliquée (GIGA) Institute, University of Liège, Liège, Belgium, [5] Groupe Interdisciplinaire de Génoprotéomique Appliquée (GIGA)-In silico Medicine, University of Liège, Liège, Belgium, [6] Laboratory of Cell and Gene Therapy, University Hospital Center of Liège and University of Liège, Liège, Belgium, [7] Department of Medico-Economic Information, University Hospital Center of Liège, Liège, Belgium, [8] University Hospital Center of Biostatistics, Faculty of Medicine, University of Liège, Liège, Belgium

OPEN ACCESS

Edited by:
Guido Moll,
Charité Universitätsmedizin
Berlin, Germany

Reviewed by:
Sairam Atluri,
Tianjin University, China
Olle Thor Hans Ringden,
Karolinska Institutet (KI), Sweden

***Correspondence:**
Céline Grégoire
celine.gregoire@chuliege.be
Yves Beguin
yves.beguin@chuliege.be

[†]These authors have contributed equally to this work and share first authorship

[‡]These authors have contributed equally to this work and share last authorship

Specialty section:
This article was submitted to Alloimmunity and Transplantation, a section of the journal Frontiers in Immunology

Received: 29 April 2022
Accepted: 30 May 2022
Published: 04 July 2022

Citation:
Grégoire C, Layios N, Lambermont B, Lechanteur C, Briquet A, Bettonville V, Baudoux E, Thys M, Dardenne N, Misset B and Beguin Y (2022) Bone Marrow-Derived Mesenchymal Stromal Cell Therapy in Severe COVID-19: Preliminary Results of a Phase I/II Clinical Trial. Front. Immunol. 13:932360. doi: 10.3389/fimmu.2022.932360

Background: Treatment of acute respiratory distress syndrome (ARDS) associated with COronaVIrus Disease-2019 (COVID-19) currently relies on dexamethasone and supportive mechanical ventilation, and remains associated with high mortality. Given their ability to limit inflammation, induce immune cells into a regulatory phenotype and stimulate tissue repair, mesenchymal stromal cells (MSCs) represent a promising therapy for severe and critical COVID-19 disease, which is associated with an uncontrolled immune-mediated inflammatory response.

Methods: In this phase I-II trial, we aimed to evaluate the safety and efficacy of 3 intravenous infusions of bone marrow (BM)-derived MSCs at 3-day intervals in patients with severe COVID-19. All patients also received dexamethasone and standard supportive therapy. Between June 2020 and September 2021, 8 intensive care unit patients requiring supplemental oxygen (high-flow nasal oxygen in 7 patients, invasive mechanical ventilation in 1 patient) were treated with BM-MSCs. We retrospectively compared the outcomes of these MSC-treated patients with those of 24 matched control patients. Groups were compared by paired statistical tests.

Results: MSC infusions were well tolerated, and no adverse effect related to MSC infusions were reported (one patient had an ischemic stroke related to aortic endocarditis). Overall, 3 patients required invasive mechanical ventilation, including one who required extracorporeal membrane oxygenation, but all patients ultimately had a favorable outcome. Survival was significantly higher in the MSC group, both at 28 and 60 days (100% vs 79.2%, p = 0.025 and 100% vs 70.8%, p = 0.0082, respectively), while no significant difference was observed in the need for mechanical ventilation nor in the number of invasive ventilation-free days, high flow nasal oxygenation-free days, oxygen support-free days and ICU-free days. MSC-treated patients also had a significantly lower

day-7 D-dimer value compared to control patients (median 821.0 µg/L [IQR 362.0-1305.0] vs 3553 µg/L [IQR 1155.0-6433.5], p = 0.0085).

Conclusions: BM-MSC therapy is safe and shows very promising efficacy in severe COVID-19, with a higher survival in our MSC cohort compared to matched control patients. These observations need to be confirmed in a randomized controlled trial designed to demonstrate the efficacy of BM-MSCs in COVID-19 ARDS.

Clinical Trial Registration: (www.ClinicalTrials.gov), identifier NCT04445454

Keywords: mesenchymal stromal cells, cellular therapy, COVID-19, SARS-CoV-2, acute respiratory distress syndrome, intensive care unit (ICU)

INTRODUCTION

Severe forms of COronaVIrus Disease-2019 (COVID-19) caused by Severe Acute Respiratory Syndrome CoronaVirus-2 (SARS-CoV-2) are associated with a mortality of up to 30% in critically ill patients hospitalized in the intensive care unit (ICU) (1). SARS-CoV-2, through its spike (S) protein, uses the angiotensin-converting enzyme 2 (ACE2) and the transmembrane protease serine 2 (TMPRSS2) to infect human cells (2). Entry of the virus and its replication within infected cells cause both epithelial and endothelial cell damages, that can result in alveolitis with pulmonary oedema and endothelial inflammation with pulmonary intravascular coagulopathy, therefore affecting both lung ventilation and perfusion (3). Release of inflammatory molecules by damaged cells and alveolar macrophages is responsible for the recruitment of neutrophils, activated monocytes and T cells (3). In most patients, disease is mild to moderate, and the initial inflammatory response is rapidly followed by a highly efficient adaptative immune response, with plasmablast proliferation and production of neutralizing antibodies, but also robust $CD4^+$ and $CD8^+$ T-cell responses (4–7). However, some patients experience a severe disease associated with high viral load (8) and inappropriate immune responses (T-cell lymphopenia and exhaustion, skewing of lung immune responses towards proinflammatory $CD8^+$ and Th17 cells and monocyte-derived proinflammatory macrophages) (5, 8–10), high amounts of cytokines and chemokines including interferon gamma-inducible protein (IP)-10, interleukin (IL)-6 and IL-10 (7), and intravascular coagulopathy indicated by high levels of D-dimers (11).

Several drugs (such as remdesivir, hydroxychloroquine, lopinavir, interferon) have failed to improve the outcome of these critically ill patients (12, 13). Neutralizing monoclonal antibodies are mostly effective in patients with non-severe disease at high risk of evolution toward a severe/critical disease, and their efficacy depends on the SARS-CoV-2 variant. To date, the only drugs that have reduced mortality in COVID-19 ARDS are anti-inflammatory/immunosuppressive drugs: dexamethasone (14), IL6 antagonists (tocilizumab or sarilumab) (15) and the JAK inhibitor baricitinib (16). In routine clinical practice, better understanding of the disease, allowing optimization of oxygen support for COVID-19 patients, and the generalized use of dexamethasone in severe COVID-19 has allowed a reduction in mortality between the first and second waves, but the ICU mortality rate remains high (17).

The interest of mesenchymal stromal cell (MSC) therapy in COVID-19 ARDS arises from their ability to both mitigate immune responses (18) and promote tissue regeneration (19). These non-hematopoietic multipotent progenitors can be easily isolated from several human tissues and have demonstrated their safety in many clinical trials in several diseases, including graft-versus-host-disease and Crohn's disease (20, 21). MSCs modulate both adaptive and innate immune cells, the main effects being on T cells and macrophages. Their potency is enhanced in inflammatory environments (mostly in the presence of IFN-γ, TNF-α, IL-1α and/or IL-1β) (22), while their migration capacities and their ability to secrete trophic factors (such as VEGF) are increased when exposed to other environmental factors such as hypoxia (23, 24).

These properties, associated with first reports of the efficacy of MSC infusions in COVID-19 pneumonia (25, 26), prompted us to initiate a phase I/II clinical trial evaluating the safety and efficacy of bone marrow (BM)-derived MSCs for severe COVID-19 infection. In this preliminary report of our study, we describe the outcome of 8 patients treated with BM-MSCs, and retrospectively compare them with matched control patients.

MATERIALS AND METHODS

Patient Selection

Patients were eligible if they met the following criteria: age between 18 and 70 years, microbiologically or radiologically confirmed COVID-19 pneumonia (as defined by an extensive interstitial pneumonia consistent with viral pneumonia on CT scan within 10 days prior to randomization, and positive result of COVID-19 polymerase chain reaction (PCR) test within 14 days prior to inclusion), and requiring oxygen administration ($SpO2 \leq 93\%$ on room air) in the ward or intensive care unit (ICU). In this first part of the study, only ICU patients were included. Exclusion criteria were: ongoing pregnancy, extracorporeal membrane oxygenation (ECMO), limitations to intensity of care, life expectancy inferior to 24 hours, known allergy to components of the investigational medicinal product (IMP), pre-existing bone marrow transplantation or immunosuppressive therapy, active secondary infection, any malignancy (except non-melanoma skin carcinoma) within 2 years before inclusion, pre-existing thrombo-embolic pathology, and participation in another clinical trial (use of anti-

viral/supportive drugs for COVID-19 infection on a compassionate use basis was not an exclusion criterion).

The study protocol conformed to the ethical guidelines of the 1975 Declaration of Helsinki and was approved by the local Ethics Committee of the University Hospital of Liège, the centralized Ethics Committee of the Cliniques Universitaires Saint-Luc, and the Belgian Federal Agency for Medicines and Health Product (EudraCT: 2020-002102-58; ClinicalTrials.gov identifier: NCT04445454). Signed informed consent was obtained from participating subjects, or – if impossible (clinical condition precluding capacity to consent) - from his/her legal representative.

Mesenchymal Stromal Cells

MSC donors were healthy adult volunteers, unrelated to the recipient. No HLA matching between patient and donor was required. Bone marrow collection and MSC expansion cultures were carried out at the Laboratory of Cell and Gene Therapy (LTCG) at the University of Liège according to good manufacturing practice (GMP) standards, as previously described (27, 28). Detailed procedures for culture and quality control are provided in **Supplementary Material**. Briefly, after bone marrow collection, mononuclear cells were isolated and the cell suspension was seeded at a density of 160,000 cells/cm^2. On day 14 and 21, MSCs were trypsinized and replated at a lower density (4,000 cells/cm^2), and cultured until passage 3, then cryopreserved. Population doubling level (calculated between passage 1 and 3) ranged from 3.6 to 6.2 (median 5.1). Quality controls included morphology, identity and purity (phenotype by flow cytometry), karyotype, viability, and immunosuppressive properties, as well as sterility tests (**Supplementary Table 1** in **Supplementary Material**). MSCs wererapidly thawed in a water bath at 37°C and diluted in the Laboratory of Cell and Gene Therapy (LTCG) and infused within 1 hour of thawing.

Design of the Study and Follow-Up

Eligible subjects were scheduled to receive 3 infusions of 1.5-3x10^6 BM-MSCs/kg, at 3 (± 1) day intervals. Patients received anticoagulant therapy, cetirizine and paracetamol before MSC infusion. Potential toxicities associated with MSC infusions were carefully monitored and recorded on the appropriate infusion form. Follow-up included daily assessment of vital status and vital signs until discharge as per institutional protocol.

The following clinical data were collected within 24 hours of ICU admission: age, body mass index (BMI), PaO_2/FiO_2 ratio, Sepsis-related Organ Failure Assessment (SOFA) score, viral load, and several biological values (including lymphocyte count, C-reactive protein (CRP), ferritin, D-dimers, creatinine). Outcomes were safety, death at day 28 and at day 60, ICU-free days (number of days out of ICU within 28 days from admission to ICU and after last discharge from ICU), need for mechanical ventilation (MV), number of invasive ventilation-free days (number of days without invasive ventilation after the last extubation within 28 days of invasive ventilation initiation), high-flow nasal oxygen (HFNO)-free days (number of days without HFNO after the last weaning within 28 days of HFNO initiation), and O_2 support-free days (number of days without any oxygen support after the last oxygen administration within 28 days of oxygen support initiation), need for noradrenaline, day-7 CRP and D-dimers values.

Using our database of COVID-19 patients treated at the University Hospital Center of Liege, we identified 247 patients requiring high-flow oxygen support within 24 hours of admission, who formed our control group. Data matching was performed based on the calculation of the propensity score, i.e the probability for a subject to be assigned to a particular group of treatment, derived from a binary logistic regression model including the following covariates: age, day-0 SOFA score, worst PaO_2/FiO_2 ratio within 24h following ICU admission, and several biological values within 48 hours of ICU admission (lymphocyte count, ferritin, D-dimers and CRP). A sample of 24 control patients matching the 8 MSC patients was selected.

Statistical Analyses

Quantitative parameters are summarized using median and interquartile range, whereas qualitative parameters are summarized using numbers (n) and frequencies (%). Comparisons of quantitative parameters between the 2 patient groups, MSC and control, were performed using the nonparametric Kruskal-Wallis test in the whole cohort and the non-parametric Wilcoxon signed ranks test in the matched sample. Qualitative parameters were compared between the two groups using the Fisher test in the whole cohort and the Mc Nemar test in the matched sample. The results were considered significant at the uncertainty level of $\alpha = 5\%$ ($p < 0.05$).

Calculations were done using SAS (version 9.4, SAS institute, Cary, NC) and RStudio (version 3.6.2, Foundation for Statistical Computing, Vienna, Austria).

RESULTS

Patients and Treatment

Between June 2020 and September 2021, 8 patients admitted to the ICU were enrolled to receive MSCs (7 men and 1 woman, aged 41 to 68 years). Their demographic characteristics are reported in **Table 1**. All patients had severe COVID-19 ARDS characterized by a WHO ordinal scale of severity score for COVID-19 of 6 (7/8) and 8 (1/8) (29). The median PaO_2/FiO_2 ratio was measured at 85.5 (IQR 77.9-93.4). At inclusion, seven patients were receiving HFNO and 1 patient required mechanical ventilation. Median SOFA score was 4 [IQR 3-5] and biological markers of inflammation were high (median CRP 171.7 mg/L [IQR 127.5-212.2], median ferritin 1,434.4 µg/L [IQR 756.4-2,742.4]), as were D-dimer levels (median 679.0 [IQR 501.5-1,713.0]). The time from first detection of SARS-CoV-2 (nasopharyngeal PCR) to admission to the hospital was 0-14 days. All included patients received their first dose of MSCs within 2 days of ICU admission.

All patients received dexamethasone (6 mg/day during 10 days) and intermediate dose anticoagulation (enoxaparin 0.5 mg/kg/12h, unless a therapeutic dose was otherwise indicated). Seven patients received the 3 scheduled MSC doses; 1 patient did not

TABLE 1 | Patient baseline characteristics.

	Normal values	MSC group (n=8)	Matched control group	n	p^1	Whole control cohort	n	p^2
Age (years)	–	50 (43-58)	54 (49.5-63)	24	0.089	67 (58-73)	247	0.0016
BMI (kg/m²)	–	31.5 (26.5-35.4)	30.1 (24.1-32.8)	19	0.34	28.7 (25. 7-31.8)	227	0.25
PaO2/FiO2	–	85.5 (77.9- 93.4)	86.5 (60.6-102.9)	24	0.89	76.6 (64.0-102.9)	242	0.33
Lymphocyte count (x10^9/L)	1.10-3.70	0.82 (0.59-0.88)	0.77 (0.49-1.06)	24	0.90	0.63 (0.41-0.90)	247	0.34
SOFA score	–	4 (3-5)	4 (3-5)	24	0.81	4 (3-6)	182	0.54
CRP (mg/L)	< 5.0	171.6 (127.5- 212.2)	126.5 (62.2-216.5)	24	0.54	119.4 (63.3- 197.1)	247	0.31
Ferritin (µg/L)	22-275	1434.4 (756.4-2742.4)	1962.6 (990.1-2875.1)	24	0.78	1523.5 (740.5- 2677.7)	132	0.97
D-dimers (µg/L)	< 500	679.0 (501.5-1713.0)	1641.5 (628.5-1641.5)	24	0.098	1047.5 (599.0- 2043.0)	206	0.38
Creatinine (mg/dL)	0.55-1.18	0.83 (0.47- 1.15)	0.84 (0.72-1.03)	24	0.39	0.85 (0.67- 1.15)	247	0.37
Viral load (cycle threshold)	–	28.63 (24.05-29.90)	28.29 (20.68-32.11)	12	0.90	25.34 (20.83-29.09)	139	0.26

Values are expressed as median (P25-P75). p^1 refers to comparisons between the MSC and matched control groups, whereas p^2 refers to comparisons between the MSC group and the whole control cohort. BMI, body mass index; SOFA, Sepsis-related Organ Failure Assessment; CRP, C-Reactive Protein.

receive the third dose after the demonstration of a cerebrovascular ischemic lesion. The median MSC dose (before thawing) was 3.15 x10^6/kg per dose (range 2.41-4.47 x10^6/kg), so that the post-thaw MSC dose of 1.5-3 x10^6 viable cells/kg was reached on each occasion. Post-thawing viability ranged from 56 to 93% (median 76%). Mixed lymphocyte reaction (MLR) assays confirmed the immunosuppressive potency of MSCs post-thawing, with inhibition of lymphocyte proliferation (compared to control without MSCs) ranging from 32 to 70% (median 49%).

We compared these patients with the 247 patients admitted to the ICU of our institution during the same period who required HFNO within the first 24 hours of admission. The only difference in their baseline characteristics was age, with patients in the MSC group being younger (median 50 yrs [IQR 43-58] vs 67 yrs [IQR 58-73] in the control cohort; p=0.0016). The other baseline characteristics (day-0 SOFA score, worst PaO_2/FiO_2 ratio within 24h following ICU admission, lymphocyte count, ferritin, D-dimers, CRP, creatinine, viral load and body mass index) were similar between the two groups. As expected, no significant difference was observed between the MSC group and the control group of 24 patients selected after matching (**Table 1**).

Outcomes

Safety

MSC infusions were well tolerated. We did not observe any significant change in parameters at the time of MSC infusion and immediately afterwards, nor any sign of allergy. One patient was diagnosed with multifocal ischemic cerebral lesions after the second MSC dose and did not receive the third dose. Further evaluation revealed a splenic infarction and an aortic endocarditis occurring on a bicuspid valve, that was considered the embolic source responsible for the stroke. This event was deemed not related to the MSC infusions. No adverse event related to MSCs was reported.

Efficacy

Most patients experienced rapid improvement in respiratory exchange after MSC infusions. Of the 7 patients requiring HFNO at inclusion, 2 required mechanical ventilation after MSC infusions, including one who required ECMO. Ultimately, all patients treated with MSCs had a favorable outcome, and none died (**Figures 1**, **2**). Median durations of hospital stay and ICU stay were 30 days (range 13-109 days) and 12 days (range 3-58 days), respectively. Of note, one patient, who initially showed a favorable course after MSC injections, had a secondary deterioration in respiratory parameters due to a pneumothorax, and required readmission to the ICU (thus prolonging the length of hospital and ICU stay).

We retrospectively compared the outcomes of these MSC-treated patients with those of our cohort of 247 unmatched control patients (**Table 2**). No significant difference was observed between the survival of the MSC group and the unmatched whole control cohort (**Figure 2**).

We then performed the same analyzes after matching (8 MSC patients vs 24 control patients). When comparing these matched

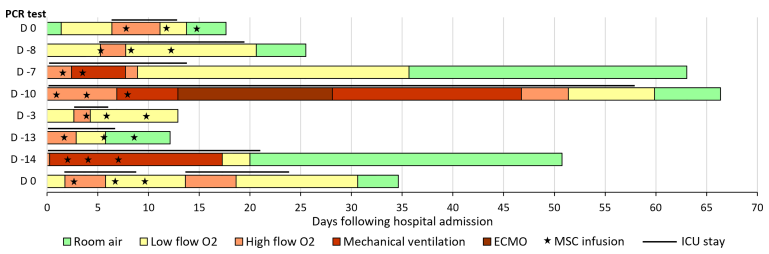

FIGURE 1 | Evolution of oxygen support in patients treated with BM-MSCs. The bars represent the length of hospitalization (in days), and the left column indicates the day of the first positive PCR test, with day 0 being the day of hospital admission. The lines above the bars represent the length of ICU stay, and the "star" symbols represent MSC administrations. ECMO, extracorporeal membrane oxygenation; MSC, mesenchymal stromal cells; ICU, intensive care unit.

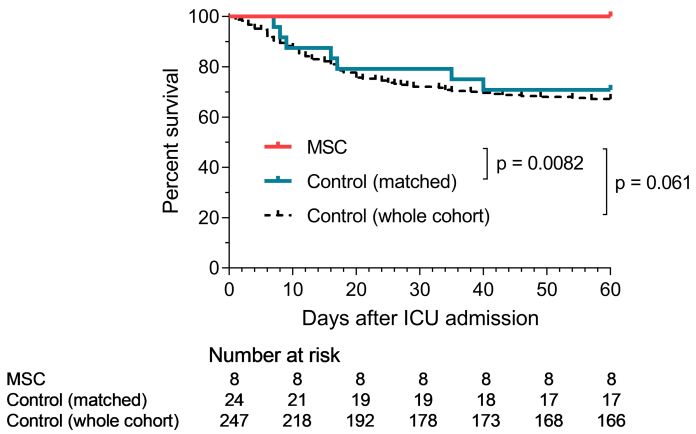

FIGURE 2 | Survival curves in MSC and control groups. p-values refers to comparisons between the MSC and control groups at day 60 (using the Fisher test for non-matched analysis and Wilcoxon test for the matched analysis).

patients, day-28 and day-60 survival was significantly superior in the MSC group (100% vs 79.2%, p = 0.025, and 100% vs 70.8%, p = 0.0082, respectively) (**Table 2** and **Figure 2**). No significant difference was observed in the percentage of patients requiring mechanical ventilation (37.5% vs 45.8%, p = 0.56), nor in the number of day-28 invasive ventilation-free days (median 11d [IQR 0-23] in the MSC group vs 0d [IQR 0-25] in the control group, p = 0.50), day-28 HFNO-free days (median 22d [IQR 10.5-26.5] in the MSC group vs 19d [IQR 0-25] in the control group, p = 0.12) or day-28 oxygen support-free days (median 19d [IQR 8.5-24.5] in the MSC group vs 18d [IQR 0-24.5] in the control group, p = 0.38). Day-28 ICU-free days was also similar in both groups (median 14d [IQR 6.5-22.0] in the MSC group vs 19d [IQR 0-23.5] in the control group, p = 0.92) (**Table 2**).

When analyzing day-7 biological inflammatory parameters, significantly lower D-dimer values were observed in the MSC group (median 821.0 µg/L [IQR 362.0-1305.0] vs 3,553 µg/L [IQR 1,155.0-6,433.5] in the control group, p = 0.0085), while CRP values remained similar between the 2 groups (median 33.2 mg/L [IQR 6.3-59.8] in the MSC group vs 20.8 mg/L [IQR 10.6-92.1] in the control group, p = 0.25) (**Table 2**, **Figure 3**).

DISCUSSION

The COVID pandemic has resulted in significant morbidity and mortality worldwide, and is a significant burden on health care, particularly ICUs. Although significant regional, temporal and center-dependent discrepancies in outcomes have been reported, mortality of critically ill patients in ICU remains high (1). The overall case fatality rate for mechanically ventilated patients is 40-45%, with even worse results in pooled analyses of elderly patients or those with comorbidities (30). In addition, among patients surviving after severe COVID-19, more than 50% experience a substantial reduction in activities of daily living and physical performance (31, 32). The societal cost of ARDS was estimated in a recent systematic review to be approximately €70,000 per case (33). It is therefore essential to identify new therapies for the prevention and treatment of severe forms of COVID-19.

Given their anti-inflammatory and regenerative properties, MSCs represent a promising therapy for many immune and inflammatory disorders, and particularly pulmonary diseases. Indeed, several studies have demonstrated the early trapping of

TABLE 2 | Clinical and biological outcomes.

	MSC group (n=8)	Matched control group (n=24)	p^1	Whole control cohort (n=247)	p^2
28-d mortality	0 (0%)	5 (20.8%)	0.025	65 (26.3%)	0.21
60-d mortality	0 (0%)	7 (29.2%)	0.0082	79 (32.0%)	0.061
ICU-free days	14 (7-22)	19 (0-24)	0.92	13 (0-23)	0.64
Need for MV	3 (37.5%)	11 (45.8%)	0.56	109 (44.1%)	1.00
Invasive ventilation-free days	11 (0-23)	0 (0-25)	0.50	0 (0-17)	0.54
HFNO support-free days	22 (11-27)	19 (0-25)	0.12	16 (0-24)	0.13
O2 support-free days	19 (9-25)	18 (0-25)	0.38	15 (0-24)	0.35
Need for noradrenaline	2 (25.0%)	11 (45.8%)	0.13	97 (39.3%)	0.49
Day-7 CRP (mg/L)	33.2 (6.3-59.8)	20.8 (10.6-92.1)	0.25	35.8 (12.2-94.5)	0.36
Day-7 D-dimers (µg/L)	821.0 (362.0-1,305.0)	3,553.0 (1,155.0-6,433.5)	0.0085	1,315.0 (675.0-3,425.0)	0.14

Values are expressed as median (P25-P75) for quantitative parameters and number (frequencies) for qualitative parameters. p^1 refers to comparisons between the MSC and matched control groups, whereas p^2 refers to comparisons between the MSC group and the whole control cohort. ICU, intensive care unit; MV, mechanical ventilation; HFNO, high flow nasal oxygen.

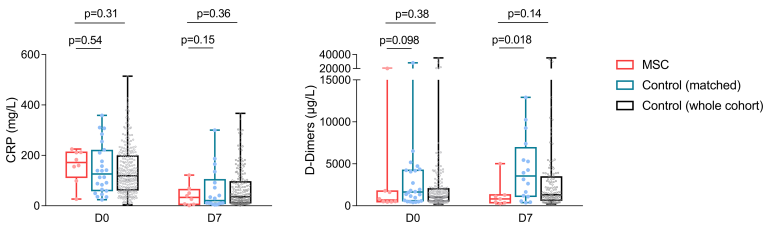

FIGURE 3 | Day-0 and day-7 CRP and D-dimer values in the MSC and control groups. Boxes extend from the 25th to 75th percentiles, and the line in the box is plotted at the median, while whiskers represent minimum and maximum, and points represent individual values.

MSCs in the lung microvasculature, where they interact with cytolytic cells and phagocytes and secrete soluble factors responsible for paracrine and systemic effects (34, 35). MSC therapy has demonstrated its efficacy in several animal models of ARDS, induced mostly by LPS, bacteria, bleomycin or hyperoxia, but also by influenza A H5N1 or after ventilator-induced lung injury (36). In these models, MSC administration mitigated inflammation, resulting in reduced pulmonary edema, increased alveolar fluid clearance, decreased epithelial and vascular permeability, improved oxygenation and longer survival. These improvements were associated with decreased levels of several inflammatory mediators (IL-1β, IL-6, IL-8, IFN-γ and TNF-α) and increased levels of anti-inflammatory and trophic factors (IL-1RA, IL-10, prostaglandin E2, TSG-6). MSCs also induced a shift from pro-inflammatory M1 to anti-inflammatory M2 monocytes/macrophages with enhanced phagocytic capacities and from pro-inflammatory Th17 cells to Tregs. Prior to the COVID-19 pandemic, 3 small phase 1/2 clinical trials had evaluated the use of MSCs in ARDS, but, despite encouraging preliminary results, neither adipose tissue-derived (AT)-MSC ($1x10^6$/kg) nor BM-MSCs ($10x10^6$/kg) have so far demonstrated their ability to significantly improve survival in ARDS (37–40).

Very early in the COVID-19 pandemic, several groups conducted small phase 1 trials evaluating the use of MSCs, mostly derived from umbilical cord (UC), in patients with COVID-19 of varying severity, confirming the absence of adverse effects and suggesting favorable outcomes (25, 41–43). A few groups described outcomes in series of critically ill COVID-19 patients in intensive care, in whom MSC therapy was also found to be safe (44–47). Five randomized trials evaluating UC-MSCs in COVID-19 patients have been reported since then, with heterogenous methodology and results. Lanzoni et al. (48) and Monsel et al. (49) included only patients with ARDS, requiring at least high-flow oxygen, whereas the patient groups were more disparate (or less well described) in the 3 other studies (50–52). MSC dose and administration scheme also differed between the studies, with overall lower doses than in our trial. Outcomes were favorable in three of these trials, with improved survival in two trials (48, 51); Shi et al. however only reported radiological and functional outcomes (50). On the contrary, Monsel et al. found that 3 infusions of $1x10^6$ UC-MSCs/kg in the early phase of COVID-19 ARDS did not improve PaO2/FiO2-ratio between D0 and D7, which was the primary endpoint. No significant differences were observed regarding the secondary endpoints either, including day-28 ventilation-free days (median 17 vs 12 days) nor day-28 mortality (26.3% vs 18.2%) (49).

In our study, 3 infusions of $1.5\text{-}3x10^6$ BM-MSC/kg in the early phase of COVID-19 ARDS were safe, and resulted in 100% survival, which was significantly superior to that of matched control patients treated in our institution during the same period. However, MSC therapy did not significantly reduce the ICU-free days, need for hemodynamic or invasive respiratory support, and duration of oxygen support. We observed significantly lower day-7 D-dimer values compared to those in the matched control patients, which is an important finding since high levels of D-dimers are associated with worse outcomes in COVID-19 ARDS (11, 53).

Unlike most studies that used UC-MSCs in COVID-19 ARDS, we chose to use BM-MSCs. Indeed, few safety data on MSCs in COVID-19 were available when we initiated this study, and BM-MSCs have been more widely used in clinical studies (notably in GVHD, Crohn's disease or organ transplantation), with an excellent safety profile. In addition, the procoagulant nature of MSCs, through tissue factor (TF) expression, was a concern given the known tendency for thrombosis in COVID-19, and BM-MSCs, which have low TF expression, activate coagulation to a much lesser extent than UC- and especially AT-MSCs (54–56). Several studies have now reported no increased thrombotic risk associated with UC-MSCs in COVID-19, which may be related to the wide use of higher doses of low molecular weight heparin in these patients (57). Similarly, patients in our study received at least intermediate-dose prophylactic anticoagulation as part of our institutional protocol in COVID-19 patients admitted to the ICU. Importantly, we observed lower D-dimer concentrations at D7 in the MSC group compared with our matched control group, confirming the absence of a systemic or prolonged procoagulant effect of BM-MSCs in this setting. The hemocompatibility of MSCs is crucial for safety in case of intravenous use, especially in hypercoagulable situations, and further evaluation of TF expression and hemocompatibility might be required to assess the suitability of MSC products (especially when isolated from other sources that the BM) in future clinical studies (56, 58). Furthermore, it has been shown that MSC infusion could be accompanied by a transient elevation of IL-6, and that this effect was more pronounced with UC-MSCs than BM-MSCs (54, 59). Given the importance of IL-6 in the pathophysiology of COVID-19-related ARDS, this could have a negative impact on patient outcome. MSCs from different origins also have different

immunomodulatory effects, and this could influence the efficacy of MSC therapy in COVID-19, but further studies are required to assess the importance of this parameter. Nevertheless, the procoagulant effects and IL6 secretion of MSCs may limit the benefits of their immunomodulatory and regenerative properties, and BM-MSCs may be a better choice than UC-MSCs in these regards.

The optimal dose and schedule of administration of MSCs is unknown. We chose to repeat MSC infusions 3 times at 3-day intervals given the short persistence of these cells after systemic administration, and infused higher doses of MSCs (1.5-3x10^6/kg/injection) than in most other trials, based on preclinical and preliminary clinical results in ARDS suggesting that higher doses (total dose up to 10x10^6/kg) might provide increased clinical benefits (38). However, we lack dose-escalation studies to assess whether this approach is optimal. Another potentially important parameter is the impact of cryopreservation and freezing-thawing on the viability and therapeutic properties of MSCs. Cryopreserved "off-the-shelf" MSCs are easy to use and immediately available, which is particularly important in acute situations such as rapidly progressive COVID-19 ARDS. However, immediately after thawing, MSCs exhibit partially reduced immunosuppressive properties *in vitro*, as well as reduced homing properties and increased complement-mediated lysis and coagulation activation (40, 60). Whether these alterations negatively impact the MSC therapeutic effect has yet to be evaluated in clinical trials, and probably depends on the MSC product and the mechanisms of action of MSCs in each disease. Indeed, MSC viability is essential for several of their functions, but phagocytosis of apoptotic MSCs by host immune cells has also been identified as an important mechanism of action (34). Suboptimal viability of MSCs after thawing has been suggested to be responsible for the failure of the START-1/2 trial in ARDS, as outcomes seemed more favorable in patients receiving BM-MSCs with intermediate (57-69%) or high (80-85%) viability (which is similar to the 56-93% viability in our study), compared to those receiving BM-MSCs with low viability (36-56%) (39). On the other hand, UC-MSCs did not improve COVID-19 ARDS in the study by Monsel et al. despite a high post-thawing viability (≥ 70%), suggesting that a high viability is important but not sufficient for the therapeutic efficacy of MSC in COVID-19 ARDS. Finally, we chose to treat patients within 48 hours of ICU admission, in the early phase of ARDS, in an attempt to stop the inflammatory process before it becomes irreversible. Contrary to the negative trial of Monsel et al. (49), most of our patients were receiving HFNO at inclusion (only one received invasive mechanical ventilation at the time of MSC infusion), indicating a less severe condition or an earlier intervention, which might account for the better outcomes.

The main limitations of this study are the small sample size and the lack of randomization. Inclusion in our study was hampered by the concurrent availability of other phase 2 or 3 studies in our hospital, and by the kinetics of arrival of COVID-19 cases in waves. Moreover, since the introduction of SARS-CoV-2 vaccination (with excellent coverage in Belgium), the number of severe cases has decreased, and it is now mainly immunocompromised patients who remain at risk of critical COVID-19 infection, but they were initially excluded from our study. For the continuation of the study, given the good safety of MSCs and the encouraging results in immunocompetent patients, we amended the study protocol to also include immunocompromised patients. The design of the study, which is non-randomised, is also an important limitation, and does not allow us to conclude that BM-MSCs are effective in this indication. However, the 100% survival rate in patients treated with MSCs is particularly high compared to the figures reported in the literature for patients with the same severity of disease and compared to our large control group treated concurrently in our institution. The main strengths of this study are: (1) the use of BM-MSCs, unlike previous studies that have predominantly used UC-MSCs (only one small study reported the benefit of pooled BM-MSCs in 5 critically-ill COVID patients), (2) the description of a relatively homogeneous group of patients in terms of respiratory parameters and adjuvant treatment (only dexamethasone in all patients) and (3) the comparison to a large database of similarly treated patients at the same institution.

In conclusion, we report positive results of BM-MSCs on survival of patients with severe COVID-19, along with satisfactory safety, which will need to be confirmed in randomized placebo-controlled trials. Several issues will need to be addressed in future studies, including the optimal treatment conditions (timing, dose, provenance of MSCs), the interaction between MSCs and concomitant treatments (dexamethasone, anti-IL6 or JAK inhibitors), and the exact mechanisms of action of MSCs in COVID-19 ARDS. Furthermore, it will be interesting to investigate whether efficacy is maintained in immuno compromised patients in the continuation of our trial. Indeed, it has been suggested that a key factor determining the efficacy of MSC therapy is the ability of host immune system to interact with MSCs (notably the ability of lung-resident cytotoxic and phagocytic cells to induce MSC apoptosis and to engulf apoptotic MSCs) (34). Ultimately, the scientific and medical efforts deployed to fight this COVID-19 pandemic may lead to advances in other pathologies, and it would be interesting to further investigate the interest of BM-MSCs in non-COVID ARDS and in pulmonary fibrosis.

DATA AVAILABILITY STATEMENT

The study protocol and individual participant data that underlie the results reported in this article, after deidentification, can be shared with investigators whose proposed use of the data has been approved by the ethic committee of the University Hospital of Liège. Data can be provided for meta-analysis or other projects comparing MSC efficacy in COVID-19. Requests should be addressed to Yves Beguin.

ETHICS STATEMENT

The study protocol conformed to the ethical guidelines of the 1975 Declaration of Helsinki and was approved by the local Ethics Committee of the University Hospital of Liège, the

centralized Ethics Committee of the Cliniques Universitaires Saint-Luc, and the Belgian Federal Agency for Medicines and Health Product (EudraCT: 2020-002102-58; ClinicalTrials.gov identifier: NCT04445454). Signed informed consent was obtained from participating subjects, or - if impossible (clinical condition precluding capacity to consent) - from his/her legal representative.

AUTHOR CONTRIBUTIONS

CG and YB designed the study. NL, BL, and BM contributed to conception and designing of the study. NL and BL recruited the patients. CL, AB, VB, and EB isolated and cultured the MSCs. CG, NL, BL, and BM analysed and interpreted the data. MT organized the database and extracted the data. ND performed the statistical analyses. CG wrote the first draft of the manuscript with contributions of NL. All authors contributed to manuscript revision, read and approved the submitted version.

FUNDING

This study was supported by funds from Leon Fredericq Foundation.

SUPPLEMENTARY MATERIAL

The Supplementary Material for this article can be found online at: https://www.frontiersin.org/articles/10.3389/fimmu.2022.932360/full#supplementary-material

REFERENCES

1. COVID-ICU Group on behalf of the REVA Network and the COVID-ICU Investigators. Clinical Characteristics and Day-90 Outcomes of 4244 Critically Ill Adults With COVID-19: A Prospective Cohort Study. *Intensive Care Med* (2021) 47(1):60–73. doi: 10.1007/s00134-020-06294-x
2. Hoffmann M, Kleine-Weber H, Schroeder S, Krüger N, Herrler T, Erichsen S, et al. SARS-CoV-2 Cell Entry Depends on ACE2 and TMPRSS2 and Is Blocked by a Clinically Proven Protease Inhibitor. *Cell* (2020) 181(2):271–80.e8. doi: 10.1016/j.cell.2020.02.052
3. Osuchowski MF, Winkler MS, Skirecki T, Cajander S, Shankar-Hari M, Lachmann G, et al. The COVID-19 Puzzle: Deciphering Pathophysiology and Phenotypes of a New Disease Entity. *Lancet Respir Med* (2021) 9(6):622–42. doi: 10.1016/S2213-2600(21)00218-6
4. Grifoni A, Weiskopf D, Ramirez SI, Mateus J, Dan JM, Moderbacher CR, et al. Targets of T Cell Responses to SARS-CoV-2 Coronavirus in Humans With COVID-19 Disease and Unexposed Individuals. *Cell* (2020) 181(7):1489–501.e15. doi: 10.1016/j.cell.2020.05.015
5. Liao M, Liu Y, Yuan J, Wen Y, Xu G, Zhao J, et al. Single-Cell Landscape of Bronchoalveolar Immune Cells in Patients With COVID-19. *Nat Med* (2020) 26(6):842–4. doi: 10.1038/s41591-020-0901-9
6. Robbiani DF, Gaebler C, Muecksch F, Lorenzi JCC, Wang Z, Cho A, et al. Convergent Antibody Responses to SARS-CoV-2 in Convalescent Individuals. *Nature* (2020) 584(7821):437–42. doi: 10.1038/s41586-020-2456-9
7. Laing AG, Lorenc A, Del Molino Del Barrio I, Das A, Fish M, Monin L, et al. A Dynamic COVID-19 Immune Signature Includes Associations With Poor Prognosis. *Nat Med* (2020) 26(10):1623–35. doi: 10.1038/s41591-020-1038-6
8. Bermejo-Martin JF, González-Rivera M, Almansa R, Micheloud D, Tedim AP, Domínguez-Gil M, et al. Viral RNA Load in Plasma is Associated With Critical Illness and a Dysregulated Host Response in COVID-19. *Crit Care* (2020) 24(1):691. doi: 10.1186/s13054-020-03398-0
9. De Biasi S, Meschiari M, Gibellini L, Bellinazzi C, Borella R, Fidanza L, et al. Marked T Cell Activation, Senescence, Exhaustion and Skewing Towards TH17 in Patients With COVID-19 Pneumonia. *Nat Commun* (2020) 11 (1):3434. doi: 10.21203/rs.3.rs-23957/v1
10. Mathew D, Giles JR, Baxter AE, Oldridge DA, Greenplate AR, Wu JE, et al. Deep Immune Profiling of COVID-19 Patients Reveals Distinct Immunotypes With Therapeutic Implications. *Science* (2020) 369(6508):eabc8511. doi: 10.1126/science.abc8511
11. Grasselli G, Tonetti T, Protti A, Langer T, Girardis M, Bellani G, et al. Pathophysiology of COVID-19-Associated Acute Respiratory Distress Syndrome: A Multicentre Prospective Observational Study. *Lancet Respir Med* (2020) 8(12):1201–8. doi: 10.1016/S2213-2600(20)30370-2
12. Ader F, Bouscambert-Duchamp M, Hites M, Peiffer-Smadja N, Poissy J, Belhadi D, et al. Remdesivir Plus Standard of Care Versus Standard of Care Alone for the Treatment of Patients Admitted to Hospital With COVID-19 (DisCoVeRy): A Phase 3, Randomised, Controlled, Open-Label Trial. *Lancet Infect Dis* (2022) 22(2):209–21. doi: 10.1016/S1473-3099(21)00485-0
13. Pan H, Peto R, Henao-Restrepo AM, Preziosi MP, Sathiyamoorthy V, Abdool Karim Q, et al. Repurposed Antiviral Drugs for Covid-19 - Interim WHO Solidarity Trial Results. *N Engl J Med* (2021) 384(6):497–511. doi: 10.1056/NEJMoa2023184
14. RECOVERY Collaborative Group, Horby P, Lim WS, Emberson JR, Mafham M, Bell JL, et al. Dexamethasone in Hospitalized Patients With Covid-19. *N Engl J Med* (2021) 384(8):693–704. doi: 10.1056/NEJMoa2021436
15. World Health Organization (WHO) Rapid Evidence Appraisal for COVID-19 Therapies (REACT) Working Group. Association Between Administration of IL-6 Antagonists and Mortality Among Patients Hospitalized for COVID-19: A Meta-Analysis. *JAMA* (2021) 326(6):499–518. doi: 10.1001/jama.2021.11330
16. Ely EW, Ramanan AV, Kartman CE, de Bono S, Liao R, Piruzeli MLB, et al. Efficacy and Safety of Baricitinib Plus Standard of Care for the Treatment of Critically Ill Hospitalised Adults With COVID-19 on Invasive Mechanical Ventilation or Extracorporeal Membrane Oxygenation: An Exploratory, Randomised, Placebo-Controlled Trial. *Lancet Respir Med* (2022) 10 (4):327–36. doi: 10.1016/S2213-2600(22)00006-6
17. Lambermont B, Rousseau AF, Seidel L, Thys M, Cavalleri J, Delanaye P, et al. Outcome Improvement Between the First Two Waves of the Coronavirus Disease 2019 Pandemic in a Single Tertiary-Care Hospital in Belgium. *Crit Care Explor* (2021) 3(5):e0438. doi: 10.1097/CCE.0000000000000438
18. Le Blanc K, Mougiakakos D. Multipotent Mesenchymal Stromal Cells and the Innate Immune System. *Nat Rev Immunol* (2012) 12(5):383–96. doi: 10.1038/nri3209
19. Rohban R, Pieber TR. Mesenchymal Stem and Progenitor Cells in Regeneration: Tissue Specificity and Regenerative Potential. *Stem Cells Int* (2017) 2017:5173732. doi: 10.1155/2017/5173732
20. Servais S, Grégoire C, Baron F, Willems E, Briquet A, Baudoux E, et al. Multipotent Mesenchymal Stromal Cell Therapy for Steroid-Refractory Acute Graft-Versus-Host Disease After Allogeneic Stem Cell Transplantation. *Belgian J Hematol* (2016) 7:229–35.
21. Grégoire C, Lechanteur C, Briquet A, Baudoux E, Baron F, Louis E, et al. Review Article: Mesenchymal Stromal Cell Therapy for Inflammatory Bowel Diseases. *Aliment Pharmacol Ther* (2017) 45(2):205–21. doi: 10.1111/apt.13864
22. Ren G, Zhang L, Zhao X, Xu G, Zhang Y, Roberts AI, et al. Mesenchymal Stem Cell-Mediated Immunosuppression Occurs *via* Concerted Action of Chemokines and Nitric Oxide. *Cell Stem Cell* (2008) 2(2):141–50. doi: 10.1016/j.stem.2007.11.014
23. Hung SC, Pochampally RR, Hsu SC, Sanchez C, Chen SC, Spees J, et al. Short-Term Exposure of Multipotent Stromal Cells to Low Oxygen Increases Their Expression of CX3CR1 and CXCR4 and Their Engraftment In Vivo. *PloS One* (2007) 2(5):e416. doi: 10.1371/journal.pone.0000416
24. Hung SC, Pochampally RR, Chen SC, Hsu SC, Prockop DJ. Angiogenic Effects of Human Multipotent Stromal Cell Conditioned Medium Activate the PI3K-

Akt Pathway in Hypoxic Endothelial Cells to Inhibit Apoptosis, Increase Survival, and Stimulate Angiogenesis. *Stem Cells* (2007) 25(9):2363–70. doi: 10.1634/stemcells.2006-0686
25. Leng Z, Zhu R, Hou W, Feng Y, Yang Y, Han Q, et al. Transplantation of ACE2- Mesenchymal Stem Cells Improves the Outcome of Patients With COVID-19 Pneumonia. *Aging Dis* (2020) 11(2):216–28. doi: 10.14336/AD.2020.0228
26. Atluri S, Manchikanti L, Hirsch JA. Expanded Umbilical Cord Mesenchymal Stem Cells (UC-MSCs) as a Therapeutic Strategy in Managing Critically Ill COVID-19 Patients: The Case for Compassionate Use. *Pain Phys* (2020) 23 (2):E71–83.
27. Lechanteur C, Briquet A, Giet O, Delloye O, Baudoux E, Beguin Y. Clinical-Scale Expansion of Mesenchymal Stromal Cells: A Large Banking Experience. *J Trans Med* (2016) 14(1):145–. doi: 10.1186/s12967-016-0892-y
28. Lechanteur C, Briquet A, Bettonville V, Baudoux E, Beguin Y. MSC Manufacturing for Academic Clinical Trials: From a Clinical-Grade to a Full GMP-Compliant Process. *Cells* (2021) 10(6):1320. doi: 10.3390/cells10061320
29. WHO Working Group on the Clinical Characterisation and Management of COVID-19 infection. A Minimal Common Outcome Measure Set for COVID-19 Clinical Research. *Lancet Infect Dis* (2020) 20(8):e192–e7. doi: 10.1016/S1473-3099(20)30483-7
30. Lim ZJ, Subramaniam A, Ponnapa Reddy M, Blecher G, Kadam U, Afroz A, et al. Case Fatality Rates for Patients With COVID-19 Requiring Invasive Mechanical Ventilation. A Meta-Analysis. *Am J Respir Crit Care Med* (2021) 203(1):54–66. doi: 10.1164/rccm.202006-2405OC
31. Aranda J, Oriol I, Martín M, Feria L, Vázquez N, Rhyman N, et al. Long-Term Impact of COVID-19 Associated Acute Respiratory Distress Syndrome. *J Infect* (2021) 83(5):581–8. doi: 10.1016/j.jinf.2021.08.018
32. Rousseau AF, Minguet P, Colson C, Kellens I, Chaabane S, Delanaye P, et al. Post-Intensive Care Syndrome After a Critical COVID-19: Cohort Study From a Belgian Follow-Up Clinic. *Ann Intensive Care* (2021) 11(1):118. doi: 10.1186/s13613-021-00910-9
33. Boucher PE, Taplin J, Clement F. The Cost of ARDS: A Systematic Review. *Chest* (2022) 161(3):684–96. doi: 10.1016/j.chest.2021.08.057
34. Galleu A, Riffo-Vasquez Y, Trento C, Lomas C, Dolcetti L, Cheung TS, et al. Apoptosis in Mesenchymal Stromal Cells Induces *In Vivo* Recipient-Mediated Immunomodulation. *Sci Trans Med* (2017) 9(416):eaam7828–eaam. doi: 10.1126/scitranslmed.aam7828
35. Lee RH, Pulin AA, Seo MJ, Kota DJ, Ylostalo J, Larson BL, et al. Intravenous hMSCs Improve Myocardial Infarction in Mice Because Cells Embolized in Lung are Activated to Secrete the Anti-Inflammatory Protein TSG-6. *Cell Stem Cell* (2009) 5(1):54–63. doi: 10.1016/j.stem.2009.05.003
36. Lopes-Pacheco M, Robba C, Rocco PRM, Pelosi P. Current Understanding of the Therapeutic Benefits of Mesenchymal Stem Cells in Acute Respiratory Distress Syndrome. *Cell Biol Toxicol* (2020) 36(1):83–102. doi: 10.1007/s10565-019-09493-5
37. Zheng G, Huang L, Tong H, Shu Q, Hu Y, Ge M, et al. Treatment of Acute Respiratory Distress Syndrome With Allogeneic Adipose-Derived Mesenchymal Stem Cells: A Randomized, Placebo-Controlled Pilot Study. *Respir Res* (2014) 15(1):39. doi: 10.1186/1465-9921-15-39
38. Wilson JG, Liu KD, Zhuo H, Caballero L, McMillan M, Fang X, et al. Mesenchymal Stem (Stromal) Cells for Treatment of ARDS: A Phase 1 Clinical Trial. *Lancet Respir Med* (2015) 3(1):24–32. doi: 10.1016/S2213-2600(14)70291-7
39. Matthay MA, Calfee CS, Zhuo H, Thompson BT, Wilson JG, Levitt JE, et al. Treatment With Allogeneic Mesenchymal Stromal Cells for Moderate to Severe Acute Respiratory Distress Syndrome (START Study): A Randomised Phase 2a Safety Trial. *Lancet Respir Med* (2019) 7(2):154–62. doi: 10.1016/S2213-2600(18)30418-1
40. Ringdén O, Moll G, Gustafsson B, Sadeghi B. Mesenchymal Stromal Cells for Enhancing Hematopoietic Engraftment and Treatment of Graft-Versus-Host Disease, Hemorrhages and Acute Respiratory Distress Syndrome. *Front Immunol* (2022) 13:839844. doi: 10.3389/fimmu.2022.839844
41. Meng F, Xu R, Wang S, Xu Z, Zhang C, Li Y, et al. Human Umbilical Cord-Derived Mesenchymal Stem Cell Therapy in Patients With COVID-19: A Phase 1 Clinical Trial. *Signal Transduct Target Ther* (2020) 5(1):172. doi: 10.1038/s41392-020-00286-5
42. Guo Z, Chen Y, Luo X, He X, Zhang Y, Wang J. Administration of Umbilical Cord Mesenchymal Stem Cells in Patients With Severe COVID-19 Pneumonia. *Crit Care* (2020) 24(1):420. doi: 10.1186/s13054-020-03142-8
43. Xu X, Jiang W, Chen L, Xu Z, Zhang Q, Zhu M, et al. Evaluation of the Safety and Efficacy of Using Human Menstrual Blood-Derived Mesenchymal Stromal Cells in Treating Severe and Critically Ill COVID-19 Patients: An Exploratory Clinical Trial. *Clin Transl Med* (2021) 11(2):e297. doi: 10.1002/ctm2.297
44. Hashemian SR, Aliannejad R, Zarrabi M, Soleimani M, Vosough M, Hosseini SE, et al. Mesenchymal Stem Cells Derived From Perinatal Tissues for Treatment of Critically Ill COVID-19-Induced ARDS Patients: A Case Series. *Stem Cell Res Ther* (2021) 12(1):91. doi: 10.1186/s13287-021-02165-4
45. Iglesias M, Butrón P, Torre-Villalvazo I, Torre-Anaya EA, Sierra-Madero J, Rodriguez-Andoney JJ, et al. Mesenchymal Stem Cells for the Compassionate Treatment of Severe Acute Respiratory Distress Syndrome Due to COVID 19. *Aging Dis* (2021) 12(2):360–70. doi: 10.14336/AD.2020.1218
46. Häberle H, Magunia H, Lang P, Gloeckner H, Körner A, Koeppen M, et al. Mesenchymal Stem Cell Therapy for Severe COVID-19 ARDS. *J Intensive Care Med* (2021) 36(6):681–8. doi: 10.1177/0885066621997365.
47. Ercelen N, Pekkoc-Uyanik KC, Alpaydin N, Gulay GR, Simsek M. Clinical Experience on Umbilical Cord Mesenchymal Stem Cell Treatment in 210 Severe and Critical COVID-19 Cases in Turkey. *Stem Cell Rev Rep* (2021) 17 (5):1917–25. doi: 10.1007/s12015-021-10214-x
48. Lanzoni G, Linetsky E, Correa D, Messinger Cayetano S, Alvarez RA, Kouroupis D, et al. Umbilical Cord Mesenchymal Stem Cells for COVID-19 Acute Respiratory Distress Syndrome: A Double-Blind, Phase 1/2a, Randomized Controlled Trial. *Stem Cells Transl Med* (2021). doi: 10.1002/sctm.20-0472
49. Monsel A, Hauw-Berlemont C, Mebarki M, Heming N, Mayaux J, Nguekap Tchoumba O, et al. Treatment of COVID-19-Associated ARDS With Mesenchymal Stromal Cells: A Multicenter Randomized Double-Blind Trial. *Crit Care* (2022) 26(1):48. doi: 10.1186/s13054-022-03930-4
50. Shi L, Huang H, Lu X, Yan X, Jiang X, Xu R, et al. Effect of Human Umbilical Cord-Derived Mesenchymal Stem Cells on Lung Damage in Severe COVID-19 Patients: A Randomized, Double-Blind, Placebo-Controlled Phase 2 Trial. *Signal Transduct Target Ther* (2021) 6(1):58. doi: 10.1038/s41392-021-00488-5
51. Dilogo IH, Aditianingsih D, Sugiarto A, Burhan E, Damayanti T, Sitompul PA, et al. Umbilical Cord Mesenchymal Stromal Cells as Critical COVID-19 Adjuvant Therapy: A Randomized Controlled Trial. *Stem Cells Transl Med* (2021) 10(9):1279–87. doi: 10.1002/sctm.21-0046
52. Shu L, Niu C, Li R, Huang T, Wang Y, Huang M, et al. Treatment of Severe COVID-19 With Human Umbilical Cord Mesenchymal Stem Cells. *Stem Cell Res Ther* (2020) 11(1):361. doi: 10.1186/s13287-020-01875-5
53. Bikdeli B, Madhavan MV, Jimenez D, Chuich T, Dreyfus I, Driggin E, et al. COVID-19 and Thrombotic or Thromboembolic Disease: Implications for Prevention, Antithrombotic Therapy, and Follow-Up: JACC State-Of-the-Art Review. *J Am Coll Cardiol* (2020) 75(23):2950–73. doi: 10.1016/j.jacc.2020.04.031
54. Grégoire C, Ritacco C, Hannon M, Seidel L, Delens L, Belle L, et al. Comparison of Mesenchymal Stromal Cells From Different Origins for the Treatment of Graft-Vs.-Host-Disease in a Humanized Mouse Model. *Front Immunol* (2019) 10:619. doi: 10.3389/fimmu.2019.00619
55. Moll G, Ignatowicz L, Catar R, Luecht C, Sadeghi B, Hamad O, et al. Different Procoagulant Activity of Therapeutic Mesenchymal Stromal Cells Derived From Bone Marrow and Placental Decidua. *Stem Cells Dev* (2015) 24 (19):2269–79. doi: 10.1089/scd.2015.0120
56. Moll G, Drzeniek N, Kamhieh-Milz J, Geissler S, Volk H-D, Reinke P. MSC Therapies for COVID-19: Importance of Patient Coagulopathy, Thromboprophylaxis, Cell Product Quality and Mode of Delivery for Treatment Safety and Efficacy. *Front Immunol* (2020) 11:1091. doi: 10.3389/fimmu.2020.01091.
57. Wiersinga WJ, Rhodes A, Cheng AC, Peacock SJ, Prescott HC. Pathophysiology, Transmission, Diagnosis, and Treatment of Coronavirus Disease 2019 (COVID-19): A Review. *JAMA* (2020) 324(8):782–93. doi: 10.1001/jama.2020.12839
58. Moll G, Ankrum JA, Olson SD, Nolta JA. Improved MSC Minimal Criteria to Maximize Patient Safety: A Call to Embrace Tissue Factor and Hemocompatibility Assessment of MSC Products. *Stem Cells Trans Med* (2022) 11(1):2–13. doi: 10.1093/stcltm/szab005

59. Pires AO, Mendes-Pinheiro B, Teixeira FG, Anjo SI, Ribeiro-Samy S, Gomes ED, et al. Unveiling the Differences of Secretome of Human Bone Marrow Mesenchymal Stem Cells, Adipose Tissue-Derived Stem Cells, and Human Umbilical Cord Perivascular Cells: A Proteomic Analysis. *Stem Cells Dev* (2016) 25(14):1073–83. doi: 10.1089/scd.2016.0048
60. Cottle C, AP P, Lipat A, Turner-Lyles C, Nguyen J, Moll G, et al. Impact of Cryopreservation and Freeze-Thawing on Therapeutic Properties of Mesenchymal Stromal/Stem Cells and Other Common Cellular Therapeutics. *Curr Stem Cell Rep* (2022) 8(2):72–92. doi: 10.1007/s40778-022-00212-1

Conflict of Interest: The authors declare that the research was conducted in the absence of any commercial or financial relationships that could be construed as a potential conflict of interest.

frontiers | Frontiers in Immunology

ORIGINAL RESEARCH
published: 06 July 2022
doi: 10.3389/fimmu.2022.874698

Enhancing Mesenchymal Stromal Cell Potency: Inflammatory Licensing *via* Mechanotransduction

Max A. Skibber[1], *Scott D. Olson*[1]*, *Karthik S. Prabhakara*[1], *Brijesh S. Gill*[2]* *and Charles S. Cox Jr*[1]*

[1] Department of Pediatric Surgery, McGovern Medical School, University of Texas Health Science Center at Houston, Houston, TX, United States, [2] Department of Surgery, McGovern Medical School, University of Texas Health Science Center At Houston, Houston, TX, United States

Mesenchymal stromal cells (MSC) undergo functional maturation upon their migration from bone marrow and introduction to a site of injury. This inflammatory licensing leads to heightened immune regulation *via* cell-to-cell interaction and the secretion of immunomodulatory molecules, such as anti-inflammatory mediators and antioxidants. Pro-inflammatory cytokines are a recognized catalyst of inflammatory licensing; however, biomechanical forces, such as fluid shear stress, are a second, distinct class of stimuli that incite functional maturation. Here we show mechanotransduction, achieved by exposing MSC to various grades of wall shear stress (WSS) within a scalable conditioning platform, enhances the immunomodulatory potential of MSC independent of classical pro-inflammatory cytokines. A dose-dependent effect of WSS on potency is evidenced by production of prostaglandin E2 (PGE_2) and indoleamine 2,3 dioxygenase 1 (IDO1), as well as suppression of tumor necrosis factor-α (TNF- α) and interferon-γ (IFN-γ) production by activated immune cells. Consistent, reproducible licensing is demonstrated in adipose tissue and bone marrow human derived MSC without significant impact on cell viability, cellular yield, or identity. Transcriptome analysis of WSS-conditioned BM-MSC elucidates the broader phenotypic implications on the differential expression of immunomodulatory factors. These results suggest mechanotransduction as a viable, scalable pre-conditioning alternative to pro-inflammatory cytokines. Enhancing the immunomodulatory capacity of MSC *via* biomechanical conditioning represents a novel cell therapy manufacturing approach.

Keywords: mesenchymal stem cell, mechanotranduction, bioreactor, immunomodulation, inflammatory licensing, wall shear stress, biomechanical culture, parallel-plate bioreactor

OPEN ACCESS

Edited by:
Sowmya Viswanathan, University Health Network, Canada

Reviewed by:
Janosch Schoon, University Medicine Greifswald, Germany
Lorena Braid, Simon Fraser University, Canada

***Correspondence:**
Scott D. Olson
scott.d.olson@uth.tmc.edu
Brijesh S. Gill
Brijesh.s.gill@uth.tmc.edu
Charles S. Cox Jr
charles.s.cox@uth.tmc.edu

Specialty section:
This article was submitted to Vaccines and Molecular Therapeutics, a section of the journal Frontiers in Immunology

Received: *12 February 2022*
Accepted: *02 June 2022*
Published: *06 July 2022*

Citation:
Skibber MA, Olson SD, Prabhakara KS, Gill BS and Cox CS Jr (2022) Enhancing Mesenchymal Stromal Cell Potency: Inflammatory Licensing via Mechanotransduction. Front. Immunol. 13:874698. doi: 10.3389/fimmu.2022.874698

INTRODUCTION

Mesenchymal stromal cell (MSC) anti-inflammatory function and role in injury resolution have led to their therapeutic application for a number of indications characterized by pathological inflammation. MSC are thought to mobilize to a site of injury (1, 2) and engage in paracrine crosstalk with immune effector cells through cell-cell contact and locally secreted factors (3). These

interactions result in broad downstream effects often suppressing cytokine production, proliferation, chemotaxis, and skewing differentiation of different immune cells to anti-inflammatory phenotypes (2, 4–6). Despite early promise in pre-clinical studies and some initial clinical trials, many studies have struggled to demonstrate significant efficacy at scale. This is likely due to the interaction of many factors, including donor heterogeneity, lot-to-lot variability in MSC preparations, limited predictive value of existing disease-specific potency markers, an incomplete understanding of critical characteristics that dictate clinical benefit, and the dynamic nature of many MSC applications, particularly when used to treat acute injury and trauma (3, 7–9).

In an effort to improve their efficacy, some studies manipulate MSC in culture to simulate inflammatory licensing (1, 10–12). This strategy aims to mimic conditions after injury when endogenous MSC are exposed to various damage signals and inflammatory cues. Anti-inflammatory changes to the MSC secretome have been reported following *in-vitro* exposure to pro-inflammatory cytokines, such as interleukin-1 beta (IL-1β) (13–15), tumor necrosis factor alpha (TNF-α) (4, 16), interferon gamma (IFN-γ) (4, 17, 18), lipopolysaccharide (LPS) (19, 20), and Polyinosinic:polycytidylic acid (Poly I:C) (21, 22). Not wholly anti-inflammatory, the MSC response elicited by these cytokines can include classical pro-inflammatory signals, such as chemokines, metalloproteins, and TNF-α (4, 10, 12, 13, 22). Other priming studies have employed culture manipulations to pre-activate MSC including the use of hypoxia (23, 24) and low serum (25, 26). While promising, these approaches carry additional associated costs as well as down-stream complications to large-scale cell manufacturing regulatory approval (5, 8, 12). When resolved, primed MSC attained by *in vitro* licensing are often considered the next generation of MSC therapies to treat acute and sub-acute inflammation-associated injuries, such as traumatic brain injury (TBI) and ischemic stroke (3, 7, 9, 27).

In-vitro mechanotransduction, replicating the wall shear stress (WSS) exposure that MSC might withstand during development or after injury-induced migration, exists as a novel pre-conditioning technique (28–30). Biomechanical cues, such as WSS, have demonstrated profound effects on MSC immunomodulatory potential and paracrine signaling (28). Various magnitudes of WSS exist throughout vasculature and different shear stress patterns are reported to have distinct implications on MSC phenotype and secretome profiles (31). Both, the bone marrow and lymphoid tissues where MSC might dwell or become arrested after egress place MSC at a solid-fluid interface. From this boundary, MSC not only engage in molecular crosstalk but react to extrinsic, biophysical cues by altering transcriptional patterns (6, 32–35). Notably, our group found that a three-hour exposure to 15 dyne/cm^2 strongly promoted the immune regulatory function of five human bone marrow MSC (hBM-MSC) cell lines. This was evidenced by increased transcription of *PTGS2, HMOX1, NFκB, IL1RN*, and *TGFβ1/2*, secretion of prostaglandin E_2 (PGE_2), and suppression of TNF-α production in a splenocyte co-culture (28).

The current study builds on our previous work by investigating how a range of physiologic WSS magnitudes affect the prospective cell therapy's clinical translatability in a bioreactor scaled up for research purposes. Here we demonstrate a dose-dependence of mesenchymal stromal cells' anti-inflammatory potential on WSS magnitude in a scalable system. Using a novel parallel-plate bioreactor (PPB) designed for accurate WSS application, we exposed adherent human adipose tissue derived MSC (hAD-MSC) and hBM-MSC to shear stress magnitudes of 0, 4, 8, and 12 dyne/cm^2. The mechanotransduced MSC (WSS-MSC) were compared to MSC grown in conventional tissue culture flasks (Static-MSC) by viability, cellular yield after WSS exposure, PGE_2 production, and indoleamine 2,3 dioxygenase 1 (IDO1) production criteria. The optimal WSS magnitude (8 dyne/cm^2) was selected and further studied using a cGMP-compliant hBM-MSC product, confirming that WSS-MSC reduced inflammatory cytokine secretion by activated splenocytes. The effects of WSS on the transcriptome were then evaluated using RNA-seq. Optimizing fluid shear stress magnitude by assessing a matrix of viability, yield, identity, and immunomodulatory potential represent the initial considerations of translating a mechanotransduction-based preconditioning strategy for clinical applications.

MATERIALS AND METHODS

Cell Culture

MSC culturing was carried out according to previously published efforts (28, 36, 37). Xeno-free human bone marrow MSC (hBM-MSC) were obtained from RoosterBio, Inc (Frederick, MD), specifically from their cGMP-simulated cell bank mirroring their cGMP-compliant products. The hBM-MSC acquired were from a single donor. The hBM-MSC were expanded according to manufacturer's suggestion in RoosterNourish-MSC-XF medium. Once cultures had reached 70% confluency, RoosterNourish-MSC-XF medium was removed, the cells were washed with phosphate-buffered saline (PBS; Life Technologies), and the adherent cells population was harvested with TrypLE Express (Gibco, Grand Island, NJ) for five minutes at 37°C. Then, 10^6 cells/mL aliquots were frozen in Cryostor CS10 (STEMCELL Technologies, Cambridge, MA) and representative aliquots were characterized according to previously published protocols (36). A single hBM-MSC cell line was utilized throughout the entirety of this investigation.

Human adipose tissue MSC (hAD-MSC) from a single donor were isolated according to a previously described methodology (37). To isolate hAD-MSC, subcutaneous adipose tissue samples were repeatedly washed with α-MEM (Life Technologies, Grand Island, NY) containing 50 μg/mL gentamicin and minced into 5 mm pieces. The samples were digested using a buffer of α-MEM, 300 IU/mL Collagenase Type II (Worthington Biochemicals, Lakewood, NJ), 1% bovine serum albumin (Gibco, Grand Island, NJ), and 50 μg/mL gentamicin for 55 minutes in a standard incubator environment. The liberated cells were then resuspended and expanded in a complete culture medium (CCM) consisting of α-MEM, 5% Stemulate human platelet lysate (hPL; Cook Regentec, Indianapolis, IN), 1%

Glutamax (Gibco, Waltham, MA), and 10 μg/mL gentamicin (Gibco). Cultures were grown at 37°C/5% CO2 and media replenished every three days until 70% confluency was reached and subcultured to passage 3 (PDL 16.2). The adherent cells were harvested with TrypLE Express and frozen at 10^6 cells per mL in Cryostor CS10 for future experiments.

Computational Fluid Dynamics Studies

Individual components of the PPB, including plates, gaskets, and flow ports, were designed and assembled using the computer-aided design software SolidWorks (Dassault Systems, Waltham, MA). Computational fluid dynamic (CFD) simulation studies of the assembly were conducted in SolidWorks' Flow Simulation package. Boundary conditions of inlet volumetric flow rate (0.5185 cm^3/s for 4 dyne/cm^2, 1.0370 cm^3/s for 8 dyne/cm^2, and 1.556 cm^3/s for 12 dyne/cm^2) and outlet pressure (3 mmHg) were assigned to the bioreactor assembly. A user-defined liquid representing CCM at 37°C was defined (density: 1.007 g/mL, dynamic viscosity: 0.0072 dyne*s/cm^2, specific heat: 4.2 x 10^3 J/Kg*K). As the perfusing media contained no cells or serum, it was characterized as a Newtonian liquid. Other assumptions and conditions included adiabatic wall thermal conditions, laminar and turbulent flow, gravity, and a PMMA surface roughness of 0.12 μm. Settings allowed for a high level of global and local mesh refinement as the simulation iteratively sought to reach convergence of velocity, flow rate, and shear stress calculations. 346,307 fluid cells described the study's fluid flow. Results were displayed on a shear stress gradient heatmap. From the fluid shear stress heatmap, the surface area described by a target shear stress ± 1 dyne/cm^2 was calculated. Velocity vector lines, in CFD simulations and the assembled device, were inspected to assess laminar versus turbulent flow.

WSS Conditioning

Fluid shear stress was imposed in a similar manner as previously published work (28). Small-scale and large-scale bioreactors were manufactured in a similar manner. Each PPB was constructed from optically transparent polymethyl-methacrylate (PMMA; McMaster-Carr, Atlanta, GA) milled on an OM2 Haas computer numerical control machine (CNC, Haas Automation Inc, Oxnard, CA). Photopolymer (Digital ABS Plus, Stratasys, Eden Prairie, MN) gaskets printed on a J750 3D Printer (Stratasys) were placed between PMMA plates to establish individual channel height, while 3D-printed ports (VeroClear, Stratasys) distributed or collected fluid flow at the channel extremes. The PPB assembly includes two acrylic plates milled to a uniform size enclosed around the 3D-printed gasket (Digital ABS Plus). The assembly is completed by inserting translucent 3D-printed ports (VeroClear) into cutouts on the top acrylic plates. Individual components and luer lock connectors are bonded together with medical-grade epoxy (Henkel, Rocky Hill, CT). Each component is sequentially washed in detergent (Liquinox, Alconox Inc, White Plains, NY), 91% isopropyl alcohol, and DI water baths and dried in a laminar flow hood. Final assembly and bonding are carried out in the same laminar flow hood. After sterilization *via* ethylene oxide exposure or autoclaving, the PPB and flow-loop were handled within a tissue culture hood.

After three PBS washes to remove any remaining particulate and the PMMA was coated with human plasma fibronectin at a concentration of 10 μg/mL overnight (Gibco). Then, passage 4 hBM-MSC (PDL 17.5) or hAD-MSC (PDL 21.8) were loaded to a target concentration of 30,000 cells/cm^2 (3.6 X 10^6 MSC per PPB) and allowed to adhere to the bottom surface of conditioning chambers over a three-hour period. The optically transparent PMMA plates allowed for inspection of MSC at each step. Seeded bioreactors were coupled to a MasterFlex L/S Series Peristaltic Pump (Cole Parmer, Vernon Hills, IL) and continuously perfused in a unidirectional manner for three hours at a WSS of 4, 8, or 12 dyne/cm^2. Requisite pump flow rate was calculated using the equation $\tau_W = -\mu \frac{du}{dy}$, where μ is the fluid dynamic viscosity of CCM, u is the linear velocity of fluid flow, and y the distance from the channel's boundary. After conditioning, the adherent cell population was washed with PBS and detached from the culture plastic using TrypLE Express.

The quantity and viability of MSC collected from each bioreactor was assessed with a NucleoCounter NC-200 using Via1 cassettes (Chemometec, Denmark). Static MSC cultured in filtered T-225 tissue culture plastic flasks (Nunc) were plated and harvested in parallel with the bioreactors. PPB were inspected by phase contrast light microscopy at each stage and after harvest.

Measurements of PGE_2 and IDO Production

Following WSS conditioning, cells were suspended at a concentration of 200,000/mL in CCM and dispensed as 1 mL per well (200,000 cells) into 6-well dishes that were then incubated for 18 hrs before the conditioned media was collected. PGE_2 and IDO1 secreted by MSC into the culture medium were quantified using ELISA kits (Cayman Chemical, Ann Arbor, MI) in accordance with the manufacturer's guidelines. Standard curves were processed in parallel for individual replicates. The resulting concentrations of PGE_2 and IDO1 were calculated using regression analysis.

Flow Cytometry

Suspended MSC samples were identified using a pre-mixed antibody panel of CD31, CD34, CD4, CD73, CD90, CD105, and CD146 (DURAClone SC Mesenchymal Stem Cell Panel, Beckman Coulter, Indianapolis, IN) as established by The International Society for Cellular Therapy as a minimal criteria (38). Data was acquired using an LSR II flow cytometer (BD Biosciences) and analyzed *via* Kaluza software (Beckman Coulter). Results are reported as a percentage of MSC expressing a given surface marker.

Splenocyte Activation

Splenocyte isolation was performed as previously described (28, 34, 36, 39). After harvesting a fresh spleen from male Sprague Dawley rats under anesthesia, the organ was morselized using a 70 μm mesh filter. The collected material was suspended in ice cold PBS and centrifuged at 400 x *g* for 8 minutes. The supernatant was disposed of and the sample re-suspended in 10 mL red blood cell lysis buffer (Sigma-Aldrich, St. Louis, MO), undergoing perturbation for 5 min while still on ice. The sample

was diluted with PBS and re-centrifuged at 400 x *g* for 8 min. The supernatant was disposed of and the pellet was suspended in phenol red-free RPMI with 10% FBS. The splenocytes were quantified and their viability assessed using a NucleoCounter NC-200. Splenocytes ($2x10^6$ cells/mL) were left inactivated or activated with lipopolysaccharide (LPS) or concanavalin A (ConA). MSC-splenocyte cocultures were plated in wells at ratios of 1:80 or 1:20 (MSC : Splenocyte) for LPS and ConA cocultures, respectively. Culture supernatants were collected at 24 hrs after LPS administration or 48 hrs after ConA administration. The samples were analyzed using TNF-α or IFN-γ ELISA kits (Abnova, Taipei, Taiwan) following manufacturer's guidelines. The hBM-MSC cell line tested was the same used in previous sections.

RNA Extraction and RNA Analysis

Aliquots of 1 million cells were pelleted and snap-frozen in LN_2 and submitted to Cancer Genomics Center core facility at The University of Texas Health Science Center at Houston (CPRIT RP180734). Total RNA was exacted by RNeasy Mini Kit (Qiagen, Hilden, Germany) and quality-checked using Agilent RNA 6000 Pico kit by Agilent Bioanalyzer 2100 (Agilent Technologies, Santa Clara, USA). All samples used in this study had an RNA integrity number greater than 7 and were subsequently used for library preparation. rRNA of 400ng total RNA were depleted with NEBNext rRNA Depletion Kit (New England Biolabs, Ipswich, MA) following the manufacturer's instructions. The RNAs with more than 70nts were selected for preparation with NEBNext Ultra II Directional RNA Library Prep Kit for Illumina (New England Biolabs, Ipswich, MA) and NEBNext Multiplex Oligos for Illumina (New England Biolabs) following the manufacturer's instructions. The quality of the final libraries was examined using Agilent High Sensitive DNA Kit by Agilent Bioanalyzer 2100 (Agilent Technologies), and the library concentrations were determined by qPCR using Collibri Library Quantification kit (Thermo Fisher Scientific). The libraries were pooled evenly and analyzed using paired-end 75-cycle sequencing on an Illumina NextSeq 550 System (Illumina, Inc., San Diego, CA, USA) using High Output Kit v2.5 (Illumina, Inc.).

All processing was done using Galaxy (40). Sequence files were processed using fastp to remove adapter sequences (41). HISAT2 was then used to align sequences to the hg38 canonical sequence (42). The alignment files were then sorted and merged using Samtools (43) and evaluated for quality using QualiMap for BamQC (44). A count file was then generated using featureCounts (45) which was then used for differential gene expression analysis using DeSeq2 (46). The resulting normalized counts were then used to determine the abundance of specific transcripts of interest.

The relevant data sets are available from the sequence read archive (SRA) as BioProject PRJNA814337.

Statistical Analysis

Statistical analyses were conducted for independent replicates of 3 or more using two-tailed t-tests or one-way ANOVA with Tukey *post-hoc* analyses for multiple comparisons. A minimum significance level of 5% was used. Each mean is presented with the standard deviation and number of independent experiments (n). Unless stated otherwise, samples from a single bioreactor unit represent a single biological replicate. When appropriate, percent or fold difference from the control is presented. Graphpad Prism software (GraphPad, San Diego, CA) was used for statistical analysis.

RESULTS

The MSC-Conditioning System Facilitates Uniform Fluid Dynamics

We designed, as part of a larger cell culture and validation pipeline, a scalable device to impose accurate WSS within a closed-loop system (**Figure 1**). The fluid dynamics of the resulting PPB and its ports were studied with computational simulations across a range of flow rates and operating conditions to generate continuous and consistent WSS. As the port geometry is the major influence on channel fluid dynamics, we iteratively designed and evaluated various geometries.

The final design was used for simulations to generate a shear stress gradient heatmap (**Figure 2**). From each heatmap, the surface area withstanding appropriate WSS magnitudes within ± 1 dyne/cm^2 of the target magnitude was calculated. When using a calibrated pump with precise flow rate control, we predicted 99.8% of the surface is within the target range at 4 ± 1 dyne/cm^2 conditions, 99.3% at 8 ± 1 dyne/cm^2 conditions, and 96.67% at 12 ± 1 dyne/cm^2 conditions. Little to no turbulent flow was produced by the entrance and exit geometries, regardless of flow rate. These simulations informed the construction of our final PPB used for uniform MSC mechanotransduction, illustrated in **Figure 1C**. The lack of turbulent flow was confirmed with dye-injection studies and visual inspection through the optically transparent PPB channels. Small-scale (20 cm^2) and large-scale (120 cm^2) PPB were manufactured for characterization at different experimental stages.

Fluid Shear Stress Affects Cellular Viability and Attachment

To assess cellular viability and harvest yield, we plated hAD-MSC or hBM-MSC within chambers of our small-scale bioreactor or conventional tissue culture flasks. Adherent cells in a PPB were exposed to a range of fluid shear stress (4, 8, or 12 dyne/cm^2) mimicking physiological conditions for 3 hrs, while the tissue culture flasks were left static (0 dyne/cm^2). Our previous mechanotransduction studies, where a 3 hr conditioning period resulted in consequential functional enhancement, led us to use this schedule (28, 34).

The experiment was first conducted with hAD-MSC, which showed a small but significant impact on viability after WSS exposure at 8 and 12 dyne/cm^2 (**Figure 3A**). The cellular viability at 0 dyne/cm^2 and 8 dyne/cm^2 were 89.1% ± 2.7% and 83.9% ± 2.0%, respectively (p=0.0408). 12 dyne/cm^2 conditions decreased viability to 82.7% ± 3.2% (p=0.0119 versus static).

The effect of WSS on hAD-MSC yield was more profound at high WSS magnitudes (**Figure 3C**). The percentage of cells

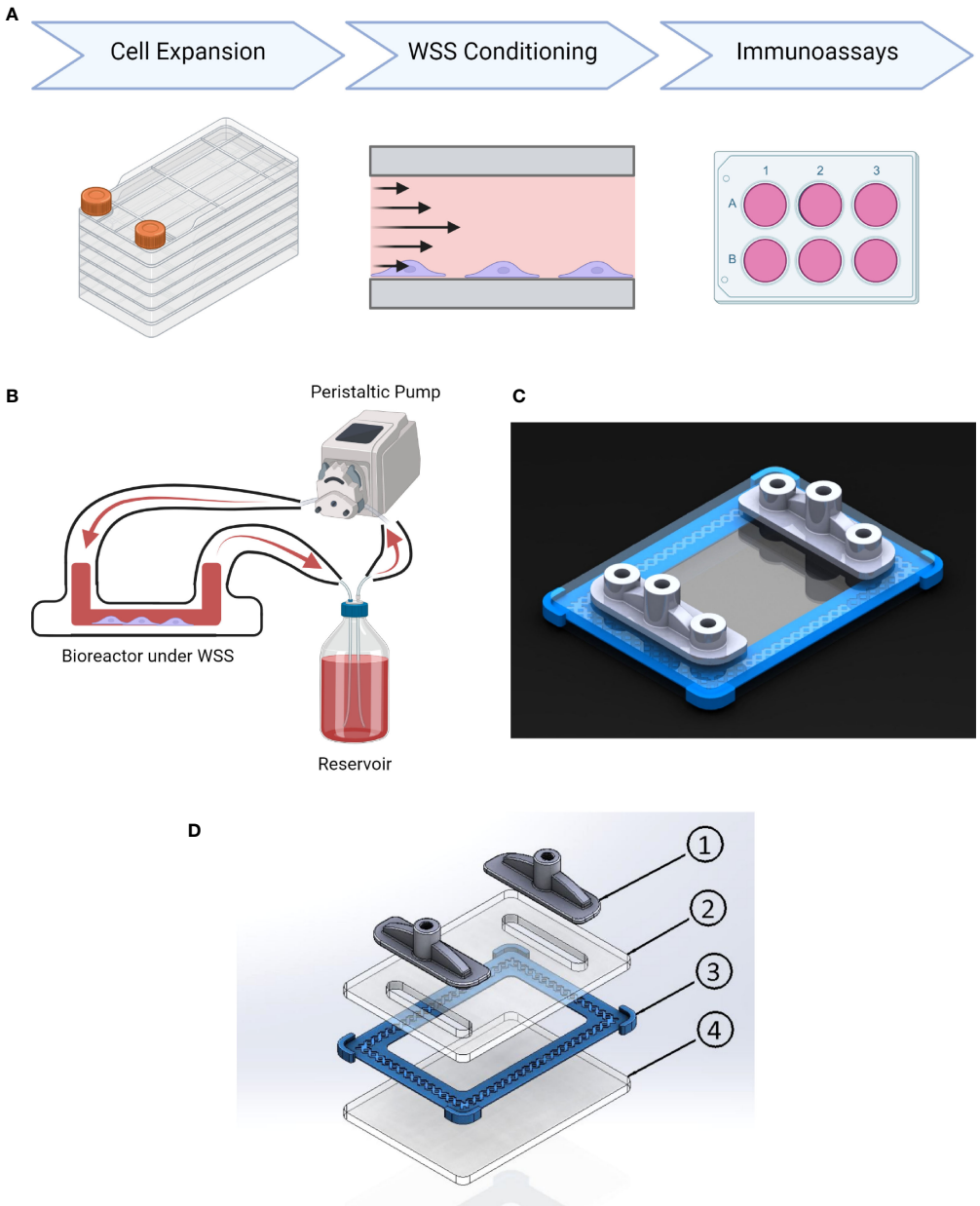

FIGURE 1 | Conditioning platform design and procedure. **(A)** Experimental timeline. MSC undergo cell expansion in large volume tissue culture plastic under xeno-free conditions using cGMP-comparable methods and reagents. Next WSS conditioning is performed on adherent MSC in the parallel plate bioreactor at 4, 8, or 12 dyne/cm^2 for 3 hrs. The resulting cells are then immunoassayed for their ability to modulate inflammation in a panel of assays. **(B)** Schematic of platform configuration, including PPB, media reservoir, and peristaltic pump. **(C)** Rendering of parallel-plate bioreactor displaying transparent PMMA plates fabricated using a CNC mill, 3D-printed gasket (blue), and 3D-printed inlet/outlet manifolds with sampling ports (grey). **(D)** Schematic of parallel plate bioreactor: (1) 3D Printed Inlet/Outlet Ports, (2) PMMA Top Plate, (3) 3D Printed Gasket, (4) PMMA Base Plate.

recovered following harvest from static and 4 dyne/cm^2 cultures were similar at 88.64% ± 6.0% and 84.8% ± 4.4%, respectively (p=0.8703). 8 dyne/cm^2 and 12 dyne/cm^2 conditions significantly decreased yield to 71.7% ± 9.7% and 51.5% ± 8.1%, respectively (p=0.0152 and p=<0.0001 versus static group, respectively).

We repeated the experiment with hBM-MSC. The viability of hBM-MSC cultured statically was 95.2% ± 2.2%, while 4 and 8 dyne/cm^2 conditions decreased viability to 81.0% ± 5.9% and 83.5% ± 5.6%, respectively (p= 0.0077 and p=0.0299 versus static, respectively) (**Figure 3B**). 12 dyne/cm^2 resulted in the greatest viability decrease relative to static culture (78.1% ± 6.6%, p=0.0017).

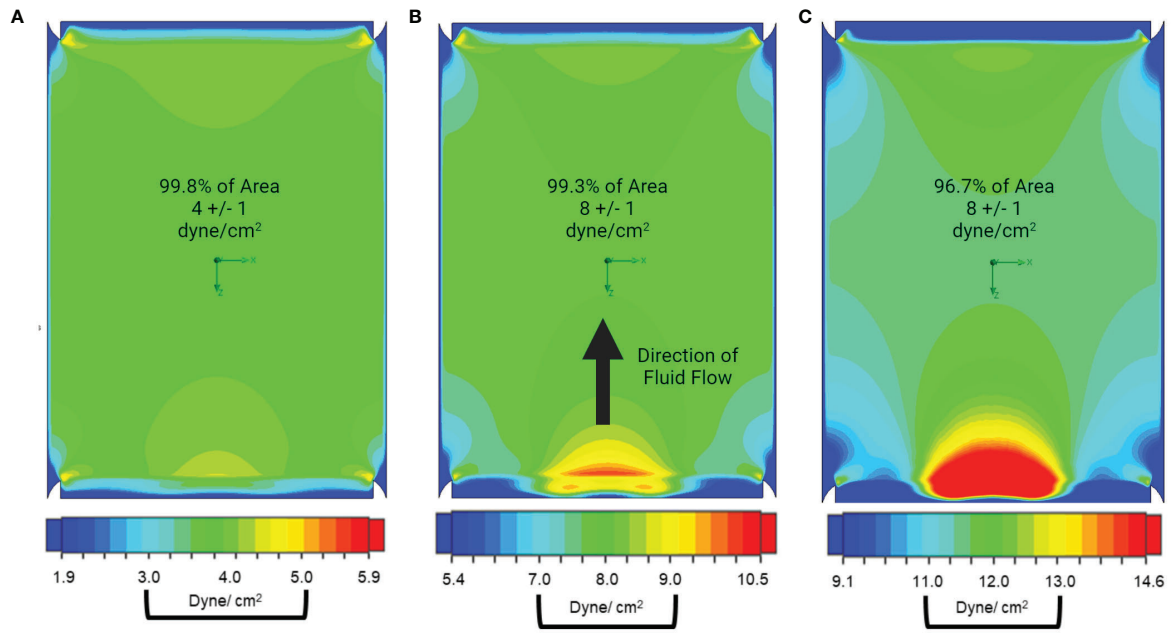

FIGURE 2 | Our parallel plate bioreactor geometry facilitates uniform fluid dynamics and shear stress. Pseudocolor heatmaps of shear stress distribution across the growth surface of the bioreactor were generated using computer modeling. In this presentation, the fluid is flowing towards the top of the page and areas of low shear are presented in shades of blue, high shear is presented in shades of red, while the targeted shear +/- 1 dyne/cm^2 are presented in shades of green. **(A)** When the operating conditions for 4 dyne/cm^2 are simulated, we find that 99.8% of the surface area is between 3-5 dyne/cm^2. **(B)** When the system is modeled at 8 dyne/cm^2 99.3% of channel surface area is within target wall shear stress and **(C)** 96.7% of channel surface area is within target when the operating conditions for 12 dyne/cm^2 are simulated.

hBM-MSC exhibited a yield reduction similar to hAD-MSC at higher WSS. Static and 4 dyne/cm^2 culture conditions resulted in yields of 93.0% ± 6.2% and 98.4% ± 11.5%, respectively. Applying 8 dyne/cm^2 led to a harvest of 81.4% ± 8.9% (p= 0.1672 versus static). After exposure to 12 dyne/cm^2, there was a significant drop in yield relative to static cultures (60.9% ± 6.7%, p=0.0001) (**Figure 3D**).

Microscopic examination of hBM-MSC after a 3 hr seeding period in the bioreactors shows cells readily adhering in a monolayer (**Figure 3E**). Re-examination of the same cell population after subsequent conditioning at 8 dyne/cm^2 revealed slight changes in cell morphology (**Figure 3F**).

WSS Induces Immunomodulatory Mechanisms in MSC

Conditioned media from hAD-MSC exposed to 0, 4, 8, and 12 dyne/cm^2 was generated by plating 200,000 cells per well into a 6 well plate and incubating for 18hrs to measure the production and accumulation of PGE_2 and IDO1. Of the WSS magnitudes tested, 4 dyne/cm^2 significantly increased PGE_2 production relative to static culture (**Figure 4A**, 358.2 ± 34.2 pg/mL versus 245.9 ± 45.1 pg/mL, p=0.0264). The PGE_2 concentrations of 8 and 12 dyne/cm^2 cultures (362.5 ± 73.3 pg/mL and 350.9 ± 125.6 pg/mL, respectively) were not significantly different from the static group (p=0.0788 and p=0.2444, respectively).

hAD-MSC IDO1 production significantly increased after exposure to 8 dyne/cm^2 from 80.8 ± 6.0 pg/mL to 222.9 ± 47.2 pg/mL (**Figure 4C**, p=0.0016). The average IDO1 concentration in 12 dyne/cm^2 wells was measured at 420.5 ± 215.9 pg/mL, which also reached significance (p=0.0225).

Relative to the hAD-MSC line, the naïve hBM-MSC line produced more PGE_2 (**Figures 4A, B**). Also, the hBM-MSC line exhibited a greater response to fluid shear stress exposure as reflected by a larger fold-change. PGE_2 secretion increased after conditioning hBM-MSC with 8 dyne/cm^2 from 2731.3 ± 645.4 pg/mL to 8657.7 ± 3189.0 pg/mL (**Figure 4B**, p=0.0135).

Mechanotransduction with 8 dyne/cm^2 significantly increased hBM-MSC production of IDO1 from 462.8 ± 35.6 pg/mL to 710.0 ± 148.5 pg/mL (**Figure 4D**, p=0.0485). Conditioning with 12 dyne/cm^2 actually decreased IDO1 with a concentration of 295.9 ± 67.4 pg/mL measured (p=0.0192). As with PGE_2, the hBM-MSC line produced more IDO1 at baseline than the hAD-MSC line (**Figures 4C, D**).

Wall-Shear Stress Does Not Alter MSC Phenotype

The previous section shows mechanotransduction enhances anti-inflammatory protein production in a shear-dependent manner. This data, in combination with viability and cellular yield findings, led us to select 8 dyne/cm^2 as an optimal WSS for further evaluation. The PPB was scaled to create a 120 cm^2 surface area to facilitate

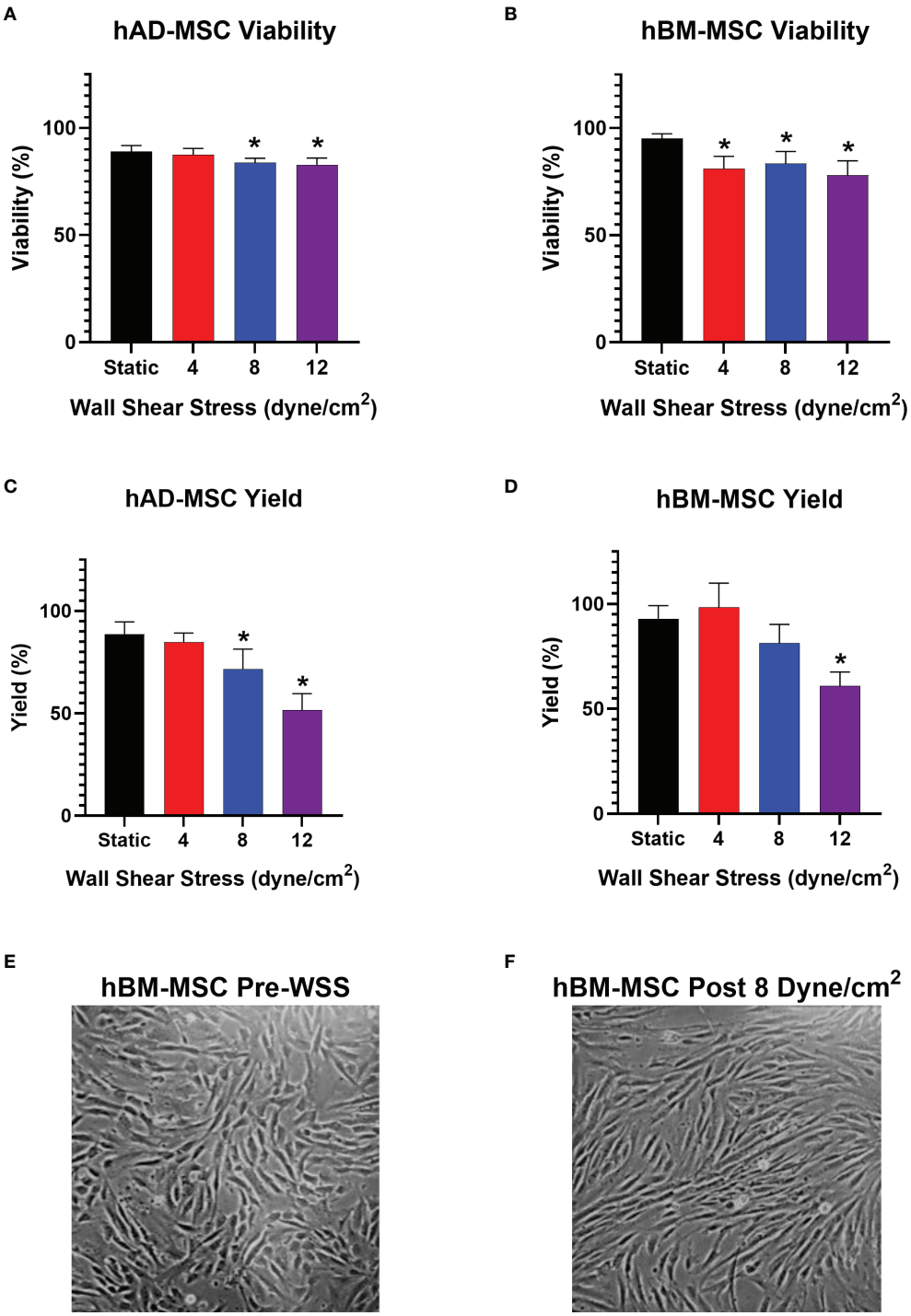

FIGURE 3 | WSS-exposure impacts cellular yield, without affecting MSC viability. **(A)** Viability of harvested hAD-MSC after exposure to 4, 8, or 12 dyne/cm^2 compared to static control culture (n=5 independent experiments; one-way ANOVA with Tukey's multiple comparison test, *p<0.05 versus static group). Data represent Mean ± SD. **(B)** Viability of harvested hBM-MSC after exposure to 4, 8, or 12 dyne/cm^2 (n=5 independent experiments for all groups, except n=4 in static group; one-way ANOVA with Tukey's multiple comparison test, *p<0.05 versus static group). **(C)** Percent yield of hAD-MSC collected after exposure to 4, 8, or 12 dyne/cm^2 compared to static control culture (n=5 independent experiments for all groups, except n=4 in 4 dyne/cm^2 group; one-way ANOVA with Tukey's multiple comparison test, *p<0.05 versus static group). **(D)** Percent yield of hBM-MSC collected after exposure to 4, 8, or 12 dyne/cm^2 compared to static control culture (n=5 independent experiments for all groups, except n=4 in 4 dyne/cm^2 group; one-way ANOVA with Tukey's multiple comparison test, *p<0.05 versus static group). **(E, F)** Phase microscopy image (10x) taken 3 hrs after injecting hBM-MSC into fibronectin-coated bioreactor and after exposure to 8 dyne/cm^2 for 3 hrs, respectively.

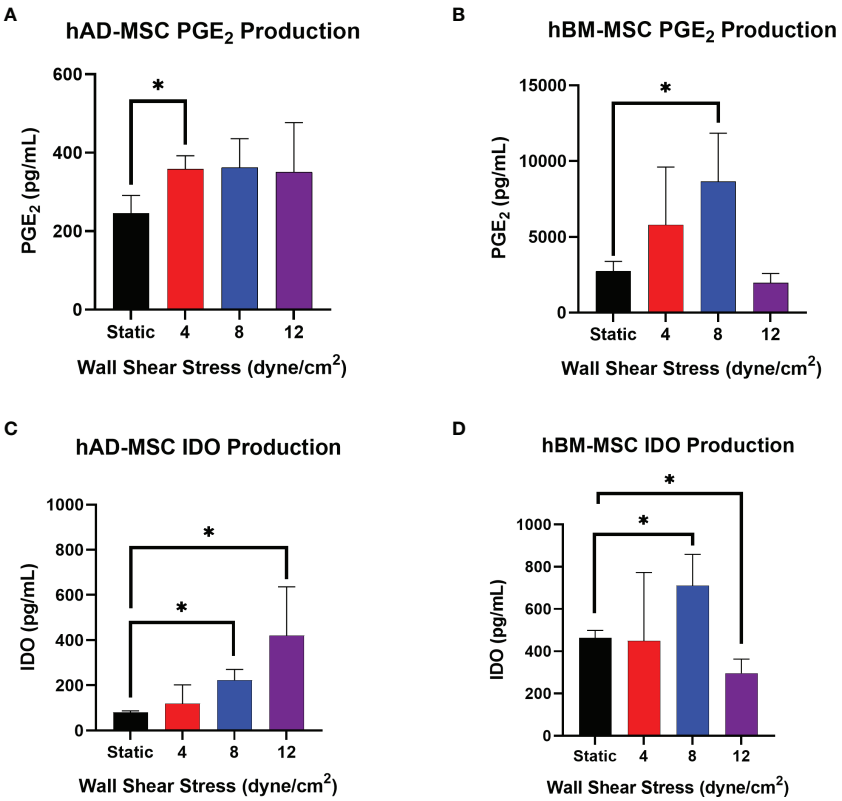

FIGURE 4 | Select WSS-exposure enhances production of PGE_2 and IDO by hAD-MSC and hBM-MSC. **(A, B)** The accumulation of PGE_2 in conditioned media from hAD-MSC and hBM-MSC cultures, respectively, plated at 200,000/mL, was assayed after an 18 hr incubation using ELISA (n=3 independent experiments; unpaired t-test, *p<0.05). Data represent Mean ± SD. **(C, D)** The concentration of IDO in conditioned media from hAD-MSC and hBM-MSC cultures plated at 200,000/mL was determined after 18 hrs incubation using ELISA (n=3 independent experiments; unpaired t-test, *p<0.05).

larger cell numbers for the following experiments (unless otherwise noted). Additionally, we focused on the use of a cGMP-simulated cell line to facilitate future translational applications.

We evaluated the expression of classic MSC markers CD73, CD90, CD105, and CD146 on mechanotransduced hBM-MSC using a pre-mixed antibody panel (39). An established reference BM-MSC cell line (hBMMSC 5204, PDL 12.9) and non-mechanotransduced hBM-MSC served as controls (Roo205 Static). WSS-MSC were negative for the hematopoietic lineage markers CD31, CD34, and CD45 (**Table 1**). Less than 1% of the WSS-MSC population expressed CD31, CD34, and CD45. These findings were comparable to the external reference hBM-MSC, which expressed CD31, CD34, and CD45 at rates of 0.69%, 0.10%, and 3.28%, respectively. Greater than 98% of WSS-MSC expressed the positive hMSC immunophenotypic markers CD73, CD90, and CD105. Over 87% of the hBM-MSC expressed CD146. At least 10,000 events were evaluated for each population.

Mechanotransduced hBM-MSC Suppress Inflammatory Cytokine Release From Activated Splenocytes *In Vitro*

Similar to previously published work, hBM-MSC conditioned with 8 dyne/cm^2 were studied using a superantigen-activated splenocyte coculture assay, a functional assay that simulates some of the complex MSC-immune effector cell interactions expected *in vivo* (28, 34, 36, 39). Two independent large-scale bioreactors were run side-by-side to compare performance (Roo205 8.1 and Roo205 8.2). The resulting WSS-MSC and splenocyte cocultures were performed in triplicate, which are presented as replicates from each PPB. Previous studies influenced the choice of MSC:splenocyte ratio for the LPS and ConA-stimulated cultures (28, 36, 47, 48).

MSC were cocultured with LPS-stimulated splenocytes at a ratio of 1:80 and incubated for 24 hrs before the supernatant was collected. WSS-MSC from the two PPB significantly reduced TNF-α production by LPS-stimulated splenocyte from 234.4 ± 7.0 pg/mL to 166.7 ± 27.6 pg/mL and 149.2 ± 7.1 pg/mL (**Figure 5A**, p=0.0095 and p=0.0019, respectively). Coculturing with Static-MSC did not significantly reduce the average supernatant concentration (195.5 ± 30.6 pg/mL, p=0.1643 versus activated-splenocyte).

MSC were cocultured with ConA-stimulated splenocytes at a ratio of 1:20 and incubated for 48 hrs before the supernatant was collected. Both, WSS-MSC and Static-MSC significantly reduced IFN-γ production (**Figure 5B**). Static-MSC decreased the measured concentration from 10,749.0 ± 111.7 pg/mL in activated splenocyte

TABLE 1 | hBM-MSC cell surface marker expression is unaltered after mechanotransduction.

Table of MSC Markers (% positive)

	Negative Markers			Positive Markers			
	CD31	CD34	CD45	CD73	CD90	CD105	CD146
Reference hBM-MSC	0.69	0.10	3.28	99.65	99.64	99.56	97.75
Roo205p4 (static culture)	0.14	0.03	0.46	99.69	99.68	99.55	93.75
Roo205p4 (small PPB) 8.1	0.48	0.00	0.12	98.76	98.93	98.29	90.08
Roo205p4 (small PPB) 8.2	0.29	0.15	0.00	99.34	99.39	98.54	87.57
Roo205p4 (Full PPB) 8.1	0.18	0.07	0.11	99.72	99.61	99.15	89.11
Roo205p4 (Full PPB) 8.2	0.35	0.05	0.02	99.08	99.00	98.44	88.12

The phenotype of each cell population was determined using a panel of markers used to identify and define MSCs. Typical expression of the markers is provided by an external bone marrow MSC. The experimental populations consist of the non-sheared control group, Roo205p4 (static culture), the replicate cultures treated with WSS generated using the initial small scale PPB, Roo205p4 (small PPB) 8.1 and 8.2, and the replicate cultures treated with WSS using the large scale PPB, Roo205p4 (large PPB) 8.1 and 8.2.

cultures to 2260.4 ± 660.8 pg/mL (p<0.0001). The IFN- γ concentrations in Roo205 8.1 and Roo205 8.2 cocultures were measured at 2176.7 ± 254.4 pg/mL and 1427.8 ± 329.8 pg/mL, respectively (p<0.0001 versus activated-splenocyte, for both groups).

Mechanotransduction Results in Differential Gene Expression of Immunomodulatory Factors

We performed whole exome sequencing on duplicate cultures of hBM-MSC conditioned with 8 dyne/cm^2 followed by differential gene expression analysis comparing them to static cultures. Principal component analysis (PCA) of the samples displays that WSS-exposure resulted in a much larger distribution of differentially expressed genes (PC1) compared with the variation between replicates (PC2) (**Figure 6A**). After biomechanical pre-conditioning, 988 genes exhibited differential expression (**Figure 6B**, p-adj < 0.05) (49, 50). 646 of these differentially expressed genes were upregulated (65.4%). Differential gene expression analysis demonstrated 313 genes with a p-adj < 0.01. This limited subset of transcripts features a number of immunomodulatory genes.

We evaluated expression of immunologically influential genes often discussed as therapeutic mechanisms for MSC: *NF-κB, PTGS2, HMOX-1, TNFAIP6*, *ICAM-1, TIMP-3, TNF-α*, and *CXCL1* (**Figure 6D**). The genes *NF-κB, PTGS2, HMOX-1, TNFAIP6*, and *ICAM-1* were significantly upregulated (p-adj<0.05), while *TIMP-3* was similarly expressed by the WSS-MSC and Static-MSC (p-adj= 0.7246). As expected, genes for typical proinflammatory cytokines, such as TNF-α and CXCL1, were not affected by WSS and detected at low levels (p-adj = 0.8945 and 0.7897, respectively).

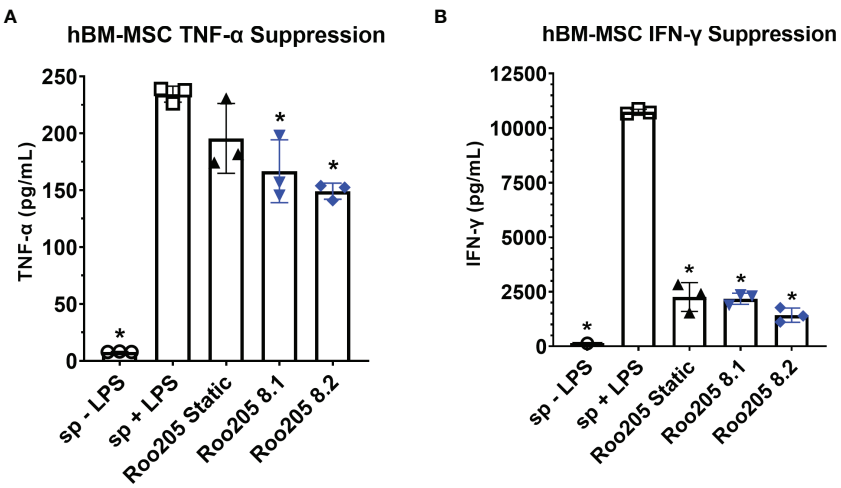

FIGURE 5 | WSS-conditioned hBM-MSC suppress activated splenocyte cytokine production. **(A)** The TNF-α concentration produced by LPS-activated splenocyte in co-culture with MSC at a ratio of 1 MSC: 20 splenocytes, after 24 hrs incubation determined using a rat-specific ELISA (n=3 independent experiments; one-way ANOVA with Tukey's multiple comparison test, *p<0.05, LPS-activated splenocytes versus other groups). Data represent Mean ± SD. **(B)** The IFN-γ concentration produced by ConA-activated splenocyte in co-culture with MSC at a ratio of 1:80 MSC to splenocyte, after 48 hrs incubation determined using a rat specific ELISA (n=3 independent experiments; one-way ANOVA with Tukey's multiple comparison test, *p<0.05, ConA-activated splenocytes versus other groups). Data represent Mean ± SD.

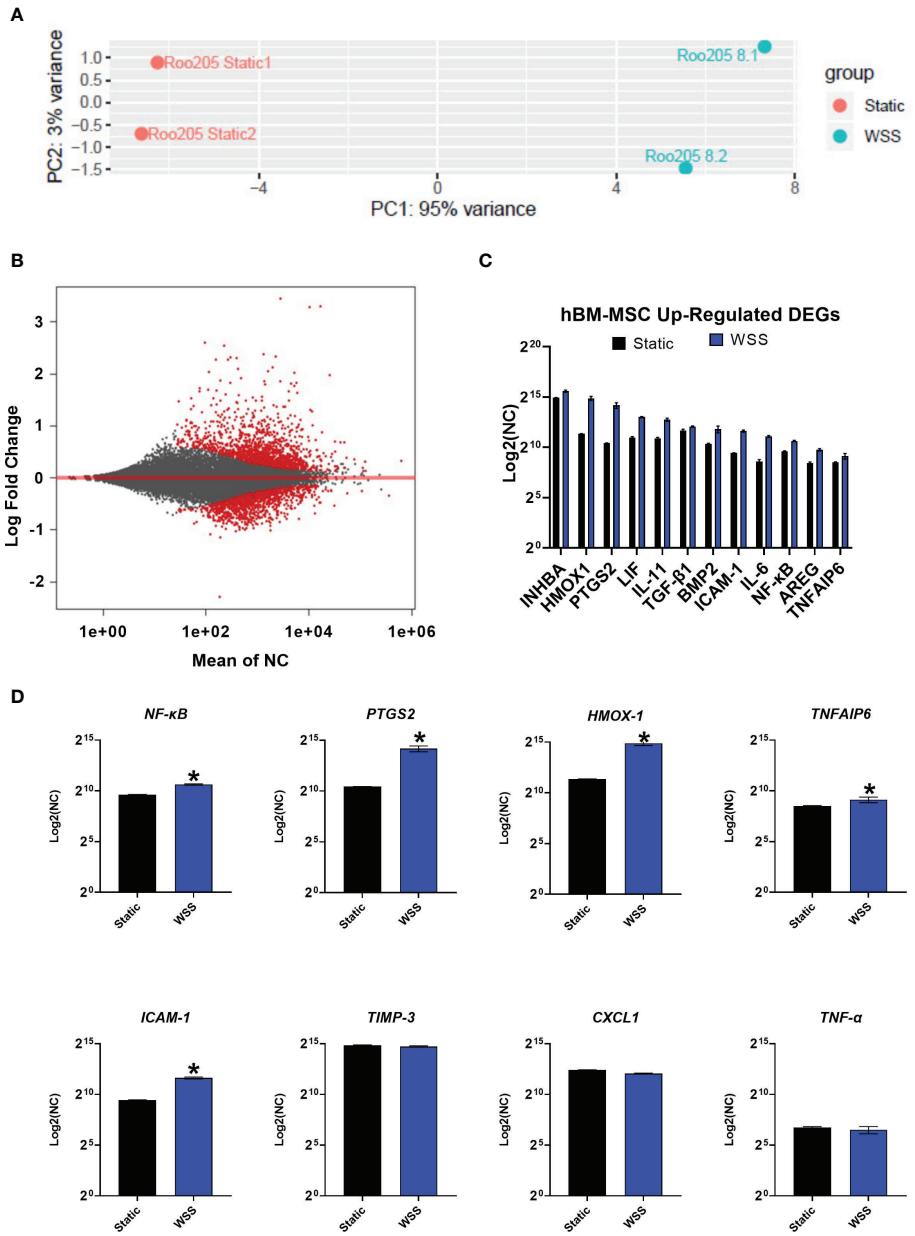

FIGURE 6 | Transcriptome analysis of mechanotransduced hBM-MSC shows enhanced expression of immune mediators. **(A)** Principal component analysis of conventionally cultured (Static) and 8 dyne/cm^2 conditioned hBM-MSC (WSS) (n=2). Samples are plotted by variance across the two primary principal components (PC1, PC2). **(B)** MA Plot depicting distribution of differentially expressed genes (DEG, in red) plotted by the mean normalized count (NC) against the log fold change. **(C)** A curated list of WSS-induced, up-regulated differentially expressed genes. Y-axis depicts NC by DESeq2 (n=2). **(D)** Expression of established inflammatory mediators. Y-axis depicts NC (n=2, *p-adj<0.05). *INHBA*, Inhibin Subunit Beta A; *HMOX1*, Heme oxygenase 1; *PTGS2*, Prostaglandin-Endoperoxide Synthase 2; *LIF*, Leukemia Inhibitory Factor; *IL-11*, Interleukin 11; *TGF-β1*, Transforming Growth Factor Beta 1; *BMP2*, Bone Morphogenetic Protein 2; *ICAM-1*, Intracellular Adhesion Molecule 1; *IL-6*, Interleukin 6; *NF-κB*, Nuclear Factor Kappa B; *AREG*, Amphiregulin; *TNFAIP6*, Tumor Necrosis Factor-Inducible Protein 6; *TIMP-3*, Tissue Inhibitor of Metalloproteinase 3; *CXCL1*, C-X-C Motif Chemokine Ligand 1; *TNF-α*, Tumor Necrosis Factor Alpha.

Finally, we screened the list of up-regulated, differentially expressed genes (p-adj <0.05) for commonly reported immune modulators. Genes of interest included *INHB1, VEGFA, LIF, IL-11, SERPINB2, TGF-β1, BMP2, IL-6, MT1X, AREG, ATF3*, and *FGF11* (**Figure 6C**).

DISCUSSION

This study describes a set of experiments that are proof-of-concept and the first steps in realizing a clinically translatable mechanotransduction strategy. We designed a scaled parallel

plate bioreactor to exert uniform WSS on adherent cells in culture and then performed a series of experiments to evaluate changes in MSC immunomodulatory potential after conditioning with fluid shear stress. We utilized computer modeling to generate PPB where >96% of the surface area was within 1 dyne/cm^2 of our target WSS value. After manufacturing our PPB, we found that human MSC from two different tissues (adipose tissue and bone marrow) exhibited high viability across the WSS range studied, although 12 dyne/cm^2 resulted in a lower cellular yield. The WSS mechanotransduction increased expression of PGE_2 and IDO1 consistently at 8 dyne/cm^2, similar to smaller scale experiments utilizing multiple cell lines (28, 34). 8 dyne/cm^2 was selected as an optimal WSS for additional characterization of hBM-MSC. We found that WSS increased the ability to reduce TNF-α production by activated splenocytes compared to static hBM-MSC cultures. All groups tested drastically reduced IFN-γ production by ConA-stimulated splenocytes. RNAseq analysis found a subset of differentially expressed genes that contained known therapeutic mechanisms of action by MSC. Over the course of our mechanotransduction studies, we've used many PPB iterations, some of which were used in studies demonstrating increased potency in multiple MSC cell lines (28, 34). This particular PPB model conditions an exponentially larger cell population than previously attempted and is the first step in scaling the concept. During its development and characterization, we used over 25 devices. The consistent maturation of WSS-MSC products validates our novel, scalable platform.

The concept of inflammatory licensing pervades the field of MSC biology. Previous studies by our group and others have evaluated the effects of inflammatory cytokines (4, 12, 14–16, 21, 24, 39, 51), hypoxia (23, 24), serum starvation (25, 26), and numerous other culture manipulations. Mechanotransduction of MSC is particularly interesting for several reasons. First, MSC are abruptly exposed to vascular fluid dynamics when migrating or when infused intravenously or intra-arterially (6, 29, 31, 33, 52–55). Previous studies evaluating the response of numerous cell lines indicate that MSC respond to this shear stress by expressing a number of potentially therapeutic mechanisms (28, 31, 32, 34). Finally, the application of WSS does not require the use of potentially dangerous culture additives that may complicate future clinical applications (2, 8, 11, 12). A WSS-conditioning strategy is an intrinsically simpler approach to increasing potency than genetic manipulation or molecular licensing, necessitating minimal adjustments to a cell therapy manufacturing pipeline and reagent list.

In previous work, our group found that mechanotransduced hBM-MSC were primed towards anti-inflammatory activity based on WSS-dependent focal adhesion kinase (FAK) signaling and described the resulting functional potentiation (28, 32, 34). Specifically, fluid shear stress activates the FAK/NF-κB signaling pathway to enhance production of proteins implicated in anti-inflammatory immune modulation, such as heme oxygenase-1 (HO-1) and PGE_2 in three independent hBM-MSC donor cell lines (34). Finally, an *in vivo* study evaluating five hBM-MSC cell lines demonstrated the increased potency of WSS-MSC in a rat TBI model, finding that WSS-MSC decreased apoptotic and M1-type activated microglia after injury (28).

Given their increased *in-vivo* potency, WSS-MSC might reduce the cell dose needed to treat, thereby easing manufacturing burden and associated costs compared to naïve MSC. With this in mind, we redesigned the WSS platform used in our previous studies to create a scalable, clinically-translatable mechanotransduction device and replicate relevant characterization assays (28, 34).

A fully sterilizable closed-circuit flow loop containing a PPB, commercially available connectors, and tubing was engineered to facilitate sterile media transfer and sampling. The custom bioreactor was iteratively designed using CFD studies to apply reproducible, accurate fluid shear stress on adherent MSC populations. While the PPB's components were individually fabricated for this study and hand-assembled, the components are compatible with large-scale injection molding and automated assembly processes. Furthermore, the bioreactor's length can be increased to accommodate more surface area and cells without drastic alteration of the reactor fluid dynamics.

As MSC manufacturing has significant bottlenecks and real-world financial constraints, it is important to optimize the number of viable cells harvested from a PPB. Our composite results from hAD-MSC and hBM-MSC suggest a strong negative correlation between WSS and cellular yield, with a smaller effect size on viability. These findings agree with a great deal of literature concerning MSC biomanufacturing and the inverse relationship between flow rate and cellular attachment (8, 56, 57). The findings suggested precluding WSS magnitudes ≥12 dyne/cm^2 due to diminishing returns.

Next, we assayed the changes of selected MSC therapeutic mechanisms and immunomodulatory activity after exposure to physiologically relevant shear stress magnitudes. PGE_2 and IDO1 are two well described mechanisms by which MSC exert anti-inflammatory activity on various immune (4, 12, 28, 36, 58). PGE_2, an eicosanoid with pleiotropic effects, is upregulated in response to many cytokines, mitogens, and pharmacological agents (12). The paracrine signaling molecule contributes to the resolution of neutrophil-mediated inflammation, attenuation of natural killer cell activity, suppression of pro-inflammatory macrophages, and inhibition of CD8+ T cells (5, 7, 10, 28). IDO1, classically secreted by MSC in response to IFN- γ stimulation, metabolizes tryptophan into kynurenine metabolites. The depletion of tryptophan induces CD8+ and CD4+ Th1 T cell anergy, suppresses allogeneic T-cell responses, and induces proliferation of T-regulatory cells (4, 59).

Fluid shear stress enhanced PGE_2 and IDO secretion in two different MSC derivations, supporting the conservation of mechanotransduction effect after scaling. There was a magnitude-dependent relationship between shear stress and PGE_2/IDO1 production that resulted in diminished returns at 12 dyne/cm^2. Our preparations of hBM-MSC and hAD-MSC exhibited similar relative responses to WSS, although hBM-MSC produced higher amounts of PGE_2 and IDO. This difference could be solely due to a limited number of samples assayed, and literature regarding PGE_2 production by the two derivations is

inconclusive (60–63). Increased PGE_2 and IDO1 production, two soluble factors with established *in vivo* mechanisms of action, indicates that WSS-MSC exhibit some of the secretome patterns of licensed MSC (1, 2, 4, 5, 7, 12, 49, 58). These findings guided our selection of 8 dyne/cm^2 and hBM-MSC for further investigation.

We evaluated the *in vitro* potency of hBM-MSC mechanotransduced with 8 dyne/cm^2*via* a cytokine suppression assay using antigen-stimulated primary rat splenocytes. The assay serves as an approximation of *in vivo* immune relations and includes the complexity of cell-to-cell interaction in a mixed leukocyte population (28). Cells of monocyte lineage are the prime producers of short-term TNF-α when stimulated with LPS activation (64). The secretion of TNF-α correlates with severity of inflammation and the innate immune system response (5, 11). In a similar set of experiments, ConA primarily activates T cells resulting in the accumulation of IFN- γ over a slightly longer period, thus cultures were sampled at 48 hrs. IFN-γ,classically associated with Th1 response and CD8+ T cell activation, served as a general indicator of the adaptive immune system (5).

Indeed, mechanotransduced hBM-MSC dampened TNF-α and IFN-γ production by activated splenocytes. In the case of TNF-α, the reduction in the WSS-MSC coculture was significant. Static-MSC contributed to a modest, but not statistically significant decrease. This enhanced suppression of TNF-α by WSS-MSC relative to Static-MSC is evidence of functional augmentation *via* mechanotransduction and successful scaling of the priming methodology. Both MSC groups significantly decreased IFN-γ concentrations, nearly to the level measured in unstimulated splenocyte cultures. Notably, little functional difference was observed between cells conditioned in independent bioreactors.

We carried out RNASeq on BM-MSC conditioned with 8 dyne/cm^2 to elucidate the effect of mechanotransduction on the transcriptome of MSC. This sequencing provides an initial analysis of the WSS-MSC transcriptional signature. PCA and MA plots depict a robust effect with transcriptional patterns shifting after WSS conditioning.

Focused RNASeq analysis found the genes *NF-κB* and *PTGS2*, both commonly associated with immune modulation mechanisms (1, 3, 5, 9, 11, 49), increased after WSS. Activation of the NF-κB-COX2-PGE_2 pathway is a recognized component of MSC potency, especially in regard to monocyte and T-cell inhibition (11, 34) and is a primary consequence of biomechanically stimulated FAK signaling (34). *PTGS2* encodes for cyclooxygenase-2, the rate-limiting enzyme in PGE_2 production, and its increased expression further confirms the observed increase in PGE_2 secretion.

Other known therapeutic mechanisms of MSC were increased including *TNFAIP6, ICAM-1*, and *HMOX-1.TNFAIP6*, or TNF-α inducible protein 6, encodes for TSG-6, a hyaluronan-binding protein that induces macrophage plasticity (65). Increased TSG-6 production is reported to ameliorate proinflammatory-driven neuroinflammation in stroke and lung injury models (65–67). The adhesion molecule ICAM-1 provides the means for direct cell-to-cell contact between MSC and immune effector cells. Upregulation of ICAM-1 is an indicator of enhanced MSC immunomodulatory capacity (49). Once engaged with monocytes or T cells, MSC can provide direct signals to induce apoptosis, cell cycle arrest, or class-switching switching (39, 49). *HMOX-1*, encoding the antioxidant HO-1, was also significantly upregulated after mechanotransduction. HO-1 is the rate-limiting enzyme in heme degradation (68). The stress-induced protein not only plays a critical role in oxidative stress protection and iron detoxification but has been shown to prevent allograft rejection and promote anti-inflammatory T cell responses through induction of IL-10 (51, 68). The upregulation of these genes should be studied in the context of disease-specific clinical applications.

Broader transcriptome analysis yielded a list of mechanically-stimulated, differentially expressed genes that are yet to be conclusively associated with mechanotransduction. This includes IL-6, leukemia inhibitory factor (LIF), and IL-11. These members of the IL-6 family, heavily regulated by NF-κB, were each differentially expressed after mechanical conditioning. These immune modulators provide neuroprotection after ischemic CNS injury by inhibiting microglia activation, regulating adaptive immune system tolerance, and influencing CD4+ T Cell lineage (49, 69–73). Members of the TGF-β family (Activin A, TGF-β1, and BMP2) were also differentially upregulated. This family is classically associated with injury resolution, anti-apoptotic signaling, enhanced T regulatory cell differentiation, microglia suppression, and CNS neurogenesis after excitotoxic neurodegeneration (7, 69, 74, 75). These findings highlight MSC's role as soluble factor generators, exerting their immunomodulatory influence through a myriad of mechanisms (49, 50, 76). A broader analysis with more experimental groups is required to evaluate this further.

A limitation to this study was its use of a single donor for each MSC tissue derivation. The number of samples and replicates were limited by the number and size of PPBs available, as each reactor was custom built, assembled, sterilized, and tested for this study. As the bioreactors move towards a final production process and become more available, we will replicate and confirm our findings across additional tissue sources, donors, and production lots of MSCs. Based on previous work comparing independent donor cell lines, WSS enhances the protein production and immunomodulatory potential different cell lines to varying degrees, which must be further quantified (34). In this study, other protocol variables were not studied (e.g., time, waveform frequency, etc.) that could further optimize the effects of WSS on MSC potency. Also, more research must be done to evaluate the duration of the mechanotransduction effect, specifically concerning conservation after a freeze-thaw cycle to facilitate acute and sub-acute applications. While the *in-vitro* splenocyte assay demonstrated various WSS-MSC immunomodulatory properties, the cell therapy must be assessed in a disease-specific animal model for more generalizable findings. Finally, we anticipate that the system will require additional scaling of the bioreactor, increasing channel surface area and the number of channels per bioreactor, to accommodate larger human dosages (between 1-10 million cells/kg).

The application of fluid shear stress to an adherent MSC population within a PPB is a scalable preconditioning methodology that requires little manipulation beyond the addition of fluid dynamics, capable of being adapted and applied for future clinical MSC products. We assessed several critical parameters of cellular manufacturing including viability, yield, identity, and immunomodulatory potential after WSS conditioning. The findings of this characterization support the feasible manufacturing of biomechanically conditioned MSC. Future efforts should confirm the attributes of a standardized, mechanotransduced MSC therapy and reduction to phenotypic heterogeneity in other cell lines. Leveraging the responsiveness of MSC to biophysical cues might yield a novel licensing approach and enhanced therapy for inflammatory indications.

DATA AVAILABILITY STATEMENT

The data presented in the study are deposited in the sequence read archive (SRA) repository, BioProject PRJNA8143337, accession numbers SAMN26548527, SAMN26548528, SAMN26548529, and SAMN26548530.

AUTHOR CONTRIBUTIONS

Conception and design: MS, SO, BG, and CC. Collection and/or assembly of data: MS, SO, and KP. Data Analysis and interpretation: MS, SO, KP, BG, and CC. Manuscript writing: MS, SO, BG, and CC. Final approval of manuscript: MS, SO, BG, and CC.

FUNDING

This study is supported by the Clare A Glassell Family Pediatric Surgery Research Fund; Alpha Omega Alpha Carolyn L. Kuckein Student Research Fellowship; NIH NINDS R21NS116302. The authors declare that this study also received funding from Cellvation. The funder was not involved in the study design, collection, analysis, interpretation of data, the writing of this article or the decision to submit it for publication.

ACKNOWLEDGMENTS

We would like to thank the Cancer Genomics Center at The University of Texas Health Science Center at Houston (CPRIT RP180734) for their support of this work. Supported in part by an Alpha Omega Alpha Carolyn L. Kuckein Student Research Fellowship. Thanks to the Claire Glassell Pediatric Fund for their generous support. Some illustrations were created in BioRender.com

SUPPLEMENTARY MATERIAL

The Supplementary Material for this article can be found online at: https://www.frontiersin.org/articles/10.3389/fimmu.2022.874698/full#supplementary-material

REFERENCES

1. Krampera M. Mesenchymal Stromal Cell 'Licensing': A Multistep Process. *Leukemia* (2011) 25:1408–14. doi: 10.1038/leu.2011.108
2. Murphy MB, Moncivais K, Caplan AI. Mesenchymal Stem Cells: Environmentally Responsive Therapeutics for Regenerative Medicine. *Exp Mol Med* (2013) 45:e54–4. doi: 10.1038/emm.2013.94
3. Cunningham CJ, Redondo-Castro E, Allan SM. The Therapeutic Potential of the Mesenchymal Stem Cell Secretome in Ischaemic Stroke. *J Cereb Blood Flow Metab* (2018) 38:1276–92. doi: 10.1177/0271678X18776802
4. Prasanna SJ, Gopalakrishnan D, Shankar SR, Vasandan AB. Pro-Inflammatory Cytokines, IFNgamma and TNFalpha, Influence Immune Properties of Human Bone Marrow and Wharton Jelly Mesenchymal Stem Cells Differentially. *PloS One* (2010) 5:e9016. doi: 10.1371/journal.pone.0009016
5. English K. Mechanisms of Mesenchymal Stromal Cell Immunomodulation. *Immunol Cell Biol* (2013) 91:19–26. doi: 10.1038/icb.2012.56
6. Fu X, Liu G, Halim A, Ju Y, Luo Q, Song AG. Mesenchymal Stem Cell Migration and Tissue Repair. *Cells* (2019) 8(8):784. doi: 10.3390/cells8080784
7. Schäfer R, Spohn G, Baer PC. Mesenchymal Stem/Stromal Cells in Regenerative Medicine: Can Preconditioning Strategies Improve Therapeutic Efficacy. *Transfusi Med Hemother* (2016) 43:256–67. doi: 10.1159/000447458
8. Jossen V, Van Den Bos C, Eibl R, Eibl D. Manufacturing Human Mesenchymal Stem Cells at Clinical Scale: Process and Regulatory Challenges. *Appl Microbiol Biotechnol* (2018) 102:3981–94. doi: 10.1007/s00253-018-8912-x
9. Zhang S, Lachance BB, Moiz B, Jia X. Optimizing Stem Cell Therapy After Ischemic Brain Injury. *J Stroke* (2020) 22:286–305. doi: 10.5853/jos.2019.03048
10. Waterman RS, Tomchuck SL, Henkle SL, Betancourt AM. A New Mesenchymal Stem Cell (MSC) Paradigm: Polarization Into a Pro-Inflammatory MSC1 or an Immunosuppressive MSC2 Phenotype. *PloS One* (2010) 5:e10088. doi: 10.1371/journal.pone.0010088
11. Gao F, Chiu SM, Motan DA, Zhang Z, Chen L, Ji HL, et al. Mesenchymal Stem Cells and Immunomodulation: Current Status and Future Prospects. *Cell Death Dis* (2016) 7:e2062. doi: 10.1038/cddis.2015.327
12. Noronha NC, Mizukami A, Caliari-Oliveira C, Cominal JG, Rocha JLM, Covas DT, et al. Priming Approaches to Improve the Efficacy of Mesenchymal Stromal Cell-Based Therapies. *Stem Cell Res Ther* (2019) 10:131. doi: 10.1186/s13287-019-1224-y
13. Carrero R, Cerrada I, Lledó E, Dopazo J, García-García F, Rubio M-P, et al. Il1β Induces Mesenchymal Stem Cells Migration and Leucocyte Chemotaxis Through NF-κb. *Stem Cell Rev Rep* (2012) 8:905–16. doi: 10.1007/s12015-012-9364-9
14. Fan H, Zhao G, Liu L, Liu F, Gong W, Liu X, et al. Pre-Treatment With IL-1β Enhances the Efficacy of MSC Transplantation in DSS-Induced Colitis. *Cell Mol Immunol* (2012) 9:473–81. doi: 10.1038/cmi.2012.40
15. Redondo-Castro E, Cunningham C, Miller J, Martuscelli L, Aoulad-Ali S, Rothwell NJ, et al. Interleukin-1 Primes Human Mesenchymal Stem Cells Towards an Anti-Inflammatory and Pro-Trophic Phenotype *In Vitro*. *Stem Cell Res Ther* (2017) 8:79. doi: 10.1186/s13287-017-0531-4
16. François M, Romieu-Mourez R, Li M, Galipeau J. Human MSC Suppression Correlates With Cytokine Induction of Indoleamine 2,3-Dioxygenase and Bystander M2 Macrophage Differentiation. *Mol Ther* (2012) 20:187–95. doi: 10.1038/mt.2011.189
17. Wang Q, Yang Q, Wang Z, Tong H, Ma L, Zhang Y, et al. Comparative Analysis of Human Mesenchymal Stem Cells From Fetal-Bone Marrow, Adipose Tissue, and Warton's Jelly as Sources of Cell Immunomodulatory

Therapy. *Hum Vaccines Immunother* (2016) 12:85–96. doi: 10.1080/21645515.2015.1030549
18. Chinnadurai R, Rajan D, Ng S, Mccullough K, Arafat D, Waller EK, et al. Immune Dysfunctionality of Replicative Senescent Mesenchymal Stromal Cells Is Corrected by Ifnγ Priming. *Blood Adv* (2017) 1:628–43. doi: 10.1182/bloodadvances.2017006205
19. Lin T, Pajarinen J, Nabeshima A, Lu L, Nathan K, Jämsen E, et al. Preconditioning of Murine Mesenchymal Stem Cells Synergistically Enhanced Immunomodulation and Osteogenesis. *Stem Cell Res Ther* (2017) 8:277. doi: 10.1186/s13287-017-0730-z
20. Kurte M, Vega-Letter AM, Luz-Crawford P, Djouad F, Noël D, Khoury M, et al. Time-Dependent LPS Exposure Commands MSC Immunoplasticity Through TLR4 Activation Leading to Opposite Therapeutic Outcome in EAE. *Stem Cell Res Ther* (2020) 11:416. doi: 10.1186/s13287-020-01840-2
21. Zhao X, Liu D, Gong W, Zhao G, Liu L, Yang L, et al. The Toll-Like Receptor 3 Ligand, Poly(I:C), Improves Immunosuppressive Function and Therapeutic Effect of Mesenchymal Stem Cells on Sepsis *via* Inhibiting MiR-143. *Stem Cells* (2014) 32:521–33. doi: 10.1002/stem.1543
22. Lim J-Y, Kim B-S, Ryu D-B, Kim TW, Park G, Min C-K. The Therapeutic Efficacy of Mesenchymal Stromal Cells on Experimental Colitis Was Improved by the IFN-γ and Poly(I:C) Priming Through Promoting the Expression of Indoleamine 2,3-Dioxygenase. *Stem Cell Res Ther* (2021) 12:37. doi: 10.1186/s13287-020-02087-7
23. Leroux L, Descamps B, Tojais NF, Séguy B, Oses P, Moreau C, et al. Hypoxia Preconditioned Mesenchymal Stem Cells Improve Vascular and Skeletal Muscle Fiber Regeneration After Ischemia Through a Wnt4-Dependent Pathway. *Mol Ther J Am Soc Gene Ther* (2010) 18:1545–52. doi: 10.1038/mt.2010.108
24. Saparov A, Ogay V, Nurgozhin T, Jumabay M, Chen WCW. Preconditioning of Human Mesenchymal Stem Cells to Enhance Their Regulation of the Immune Response. *Stem Cells Int* (2016) 2016:3924858. doi: 10.1155/2016/3924858
25. Ishiuchi N, Nakashima A, Doi S, Kanai R, Maeda S, Takahashi S, et al. Serum-Free Medium and Hypoxic Preconditioning Synergistically Enhance the Therapeutic Effects of Mesenchymal Stem Cells on Experimental Renal Fibrosis. *Stem Cell Res Ther* (2021) 12:472. doi: 10.1186/s13287-021-02548-7
26. Nagasaki K, Nakashima A, Tamura R, Ishiuchi N, Honda K, Ueno T, et al. Mesenchymal Stem Cells Cultured in Serum-Free Medium Ameliorate Experimental Peritoneal Fibrosis. *Stem Cell Res Ther* (2021) 12:203. doi: 10.1186/s13287-021-02273-1
27. Pischiutta F, Caruso E, Lugo A, Cavaleiro H, Stocchetti N, Citerio G, et al. Systematic Review and Meta-Analysis of Preclinical Studies Testing Mesenchymal Stromal Cells for Traumatic Brain Injury. *NPJ Regener Med* (2021) 6:71. doi: 10.1038/s41536-021-00182-8
28. Diaz MF, Vaidya AB, Evans SM, Lee HJ, Aertker BM, Alexander AJ, et al. Biomechanical Forces Promote Immune Regulatory Function of Bone Marrow Mesenchymal Stromal Cells. *Stem Cells* (2017) 35:1259–72. doi: 10.1002/stem.2587
29. Chen WT, Hsu WT, Yen MH, Changou CA, Han CL, Chen YJ, et al. Alteration of Mesenchymal Stem Cells Polarity by Laminar Shear Stimulation Promoting Beta-Catenin Nuclear Localization. *Biomaterials* (2019) 190-191:1–10. doi: 10.1016/j.biomaterials.2018.10.026
30. Li JZ, Meng SS, Xu XP, Huang YB, Mao P, Li YM, et al. Mechanically Stretched Mesenchymal Stem Cells Can Reduce the Effects of LPS-Induced Injury on the Pulmonary Microvascular Endothelium Barrier. *Stem Cells Int* (2020) 2020:8861407. doi: 10.1155/2020/8861407
31. Stolberg S, Mccloskey KE. Can Shear Stress Direct Stem Cell Fate? *Biotechnol Prog* (2009) 25:10–9. doi: 10.1002/btpr.124
32. Lee HJ, Li N, Evans SM, Diaz MF, Wenzel PL. Biomechanical Force in Blood Development: Extrinsic Physical Cues Drive Pro-Hematopoietic Signaling. *Differentiation* (2013) 86:92–103. doi: 10.1016/j.diff.2013.06.004
33. Huselstein C, Rahouadj R, De Isla N, Bensoussan D, Stoltz JF, Li YP. Mechanobiology of Mesenchymal Stem Cells: Which Interest for Cell-Based Treatment? *BioMed Mater Eng* (2017) 28:S47–56. doi: 10.3233/BME-171623
34. Lee HJ, Diaz MF, Ewere A, Olson SD, Cox CS Jr., Wenzel PL. Focal Adhesion Kinase Signaling Regulates Anti-Inflammatory Function of Bone Marrow Mesenchymal Stromal Cells Induced by Biomechanical Force. *Cell Signal* (2017) 38:1–9. doi: 10.1016/j.cellsig.2017.06.012
35. Wong SW, Lenzini S, Giovanni R, Knowles K, Shin JW. Matrix Biophysical Cues Direct Mesenchymal Stromal Cell Functions in Immunity. *Acta Biomater* (2021) 133:126–38. doi: 10.1016/j.actbio.2021.07.075
36. Kota DJ, Prabhakara KS, Toledano-Furman N, Bhattarai D, Chen Q, Dicarlo B, et al. Prostaglandin E2 Indicates Therapeutic Efficacy of Mesenchymal Stem Cells in Experimental Traumatic Brain Injury. *Stem Cells* (2017) 35:1416–30. doi: 10.1002/stem.2603
37. George MJ, Prabhakara K, Toledano-Furman NE, Wang YW, Gill BS, Wade CE, et al. Clinical Cellular Therapeutics Accelerate Clot Formation. *Stem Cells Transl Med* (2018) 7:731–9. doi: 10.1002/sctm.18-0015
38. Dominici M, Le Blanc K, Mueller I, Slaper-Cortenbach I, Marini F, Krause D, et al. Minimal Criteria for Defining Multipotent Mesenchymal Stromal Cells. The International Society for Cellular Therapy Position Statement. *Cytotherapy* (2006) 8:315–7. doi: 10.1080/14653240600855905
39. Kota DJ, Dicarlo B, Hetz RA, Smith P, Cox CS Jr., Olson SD. Differential MSC Activation Leads to Distinct Mononuclear Leukocyte Binding Mechanisms. *Sci Rep* (2014) 4:4565. doi: 10.1038/srep04565
40. Afgan E, Baker D, Batut B, Van Den Beek M, Bouvier D, Cech M, et al. The Galaxy Platform for Accessible, Reproducible and Collaborative Biomedical Analyses: 2018 Update. *Nucleic Acids Res* (2018) 46:W537–44. doi: 10.1093/nar/gky379
41. Chen S, Zhou Y, Chen Y, Gu J. Fastp: An Ultra-Fast All-in-One FASTQ Preprocessor. *Bioinformatics* (2018) 34:i884–90. doi: 10.1093/bioinformatics/bty560
42. Kim D, Paggi JM, Park C, Bennett C, Salzberg SL. Graph-Based Genome Alignment and Genotyping With HISAT2 and HISAT-Genotype. *Nat Biotechnol* (2019) 37:907–15. doi: 10.1038/s41587-019-0201-4
43. Li H, Handsaker B, Wysoker A, Fennell T, Ruan J, Homer N, et al. The Sequence Alignment/Map Format and SAMtools. *Bioinformatics* (2009) 25:2078–9. doi: 10.1093/bioinformatics/btp352
44. Garcia-Alcalde F, Okonechnikov K, Carbonell J, Cruz LM, Gotz S, Tarazona S, et al. Qualimap: Evaluating Next-Generation Sequencing Alignment Data. *Bioinformatics* (2012) 28:2678–9. doi: 10.1093/bioinformatics/bts503
45. Liao Y, Smyth GK, Shi W. Featurecounts: An Efficient General Purpose Program for Assigning Sequence Reads to Genomic Features. *Bioinformatics* (2014) 30:923–30. doi: 10.1093/bioinformatics/btt656
46. Love MI, Huber W, Anders S. Moderated Estimation of Fold Change and Dispersion for RNA-Seq Data With Deseq2. *Genome Biol* (2014) 15:550. doi: 10.1186/s13059-014-0550-8
47. Diaz-Arrastia R, Wang KK, Papa L, Sorani MD, Yue JK, Puccio AM, et al. Acute Biomarkers of Traumatic Brain Injury: Relationship Between Plasma Levels of Ubiquitin C-Terminal Hydrolase-L1 and Glial Fibrillary Acidic Protein. *J Neurotrauma* (2014) 31:19–25. doi: 10.1089/neu.2013.3040
48. Liu X, Feng T, Gong T, Shen C, Zhu T, Wu Q, et al. Human Umbilical Cord Mesenchymal Stem Cells Inhibit the Function of Allogeneic Activated Vγ9vδ2 T Lymphocytes *In Vitro*. *BioMed Res Int* (2015) 2015:317801. doi: 10.1155/2015/317801
49. Cruz-Barrera M, Florez-Zapata N, Lemus-Diaz N, Medina C, Galindo CC, Gonzalez-Acero LX, et al. Integrated Analysis of Transcriptome and Secretome From Umbilical Cord Mesenchymal Stromal Cells Reveal New Mechanisms for the Modulation of Inflammation and Immune Activation. *Front Immunol* (2020) 11:575488. doi: 10.3389/fimmu.2020.575488
50. Lu S, Qiao X. Single-Cell Profiles of Human Bone Marrow-Derived Mesenchymal Stromal Cells After IFN-Gamma and TNF-Alpha Licensing. *Gene* (2021) 771:145347. doi: 10.1016/j.gene.2020.145347
51. Mougiakakos D, Jitschin R, Johansson CC, Okita R, Kiessling R, Le Blanc K. The Impact of Inflammatory Licensing on Heme Oxygenase-1-Mediated Induction of Regulatory T Cells by Human Mesenchymal Stem Cells. *Blood* (2011) 117:4826–35. doi: 10.1182/blood-2010-12-324038
52. Dong J-D, Gu Y-Q, Li C-M, Wang C-R, Feng Z-G, Qiu R-X, et al. Response of Mesenchymal Stem Cells to Shear Stress in Tissue-Engineered Vascular Grafts. *Acta Pharmacol Sin* (2009) 30:530–6. doi: 10.1038/aps.2009.40
53. Karp JM, Leng Teo GS. Mesenchymal Stem Cell Homing: The Devil Is in the Details. *Cell Stem Cell* (2009) 4:206–16. doi: 10.1016/j.stem.2009.02.001
54. Nam J, Aguda BD, Rath B, Agarwal S. Biomechanical Thresholds Regulate Inflammation Through the NF-kappaB Pathway: Experiments and Modeling. *PloS One* (2009) 4:e5262. doi: 10.1371/journal.pone.0005262

55. Dan P, Velot É., Decot V, Menu P. The Role of Mechanical Stimuli in the Vascular Differentiation of Mesenchymal Stem Cells. *J Cell Sci* (2015) 128:2415–22. doi: 10.1242/jcs.167783
56. Angelos MG, Brown MA, Satterwhite LL, Levering VW, Shaked NT, Truskey GA. Dynamic Adhesion of Umbilical Cord Blood Endothelial Progenitor Cells Under Laminar Shear Stress. *Biophys J* (2010) 99:3545–54. doi: 10.1016/j.bpj.2010.10.004
57. Hummer J, Koc J, Rosenhahn A, Lee-Thedieck C. Microfluidic Shear Force Assay to Determine Cell Adhesion Forces. *Methods Mol Biol* (2019) 2017:71–84. doi: 10.1007/978-1-4939-9574-5_6
58. Meisel R, Zibert A, Laryea M, Gobel U, Daubener W, Dilloo D. Human Bone Marrow Stromal Cells Inhibit Allogeneic T-Cell Responses by Indoleamine 2,3-Dioxygenase-Mediated Tryptophan Degradation. *Blood* (2004) 103:4619–21. doi: 10.1182/blood-2003-11-3909
59. Wu H, Gong J, Liu Y. Indoleamine 2, 3-Dioxygenase Regulation of Immune Response (Review). *Mol Med Rep* (2018) 17:4867–73. doi: 10.3892/mmr.2018.8537
60. Najar M, Raicevic G, Boufker HI, Kazan HF, Bruyn CD, Meuleman N, et al. Mesenchymal Stromal Cells Use PGE2 to Modulate Activation and Proliferation of Lymphocyte Subsets: Combined Comparison of Adipose Tissue, Wharton's Jelly and Bone Marrow Sources. *Cell Immunol* (2010) 264:171–9. doi: 10.1016/j.cellimm.2010.06.006
61. Hegyi B, Kudlik G, Monostori É., Uher F. Activated T-Cells and Pro-Inflammatory Cytokines Differentially Regulate Prostaglandin E2 Secretion by Mesenchymal Stem Cells. *Biochem Biophys Res Commun* (2012) 419:215–20. doi: 10.1016/j.bbrc.2012.01.150
62. Ribeiro A, Laranjeira P, Mendes S, Velada I, Leite C, Andrade P, et al. Mesenchymal Stem Cells From Umbilical Cord Matrix, Adipose Tissue and Bone Marrow Exhibit Different Capability to Suppress Peripheral Blood B, Natural Killer and T Cells. *Stem Cell Res Ther* (2013) 4:125. doi: 10.1186/scrt336
63. Mattar P, Bieback K. Comparing the Immunomodulatory Properties of Bone Marrow, Adipose Tissue, and Birth-Associated Tissue Mesenchymal Stromal Cells. *Front Immunol* (2015) 6. doi: 10.3389/fimmu.2015.00560
64. Belge KU, Dayyani F, Horelt A, Siedlar M, Frankenberger M, Frankenberger B, et al. The Proinflammatory CD14+CD16+DR++ Monocytes are a Major Source of TNF. *J Immunol* (2002) 168:3536–42. doi: 10.4049/jimmunol.168.7.3536
65. Mittal M, Tiruppathi C, Nepal S, Zhao YY, Grzych D, Soni D, et al. TNFalpha-Stimulated Gene-6 (TSG6) Activates Macrophage Phenotype Transition to Prevent Inflammatory Lung Injury. *Proc Natl Acad Sci U.S.A.* (2016) 113:E8151–8. doi: 10.1073/pnas.1614935113
66. Watanabe J, Shetty AK, Hattiangady B, Kim D-K, Foraker JE, Nishida H, et al. Administration of TSG-6 Improves Memory After Traumatic Brain Injury in Mice. *Neurobiol Dis* (2013) 59:86–99. doi: 10.1016/j.nbd.2013.06.017
67. Li R, Liu W, Yin J, Chen Y, Guo S, Fan H, et al. TSG-6 Attenuates Inflammation-Induced Brain Injury *via* Modulation of Microglial Polarization in SAH Rats Through the SOCS3/STAT3 Pathway. *J Neuroinflamm* (2018) 15:231. doi: 10.1186/s12974-018-1279-1
68. Sebastián VP, Salazar GA, Coronado-Arrázola I, Schultz BM, Vallejos OP, Berkowitz L, et al. Heme Oxygenase-1 as a Modulator of Intestinal Inflammation Development and Progression. *Front Immunol* (2018) 9. doi: 10.3389/fimmu.2018.01956
69. Morganti-Kossman MC, Lenzlinger PM, Hans V, Stahel P, Csuka E, Ammann E, et al. Production of Cytokines Following Brain Injury: Beneficial and Deleterious for the Damaged Tissue. *Mol Psychiatry* (1997) 2:133–6. doi: 10.1038/sj.mp.4000227
70. Walker PA, Harting MT, Jimenez F, Shah SK, Pati S, Dash PK, et al. Direct Intrathecal Implantation of Mesenchymal Stromal Cells Leads to Enhanced Neuroprotection *via* an NFkappaB-Mediated Increase in Interleukin-6 Production. *Stem Cells Dev* (2010) 19:867–76. doi: 10.1089/scd.2009.0188
71. Metcalfe SM. LIF in the Regulation of T-Cell Fate and as a Potential Therapeutic. *Genes Immun* (2011) 12:157–68. doi: 10.1038/gene.2011.9
72. Erta M, Quintana A, Hidalgo J. Interleukin-6, a Major Cytokine in the Central Nervous System. *Int J Biol Sci* (2012) 8:1254–66. doi: 10.7150/ijbs.4679
73. Zhang B, Zhang HX, Shi ST, Bai YL, Zhe X, Zhang SJ, et al. Interleukin-11 Treatment Protected Against Cerebral Ischemia/Reperfusion Injury. *BioMed Pharmacother* (2019) 115:108816. doi: 10.1016/j.biopha.2019.108816
74. Abdipranoto-Cowley A, Park JS, Croucher D, Daniel J, Henshall S, Galbraith S, et al. Activin A is Essential for Neurogenesis Following Neurodegeneration. *Stem Cells (Dayton Ohio)* (2009) 27:1330–46. doi: 10.1002/stem.80
75. Shah NJ, Mao AS, Shih TY, Kerr MD, Sharda A, Raimondo TM, et al. An Injectable Bone Marrow-Like Scaffold Enhances T Cell Immunity After Hematopoietic Stem Cell Transplantation. *Nat Biotechnol* (2019) 37:293–302. doi: 10.1038/s41587-019-0017-2
76. Sun C, Zhang K, Yue J, Meng S, Zhang X. Deconstructing Transcriptional Variations and Their Effects on Immunomodulatory Function Among Human Mesenchymal Stromal Cells. *Stem Cell Res Ther* (2021) 12:53. doi: 10.1186/s13287-020-02121-8

Conflict of Interest: SO has received research support from Athersys, CBR Systems, Hope Bio, Generate Life Sciences, Cellvation, and Biostage. CC has received research support from Athersys, CBR Systems, Hope Bio, Biostage, Generate Life Sciences, and Cellvation, and is on the Scientific Advisory Board of Cellvation and Generate Life Sciences. BG is on the Scientific Advisory Board of Cellvation.

The remaining authors declare that the research was conducted in the absence of any commercial or financial relationships that could be construed as a potential conflict of interest.

Publisher's Note: All claims expressed in this article are solely those of the authors and do not necessarily represent those of their affiliated organizations, or those of the publisher, the editors and the reviewers. Any product that may be evaluated in this article, or claim that may be made by its manufacturer, is not guaranteed or endorsed by the publisher.

frontiers | Frontiers in Immunology

OPINION
published: 15 July 2022
doi: 10.3389/fimmu.2022.967731

Incorporating Cryopreservation Evaluations Into the Design of Cell-Based Drug Delivery Systems: An Opinion Paper

Marlene Davis Ekpo[1], *Jingxian Xie*[1], *Xiangjian Liu*[1], *Raphael Onuku*[2], *George Frimpong Boafo*[1] *and Songwen Tan*[1]*

[1] Xiangya School of Pharmaceutical Sciences, Central South University, Changsha, China, [2] Department of Pharmaceutical and Medicinal Chemistry, Faculty of Pharmaceutical Sciences, University of Nigeria, Nsukka, Nigeria

Keywords: mesenchymal stem cells, cryopreservation, cryoprotectants, chemotherapy, targeted drug delivery

OPEN ACCESS

Edited by:
Guido Moll, Charité Universitätsmedizin Berlin, Germany

Reviewed by:
Kelvin G. M. Brockbank, Cell and Tissue Systems, United States

***Correspondence:**
Songwen Tan
songwen.tan@csu.edu.cn

Specialty section:
This article was submitted to Vaccines and Molecular Therapeutics, a section of the journal Frontiers in Immunology

Received: *13 June 2022*
Accepted: *22 June 2022*
Published: *15 July 2022*

Citation:
Ekpo MD, Xie J, Liu X, Onuku R, Boafo GF and Tan S (2022) Incorporating Cryopreservation Evaluations Into the Design of Cell-Based Drug Delivery Systems: An Opinion Paper. Front. Immunol. 13:967731. doi: 10.3389/fimmu.2022.967731

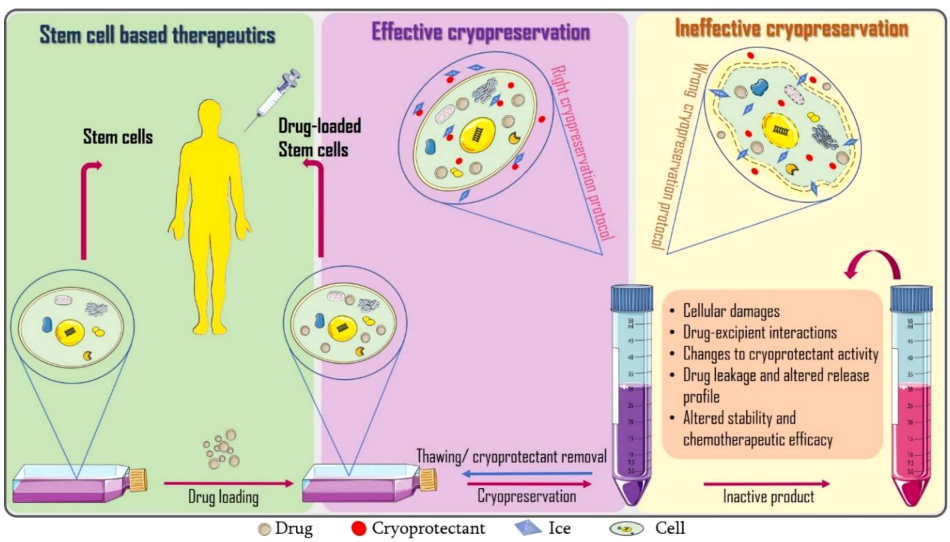

GRAPHICAL ABSTRACT | Incorporating cryopreservation evaluations into the design of cell-based drug delivery systems.

INTRODUCTION

Stem cell based therapies capitalize on the desirable features of stem cells with possible modifications to enhance their therapeutic potentials (1). In pharmaceutics and biotechnology, cells have been explored as vehicles for targeted drug delivery (2) especially in cancer treatment because conventional chemotherapy and gene therapy are still limited by factors including poor

pharmacokinetics, accumulation in non-cancerous tissues, undesirable side effects and toxicity (3). If these cell-based drug formulations become standardized, cryopreservation is currently the most probable means to ensure long-term storage (4).

Cryopreservation is an indispensable step required for the stability of cell therapies and variables including type and concentration of cryoprotectants, cooling/thawing rate and freezing temperature are critical to ensuring acceptable post-thaw recovery (4). Prior cryopreservation research has revealed that a balance in interactions between ice, water and cryoprotectants is required for optimized cryopreservation outcome. The post-cryopreservation assessments performed involves those to ascertain cell viability, function, and so on (5).

We perceive that drug loading can further alter the dynamics of ice, cryoprotectant and cell interactions resulting to failure of the dosage form. To the best of our knowledge, there are limited studies precisely aimed at assessing the post-thaw stability and therapeutic efficacy of drug loaded (stem) cells. Only few researchers like Lisini et al. (6) have reasoned in this direction. They investigated the post-cryopreservation viability, recovery and release of paclitaxel loaded mesenchymal stem cells after 21 days and suggested further studies should extend this storage time to at least 12 months. Close to evaluating the effects of cryopreservation on drug delivery systems is freeze-thaw stability studies which can provide us with insights on possible deformations to frozen drug delivery systems as presented in **Table 1**.

Here in, we opine that research aimed at determining optimal cryogenic storage conditions should be incorporated into the design of cell-based formulations. We discuss some of the parameters that should be evaluated including biocompatibility of cryoprotectants and drugs, cryoprotectant-drug-ice interactions, possible changes to drug entrapment efficacy, drug release, cell viability, and therapeutic efficacy. Suitable molecular dynamics and energy transfer models can be used to decipher the underlying mechanism(s) of drug induced changes in cryopreservation outcomes.

STEM CELLS IN DRUG DELIVERY

Conventional chemotherapy are still limited by some factors including poor pharmacokinetics, accumulation in non-cancerous tissues, and toxicity (18). Stem cells are applicable in overcoming these limitations as they can be engineered and used as carriers or vehicles for targeted drug delivery based on the proposition that mesenchymal stem cells (MSCs) undergo chemotaxis toward tumors following the release of chemo-attractants like vascular endothelial growth factor (VEGF) (19). Gao et al. showed that MSCs are promising in this regard as the stem cells carrying paclitaxel loaded nanoparticles (NPs) were able to deliver their therapeutic pay-load to murine orthotopic glioma cells (20). Furthermore, paclitaxel loaded human olfactory bulb neural stem cells (Hu-OBNSCs) and

TABLE 1 | Effects of freezing and freeze thaw stability studies of some pharmaceutical formulations.

Formulation	Evaluation	Effect of Cryopreservation/freeze-thaw	REF
Paclitaxel loaded mesenchymal stem cells	Viability, recovery, drug release.	Retained viability and potency of the formulation but loss of cell proliferation and differentiation.	(6)
Hydroxyzine- and cetirizine loaded Multilamellar vesicles (liposomes)	Entrapment efficiency	Percentage entrapment of Hydroxyzine liposomes decreased considerably after 1 month but improved by pH adjustment	(7)
Humanized monoclonal antibody (IgG1)	Freeze-thaw aggregation	Noncovalently linked aggregates composed of native-like monomers were observed after freeze-thaw.	(8)
Recombinant human growth hormone	Safety/immunotoxicity of protein aggregates	Freeze-thaw induced aggregates elicited immunogenicity in mouse model.	(9)
Ethylene glycol/water-based nanofluids containing Al_2O_3 nanoparticles	Suspension stability, particle size distribution and thermal conductivity	The assessed parameters were not affected at lower temperature	(10)
Monoclonal Antibody (IgG2)	Fluctuations in buffer pH	Buffer pH increased at below 0° C with sodium phosphate buffer having the greatest change in pH when going from 25 to -30 ° C.	(11)
Insulin loaded PVA hydrogels	Insulin release	Higher freeze-thaw cycles effected insulin release rate and total released amount (from 66 to 38%) negatively.	(12)
Gentamicin palmitate salt and gentamicin sulfate salt loaded bone grafts	Drug release rate and antibiotic activity	Antibiotic activity was not significantly altered after freezing for up to 6 months.	(13)
PLGA microspheres encapsulating FITC-labled dextran	Effect of freezing on sustained release	Freezing increased initial/burst with rapid release kinetic profiles due to high porosity of frozen microspheres.	(14)
Diflunisal loaded chitosan-PVA hydrogels	Swelling capacity, morphology, porosity, drug loading and release profile	Lower freezing temperatures or longer freezing times, resulted in higher porosity and smaller pore sizes and increased intrusion volume. Increasing the number of freezing cycles produced hydrogels with more defined pores and reduced swelling degree.	(15)
Insulin-loaded PLGA nanoparticles	Stability and bioactivity	Co-encapsulation of cryoprotectants alleviated freeze damage and preserved insulin stability and bioactivity.	(16)
Fluconazole-loaded multilamellar liposome	Stability and drug entrapment efficiency	Addition of cryoprotectants (trehalose) before lyophilization produced non-compact and easily reconstituted cakes. Fluconazole entrapment improved significantly (from 63.452% to 91.877%) on addition of trehalose.	(17)

mesenchymal stromal cells have been effective in inhibiting the progression of glioblastoma (20–22). MSCs have also been applied in the delivery of immune biomolecules like cytokines to tumor sites. For instance, transduction of MSCs with an adenoviral expression vector bearing interferon-β gene has been shown to increase the production of interferon-β at the cancer site (23). Similarly, delivery of interleukin expressing MSCs has promoted cytotoxicity to tumor cells via the activation of endogenous natural killer (NK) cells and lymphocytes (24). Extracellular vesicles released by stem cells have also been explored as cancer targeted drug delivery vesicles because of their biocompatibility and minimal immunogenicity. Abnous et al. applied exosomes as carriers in the delivery of doxorubicin to colorectal tumor and results showed that the formulation had better pharmacokinetic properties, tumor location and suppression compared to the free drug (25). These research efforts have shown tremendous potential for clinical application and would be a great drawback if the formulations are rendered inactive by cryopreservation.

POSSIBLE EFFECTS OF CRYOPRESERVATION AND ASSESSMENTS TO CONSIDER IN CRYOPRESERVATION OF CELL-BASED DRUG DELIVERY SYSTEMS

Cellular Damage

A growing body of evidence suggests conflicting results regarding the effects of cryopreservation and thawing of stem cells, including extensive physical and biological stress, apoptosis and necrosis, mitochondrial damage, changes in basal respiration and ATP production, damage to cellular structure, telomere shortening and cellular senescence (26), as well as oxidative damages (DNA damage, lipid peroxidation, protein oxidation) from reactive oxygen species released during freezing (27, 28), all of which can inadvertently lead to reduced therapeutic efficacy (29, 30). More details on the principles and protocols for evaluating stem cell viability after cryopreservation can be found in a review by Xie et al. (5). In addition to the potential cryopreservation induced cellular damage (s), we speculate that inclusion of drugs can affect cryopreservation outcome resulting to failure of the dosage form. Lisini et al. reports the loss of proliferation and differentiation in paclitaxel loaded MSCs (6).

Drug-Excipient Interactions and Changes to Cryoprotectant Activity

The activity of cryoprotectants may be affected by the inclusion of drugs and other excipients. Therefore, the drugs should be analyzed for possible effects on ice (ice recrystallization inhibition (IRI), thermal hysteresis and ice shaping). In fact, a serendipitous discovery of this sort was made by Liu et al. (31) where medium molecular weight sodium hyaluronate (MSH) devoid of prior IRI activity showed significant IRI activity in the presence of red blood cells through an unknown mechanism. The observed IRI activity would imply adjustments to the cryopreservation protocol for red blood cells using MSH. To understand how cryoprotectants, drugs, ice and other cellular components may interact, molecular dynamics modelling studies like ice crystallization (isothermal crystallization) kinetics, and heat and mass transfer modelling (32) can be performed. Furthermore, some cryoprotectants may possess some pharmacological activity that may be incompatible with the loaded drugs or react with drugs to produce toxic effects. Therefore, drug-excipient compatibility studies have to be performed at preformulation to rule out possible chemical or physical interactions that could affect quality, manufacturability and performance of the final product. Other concerns would be if the post-thaw removal of cryoprotectants (especially penetrating cryoprotectants like DMSO and proline) could affect drug entrapment and release properties as discussed in the next section.

Altered Intracellular Drug Entrapment and Drug Release

Drug release is an important determinant of stability and therapeutic effectiveness of formulations (33). If the drugs leak or the release profile is altered, therapeutic failure is imminent. Other dosage forms can provide cues on how freezing could affect drug entrapment. Kim et al. proposes that the freezing phase of freeze-drying is most probably responsible for the high porosity of polylactic-co-glycolic acid (PLGA) microspheres. Freezing converts the free water molecules present within the pores and their interconnected channels into ice crystals. Following sublimation, the empty cavities spaces retain the shape and dimension of the ice crystal. Cracking (micro-channeling) of the PLGA polymer walls can also arise from overstretching of the pores during ice recrystallization thus further increasing the porosity of the microspheres which in turn is not favorable for sustained or prolonged drug release (14). The application of cryoprotectants in stabilizing lyophilized preparations has been explored in several studies (34–37).

Figueroa-Pizano et al. utilized freezing-thawing in the fabrication of diflunisal loaded chitosan-polyvinyl alcohol (PVA) hydrogels. They discovered that the use of either lower temperatures or prolonged freezing resulted in hydrogels with higher porosity, smaller pores sizes and less swelling capacity, which may not support prolonged drug release (15). Also, freeze-thawing notably reduced the entrapment efficacy of hydroxyzine and cetirizine loaded liposomes (7). With regard to cells, any factor that causes the membrane to lose its integrity would result in drug leakage and distortion of the release profile. These factors include degradation of cell membrane proteins, puncturing of the cell membrane by ice crystals, dehydration, etc. Therefore, cryoprotectants must be carefully screened before selection. Although Lisini et al. reports preserved post-thaw release capacity of paclitaxel based on antitumor potency test (6), it would still be necessary to quantify the drug released at each time for a better understanding of the drug release kinetics and also compare the drug entrapment before and after cryopreservation.

Altered Stability and Chemotherapeutic Efficacy

Stability and therapeutic efficacy are paramount parameters to be assessed during formulation studies. But presently, there is a gap in literature to address the post-cryopreservation performance of cell-based formulations. Lisini et al. reports that efficacy of paclitaxel loaded stem cells was not significantly altered by cryopreservation (6). Fonte et al. assessed the effect of freezing on the structural stability of encapsulated insulin prior to lyophilization (16). Their results showed pH fluctuations caused by temperature-related changes to crystallization, pKas, solubility, eutectics, and cryoconcentration (11). Coraça-Huber et al. examines the post-thaw antibiotic activity of gentamicin loaded bone grafts following cryopreservation at -80°C for up to six (6) months. Results showed uncompromised antibiotic activity of the formulations against *Staphylococcus aureus* (13). Freezing and thawing can induce damage of protein therapeutics (antibodies, lipids, proteins, DNA, genes) resulting in depletion or total loss of therapeutic activity. Protein aggregation can be as a result of altered conformational stability at water–ice interface or cryoconcentration of solutes and proteins in the liquid phase (38). Cryoconcentration frequently occurs during slow freezing where various peptide components and other solutes separate from the water–ice interface creating a concentration gradient proximal to the ice front (39). The resultant phase separation and probable loss of pH buffering are key factors responsible for protein aggregation and structural damage. The concentrated solutes can also contribute to aggregation by disturbances to protein thermodynamic stability. On the other hand, less water recrystallization occurs during rapid freezing leading to the formation of smaller ice crystals causing exposure of proteins and other solutes to a greater water-ice crystal interface where they can be adsorbed and concentrated leading to increased aggregation, loss of structural integrity and therapeutic efficacy. Freeze-thaw induced protein aggregation and perturbed therapeutic activity of a model monoclonal antibody (mAb) therapeutic- Trastuzumab can be found in a study by Dash and coworkers (40). Hence, freezing protocols must be designed and optimized to favor the cryopreserved material (41). Horn et al. confirms the effectiveness of cryoprotectants for maintaining stability of immunoglobulin (IGG) solutions. They discovered significantly higher formation of monomer aggregates IGG formulations without cryoprotectants (42). Similarly, Jain et al. reports significant reduction in freeze-thaw damage of mAb-1 attained by prior optimization of cryopreservation protocols during pilot scale studies (43). Furthermore, Liu and co-authors suggest that freezing induced disturbances to the tertiary structure of mAbs are reversible or irreversible depending on the pH of the system or the type of excipients included in the formulation (44). Therefore, thorough research has to be conducted before selecting excipients (cryoprotectants and buffers) for the formulation and cryopreservation of cell-based drug delivery systems.

CONCLUSION

Based on the complexity of novel cell-based drug delivery systems, it would be detrimental to assume the absence of alterations to the formulation after cryopreservation. To achieve the desired therapeutic effect, an equilibrium must be maintained between the several factors that could influence product stability. These factors should include but are not limited to cryoprotectant type and concentration, drug type and concentration, cell type, freeze/thaw rate, mode of freezing. The optimal conditions for storage and transportation can only be determined through scalable and reproducible research. As observed from lisini et al., the paclitaxel loaded stem cells possessed appreciable chemotherapeutic activity after cryopreservation with 10% dimethyl sulfoxide (DMSO) supplemented with sodium chloride (0.9%w/v) and 5% human albumin but these results cannot be extrapolated to other cell types, cryoprotectants, drugs and storage duration. In fact, there is a growing need to find better substitutes to DMSO for cryopreservation owing to its unwanted effect on cryopreserved material and in humans after clinical application. Hopefully, future research in this direction will serve as guide to perform similar studies for other drug delivery systems that requires freezing or cryopreservation as an indispensable technique during fabrication, storage and transportation. Future studies can also investigate cryoprotectants with drug carrier properties e.g., graphene oxide, nanocellulose and PVA. If this is achievable the post-thaw removal of such cryoprotectants before clinical application would be eliminated.

AUTHOR CONTRIBUTIONS

Conceptualization, ME, ST. Writing—original draft preparation, ME, JX, RO. Writing—review and editing, ME, XL, GB, and ST. Supervision and approval, ST. All authors contributed to the article and approved the submitted version.

REFERENCES

1. Liu Z, Cheung HH. Stem Cell-Based Therapies for Parkinson Disease. *Int J Mol Sci* (2020) 21(21):8060. doi: 10.3390/ijms21218060
2. Tan S, Wu T, Zhang D, Zhang Z. Cell or Cell Membrane-Based Drug Delivery Systems. *Theranostics* (2015) 5(8):863–81. doi: 10.7150/thno.11852
3. Kusuma GD, Frith JE, Sobey CG, Lim R. Editorial: Stem Cells as Targeted Drug Delivery Vehicles. *Front Pharmacol* (2020) 11:614730. doi: 10.3389/fphar.2020.614730
4. Meneghel J, Kilbride P, Morris GJ. Cryopreservation as a Key Element in the Successful Delivery of Cell-Based Therapies-A Review. *Front Med (Lausanne)* (2020) 7:592242. doi: 10.3389/fmed.2020.592242
5. Xie J, Ekpo MD, Xiao J, Zhao H, Bai X, Liang Y, et al. Principles and Protocols For Post-Cryopreservation Quality Evaluation of Stem Cells in Novel Biomedicine. *Front Pharmacol* (2022) 13:907943. doi: 10.3389/fphar.2022.907943
6. Lisini D, Nava S, Frigerio S, Pogliani S, Maronati G, Marcianti A, et al. Automated Large-Scale Production of Paclitaxel Loaded Mesenchymal

Stromal Cells for Cell Therapy Applications. *Pharmaceutics* (2020) 12(5):411. doi: 10.3390/pharmaceutics12050411
7. Elzainy AA, Gu X, Simons FE, Simons KJ. Hydroxyzine- and Cetirizine-Loaded Liposomes: Effect of Duration of Thin Film Hydration, Freeze-Thawing, and Changing Buffer pH on Encapsulation and Stability. *Drug Dev Ind Pharm* (2005) 31(3):281–91. doi: 10.1081/ddc-52070
8. Hawe A, Kasper JC, Friess W, Jiskoot W. Structural Properties of Monoclonal Antibody Aggregates Induced by Freeze-Thawing and Thermal Stress. *Eur J Pharm Sci* (2009) 38(2):79–87. doi: 10.1016/j.ejps.2009.06.001
9. Fradkin AH, Carpenter JF, Randolph TW. Immunogenicity of Aggregates of Recombinant Human Growth Hormone in Mouse Models. *J Pharm Sci* (2009) 98(9):3247–64. doi: 10.1002/jps.21834
10. Choi TJ, Jang SP, Jung DS, Lim HM, Byeon YM, Choi IJ. Effect of the Freeze-Thaw on the Suspension Stability and Thermal Conductivity of EG/Water-Based Al2O3 Nanofluids. *J Nanomaterials* (2019) 2019:1–8. doi: 10.1155/2019/2076341
11. Kolhe P, Amend E, Singh SK. Impact of Freezing on pH of Buffered Solutions and Consequences for Monoclonal Antibody Aggregation. *Biotechnol Prog* (2010) 26(3):727–33. doi: 10.1002/btpr.377
12. Cai Y, Che J, Yuan M, Shi X, Chen W, Yuan WE. Effect of Glycerol on Sustained Insulin Release From PVA Hydrogels and Its Application in Diabetes Therapy. *Exp Ther Med* (2016) 12(4):2039–44. doi: 10.1155/2019/2076341
13. Coraca-Huber DC, Wurm A, Fille M, Hausdorfer J, Nogler M, Kuhn KD. Effect of Freezing on the Release Rate of Gentamicin Palmitate and Gentamicin Sulfate From Bone Tissue. *J Orthop Res* (2014) 32(6):842–7. doi: 10.1002/jor.22602
14. Kim TH, Park TG. Critical Effect of Freezing/Freeze-Drying on Sustained Release of FITC-Dextran Encapsulated Within PLGA Microspheres. *Int J Pharm* (2004) 271(1-2):207–14. doi: 10.1016/j.ijpharm.2003.11.021
15. Figueroa-Pizano MD, Velaz I, Penas FJ, Zavala-Rivera P, Rosas-Durazo AJ, Maldonado-Arce AD, et al. Effect of Freeze-Thawing Conditions for Preparation of Chitosan-Poly (Vinyl Alcohol) Hydrogels and Drug Release Studies. *Carbohydr Polym* (2018) 195:476–85. doi: 10.1016/j.carbpol.2018.05.004
16. Fonte P, Andrade F, Azevedo C, Pinto J, Seabra V, van de Weert M, et al. Effect of the Freezing Step in the Stability and Bioactivity of Protein-Loaded PLGA Nanoparticles Upon Lyophilization. *Pharm Res* (2016) 33(11):2777–93. doi: 10.1007/s11095-016-2004-3
17. El-Nesr OH, Yahiya SA, El-Gazayerly ON. Effect of Formulation Design and Freeze-Drying on Properties of Fluconazole Multilamellar Liposomes. *Saudi Pharm J* (2010) 18(4):217–24. doi: 10.1016/j.jsps.2010.07.003
18. Senapati S, Mahanta AK, Kumar S, Maiti P. Controlled Drug Delivery Vehicles for Cancer Treatment and Their Performance. *Signal Transduct Target Ther* (2018) 3(1):7. doi: 10.1038/s41392-017-0004-3
19. Szewc M, Radzikowska-Buchner E, Wdowiak P, Kozak J, Kuszta P, Niezabitowska E, et al. MSCs as Tumor-Specific Vectors for the Delivery of Anticancer Agents-A Potential Therapeutic Strategy in Cancer Diseases: Perspectives for Quinazoline Derivatives. *Int J Mol Sci* (2022) 23(5):2745. doi: 10.3390/ijms23052745
20. Wang X, Gao J, Ouyang X, Wang J, Sun X, Lv Y. Mesenchymal Stem Cells Loaded With Paclitaxel-Poly(Lactic-Co-Glycolic Acid) Nanoparticles for Glioma-Targeting Therapy. *Int J Nanomed* (2018) 13:5231–48. doi: 10.2147/IJN.S167142
21. Marei H, Casalbore P, Althani A, Coccè V, Cenciarelli C, Alessandri G, et al. Human Olfactory Bulb Neural Stem Cells (Hu-OBNSCs) Can Be Loaded With Paclitaxel and Used to Inhibit Glioblastoma Cell Growth. *Pharmaceutics* (2019) 11(1):45. doi: 10.3390/pharmaceutics11010045
22. Pacioni S, D'Alessandris QG, Giannetti S, Morgante L, De Pascalis I, Coccè V, et al. Mesenchymal Stromal Cells Loaded With Paclitaxel Induce Cytotoxic Damage in Glioblastoma Brain Xenografts. *Stem Cell Res Ther* (2015) 6:194. doi: 10.1186/s13287-015-0185-z
23. Javan MR, Khosrojerdi A, Moazzeni SM. New Insights Into Implementation of Mesenchymal Stem Cells in Cancer Therapy: Prospects for Anti-Angiogenesis Treatment. *Front Oncol* (2019) 9:840. doi: 10.3389/fonc.2019.00840
24. Okada H, Pollack IF. Cytokine Gene Therapy for Malignant Glioma. *Expert Opin Biol Ther* (2004) 4(10):1609–20. doi: 10.1517/14712598.4.10.1609
25. Bagheri E, Abnous K, Farzad SA, Taghdisi SM, Ramezani M, Alibolandi M. Targeted Doxorubicin-Loaded Mesenchymal Stem Cells-Derived Exosomes as a Versatile Platform for Fighting Against Colorectal Cancer. *Life Sci* (2020) 261:118369. doi: 10.1016/j.lfs.2020.118369
26. Cottle C, Porter AP, Lipat A, Turner-Lyles C, Nguyen J, Moll G, et al. Impact of Cryopreservation and Freeze-Thawing on Therapeutic Properties of Mesenchymal Stromal/Stem Cells and Other Common Cellular Therapeutics. *Curr Stem Cell Rep* (2022) 8(2):72–92. doi: 10.1007/s40778-022-00212-1
27. Davies OG, Smith AJ, Cooper PR, Shelton RM, Scheven BA. The Effects of Cryopreservation on Cells Isolated From Adipose, Bone Marrow and Dental Pulp Tissues. *Cryobiology* (2014) 69(2):342–7. doi: 10.1016/j.cryobiol.2014.08.003
28. Karimi-Busheri F, Rasouli-Nia A, Weinfeld M. Key Issues Related to Cryopreservation and Storage of Stem Cells and Cancer Stem Cells: Protecting Biological Integrity. *Adv Exp Med Biol* (2016) 951:1–12. doi: 10.1007/978-3-319-45457-3_1
29. Moll G, Alm JJ, Davies LC, von Bahr L, Heldring N, Stenbeck-Funke L, et al. Do Cryopreserved Mesenchymal Stromal Cells Display Impaired Immunomodulatory and Therapeutic Properties? *Stem Cells* (2014) 32(9):2430–42. doi: 10.1002/stem.1729
30. François M, Copland IB, Yuan S, Romieu-Mourez R, Waller EK, Galipeau J. Cryopreserved Mesenchymal Stromal Cells Display Impaired Immunosuppressive Properties as a Result of Heat-Shock Response and Impaired Interferon-γ Licensing. *Cytotherapy* (2012) 14(2):147–52. doi: 10.3109/14653249.2011.623691
31. Liu X, Hu Y, Pan Y, Fang M, Tong Z, Sun Y, et al. Exploring the Application and Mechanism of Sodium Hyaluronate in Cryopreservation of Red Blood Cells. *Mater Today Bio* (2021) 12:100156. doi: 10.1016/j.mtbio.2021.100156
32. Geng H, Liu X, Shi G, Bai G, Ma J, Chen J, et al. Graphene Oxide Restricts Growth and Recrystallization of Ice Crystals. *Angew Chem Int Ed Engl* (2017) 56(4):997–1001. doi: 10.1002/anie.201609230
33. Lu X-Y, Wu D-C, Li Z-J, Chen G-Q. Polymer nanoparticles. *Prog Mol Biol Transl Sci*(2011)104:299–233. doi: 10.1016/B978-0-12-416020-0.00007-3
34. Amis T, Renukuntla J, Bolla PK, Clark B. Selection of Cryoprotectant in Lyophilization of Progesterone-Loaded Stearic Acid Solid Lipid Nanoparticles. *Pharmaceutics* (2020) 12:892. doi: 10.3390/pharmaceutics12090892
35. Bodzen A, Jossier A, Dupont S, Mousset P-Y, Beney L, Lafay S, et al. Design of a New Lyoprotectant Increasing Freeze-Dried Lactobacillus Strain Survival to Long-Term Storage. *BMC Biotechnol* (2021) 21(1):66. doi: 10.1186/s12896-021-00726-2
36. Lee H, Jiang D, Pardridge WM. Lyoprotectant Optimization for the Freeze-Drying of Receptor-Targeted Trojan Horse Liposomes for Plasmid DNA Delivery. *Mol Pharm* (2020) 17(6):2165–74. doi: 10.1021/acs.molpharmaceut.0c00310
37. Li J, Hu M, Xu H, Yu X, Ye F, Wang K, et al. Influence of Type and Proportion of Lyoprotectants on Lyophilized Ginsenoside Rg3 Liposomes. *J Pharm Pharmacol* (2016) 68(1):1–13. doi: 10.1111/jphp.12489
38. Cordes AA, Carpenter JF, Randolph TW. Accelerated Stability Studies of Abatacept Formulations: Comparison of Freeze-Thawing- and Agitation-Induced Stresses. *J Pharm Sci* (2012) 101(7):2307–15. doi: 10.1002/jps.23150
39. Rathore N, Rajan RS. Current Perspectives on Stability of Protein Drug Products During Formulation, Fill and Finish Operations. *Biotechnol Prog* (2008) 24(3):504–14. doi: 10.1021/bp070462h
40. Dash R, Rathore AS. Freeze Thaw and Lyophilization Induced Alteration in mAb Therapeutics: Trastuzumab as a Case Study. *J Pharm BioMed Anal* (2021) 201:114122. doi: 10.1016/j.jpba.2021.114122
41. Le Basle Y, Chennell P, Tokhadze N, Astier A, Sautou V. Physicochemical Stability of Monoclonal Antibodies: A Review. *J Pharm Sci* (2020) 109(1):169–90. doi: 10.1016/j.xphs.2019.08.009
42. Horn J, Jena S, Aksan A, Friess W. Freeze/thaw of IGG Solutions. *Eur J Pharm Biopharm* (2019) 134:185–9. doi: 10.1016/j.ejpb.2018.12.001
43. Jain K, Salamat-Miller N, Taylor K. Freeze-Thaw Characterization Process to Minimize Aggregation and Enable Drug Product Manufacturing of Protein Based Therapeutics. *Sci Rep* (2021) 11(1):11332. doi: 10.1038/s41598-021-90772-9

44. Liu L, Braun LJ, Wang W, Randolph TW, Carpenter JF. Freezing-Induced Perturbation of Tertiary Structure of a Monoclonal Antibody. *J Pharm Sci* (2014) 103(7):1979–86. doi: 10.1002/jps.24013

Conflict of Interest: The authors declare that the research was conducted in the absence of any commercial or financial relationships that could be construed as a potential conflict of interest.

Publisher's Note: All claims expressed in this article are solely those of the authors and do not necessarily represent those of their affiliated organizations, or those of the publisher, the editors and the reviewers. Any product that may be evaluated in this article, or claim that may be made by its manufacturer, is not guaranteed or endorsed by the publisher.

frontiers | Frontiers in Immunology

TYPE Erratum
PUBLISHED 31 August 2022
DOI 10.3389/fimmu.2022.1020829

OPEN ACCESS

APPROVED BY
Frontiers Editorial Office,
Frontiers Media SA, Switzerland

*CORRESPONDENCE
Frontiers Production Office
production.office@frontiersin.org

SPECIALTY SECTION
This article was submitted to Vaccines and Molecular Therapeutics, a section of the journal Frontiers in Immunology

RECEIVED 16 August 2022
ACCEPTED 16 August 2022
PUBLISHED 31 August 2022

CITATION
Frontiers Production Office (2022) Erratum: Incorporating cryopreservation evaluations into the design of cell-based drug delivery dystems: An opinion paper. *Front. Immunol.* 13:1020829. doi: 10.3389/fimmu.2022.1020829

Erratum: Incorporating cryopreservation evaluations into the design of cell-based drug delivery dystems: An opinion paper

Frontiers Production Office*

Frontiers Media SA, Lausanne, Switzerland

KEYWORDS

mesenchymal stem cells, cryopreservation, cryoprotectants, chemotherapy, targeted drug delivery

An erratum on:

Incorporating cryopreservation evaluations into the design of cell-based drug delivery systems: an opinion paper.

By Ekpo MD, Xie J, Liu X, Onuku R, Boafo GF and Tan S (2022) Front. Immunol. 13:967731.doi: 10.3389/fimmu.2022.967731

Due to a production error, there was a mistake in affiliation two of this article. Instead of "School of Pharmacy, Taipei Medical University, Taipei, Taiwan", it should be "Department of Pharmaceutical and Medicinal Chemistry, Faculty of Pharmaceutical Sciences, University of Nigeria, Nsukka, Nigeria".

The publisher sincerely apologizes for this mistake.

The original version of this article has been updated.

frontiers | Frontiers in Immunology

ORIGINAL RESEARCH
published: 18 July 2022
doi: 10.3389/fimmu.2022.917790

Cytokine Activation Reveals Tissue-Imprinted Gene Profiles of Mesenchymal Stromal Cells

Danielle M. Wiese[1], *Catherine A. Wood*[1], *Barry N. Ford*[2] *and Lorena R. Braid*[1,3]*

[1] Aurora BioSolutions Inc., Medicine Hat, AB, Canada, [2] Defence Research and Development Canada Suffield Research Centre, Casualty Management Section, Medicine Hat, AB, Canada, [3] Simon Fraser University, Department of Molecular Biology and Biochemistry, Burnaby, BC, Canada

Development of standardized metrics to support manufacturing and regulatory approval of mesenchymal stromal cell (MSC) products is confounded by heterogeneity of MSC populations. Many reports describe fundamental differences between MSCs from various tissues and compare unstimulated and activated counterparts. However, molecular information comparing biological profiles of activated MSCs across different origins and donors is limited. To better understand common and source-specific mechanisms of action, we compared the responses of 3 donor populations each of human umbilical cord (UC) and bone marrow (BM) MSCs to TNF-α, IL-1β or IFN-γ. Transcriptome profiles were analysed by microarray and select secretome profiles were assessed by multiplex immunoassay. Unstimulated (resting) UC and BM-MSCs differentially expressed (DE) 174 genes. Signatures of TNF-α-stimulated BM and UC-MSCs included 45 and 14 new DE genes, respectively, while all but 7 of the initial 174 DE genes were expressed at comparable levels after licensing. After IL-1β activation, only 5 of the 174 DE genes remained significantly different, while 6 new DE genes were identified. IFN-γ elicited a robust transcriptome response from both cell types, yet nearly all differences (171/174) between resting populations were attenuated. Nine DE genes predominantly corresponding to immunogenic cell surface proteins emerged as a BM-MSC signature of IFN-γ activation. Changes in protein synthesis of select analytes correlated modestly with transcript levels. The dynamic responses of licensed MSCs documented herein, which attenuated heterogeneity between unstimulated populations, provide new insight into common and source-imprinted responses to cytokine activation and can inform strategic development of meaningful, standardized assays.

Keywords: mesenchymal stromal cells (MSC), TNF-α, IL1-β, IFN-γ, licensing, activation, transcriptome, gene profiles

OPEN ACCESS

Edited by:
Guido Moll,
Charité Universitätsmedizin Berlin, Germany

Reviewed by:
Takeo Mukai,
The University of Tokyo, Japan
Helder Cruz,
Theraproteins, Portugal

***Correspondence:**
Lorena R. Braid
lorena@aurorabiosolutions.com;
lrbraid@sfu.ca

Specialty section:
This article was submitted to Vaccines and Molecular Therapeutics, a section of the journal Frontiers in Immunology

Received: *11 April 2022*
Accepted: *10 June 2022*
Published: *18 July 2022*

Citation:
Wiese DM, Wood CA, Ford BN and Braid LR (2022) Cytokine Activation Reveals Tissue-Imprinted Gene Profiles of Mesenchymal Stromal Cells. Front. Immunol. 13:917790. doi: 10.3389/fimmu.2022.917790

INTRODUCTION

Mesenchymal stromal cells (MSCs) are potential therapeutics for numerous clinical indications, particularly those that exploit the immunomodulatory properties of the cells. Recent clinical advances in MSC-based therapeutics have revealed a need for standardized tests that correlate predictive markers of immunomodulation, regeneration and homing properties with therapeutic efficacy (1–5). Robust and validated potency assays are required by regulatory authorities to fulfill

performance criteria for advanced clinical trials and eventual product approval (1, 2, 6). Comparison of stimulus-provoked biomarkers from cytokine-activated MSCs versus unstimulated MSC controls has been proposed as predictive metrics of therapeutic potential (7, 8). Measured biomarkers, or mechanism-of-action surrogates, could include cell surface markers, secreted proteins and expressed transcripts.

MSCs are progenitor cells that reside in the stroma of most tissues and organs. Although MSCs derived from various tissues share core properties and were originally believed to be comparable, source-specific distinctions between MSC populations are increasingly reported. Tissue and donor origin have been linked to unique transcriptome (9–13), secretome (14, 15) and surfaceome (15–18) profiles, as well as variable therapeutic potential (12, 19, 20). Cell isolation and cultivation protocols (reviewed in (4, 5, 21, 22)), including media formulation, can also influence these properties (23, 24). This heterogeneity complicates development of standardized potency assays.

Many studies have explored the biological responses of culture-adapted MSCs to specific inflammatory stimuli, both as a predictor of their response after administration for inflammatory diseases and conditions, and to pre-activate or prime the cells to enhance their therapeutic potential (12, 17, 25–29). There are substantial data describing differences between culture adapted MSCs from different sources, and studies comparing unstimulated and activated counterparts. However, molecular data describing the biological profiles and properties of activated MSCs derived from different origins and donors are limited. Comparative studies addressing this topic have focused on relatively few, select immune-modulatory transcripts, cell surface markers, secreted factors or functions (16, 30–32).

Here we undertook a transcriptome profiling approach to compare the responses of umbilical cord-derived (UC) and bone marrow-derived (BM) MSCs to 3 common inflammatory mediators that activate MSCs via independent signalling pathways. Three representative donor populations, balanced for sex and *in vitro* age, from each MSC source were included to generate a heterogeneous data set. MSC polarization as a result of cytokine activation was assessed at the level of gene expression by microarray, and by secreted output of a panel of cytokines and growth factors. We postulated that licensing of cultured MSCs by pro-inflammatory signals might drive MSCs with underlying differences towards a synchronized phenotype or amplify their differences to produce more distinct cell populations. Understanding these dynamics will enable rational development of robust, standardized MSC potency assays employing activation and functional polarization strategies.

MATERIALS AND METHODS

Cell Source

High quality MSC populations were obtained from commercial sources and qualified by tri-lineage differentiation and cell surface marker profiles as previously described (33) in accordance with internationally accepted minimal criteria (34). UC-MSCs (35) cryopreserved at mean population doubling level (mPDL) 10, were provided by Tissue Regeneration Therapeutics (TRT), Inc. (Toronto, Canada). UC-MSCs are isolated from the perivascular Wharton's jelly (36) of healthy term (>37 weeks) umbilical cords delivered by C-section, and cultivated in Mesenchymal Stem Cell Growth Media – Chemically Defined™ (MSCGM-CD™; Lonza, Walkersville, MD). BM-MSCs from donors 18-30 years of age, cryopreserved at mPDL 9, were obtained from RoosterBio Inc. (Frederick, MD).

Cell Culture

For cell expansion, MSCs were seeded at a density of 1333 cells/cm^2 in RoosterNourish™-MSC-XF (RoosterBio Inc.). Cells were incubated at 37° C, 5% CO_2 with media changes every 3-4 days and passaged once the monolayer reached 70-80% confluence. Culture media was aspirated and cells washed with $DPBS^{-/-}$ (ThermoFisher Scientific, Waltham, MA), then enzymatically detached using TrypLE™ Select (ThermoFisher Scientific, Waltham, MA). Once cells were dissociated, an equal volume of media was added to the suspension and cells were counted with a Millipore Scepter cell counter using 60 μm probes (MilliporeSigma, Billerica, MA). Cells were centrifuged at 149 x *g* for 5 minutes, and the cell pellet re-suspended in fresh media and seeded in new culture vessels at a density of 1333 cells/cm^2.

Cytokine Stimulation

Three donor populations of UC-MSCs and BM-MSCs (2 male and 1 female each) were tested independently, in 3 replicate experiments. MSCs at passage 4 (mPDL 14.6-16.5) were seeded in 25 cm^2 flasks at a density of 13 333 cells/cm^2 in 3ml RoosterNourish™-MSC-XF and allowed to adhere overnight. After 18 hours, nearly all cells had adhered and exhibited a normal fibroblastic morphology, generating a monolayer with ~70% confluence. Purified recombinant human cytokines (PeproTech, Inc., Rocky Hill, NJ) were diluted in protein-free (PF) RoosterBasal™-PF media (RoosterBio Inc.) at the following concentrations: TNF-α (50 ng/ml), IL-1β (80 pg/ml) and IFN-γ (50 ng/ml). Complete media was removed from the monolayers and replaced with 2 ml of cytokine solution. Unstimulated cultures received 2 ml of RoosterBasal™-PF without cytokine supplements. To quantify media background, 2 ml of unsupplemented or cytokine-supplemented PF media was added to 25 cm^2 flasks. All flasks were incubated at 37°C, 5% CO_2 for 24 hours.

After 24 hours, conditioned media (CM) was collected and stored in small aliquots at -80°C until analysis. To collect mRNA, cells were enzymatically detached from the culture vessel and pelleted by centrifugation as described above, then re-suspended in 0.5 ml of RNAprotect® Cell Reagent (Qiagen, Germantown, MD) for short-term storage at -80°C.

RNA Extraction

Cell pellets from technical replicates (n = 3 for each donor population) were combined to produce a single RNA sample. RNA was extracted using Qiagen RNeasy® Plus Mini Kits (Qiagen) according to manufacturer's recommendations. 20 μl

of 2 M β-mercaptoethanol was added per ml of kit buffer (RLT buffer) and 600 µl RLT buffer was used for each sample. RNA concentration and purity were assessed in 96 well plates using a BioTek Synergy HT microplate reader (BioTek Instruments Inc., Winooski, VT) and Gen5 2.05 software with path length correction.

Microarray Processing

RNA expression was analyzed using GeneChip™ U133A 2.0 arrays (Affymetrix, ThermoFisher Scientific) as previously described [28]. Briefly, RNA was amplified and labeled using GeneChip™ 3' IVT Plus kits (Affymetrix, ThermoFisher Scientific), and hybridized to arrays for 16 hours at 45°C, 60 RPM in a GeneChip™ Hybridization Oven 640 (Affymetrix, ThermoFisher Scientific). Chips were scanned using a GeneChip™ 3000 7G Scanner (Affymetrix, ThermoFisher Scientific) and the resulting images reviewed for quality in GeneChip™ Control Console Viewer.

Gene Expression Data Analyses

24 microarray .CEL files were analyzed using Bioconductor (37) packages in R version 3.4.2 (38). Pre-processing (GCRMA background adjustment, normalization, $\log_2$ expression matrix output) was performed using gcrma (39) and Affymetrix U133A 2.0 probe affinity data. Data quality was interrogated using simpleaffy (39–41) following GeneChip™ guidelines (42). To minimize batch influences on data collected, MSC type and cell donor sex were equally distributed (with the exception of 1/24) amongst two culture and stimulation periods, and three RNA extraction and microarray processing batches. Nevertheless, any batch effects were explored by evaluating all BatchQC (43) metrics with and without ComBat (44) adjustment, and subsequently the data was left unadjusted. Using genefilter (45), pre-processed probe sets were filtered to only include those that were expressed greater than 2-fold above background signal on at least 3 arrays; 3 is the smallest number of arrays assigned to a condition (cytokine stimulation within a MSC type). Sixty-two percent of probe sets were included for differential expression analysis.

Limma (46) was used for linear modeling of comparisons and differential expression assessment. Comparisons of resting MSC types, resting versus activated UC-MSCs and BM-MSCs separately, and activated MSC types utilized TREAT (47) to simultaneously select significantly differentially expressed (DE) probe sets having both a Benjamini-Hochberg (48) false discovery rate (FDR)-adjusted p-value (p) of <0.05 and a >2-fold change. Annotation information was accessed through AnnotationDbi (49, 50) and heat maps were created using ComplexHeatmap (51).

Functional analysis was carried out using DAVID (52, 53) by querying DE gene lists' Entrez identifiers for enriched (FDR 5%) Gene Ontology (GO) Biological Process terms (54, 55) and Kyoto Encyclopedia of Genes and Genomes (KEGG) pathways (56, 57). All non-specific probe sets were addressed by eliminating included Entrez identifiers of read-through transcripts, microRNAs and additional members of the same gene family. The data have been deposited in NCBI's Gene Expression Omnibus (GEO) database (58, 59), available through accession number GSE129165.

Reverse Transcription-Quantitative Polymerase Chain Reaction and Analysis

RT-qPCR was performed in triplicate wells using Quantinova SYBR green kits (Qiagen) read by CFX Connect Real-Time System (Bio-Rad, Hercules, CA). Sequences for *ACTB*, *CXCL12*, *GAPDH*, *HLA-DRA*, *IDO1*, *PTGS2*, *TNFAIP6* and *YWHAZ* primers (MilliporeSigma) are listed in **Supplementary Figure 1A**. Non-detects, due to failure to amplify by cycle 40, had C_q values imputed using R packages HTqPCR (60) and nondetects (61); valid undetected values (imputed value <0 across replicates) were subsequently substituted with $C_{q\ (max)}$+1 (62). *ACTB*, *GAPDH* and *YWHAZ* were used as reference genes for normalization due to greatest stability amongst RefFinder (63) ranking of Reference Genes H96 PrimerPCR Pathway Plate (Bio-Rad) results (data not shown). Relative expression was calculated using $2^{Cq(\text{reference gene mean})-Cq(\text{target})}$ (64).

Multiplex Immunoassay

A subset of inflammatory mediators was quantified in CM samples using commercially available multiplex immunoassays. Test samples were thawed at 4°C and used within 24 hours; any remaining sample was discarded. Each of three 25 cm^2 flask replicate samples per MSC donor were analyzed by Bio-Plex Pro™ (Bio-Rad) Human Cytokine Panel Group I 27-plex and Human TGF-β 3-plex kits, run undiluted and at a final dilution of 1:5 with 0.625% BSA respectively. The observed concentration of samples was exported from Bio-Plex Manager™ 6.1 software and normalized to concentration (pg/ml) per one million cells at CM collection.

Multiplex Immunoassay Statistical Analysis

The mean analyte concentrations for each MSC donor were used to compare unstimulated MSC types, resting versus licensed UC-MSCs and BM-MSCs separately, and licensed MSC types. Statistical significance was determined by multiple t-tests since the range of analyte concentrations across the assay covered several orders of magnitude. An FDR-adjusted $p<0.05$ was deemed statistically significant. All analysis was performed using GraphPad Prism version 7 (GraphPad Software, La Jolla, CA).

RESULTS

Unstimulated UC and BM-MSCs Differentially Express Immune- and Inflammation-Related Genes

The transcriptome profiles of unstimulated UC and BM-MSCs were first established. Of 14,500 assayed genes, 174 exhibited significant expression differences between MSC types. UC-MSCs solely expressed 30 genes, and significantly higher levels of 46 genes compared to BM-MSCs (**Figure 1A**; **Table S1**); few of

these differentially expressed (DE) genes could be connected by function or pathway. Several genes contribute to enrichment of the rheumatoid arthritis KEGG pathway and positive regulation of angiogenesis GO function (**Figure 1B**). BM-MSCs uniquely expressed 46 genes, and 52 genes at significantly higher levels than UC-MSCs (**Figure 1A**; **Table S1**). Subsets of these DE genes are linked to extracellular matrix organization, cell adhesion and skeletal system development GO functions (**Figure 1B**). Other DE genes between UC and BM-MSCs included various collagens, phospholipase, integrin subunit, sialyltransferase enzyme and solute carrier family member transcripts (**Table S1**).

DE genes linked to GO immune and/or inflammatory responses were comparably enriched in UC-MSCs (8 genes) and BM-MSCs (7 genes) (**Figure 1A**). Expression of other important immune-related genes was also interrogated (**Figures 1C, D**). Both MSC types expressed major histocompatibility complex (MHC) class I chain paralogues at moderate to high levels and did not express MHC class II paralogues except for *HLA-DPA1* and *HLA-DPB1* (**Figure 1C**). *HLA-DMA* was detected in 2 BM-MSC populations but was only substantial in 1. (**Figure 1C**). The metabolic immunomodulatory gene *IDO1* was detected in only 1 unstimulated UC-MSC population (**Figure 1D**). *CD200*, a disputed surrogate marker for immunosuppression (2, 16), and *PTGS2* (COX-2), which preferentially produces the T-cell inhibitor PGE2 in MSCs (17, 65), were significantly expressed by UC-MSCs but not detected in BM-MSCs (**Figure 1D**). *IL1B* and *LIF*, purportedly linked to the superior immunomodulatory performance of native UC-MSCs compared to BM-MSCs (66), were expressed significantly more by UC-MSCs (**Figures 1A, D**; **Table S1**).

Next, MSCs were strategically activated with inflammatory mediators to assess the continuity of their gene expression and

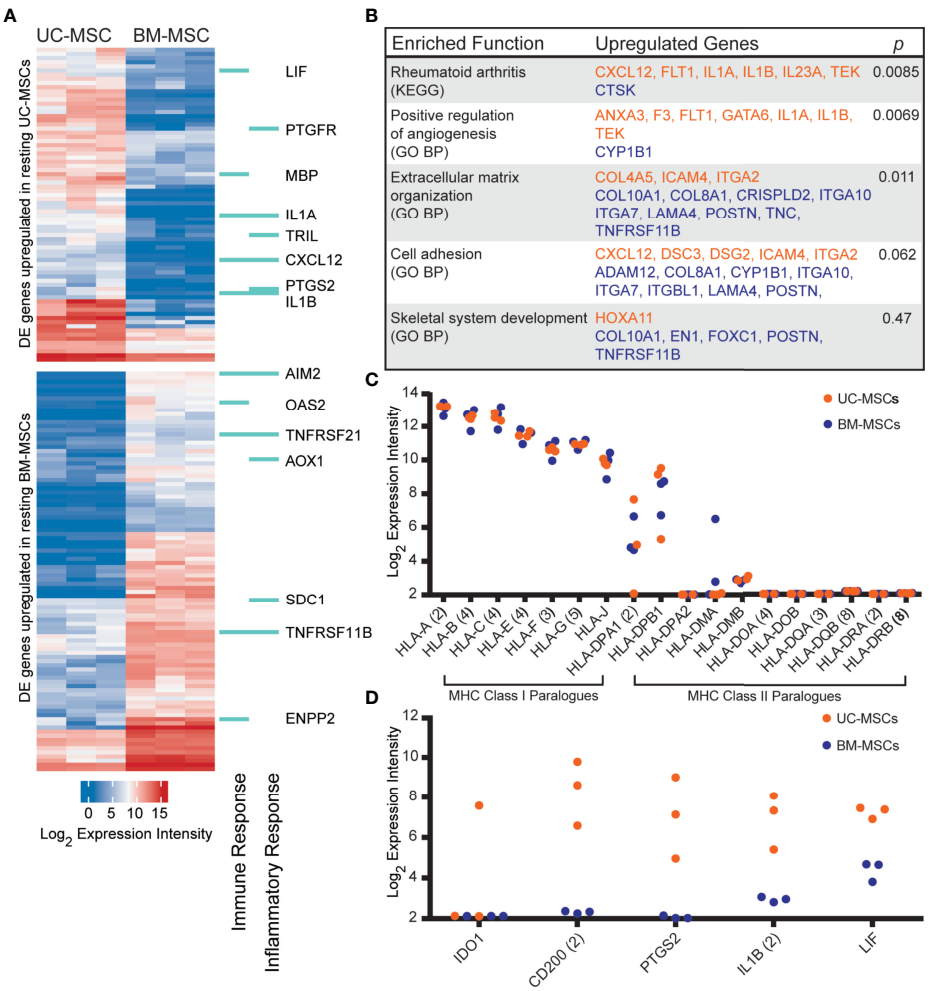

FIGURE 1 | The transcriptomes of unstimulated UC and BM-MSCs exhibit significant differences. **(A)** Seventy-six genes are preferentially expressed by UC-MSCs, while 98 genes are enriched in BM-MSCs. A subset are components of immune and inflammatory responses, as specified by GO. **(B)** Few DE genes exhibit functional co-registration. Genes DE by UC (orange) and BM (purple) MSCs contribute to few enriched ($p<0.05$) functional annotations. **(C)** UC and BM-MSCs similarly express MHC-I paralogues and lack most MHC-II paralogues. **(D)** Key immunomodulatory genes are more highly expressed in resting UC-MSCs. BM, bone marrow; DE, differentially expressed; GO BP, Gene Ontology Biological Process annotation; KEGG, Kyoto Encyclopedia of Genes and Genomes pathway annotation; MSC, mesenchymal stromal cell; UC, umbilical cord.

secreted responses to controlled stimulation. TNF-α is a multi-functional inflammatory mediator implicated in numerous signalling and functional pathways. IL-1β is a potent low-abundance cytokine with activity more refined to acute injury or infection, while IFN-γ stimulates the innate and adaptive immune responses to pathogens. MSCs were dosed with a physiologically relevant amount of cytokine, estimated from circulating or local levels reported in clinical samples (67, 68).

TNF-α Evokes Source-Specific Gene Profiles Related to Inflammation and Immunity

Sixty-one genes were upregulated to comparable levels between TNF-α activated UC- and BM-MSCs (**Figure 2A**; **Table S2**), most of which were linked to GO immune and inflammatory processes (**Figure 2B**). Only 7 of the 174 genes that were DE between unstimulated MSC types remained significantly DE between TNF-α activated MSC types (**Table 1**). However, TNF-α evoked fifty-nine newly significantly DE genes between TNF-α licensed UC and BM MSCs (**Table 1**; **Figures 2C, D**). Fourteen genes preferentially expressed by TNF-α polarized UC-MSCs are primarily involved in inflammation or immunity (*CCL2, CCL7*, *CCR10*, *GPRC5B*, *MAP3K8*; **Figures 2C, E**), or structure or adhesion (*FNBP1L*, *FRY*, *JUP*, *KRT19*, *LAMC2*). Forty-five of 59 DE genes more abundant in BM-MSCs are linked to the following enriched GO functions: innate immunity, viral defense, including negative regulation of viral genome replication and type I interferon (IFN) signalling, with negative regulation of type I IFN production and positive regulation of IFN-α and IFN-β production (**Figures 2D, F**). Notably, none of the 14 genes DE by UC-MSCs are involved in these functions (**Figure 2E**). Taken together, the differences between resting UC and BM-MSCs are attenuated by TNF-α stimulation, accompanied by the introduction of new source-specific transcriptome signatures (**Table 1**), most notably the preferential activation of Type I IFN signalling in BM-MSCs.

IL-1β Drives UC and BM-MSCs Towards A Similar Transcriptome Profile With Few Signature Differences

Only 33 genes were significantly responsive to IL-1β priming, 15 of which increased in both MSC types to comparable expression intensities (**Figure 3A** and **Table S3**). These genes have defined roles in immune and inflammation responses. KEGG pathway analysis of all responsive genes revealed enrichment for TNF signaling (12 genes), chemokine signaling (8 genes), NF-κB signaling (8 genes), cytokine-cytokine receptor interaction (5 genes), NOD-like receptor signaling (5 genes) and Toll-like receptor signaling (6 genes) (**Figure 3B**). Top enriched GO functions included inflammatory response (13 genes), immune response (12 genes) and chemotaxis (6 genes) (**Figure 3B** and **Table S4**).

Interestingly, only 5 of the 174 DE genes (*KRTAP1-1, B3GALT2, COL10A1*, *PTGS2* and *IL1A*) remained significantly different between IL-1β licensed UC and BM-MSCs (**Table 1** and **Figure 3C**), although the fold-difference was reduced. Six new DE genes emerged following IL-1β dosing (**Table 1** and **Figure 3D**). *BST2, STAT4, WISP1, MMP3, MAPK3K8* and *GPRC5B* are either not expressed or expressed at similarly modest intensities in unstimulated MSCs. After IL-1β exposure, these genes were upregulated in only 1 or the other MSC type, resulting in unique signatures between MSC types (**Figure 3D**). The signature of IL-1β polarized UC-MSCs includes *MAP3K8* and *GPRC5B*, while polarized BM-MSCs uniquely express *BST2, STAT4, WISP1* and *MMP3* (**Table 1**).

Source-Specific Transcriptome Profiles of IFN-γ Licensed UC and BM-MSCs Are Linked to Immune Processes

Dynamic transcriptome changes in UC and BM-MSCs following IFN-γ exposure also resulted in a striking convergence of transcriptome profiles (**Figure 4A**), leaving only 3 (*BAALC, CCNA1* and *CXCL12*) of the 174 DE genes between unstimulated MSC types significantly different (**Table 1**). Many responsive genes contribute to enriched KEGG pathways for antigen processing and presentation (15 genes) and cell adhesion molecules (10 genes), among others (**Figure 4B**). The top 5 enriched GO terms for this group of genes were the type I IFN signalling pathway (18 genes), IFN-γ-mediated signaling pathway (16 genes), immune response (21 genes), defense response to virus (14 genes) and antigen processing and presentation (9 genes) (**Figure 4B** and **Table S4**). In both MSC types, IFN-γ significantly induced *IDO1*, genes encoding MHC-II chain paralogues (*HLA-DRA*, *-DRB1/4/5*, *-DMA, -DMB*) and MHC-associated *CIITA*, as well as increased expression of *HLA-B/C/E/F* (MHC-I) and *BTN3A1* (**Table S5**). Notably, TNF-α and IL-1β did not have this effect. The only significantly downregulated transcript common to both stimulated MSC types was *GLS*, which encodes glutaminase. (**Table S5**).

Nine source-specific DE genes emerged as a consequence of IFN-γ polarization (**Table 1** and **Figures 4C, D**). Expression of *HLA-DRA* and *KCTD14* and *OASL* increased more substantially in BM-MSCs compared to UC-MSCs (**Figures 4C, D**), while *TLR2*, *ACKR4*, *CMAHP*, *HLA-DQA1, -2* and *HLA-DQB1* were specifically induced in BM-MSCs (**Figure 4D**). Stimulated UC-MSCs produced significantly higher levels of *RIMS2 and CXCL12*, which were undetected in both resting and activated BM-MSCs (**Figure 4D**). Overall, a small panel of DE genes predominantly corresponding to immunogenic cell surface proteins emerged as a BM-MSC signature, while UC-MSC uniquely express *CXCL12* and *RIMS2*.

Confirmation of Array Data by RT-qPCR

Transcript levels for select genes of interest were validated using RT-qPCR (**Supplementary Figures 1A, B**). Consistent with the array data, *IDO1* was detected in only one resting UC-MSC population and was upregulated in all IFN-γ activated MSCs. Specific *HLA-DRA* induction by IFN-γ was also verified by RT-qPCR; *HLA-DRA* was also confirmed at higher levels in IFN-γ activated BM-MSCs. RT-qPCR also verified the source-specific regulation of *CXCL12* revealed by microarray; *CXCL12* transcript was more abundant in unstimulated UC-MSCs, upregulated in IFN-γ polarized UC-MSCs,

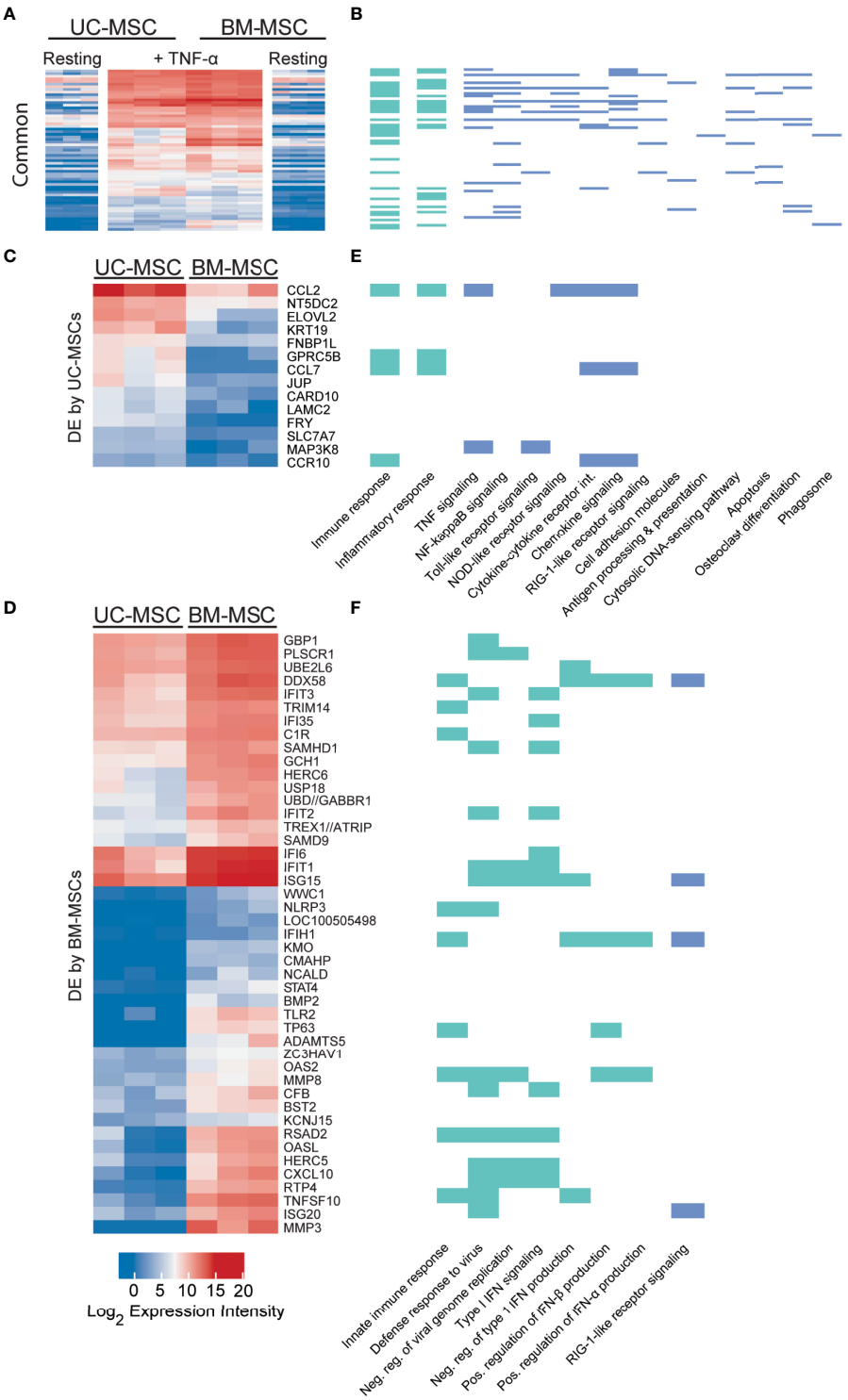

FIGURE 2 | TNF-α resolves all but 7 differentially expressed genes in unstimulated MSCs and evokes source-specific activation signatures. **(A)** Sixty-one genes are activated to comparable levels after licensing of UC and BM-MSCs by TNF-α. **(B)** Most of these genes are linked to enriched GO Biological Process terms are indicated in (green), and enriched KEGG pathways (blue ($p<0.05$) related to immunity and inflammation. **(C)** Thirteen genes are upregulated in TNF-α licensed UC-MSCs statistically higher than activated BM-MSCs. **(D)** Forty-five genes are statistically upregulated in DE genes TNF-α licensed BM-MSCs. **(E)** UC-MSCs preferentially express genes linked to immunity, inflammation and cytokine and chemokine signaling, while **(F)** BM-MSCs increase expression of genes linked to innate immune function and Type I IFN signalling. BM, bone marrow; DE, differentially expressed; MSC, mesenchymal stromal cell; UC, umbilical cord.

TABLE 1 | Statistically significant differences between UC-MSCs and BM-MSCs after cytokine activation.

Different:	In resting and licensed cells (unchanged by activation)	After licensing only (changes induced by activation)
+ TNF-α		
↑ in UC-MSCs	*MBP*, *ST6GALNAC5*, *TEK*	*CARD10, CCL2, CCL7, CCR10, ELOVL2, FNBP1L, FRY, GPRC5B, JUP, KRT19, LAMC2, MAP3K8, NT5DC2, SLC7A7*
↑ in BM-MSCs	*CPM*, *IFI44L*, *KRTAP1-1*, *MMP13*	*ADAMTS5, BMP2, BST2, C1R, CFB, CMAHP, CXCL10, DDX58, GBP1, GCH1, HERC5, HERC6, IFI35, IFI6, IFIH1, IFIT1, IFIT2, IFIT3, ISG15, ISG20, KCNJ15, KMO, LOC100505498, MMP3, MMP8, NCALD, NLRP3, OAS2, OASL, PLSCR1, RSAD2, RTP4, SAMD9, SAMHD1, STAT4, TLR2, TNFSF10, TP63, TREX1//ATRIP, TRIM14, UBD//GABBR1, UBE2L6, USP18, WWC1, ZC3HAV1*
	IL-10, IL-12, IL-13, VEGF	IL-7, RANTES
+ IL-1β		
↑ in UC-MSCs	*IL1A*, *PTGS2*	*GPRC5B*, *MAP3K8*
↑ in BM-MSCs	*B3GALT2*, *COL10A1*, *KRTAP1-1*	*BST2*, *MMP3*, *STAT4*, *WISP1*
	IL-10, IL-12, IL-13, VEGF	IL-7, IP-10
+ IFN-γ		
↑ in UC-MSCs	*CCNA1*, *CXCL12*	*RIMS2*
↑ in BM-MSCs	*BAALC* IL-13	*ACKR4*, *CMAHP*, *HLA-DQA1//HLA-DQA2*, *HLA-DQB1*, *HLA-DRA*, *KCTD14*, *OASL*, *TLR2*

↑, *DE by specified MSC type. UC, umbilical cord-derived MSCs. BM, bone marrow-derived MSCs. //, non-specific probe set. Italicized font denotes a transcript; regular font denotes a soluble protein.*

and downregulated in TNF-α or IL-1β polarized UC-MSCs. *PTGS2* also proved to be specifically expressed by unstimulated UC-MSCs, and ubiquitously upregulated in response to all 3 cytokines although IL-1β elicited the strongest response. *TNFAIP6* (TSG-6), which is important for MSC immunosuppressive activity [65,66], was found to be modestly increased in response to IL-1β and IFN-γ and substantially upregulated in TNF-α activated BM-MSCs by microarray and RT-qPCR.

Unstimulated and Activated UC and BM-MSCs Exhibit Unique Chemokine and Cytokine Secretion Profiles

The secreted protein profiles of cytokine-activated UC and BM-MSCs was next queried using a panel of 30 human cytokines and growth factors. The UC-MSCs proliferated faster than the BM-MSCs during the 24-hour activation period (**Supplementary Figure 2A**), so analyte concentration was normalized to the number of cells quantified at sample collection. The licensing cytokines were not detected in unconditioned media controls after the 24-hour incubation period (**Supplementary Figure 2B**). Experiments were performed in a protein-free media formulation to minimize confounding effects from background levels or signalling interactions caused by growth factors present in expansion media.

Unstimulated UC and BM-MSCs secreted substantial levels of TGF-β1 and RANTES and did not produce GM-CSF, IL-2, or PDGF-2 until stimulated (**Figure 5**). TGF-β2 and IL-17 were similarly expressed by resting and stimulated UC and BM-MSCs, although substantial donor variability for these analytes confounded statistical analysis (**Supplementary Figure 2C**). TGF- β3 and IL-5 were never detected (not shown).

Thirteen cytokines were more abundantly secreted ($p<0.05$) by unstimulated BM-MSCs (**Table S6** and **Figure 5**), including VEGF, IL-12, G-CSF and IP-10. Nine other cytokines, IL-10, IL-13, TNF-α, IFN- γ, eotaxin, IL-9, IL-1β, IL-4, and MIP-1β, were secreted at low concentrations (<10 pg/ml/million cells) by BM-MSCs, but ranged from undetectable to <2 pg/ml/million cells in CM from UC-MSCs (**Table S6** and **Figure 5**). Unstimulated UC-MSCs secreted more FGF-2 (1.9-fold higher, $p<0.05$) than BM-MSCs, and more IL-6, IL-8 and MCP-1 albeit at non-significant levels ($p>0.05$) due to donor variability (**Figure 5** and **Table S6**).

TNF-α elicited a significant secretory response from both UC and BM-MSCs. Production of 17 soluble proteins increased from both MSC types. Final concentrations of TNF-α, G-CSF, IFN-γ, eotaxin, IL-9, IL-1β, IL-4, MIP-1β and FGF-2 were similar between UC and BM-MSCs (**Figure 5** and **Table S7**). By contrast, TNF-α activated BM-MSCs secreted significantly higher amounts of IL-7 and RANTES, which UC-MSCs significantly reduced IL-7 synthesis (**Table 1** and **Figure 5**). TNF-α did not modulate IL-10, IL-12, IL-13 or VEGF output from either cell type; these remained more highly secreted by BM-MSCs (**Figure 5**, **Table 1** and **Table S7**).

IL-1β stimulated production of analytes similar to TNF-α (**Figure 5**). However, we documented substantial donor variability in protein-level responses to IL-1β which was not evident on the gene level or in response to TNF-α or IFN-γ. Interestingly, UC-MSCs reduced IL-7 and IP-10 output in response to IL-1β, while BM-MSCs substantially increased secretion of these proteins (**Figure 5** and **Table S7**).

IFN-γ had little detectable effect on the selected panel of pro-inflammatory cytokines (**Figure 5**). Both UC and BM-MSCs substantially increased IFN-γ secretion via positive feedback (**Supplementary Figure 2B** and **Figure 5**). IP-10 also increased >2-fold in both IFN-γ activated MSC types but did not meet statistical significance criteria (**Figure 5** and **Table S7**). IL-13 was found to be significantly different between IFN-γ activated MSC types, but all measured CM concentrations were <1pg/ml (**Figure 5**).

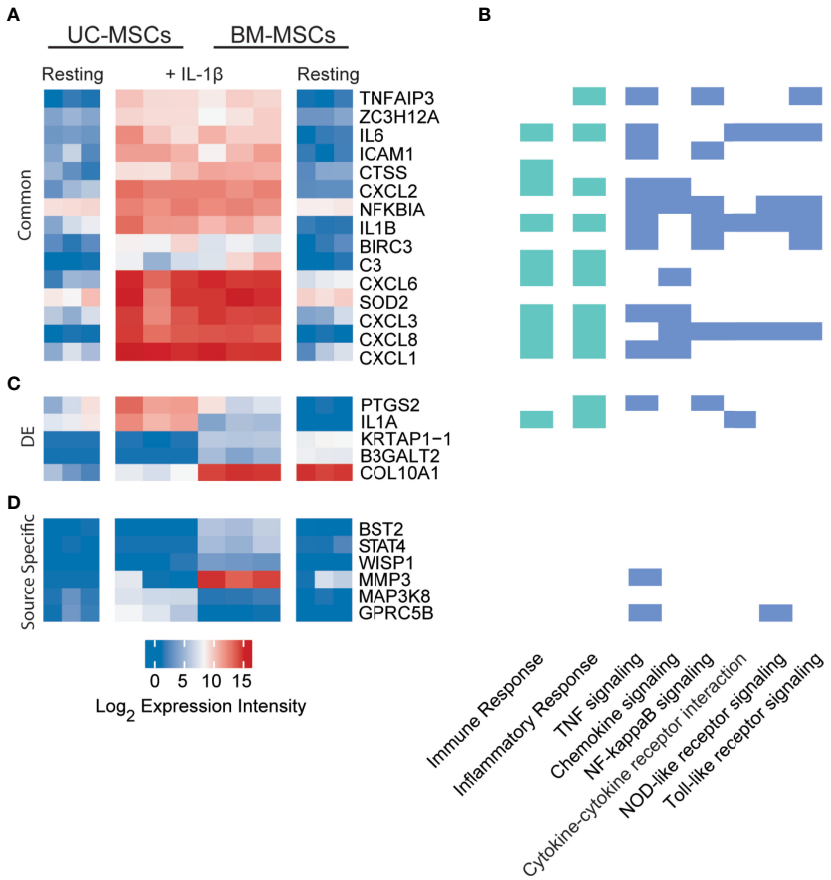

FIGURE 3 | Expression profiles of IL-1β licensed UC and BM-MSCs include 15 common genes and 6 source-imprinted genes. **(A)** Fifteen genes are significantly upregulated to comparable levels in UC and BM-MSCs activated by IL-1β. **(B)** Genes responsive to IL-1β are involved in many immune and inflammatory processes, as determined by GO (green; see complete enriched list in **Table S4**), as well as 6 enriched KEGG pathways (blue) ($p<0.05$). **(C)** Only 5 of the 74 genes DE between unstimulated UC and BM-MSCs are still expressed at significantly levels after dosing with IL-1β. **(D)** Four genes are specifically upregulated in IL-1β licensed BM-MSCs, while 2 genes are specifically upregulated in IL-1β activated UC-MSCs. BM, bone marrow; DE, differentially expressed; IL, interleukin; MSC, mesenchymal stromal cell; UC, umbilical cord.

Gene and Protein Expression Profiles Are Not Consistent

We next assessed the correlation between gene expression and protein output. Of the assayed proteins, concomitant abundance of transcripts after licensing were evident for IL-6, IL-8, VEGF, FGF-basic, MCP-1 and TGF- β1 (**Supplementary Figure 3**). Others, like RANTES, were only correlative in a subset of activating conditions. This data shows that only a subset of gene and protein biomarkers of MSC activation can be used interchangeably.

DISCUSSION

Tissue and donor-influenced variability between MSC populations has been well established (9–11, 14–19). However, phenotypic and functional assessments have predominantly been performed on unstimulated cells (12, 69–72). Once administered to a patient, MSCs respond to the wounded or diseased environment and become polarized, adopting an activated phenotype. Van Megen et al. reported that the surface profiles of BM-MSCs still meet MSC minimal criteria after activation by IFN-γ (73). We also found that activated phenotype of MSCs did not influence MSC surface marker profiles (data not shown). We postulated that evaluation of polarized MSC populations after cytokine activation might provide important insights into their functional efficacy and inform development of cellular therapies and quality control assays across donors and tissue of origin.

Our data show remarkable synchronization of UC and BM-MSC transcriptomes upon activation with each of the selected cytokines, although responses to each cytokine were different. Multiple trajectories of change in gene expression markedly resolved the heterogeneity between unstimulated cell populations. These transcriptome shifts suggest that polarized MSCs may share many fundamental mechanisms of action. Consistent with this notion, Szabó et al. reported that IFN-γ and TNF-α pre-conditioning synchronized murine MSCs and attenuated donor-imprinted functional heterogeneity (73). Pre-activation of MSCs has been shown to improve therapeutic

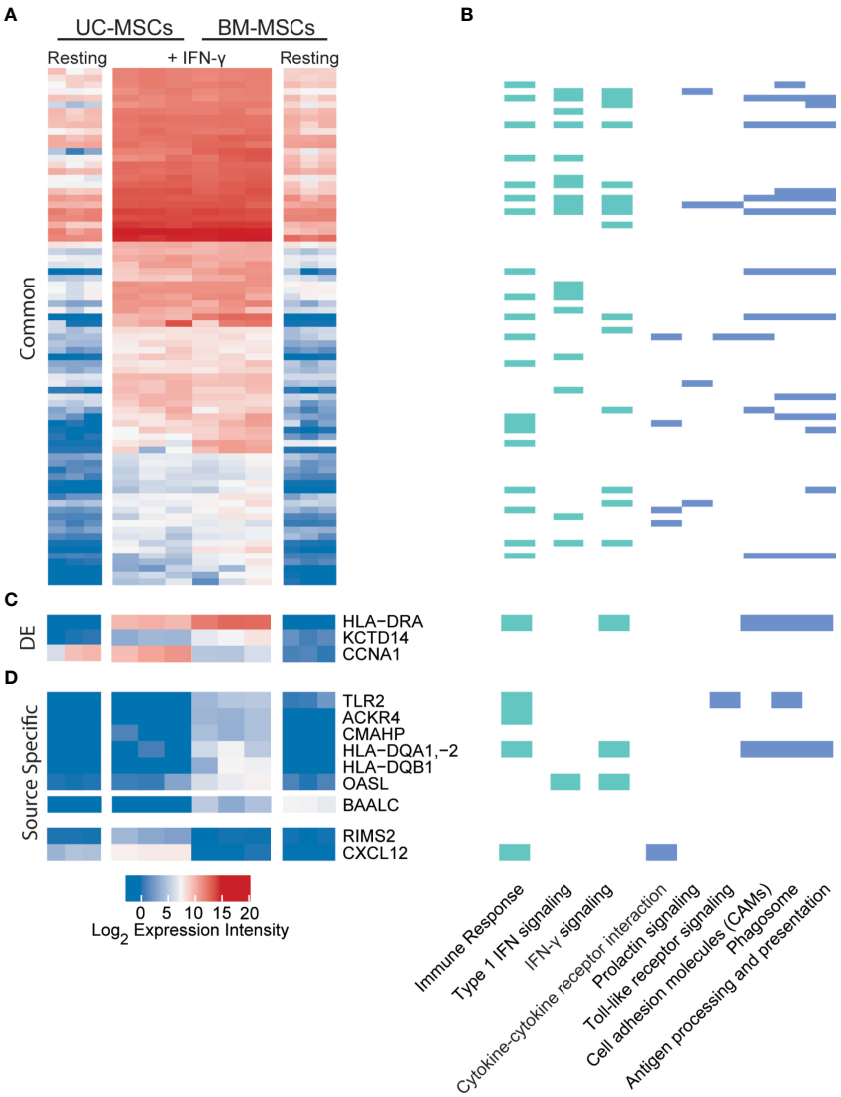

FIGURE 4 | UC and BM-MSCs exhibit robust and highly similar transcriptome responses to to IFN-γ. **(A)** Seventy-eight DE genes were significantly upregulated in both MSC types by IFN-γ activation. **(B)** IFN-γ activation results in functional enrichment of immune and IFN signaling GO processes (green), among others (see complete list in **Table S4**), and 6 KEGG pathways (blue). **(C)** Three genes were upregulated by both UC and BM-MSCs but to significantly different levels. **(D)** Nine genes were expressed in a source-specific manner. 6 were upregulated specifically in BM-MSCs, while 2 were solely increased in UC-MSCs. One gene, *BAALC*, was downregulated in BM-MSCs but remained undetected in UC-MSCs. BM, bone marrow; DE, differentially expressed; IFN, interferon; MSC, mesenchymal stromal cell; UC, umbilical cord.

potency and reproducibility (5, 27, 74–81), to restore functionality of senescent cells (82), and to support context-dependent recovery of functional cells from cryopreservation (83, 84). The reported variable outcomes in manufacturing and therapeutic success between MSC sources (8, 69, 70, 72) may therefore be the consequence of a small cohort of functionally relevant factors differentially expressed after licensing or *in vivo* deployment, rather than the non-specific heterogeneity found in unstimulated cells. Conversely, controlled stimulation with selected cytokines or other defined stressors could be leveraged to strategically manipulate specific therapeutic properties of MSCs.

TNF-α stimulation revealed a cohort of genes involved in viral immunity and the Type 1 IFN signalling pathway that were specifically upregulated in activated BM-MSCs, although they had been similarly expressed in resting UC and BM-MSCs. In addition, *bone marrow stromal antigen 2* (*BST2;* tetherin), *matrix metalloprotease 3* (*MMP3)* and *signal transducer and activator of transcription 4* (*STAT4)* were DE by BM-MSCs after TNF-α and IL-1β activation, suggesting that they may be functional mediators important to BM-specific mechanisms of action. By contrast, *G-protein coupled receptor family C group 5 member B* (*GPRC5B)* and *mitogen-activated protein kinase kinase kinase 8* (*MAP3K8)* were reproducibly DE by UC-MSCs in response to

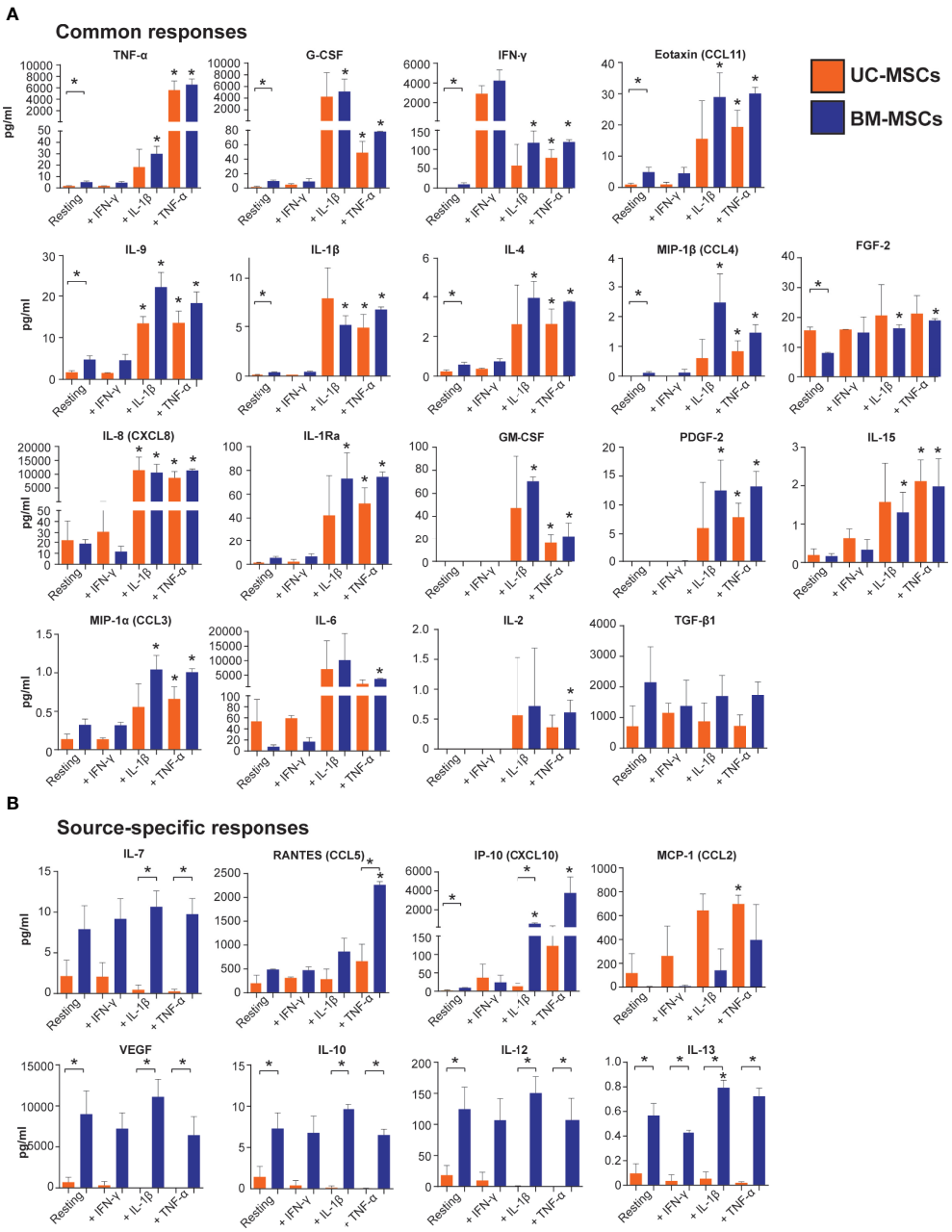

FIGURE 5 | Output of inflammatory mediators by licensed UC and BM-MSCs has some source-specific differences. **(A)** Eighteen proteins exhibited similar expression patterns in unstimulated and licensed MSCs. **(B)** Nine proteins displayed source-specific expression patterns. Seven proteins were specifically produced at significantly higher concentrations by licensed BM-MSCs, while MCP-1 was uniquely upregulated by activated UC-MSCs. Protein concentration was normalized to per million cells at harvest after 24-hour activation. Bracketed asterisks denote significantly different means between MSC types, and unbracketed asterisks denote significantly different means between activated and resting MSCs of the same type, as determined by FDR-adjusted $p<0.05$. BM, bone marrow; MSC, mesenchymal stromal cell; UC, umbilical cord.

TNF-α and IL-1β. Intriguingly, *regulating synaptic membrane exocytosis protein 2* (*RIMS2*) was only induced in UC-MSCs following IFN-γ exposure, while several human leukocyte antigen (HLA) receptors, involved in antigen presentation, and *toll like receptor 2* (*TLR2*), which recognizes pathogenic peptides, were specifically upregulated in BM-MSCs.

CXCL12 emerged as a dynamic signature gene unique to UC-MSCs. *CXCL12* was expressed by unstimulated UC-MSCs, but not BM-MSCs. Upon activation by TNF-α and IL-1β, expression intensity of *CXCL12* decreased, most substantially in response to IL-1β, and remained off in BM-MSCs. IFN-γ stimulated significant upregulation of *CXCL12* from UC-MSCs, and a

mild upregulation from BM-MSCs, but only to within the detectable range. *CXCL12* encodes Stromal Derived Factor (SDF-1), a chemotactic molecule for lymphocytes and MSCs. We have documented that UC-MSCs increase SDF-1 production in response to full-thickness burns (Braid et al, 2022, in prep), supporting the notion that *CXCL12* is an important factor relevant to therapeutic efficacy and potentially UC-MSC-specific treatment outcomes.

The data also provide evidence that MSCs from different sources may achieve similar functional outcomes by different mechanisms. MCP-1, VEGF, and IL-6 are important for MSC-mediated angiogenesis (85), in addition to other functions. In this study, unstimulated BM-MSCs produced significantly higher amounts of VEGF, while resting UC-MSCs produced higher amounts of MCP-1 and IL-6. Thus, CM isolated from either unstimulated MSC type possesses pro-angiogenic factors of different identity. Following TNF-α or IL-1β activation, however, BM-MSCs and UC-MSCs secreted comparable levels of IL-6, while UC-MSCs produced more MCP-1 than BM-MSCs which exhibited donor-influenced increases in MCP-1 output. By contrast, VEGF production by either MSC type was largely unaffected by any priming condition. The functional efficacy of the activated cells and resulting CM produced in this study are being evaluated to better understand the functional relationship between the changes documented here.

The current standard for establishing immune-modulatory potency of MSCs is the T-cell suppression assay, in which MSCs are co-cultured with lymphocytes and reduced T-cell proliferation correlates to MSC potency. Chinnadurai et al. identified a panel of genes upregulated by both IFN-γ activated MSCs and MSCs exhibiting immune-suppressive activity in T-cell suppression assays (86). Chinnadurai's study suggests that a simplified assay for MSC immunosuppressive potency or activation status is possible, since IFN-γ activation can be used as a surrogate model for the more complex and costly co-culture assay (86). Here, IFN-γ evoked highly similar and convergent transcriptome responses from UC and BM-MSCs, supporting IFN-γ activation as a surrogate assay applicable to multiple MSC types. The lack of secretory response to IFN-γ found here is likely a consequence of analyte selection, since many of the hallmark IFN-γ responsive proteins were not represented on the panel.

IFN-γ-mediated activation has also been proposed as a "universal" surrogate to assess general MSC potency (1). However, our study revealed minimal overlap in secreted markers between the TNF-α, IL-1β and IFN-γ activation states. We also noted that 1 population each of UC-MSCs and BM-MSCs were significantly more responsive to IL-1β than the other populations tested. Interestingly, these 2 populations did not exhibit such sensitivity to either TNF-α or IFN-γ. Redondo-Castro et al. reported that IL-1β stimulated higher levels of IL-6 and G-CSF from BM-MSCs than TNF-α or IFN-γ (87). We documented the same pattern here, for both UC and BM-MSCs. In Redondo-Castro's study, CM from IL-1β-activated BM-MSCs reduced synthesis of pro-inflammatory cytokines secreted by inflamed microglial cells via G-CSF, while CM from TNF-α or IFN-γ-licensed BM-MSCs did not (87). These findings suggest that MSC responses to IFN-γ alone may not adequately predict responsiveness to other activation pathways or mechanisms of action, and support development of potency assays based on the MSCs' proposed utility (8).

Differences in the fundamental properties of UC and BM-MSCs make certain comparisons challenging. For example, the doubling time of UC-MSCs is shorter than BM-MSCs (19, 71, 88). Although cells were seeded at the same density in our experiments, significantly more UC-MSCs were harvested 36 hours later, at the time of collection. Raw data from the CM analysis showed that analyte concentrations in the UC-MSC CM were substantially higher than in CM from BM-MSCs. However, once the results were normalized to the number of cells at the time of collection, resting and activated BM-MSCs emerged as more substantial producers of many of the soluble mediators analyzed. A recent study showed that UC-MSCs are more responsive than BM-MSCs to TNF-α stimulation (89). In that study, UC-MSCs rapidly produced TSG-6, and then TSG-6 expression tapered off over a 24-hour period. Conversely, secretion of TSG-6 from BM-MSCs took longer to initiate and peaked at 24 hours. Thus, it is difficult to extrapolate the functional relevance of absolute analyte values documented in this study which may vary depending on the sampling time point. However, clear trends emerged from the data. VEGF, TGF-β1, IL-7, IL-10, IL-12 and IL-13 were consistently secreted at higher protein to cell ratios by BM-MSCs, independent of priming condition. Moreover, secretion of these factors was mainly unaffected by any of the priming conditions for both MSC types. With the exceptions of IP-10, RANTES and MCP-1, the soluble responses of UC and BM-MSCs were similar in both identity and amplitude for the remaining analytes.

Our results suggest that assessments of variability between unstimulated MSCs or resting and polarized counterparts may not be fully predictive of tissue or donor-imprinted differences in therapeutic efficacy or mechanisms of action. *IDO1* is an accepted surrogate marker of immunosuppressive activity for MSCs. IFN-γ stimulates *IDO1* expression, and the degree of responsiveness to IFN-γ purportedly predicts MSC immune-modulatory potency (90). Using this paradigm, however, one potent UC-MSC population would have been discarded as "unresponsive". Unlike the other MSC populations used in this study, unstimulated cells from this UC-MSC donor robustly expressed *IDO1*. In response to IFN-γ, the other MSC populations increased *IDO1* to levels that matched the pre-stimulation *IDO1* levels from this donor population. Evaluation of the pre-activation or resting state would have predicted this donor population to have superior immunosuppressive function, when in fact it generated comparable *IDO1* levels in response to all the IFN-γ activated MSC. Conversely, fold-change metrics would have marked this population as an unsuitable non-responder.

Development of reliable assays to qualify MSCs based on identity and functional utility have been hindered by the overwhelming heterogeneity of MSC populations derived from different donors and tissues. The remarkable transcriptome convergence documented in this study implies that a

substantial proportion of the heterogeneity in unstimulated cells may simply be noise (70). Once activated, this background is resolved and the meaningful differences between MSC populations emerge. We propose that focused assessment of activated MSC phenotypes can refine and expedite the development of robust surrogate assays and release criteria that clearly distinguish MSC populations with different functional properties.

DATA AVAILABILITY STATEMENT

The datasets presented in this study can be found in online repositories. The names of the repository/repositories and accession number(s) can be found in: NCBI's Gene Expression Omnibus (GEO), accession number GSE129165.

AUTHOR CONTRIBUTIONS

DW: Collection and/or assembly of data, data analysis and interpretation, manuscript writing, final approval of the manuscript. CW: Collection and/or assembly of data, final approval of the manuscript. BF: Financial support, final approval of the manuscript. LB: Conception and design, collection and/or assembly of data, data analysis and interpretation, manuscript writing, final approval of the manuscript.

FUNDING

This work was funded by Public Service and Procurement Canada contracts W7702 175853 and W7714 196914 to Aurora BioSolutions Inc.

ACKNOWLEDGMENTS

The authors wish to thank Cindy Ruttan for technical support for RNA preparation and array analysis, and Tissue Regeneration Therapeutics Inc., Toronto, Canada for provision of HUCPVCs.

SUPPLEMENTARY MATERIAL

The Supplementary Material for this article can be found online at: https://www.frontiersin.org/articles/10.3389/fimmu.2022.917790/full#supplementary-material

Supplementary Figure 1 | (A) Primer sequences used in RT-qPCR for 3 reference genes and 5 genes of interest. **(B)** Relative expression of genes of interest found by RT-qPCR, displayed as mean ± SEM of 3 donors, confirms their microarray expression. BM, bone marrow; F, forward; MSCs, mesenchymal stromal cells; R, reverse; ref, reference gene; UC, umbilical cord.

Supplementary Figure 2 | (A) UC and BM-MSC donor populations exhibit different doubling kinetics during the activation and CM collection period. Secreted analyte concentration was normalized to cell number at harvest and analyzed using units of pg/ml/million cells. **(B)** Dosed cytokines were not detected in UM after the 24-hour activation period. **(C)** Substantial MSC donor variability in secretion of TGF-β2 and IL-17 precluded statistical analysis. BM, bone marrow; CM, conditioned media; MSC, mesenchymal stromal cell; UC, umbilical cord; UM, unconditioned media.

Supplementary Figure 3 | Correlation between transcriptome and secreted responses of resting and activated UC (orange) and BM-MSCs (blue). **(A)** A modest relationship exists between transcriptome expression and secreted protein concentration in CM from resting MSCs. When MSCs are primed with **(B)** TNF-α, **(C)** IL1-β or **(D)** IFN-γ, substantial changes in protein expression are often not coupled to a measured increase in corresponding transcript abundance and vice versa. BM, bone marrow; CM, conditioned media; MSC, mesenchymal stromal cell; UC, umbilical cord.

REFERENCES

1. Galipeau J, Krampera M, Barrett J, Dazzi F, Deans RJ, DeBruijn J, et al. International Society for Cellular Therapy Perspective on Immune Functional Assays for Mesenchymal Stromal Cells as Potency Release Criterion for Advanced Phase Clinical Trials. *Cytotherapy* (2015) 18:151–59. doi: 10.1016/j.jcyt.2015.11.008
2. de Wolf C, van de Bovenkamp M, Hoefnagel M. Regulatory Perspective on *in Vitro* Potency Assays for Human Mesenchymal Stromal Cells Used in Immunotherapy. *Cytotherapy* (2017) 19:784–97. doi: 10.1016/j.jcyt.2017.03.076
3. Samsonraj RM, Raghunath M, Nurcombe V, Hui JH, van Wijnen AJ, Cool SM. Concise Review: Multifaceted Characterization of Human Mesenchymal Stem Cells for Use in Regenerative Medicine. *Stem Cells Transl Med* (2017) 6 (12):2173–85. doi: 10.1002/sctm.17-0129
4. Robb KP, Fitzgerald JC, Barry F, Viswanathan S. Mesenchymal Stromal Cell Therapy: Progress in Manufacturing and Assessments of Potency. *Cytotherapy* (2019) 21(3):289–306. doi: 10.1016/j.jcyt.2018.10.014
5. Yin JQ, Zhu J, Ankrum JA. Manufacturing of Primed Mesenchymal Stromal Cells for Therapy. *Nat Biomed Eng* (2019) 3:90–104 . doi: 10.1038/s41551-018-0325-8
6. Le Blanc K, Davies LC. MSCs—Cells With Many Sides. *Cytotherapy* (2018) 20:273–78 . doi: 10.1016/j.jcyt.2018.01.009
7. Viswanathan S, Keating A, Deans R, Hematti P, Prockop D, Stroncek DF, et al. Soliciting Strategies for Developing Cell-Based Reference Materials to Advance Mesenchymal Stromal Cell Research and Clinical Translation. *Stem Cells Dev* (2014) 23:1157–67 . doi: 10.1089/scd.2013.0591
8. Viswanathan S, Shi Y, Galipeau J, Krampera M, Leblanc K, Martin I, et al. Mesenchymal Stem Versus Stromal Cells: International Society for Cell & Gene Therapy (ISCT®) Mesenchymal Stromal Cell Committee Position Statement on Nomenclature. *Cytotherapy* (2019) 21:1019–24 . doi: 10.1016/j.jcyt.2019.08.002
9. Fong CY, Chak LL, Biswas A, Tan JH, Gauthaman K, Chan WK, et al. Human Wharton's Jelly Stem Cells Have Unique Transcriptome Profiles Compared to Human Embryonic Stem Cells and Other Mesenchymal Stem Cells. *Stem Cell Rev Rep* (2011) 7(1):1–16. doi: 10.1007/s12015-010-9166-x
10. Cho KA, Park M, Kim YH, Woo SY, Ryu KH. RNA Sequencing Reveals a Transcriptomic Portrait of Human Mesenchymal Stem Cells From Bone Marrow, Adipose Tissue, and Palatine Tonsils. *Sci Rep* (2017) 7(1):1–9. doi: 10.1038/s41598-017-16788-2
11. Alhattab D, Jamali F, Ali D, Hammad H, Adwan S, Rahmeh R, et al. An Insight Into the Whole Transcriptome Profile of Four Tissue-Specific Human Mesenchymal Stem Cells. *Regen Med* (2019) 14:841–65. doi: 10.2217/rme-2018-0137
12. Ménard C, Dulong J, Roulois D, Hébraud B, Verdière L, Pangault C, et al. Integrated Transcriptomic, Phenotypic, and Functional Study Reveals Tissue-Specific Immune Properties of Mesenchymal Stromal Cells. *Stem Cells* (2020) 38(1):146–59. doi: 10.1002/stem.3077
13. Medrano-Trochez C, Chatterjee P, Pradhan P, Stevens HY, Ogle ME, Botchwey EA, et al. Single-Cell RNA-Seq of Out-of-Thaw Mesenchymal Stromal Cells Shows Tissue-Of-Origin Differences and Inter-Donor Cell-Cycle Variations. *Stem Cell Res Ther* (2021) 12(1):565. doi: 10.1186/s13287-021-02627-9
14. Pires AO, Mendes-Pinheiro B, Teixeira FG, Anjo SI, Ribeiro-Samy S, Gomes ED, et al. Unveiling the Differences of Secretome of Human Bone Marrow

Mesenchymal Stem Cells, Adipose Tissue-Derived Stem Cells, and Human Umbilical Cord Perivascular Cells: A Proteomic Analysis. *Stem Cells Dev* (2016) 25(14):1073–83. doi: 10.1089/scd.2016.0048
15. Lv F, Lu M, Cheung KMC, Leung VYL, Zhou G. Intrinsic Properties of Mesemchymal Stem Cells From Human Bone Marrow, Umbilical Cord and Umbilical Cord Blood Comparing the Different Sources of MSC. *Curr Stem Cell Res Ther* (2012) 7(6):389–99. doi: 10.2174/157488812804484611
16. Najar M, Raicevic G, Jebbawi F, De Bruyn C, Meuleman N, Bron D, et al. Characterization and Functionality of the CD200-CD200R System During Mesenchymal Stromal Cell Interactions With T-Lymphocytes. *Immunol Lett* (2012) 146:50–6. doi: 10.1016/j.imlet.2012.04.017
17. Najar M, Krayem M, Merimi M, Burny A, Meuleman N, Bron D, et al. Insights Into Inflammatory Priming of Mesenchymal Stromal Cells: Functional Biological Impacts. *Inflamm Res* (2018) 67(6):467–77. doi: 10.1007/s00011-018-1131-1
18. Maleki M, Ghanbarvand F, Behvarz MR, Ejtemaei M, Ghadirkhomi E. Comparison of Mesenchymal Stem Cell Markers in Multiple Human Adult Stem Cells. *Int J Stem Cells* (2014) 7(2):118–26. doi: 10.15283/ijsc.2014.7.2.118
19. El Omar R, Beroud J, Stoltz J-F, Menu P, Velot E, Decot V. Umbilical Cord Mesenchymal Stem Cells: The New Gold Standard for Mesenchymal Stem Cell-Based Therapies? *Tissue Eng Part B Rev* (2014) 20(5):523–44. doi: 10.1089/ten.teb.2013.0664
20. Ma Y, Wang L, Yang S, Liu D, Zeng Y, Lin L, et al. The Tissue Origin of Human Mesenchymal Stem Cells Dictates Their Therapeutic Efficacy on Glucose and Lipid Metabolic Disorders in Type II Diabetic Mice. *Stem Cell Res Ther* (2021) 12(1):385. doi: 10.1186/s13287-021-02463-x
21. Iyer RK, Bowles PA, Kim H, Dulgar-Tulloch A. Industrializing Autologous Adoptive Immunotherapies: Manufacturing Advances and Challenges. *Front Med* (2018) 5:150. doi: 10.3389/fmed.2018.00150
22. Jossen V, van den Bos C, Eibl R, Eibl D. Manufacturing Human Mesenchymal Stem Cells at Clinical Scale: Process and Regulatory Challenges. *Appl Microbiol Biotechnol* (2018) 102(9):3981–94. doi: 10.1007/s00253-018-8912-x
23. Abdelrazik H, Spaggiari GM, Chiossone L, Moretta L. Mesenchymal Stem Cells Expanded in Human Platelet Lysate Display a Decreased Inhibitory Capacity on T- and NK-Cell Proliferation and Function. *Eur J Immunol* (2011) 41(11):3281–90. doi: 10.1002/eji.201141542
24. Kasoju N, Wang H, Zhang B, George J, Gao S, Triffitt JT, et al. Transcriptomics of Human Multipotent Mesenchymal Stromal Cells: Retrospective Analysis and Future Prospects. *Biotechnol Adv* (2017) 35:407–18. doi: 10.1016/j.biotechadv.2017.04.005
25. Krampera M. Mesenchymal Stromal Cell Licensing: A Multistep Process. *Leukemia* (2011) 25(9):1408–14. doi: 10.1038/leu.2011.108
26. Zachar L, Bačenková D, Rosocha J. Activation, Homing, and Role of the Mesenchymal Stem Cells in the Inflammatory Environment. *J Inflamm Res* (2016) 9:231–40. doi: 10.2147/JIR.S121994
27. Ferreira JR, Teixeira GQ, Santos SG, Barbosa MA, Almeida-Porada G, Gonçalves RM. Mesenchymal Stromal Cell Secretome: Influencing Therapeutic Potential by Cellular Pre-Conditioning. *Front Immunol* (2018) 9:2837. doi: 10.3389/fimmu.2018.02837
28. Sun C, Zhang K, Yue J, Meng S, Zhang X. Deconstructing Transcriptional Variations and Their Effects on Immunomodulatory Function Among Human Mesenchymal Stromal Cells. *Stem Cell Res Ther* (2021) 12(1):53. doi: 10.1186/s13287-020-02121-8
29. Corbett JM, Hawthorne I, Dunbar H, Coulter I, Chonghaile MN, Flynn CM, et al. Cyclosporine A and Ifnγ Licencing Enhances Human Mesenchymal Stromal Cell Potency in a Humanised Mouse Model of Acute Graft Versus Host Disease. *Stem Cell Res Ther* (2021) 12(1):238. doi: 10.1186/s13287-021-02309-6
30. Prasanna SJ, Gopalakrishnan D, Shankar SR, Vasandan AB, Pro-Inflammatory Cytokines. *IFNγ TNFα Influence Immune Properties Hum Bone Marrow Wharton Jelly Mesenchymal Stem Cells Differentially PloS One* (2010) 5:1–16. doi: 10.1371/journal.pone.0009016
31. Hemeda H, Jakob M, Ludwig A-K, Giebel B, Lang S, Brandau S. Interferon-γ and Tumor Necrosis Factor-α Differentially Affect Cytokine Expression and Migration Properties of Mesenchymal Stem Cells. *Stem Cells Dev* (2010) 19 (5):693–706. doi: 10.1089/scd.2009.0365
32. Kim J-H, Jo CH, Kim H-R, Hwang Y. Comparison of Immunological Characteristics of Mesenchymal Stem Cells From the Periodontal Ligament, Umbilical Cord, and Adipose Tissue. *Stem Cells Int* (2018) 2018:1–12. doi: 10.1155/2018/8429042
33. Wiese DM, Ruttan CC, Wood CA, Ford BN, Braid LR. Accumulating Transcriptome Drift Precedes Cell Aging in Human Umbilical Cord-Derived Mesenchymal Stromal Cells Serially Cultured to Replicative Senescence. *Stem Cells Transl Med* (2019) 8(9):946–58 . doi: 10.1002/sctm.18-0246
34. Dominici M, Le Blanc K, Mueller I, Slaper-Cortenbach I, Marini FC, Krause DS, et al. Minimal Criteria for Defining Multipotent Mesenchymal Stromal Cells. The International Society for Cellular Therapy Position Statement. *Cytotherapy* (2006) 8(4):315–7. doi: 10.1080/14653240600855905
35. Sarugaser R, Lickorish D, Baksh D, Hosseini MM, Davies JE. Human Umbilical Cord Perivascular (HUCPV) Cells: A Source of Mesenchymal Progenitors. *Stem Cells* (2005) 23(2):220–9. doi: 10.1634/stemcells.2004-0166
36. Davies JE, Walker JT, Keating A. Concise Review: Wharton's Jelly: The Rich, But Enigmatic, Source of Mesenchymal Stromal Cells. Stem Cells Transl. *Med* (2017) 6(7):1620–30. doi: 10.1002/sctm.16-0492
37. Huber W, Carey VJ, Gentleman R, Anders S, Carlson M, Carvalho BS, et al. Orchestrating High-Throughput Genomic Analysis With Bioconductor. *Nat Methods* (2015) 12(2):115–21. doi: 10.1038/nmeth.3252
38. R Core Team. *R: A Language and Environment for Statistical Computing*. Vienna, Austria: R Foundation for Statistical Computing (2017).
39. Wu J, Irizarry R, MacDonald J, Gentry J. *Gcrma: Background Adjustment Using Sequence Information*. (2017). https://www.bioconductor.org/packages/devel/bioc/manuals/gcrma/
40. Wilson CL, Miller CJ. Simpleaffy: A BioConductor Package for Affymetrix Quality Control and Data Analysis. *Bioinformatics* (2005) 21(18):3683–5. doi: 10.1093/bioinformatics/bti605
41. Miller CJ. *Simpleaffy: Very Simple High Level Analysis of Affymetrix Data*. (2017).
42. Affymetrix Inc. *GeneChip ® Expression Analysis Data Analysis Fundamentals GENECHIP ® EXPRESSION ANALYSIS*. http://tools.thermofisher.com/content/sfs/manuals/data_analysis_fundamentals_manual.pdf
43. Manimaran S, Selby HM, Okrah K, Ruberman C, Leek JT, Quackenbush J, et al. BatchQC: Interactive Software for Evaluating Sample and Batch Effects in Genomic Data. *Bioinformatics* (2016) 32(24):3836–8. doi: 10.1093/bioinformatics/btw538
44. Johnson WE, Li C, Rabinovic A. Adjusting Batch Effects in Microarray Expression Data Using Empirical Bayes Methods. *Biostatistics* (2007) 8 (1):118–27. doi: 10.1093/biostatistics/kxj037
45. Gentleman R, Carey VJ, Huber W, Hahne F. *Genefilter: Methods for Filtering Genes From High-Throughput Experiments*. R package version 1.68.0 (2019). https://bioconductor.org/packages/release/bioc/html/genefilter.html
46. Ritchie ME, Phipson B, Wu D, Hu Y, Law CW, Shi W, et al. Limma Powers Differential Expression Analyses for RNA-Sequencing and Microarray Studies. *Nucleic Acids Res* (2015) 43(7):e47–59. doi: 10.1093/nar/gkv007
47. Mccarthy DJ, Smyth GK. Testing Significance Relative to a Fold-Change Threshold Is a TREAT. *Bioinformatics* (2009) 25:765–71 . doi: 10.1093/bioinformatics/btp053
48. Benjamini Y, Hochberg Y. Controlling the False Discovery Rate: A Practical and Powerful Approach to Multiple Testing. *J R Stat Soc Ser B Methodol* (1995) 57(1):289–300. doi: 10.1111/j.2517-6161.1995.tb02031.x
49. Pagès H, Carlson M, Falcon S, Li N. *AnnotationDbi: Annotation Database Interface*. (2017). https://bioconductor.org/packages/release/bioc/html/AnnotationDbi.html
50. Carlson M. *Hgu133a2.Db: Affymetrix Human Genome U133A 2.0 Array Annotation Data (Chip Hgu133a2)*. (2016) https://bioconductor.org/packages/release/data/annotation/html/hgu133a2.db.html.
51. Gu Z, Eils R, Schlesner M. Complex Heatmaps Reveal Patterns and Correlations in Multidimensional Genomic Data. *Bioinformatics* (2016) 32:2847–284 . doi: 10.1093/bioinformatics/btw313
52. Huang DW, Sherman BT, Lempicki RA. (2009) 37(1):1–13. doi: 10.1093/nar/gkn923
53. Huang DW, Sherman BT, Lempicki RA. Systematic and Integrative Analysis of Large Gene Lists Using DAVID Bioinformatics Resources. *Nat Protoc* (2009) 4(1):44–57. doi: 10.1038/nprot.2008.211
54. Ashburner M, Ball CA, Blake JA, Botstein D, Butler H, Cherry JM, et al. Gene Ontology: Tool for the Unification of Biology. *Nat Genet* (2000) 25:25–29. doi: 10.1038/75556

55. Carbon S, Douglass E, Dunn N, Good B, Harris NL, Lewis SE, et al. The Gene Ontology Resource: 20 Years and Still GOing Strong. *Nucleic Acids Res* (2019) 47(D1):D330–8. doi: 10.1093/nar/gky1055
56. Kanehisa M, Goto S. Yeast Biochemical Pathways. KEGG: Kyoto Encyclopedia of Genes and Genomes. *Nucleic Acids Res* (2000) 28:27–30. doi: 10.1093/nar/28.1.27
57. Kanehisa M, Sato Y, Furumichi M, Morishima K, Tanabe M. New Approach for Understanding Genome Variations in KEGG. *Nucleic Acids Res* (2019) 8: D590–D59. doi: 10.1093/nar/gky962
58. Edgar R, Domrachev M, Lash AE. Gene Expression Omnibus: NCBI Gene Expression and Hybridization Array Data Repository. *Nucleic Acids Res* (2002) 30(1):207–10. doi: 10.1093/nar/30.1.207
59. Barrett T, Wilhite SE, Ledoux P, Evangelista C, Kim IF, Tomashevsky M, et al. NCBI GEO: Archive for Functional Genomics Data Sets - Update. *Nucleic Acids Res* (2013) 41:D991–D995. 10.1093/nar/gks1193.
60. Dvinge H, Bertone P. HTqPCR: High-Throughput Analysis and Visualization of Quantitative Real-Time PCR Data in R. *Bioinformatics* (2009) 25(24):3325–6. doi: 10.1093/bioinformatics/btp578
61. McCall MN, McMurray HR, Land H, Almudevar A. On Non-Detects in QPCR Data. *Bioinformatics* (2014) 30(16):2310–6. doi: 10.1093/bioinformatics/btu239
62. De Ronde MWJ, Ruijter JM, Lanfear D, Bayes-Genis A, Kok MGM, Creemers EE, et al. Practical Data Handling Pipeline Improves Performance of QPCR-Based Circulating MiRNA Measurements. *Rna* (2017) 23(5):811–21. doi: 10.1261/rna.059063.116
63. Xie F, Xiao P, Chen D, Xu L, Zhang B. MiRDeepFinder: A MiRNA Analysis Tool for Deep Sequencing of Plant Small RNAs. *Plant Mol Biol* (2012) 80 (1):75–84. doi: 10.1007/s11103-012-9885-2
64. Bio-Rad Laboratories Inc. *Real-Time PCR Applications Guide*. (2006). pp. 1–100. https://www.bio-rad.com/webroot/web/pdf/lsr/literature/Bulletin_5279.pdf
65. Chen K, Wang D, Du WT, Han ZB, Ren H, Chi Y, et al. Human Umbilical Cord Mesenchymal Stem Cells HUC-MSCs Exert Immunosuppressive Activities Through a PGE2-Dependent Mechanism. *Clin Immunol* (2010) 135:448–58. doi: 10.1016/j.clim.2010.01.015
66. Bárcia RN, Santos JM, Filipe M, Teixeira M, Martins JP, Almeida J, et al. What Makes Umbilical Cord Tissue-Derived Mesenchymal Stromal Cells Superior Immunomodulators When Compared to Bone Marrow Derived Mesenchymal Stromal Cells? *Stem Cells Int* (2015) 2015:1–14. doi: 10.1155/2015/583984
67. Van Den Broek LJ, Kroeze KL, Waaijman T, Breetveld M, Sampat-Sardjoepersad SC, Niessen FB, et al. Differential Response of Human Adipose Tissue-Derived Mesenchymal Stem Cells, Dermal Fibroblasts, and Keratinocytes to Burn Wound Exudates: Potential Role of Skin-Specific Chemokine Ccl27. *Tissue Eng - Part A* (2014) 20(1–2):197–209. doi: 10.1089/ten.tea.2013.0123
68. Hur J, Yang HT, Chun W, Kim JH, Shin SH, Kang HJ, et al. Inflammatory Cytokines and Their Prognostic Ability in Cases of Major Burn Injury. *Ann Lab Med* (2015) 35:105–10. doi: 10.3343/alm.2015.35.1.105
69. Ketterl N, Brachtl G, Schuh C, Bieback K, Schallmoser K, Reinisch A, et al. A Robust Potency Assay Highlights Significant Donor Variation of Human Mesenchymal Stem/Progenitor Cell Immune Modulatory Capacity and Extended Radio-Resistance. *Stem Cell Res Ther* (2015) 6(1):1–11. doi: 10.1186/s13287-015-0233-8
70. Paladino FV, Sardinha LR, Piccinato CA, Goldberg AC. Intrinsic Variability Present in Wharton's Jelly Mesenchymal Stem Cells and T Cell Responses May Impact Cell Therapy. *Stem Cells Int* (2017) 2017:1–12. doi: 10.1155/2017/8492797
71. Donders R, Bogie JFJ, Ravanidis S, Gervois P, Vanheusden M, Marée R, et al. Human Wharton's Jelly-Derived Stem Cells Display a Distinct Immunomodulatory and Proregenerative Transcriptional Signature Compared to Bone Marrow-Derived Stem Cells. *Stem Cells Dev* (2018) 27:65–84 . doi: 10.1089/scd.2017.0029
72. Heathman TRJJ, Rafiq QA, Chan AKCC, Coopman K, Nienow AW, Kara B, et al. Characterization of Human Mesenchymal Stem Cells From Multiple Donors and the Implications for Large Scale Bioprocess Development. *Biochem Eng J* (2016) 108:14–23. doi: 10.1016/j.bej.2015.06.018
73. Szabó E, Fajka-Boja R, Kriston-Pál É, Hornung Á, Makra I, Kudlik G, et al. Licensing by Inflammatory Cytokines Abolishes Heterogeneity of Immunosuppressive Function of Mesenchymal Stem Cell Population. *Stem Cells Dev* (2015) 24(18):2171–80. doi: 10.1089/scd.2014.0581
74. Van Megen KM, Van 't Wout EJT, Motta JL, Dekker B, Nikolic T, Roep BO. Activated Mesenchymal Stromal Cells Process and Present Antigens Regulating Adaptive Immunity. *Front Immunol* (2019) 10:694(APR). doi: 10.3389/fimmu.2019.00694
75. Noronha NDC, Mizukami A, Caliári-Oliveira C, Cominal JG, Rocha JLM, Covas DT, et al. Correction to: Priming Approaches to Improve the Efficacy of Mesenchymal Stromal Cell-Based Therapies (Stem Cell Research and Therapy. *Stem Cell Res Ther* (2019) 10(1):1–21. doi: 10.1186/s13287-019-1259-0
76. Wobma HM, Kanai M, Ma SP, Shih Y, Li HW, Duran-Struuck R, et al. Dual IFN-γ/Hypoxia Priming Enhances Immunosuppression of Mesenchymal Stromal Cells Through Regulatory Proteins and Metabolic Mechanisms. *J Immunol Regen Med* (2018) 1:45–56. doi: 10.1016/j.regen.2018.01.001
77. Huang Y, Li Q, Zhang K, Hu M, Wang Y, Du L, et al. Single Cell Transcriptomic Analysis of Human Mesenchymal Stem Cells Reveals Limited Heterogeneity. *Cell Death Dis* (2019) 10(5):1–12. doi: 10.1038/s41419-019-1583-4
78. De Witte SFH, Merino AM, Franquesa M, Strini T, Van Zoggel JAA, Korevaar SS, et al. Cytokine Treatment Optimises the Immunotherapeutic Effects of Umbilical Cord-Derived MSC for Treatment of Inflammatory Liver Disease. *Stem Cell Res Ther* (2017) 8(1):1–12. doi: 10.1186/s13287-017-0590-6
79. Domenis R, Cifù A, Quaglia S, Pistis C, Moretti M, Vicario A, et al. Pro Inflammatory Stimuli Enhance the Immunosuppressive Functions of Adipose Mesenchymal Stem Cells-Derived Exosomes. *Sci Rep* (2018) 8(1):1–11. doi: 10.1038/s41598-018-31707-9
80. Kim DS, Jang IK, Lee MW, Ko YJ, Lee DH, Lee JW, et al. Enhanced Immunosuppressive Properties of Human Mesenchymal Stem Cells Primed by Interferon-γ. *EBioMedicine* (2018) 28:261–73. doi: 10.1016/j.ebiom.2018.01.002
81. Boland L, Burand AJ, Brown AJ, Boyt D, Lira VA, Ankrum JA. IFN-γ and TNF-α Pre-Licensing Protects Mesenchymal Stromal Cells From the Pro-Inflammatory Effects of Palmitate. *Mol Ther* (2018) 26(3):860–73. doi: 10.1016/j.ymthe.2017.12.013
82. Chinnadurai R, Rajan D, Ng S, McCullough K, Arafat D, Waller EK, et al. Immune Dysfunctionality of Replicative Senescent Mesenchymal Stromal Cells Is Corrected by IFNg Priming. *Blood Adv* (2017) 1(11):628–43. doi: 10.1182/bloodadvances.2017006205
83. Chinnadurai R, Copland IB, Garcia MA, Petersen CT, Lewis CN, Waller EK, et al. Cryopreserved MSCs Are Susceptible to T-Cell Mediated Apoptosis Which Is Partly Rescued by Ifnγ Licensing Raghavan. *Stem Cells* (2016) 34 (9):2429–42. doi: 10.1002/stem.2415.Cryopreserved
84. Burand AJ, Gramlich OW, Brown AJ, Ankrum JA. Function of Cryopreserved Mesenchymal Stromal Cells With and Without Interferon-γ Prelicensing Is Context Dependent. *Stem Cells* (2017) 35(5):1437–9. doi: 10.1002/stem.2528
85. Kwon HM, Hur SM, Park KY, Kim CK, Kim YM, Kim HS, et al. Multiple Paracrine Factors Secreted by Mesenchymal Stem Cells Contribute to Angiogenesis. *Vasc Pharmacol* (2014) 63:19–28. doi: 10.1016/j.vph.2014.06.004
86. Chinnadurai R, Rajan D, Qayed M, Arafat D, Garcia M, Liu Y, et al. Potency Analysis of Mesenchymal Stromal Cells Using a Combinatorial Assay Matrix Approach. *Cell Rep* (2018) 22:2504–17. doi: 10.1016/j.celrep.2018.02.013
87. Redondo-Castro E, Cunningham C, Miller J, Martuscelli L, Aoulad-Ali S, Rothwell NJ, et al. Interleukin-1 Primes Human Mesenchymal Stem Cells Towards an Anti-Inflammatory and Pro-Trophic Phenotype in Vitro. *Stem Cell ResTher* (2017) 8(79):1–17. doi: 10.1186/s13287-017-0531-4
88. Mennan C, Garcia J, Roberts S, Hulme C, Wright K. A Comprehensive Characterisation of Large-Scale Expanded Human Bone Marrow and Umbilical Cord Mesenchymal Stem Cells. *Stem Cell Res Ther* (2019) 10 (1):1–15. doi: 10.1186/s13287-019-1202-4
89. Jahromi SH, Li Y, Davies JE. Effect of Tumor Necrosis Factor Alpha Dose and Exposure Time on Tumor Necrosis Factor Induced Gene-6 Activation by Neonatal and Adult Mesenchymal Stromal Cells. *Stem Cells Dev* (2018) 27 (1):44–54. doi: 10.1089/scd.2017.0179
90. Meisel R, Zibert A, Laryea M, Göbel U, Däubener W, Dilloo D. Human Bone Marrow Stromal Cells Inhibit Allogeneic T-Cell Responses by Indoleamine

2,3-Dioxygenase-Mediated Tryptophan Degradation. *Blood* (2004) 103 (12):4619–21. doi: 10.1182/blood-2003-11-3909

Conflict of Interest: LB is an officer and a shareholder of Aurora BioSolutions Inc. DW and CW are employees of Aurora BioSolutions Inc.

The remaining authors declare that the research was conducted in the absence of any commercial or financial relationships that could be construed as a potential conflict of interest.

Publisher's Note: All claims expressed in this article are solely those of the authors and do not necessarily represent those of their affiliated organizations, or those of the publisher, the editors and the reviewers. Any product that may be evaluated in this article, or claim that may be made by its manufacturer, is not guaranteed or endorsed by the publisher.

frontiers | Frontiers in Immunology

TYPE Original Research
PUBLISHED 19 August 2022
DOI 10.3389/fimmu.2022.976511

OPEN ACCESS

EDITED BY
Guido Moll,
Charité Universitätsmedizin Berlin, Germany

REVIEWED BY
Takeo Mukai,
The University of Tokyo, Japan
Tokiko Nagamura-Inoiue,
The University of Tokyo, Japan

*CORRESPONDENCE
Karen Bieback
Karen.bieback@medma.uni-heidelberg.de
Richard Schäfer
richard.schaefer@uniklinik-freiburg.de

†These authors have contributed equally to this work and share senior authorship

SPECIALTY SECTION
This article was submitted to Vaccines and Molecular Therapeutics, a section of the journal Frontiers in Immunology

RECEIVED 23 June 2022
ACCEPTED 27 July 2022
PUBLISHED 19 August 2022

CITATION
Willer H, Spohn G, Morgenroth K, Thielemann C, Elvers-Hornung S, Bugert P, Delorme B, Giesen M, Schmitz-Rixen T, Seifried E, Pfarrer C, Schäfer R and Bieback K (2022) Pooled human bone marrow-derived mesenchymal stromal cells with defined trophic factors cargo promote dermal wound healing in diabetic rats by improved vascularization and dynamic recruitment of M2-like macrophages.
Front. Immunol. 13:976511.
doi: 10.3389/fimmu.2022.976511

Pooled human bone marrow-derived mesenchymal stromal cells with defined trophic factors cargo promote dermal wound healing in diabetic rats by improved vascularization and dynamic recruitment of M2-like macrophages

Hélène Willer[1,2], Gabriele Spohn[3], Kimberly Morgenroth[3], Corinna Thielemann[1], Susanne Elvers-Hornung[1], Peter Bugert[1], Bruno Delorme[4], Melanie Giesen[4], Thomas Schmitz-Rixen[5], Erhard Seifried[3], Christiane Pfarrer[2], Richard Schäfer[3,6,7*†] and Karen Bieback[1,8,9*†]

[1]Institute of Transfusion Medicine and Immunology, Medical Faculty Mannheim, Heidelberg University, German Red Cross Blood Donor Service Baden-Württemberg - Hessen, Mannheim, Germany, [2]Institute for Anatomy, University of Veterinary Medicine Hannover, Hannover, Germany, [3]Institute for Transfusion Medicine and Immunohaematology, German Red Cross Blood Service Baden-Württemberg-Hessen, Frankfurt am Main, Germany, [4]Macopharma, Mouvaux, France, [5]German Society of Surgery, Berlin, Germany, [6]Institute for Transfusion Medicine and Gene Therapy, Medical Center – University of Freiburg, Freiburg, Germany, [7]Center for Chronic Immunodeficiency (CCI), Medical Center – University of Freiburg, Freiburg, Germany, [8]Mannheim Institute for Innate Immunoscience, Medical Faculty Mannheim, Heidelberg University, Mannheim, Germany, [9]FlowCore, Medical Faculty Mannheim, Heidelberg University, Mannheim, Germany

Human Mesenchymal Stromal Cells (hMSCs) are a promising source for cell-based therapies. Yet, transition to phase III and IV clinical trials is remarkably slow. To mitigate donor variabilities and to obtain robust and valid clinical data, we aimed first to develop a manufacturing concept balancing large-scale production of pooled hMSCs in a minimal expansion period, and second to test them for key manufacture and efficacy indicators in the clinically highly relevant indication wound healing. Our novel clinical-scale manufacturing concept is comprised of six single donor hMSCs master cell banks that are pooled to a working cell bank from which an extrapolated number of 70,000 clinical doses of $1x10^6$ hMSCs/cm^2 wound size can be manufactured within only three passages. The pooled hMSC batches showed high stability of key manufacture indicators such as morphology, immune phenotype, proliferation, scratch wound healing, chemotactic migration and angiogenic support. Repeated topical hMSCs administration significantly accelerated the wound healing in a diabetic rat model by delivering a defined growth factor cargo

(specifically BDNF, EGF, G-CSF, HGF, IL-1α, IL-6, LIF, osteopontin, VEGF-A, FGF-2, TGF-β, PGE-2 and IDO after priming) at the specific stages of wound repair, namely inflammation, proliferation and remodeling. Specifically, the hMSCs mediated epidermal and dermal maturation and collagen formation, improved vascularization, and promoted cell infiltration. Kinetic analyses revealed transient presence of hMSCs until day (d)4, and the dynamic recruitment of macrophages infiltrating from the wound edges (d3) and basis (d9), eventually progressing to the apical wound on d11. In the wounds, the hMSCs mediated M2-like macrophage polarization starting at d4, peaking at d9 and then decreasing to d11. Our study establishes a standardized, scalable and pooled hMSC therapeutic, delivering a defined cargo of trophic factors, which is efficacious in diabetic wound healing by improving vascularization and dynamic recruitment of M2-like macrophages. This decision-making study now enables the validation of pooled hMSCs as treatment for impaired wound healing in large randomized clinical trials.

KEYWORDS

mesenchymal stromal cells (MSCs), pooling, chronic wound healing, potency, efficacy, clinical scale production, platelet lysate, pathogen-inactivation

Introduction

Despite advances in patient stratification and treatments, chronic wounds are still an unmet clinical challenge for an increasing number of patients. Non-healing wounds are a particularly serious health problem for an aging population with severe comorbidities such as obesity, diabetes or cardiovascular diseases (1). The WHO reports 422 million patients with diabetes of whom 15-25% develop chronic wounds (https://www.who.int) (2).

Human Mesenchymal Stromal Cells (hMSCs) have been widely investigated in cellular therapies for the treatment of autoimmune, inflammatory, and vascular diseases (3, 4). Specifically, MSCs can improve wound healing, most likely by secreting factors associated with chemoattraction, cell proliferation and differentiation, immunomodulation, angiogenesis, anti-apoptosis, anti-fibrosis, and even anti-microbial effects (1, 5–7). This has led to several promising preclinical studies, as well as phase I and II clinical trials targeting chronic skin wounds, venous ulcers and epidermolysis bullosa (8–11). Yet, transition to phase III and IV clinical trials, or even marketing authorization, is remarkably slow. Next to safety and efficacy issues, often related to inconsistent study results, the so far tested hMSC therapies have been proven neither cost-effective, nor competitive against best-practice therapies (12). Next to technical obstacles (e.g. up-scaling and cryopreservation), issues pertaining to hMSC biology, such as donor variabilities, functional senescence, and the large variety of proposed mechanisms of action (MoAs), are increasing the complexity even further (13). Thus, to obtain robust and valid clinical data, it is of utmost importance to manufacture a substantial amount of hMSC doses from highly reproducible clinical hMSC products that can be tested in large randomized clinical trials. Furthermore, these products and their clinical evaluation require approval by the competent regulatory authorities. These expect a thorough scientific approach addressing GMP-compatible manufacturing, comprehensive quality control and in-depth preclinical efficacy and safety testing (13).

Upscaling issues of hMSCs were intensely discussed when a large phase III clinical trial failed to meet its clinical endpoint: the respective product "Prochymal™", an allogeneic hMSC therapeutic, expanded *in vitro* to produce numerous clinical doses, lacked efficacy. In contrast, other allogeneic hMSC products, expanded to only few clinical doses, reproducibly showed efficacy in trials for steroid-refractory graft-versus-host-disease (GvHD) (14). This suggests that hMSCs manufacture should be carefully balanced to yield a sufficient number of clinical doses, but with only few population doublings during *ex vivo* production.

Inconsistent results from clinical trials may also result from donor-to-donor variability when hMSCs are manufactured from single donors (15). To address this, hMSC pooling concepts were developed. As one example, the product "MSC-FFM" was manufactured from pooled bone marrow (BM) mononuclear cells (MNCs), containing hMSC precursors as well as alloreactive immune cells of eight healthy 3rd-party donors (16). Besides reducing donor variability, an allogeneic immune reaction was intended to produce immunologically primed

hMSCs with higher immunosuppressive strength. Indeed, for these cells beneficial effects in children and adults with severe steroid-refractory GvHD were reported (17, 18). Yet, highly immunosuppressive hMSCs may not be the first choice when aiming at chronic wound healing. Another example of a pooled hMSC product is "Stempeucel®", successfully evaluated in critical limb ischemia. Here, a donor master cell bank (MCB) of single donor hMSCs after passage 1 was established (19). Next, a working cell bank (WCB) was generated by pooling hMSCs from three donors. This was then further expanded for five passages until the final product was cryopreserved. While the pooled "MSC-FFM" product requires establishing a new pooled hMSC MCB from scratch, the single-donor "Stempeucel®" hMSCs MCB concept allows high batch-to-batch consistency as recently shown (20). Yet, replicative aging within the five passages until reaching final product formulation may affect the quality of the clinical product (21).

To balance the needs for reproducible clinical results with consistent cell batches without extensive cell expansion, we developed a novel pooling concept based on various single donor MCBs, and pooled WCBs for final dose manufacture. We pooled six donors to efficiently level out donor-to-donor heterogeneity while keeping donor exposure low (22). In detail, we expanded the hMSCs from single donors in passage 0 and cryopreserved them as single donor MCBs. After thawing, we pooled single donor-derived hMSCs at different passages achieving a pooled hMSC MCB and expanded these as pooled hMSC WCBs up to passage 3. This concept allows identifying the pooled WCB with the best potential to manufacture maximal dose numbers at considerably low passage.

Human platelet lysate (hPL) is an increasingly used media supplement for cell therapies manufacture that promotes hMSC expansion *ex vivo* (23, 24). Yet, platelet donor variability and batch inconsistencies may hamper the implementation of robust manufacture concepts (13). To maximize consistency and ensure comparability, we used a large hPL batch pooled from 70 donors for the entire hMSC production series in our study. Pooling platelet donations equilibrates the hPL donor variability; yet, multi-donor exposure may increase the risk for transmitting infectious agents, which in turn can be addressed by pathogen reduction treatment (PRT) (22). Therefore, the pooled hPL batch used in this study was treated by high-dose gamma irradiation for pathogen reduction (25). The main advantages of gamma irradiation are that it does not involve any additives, and thus no residues, and that it can be directly applied to the final homogeneous and standardized pooled hPL batches. High-dose gamma irradiation (35 kGy) can efficiently inactivate both enveloped and non-enveloped viruses, meeting the current regulatory requirements (26), and irradiated hPL was shown to maintain hMSC proliferation capacity and function (25).

In addition to donor-to-donor variance and extensive expansion, cryodamage and dosing issues are discussed to compromise the success of hMSCs clinical translation. To ease manufacturing and delivery, hMSCs are typically expanded *ex vivo* and then cryopreserved as clinical products, which are then shipped to the patient´s bedside, where they are administered directly after thawing. Yet, cryopreservation may affect clinical potency associated with a heat-shock response, reduced immunomodulatory and homing capacity (27–29) and increased tissue factor expression (30).

To evaluate our novel hMSC product, we compared pools generated at passage 1, 2 and 3 (Pool 1, 2 and 3, respectively). Pools were first assessed *in vitro* for cell yield (clinical doses/batch), morphology, immune phenotype, growth factor content, proliferation, scratch/wound healing, chemotactic migration and angiogenic support. Based on highest yield and acceptable *in vitro* functions, we selected Pool 2 hMSCs for testing their wound healing capacity within a preclinical wound healing model *in vivo*. Zucker diabetic fatty rats were chosen as model of impaired and delayed wound healing (31). One million hMSCs/cm^2 were topically applied within a diluted fibrin glue, previously shown to support cell viability and migration into the wounds (8, 9). In a series of pilot experiments, we compared possible cryodamage of freshly thawed hMSCs to hMSCs from rescue culture, and single versus 3-times repeated hMSC administration to target the different wound healing phases, respectively. Further, we assessed eventual systemic effects. The hMSC-treated wounds showed accelerated wound healing, accompanied by better wound indices (epidermal and dermal regeneration and collagen deposition), improved angiogenesis and increased macrophage infiltration and M2-like polarization.

Methods and materials

BM-derived hMSCs: Isolation, cultivation and characterization

Human BM-MNCs were obtained by puncturing the iliac crest of healthy BM donors (ethical vote # 329/10, ethics committee, University Hospital Frankfurt am Main, Germany). The hBM-MNCs were seeded at a density of 100,000 cells/cm^2 in Nunclon™ Delta flasks in 93% alpha-MEM with Glutamin (Lonza, Cologne, Germany), 6% pooled virally inactivated human platelet lysate (hPL) (MultiPL´100i, Macopharma, Tourcoing, France), 1% Penicillin/Streptomycin (Thermo Fisher Scientific, Darmstadt, Germany) and 2 IU Heparin (Ratiopharm GmbH, Ulm, Germany). After 24h, the non-adherent cells were removed by rinsing with PBS (Thermo Fisher Scientific) and culture medium exchange, and hMSCs were grown from the adherent cell fraction (15). For scale-up and GMP-compatible manufacture, hMSCs were also cultured in CellStacks with a larger culture surface enabling seeding, media exchange and harvest in a closed system (MC3 system, Macopharma). After reaching subconfluence, hMSCs were split using TrypLE™ Select (Thermo Fisher Scientific) and seeded at

a density of 1,000 cells/cm^2, or cryopreserved in 33% hPL, 5% DMSO (Sigma-Aldrich, Taufkirchen, Germany) in alpha-MEM as single donor-MCB. To level out individual differences, single donor hMSCs from six randomly chosen donors were then thawed and pooled at equal cell numbers (e.g. 6 times 1x10^6 hMSCs), either at beginning of passage 1, 2 or 3 (Pool 1, 2 and 3, respectively). End of passage 3, hMSCs were cryopreserved as final ("clinical") product. Pool 1 and 2 served as pooled WCBs (Figure 1A).

The hMSCs were verified to be mycoplasma- (Venor® GeM Classic, Minerva Biolabs GmbH, Berlin, Germany) and endotoxin-free (Endosafe® nexgen-PTS™, Charles River Laboratories, Freiburg, Germany).

Population doublings were calculated using the formula:

$$Population\ \ doublings\ \ (PD) = \frac{\ln(\frac{harvest}{seed})}{ln2}$$

and maximum achievable cell number by

$$maximum\ \ achievable\ \ cell\ \ number = input{\star}2^{population\ \ doubling}$$

Maximum achievable cell numbers at end of passage 3 and target cell dose equivalents (1x10^6 hMSCs/cm^2 wound size) were extrapolated for Pools 1 -3, respectively (32).

The hMSCs were characterized by a battery of *in vitro* test systems: First, marker expression (binary markers, either absent or present on hMSCs (33)) was assessed by flow cytometry (32). Second, adipogenic differentiation was induced using the hMSC Adipogenic Differentiation Medium BulletKit™ (Lonza, Basel, Switzerland) and osteogenic differentiation using osteogenic medium composed of alpha-MEM, 10% FBS supplemented with 1 µM dexamethasone, 50 µM ascorbic acid and 10 mM β-glycerolphosphate (Sigma-Aldrich), respectively. After three weeks of differentiation cells were lineage specifically stained: lipid vacuoles in adipogenic differentiation cultures were stained with Oil Red O, calcium deposits of osteogenic differentiated cells with Alizarin Red, respectively. Third, the hMSCs' capacity to inhibit T cell proliferation *in vitro* was assessed (32). Briefly, hMSCs were pre-seeded and CellTrace™ Violet (Thermo Fisher)-labeled pooled peripheral blood mononuclear cells (PBMNCs) were added, and further stimulated with phytohemagglutinin-L (PHA-L, 10 µg/mL, Sigma-Aldrich), or kept as non-stimulated controls. Proliferation of PBMNCs was assessed after 5 days using flow cytometry and hMSC-mediated inhibition was calculated. Fourth, live cell imaging using the Incucyte® Zoom device (Sartorius AG, Hertfordshire, United Kingdom) was performed and analyzed using Incucyte® analysis algorithms. First, hMSCs proliferation was assessed by seeding 200 hMSCs/cm^2 and monitoring the increase in cell confluence over time. The 96h time point was chosen to compare Pools 1-3. Second, a scratch wound healing assay of hMSC monolayer was performed. In detail, hMSCs were seeded at 60,000 cells/cm^2 and incubated overnight. Then, wound scratches were applied using

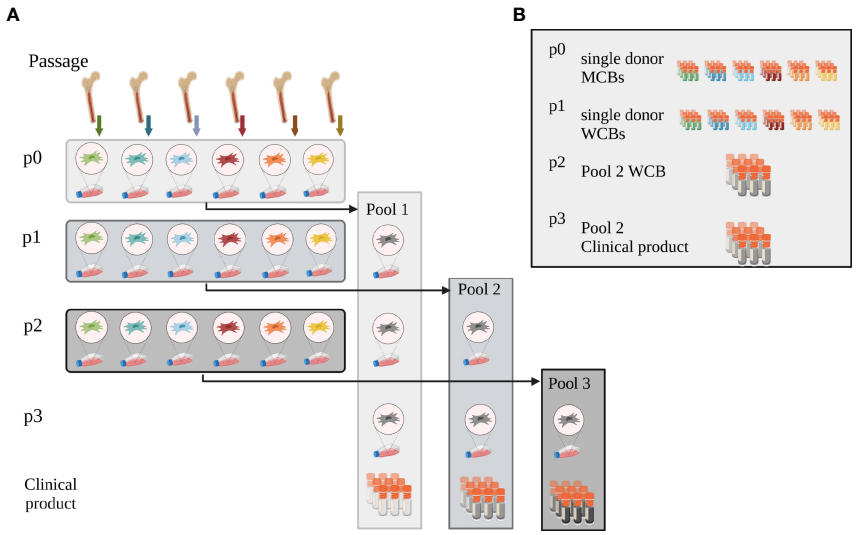

FIGURE 1
Pooling concept. **(A)** Pooling concept: hMSCs were isolated and expanded from bone marrow from six individual donors (passage p0). To initiate passage 1 expansion, single donor hMSCs were then thawed and either pooled at the onset of passage 1 (Pool 1) or expanded as single-donor hMSCs individually. These were then either pooled at the onset of passage 2 (Pool 2) or 3 (Pool 3), respectively. Pooled hMSCs at the end of passage 3 were cryopreserved, formulated as clinical product. **(B)** Master and Working Cell Bank concept: at the end of passage 0, single donor-derived hMSCs were cryopreserved as single donor MCBs. Single donor MSCs expanded in passage 1 were cryopreserved when harvested after passage 1 and served as WCBs. Pool 2 hMSCs, pooled at the onset of passage 2, were cryopreserved as working cell bank (WCB Pool 2) at the end of passage 2. Aliquots from this WCB were thawed and expanded one further passage to yield the potential clinical product end of passage 3. These cells were thawed and used for all experiments. Created with BioRender.com.

the 96-pin Incucyte® woundmaker tool. The wound closure (wound density at different time points relative to initial wound size) was calculated over time and values at 24h used for comparison. Third, angiogenic tube network formation on hMSCs monolayers was assessed, as described previously (34). hMSCs were seeded at 60,000 cells/cm^2 and after 60min 15,000 green fluorescent protein (GFP)+ human umbilical vein endothelial cells (HUVECs) were added. Human adipose-derived stromal cells (hASCs) served as positive control and were used for normalization of individual experiments. Network length (mm/mm^2) was chosen as parameter for quantitative analysis. Fourth, chemotactic migration of hMSCs was assessed (35). Briefly, the insert plate of an Incucyte® ClearView 96 well plate was coated with fibronectin. Subsequently, 1,000 hMSCs were seeded and the plate was mated with the reservoir plate containing serum-free or hPL-containing medium. hMSCs migration was monitored for 48h and analyzed as "count normalized to initial top value".

Trophic factors of hMSCs lysate were quantified using Luminex and ELISA technologies (32). Briefly, 1-10 x 10^6 hMSCs were harvested. hMSC pellets were lysed with ice-cold ProcartaPlex™ Cell Lysis Buffer, centrifuged at maximum speed and supernatant stored at -80°C until assays were performed. Transforming growth factor beta 1 (TGF-β1) and Prostaglandin E2 (PGE2) were analyzed by ELISA (Biorbyt Ltd., Cambridge, UK and Cayman Chemical, Ann Arbor, MI, USA, resp.), Fibroblast growth factor 2 (FGF2) was analyzed by singleplex and all other trophic factors using a ProcartaPlex™ custom multiplex panel (Thermo Fisher Scientific).

hMSCs' IDO-1 production was stimulated by tumor necrosis factor- α (TNF-α), interleukin-1β (IL-1β), and interferon-ɣ (IFN-ɣ), each 20 ng/mL for 48h. Subsequently, hMSCs were harvested and counted. Pellets were lysed (300 mM NaCl, 50 mM Tris, 2 mM $MgCl_2$, 0.05% NP40, 1x Protease/Phosphatase Inhibitor), centrifuged at maximum speed and supernatant stored at -80°C until ELISA (Cloud-Clone Corp., Katy, TX, United States) was performed.

To assess the trophic factors content in the pooled hPL batch used in this study (MultiPL'100i; batch number 11219267DM), two different bags were tested by ELISA (Bio-techne; FGF (#SFB50), vascular endothelial growth factor-A (VEGF-A; #SVE00), epidermal growth factor (EGF; #SEG00), platelet-derived growth factor-AB (PDGF-AB) (#SHD00C), insulin-like growth factor-1 (IGF-1) (#SG100) and TGF-β1 (#SB100B)).

Wound healing model

Animal experiments were approved by the local ethics committee (G142-19, Regierungspräsidium Karlsruhe, Germany). Zucker diabetic rats were chosen as model of impaired wound healing (31). In total, 66 six weeks old male rats (ZDF (obese fa/fa), ZDF-Leprfa/Crl; Charles River Laboratories, Châtillon, France) were used. Upon arrival, rats were kept in groups of two and fed ad libitum with a special high-fat diet (Purina #5008, ssniff Spezialdiät GmbH, Soest, Germany) for 6 weeks to induce diabetes type II (Figure 2A). Rats were weighed every 2 days and non-fasted blood glucose was measured once a week (Accu-Chek® Aviva, Roche Diabetes Care, Mannheim, Germany). Animals were considered diabetic with a glucose level of 300 mg/dL, typically reached 3 weeks after initiating diet. Only diabetic rats were used for the wound healing experiments. Rats with blood glucose levels above 600 mg/dL were fed with the normal food until blood glucose levels dropped.

At 12 weeks of age, rats were anaesthetized with isoflurane (CP-Pharma 1 mL/mL, induction with 5% isoflurane plus 5 L/min oxygen and maintenance with 2-3% isoflurane plus 1 L/min oxygen) and 0.8 mL of blood were taken. For wound setting the rats were shaved on the back, the surgery field was disinfected and two wounds were set 1.5 cm behind the shoulder blades and 1.5 cm right and left from the spine with an 8 mm skin biopsy punch (WDT®, Garbsen, Germany). Only the skin was removed, the skeletal muscle fascia was left intact. Depending on the experimental setting, control animals were either left completely untreated or one wound was untreated and the other treated with cell-free fibrin glue. In other animals, one wound was treated with fibrin glue plus hMSCs, whereas the contralateral wound served as control, left untreated or treated with cell-free fibrin glue (Figure 2B). Post-surgery 10 mL of physiological saline was injected subcutaneously to avoid dehydration and allow faster recovery after anaesthesia. To protect wounds from contamination or mutilation, a wound dressing was applied (Curapor®, Lohmann-Rauscher, Rengsdorf, Germany). This dressing was changed every other day. 200 mg/kg of metamizole sodium was used for analgesia (Novaminsulfon® solution for injection 500 mg/mL, Bela-pharm, Vechta, Germany) given for 4 days by subcutaneous injection.

For topical cell application, a commercial fibrin sealant syringe system was used (TISSEEL, Baxter Deutschland GmbH, Unterschleißheim, Germany). hMSCs were either thawed (cryo) or trypsinized after a short rescue culture (fresh; cells were thawed, cultured for up to two days to recover from eventual cryo-damage and to re-boot their metabolism), washed, counted and formulated at a density of 5x10^5 viable hMSCs in 50 µL prediluted fibrinogen/aprotinin solution (final concentration 5 mg/mL) (9). Immediately before the application to the wounds, the cell suspension was drawn in one syringe of the duplojet device, while the other syringe contained prediluted thrombin solution (final concentration 25 mg/mL). Both components were combined using the TISSEEL duplojet system to formulate the fibrin glue. For each wound, 50 µL fibrinogen with hMSCs and 50 µL thrombin were then applied onto the wound, resulting in a dose of 1x10^6 hMSCs/cm^2 wound. The glue was allowed to polymerize in the air for 7 minutes before applying the wound dressing.

To assess the capacity of the hMSCs to migrate out of the gel, an *in vitro* migration assay was performed. Briefly, fibrin glue

with hMSCs was applied into a well of a 24-well plate. Subsequently, the hMSCs` migration towards hPL-supplemented culture medium as attractant, or serum-free medium as control, was evaluated microscopically.

Three pilot studies were performed, according to the 6R principles with each 3-5 animals. First, to pretest eventual cryopreservation damage we compared freshly thawed (cryo) hMSCs against rescue culture post-thaw (fresh) hMSCs (28–30). Second, we compared single dose injection (d0) against repeated hMSCs administration (days 0, 4 and 8) to apply hMSCs at the inflammation, proliferation and remodeling phase respectively (Figure 2A). Of note, despite smaller wound sizes, we applied the same cell dose as on d0. Third, we investigated eventual systemic effects of hMSCs. Here, single rats were allocated into one group where the contralateral site served as control, and the lateral site was treated with hMSCs and compared to a group of animals with only control-treated wounds.

With the results from the pilot study, a power analysis was performed to calculate the sample size for the main study. Here, culture-adapted fresh hMSCs were applied repeatedly, but treatments of the two wounds were chosen randomly (in total, n= 42 rats in the main study). To overcome potential breed-specific biases, experiments were performed in different experimental cohorts.

Furthermore, a biodistribution study was performed where animals were sacrificed on day 1, 2, 3, 4, 9 and 11 (each one animal per group). Here, both wounds served as either control (untreated/fibrin group) or were hMSCs-treated. Wound, liver, spleen and lungs were harvested, snap-frozen and then analyzed for the presence of human cells by immunohistochemical staining and digital PCR (dPCR).

For each animal, every other day upon wound dressing change, the wounds were scaled and photographed with a perpendicular angle. Wound area was measured using ImageJ (36). In addition, blood samples were taken after 14 days before the animals were sacrificed and a blood count performed (CELL-DYN Ruby, Abbott GmbH, Wiesbaden, Germany). First, the rats were fully anaesthetized with isoflurane and then 100 mg/kg ketamine and 5 mg/kg xylazine were injected intracardially. To avoid autolysis, wounds and organs were removed immediately.

A

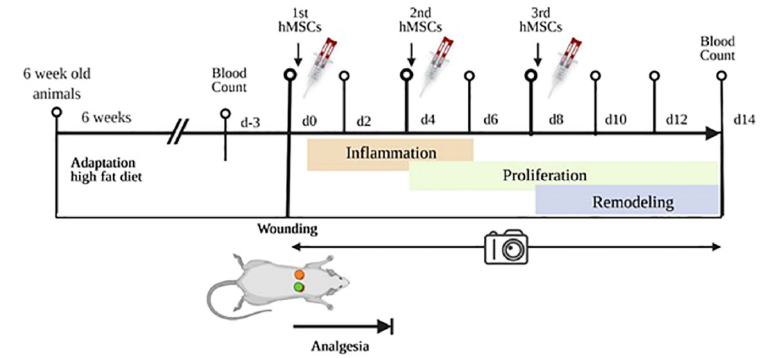

B

		Groups	Lateral wound	Contralateral wound
Pilot studies	1.1x; fresh or cryo ? 2.Fresh;1x or 3x ? 3.Systemic effect?	Untreated	Untreated	Untreated
		Fibrin glue	Fibrin glue	Untreated
		hMSCs	hMSCs	Untreated
Main Study	hMSCs fresh, 3x	Untreated	Untreated	Untreated
		Fibrin glue	Fibrin glue	Untreated
		hMSCs	hMSCs	Untreated
	Reduce animal numbers (6Rs) (e.g. biodistribution)	Untreated/ Fibrin glue	Fibrin glue	Untreated
		hMSCs	hMSCs	hMSCs

FIGURE 2
Schematic of *in vivo* wound healing assay. **(A)** Diabetic ZDF rats were wounded and treated topically with hMSCs ($1x10^6/cm^2$ wound) in diluted fibrin glue. Untreated and cell-free fibrin glue-treated wounds served as control (created with BioRender.com). **(B)** Table representing animal allocation. fresh, MSCs from max. 2 days of rescue-culture before administration to the wounds; cryo, MSCs thawed immediately before application; 1x, single application day 0; 3x, repeated application d0, day 4 and day 8.

Wounds were cut in half to perform all analyses at the wounds center and were either paraformaldehyde (PFA)-fixed and paraffin-embedded or snap-frozen in Tissue-Tek® and cryomolds.

Histological and immunohistochemical analysis

Standard hematoxylin-eosin (HE) and Azan staining was performed on 5 µm thick cuts after organ fixation in 4% PFA and paraffin embedding.

To investigate whether hMSCs promote host cell infiltration into the wound, artificial intelligence and QuPath algorithms (37) based on a random tree classifier were used for analyzing HE stains. First, the wound was defined as region of interest. Second, an automatic cell detection was run to determine the total cell count in this area. Using QuPath-based cell classification, fibroblasts and lymphocytes were discriminated based on nuclear stain (more homogenous and intense in lymphocytes than fibroblasts) and cellular morphology (round lymphocytes versus elongated fibroblasts). In addition, a "composite classifier" was used to improve the differentiation of lymphocytes characterized by their very pronounced circularity compared to fibroblasts.

Heidenhain's Azan trichrome stain was performed to assess collagen fiber deposition. Mean blue intensity was taken as measure of collagen density and dermis maturation. For this the "intensity mean value: blue" feature was used (Zeiss Zen 3.0 blue edition, Carl Zeiss Microscopy, Oberkochen, Germany). This tool calculates the average brightness (pixel value) of the selected region of interest. Dark blue colors reflecting high collagen density have lower pixel values than the lighter blue stains of wounds with fewer collagen fibers. Pixel values of the wound tissue were compared with those of the surrounding not injured dermis, with lower intensity equivalent to more collagen deposition in the granulation tissue.

$$\text{Blue mean intensity in \%} = \frac{\text{wound intensity mean blue value} * 100}{\text{not injured dermis intensity mean blue value}}$$

Immunohistochemical staining was performed to assess the degree of vascularization (CD31+ endothelial cells), immune cell infiltration (CD68+ and CD163+ macrophages) and presence of the transplanted hMSCs (human Ku80+ cells (38)). Cryosections (10 µm) were fixed in 4 % PFA for 10 minutes. Nonspecific binding sites were blocked using 1 % bovine serum albumin (BSA, PAN-Biotech, Aidenbach, Germany), 0.2 % fish skin gelatin (Sigma-Aldrich) and 0.1 % Triton X (Carl Roth, Karlsruhe, Germany) in Tris-Buffer saline. Antibodies were then added and incubated overnight (each 1:1,000 for mouse anti-rat monoclonal CD31 (Ab64543), Abcam, Cambridge, UK, rabbit anti-rat polyclonal CD68 (Ab125212) Abcam, mouse anti-rat monoclonal CD163 (MCA342GA) BioRad, Feldkirchen, Germany, and 1:250 rabbit anti-human monoclonal Ku80 (EPR3468), Abcam). After washing, endogenous peroxidase was blocked in 3 % H_2O_2. Then, the secondary biotinylated antibody was added for 30 min (1:100 anti-mouse and anti-rabbit Ig, (RPN1001V, RPN1004V1) GE-healthcare, Solingen, Germany). Then 1 % streptavidin peroxidase (GE-healthcare) was added. Histogreen was used as substrate chromogen (Linaris GmbH, Dossenheim, Germany). Nuclei were counterstained with Mayer's hematoxylin and sections mounted after dehydration in 99 % ethanol, tissue clear and n-butyl acetate. Control slides were either left unstained to evaluate Histogreen background signal or stained with only the 2nd antibody. Slides were scanned (Zeiss AXIO Scan.Z1) and analyzed using QuPath open software (36), creating a color filter to quantify histogreen-positive area in the entire wound previously defined as region of interest.

hKu80 staining in the organs was validated using Alexa Fluor 488- or Alexa Fluor 568-labeled secondary antibodies, (1:1,000; Life Technologies, Thermo Fisher Scientific) and TO-PRO-3 nuclear stain (Thermo Fisher Scientific) and assessed by confocal microscopy.

Histology scoring system

Epidermal Thickness Index (ETI)

In 14 days old wounds, the average thickness of the wound epidermis was calculated for five locations and compared to the average thickness of the non-lesioned epidermis.

$$ETI = \frac{\text{average epidermis thickness in wound area} * 100}{\text{average epidermis thickness in uninjured skin}}$$

An ETI > 105 % is considered hypertrophic and mostly observed during the re-epithelialization phase and is an indicative of healing. A return of the epidermis thickness close to non-injured skin (95%<ETI<105 %) is only observed after remodeling stage (39).

Scar elevation Index (SEI)

In 14 days old wounds, the average thickness of the dermis was calculated using five areas and compared to the average thickness of the unwounded dermis.

$$SEI = \frac{\text{average dermis thickness in wound area} * 100}{\text{average dermis thickness in uninjured skin}}$$

A hypertrophic dermis in the wound (SEI>105 %) can reflect excessive collagen deposition and is therefore an indirect indicator of scar formation. A hypotrophic dermis with a SEI<95 % is typically reported in early stages of healing wounds and reflects an underdeveloped dermis. A 95<SEI<105 % characterizes a wound dermis whose thickness has returned to normal and is only observed in the final stage of healing (39).

Chip-based dPCR to detect residual human cells

To follow the fate of the topically applied hMSCs, wounds and organs were analyzed for human DNA using a sensitive dPCR method (40).

The dPCR assay was designed for detection of the single locus gene *GAPDH* in the rat and the human genome with specific primers and TaqMan™ probes with minor groove binding (MGB) modification at the 3'-end. For human *GAPDH*: forward primer, 5'-ccccacacacatgcacttacc-3'; reverse primer, 5'-cctagtcccagggctttgatt-3'; VIC-labeled probe, 5'-taggaaggacaggcaac-3'; for mouse/rat *GAPDH*: forward primer, 5'-gaatataaaattagatctctttggac-3'; reverse primer, 5'-gttgaatgcttggatgtacaacc-3'; FAM-labeled probe, 5'-taggaaggacaggcaac-3'. The human/rat GAPDH assay was prepared as 40x concentrated mixture containing 9 µmol of each primer and 5 µmol of each probe resulting in a final concentration of 225 nmol of each primer and 125 nmol of each probe.

The dPCR (QuantStudio® 3D; Thermo Fisher Scientific) was performed on chips with 20,000 reaction wells each with 755 pL volume. For each dPCR analysis 7.1 µL DNA was mixed with 0.375 µL 40x GAPDH assay and 7.5 µL dPCR Master Mix V2 containing ROX as reference dye (Thermo Fisher Scientific). The cycling program started with 10 min at 96 °C, followed by 40 cycles with 30 sec at 98 °C and 2 min at 52 °C. After cycling the dPCR chips were scanned for the FAM and VIC signals (QuantStudio® 3D Chip Reader; Thermo Fisher Scientific) and the data were analyzed using the QuantStudio 3D AnalysisSuite cloud software (https://apps.thermofisher.com/quantstudio3d). Based on the fluorescence signals and statistical correction using Poisson distribution the software enabled calculation of target copies per µL and target/total (%) values. For validation of the assay, human and rat genomic DNA was used pure and mixed at defined ratios (1:10, 1:20, 1:50). Human DNA was reliably detectable in the 1:50 mixture (detection limit 2 %; approx. 4 copies/µL), whereas, pure rat DNA showed a background signal of 0.2% (approx. 0.4 copies/µL). 0.5 copies/µl were calculated as cut-off for positive signals.

Statistics

Quantitative data are presented as means ± standard deviation (SD) and were compared with analysis of variance (ANOVA) and *post hoc* tests as specified in the figures using GraphPad Prism (La Jolla, CA, USA). Values of $p < 0.05$ were considered as statistically significant.

Results

Closed system and pooled hPL allow scale-up manufacture of pooled hMSC doses with defined trophic factors content

For scale-up and GMP-compatible manufacture, hMSCs were simultaneously cultured in standard Nunclon™ Delta flasks (175 cm^2 per flask) as well as in CELLSTACK™ with a larger culture surface (636 cm^2 per stack) enabling seeding, media exchange and harvest in the closed MC3 system. Growth kinetics and hMSC surface marker expression were identical (not shown). Production of clinical-scale doses was more feasible with the closed MC3 system due to optimized handling for media changes and passaging/harvest particularly reducing hands-on time in the cell culture.

The extrapolated maximum of cell numbers that could be produced in line with highest number of target cell doses (~70,000 extrapolated doses) was achieved with Pool 2 hMSCs compared to Pool 1 (~6,000 extrapolated doses) and 3 (~50,000 extrapolated doses) hMSCs (Figures 1A, B, 3A, B). For all hMSC pools, the expression of binary (absent or present) MSC markers was identical, consistent with guidelines set by the International Society for Cellular Therapy (Figure 3C). The functional characterization of the hMSC pools proved similar regarding their adipogenic and osteogenic differentiation potential (Supplementary Figure 1) and their immunomodulatory strength measured by their inhibition of PHA-driven T cell proliferation (Figure 3D). Proliferation, scratch wound healing, vascular tube formation support and chemotactic migration assessed by live cell imaging showed also no differences between the hMSC pools (Figures 3E–H). Yet, due to apparent day-to-day and operator-to-operator related variations in the latter assays, the need for better assay standardization became obvious.

Given that Pool 2 hMSCs achieved the highest calculated numbers of extrapolated clinical doses with similar characteristics compared to Pool 1 and 3 hMSCs, we elected Pool 2 hMSCs for further preclinical evaluation.

The delivery of trophic factors is a key MoA of hMSCs (13). Therefore, we quantitatively evaluated trophic factor candidates for wound healing. Of note, we analyzed the hMSC lysates reflecting the actual clinical product, rather than mere cell culture supernatant collected during expansion. Specifically, we detected BDNF, EGF, G-CSF, HGF, IL-1α, IL-6, LIF, osteopontin, VEGF-A, FGF-2, TGF-β, PGE-2 and inducible IDO-1 in the hMSCs and calculated their contents per applied hMSC dose (Table 1). GM-CSF, IL-1β, NGF-β, angiopoietin, IFN-γ, IL-2 and TNF-α were below the detection limit of the assay. These growth factors are active in different phases of wound healing.

Given that the media supplement influences the final trophic factors composition of the hMSC lysates (54), we tested also the hPL batch used in this study (Supplementary Table 1). Here, we detected high concentrations of TGF-β1, EGF, PDGF-AB and VEGF-A, mirrored by the relatively high amounts of TGF- β1 and VEGF-A in the hMSC dose (Table 1).

hMSCs migrate from the fibrin glue and improve skin wound healing in diabetic rats

For cell application, we used a protocol established by Yufit et al. using 1:10 diluted TISSEEL fibrin glue as cell carrier (9). In

10.3389/fimmu.2022.976511

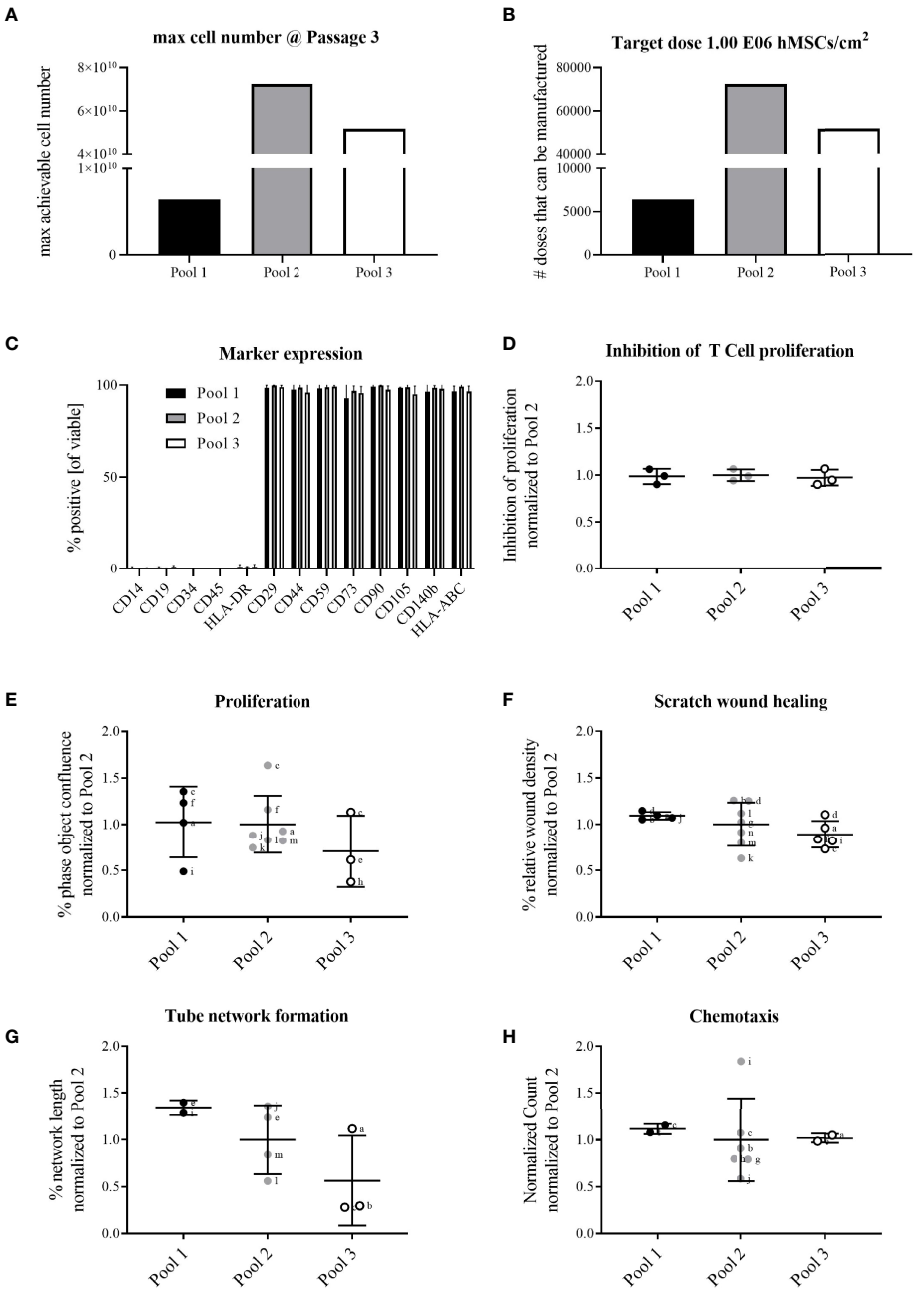

FIGURE 3
All hMSC pools featured similar proliferation capacity, yet with Pool 2 hMSCs the highest number of extrapolated clinical doses could be achieved. All pools exerted similar functional characteristics. Calculation of **(A)** maximally achievable cell doses/manufacturing batch and **(B)** cell doses manufactured/batch (1x10^6 hMSCs/cm^2 wound size) for hMSCs pooled at either passage 1 (Pool 1), passage 2 (Pool 2) or passage 3 (Pool 3). **(C)** Flow cytometry characterization of binary (absent or present) hMSCs markers. **(D-H)** Functional characterization of hMSC pools. Data are shown as normalized to the average of Pool 2. **(D)** hMSCs-mediated inhibition of PHA-driven T cell proliferation. **(E–H)** Live cell imaging analyses of functional hMSC attributes: **(E)** proliferation; phase object confluence 96h post-seeding; **(F)** scratch wound healing: relative wound density at 24h post-wounding; **(G)** tube network formation: hMSCs were seeded as monolayer and fluorescently-labeled endothelial cells (HUVEC) were seeded on top. Tube length was assessed 48h post-seeding and calculated as percent of human adipose stromal cell-mediated tube formation; **(H)** chemotactic migration to hPL-supplemented medium in bottom chamber. Counts of migrated cells in bottom wells were normalized to initial top-well values. Serum-free medium served as negative control. **(E–H)** Small letters indicate experimental replicates performed on different days by different operators. All data are shown as data from individual experimental replicates, indicating mean ± SD.

TABLE 1 Trophic factors in Pool 2 hMSC lysate, calculated per hMSCs dose.

	pg/applied hMSCs dose	Wound healing function	References
Luminex			
BDNF	3.06	Acts proangiogenic	(41)
EGF	0.58	Induces migration, proliferation, plasticity of epithelial cells, fibroblast function, formation of granulation tissue	(42, 43)
G-CSF	1.99	Accelerates wound healing, promotes neutrophil infiltration	(44)
HGF	122.68	Induces migration, proliferation, and matrix metalloproteinase production of keratinocytes, acts proangiogenic	(42, 45)
IL-1*a*	2.33	Stimulates keratinocyte and fibroblast proliferation, extracellular matrix remodeling, fibroblast chemotaxis, regulates the immune response	(46)
IL-6	23.08	Mitogenic for keratinocytes, promotes neutrophil attraction	(42)
LIF	6.94	Enhances proangiogenic potential of hMSCs	(47)
Osteopontin	21.63	Regulates ECM, myofibroblast differentiation	(41, 42)
VEGF-A	174.43	Acts proangiogenic	(41)
FGF2	2.69	Acts proangiogenic, mitogenic for fibroblasts and keratinocytes	(42)
GM-CSF	below detection limit	Mitogenic for keratinocytes, induces migration and proliferation of endothelial cells, regulates macrophage polarization	(41, 42)
IL-1β	below detection limit	Acts proinflammatory	(41)
NGF-*b*	below detection limit	Stimulates nerve ingrowth	(42)
Angiopoietin	below detection limit	Induces vessel stabilization and remodeling	(42)
IFN-γ	below detection limit	Modulates cell-mediated immunity, neutrophil inflammatory response, M1 polarization, can impair wound healing	(48, 49)
IL-2	below detection limit	Attracts immune cells	(50, 51)
TNF-α	below detection limit	Proinflammatory, inhibits myofibroblast differentiation	(41)
ELISA			
TGF-*β*1	162.29	Promotes chemoattraction, angiogenesis, M2 macrophage polarization, myofibroblast differentiation, mitogenic for fibroblasts, inhibits proliferation of keratinocytes, stimulates ECM proteins and integrin expression	(41, 42)
PGE2	26.57	Induces anti-inflammatory responses, M2 macrophage polarization, is proangiogenic, reduces pathological scar formation	(52)
IDO-1 (after stimulation for 48h with TNF-*a*, IL-1β, IFN-γ)	555.07	Modulates immune responses	(53)

BDNF, brain-derived neurotrophic factor; EGF, epidermal growth factor; G-CSF, granulocyte colony stimulating factor; HGF, hepatocyte growth factor; IL-1*a*, interleukin 1 alpha; IL-6, interleukin 6; LIF, leukemia inhibitory factor; VEGF-A, vascular endothelial growth factor A; FGF2, fibroblast growth factor 2; GM-CSF, granulocyte-macrophage colony-stimulating factor; IL-1β, interleukin 1 beta; NGF-β, nerve growth factor beta; IFN-γ, interferon gamma; IL-2, interleukin 2; TNF-*a*, tumor necrosis factor alpha; TGF-β1, transforming growth factor beta 1; PGE2, prostaglandin E2; IDO-1, indoleamine 2,3-dioxygenase.

a pilot *in vitro* experiment, we verified that hMSCs formulated in the 1:10 diluted fibrin glue were able to egress and migrate from the glue. The diluted fibrin glue needed about 7 minutes to polymerize to a gel. After 4.5 hours the hMSCs started to migrate from the glue into the culture vessel, and hMSC migration increased over time (Supplementary Figure 2). Of note, no migration was induced in serum-free conditions indicating targeted migration of hMSCs.

For the *in vivo* evaluation of the wound healing potential of pooled hMSCs, three pilot studies were performed in preparation for the main study. In each study, two circular wounds of 8 mm diameter were set per one animal and either left untreated, treated with cell-free fibrin glue, or with hMSCs-formulated fibrin glue (Figures 2A, B).

In pilot study 1, we evaluated an eventual cryodamage comparing just thawed hMSCs (cryo) with hMSCs from a rescue culture (fresh). From day 4 on, wounds treated with fresh hMSCs healed slightly better than hMSCs cryo (Figure 4B). On day 12, a significantly smaller wound size was calculated in hMSC cryo-treated wounds compared to untreated wounds. Cell-free fibrin glue per se, compared to untreated wounds, promoted wound healing, but slightly delayed compared to hMSCs-treated wounds (d10 and d12, Figure 4B). Based on these data, we concluded that hMSCs show a slight cryodamage

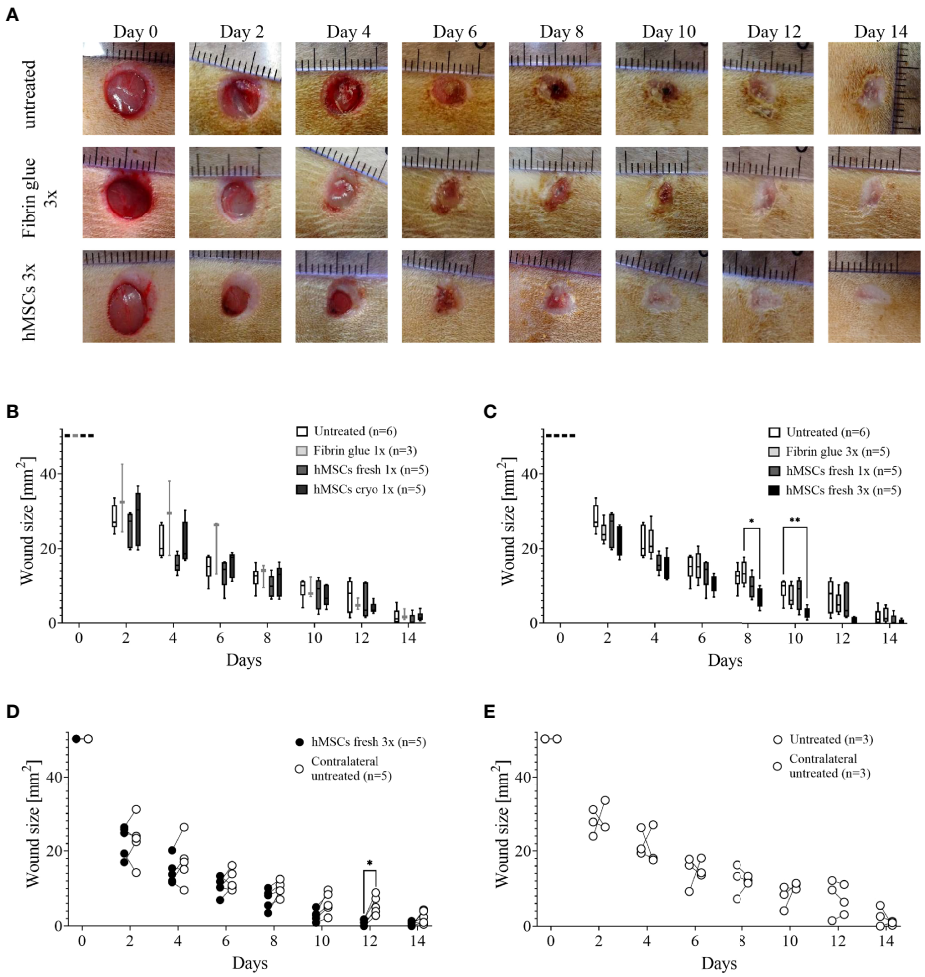

FIGURE 4
Pilot studies 1-3 to assess cryodamage, dose finding and systemic wound healing effects. **(A)** Representative images of wounded skin after single topical treatment with either hMSCs in fibrin glue, cell-free fibrin glue or untreated at d0 after wounding. **(B)** Wound area reduction after topical treatment with either untreated, cell-free fibrin glue and hMSCs thawed (cryo) or from rescue culture (fresh), **(C)** Single versus 3-times repeated hMSCs administration (1x versus 3x fresh, d0, 4 and 8). Quantification of wound areas relative to initial wound area was performed with Image J. Data are presented as min to max box-whisker plots denoting the median. **(D, E)** Comparison of wound size reduction of contralateral untreated wounds with lateral either hMSCs **(D)** or untreated wounds **(E)**. Side-by side comparison of hMSCs fresh vs. contralateral untreated and untreated vs. contralateral untreated shown. *p≤ 0.05, **p≤ 0.01 as calculated using two-way ANOVA und Tukey multiple comparisons. fresh, MSCs from max. 2 days of rescue-culture before administration to the wounds; cryo, MSCs thawed immediately before application; 1x, single application day 0; 3x, repeated application d0, day 4 and day 8.

and favored the use of rescue-cultured fresh hMSCs for the subsequent experiments.

In pilot study 2, we evaluated whether repeated application on days 0, 4 and 8 of fresh hMSC doses could further accelerate wound healing. Given that the hMSC therapeutic contained a large variety of growth factors, known to be active, and thus, being required, during the inflammation, proliferation and remodeling phase of wound healing, we applied hMSCs at respective time points, d0, d4 and d8 reflecting the different wound healing phases (Figure 2A). Starting at day 4, wounds treated with hMSCs trended smaller than control-treated wounds, but from day 8 on, wounds treated 3 times with hMSCs were significantly smaller compared to controls (Figures 4A, C).

Topically applied hMSCs do not exert systemic wound healing effects

Further, blood samples collected during the pilot studies were analyzed comparing white blood cells (WBCs), neutrophil, lymphocyte and platelet counts on day 0 and day 14. In the control settings, all blood cell counts appeared to be increased at

day 14. Yet, WBCs and especially lymphocyte counts in 9 out of 15 hMSCs-treated animals were decreased compared to d0. This effect was more pronounced after repeated hMSCs application (not shown). None of the control animals showed this trend.

Accordingly, we asked in pilot study 3 whether hMSCs would exert systemic effects and could affect healing of the contralateral wound where no hMSCs were applied topically. Statistical analysis revealed that only the wounds that were topically treated with three hMSC doses at the different time points significantly improved healing. The contralateral untreated site showed comparable healing as untreated wounds (Figures 4D, E; Supplementary Figure 3). These data suggest that topically applied hMSCs exert their therapeutic wound healing effects only locally.

Based on the results from these pilot studies and a power-based sample size calculation, the main study was designed (i) using fresh, rescue-cultured hMSCs, (ii) repeated application of hMSC doses on day 0, 4 and 8, and (iii) reduced numbers of control wounds according to the 6Rs principles, as systemic effects were excluded.

Results from the main study supported the significant wound healing effect of hMSCs. Wounds treated with three sequential hMSC doses were significantly smaller on days 10, 12 and 14 compared to both controls (Figures 5A, B). Importantly, some wounds treated with hMSCs were already closed on day 12 after wound setting. In both control groups the first wounds were completely healed only at day 14. We found that both control wounds, untreated and cell-free fibrin glue-treated, showed similar wound healing rates. In these series of experiments, we observed extensive crust formation in fibrin glue-treated wounds, but not the hMSC-fibrin glue-treated wounds (Figure 5).

The data from the pilot and the main studies documented that hMSCs significantly improved wound healing compared to both control groups. Yet, the initially observed trend of decreased circulating lymphocytes within peripheral blood after topical hMSCs application was not confirmed.

hMSCs increase CD31-positive capillaries and recruit CD68- and CD163-positive macrophages into healing wounds

Having observed accelerated wound healing in hMSCs-treated wounds, histological analysis was performed. To gain insight into cell infiltration to the wounds, cells in total, lymphocytes and fibroblasts were identified based on their typical nuclear and cell phenotypic features (Figure 6A). In the hMSCs-treated wounds more lymphocytes could be detected compared to untreated and fibrin glue-treated wounds, whereas fibroblast and total cell numbers seemed unaffected by hMSCs treatment (Figure 6A).

In a next step, immunohistochemical staining of CD31, indicative of tissue vascularization, CD68 as pan-macrophage marker and CD163 as marker for M2-subtype anti-inflammatory macrophages, activated in murine wound healing promoting to anti-inflammatory functions, extracellular matrix formation and angiogenesis (55), was performed. We found an increase in CD31+ capillaries in the wounds repeatedly treated by hMSCs doses compared to untreated controls and fibrin glue-treated controls (Figures 6B, C). The hMSCs-treated wounds showed also a higher proportion of CD68+ and CD163+ infiltrated macrophages, compared to both control groups (Figures 6D, E). Detailed microscopic wound assessment at different time points after wound setting (part of the biodistribution study) revealed gradual infiltration of macrophages from the wound edges (d3), then the basal wound area (d9), eventually progressing to the apical wound tissue on d11 (Figure 7). In the hMSCs-treated wounds, CD68+ cell infiltration extended more towards the apical layers than in both controls (Figures 7C, E). This infiltration was accelerated in hMSCs-treated wounds at day 9 to then drop to similar levels as both controls on d11 (Figure 7A). Starting at day 4, hMSCs promoted infiltration/differentiation of CD163-expressing macrophages, whereas both control-treated wounds revealed no increase in CD163-positive cells. Only in hMSC-treated wounds the CD163+ signal peaked at day 9 (Figure 7B) with positive signals in the entire wound area extending to the apical layer (Figures 7D, F).

hMSCs improve epithelial thickness, reduce scar elevation and increase collagen density in healing wounds

Having documented that hMSCs led to an increase in vascularization and induced CD68-, but also CD163-positive macrophage infiltration, we aimed to gain more insights into the healing dynamics of the wounds. Here, a histology scoring system was used (39). First, an epithelial thickness index was calculated (Figure 6F). Almost all wounds demonstrated hypertrophy of the epithelium, indicative for their healing stage (39). Without statistical significance, mean values suggested that the hMSCs-treated wounds showed the least epithelial thickness, followed by fibrin and then untreated wounds (Figure 6F). Second, a scar elevation index was calculated. All wounds demonstrated hypoplasia of the dermis, yet hMSCs-treated wounds were already close to a normal state, significantly different to the untreated wounds, indicating an already better-developed wound compared to both controls (Figure 6G). Third, collagen density was calculated based on intensity of blue Azan stain and compared to the respective non-wounded dermis. After migration into the wound, fibroblasts gradually produce ECM and collagen fibers. During wound healing, especially during proliferation stage, collagen accumulates in wounds, resulting in a darker blue Azan stain. Our results indicated a significantly higher collagen deposition and density in hMSCs-treated wounds on day 14 of our experiment compared to controls indicative of improved collagen deposition (Figure 6H).

10.3389/fimmu.2022.976511

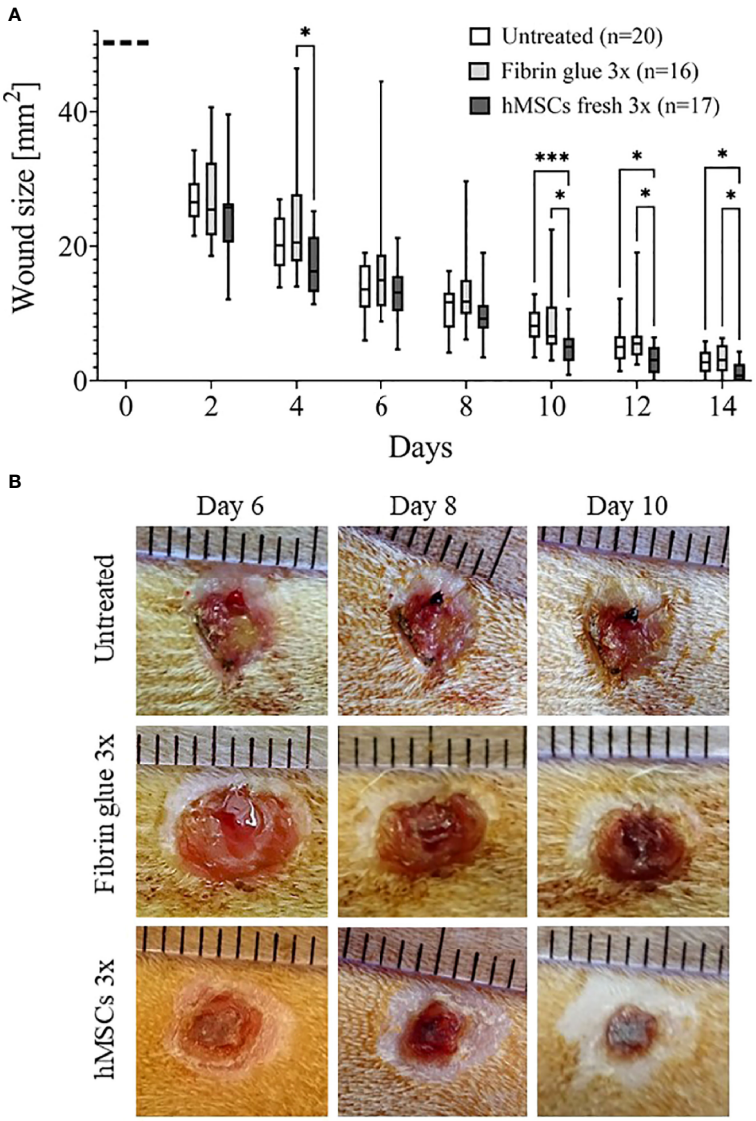

FIGURE 5
hMSCs improve wound healing. **(A)** Wound size reduction after 3-times repeated topical treatment with either hMSCs ($1x10^6/cm^2$) in fibrin glue, cell-free fibrin glue or untreated at d0, d4 and d8 after wounding. Quantification of wound areas relative to initial wound area was performed with Image J. * $p \leq 0.05$, *** $p \leq 0.001$, as calculated using two-way ANOVA and Tukey multiple comparisons. **(B)** Representative images of wounded skin after 3-times repeated topical treatment with either hMSCs in fibrin glue, cell-free fibrin glue or untreated depicting crust formation, especially in fibrin glue-treated wounds.

hMSCs are only transiently detectable in wounds

To assess the fate and biodistribution of topically applied hMSCs over time within the wounds and in distant organs, animals were sacrificed on day 1, 2, 3, 4, 9 and day 11, followed by histological as well as dPCR-based quantification of human cells.

Staining the wound sections for human nuclear Ku80 expression (38), we identified topically applied hMSCs on day 3 and 4 within the area of the fibrin glue interspersed within non-human tissue, yet hMSCs were undetectable at later time points (Figure 8A).

Accordingly, we confirmed the presence of human DNA in hMSCs-treated wounds. Levels decreased over time suggesting that the hMSCs were gradually eliminated from the wounds

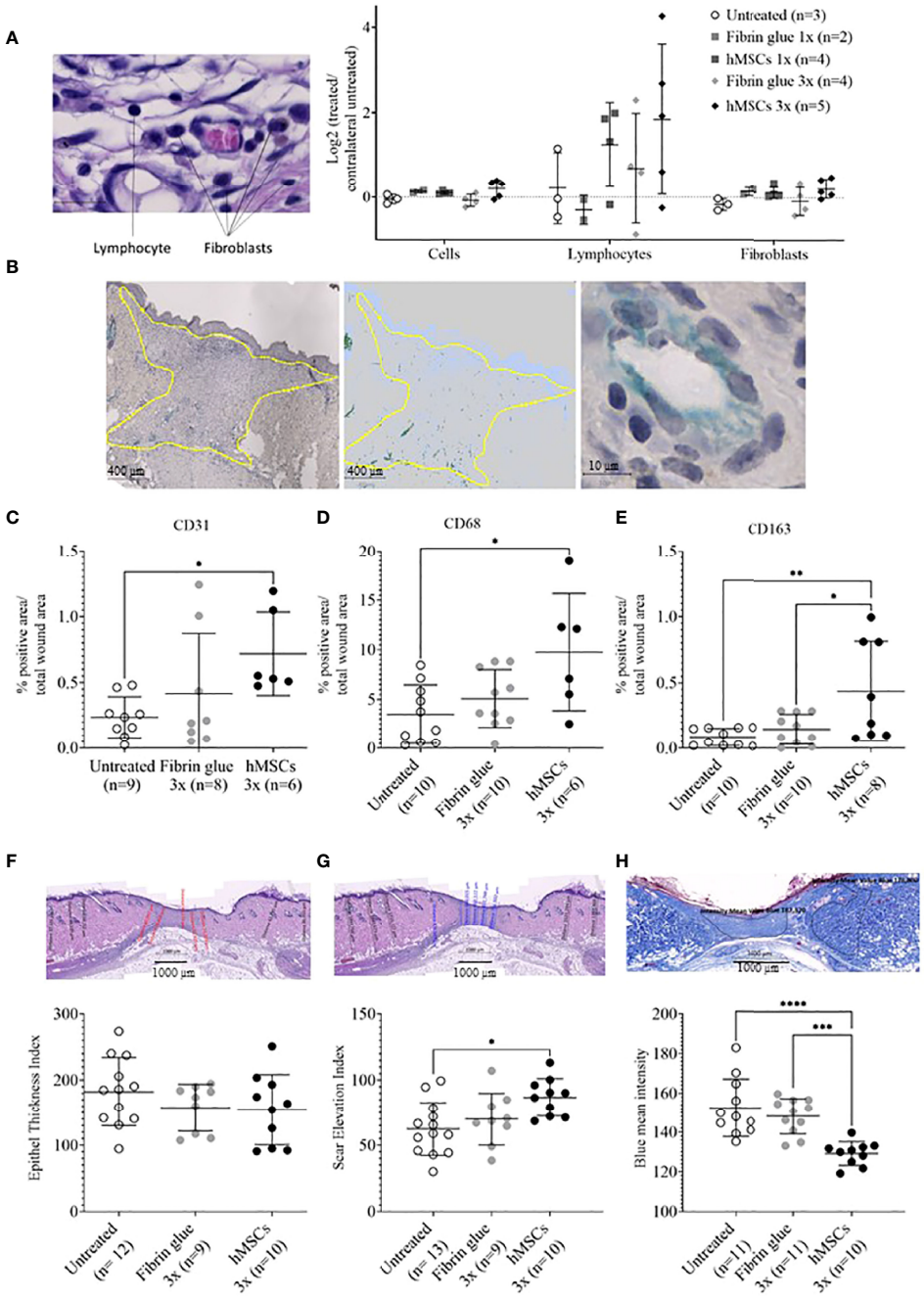

FIGURE 6
hMSCs tend to increase lymphocyte infiltration, CD31+ vascularization and CD68- and CD163-positive macrophage infiltration, and to improve wound healing indices. Wound skin was harvested at d14 and histologically analyzed. **(A)** Frequencies of total cells, lymphocytes and fibroblasts within wounds analyzed by QuPath algorithm on HE stains. Values were normalized against the untreated contralateral site. **(B)** Representative images of CD31-positive structures and calculation relative to the total wound area outlined in yellow. **(C–E)** Frequencies of **(C)** CD31+, **(D)** CD68+ and **(E)** CD163+ cells were determined by immunohistochemical staining relative to the total wound area. **(F–H)** Histological wound healing indices: **(F)** Epithelial thickness index (ETI) calculated by comparing epithelial thickness in the uninjured skin and wounded area, **(G)** scar elevation index (SEI) calculated by comparing the dermis thickness in the uninjured skin and wounded area and **(H)** collagen density after Azan staining in the uninjured skin and wounded area. Quantification was done using QuPath algorithms. Data from individual wounds are shown. *p≤ 0.05, **p≤ 0.01, ***p ≤ 0.001, **** p ≤ 0.0001, as calculated using one-way ANOVA und Tukey-Test.

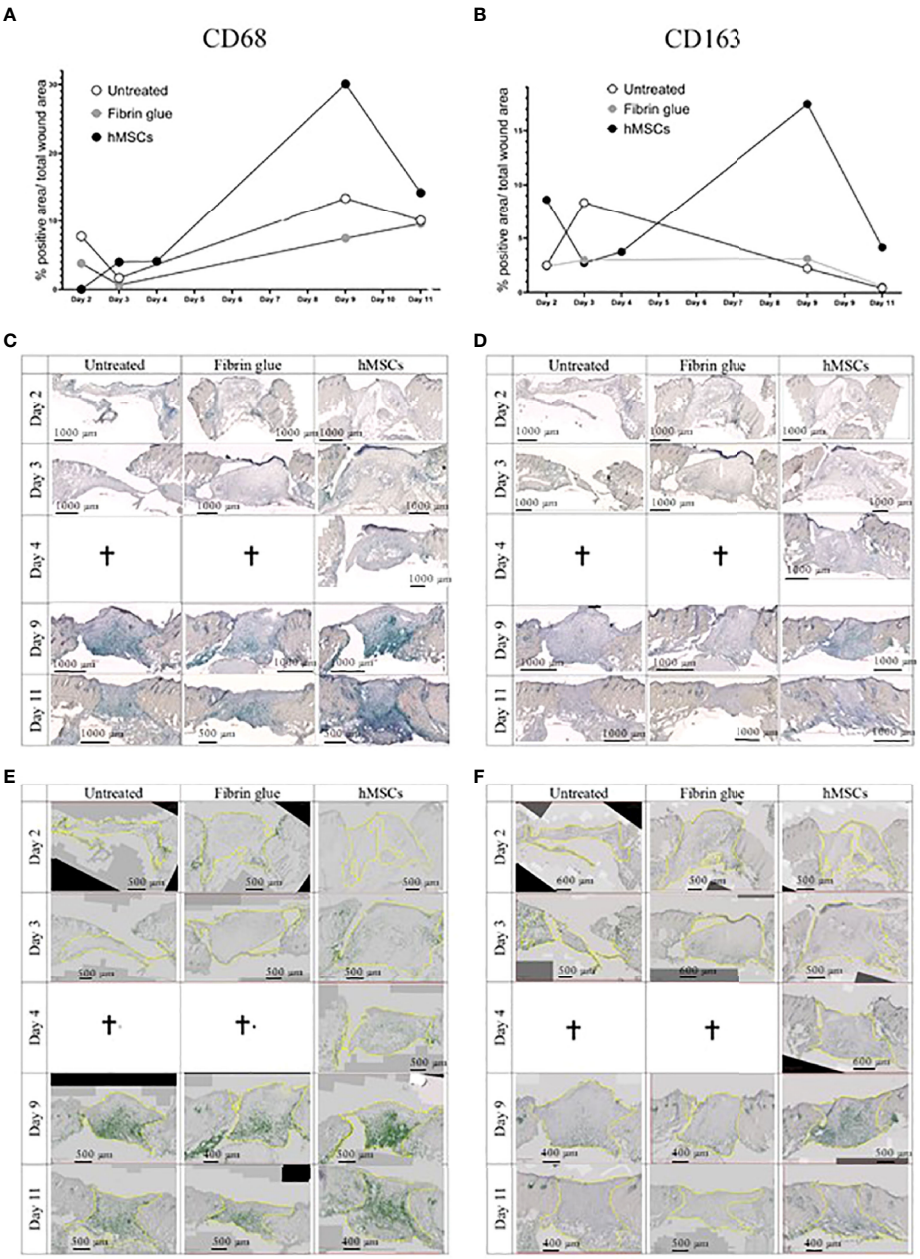

FIGURE 7
hMSCs rapidly recruit macrophages, infiltrating wounds from the wound edges and basis. Immunohistochemical staining of **(A, C, E)** CD68- and **(B, D, F)** CD163-positive macrophages. **(A, B)** Quantification as described in Figure 4. **(C, D)** Representative images are shown. **(E, F)** Wound margins are indicated in yellow, the histogreen-positive signal is highlighted and the histogreen-negative background signal reduced to visualize macrophage recruitment kinetics and routes.

(Figure 8B). Interestingly, traces of human DNA were also detected in cell-free fibrin glue-treated wounds, but never in untreated wounds, suggesting that the fibrin glue might contain low levels of human DNA. Human DNA was also detected in the livers of hMSCs-treated rats on day 1, 2, 4 and 11. The histological crosscheck revealed that the hKu80 signal was located in the cytoplasm, but not in the nucleus of the rat hepatocytes (Figure 8C).

A

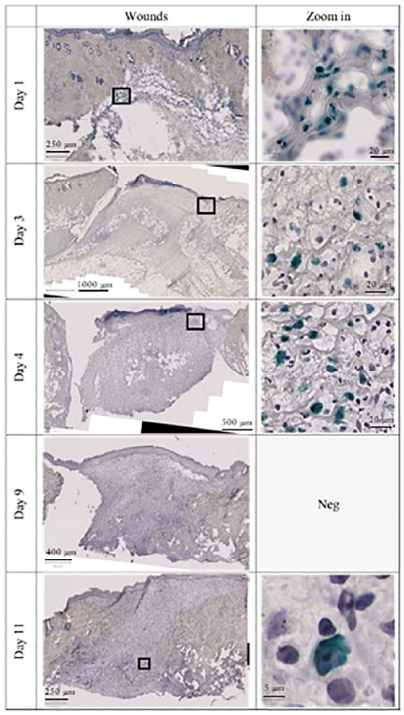

B

		d1	d2	d3	d11
Wound	Untreated	Neg.	Neg.	†	Neg.
	Fibrin glue	0.52	0.65	†	0.71
	hMSCs	44.87	14.73	30.16	0.95
Liver	Untreated/ fibrin glue	0.55	0.53	†	0.53
	hMSCs	0.74	1.78	0.98	0.57
Spleen	Untreated/ fibrin glue	1.18	Neg.	†	Neg.
	hMSCs	0.69	Neg.	0.89	0.80
Lung	Untreated/ fibrin glue	Neg.	Neg.	†	Neg.
	hMSCs	1.31	0.55	Neg.	Neg.

C

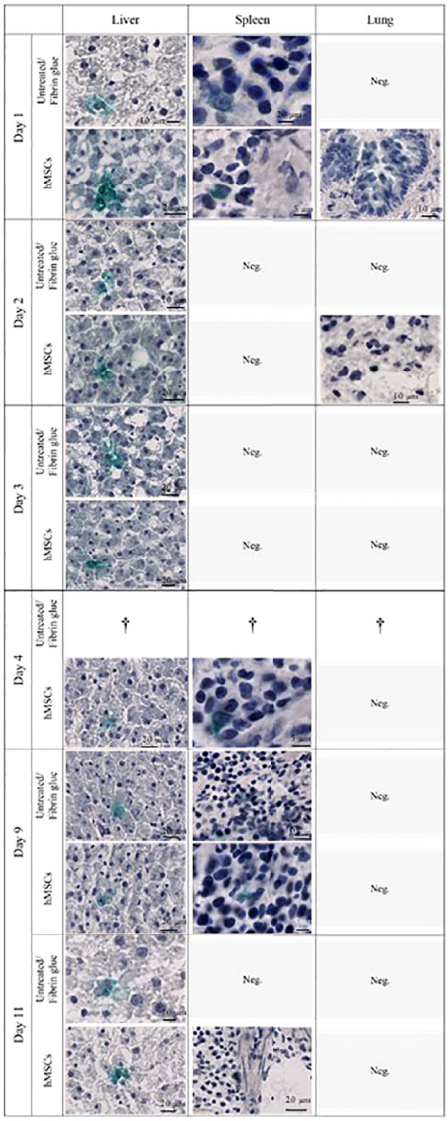

FIGURE 8
hMSCs are only transiently detectable in wounds. **(A)** Human Ku80-Histogreen staining in wound cross-sections. Left: Cross section of the entire wound. Right: Zoom on hKu80-positive cells. On day 1, wound edges with fibrin glue containing hMSCs located under the intact dermis are shown. Day 3 and 4 after hMSCs application, intact hMSCs were located in the fibrin glue top of the wound. Despite detection of human DNA in the wounds by dPCR on day 9, no hKu80 signal was detected in the histological sections. On day 11, very few hKu80-positive cells were found in the basal part of the wounds. **(B)** dPCR results of human DNA in rat wounds and organs. A value of ≥ 0.5 copies/µl was taken as positive result. **(C)** hKu80 expression in cryosections of analyzed organs: representative microphotographs are shown for samples where human cells were detected; no microphotographs are shown for negative samples.

We also detected traces of human DNA in livers of rats having one of their wounds treated with fibrin (Figure 8B). These results were confirmed by histological analysis. Again, the hKu80 stain was cytoplasmic (Figure 8C). It appears that not only hMSCs, but also the fibrin glue fragments, to a lesser extent, were transported from the wound site to the liver for phagocytosis by hepatocytes. Traces of human DNA were also found in the spleen of hMSCs-treated rats on days 1, 4 and 11 and in the spleens of animals with a fibrin glue-treated wound on day 1. Histological analysis confirmed this result as well (Figure 8C). On day 1 and 2, dPCR detected the presence of human DNA in the lungs of hMSCs-treated rats. No human DNA was found in the lungs of fibrin glue-treated rats.

Discussion

A well-standardized MSC therapeutic can improve the validity of clinical studies. Yet, the transfer of lab-scale protocols for hMSC manufacture to sustainable clinical adoption is laden with technical obstacles, issues pertaining to hMSC biology and variable MoAs (13). Here, we propose a GMP-compliant protocol, which allows for scalable and reproducible manufacturing of qualified clinical hMSCs batches at minimal *in vitro* expansion. All steps performed use only one batch of pooled pathogen-inactivated platelet lysate (25). We demonstrate that these pooled hMSCs, when topically applied, are potent in accelerating wound healing in a preclinical rat model without systemic effects. In this decision-making approach, we prepare the grounds for clinical wound healing studies: i) apply hMSC topically in a fibrin glue matrix, ii) preferably use fresh hMSCs, and iii) perform repeated application.

Donor-to-donor variability and extensive *in vitro* expansion are major drivers of inconsistent results from clinical trials, particularly when hMSCs batches are manufactured from single donors (3, 56). Pooling single donations, a concept implemented for platelet concentrates for many years (57), has been introduced recently for both hMSC and hPL products (13, 16, 19, 20, 25, 58). To balance the needs for scale-up and low-level expansion of a pooled hMSC product, our concept starts with MCBs from single donor hMSCs. From these, pooled hMSCs WCBs can be repeatedly manufactured, thus maximizing the starting material for clinical doses within only three passages (Figure 9). We argued about the best pooling time point. Contrary to "MSC-FFM", pooled as MNCs, and "Stempeucel®", pooled at passage 1 followed by five to six expansion passages (17, 20), we compared pooling at passage 1, 2 and 3. As expected, the *in vitro* tests showed that quality did not differ significantly between the different hMSC pools. Pool 2 was chosen based on the potential to produce up to 70,000 clinical doses ($1x10^6$ hMSCs/cm^2 wound size) at minimal *in vitro* expansion burden.

Exposure to multiple donors, however, may increase the risk of transmitting infectious agents. We propose to address this by i) rigorous donor testing according to blood banking standards (e.g. individual donor nucleic acid testing for HIV, HBV, HCV with increased sensitivity), by ii) pooling only a limited number of donors (we decided on six), and iii) a thorough MCB evaluation that includes re-testing for infectious agents. Our concept of six separate single donor MCBs and one pooled hMSCs WCB ascertains individual release testing of each cell bank. This ensures that the hMSCs from each donor are re-tested before being formulated as clinical product. For unknown infectious agents, though, a risk remains. In general, this pertains to pooled hPL as well. Here, however, PRT can be applied (22). In this case, we used hPL treated by high-dose gamma irradiation. The large hPL batch we used in this study was pooled from 70 single donors, allowing to produce this substantial number of clinical hMSC doses and for leveling-out single hPL donor variances (25).

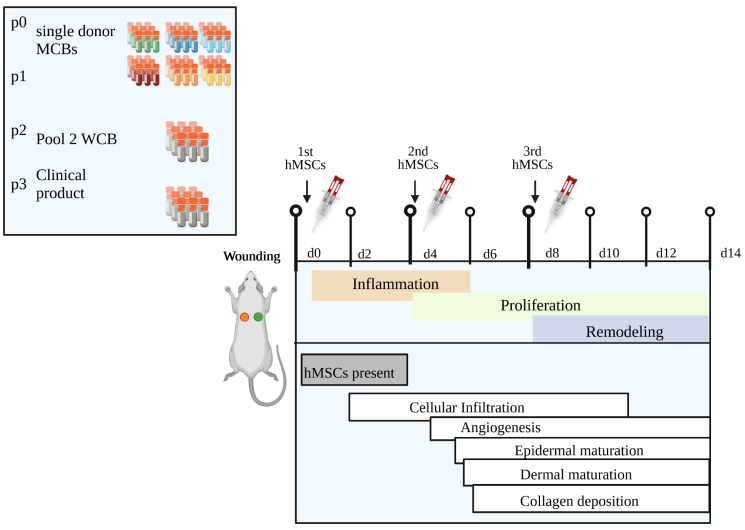

FIGURE 9
Summary of key findings. Our novel clinical-scale manufacturing concept is comprised of six single donor hMSCs master cell banks that are pooled to a working cell bank from which an extrapolated number of 70,000 clinical doses of $1x10^6$ hMSCs/cm^2 wound size can be manufactured within only three passages. Repeated topical hMSCs administration significantly accelerated the wound healing in a diabetic rat model by delivering a defined growth factor cargo at the specific stages of wound repair, namely inflammation, proliferation and remodeling. Specifically, the hMSCs mediated epidermal and dermal maturation and collagen formation, improved vascularization, and promoted cell infiltration, especially a dynamic recruitment of M2 macrophages. Created with Biorender.com.

Furthermore, we scaled-up the manufacturing process by expanding the pooled hMSCs in a closed cell culture system, where all media change and harvest steps are performed *via* sterile-connected bags. This reduces the hands-on time as well as open handling steps and allows direct transfer to clinical production according to GMP.

Successfully having addressed challenges of hMSC product manufacturing, we next moved to testing their preclinical efficacy in a diabetic wound healing rat model, known for their impaired wound healing capacity reflecting chronic healing defects in patients. The wound healing process is composed of three overlapping phases: inflammation, proliferation and remodeling (5). Pro-inflammatory macrophages, simplified referred to as M1 macrophages, infiltrate the wound at first to sanitize it from debris. In healing wounds, anti-inflammatory and pro-regenerative macrophages (M2) take over mediating migration and proliferation of fibroblasts, keratinocytes, and endothelial cells to restore dermis, epidermis and vasculature (55). Chronic wounds fail to heal because they remain in the early inflammation phase. We show that pooled hMSCs accelerated wound healing with significant reduced wound sizes already at day 4. Assuming that hMSCs mediate wound repair by delivering their trophic factors cargo, we calculated the trophic factors content per dose of the hMSC product, eventually allowing for a correlation between the trophic factor content in the clinical product and the strength of its therapeutic efficacy. Our hMSC product contains a variety of trophic factors known to promote the different phases of wound healing at stable concentrations in different batches. Repeated treatment with pooled hMSCs promoted cell infiltration and M2 macrophage recruitment, improved vascularization and induced epidermal and dermal maturation and collagen formation. We propose that the repeated hMSCs application not only increases the cumulative factors dose, but also importantly provides the different factors each at the right time during the different wound healing phases. G-CSF, IL-1α, IL-6, TGF-β, PGE-2 and inducible IDO-1 likely contributed to the observed immune infiltration and the consequent important inflammation phase. As per their known functions, TGF-β, PGE-2 and LIF mediate dynamic recruitment and polarization of macrophages. Further, it is reasonable to assume that VEGF-1, FGF-2, BDNF and HGF are responsible for the increased vessel density, and EGF, HGF, IL-1α, osteopontin and FGF-2 for keratinocyte and fibroblast proliferation/differentiation and ECM remodeling as indicated by the improved epithelial thickness, scar elevation and collagen density (Figure 9).

To the best of our knowledge, we describe for the first time in detail the dynamics of macrophage recruitment and polarization in hMSC-treated wounds. Specifically, hMSCs recruited more CD68+ and CD163+ macrophages gradually into all wound layers, first from the wound edges (d3), then the basal wound area (d9), finally progressing to the apical wound tissue on d11. This indicates an increased motility of these recruited macrophages. By chemotactically attracting macrophages and polarizing them to pro-regenerative M2 macrophages, hMSCs orchestrate the dysbalanced immune response within the wound (55, 59, 60).

We detected hMSCs in the wounds for up to 4 days by both dPCR and hKu80 nuclear staining. Yet, they apparently failed to persist and to differentiate *in situ* into endothelial cells or keratinocytes, as observed previously (8, 61). However, we found traces of human DNA in various organs already one day after topical application, of note, both in hMSCs-treated and human fibrin glue-treated animals. Histological staining verified the presence of hKu80 protein in these organs, confirming the dPCR results. This may indicate that human DNA and protein were removed from the wounds by phagocytes and then rapidly distributed to lung, spleen and liver. Yet, we cannot exclude that few intact human cells may have found their way to these organs. Here, however, the Ku80 signal was located in the cytoplasm. This may suggest that these human cells were oxidatively stressed (62).

The transient presence of hMSCs within the wounds could be explained by macrophage-mediated immunological clearance of xenogeneic hMSCs. In fact, Galleu et al. suggested the efferocytosis of allogeneic hMSCs as key for clinical efficacy, at least in the context of GvHD (63). In the GvHD setting, only those patients capable of immunologically clearing hMSCs benefitted from the hMSC therapy.

An adverse immune response may occur after repeated application of allogeneic or xenogeneic cells. A recent trial evaluating intravenously injected ABCB5+ allogeneic skin-derived hMSCs in patients with epidermolysis bullosa reported two patients with severe, yet transient and manageable, hypersensitivity reactions (11). We, however, even after repeated topical application (three subsequent doses), found no or only mild signs of an adverse immune response in our preclinical model, similar to previous studies (10, 64, 65). Ardanaz et al. conclude that once no hypersensitivity response to a second pooled allogeneic BM-MSC injection is observed, repeated treatments are possible to potentiate the benefit of hMSC therapy (66).

Given that hMSCs exert their therapeutic MoAs on various levels, we propose a matrix of potency assays for product release, combining trophic factors concentrations (min/max ranges) with functional and quality control tests that predict clinical efficacy. An example for this matrix approach is the measure of i) IL-1RA secretion in response to stimulation by M1-polarized macrophages, ii) pro-angiogenic VEGF secretion after 48h hypoxia, and iii) tube formation of hMSCs on matrigel as potency test matrix for ABCB5+ skin-derived hMSCs for treatment of chronic venous ulcers, epidermolysis bullosa, and liver disease (67).

For purity testing, we used binary marker expression as typically assessed by flow cytometry. Our hMSCs, single donor- and pool-derived, followed the consented hMSCs binary marker

profile (33). To predict immunomodulatory capacity, we documented their T cell inhibitory potential and inducible IDO-1 expression with highly reproducible results. As novel assays, we introduced an angiogenesis support assay and further, to control hMSCs fitness, a scratch wound healing and a chemotaxis assay. Yet, for these three assays day-to-day and operator-to-operator-variations were apparent calling for better standardization. A cell ruler could improve individual assay run reproducibility and thus improve batch-release testing (68). The need for thorough in-house protocol standardization, but also transfer and training to other sites, is confirmed by a recent multicenter study, which reports that the factor "production site" contributed more to variations in hMSC cultures than the source material used for hMSC production (69).

Within this decision making study, we prepared the fundament for a clinical study assessing pooled hMSCs efficacy in chronic wound healing. We not only provide data of a scalable manufacturing protocol, but also evidence for preclinical efficacy of the pooled hMSC product acting on different phases of wound healing. We reproduced a protocol for clinical administration of hMSCs to the wounds using fibrin glue. In the preclinical model with relatively small wounds, we applied the hMSCs topically in fibrin glue *via* a syringe. However, Falanga et al. already showed that for large wounds this administration works even well when applied as spray (8). Besides providing a stable matrix for the hMSCs, fibrin clot formation is an essential component of physiological wound healing. We speculated that the cell-free fibrin glue might per se improve wound healing. Yet, this was not observed in the ZDF model, possibly related to the 1:10 dilution. Interestingly, fibrin glue-treated wounds showed increased crust formation compared to hMSCs-fibrin glue-treated wounds. As ZDF rats are known for impaired wound contraction, increased inflammation and abundant crust production (31), the reduced crust formation in the hMSC group may be attributed to their known fibrinolytic activity (70). Furthermore, improved crust degradation may indicate the accelerated wound healing by hMSCs.

Given that preclinical models lack to reflect fully the complexity of human chronic non-healing wounds, well-designed clinical trials are required. We suggest a manufacturing protocol yielding in hMSCs of proven biological potency that can be instantly manufactured as an off-the-shelf product at clinical scale. As a pooled product, it levels-out donor heterogeneity. It further allows for scaled and reliable production of standardized clinical cell batches, based on the MCB/WCB concept and the use of a pathogen-inactivated pooled hPL. We confirm data that hMSCs applied in a fibrin glue are therapeutically active in accelerating wound healing, best when obtained from a rescue-culture and applied repeatedly.

In conclusion, we provide scientific evidence for a standardized, scalable and, importantly, efficacious pooled hMSC product. We show that these pooled hMSCs with a defined wound healing factor cargo accelerated the dermal wound healing in diabetic rats by improving vascularization and dynamically recruiting M2-like macrophages (Figure 9). The next steps to acquire a manufacturing license as an advanced therapy medicinal product (ATMP) for clinical use, are i) validate the *in vitro* assays for batch qualification and release testing, ii) perform a thorough preclinical biodistribution, toxicity, and tumorigenicity study program and iii) finally a clinical trial.

Data availability statement

The raw data supporting the conclusions of this article will be made available by the authors, without undue reservation.

Ethics statement

The studies involving human participants were reviewed and approved by 329/10, ethics committee, University Hospital Frankfurt am Main, Germany. The patients/participants provided their written informed consent to participate in this study. The animal study was reviewed and approved by G142-19, Regierungspräsidium Karlsruhe, Germany.

Author contributions

All authors contributed to gathering of data, writing, editing, and revising of the manuscript.

Funding

We acknowledge the financial support of the German Red Cross Blood Donor Service Baden-Württemberg - Hessen. This work was supported by a grant from the Deutsche Forschungsgemeinschaft (DFG GRK 1874-2 DIAMICOM, SP6 – HW and KB). For the publication fee we acknowledge financial support by Deutsche Forschungsgemeinschaft within the funding programme "Open Access Publikationskosten" as well as by Heidelberg University.

Acknowledgments

We acknowledge the support from Stefanie Uhlig, Flow Core Mannheim, Core Facility Platform Mannheim (CFPM), Silke Vorwald, Institute of Neuroanatomy, Dr. Bettina Kränzlin and the entire core facility Preclinical Models and the LIMa Live Cell Imaging Mannheim core, both CFPM, Medical Faculty Mannheim, Heidelberg University.

Conflict of interest

BD and MG are employees of Macopharma.

The remaining authors declare that the research was conducted in the absence of any commercial or financial relationships that could be construed as a potential conflict of interest.

The authors declare that this study received funding from Macopharma. The funder had the following involvement in the study: provision of funding and material; manuscript writing and review of the final manuscript. Macopharma also provided high-dose gamma irradiated pooled hPL.

Publisher's note

Supplementary material

The Supplementary Material for this article can be found online at: https://www.frontiersin.org/articles/10.3389/fimmu.2022.976511/full#supplementary-material

SUPPLEMENTARY FIGURE 1
All hMSC pools display similar adipogenic and osteogenic differentiation potential. hMSCs were seeded at a density of 1,000 cells/cm^2 and grown to subconfluency. Adipogenic differentiation was induced using the hMSC Adipogenic Differentiation Medium BulletKit (Lonza), or osteogenic differentiation was induced using osteogenic medium composed of α-MEM/10% FBS supplemented with 1 μM dexamethasone, 50 μM ascorbic acid, and 10 mM β-glycerolphosphate (Sigma–Aldrich). After 3 weeks under differentiation conditions, lipid vacuoles in adipogenic cultures were stained with oil red O and calcium deposits of osteogenic cultures with alizarin red S, respectively.

SUPPLEMENTARY FIGURE 2
hMSCs migrate out of diluted fibrin glue. Instead of being applied to a wound, hMSCs were seeded in fibrin glue into a cell culture well plate and cultivated in medium supplemented with hPL versus serum-free medium as control. 4.5 hours post-seeding, hMSCs migrated from the glue attaining their typical fibroblast-like morphology. hMSCs in serum-free medium showed no migration out of the gel. (Axio Vert.A1, 5-fold magnification).

SUPPLEMENTARY FIGURE 3
No systemic wound healing effect after topical hMSCs application. Rats were wounded and hMSCs applied topically in diluted fibrin glue. Comparison of wound size reduction of contralateral untreated wounds with lateral either **(A)** untreated, **(B)** hMSCs cryo single application, **(C)** fibrin glue single application, **(D)** single application hMSCs fresh, **(E)** repeated application of fibrin glue or **(F)** repeated application of hMSCs fresh d0, 4 and 8. Quantification of the wound area was performed with Image J. ** p≤ 0.01, as calculated using two-way ANOVA und Sidak-Test.

SUPPLEMENTARY TABLE 1
Trophic factors content in hPL MultiPL'100i (batch 11219267DM), including batch release test results. Experiments performed on two different bags (#209 and 221) from the used MultiPL'100i batch 11219267DM, means and standard deviations are shown. [1] Experiments repeated twice with different controls and verified using ELISA kits from two different companies. bFGF, basic fibroblast growth factor; IGF, insulin-like growth factor 1; TGF-β1, transforming growth factor beta 1; EGF, epidermal growth factor; PDGF-AB, platelet-derived growth factor AB; VEGF, vascular endothelial growth factor; TNF-*a*, tumor necrosis factor alpha; IFN-γ, interferon gamma; LAL, limulus amebocyte lysate; NTU, nephelometric turbidity unit.

References

1. Otero-Vinas M, Falanga V. Mesenchymal stem cells in chronic wounds: The spectrum from basic to advanced therapy. *Adv Wound Care (New Rochelle)* (2016) 5(4):149–63. doi: 10.1089/wound.2015.0627

2. Gianino E, Miller C, Gilmore J. Smart wound dressings for diabetic chronic wounds. *Bioengineering (Basel)* (2018) 5(3):51. doi: 10.3390/bioengineering5030051

3. Galipeau J, Sensebe L. Mesenchymal stromal cells: Clinical challenges and therapeutic opportunities. *Cell Stem Cell* (2018) 22(6):824–33. doi: 10.1016/j.stem.2018.05.004

4. Krampera M, Le Blanc K. Mesenchymal stromal cells: Putative microenvironmental modulators become cell therapy. *Cell Stem Cell* (2021) 28 (10):1708–25. doi: 10.1016/j.stem.2021.09.006

5. Maxson S, Lopez EA, Yoo D, Danilkovitch-Miagkova A, Leroux MA. Concise review: role of mesenchymal stem cells in wound repair. *Stem Cells Transl Med* (2012) 1(2):142–9. doi: 10.5966/sctm.2011-0018

6. Huang YZ, Gou M, Da LC, Zhang WQ, Xie HQ. Mesenchymal stem cells for chronic wound healing: Current status of preclinical and clinical studies. *Tissue Eng Part B Rev* (2020) 26(6):555–70. doi: 10.1089/ten.teb.2019.0351

7. Marx C, Gardner S, Harman RM, Wagner B, Van de Walle GR. Mesenchymal stromal cell-secreted CCL2 promotes antibacterial defense mechanisms through increased antimicrobial peptide expression in keratinocytes. *Stem Cells Transl Med* (2021) 10(12):1666–79. doi: 10.1002/sctm.21-0058

8. Falanga V, Iwamoto S, Chartier M, Yufit T, Butmarc J, Kouttab N, et al. Autologous bone marrow-derived cultured mesenchymal stem cells delivered in a fibrin spray accelerate healing in murine and human cutaneous wounds. *Tissue Eng.* (2007) 13(6):1299–312. doi: 10.1089/ten.2006.0278

9. Yufit T, Carson P, Falanga V. Topical delivery of cultured stem cells to human non-healing wounds: GMP facility development in an academic setting and FDA requirements for an IND and human testing. *Curr Drug Deliv* (2014) 11 (5):572–81. doi: 10.2174/1567201811310990035

10. Kerstan A, Dieter K, Niebergall-Roth E, Dachtler AK, Kraft K, Stucker M, et al. Allogeneic ABCB5(+) mesenchymal stem cells for treatment-refractory chronic venous ulcers: a phase I/IIa clinical trial. *JID Innov* (2022) 2(1):100067. doi: 10.1016/j.xjidi.2021.100067

11. Kiritsi D, Dieter K, Niebergall-Roth E, Fluhr S, Daniele C, Esterlechner J, et al. Clinical trial of ABCB5+ mesenchymal stem cells for recessive dystrophic epidermolysis bullosa. *JCI Insight* (2021) 6(22):e151922. doi: 10.1172/jci.insight.151922

12. Armstrong JPK, Keane TJ, Roques AC, Patrick PS, Mooney CM, Kuan WL, et al. A blueprint for translational regenerative medicine. *Sci Transl Med* (2020) 12 (572):eaaz2253. doi: 10.1126/scitranslmed.aaz2253

13. Bieback K, Kuci S, Schafer R. Production and quality testing of multipotent mesenchymal stromal cell therapeutics for clinical use. *Transfusion* (2019) 59 (6):2164–73. doi: 10.1111/trf.15252

14. Galipeau J. The mesenchymal stromal cells dilemma–does a negative phase III trial of random donor mesenchymal stromal cells in steroid-resistant graft-versus-host disease represent a death knell or a bump in the road? *Cytotherapy* (2013) 15(1):2–8. doi: 10.1016/j.jcyt.2012.10.002

15. Siegel G, Kluba T, Hermanutz-Klein U, Bieback K, Northoff H, Schafer R. Phenotype, donor age and gender affect function of human bone marrow-derived mesenchymal stromal cells. *BMC Med* (2013) 11:146. doi: 10.1186/1741-7015-11-146

16. Kuci Z, Bonig H, Kreyenberg H, Bunos M, Jauch A, Janssen JW, et al. Mesenchymal stromal cells from pooled mononuclear cells of multiple bone marrow donors as rescue therapy in pediatric severe steroid-refractory graft-versus-host disease: a multicenter survey. *Haematologica* (2016) 101(8):985–94. doi: 10.3324/haematol.2015.140368

17. Bader P, Kuci Z, Bakhtiar S, Basu O, Bug G, Dennis M, et al. Effective treatment of steroid and therapy-refractory acute graft-versus-host disease with a novel mesenchymal stromal cell product (MSC-FFM). *Bone Marrow Transplant* (2018) 53(7):852–62. doi: 10.1038/s41409-018-0102-z

18. Bonig H, Kuci Z, Kuci S, Bakhtiar S, Basu O, Bug G, et al. Children and adults with refractory acute graft-versus-Host disease respond to treatment with the mesenchymal stromal cell preparation "MSC-FFM"-Outcome report of 92 patients. *Cells* (2019) 8(12):1577. doi: 10.3390/cells8121577

19. Gupta PK, Krishna M, Chullikana A, Desai S, Murugesan R, Dutta S, et al. Administration of adult human bone marrow-derived, cultured, pooled, allogeneic mesenchymal stromal cells in critical limb ischemia due to buerger's disease: Phase II study report suggests clinical efficacy. *Stem Cells Transl Med* (2017) 6(3):689–99. doi: 10.5966/sctm.2016-0237

20. Thej C, Balasubramanian S, Rengasamy M, Walvekar A, Swamynathan P, Raj SS, et al. Human bone marrow-derived, pooled, allogeneic mesenchymal stromal cells manufactured from multiple donors at different times show comparable biological functions *in vitro*, and *in vivo* to repair limb ischemia. *Stem Cell Res Ther* (2021) 12(1):279. doi: 10.1186/s13287-021-02330-9

21. Bieback K, Hecker A, Schlechter T, Hofmann I, Brousos N, Redmer T, et al. Replicative aging and differentiation potential of human adipose tissue-derived mesenchymal stromal cells expanded in pooled human or fetal bovine serum. *Cytotherapy* (2012) 14(5):570–83. doi: 10.3109/14653249.2011.652809

22. Blumel J, Schwantes A, Baylis SA, Stuhler A. Strategies toward virus and prion safe human platelet lysates. *Transfusion* (2020) 60(1):219–20. doi: 10.1111/trf.15581

23. Burnouf T, Strunk D, Koh MB, Schallmoser K. Human platelet lysate: Replacing fetal bovine serum as a gold standard for human cell propagation? *Biomaterials* (2016) 76:371–87. doi: 10.1016/j.biomaterials.2015.10.065

24. Astori G, Amati E, Bambi F, Bernardi M, Chieregato K, Schafer R, et al. Platelet lysate as a substitute for animal serum for the ex-vivo expansion of mesenchymal stem/stromal cells: present and future. *Stem Cell Res Ther* (2016) 7 (1):93. doi: 10.1186/s13287-016-0352-x

25. Viau S, Eap S, Chabrand L, Lagrange A, Delorme B. Viral inactivation of human platelet lysate by gamma irradiation preserves its optimal efficiency in the expansion of human bone marrow mesenchymal stromal cells. *Transfusion* (2019) 59(3):1069–79. doi: 10.1111/trf.15205

26. The European Agency for the Evaluation of Medicinal Products. *Human medicines evaluation unit. note for guidance on virus validation studies: The disgn, contribution and interpretation of studies validating the inactivation and removal of vriuses*. (1996) EMEA: London UK.

27. Francois M, Copland IB, Yuan S, Romieu-Mourez R, Waller EK, Galipeau J. Cryopreserved mesenchymal stromal cells display impaired immunosuppressive properties as a result of heat-shock response and impaired interferon-gamma licensing. *Cytotherapy* (2012) 14(2):147–52. doi: 10.3109/14653249.2011.623691

28. Chinnadurai R, Copland IB, Garcia MA, Petersen CT, Lewis CN, Waller EK, et al. Cryopreserved mesenchymal stromal cells are susceptible to T-cell mediated apoptosis which is partly rescued by IFNgamma licensing. *Stem Cells* (2016) 34 (9):2429–42. doi: 10.1002/stem.2415

29. Chinnadurai R, Garcia MA, Sakurai Y, Lam WA, Kirk AD, Galipeau J, et al. Actin cytoskeletal disruption following cryopreservation alters the biodistribution of human mesenchymal stromal cells in vivo. *Stem Cell Rep* (2014) 3(1):60–72. doi: 10.1016/j.stemcr.2014.05.003

30. Moll G, Geissler S, Catar R, Ignatowicz L, Hoogduijn MJ, Strunk D, et al. Cryopreserved or fresh mesenchymal stromal cells: Only a matter of taste or key to unleash the full clinical potential of MSC therapy? *Adv Exp Med Biol* (2016) 951:77–98. doi: 10.1007/978-3-319-45457-3_7

31. Slavkovsky R, Kohlerova R, Tkacova V, Jiroutova A, Tahmazoglu B, Velebny V, et al. Zucker diabetic fatty rat: a new model of impaired cutaneous wound repair with type II diabetes mellitus and obesity. *Wound Repair Regen* (2011) 19(4):515–25. doi: 10.1111/j.1524-475X.2011.00703.x

32. Spohn G, Witte AS, Kretschmer A, Seifried E, Schafer R. More human BM-MSC with similar subpopulation composition and functional characteristics can be produced with a GMP-compatible fabric filter system compared to density gradient technique. *Front Cell Dev Biol* (2021) 9:638798. doi: 10.3389/fcell.2021.638798

33. Dominici M, Le Blanc K, Mueller I, Slaper-Cortenbach I, Marini F, Krause D, et al. Minimal criteria for defining multipotent mesenchymal stromal cells. The international society for cellular therapy position statement. *Cytotherapy* (2006) 8 (4):315–7. doi: 10.1080/14653240600855905

34. Kremer H, Gebauer J, Elvers-Hornung S, Uhlig S, Hammes HP, Beltramo E, et al. Pro-angiogenic activity discriminates human adipose-derived stromal cells from retinal pericytes: Considerations for cell-based therapy of diabetic retinopathy. *Front Cell Dev Biol* (2020) 8:387. doi: 10.3389/fcell.2020.00387

35. Wuhrer A, Uhlig S, Tuschy B, Berlit S, Sperk E, Bieback K, et al. Wound fluid from breast cancer patients undergoing intraoperative radiotherapy exhibits an altered cytokine profile and impairs mesenchymal stromal cell function. *Cancers (Basel)* (2021) 13(9):2140. doi: 10.3390/cancers13092140

36. Schneider CA, Rasband WS, Eliceiri KW. NIH Image to ImageJ: 25 years of image analysis. *Nat Methods* (2012) 9(7):671–5. doi: 10.1038/nmeth.2089

37. Bankhead P, Loughrey MB, Fernandez JA, Dombrowski Y, McArt DG, Dunne PD, et al. QuPath: Open source software for digital pathology image analysis. *Sci Rep* (2017) 7(1):16878. doi: 10.1038/s41598-017-17204-5

38. Rigon M, Horner SJ, Straka T, Bieback K, Gretz N, Hafner M, et al. Effects of ASC application on endplate regeneration upon glycerol-induced muscle damage. *Front Mol Neurosci* (2020) 13:107. doi: 10.3389/fnmol.2020.00107

39. van de Vyver M, Boodhoo K, Frazier T, Hamel K, Kopcewicz M, Levi B, et al. Histology scoring system for murine cutaneous wounds. *Stem Cells Dev* (2021) 30 (23):1141–52. doi: 10.1089/scd.2021.0124

40. Eryilmaz M, Muller D, Rink G, Kluter H, Bugert P. Introduction of noninvasive prenatal testing for blood group and platelet antigens from cell-free plasma DNA using digital PCR. *Transfus Med Hemother* (2020) 47(4):292–301. doi: 10.1159/000504348

41. Rodrigues M, Kosaric N, Bonham CA, Gurtner GC. Wound healing: A cellular perspective. *Physiol Rev* (2019) 99(1):665–706. doi: 10.1152/physrev.00067.2017

42. Werner S, Grose R. Regulation of wound healing by growth factors and cytokines. *Physiol Rev* (2003) 83(3):835–70. doi: 10.1152/physrev.2003.83.3.835

43. Hardwicke J, Schmaljohann D, Boyce D, Thomas D. Epidermal growth factor therapy and wound healing - past, present and future. *Surg-J R Coll Surg E* (2008) 6(3):172–7. doi: 10.1016/S1479-666X(08)80114-X

44. Jimi S, Sato K, Kimura M, Suzumiya J, Hara S, De Francesco F, et al. G-CSF administration accelerates cutaneous wound healing accompanied with increased pro-hyp production in db/db mice. *Clin Res Dermatol: Open Access* (2017) 4(2):1–9. doi: 10.15226/2378-1726/4/2/00155

45. Conway K, Ruge F, Price P, Harding KG, Jiang WG. Hepatocyte growth factor regulation: an integral part of why wounds become chronic. *Wound Repair Regen* (2007) 15(5):683–92. doi: 10.1111/j.1524-475X.2007.00296.x

46. Robertson FM, Pellegrini AE, Ross MS, Oberyszyn AS, Boros LG, Bijur GN, et al. Interleukin-1alpha gene expression during wound healing. *Wound Repair Regen* (1995) 3(4):473–84. doi: 10.1046/j.1524-475X.1995.30412.x

47. Santos GC, Silva DN, Fortuna V, Silveira BM, Orge ID, de Santana TA, et al. Leukemia inhibitory factor (LIF) overexpression increases the angiogenic potential of bone marrow mesenchymal Stem/Stromal cells. *Front Cell Dev Biol* (2020) 8:778. doi: 10.3389/fcell.2020.00778

48. Kanno E, Tanno H, Masaki A, Sasaki A, Sato N, Goto M, et al. Defect of interferon gamma leads to impaired wound healing through prolonged neutrophilic inflammatory response and enhanced MMP-2 activation. *Int J Mol Sci* (2019) 20(22):5657. doi: 10.3390/ijms20225657

49. Miles RH, Paxton TP, Zacheis D, Dries DJ, Gamelli RL. Systemic administration of interferon-gamma impairs wound-healing. *J Surg Res* (1994) 56(3):288–94. doi: 10.1006/jsre.1994.1045

50. Seraphim PM, Leal EC, Moura J, Goncalves P, Goncalves JP, Carvalho E. Lack of lymphocytes impairs macrophage polarization and angiogenesis in diabetic wound healing. *Life Sci* (2020) 254:117813. doi: 10.1016/j.lfs.2020.117813

51. Doersch KM, DelloStritto DJ, Newell-Rogers MK. The contribution of interleukin-2 to effective wound healing. *Exp Biol Med* (2017) 242(4):384–96. doi: 10.1177/1535370216675773

52. Cheng H, Huang H, Guo Z, Chang Y, Li Z. Role of prostaglandin E2 in tissue repair and regeneration. *Theranostics* (2021) 11(18):8836–54. doi: 10.7150/thno.63396

53. Ito H, Ando T, Ogiso H, Arioka Y, Saito K, Seishima M. Inhibition of indoleamine 2,3-dioxygenase activity accelerates skin wound healing. *Biomaterials* (2015) 53:221–8. doi: 10.1016/j.biomaterials.2015.02.098

54. Bieback K, Hecker A, Kocaomer A, Lannert H, Schallmoser K, Strunk D, et al. Human alternatives to fetal bovine serum for the expansion of mesenchymal stromal cells from bone marrow. *Stem Cells* (2009) 27(9):2331–41. doi: 10.1002/stem.139

55. Krzyszczyk P, Schloss R, Palmer A, Berthiaume F. The role of macrophages in acute and chronic wound healing and interventions to promote pro-wound healing phenotypes. *Front Physiol* (2018) 9:419. doi: 10.3389/fphys.2018.00419

56. Martin I, Galipeau J, Kessler C, Le Blanc K, Dazzi F. Challenges for mesenchymal stromal cell therapies. *Sci Transl Med* (2019) 11(480):eaat2189. doi: 10.1126/scitranslmed.aat2189

57. Schrezenmeier H, Seifried E. Buffy-coat-derived pooled platelet concentrates and apheresis platelet concentrates: which product type should be preferred? *Vox Sang* (2010) 99(1):1–15. doi: 10.1111/j.1423-0410.2009.01295.x

58. Kerstan A, Niebergall-Roth E, Esterlechner J, Schroder HM, Gasser M, Waaga-Gasser AM, et al. *Ex vivo*-expanded highly pure ABCB5(+) mesenchymal stromal cells as good manufacturing practice-compliant autologous advanced therapy medicinal product for clinical use: process validation and first in-human data. *Cytotherapy* (2021) 23(2):165–75. doi: 10.1016/j.jcyt.2020.08.012

59. Chen L, Tredget EE, Wu PY, Wu Y. Paracrine factors of mesenchymal stem cells recruit macrophages and endothelial lineage cells and enhance wound healing. *PloS One* (2008) 3(4):e1886. doi: 10.1371/journal.pone.0001886

60. Fontaine MJ, Shih H, Schafer R, Pittenger MF. Unraveling the mesenchymal stromal cells' paracrine immunomodulatory effects. *Transfus Med Rev* (2016) 30 (1):37–43. doi: 10.1016/j.tmrv.2015.11.004

61. Wu Y, Chen L, Scott PG, Tredget EE. Mesenchymal stem cells enhance wound healing through differentiation and angiogenesis. *Stem Cells* (2007) 25 (10):2648–59. doi: 10.1634/stemcells.2007-0226

62. Song JY, Lim JW, Kim H, Morio T, Kim KH. Oxidative stress induces nuclear loss of DNA repair proteins Ku70 and Ku80 and apoptosis in pancreatic acinar AR42J cells. *J Biol Chem* (2003) 278(38):36676–87. doi: 10.1074/jbc.M303692200

63. Galleu A, Riffo-Vasquez Y, Trento C, Lomas C, Dolcetti L, Cheung TS, et al. Apoptosis in mesenchymal stromal cells induces *in vivo* recipient-mediated immunomodulation. *Sci Transl Med* (2017) 9(416):eaam7828. doi: 10.1126/scitranslmed.aam7828

64. Ankrum JA, Ong JF, Karp JM. Mesenchymal stem cells: immune evasive, not immune privileged. *Nat Biotechnol* (2014) 32(3):252–60. doi: 10.1038/nbt.2816

65. Avivar-Valderas A, Martin-Martin C, Ramirez C, Del Rio B, Menta R, Mancheno-Corvo P, et al. Dissecting allo-sensitization after local administration of human allogeneic adipose mesenchymal stem cells in perianal fistulas of crohn's disease patients. *Front Immunol* (2019) 10:1244. doi: 10.3389/fimmu.2019.01244

66. Ardanaz N, Vazquez FJ, Romero A, Remacha AR, Barrachina L, Sanz A, et al. Inflammatory response to the administration of mesenchymal stem cells in an equine experimental model: effect of autologous, and single and repeat doses of pooled allogeneic cells in healthy joints. *BMC Vet Res* (2016) 12:65. doi: 10.1186/s12917-016-0692-x

67. Ballikaya S, Sadeghi S, Niebergall-Roth E, Nimtz L, Frindert J, Norrick A, et al. Process data of allogeneic *ex vivo*-expanded ABCB5(+) mesenchymal stromal cells for human use: off-the-shelf GMP-manufactured donor-independent ATMP. *Stem Cell Res Ther* (2020) 11(1):482. doi: 10.1186/s13287-020-01987-y

68. Viswanathan S, Keating A, Deans R, Hematti P, Prockop D, Stroncek DF, et al. Soliciting strategies for developing cell-based reference materials to advance mesenchymal stromal cell research and clinical translation. *Stem Cells Dev* (2014) 23(11):1157–67. doi: 10.1089/scd.2013.0591

69. Stroncek DF, Jin P, McKenna DH, Takanashi M, Fontaine MJ, Pati S, et al. Human mesenchymal stromal cell (MSC) characteristics vary among laboratories when manufactured from the same source material: A report by the cellular therapy team of the biomedical excellence for safer transfusion (BEST) collaborative. *Front Cell Dev Biol* (2020) 8:458. doi: 10.3389/fcell.2020.00458

70. Chaires-Rosas CP, Ambriz X, Montesinos JJ, Hernandez-Tellez B, Pinon-Zarate G, Herrera-Enriquez M, et al. Differential adhesion and fibrinolytic activity of mesenchymal stem cells from human bone marrow, placenta, and wharton's jelly cultured in a fibrin hydrogel. *J Tissue Eng.* (2019) 10:2041731419840622. doi: 10.1177/2041731419840622

frontiers | Frontiers in Immunology

TYPE Original Research
PUBLISHED 14 September 2022
DOI 10.3389/fimmu.2022.959658

OPEN ACCESS

EDITED BY
Tomomi Toubai,
Yamagata University, Japan

REVIEWED BY
Takeo Mukai,
The University of Tokyo, Japan
Britt Gustafsson,
Karolinska Institutet (KI), Sweden
Timothy Devos,
University Hospitals Leuven, Belgium
Christopher D. Porada,
Wake Forest School of Medicine, United States
Yongxia Wu,
Medical College of Wisconsin, United States

*CORRESPONDENCE
Muna Qayed
muna.qayed@emory.edu

†These authors have contributed equally to this work

SPECIALTY SECTION
This article was submitted to Alloimmunity and Transplantation, a section of the journal Frontiers in Immunology

RECEIVED 01 June 2022
ACCEPTED 11 August 2022
PUBLISHED 14 September 2022

CITATION
Stenger E, Giver CR, Langston A, Kota D, Das PK, Chinnadurai R, Galipeau J, Waller EK and Qayed M (2022) Safety of autologous freshly expanded mesenchymal stromal cells for the treatment of graft-versus-host disease. *Front. Immunol.* 13:959658. doi: 10.3389/fimmu.2022.959658

Safety of autologous freshly expanded mesenchymal stromal cells for the treatment of graft-versus-host disease

Elizabeth Stenger[1], Cynthia R. Giver[2], Amelia Langston[2], Daniel Kota[2], Pankoj Kumar Das[2], Raghavan Chinnadurai[3], Jacques Galipeau[4], Edmund K. Waller[2†] and Muna Qayed[1*†]

[1]Aflac Cancer and Blood Disorders Center, Children's Healthcare of Atlanta, Emory University, Atlanta, GA, United States, [2]Bone Marrow and Stem Cell Transplant Center, Winship Cancer Institute, Emory University, Atlanta, GA, United States, [3]Department of Biomedical Sciences, Mercer University School of Medicine, Savannah, GA, United States, [4]Department of Medicine and Carbone Cancer Center, University of Wisconsin in Madison, Madison, WI, United States

Despite the curative potential of hematopoietic cell transplantation (HCT) for hematologic malignancies, graft-versus-host disease (GVHD) remains a substantial cause of morbidity and mortality, particularly if treatment is refractory. Treatment with additional immunosuppression including steroids often leads to opportunistic infections and organ dysfunction. Novel therapies are greatly needed, specifically ones that lead to responses in treatment-refractory patients and are better tolerated. Mesenchymal stromal cells (MSCs) are non-hematopoietic tolerogenic cells present in normal bone marrow (BM), which can be expanded *ex vivo* to therapeutic doses. Their safety and efficacy have been assessed in inflammatory disorders including GVHD, but heterogeneity in clinical responses has led some to examine MSC manufacturing and administration procedures, which may impact *in vivo* efficacy. We hypothesized that autologous, early-passage, and culture-recovered (after freeze and thaw) MSCs would be safe and may have superior efficacy. In this phase I single-center trial, we assessed MSC safety and early efficacy of an escalating number of doses (2×10^6/kg doses; dose level 1, single dose; dose level 2, two weekly doses; dose level 3, four weekly doses) in patients aged ≥12 years with treatment-refractory acute or chronic GVHD. Eleven enrolled patients received some or all planned MSC infusions, with a median age at enrollment of 37 years. The most common primary HCT indication was leukemia, and the median time from HCT to first MSC infusion was 2.6 years. MSC infusion was well tolerated, with all severe adverse events expected and determined to be unlikely or definitely not related to the study. Thus, no dose-limiting toxicities occurred in the three dose levels. Three of four patients with acute GVHD (or overlap with acute features) had responses seen at any timepoint, ranging from partial to complete. In those with a chronic GVHD indication (n = 7), an overall response at 3 months was partial in five, stable in one, and progressive in one. No appreciable differences were seen between dose levels in peripheral blood lymphocyte subsets. In conclusion,

autologous and culture-recovered MSCs were safe in the setting of refractory GVHD following HCT for hematologic malignancy, and clinical responses were most notable in patients with acute GVHD.

KEYWORDS

Mesechymal stromal cell, acute graft versus host disease (aGVHD), chronic graft versus host disease (GVHD), allogeneic transplant of haematopoietic stem cells, Hematologic malignancy

Introduction

Hematopoietic cell transplantation (HCT) is the only curative option for many hematologic malignancies, in which healthy donor hematopoietic stem cells (HSCs) are infused following typically high doses of chemotherapy (1). One of the main complications of HCT is graft-versus-host disease (GVHD), in which donor immune cells (particularly T lymphocytes) attack recipient organs (1). Corticosteroids remain the primary upfront therapy for GVHD, and steroid-refractory GVHD remains a major cause of morbidity and mortality (2). Second-line treatments for both acute and chronic GVHD lead to cumulative immune suppression and risk for infections. Thus, novel and effective therapies for treatment-refractory GVHD, especially without additive risk of opportunistic infections or organ dysfunction, are urgently needed.

Mesenchymal stromal cells (MSCs) are a regulatory non-hematopoietic immune cell population present in the bone marrow (BM) that can be expanded *ex vivo* to large numbers (3). Based on their ability to suppress the immune system and promote tissue regeneration, MSCs have been evaluated as a treatment for GVHD for nearly two decades (4). Positive clinical trial results have led to the approval of MSCs in Japan for the treatment of GVHD (5), and although US-based trials showed benefit in pediatric patients (6), no benefit was seen in the initial randomized, placebo-controlled trial in adult and pediatric patients (7). Inconsistency in trial results (8) is likely in part due to heterogeneity in cell manufacturing and administration procedures. Three major sources of variability that may impact the clinical efficacy of MSCs have been extensively reviewed: freeze-thawing, replication fitness, and donor source. First, most MSC products are cryopreserved post-expansion and infused immediately post-thaw. However, preclinical data suggest that MSCs are functionally stunned/impaired post-thaw, in comparison to the culture-recovered counterparts (9–11). Second, most MSC products (particularly commercial) have undergone prolonged *ex vivo* expansion, which has been shown to compromise their function. In the setting of acute GVHD treatment, late passage was significantly associated with decreased clinical response and survival (12). Finally, most MSC products have been random donor source, and while MSCs were initially thought to be immune privileged, later studies demonstrated recipient driven immune-mediated rejection (13, 14). While it is not feasible to utilize HLA-matched random donor MSCs, autologous source may be feasible in some settings including GVHD. Importantly, following HCT, the BM MSC compartment remains autologous, and our preclinical data confirm intact phenotype and function of autologous, BM-derived MSCs from patients with GVHD following HCT for hematologic malignancy (15).

By addressing all these limitations, the primary objective of this trial was to evaluate the safety and tolerability of autologous, early-passage, culture-recovered (fresh) MSCs in the setting of treatment-refractory GVHD post-HCT for hematologic malignancy. Thus, within this phase I trial, our primary endpoint was dose-limiting toxicities (DLTs) of an escalating number of weekly MSC infusions, with secondary endpoints examining GVHD response.

Methods

Study design

This was a prospective, single-center, phase I dose-escalation study of autologous MSCs for the treatment of GVHD. The trial followed a standard 3 + 3 design with a fixed MSC dose (2×10^6/kg) and three dose levels with an escalation of the number of doses administered: dose level 1, single infusion; dose level 2, two weekly infusions; dose level 3, four weekly infusions. The protocol was approved by the Emory University Institutional Review Board and the Food and Drug Administration (FDA) (IND 16191) and registered with ClinicalTrials.gov (#NCT02359929). Patients were recruited through the adult and pediatric blood and marrow transplant programs at the Winship Cancer Institute at Emory University and Children's Healthcare of Atlanta. Written informed consent was obtained prior to enrollment.

Study population

Patients aged ≥12 years with steroid-refractory or resistant GVHD post-allogeneic HCT for a hematologic malignancy were eligible. GVHD could be grade II–IV acute GVHD requiring systemic therapy and refractory/unresponsive to glucocorticoid (≥1 mg prednisone-equivalent/kg × 1 week); chronic GVHD was extensive and either not improved despite therapy with glucocorticoid (≥0.5 mg prednisone-equivalent/kg/day) and therapeutic doses of a calcineurin inhibitor for ≥4 weeks or worsened within 2 weeks, or overlap syndrome not responding to glucocorticoid treatment (≥1 mg prednisone-equivalent/kg × 1 week). Patients with active fungal infections, evidence of disease relapse, donor chimerism <50%, or oxygen requirement were not eligible to participate. Patients were permitted to receive other systemic immunosuppression per standard of care, including calcineurin inhibitors and steroids. Fifteen patients were enrolled, of whom 11 received some or all planned MSC doses. Four patients were screen failures, and three patients had MSC manufacturing failure, one of whom underwent a second BM collection and MSC expansion, with details shown for an infused product. The trial was closed prior to enrollment of the planned sixth patient on dose level 3, due to no DLTs observed in any of the treated patients (including in dose level 3) and changes in Good Manufacturing Practice (GMP) facility staffing.

Initial mesenchymal stromal cell manufacturing

BM (1 ml/kg with a maximum of 60 ml) was obtained *via* aspiration under aseptic conditions and then processed for MSC expansion in a class 10000 GMP facility at Emory University Hospital (EUH) per previously published methods (15, 16). In brief, the mononuclear cell (MNC) layer was isolated using Ficoll-Paque™ PREMIUM (MediaTech, Inc., Manassas, VA, USA) density gradient, washed, and resuspended in a complete culture medium (CCM) comprised of HyClone® Minimum Essential Medium (MEM) Alpha Modification (HyClone Laboratories, Logan, UT, USA) with 10% pooled human platelet lysate (phPL; EUH, Atlanta, GA, USA) and gentamicin (prior to P1 only; HyClone Laboratories, Logan, UT, USA). MNCs were then placed into a cellular stack (Corning®, Corning, NY, USA) and incubated at 37°C in a 5% CO_2, humidified environment for 7–10 days (Passage 0 (P0)), with media change at 72 h. MSCs were enzymatically detached and reseeded at approximately 1,000 cells/cm^2 in culture media containing 10% phPL for an additional 7–10 days (Passage 1 (P1)). If an insufficient number of cells were obtained (per assigned dose level), cells were passaged up to two additional times. Once a sufficient cell number was obtained, cells were collected enzymatically, washed, and counted. Release criteria for cryopreservation included sufficient cell number, viability, identity, negative sterility, endotoxin, and mycoplasma testing (Supplemental Table 1). Cells were then resuspended at 10×10^6 MSC/ml in freezing media (5% human serum albumin and 10% dimethyl sulfoxide (DMSO) in CCM), cryopreserved using a programmable control rate freezer, and stored in vapor phase liquid nitrogen until 72 h prior to planned infusion. All cell counting and viability were performed using an Invitrogen Countess™ automated cell counter (Invitrogen, Grand Island, NY, USA).

Mesenchymal stromal cell culture recovery

Approximately 72 h prior to planned infusion, cells were removed from vapor phase liquid nitrogen, thawed in a 37°C water bath, washed, counted, and seeded onto tissue culture treated plates at a maximum concentration of 50,000 cells/cm^2 in culture media containing 10% phPL. Media was changed at 24 h, with cells expanded for an additional 1–3 days (median 3 days total, range 2–4). Cells were then collected enzymatically, washed, counted, and resuspended at a concentration of 4×10^6 cells/ml in a solution of Plasma-Lyte A containing 0.05% human serum albumin. Release criteria for infusion included >70% viability and negative gram stain (Supplemental Table 2). When release criteria were met, cells were then injected into a standard blood transfusion bag and transported from the manufacturing facility to the site of infusion.

Mesenchymal stromal cell infusion and patient follow-up

An infusion was performed on either the inpatient unit or outpatient infusion center depending on patient condition. MSCs were infused within 4 h of release using standard blood product tubing and through a central or large bore peripheral intravenous line over 10–20 min by gravity or by a pump. Patients were pre-medicated with acetaminophen, diphenhydramine, and hydrocortisone (or if already on steroids, an equivalent dose). Vital signs were closely monitored during and after (up to 4 h) of the infusion. Targeted adverse events (AEs) were collected on all treated patients for 7 days after each MSC infusion. All serious AEs were collected through study completion. Acute GVHD staging and grading and chronic GVHD scoring were performed per published criteria (17). Patients were followed up for up to 1 year for secondary endpoints.

Longitudinal analysis of peripheral blood post-mesenchymal stromal cell infusion

Peripheral blood samples were obtained at baseline and then weekly through day 42 from study initiation. Cells were analyzed

by flow cytometry for the expression of CD3 (PE-AF594), CD4 (APC-Cy7), CD8 (FITC), CD25 (APC), CD27 (PE), CD69 (PE-Cy7), and FOXP3 (PE; BD Biosciences, San Jose, CA, USA). All samples were run on a Canto II flow cytometer (Beckman Coulter, Indianapolis, IN, USA) and analyzed using FlowJo (BD, Ashland, OR, USA). CD4 and CD8 counts (cells/mm^3) were calculated using total lymphocyte count from clinical laboratory complete blood counts obtained on the same day.

Definitions and study endpoints

Systemic reaction was defined as any untoward medical hypersensitivity-like event other than injection site reaction, occurring during or after MSC infusion, which could be at least possibly attributed to the MSC infusion. Acute systemic reactions were defined as those occurring within 2 h of infusion. DLTs were defined as any grade ≥3 adverse reaction that was unexpected or considered attributable to the MSC infusion and occurred within 1 month from the last MSC infusion. Maximum tolerated dose (MTD) was defined as the highest dose level at which at most one of six patients experience a DLT after one cycle, with the immediate higher dose level having at least two patients who experience DLTs.

Overall acute GVHD responses were categorized as complete response (CR), partial response (PR), mixed response (MR), stable disease (SD), or progressive disease (PD), which were defined per published standards. Overall "response" was defined as achieving either CR or PR, while "no response" was defined as achieving MR, SD, or PD. Organ-specific response was classified as improving, stable, progressing, or death. Overall chronic GVHD "response" was defined as a reduction in overall National Institutes of Health (NIH) score at 3 months, without worsening of any specific organ. Organ-specific responses were categorized per NIH criteria as CR, PR, SD, or PD.

The primary endpoint of this phase I trial was safety and tolerability, based on DLTs. Second endpoints included overall and organ-specific acute (at day 29, 4 weeks after the last infusion, 3 months, and 6 months) and chronic (at 3 and 6 months) GVHD responses.

Statistical analysis

Descriptive statistics were performed on subject clinical and treatment factors, disease response, and flow cytometry data (grouped by dose level). Categorical data are presented as frequency tables and percentages, while continuous data are presented as mean and standard deviation or median and range.

Results

Baseline characteristics

Eleven patients with refractory or resistant GVHD received some or all planned autologous MSC doses, with baseline characteristics shown in Table 1. The median age at enrollment was 37 years (range, 26–75 years), with most being male (73%) and white (64%). Indications for HCT included leukemia (acute, n = 3; chronic, n = 2), lymphoma (n = 3), myelodysplastic syndrome (n = 2), and myelofibrosis (n = 1), and median time from HCT to first MSC infusion was 2.6 years (range, 0.2–6.5). Most patients received

TABLE 1 Baseline patient, disease, and HCT characteristics.

Study ID	Age (years)	Sex	Race/ethnicity	HCT indication	Time from HCT (years)	Donor	HSC source	Prep regimen	GVHD ppx
EPIC2014-01	35	M	White	ALL	0.5	MUD	BM	Flu/Mel	Tac/MTX
EPIC2014-05	59	M	Native Hawaiian or Other Pacific Islander	AML	0.3	MRD	PBSC	Flu/Mel	Tac/MTX
EPIC2014-06	26	M	White	HL	0.7	MRD	PBSC	Flu/Bu	Tac/MMF
EPIC2014-07	53	M	White	AML	3.4	URD	PBSC	Bu/Cy	Tac/NR
EPIC2014-12	50	M	Black or African American	CTCL	2.6	MUD	PBSC	Flu/Mel	Tac/MTX
EPIC2014-13	34	M	White	MF	4.5	MMUD	PBSC	Bu/Cy	Tac/MTX
EPIC2014-14	55	M	Black or African American	MDS	3.1	MRD	BM	Bu/Cy	Tac/MTX
EPIC2014-15	26	M	White, Hispanic, or Latino	CML	0.4	MUD	PBSC	Bu/Cy	Tac/MTX
EPIC2014-16	28	F	White	HL	6.5	URD	PBSC	FluMel	Tac/MTX
EPIC2014-17	75	F	White	MDS	4.7	MUD	PBSC	FluTBI	Tac/MMF
EPIC2014-18	37	F	Black or African American	CML	0.6	MRD	PBSC	FluMel	Tac/MTX

HCT, hematopoietic cell transplantation; HSC, hematopoietic stem cell; Prep, preparative; GVHD, graft-versus-host disease; ppx, prophylaxis; M, male; F, female; ALL, acute lymphoblastic leukemia; AML, acute myeloid leukemia; HL, Hodgkin lymphoma; CTCL, cutaneous T-cell lymphoma; MF, myelofibrosis; MDS, myelodysplastic syndrome; MUD, matched unrelated donor; MRD, matched related donor; URD, unrelated donor; MMUD, mismatched unrelated donor; BM, bone marrow; PBSC, peripheral blood stem cells; Flu, fludarabine; Mel, melphalan; Bu, busulfan; Cy, cyclophosphamide; TBI, total body irradiation; Tac, tacrolimus; MTX, methotrexate; MMF, mycophenolate mofetil; NR, not reported.

peripheral blood stem cells (PBSC) (73%) from an unrelated donor (URD) (64%). The conditioning regimen was most commonly reduced intensity (n = 6), followed by myeloablative (n = 5); all patients received tacrolimus in combination with mycophenolate mofetil or methotrexate for GVHD prophylaxis.

Mesenchymal stromal cell expansion and culture recovery

From a median starting BM volume of 54 ml (range, 48–60 ml), median starting white blood cell (WBC) count was 1.49e9 (range, 0.43e9–2.85e9), and total nucleated cell (TNC) post-Ficoll was 2.07e8 (range, 0.69e8–11.3e8; Supplemental Table 3). Time from initial seeding to P0 was 10 ± 1.8 days (median ± SD), and from P0 to P1, it was 6 ± 1.3 days. Seven products (most commonly those at a higher dose level, with a higher total dose) required additional time in culture, with a median time from P1 to P2 of 7 ± 1.5 days; two of these required additional passage time of 4 and 7 days. Doubling time from P0 to P1 was 1.55 ± 1.66 (median ± SD) days, and from P1 to P2, it was 1.49 ± 0.87 days. Following expansion, MSCs were cryopreserved until approximately 72 h prior to planned infusion, with a median cryopreservation time of 14 days (range, 7–35 days). MSCs were culture recovered for a median of 3 days (range, 2–4) prior to infusion.

Safety of mesenchymal stromal cell infusion

Three patients were treated on dose level 1 (single dose), three patients on dose level 2 (weekly × 2 doses), and five patients on dose level 3 (weekly × 4 doses, except one patient who received only two doses due to poor expansion). All doses were 2×10^6 MSC/kg, except for dose 1 in patient 7, who received a dose of 1.27×10^6/kg due to inadequate post-culture recovery. Targeted AEs are shown in Figure 1, with the most common being grade 1 or 2 hypertension (n = 4 events occurring in patient 16) followed by sinus tachycardia and dyspnea (each occurring in n = 2 patients). Nine severe AEs (SAEs) occurred (Figure 1), including two grade 4 sepsis events and two deaths (grade 5; patient 5 due to multi-organ failure in the setting of GVHD and patient 6 due to pneumonia and respiratory failure, at 115 and 46 days following first MSC infusion, respectively). All SAEs were expected and determined to be unlikely or definitely not related to study participation. Overall, three targeted AEs were attributed to study participation: grade 1 hypertension (probably related), grade 2 hypertension 30 min after MSC infusion (probably related), and grade 1 rash (possibly related). Thus, no DLTs occurred on any of the three dose levels, and an MTD was not reached.

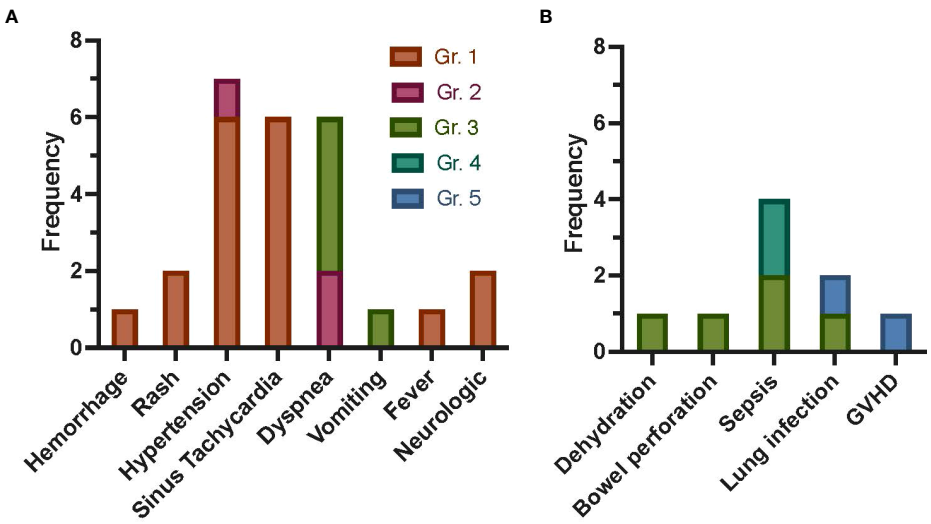

FIGURE 1
Frequency of AEs following autologous MSC infusion as treatment for refractory GVHD post-HCT for malignant disease. Targeted AEs **(A)** were captured within 7 days of each MSC infusion. Allergic reaction/hypersensitivity, sinus bradycardia, hypotension, rigors/chills, renal, and hypoxia are not shown, as no events occurred. The most common targeted AE was grade 1 or 2 hypertension, with four events occurring in one patient (16). Sinus tachycardia events were all grade 1, with two events occurring in patient 12 and four events occurring in patient 15. All dyspnea events occurred in two patients (n = 2 in patient 7, n = 4 in patient 16). Only three AEs were attributed to study participation: grade 1 rash possibly related, grade 1 rash possibly related, and grade 2 hypertension (30 min after MSC infusion) probably related. SAEs **(B)** were captured for 1 year, with the most common SAE being sepsis (n = 4). Death occurred in two patients (patients 5 and 6, due to GVHD and pneumonia and respiratory failure, respectively). All SAEs were expected and were not attributed (unlikely or definitely not related) to study participation. Gr., grade; GVHD, graft-versus-host disease; AEs, adverse events; MSC, mesenchymal stromal cell; HCT, hematopoietic cell transplantation; SAEs, severe AEs.

Graft-versus-host disease characteristics and responses

As shown in Tables 2, 3, all patients had received multiple previous lines of GVHD treatment (range, 3–9), and all were on systemic immunosuppression (with one to three agents) at the time of MSC infusion. In those with a primary indication of acute GVHD at the time of enrollment (patients 1 and 5, both of whom had chronic GVHD at the time of infusion; Table 2), responses were seen following a single infusion of MSCs (at 129 and 77 days from GVHD diagnosis, respectively). Patient 1 had skin-only acute GVHD with CR at 6 months and discontinuation of systemic steroids; patient 5 had an MR, with CR of the upper and lower gastrointestinal (LGI) (maximum stage 4) acute GVHD by 3 months but developed new stage 3 liver GVHD. Nonetheless, the systemic steroid dose was able to be decreased in patient 5. Two patients had overlap GVHD as their primary indication for MSC treatment (patients 6 and 15; first MSC infusion at 146 and 122 days from GVHD diagnosis, respectively), with acute GVHD responses seen in one patient (patient 15—on dose level 3) with PR (LGI staging improved to 1 from maximum 2 and decreased systemic steroids). Patient 6 had no response (NR) to a single dose of MSCs with continued stage 4 LGI and eventually death related to complications from GVHD. Thus, 75% of patients with acute GVHD or overlap indication had an overall "response" (at any timepoint) to autologous MSC infusion, and 25% were non-responders.

TABLE 2 Acute GVHD characteristics and response following autologous MSC infusion.

Study ID	Dose level; # doses	Time from GVHD dx (days)	Max grade; stage[1]	Treatment on day 1	Other treatments	Timepoint	Grade	Stage	Overall response	Steroid dose (mg/kg)
EPIC2014-01[2]	1; 1	129	II; 3/0/0/0	Steroid, FK, ECP	ATG	D1	II	2/0/0/0	CR	0.7→0[3]
						D8	I	1/0/0/0		
						D15	I	1/0/0/0		
						D29	I	1/0/0/0		
						D36	I	1/0/0/0		
						3 months	II	3/0/0/0		
						6 months	0	0/0/0/0		
EPIC2014-05	1; 1	77	IV; 0/1/4/0	Steroid, FK, ruxolitinib, ECP	ATG, MMF, infliximab	D1	IV	0/1/4/0	MR	0.9→0.6
						D8	IV	0/1/4/0		
						D15	II	0/0/1/0		
						D29	IV	0/0/4/0		
						D36	I	0/1/0/0		
						D42	IV	0/1/4/0		
						2 months	I	0/1/0/0		
						3 months	III	0/0/0/3		
EPIC2014-06[4]	1; 1	146	IV; 0/1/4/0	Steroid, FK	Sirolimus, MMF, ECP	D1	IV	0/0/4/0	NR	1.1→0.7
						D8	IV	0/1/4/0		
						D15	IV	0/0/4/0		
						D29	IV	0/0/4/0		
						D36	IV	0/1/4/0		
EPIC2014-15	3; 4	122	III; 0/0/2/0	Steroid, FK	Remicade, Jakafi	D1	II	0/0/1/0	PR	1.0→0
						D8	II	0/0/1/0		
						D15	II	0/0/1/0		
						D29	II	0/0/1/0		
						D36	III	0/0/2/0		
						2 months	III	0/0/2/0		
						3 months	III	0/0/2/0		
						6 months	II	0/0/1/0		
						12 months	II	0/0/1/0		

GVHD, graft-versus-host disease; MSC, mesenchymal stromal cells; Max, maximum; FK, tacrolimus; ECP, extracorporeal photopheresis; ATG, anti-thymocyte globulin; MMF, mycophenolate mofetil; CR, complete response; NR, no response; PR, partial response; UGI, upper gastrointestinal; LGI, lower GI.
(1)Stage reported as skin/UGI/LGI/liver.
(2)Chronic GVHD diagnosed on 2/24/2015. Skin GVHD developed chronic features during the study.
(3)Steroids weaned off within a few days of first MSC infusion.
(4)Overlap GVHD with acute phenotype.

10.3389/fimmu.2022.959658

TABLE 3 Chronic GVHD characteristics and response following autologous MSC infusion.

Study ID	Dose level	# Doses	Time from GVHD dx (years)	Baseline severity	Treatment on day 1	Other treatments	Severity at last f/u	Overall response[1]	Steroid dose (mg/kg)
EPIC2014-07	2	2	2.1	Severe	Steroid, FK[2]	Sirolimus, MMF, ruxolitinib, ECP, imatinib, MTX, rituximab	Severe	PR	0.3→0.3
EPIC2014-12	2	2	0.2[3]	Mod	Steroid	FK, ruxolitinib	Mod	PR	0.5→0.2
EPIC2014-13	2	2	0.5[4]	Severe	FK[5]	Steroid, ruxolitinib, ibrutinib, ECP	Severe	PD	0→0
EPIC2014-14	3	4	1.7	Severe	Steroid, FK, ruxolitinib	N/A	Severe	SD	0.1→0.1
EPIC2014-16	3	4	6.2	Severe	Steroid, sirolimus, ibrutinib[6]	FK, ECP	Severe	PR	0.6→0.4
EPIC2014-17[7]	3	2	4.4	Severe	Ruxolitinib, MMF	Steroid, rituximab, FK, MMF, imatinib, sirolimus, ECP, ruxolitinib	Mod	PR	0→0
EPIC2014-18[8]	3	4	0.2	Mild	Steroid, FK, ruxolitinib	N/A	Mild	PR	0.2→0

GVHD, graft-versus-host disease; MSC, mesenchymal stromal cells; dx, diagnosis; f/u, follow-up; mod, moderate; FK, tacrolimus; MMF, mycophenolate mofetil; ECP, extracorporeal photopheresis; MTX, methotrexate; PR, partial response; PD, progressive disease; SD, stable disease; EGD, esophagogastroduodenoscopy; UGI, upper gastrointestinal; LGI, lower GI.
(1)Overall response assessed at 3 months following first MSC infusion.
(2)Ibrutinib started 3 months following first MSC infusion.
(3)Date of diagnostic EGD, prior history of skin and nail chronic GVHD.
(4)Overlap GVHD diagnosed on 4/30/2015.
(5)Jakafi started at 9 months following first MSC infusion.
(6)Ruxolitinib started 5 months following first MSC infusion and ibrutinib discontinued.
(7)History of acute skin only GVHD, quiescent at study enrollment.
(8)At enrollment, patient had acute GVHD (stage 1 UGI, 2 LGI); at treatment, patient had only chronic GVHD.

In those with chronic GVHD as the primary indication for MSC (n = 7; Table 3 and Supplementary Table 4), an overall response at 3 months was partial in five, stable in one, and progressive in one (with an improved total score but increased GI and joint scores). In GI and lung organ systems, 50% and 33% of patients, respectively, had a CR at 3 and 6 months (Figure 2), with lung responses otherwise PR or SD, but progressive GI disease in remaining patients. Otherwise, most organ-specific

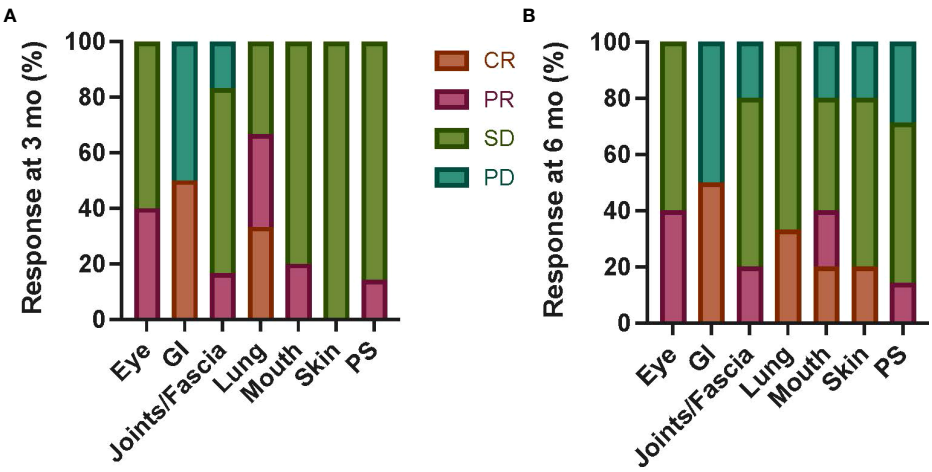

FIGURE 2
Chronic GVHD organ-specific responses following autologous MSC infusion. Organ-specific responses were assessed at 3 months **(A)** and 6 months **(B)** from first MSC infusion in six patients with primary indication of chronic GVHD regardless of dose level. CR was seen in a subset of patients with GI and lung involvement at both timepoints; otherwise, most patients had PR or SD in all organs. The proportion of patients with PD was highest in the GI system (50% at both 3 and 6 months), with a smaller proportion in joints/fascia, mouth (3 months only), and PS (3 months only) systems. Mo, months; GI, gastrointestinal; PS, performance score; CR, complete response; PR, partial response; SD, stable disease; PD, progressive disease; GVHD, graft-versus-host disease; MSC, mesenchymal stromal cell.

responses were PR or SD in most patients. PD was seen in a smaller proportion of patients with joint/fascia, mouth (6 months only), skin (6 months only), or PS (6 months only) systems involved.

Longitudinal immune profile

CD4 and CD8 lymphocyte counts and percentage of activated (CD69+) subsets are shown in Figure 3 (mean and SD), broken down by dose level. While CD4 and CD8 counts did not appear to differ between dose levels or over time, the percentage of activated CD4 and CD8 lymphocytes was the lowest at day 29 in those treated on dose level 3 (noting that dose level 1 patients had the highest percentage at baseline). No appreciable difference was detected in the percentage of regulatory T cells (FOXP3+ cells within CD3+ CD4+CD8−CD25+CD69−) between dose levels (Figure 3).

Discussion

In this phase I dose-escalation trial of autologous MSCs for treatment-refractory GVHD following HCT for hematologic malignancy, no DLTs were seen, and an MTD was not

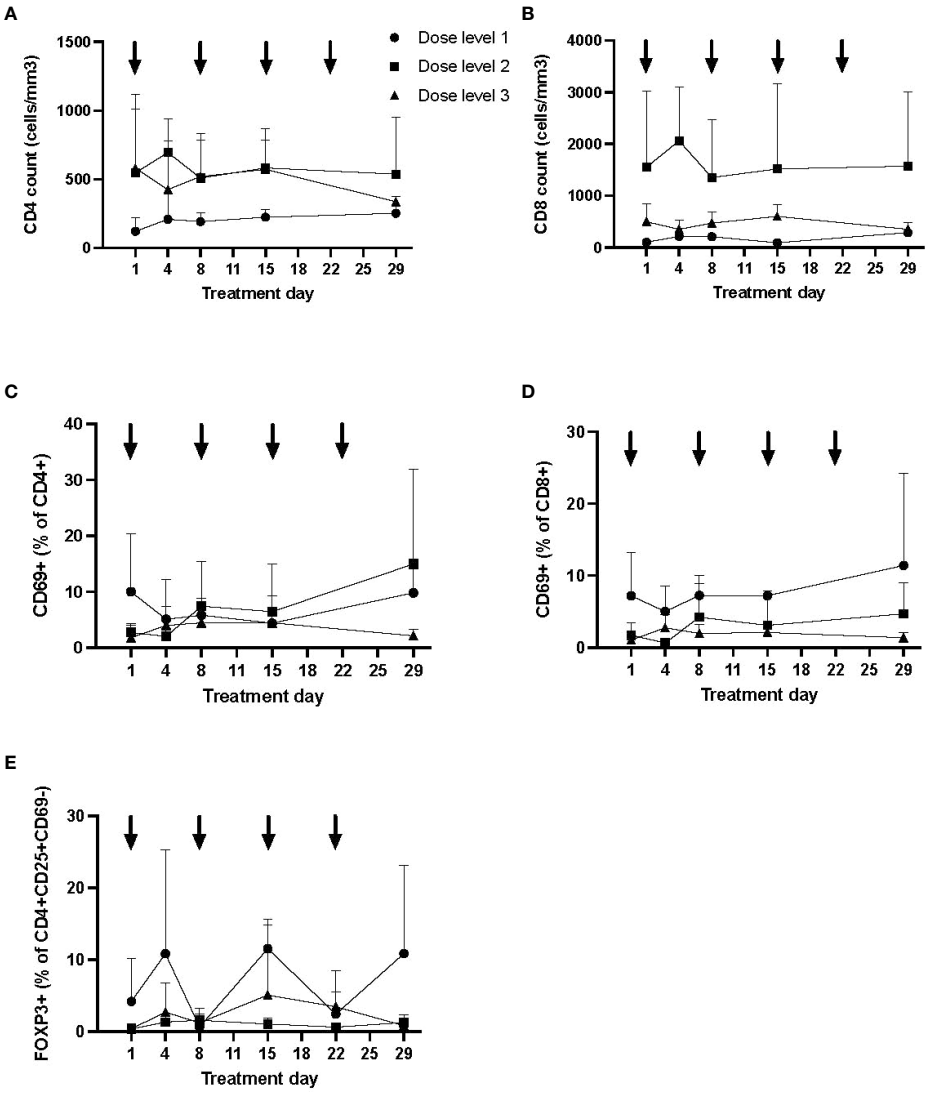

FIGURE 3
Longitudinal immune profile following autologous MSC infusion. Flow cytometry was performed to evaluate lymphocyte subsets (CD3+CD4+ and CD3+CD8+; **A**, **B**), T-cell activation (CD69+; **C**, **D**), and regulatory T cells **(E)** longitudinally. Data (mean, SD) are shown by dose level, with timing of MSC infusion designated by arrows. The proportion of activated T cells was lowest at day 29 in dose level 3, although T-cell activation was higher at baseline in dose level 1. No significant differences were otherwise seen by dose level in T-cell counts or proportion of regulatory T cells. MSC, mesenchymal stromal cell; SD, standard deviation.

reached, with the highest dose level being weekly infusions of 2×10^6/kg × 4 doses. Secondary endpoints included clinical response, and while limited by the small sample size and heterogeneity of GVHD, three of four patients with acute GVHD (or overlap with acute component) had objective responses ranging from partial to complete. Importantly, this trial demonstrates the feasibility of using autologous and culture-recovered MSCs to treat GVHD.

To our knowledge, this is the first clinical trial to evaluate autologous, fresh (culture recovered), and early-passage MSCs in the treatment of GVHD to overcome barriers in donor source and culture conditions, which may have impacted the efficacy of MSCs in previous trials. Given that most clinical trials have used cryopreserved, freshly thawed MSCs, it was important to first verify the safety of this approach. Additionally, our product likely costs considerably less than commercial MSC products such as Remestemcel-L, which has been reported to cost $195,000 in Japan. Our safety findings are consistent with previous studies, including a meta-analysis restricted to randomized controlled trials of MSCs for a variety of inflammatory conditions (18); while transient fever was associated with MSC infusion in this meta-analysis, this may have been abrogated in our population given steroid pre-treatment and concurrent immunosuppression for treatment of GVHD. Additionally, our safety and feasibility results are consistent with our previously published phase I dose-escalation trial of autologous and culture-recovered MSCs as treatment for refractory Crohn's disease, where no DLTs were seen (16).

This approach could further improve efficacy—given our phase I design, small sample size, and heterogeneity in patients (including concurrent GVHD treatment), we were limited in our ability to detect clinical responses to our MSC product. Nonetheless, our data suggest that an acute GVHD phenotype may be more responsive to MSC treatment, with the only acute GVHD patient having no response to MSCs having been on >1 mg/kg/day of steroids. Compared to the efficacy results of other MSC trials, our efficacy results in acute GVHD patients compare favorably and in chronic GVHD patients are comparable, while providing more detailed outcome data (with longitudinal organ scoring). As recently reviewed by Kelly et al. (4), MSCs have been evaluated for the treatment of GVHD in nearly 60 ongoing or completed clinical trials, primarily for steroid-refractory acute GVHD and in a single-arm, small, phase I or II clinical trials. Heterogeneity in MSC product (including starting product, passage, and dose) and definitions (including treatment-refractory GVHD and response) limit the ability to assess responses across trials. Nonetheless, in the treatment of steroid-refractory acute GVHD, responses have been mixed, with day 28 CR ranging from 8% to 75% and higher OR ranging from 42% to 100%; notably, many trials did not specify the timing of response assessment. In the two studies with a control group, responses were higher in those treated with MSCs; in those with two dose levels (n = 2), the dose response was mixed. There are limited data on MSCs as a first-line treatment for acute GVHD, with both trials showing paradoxical lower responses in those receiving a higher MSC dose. Fewer trials of MSCs for chronic GVHD treatment have been performed, all small (n = 1–14 patients) and single arm. Responses have also been mixed, with CR at day 28 ranging from 0% to 40% and OR ranging from 0% to 80%; in one trial reporting responses at 1 year, CR and OR were 80%. Across all studies (acute and chronic GVHD), overall survival post-MSC treatment was also mixed, ranging from 0% to 100%. Potentially reduced potency in post-thawed products and use of late-passage MSCs may in part explain variability in observed responses. Thus, methods to improve MSC potency and standardized product potency assays may assist in comparisons across clinical trials (19). In our study, we did not observe any changes in lymphocyte count, lymphocyte activation, or regulatory T cells in the first month to correlate with treatment exposure or response. Future trials should emphasize the performance of correlative analyses to identify pharmacodynamic evidence of MSC activity and predictors of response.

Our efficacy data also appear similar to other second-line treatments for treatment-refractory GVHD, particularly for acute GVHD. Ruxolitinib is the only agent currently approved by the FDA for the treatment of steroid-refractory acute GVHD, based on clinical trial data with CR ranging from 27% to 34% and OR ranging from 55% to 62% at day 28 (20, 21). In chronic GVHD, three agents are now approved for the treatment of refractory disease, ibrutinib, belumosudil, and ruxolitinib, with best OR ranging from 67% to 76% and CR ranging from 5% to 21% (22). Steroids remain the pillar of upfront therapy for GVHD but often lead to significant morbidity including likely impairment in epithelial healing, which can further complicate the clinical picture of GI GVHD (23). The cumulative effect of added immune suppression can lead to opportunistic infections and further toxicity. Alternative approaches focused on promoting tolerance and tissue healing may offer efficacy without additive risk for infection. In addition to MSCs, another example is the use of urinary-derived human chorionic gonadotropin/epidermal growth factor (uhCG/EGF) for the treatment of severe acute GVHD (24, 25).

The use of autologous MSCs in the setting of GVHD is limited by the timeline required for *ex vivo* expansion, especially in the treatment of acute GVHD, where the escalation of therapy is needed after 1 week if refractory to steroids. An autologous source of MSCs for chronic GVHD treatment is likely not feasible, as treatment beyond four doses is likely required, and expansion for >4 doses while maintaining early passage is not achievable. The use of early passage and culture-recovered MSCs, regardless of BM source, is likely to offer improved potency over freshly thawed and multiply passaged MSCs, though this requires further evidence from future clinical trials with associated biologic correlates. Informed by our phase I trial results and with a continued goal to improve the *in vivo* efficacy of MSC infusion, we have thus launched a clinical trial of third-party cryopreserved MSCs to evaluate interferon-gamma

priming during culture recovery, based on preclinical studies demonstrating enhanced potency (NCT04328714) (10, 26, 27).

In conclusion, we determined that autologous MSCs given weekly for four doses are safe in the setting of treatment-refractory GVHD post-HCT for hematologic malignancy. Culture recovery may reverse the deleterious impact of cryopreservation and thawing on MSC potency, and thus the safety signal in this trial supports this manufacturing approach in now ongoing and future GVHD trials.

Data availability statement

The original contributions presented in the study are included in the article/Supplementary Material. Further inquiries can be directed to the corresponding author.

Ethics statement

The studies involving human participants were reviewed and approved by Emory University IRB. Written informed consent to participate in this study was provided by the participants' legal guardian/next of kin.

Author contributions

AL, JG, EW, and MQ designed the trial. CG, AL, DK, PD, RC, JG, EW, and MQ participated in the study execution and data collection. ES, CG, PD, and MQ analyzed the data. All authors interpreted the data, critically reviewed the manuscript, and provided final approval for submission. All authors agree to be accountable for all aspects of the work, ensuring the accuracy and integrity of the publication.

Funding

Supported by: National Center for Advancing Translational Sciences (KL2TR000455) (MQ) and CURE Childhood Cancer (MQ).

Acknowledgments

The authors would like to acknowledge the contributions of Ian Copland, PhD (posthumous) and Marco Garcia.

Conflict of interest

The authors declare that the research was conducted in the absence of any commercial or financial relationships that could be construed as a potential conflict of interest.

Publisher's note

Supplementary material

The Supplementary Material for this article can be found online at: https://www.frontiersin.org/articles/10.3389/fimmu.2022.959658/full#supplementary-material

References

1. D'Souza A, Fretham C, Lee SJ, Arora M, Brunner J, Chhabra S, et al. Current use of and trends in hematopoietic cell transplantation in the united states. *Biol Blood Marrow Transplant* (2020) 26(8):e177–82. doi: 10.1016/j.bbmt.2020.04.013

2. El Jurdi N, Rayes A, MacMillan ML, Holtan SG, DeFor TE, Witte J, et al. Steroid-dependent acute GVHD after allogeneic hematopoietic cell transplantation: risk factors and clinical outcomes. *Blood Adv* (2021) 5(5):1352–9. doi: 10.1182/bloodadvances.2020003937

3. Le Blanc K, Mougiakakos D. Multipotent mesenchymal stromal cells and the innate immune system. *Nat Rev Immunol* (2012) 12(5):383–96. doi: 10.1038/nri3209

4. Kelly K, Rasko JEJ. Mesenchymal stromal cells for the treatment of graft versus host disease. *Front Immunol* (2021) 12:761616. doi: 10.3389/fimmu.2021.761616

5. Murata M, Terakura S, Wake A, Miyao K, Ikegame K, Uchida N, et al. Off-the-shelf bone marrow-derived mesenchymal stem cell treatment for acute graft-versus-host disease: real-world evidence. *Bone marrow Transplant* (2021) 56 (10):2355–66. doi: 10.1038/s41409-021-01304-y

6. Kurtzberg J, Prockop S, Chaudhury S, Horn B, Nemecek E, Prasad V, et al. Study 275: Updated expanded access program for remestemcel-l in steroid-refractory acute graft-versus-Host disease in children. *Biol Blood marrow Transplant J Am Soc Blood Marrow Transplant* (2020) 26(5):855–64. doi: 10.1016/j.bbmt.2020.01.026

7. Kebriaei P, Hayes J, Daly A, Uberti J, Marks DI, Soiffer R, et al. A phase 3 randomized study of remestemcel-l versus placebo added to second-line therapy in patients with steroid-refractory acute graft-versus-Host disease. *Biol Blood marrow Transplant* (2020) 26(5):835–44. doi: 10.1016/j.bbmt.2019.08.029

8. Galipeau J. Mesenchymal stromal cells for graft-versus-Host disease: A trilogy. *Biol Blood Marrow Transplant* (2020) 26(5):e89–91. doi: 10.1016/j.bbmt.2020.02.023

9. Francois M, Copland IB, Yuan S, Romieu-Mourez R, Waller EK, Galipeau J. Cryopreserved mesenchymal stromal cells display impaired immunosuppressive properties as a result of heat-shock response and impaired interferon-gamma licensing. *Cytotherapy* (2012) 14(2):147–52. doi: 10.3109/14653249.2011.623691

10. Chinnadurai R, Copland IB, Garcia MA, Petersen CT, Lewis CN, Waller EK, et al. Cryopreserved mesenchymal stromal cells are susceptible to T-cell mediated apoptosis which is partly rescued by IFNγ licensing. *Stem Cells* (2016) 34(9):2429–42. doi: 10.1002/stem.2415

11. Cottle C, Porter AP, Lipat A, Turner-Lyles C, Nguyen J, Moll G, et al. Impact of cryopreservation and freeze-thawing on therapeutic properties of mesenchymal Stromal/Stem cells and other common cellular therapeutics. *Curr Stem Cell Rep* (2022) 8(2):72–92. doi: 10.1007/s40778-022-00212-1

12. von Bahr L, Sundberg B, Lonnies L, Sander B, Karbach H, Hagglund H, et al. Long-term complications, immunologic effects, and role of passage for outcome in mesenchymal stromal cell therapy. *Biol Blood Marrow Transplant* (2012) 18 (4):557–64. doi: 10.1016/j.bbmt.2011.07.023

13. Eliopoulos N, Stagg J, Lejeune L, Pommey S, Galipeau J. Allogeneic marrow stromal cells are immune rejected by MHC class I- and class II-mismatched recipient mice. *Blood* (2005) 106(13):4057–65. doi: 10.1182/blood-2005-03-1004

14. Krampera M, Glennie S, Dyson J, Scott D, Laylor R, Simpson E, et al. Bone marrow mesenchymal stem cells inhibit the response of naive and memory antigen-specific T cells to their cognate peptide. *Blood* (2003) 101(9):3722–9. doi: 10.1182/blood-2002-07-2104

15. Copland IB, Qayed M, Garcia MA, Galipeau J, Waller EK. Bone marrow mesenchymal stromal cells from patients with acute and chronic graft-versus-Host disease deploy normal phenotype, differentiation plasticity, and immune-suppressive activity. *Biol Blood Marrow Transplant* (2015) 21(5):934–40. doi: 10.1016/j.bbmt.2015.01.014

16. Dhere T, Copland I, Garcia M, Chiang KY, Chinnadurai R, Prasad M, et al. The safety of autologous and metabolically fit bone marrow mesenchymal stromal cells in medically refractory crohn's disease - a phase 1 trial with three doses. *Alimentary Pharmacol Ther* (2016) 44(5):471–81. doi: 10.1111/apt.13717

17. Jagasia MH, Greinix HT, Arora M, Williams KM, Wolff D, Cowen EW, et al. National institutes of health consensus development project on criteria for clinical trials in chronic graft-versus-Host disease: I. the 2014 diagnosis and staging working group report. *Biol Blood Marrow Transplant* (2015) 21(3):389–401.e1. doi: 10.1016/j.bbmt.2014.12.001

18. Lalu MM, McIntyre L, Pugliese C, Fergusson D, Winston BW, Marshall JC, et al. Safety of cell therapy with mesenchymal stromal cells (SafeCell): a systematic review and meta-analysis of clinical trials. *PloS One* (2012) 7(10):e47559. doi: 10.1371/journal.pone.0047559

19. Chinnadurai R, Rajan D, Qayed M, Arafat D, Garcia M, Liu Y, et al. Potency analysis of mesenchymal stromal cells using a combinatorial assay matrix approach. *Cell Rep* (2018) 22(9):2504–17. doi: 10.1016/j.celrep.2018.02.013

20. Zeiser R, von Bubnoff N, Butler J, Mohty M, Niederwieser D, Or R, et al. Ruxolitinib for glucocorticoid-refractory acute graft-versus-Host disease. *New Engl J Med* (2020) 382(19):1800–10. doi: 10.1056/NEJMoa1917635

21. Jagasia M, Perales MA, Schroeder MA, Ali H, Shah NN, Chen YB, et al. Ruxolitinib for the treatment of steroid-refractory acute GVHD (REACH1): a multicenter, open-label phase 2 trial. *Blood* (2020) 135(20):1739–49. doi: 10.1182/blood.2020004823

22. Martini DJ, Chen YB, DeFilipp Z. Recent FDA approvals in the treatment of graft-Versus-Host disease. *Oncologist* (2022) 27(8):685–93. doi: 10.1093/oncolo/oyac076

23. Huang EY, Inoue T, Leone VA, Dalal S, Touw K, Wang Y, et al. Using corticosteroids to reshape the gut microbiome: implications for inflammatory bowel diseases. *Inflammatory Bowel Dis* (2015) 21(5):963–72. doi: 10.1097/mib.0000000000000332

24. Holtan SG, Hoeschen AL, Cao Q, Arora M, Bachanova V, Brunstein CG, et al. Facilitating resolution of life-threatening acute GVHD with human chorionic gonadotropin and epidermal growth factor. *Blood Adv* (2020) 4(7):1284–95. doi: 10.1182/bloodadvances.2019001259

25. Holtan SG, Ustun C, Hoeschen AL, Feola J, Cao Q, Gandhi P, et al. Phase 2 results of urinary-derived human chorionic Gonadotropin/Epidermal growth factor as treatment for life-threatening acute GVHD. *Blood* (2021) 138(1):261. doi: 10.1182/blood-2021-145008

26. Chinnadurai R, Copland IB, Patel SR, Galipeau J. IDO-independent suppression of T cell effector function by IFN-gamma-licensed human mesenchymal stromal cells. *J Immunol (Baltimore Md 1950)* (2014) 192(4):1491–501. doi: 10.4049/jimmunol.1301828

27. Guess AJ, Daneault B, Wang R, Bradbury H, La Perle KM, Fitch J, et al. Safety profile of good manufacturing practice manufactured interferon γ-primed mesenchymal Stem/Stromal cells for clinical trials. *Stem Cells Trans Med* (2017) 6(10):1868–79. doi: 10.1002/sctm.16-0485

frontiers | Frontiers in Immunology

TYPE Original Research
PUBLISHED 30 November 2022
DOI 10.3389/fimmu.2022.972095

OPEN ACCESS

EDITED BY
David Allan,
Ottawa Hospital Research Institute (OHRI), Canada

REVIEWED BY
David Andrew Hess,
Western University, Canada
Scott D. Olson,
University of Texas Health Science Center at Houston, United States

*CORRESPONDENCE
Sowmya Viswanathan
sowmya.viswanathan@uhnresearch.ca

SPECIALTY SECTION
This article was submitted to Alloimmunity and Transplantation, a section of the journal Frontiers in Immunology

RECEIVED 17 June 2022
ACCEPTED 27 September 2022
PUBLISHED 30 November 2022

CITATION
Robb KP, Audet J, Gandhi R and Viswanathan S (2022) Putative critical quality attribute matrix identifies mesenchymal stromal cells with potent immunomodulatory and angiogenic "fitness" ranges in response to culture process parameters. *Front. Immunol.* 13:972095. doi: 10.3389/fimmu.2022.972095

Putative critical quality attribute matrix identifies mesenchymal stromal cells with potent immunomodulatory and angiogenic "fitness" ranges in response to culture process parameters

Kevin P. Robb[1,2,3], Julie Audet[3], Rajiv Gandhi[1,4] and Sowmya Viswanathan[1,2,3,5]*

[1]Osteoarthritis Research Program, Division of Orthopedic Surgery, Schroeder Arthritis Institute, University Health Network, Toronto, ON, Canada, [2]Krembil Research Institute, University Health Network, Toronto, ON, Canada, [3]Institute of Biomedical Engineering, University of Toronto, Toronto, ON, Canada, [4]Department of Surgery, Division of Orthopedic Surgery, University of Toronto, Toronto, ON, Canada, [5]Department of Medicine, Division of Hematology, University of Toronto, Toronto, ON, Canada

Adipose-derived mesenchymal stromal cells (MSC(AT)) display immunomodulatory and angiogenic properties, but an improved understanding of quantitative critical quality attributes (CQAs) that inform basal MSC(AT) fitness ranges for immunomodulatory and/or angiogenic applications is urgently needed for effective clinical translation. We constructed an *in vitro* matrix of multivariate readouts to identify putative CQAs that were sensitive enough to discriminate between specific critical processing parameters (CPPs) chosen for their ability to enhance MSC immunomodulatory and angiogenic potencies, with consideration for donor heterogeneity. We compared 3D aggregate culture conditions (3D normoxic, 3D-N) and 2D hypoxic (2D-H) culture as non-genetic CPP conditions that augment immunomodulatory and angiogenic fitness of MSC(AT). We measured multivariate panels of curated genes, soluble factors, and morphometric features for MSC(AT) cultured under varying CPP and licensing conditions, and we benchmarked these against two functional and therapeutically relevant anchor assays – *in vitro* monocyte/macrophage (MΦ) polarization and *in vitro* angiogenesis. Our results showed that varying CPP conditions was the primary driver of MSC(AT) immunomodulatory fitness; 3D-N conditions induced greater MSC(AT)-mediated MΦ polarization toward inflammation-resolving subtypes. In contrast, donor heterogeneity was the primary driver of MSC(AT) angiogenic fitness. Our analysis further revealed panels of putative CQAs with minimum and maximum values that consisted of twenty MSC(AT) characteristics that informed

immunomodulatory fitness ranges, and ten MSC(AT) characteristics that informed angiogenic fitness ranges. Interestingly, many of the putative CQAs consisted of angiogenic genes or soluble factors that were inversely correlated with immunomodulatory functions (*THBS1, CCN2, EDN1, PDGFA, VEGFA, EDIL3, ANGPT1*, and *ANG* genes), and positively correlated to angiogenic functions (VEGF protein), respectively. We applied desirability analysis to empirically rank the putative CQAs for MSC(AT) under varying CPP conditions and donors to numerically identify the desirable CPP conditions or donors with maximal MSC (AT) immunomodulatory and/or angiogenic fitness. Taken together, our approach enabled combinatorial analysis of the matrix of multivariate readouts to provide putative quantitative CQAs that were sensitive to variations in select CPPs that enhance MSC immunomodulatory/angiogenic potency, and donor heterogeneity. These putative CQAs may be used to prospectively screen potent MSC(AT) donors or cell culture conditions to optimize for desired basal MSC(AT) immunomodulatory or angiogenic fitness.

KEYWORDS

mesenchymal stromal cell, immunomodulation, angiogenesis, critical quality attribute, donor heterogeneity, 3D suspension cultures, hypoxic conditioning, potency

Introduction

The immunomodulatory and pro-angiogenic functions of mesenchymal stromal cells (MSCs) make them attractive cell therapy candidates for numerous clinical indications (1). However, despite hundreds of clinical trials, mixed reports on clinical efficacy and insufficient characterization of MSC potency have continued to hamper the field, resulting in very few MSC products with regulatory and market endorsement (2). As was recently outlined by Krampera and Le Blanc (3), part of the observed heterogeneity in clinical efficacy of MSCs is likely due to the complex interactions between MSCs and the host tissue microenvironment, which is specific to a given disease as well as stage of the disease. This has further pointed to the need for defining critical quality attributes (CQAs) with established limits or ranges that enable quality checks of basal thresholds for high therapeutic potency MSCs with associated fitness levels (4). These fitness levels may be further modulated by the host disease microenvironment to ultimately determine net MSC therapeutic efficacy (3, 5), but quantifying basal MSC fitness through CQAs is a necessary starting point. Importantly, MSC CQAs must be linked to specific culture conditions, which are a critical source of variability in processing and expanding MSCs (6, 7).

Previous work has investigated MSC characteristics that carry functional significance and can serve as candidate CQAs for defining basal MSC fitness levels that correlate with clinical efficacy. Our group has demonstrated that prevalence of a panel of seven immunomodulatory markers expressed by bone marrow-derived MSCs (MSC(M)) *in vitro* (i.e., basal CQAs) correlated with improved patient-reported outcomes, suggestive of an anti-inflammatory mechanism of action in a twelve-patient knee osteoarthritis trial (8). Work by Galleu *et al.* has suggested that MSC(M) that are more susceptive to host cytotoxic activity afforded better clinical responses in graft-versus-host disease (GVHD) patients (9). Several groups have evaluated multi-dimensional characteristics of MSCs that could be considered putative CQAs, as these correlate to *in vitro* immunosuppression of T cell functions; However, the associations between this immunomodulatory ability and clinical efficacy, at least in GVHD patients, has not panned out (10). Nonetheless, work by Chinnadurai *et al.* demonstrated that interactions with peripheral blood-derived mononuclear cells (PBMCs) modulate the mRNA and secreted factor profiles (11, 12), as well as the signal transducer and activator of transcription (STAT) phosphorylation status (13) of human MSCs derived from various tissue sources, and that these signatures correlate with T cell immunosuppression. Maughon *et al.* have shown that metabolomic and cytokine profiles of human MSC(M) and induced pluripotent stem cell-derived MSCs also correlate to T cell suppression (14). Furthermore, multidimensional profiles of human MSC(M) morphological features have been linked to T cell suppression for MSC(M) stimulated with TNFα and/or IFNγ (15, 16). Notably, work by Boregowda *et al.* postulated a potential interplay between immunomodulatory and pro-angiogenic functions of human MSC(M) mediated by expression levels of the transcription factor TWIST1, and suggested that culture conditions impact the interplay between these two properties of MSCs (17).

While progress has been made in identifying candidate CQAs for MSCs (18, 19), it is important for these candidate CQAs to be measurable, quantitative and sensitive to donor heterogeneity and variations in critical processing parameters (CPPs, *i.e.*, culture parameters that influence CQAs), two major, controllable variables that impact MSC functional activity *in vitro*. Subsequent *in vivo* MSC functionality is less tractable and likely modulated by host immune cell and microenvironment interactions. Donor heterogeneity can be attributed to several factors, including donor health status, BMI, sex, and age which are known to influence MSC functional properties, such as *in vitro* clonogenic potential and paracrine functions (20–22). In addition, manufacturing strategies for MSCs vary widely, and culture conditions or CPPs can have a marked impact on cell behaviour (23, 24). For example, stimulation with pro-inflammatory cytokines, commonly referred to as "licensing" in the MSC field, has been extensively explored as a means to enhance immunoregulatory functions of MSCs and reduce donor heterogeneity (25, 26).

In terms of CPPs, we elected to focus on and compare MSCs cultured under hypoxic or 3D aggregate conditions as non-genetic, culture manipulating methods that are known to augment immunomodulatory and/or angiogenic properties of MSCs, rather than traditional parameters (medium, seeding density, etc.). The effects of hypoxic conditions on MSC function have been widely investigated, in particular for augmenting the pro-angiogenic functions of MSCs within *in vitro* and *in vivo* models (27, 28). Recent evidence has also shown that hypoxic culture may augment MSC immunomodulatory functions (29, 30). In parallel, 3D cultures of MSCs were considered as work by Bartosh et al. demonstrated that human MSC(M) spheroids had improved immunomodulatory functions within an *in vitro* mouse macrophage co-culture system and in the zymosan-induced peritonitis mouse model (31). Other studies have provided further evidence for the augmented immunomodulatory (32, 33), as well as pro-angiogenic (32, 34, 35) functions of MSCs cultured in 3D aggregates. Notably, we employed xeno-free cell culture medium for MSC expansion and generation of 3D aggregates, and previous work has suggested that 3D-cultured MSCs lose their augmented immunomodulatory function when cultured using xeno-free medium (36).

In the present study, we explored the relationship between select CPPs known to enhance immunomodulatory and/or angiogenic MSC basal fitness range and multivariate morphological, gene expression, soluble factor expression, and functional readouts against a backdrop of donor heterogeneity. Using adipose tissue-derived MSCs (MSC(AT)), we employed a statistical approach to identify a putative matrix of CQAs that are correlated with anchor functional assays. We focused on *in vitro* MΦ polarization, recognizing that MΦs are a primary effector cell type of MSCs for numerous indications (reviewed in (37)), and given clinical data from our laboratory demonstrating that MSC(M) injections modulate MΦ phenotype in knee osteoarthritis (8). To evaluate functional angiogenesis, the human umbilical vein endothelial cell (HUVEC) tube formation assay was selected as a potency assay that has been employed for clinical-grade MSC products (19, 38).

We integrated our statistical methods to identify a matrix of putative CQAs with minimum and maximum values that correlated with functional immunomodulatory and/or angiogenic readouts. This combinatorial assay matrix approach allowed us to systematically compare and rank the effects of varying CPPs on putative CQAs for MSC(AT) in terms of their immunomodulatory and angiogenic properties, two functional axes with high therapeutic relevance. The matrix of putative CQAs also allows for identification of donors with enhanced immunomodulation or angiogenic functionalities.

Methods

MSC(AT) isolation, culture, and CPPs

Subcutaneous human adipose tissue was obtained external to the knee joint in patients undergoing knee arthroscopy or from abdominal lipoaspirate (REB #18-5480 and #18-6345, see Table 1 for summary of donor characteristics). MSC(AT) were isolated and expanded using MesenCult™-ACF Plus xeno-free and antibiotic-free growth medium (StemCell Technologies, Vancouver, Canada) on standard tissue culture polystyrene flasks coated with animal component-free cell attachment substrate (StemCell Technologies) according to the manufacturer's instructions. Cells were expanded in a standard incubator at 37˚C in 5% CO_2 under ambient air. For passaging, flasks at approximately 80% confluency were washed with PBS (Wisent, St-Bruno, Canada) and harvested using TrpLE (Gibco, Waltham, USA) prior to re-plating at 5,000 cells/cm^2. All experiments were performed using MSC(AT) between passage 3 and passage 5.

At approximately 70-80% confluence, MSC(AT) were transiently (16-20 h) cultured under varied CPP conditions, including 3D normoxic (3D-N), 2D hypoxic (2D-H), or 2D normoxic (2D-N) conditions. These culture steps were performed on separate flasks cultured in parallel using MesenCult™-ACF Plus medium supplemented with 1% (v/v) human serum album (HSA; Canadian Blood Services, Ottawa, Canada). 3D-N culture was performed by harvesting MSC(AT) from adherent flasks and plating cells on ultra-low attachment surfaces (Corning, Corning, USA) at 26,700 cells/cm^2 and 200,000 cells/mL in medium supplemented with 2 ng/mL IL-6 (Peprotech, Cranbury, USA; used to support cell viability in the 3D culture), based on previously reported methods that allow spontaneous aggregation of MSCs into cell clusters (39). Flasks from the same batch of cells were cultured in parallel under 2D-N (maintained in standard tissue culture incubator) or 2D-H

TABLE 1 Summary of MSC(AT) donor characteristics.

Donor ID	Sex	Age	BMI	Depot	Procedure	Osteoarthritis location	KL grade
D1	M	46	27.3	Knee	Arthroscopy	None	N/A
D2	F	38	22.0	Knee	Arthroscopy	Knee	2
D3	M	28	26.9	Knee	Arthroscopy	Knee	1
D4	F	52	22.4	Knee	Arthroscopy	Knee	1
D5	M	54	30.1	Abdomen	Lipoaspirate	Hand	N/A

Subcutaneous adipose tissue was collected from human donors. Depot column indicates anatomical location of adipose tissue collection. Procedure column indicates the procedure the donor underwent for the adipose tissue collection. All patients (except D1) had been diagnosed with knee or hand osteoarthritis. M: Male, F: Female, BMI: Body Mass Index, KL: Kellgren-Lawrence grade.

conditions (38 mmHg O_2, *i.e.*, 5% O_2 under standard atmospheric pressure) using a HypoxyLab workstation (Oxford Optronix, Milton, UK) for the same duration as 3D culture.

Prior to experiments, 3D cell aggregates were collected from ultra-low attachment flasks. Following multiple PBS washes of the flask and mixing, samples were removed for cell counting. Cell enumeration was performed after dissociating the aggregates using Accumax™ solution (Sigma, St. Louis, USA), according to previously published methods (40). For MSC(AT) cultured under 2D-N and 2D-H conditions, flasks were washed with PBS and incubated in TrpLE solution, followed by neutralization with complete medium and cell counting. All cell counts were performed using the Vi-Cell XR Cell Counter (Beckman Coulter, Brea, USA). Prior to plating cells for experiments, excess PBS was added to cell suspensions to dilute residual growth factors/cytokines before centrifugation (350 x g, 5 min) to pellet the cells.

Morphometric and surface marker characterization of MSC(AT)

Cell diameter and circularity was measured for single cell suspensions using the Vi-Cell XR Cell Counter (Beckman Coulter). 3D-N MSC(AT) were dissociated into single cell suspensions as described above. To analyze maximum feret diameters and circularity of whole intact 3D-N MSC(AT) aggregates, 10X phase-contrast images were captured using an EVOS XL Core Cell Imaging System (ThermoFisher, Waltham, USA). A semi-automated algorithm was developed in ImageJ (41) based on rolling ball subtraction to create binary images for particle analysis, and a minimum of 230 aggregate measurements were performed per donor and condition.

Surface marker expression of MSC(AT) was measured following previously established protocols (8) and in accordance with IFATS/ISCT guidelines (positive marker threshold: >80%, negative marker threshold: <2%) (42). The following PE-conjugated anti-human antibodies from BioLegend (San Diego, USA) were used: anti-CD90 (cat. 328109), anti-CD73 (cat. 344004), anti-CD44 (cat. 338807), anti-CD29 (cat. 303003), anti-CD13 (cat. 301703), anti-CD34 (cat. 343506), anti-CD31 (cat. 303105), anti-CD45 (cat. 304008), and anti-CD105 (cat. 323205). For staining, single cell suspensions of 2D-H and 2D-N MSC(AT) were obtained by TrpLE dissociation, while 3D-N aggregates were digested using Accumax™ solution as described above. To evaluate the effects of Accumax™ digestion on the surface marker profile of 2D MSC(AT), a subset of 2D-N MSC(AT) were digested using the same Accumax™ digestion protocol as used for 3D cell aggregates. Samples were characterized using the FC500 flow cytometer (Beckman Coulter) and analyzed using FlowJo version 10 software (Ashland, USA).

Western blotting

Western blot analysis was performed to confirm CD105 expression in MSC(AT) cultured under varying CPP conditions. Cells were lysed using a buffer containing 50 mM Tris–HCl (pH 7.5), 1mM EGTA, 1mM EDTA, 1% (w/v) Nonidet P40, 1mM sodium orthovanadate, 50 mM sodium fluoride, 5 mM sodium pyrophosphate, 0.27 M sucrose, and a protease inhibitor cocktail (Roche). Protein concentration of all samples was measured using the Pierce BCA protein assay (ThermoFisher). Protein samples were loaded in a 10% polyacrylamide gel (20 µg/well) for electrophoresis followed by transfer to nitrocellulose membranes. Membranes were then blocked with TBS-T containing 5% (w/v) BSA and they were immunoblotted in the same buffer overnight at 4°C with an anti-CD105 primary antibody (cat. 323205, BioLegend, 1:1,000 dilution), or for 2 h with an anti-β-actin antibody (Sigma, 1:10,000 dilution) used for the loading control. Washes were then performed with TBS-T and the blots were then incubated with secondary HRP-conjugated antibodies in 5% skimmed milk. The blots were washed in TBS-T and the signal was detected with the enhanced chemiluminescence reagent (ECL; GE Healthcare, Chicago, USA) and using a chemiluminescent imaging system (Bio-Rad, Hercules, USA).

Gene expression and soluble factor measurements

After harvesting cells from 2D-N, 2D-H, and 3D-N conditions, cells were added to 24-well plates at 60,000 cells/well in MesenCult™-ACF Plus medium supplemented with 1% HSA (v/v) with or without addition of pro-inflammatory licensing cytokines. The licensing cytokines (all purchased from Peprotech) consisted of IFNγ (30 ng/mL), TNFα (10 ng/mL), and IL-1β (5 ng/mL). Cells harvested from 2D-N or 2D-H conditions were maintained under normoxic or hypoxic (38 mmHg O_2) conditions for 24 h, respectively, while cell aggregates from the 3D-N condition were plated on ultra-low attachment 24-well plates (Corning) without dissociation. After the culture period, conditioned medium was collected, centrifuged (1,000 x g, 5 min) and frozen at -80°C. The remaining cells were washed in PBS and RNA was extracted using a RNeasy Mini kit (Qiagen, Hilden, Germany) according to the manufacturer's instructions. RNA concentration and purity was measured using a DS-11 Spectrophotometer (DeNovix, Wilmington, USA).

The nCounter platform (NanoString, Seattle, USA) was used as a highly sensitive tool that detects target mRNAs with high specificity and without amplification. Samples (100 ng RNA/sample) were run on the nCounter MAX Analysis system (St. Michael's Genomics Molecular Biology Core facility) according to the manufacturer's instructions using a custom CodeSet 58-gene panel. The data was processed using the nSolver version 4.0 software (NanoString) according to the manufacturer's instructions to obtain mRNA counts normalized to the synthetic positive control probes and to reference genes. The following were measured as potential reference genes: *ABCF1*, *GAPDH*, *GUSB*, *HPRT1*, *LDHA*, *RPL19*, *RPLP0*, *TUBB*, *POLR1B*, and *TBP*. Reference gene stability was evaluated using geNorm analysis in the nSolver software; *POLR1B* and *TBP* were subsequently discarded as reference genes and not used for normalization. Normalized mRNA counts below 20 were assigned values of 1 if >33% of samples were within range. The following genes were undetectable (<33% of samples were within range) under both licensed and unlicensed conditions: *ANGPT2*, *BDNF*, *BMP7*, *CCR7*, *CD200*, *CTLA4*, *CXCR4*, *IGF1*, *IL10*, *IL12A*, *NGF*, *PDGFB*, *PROK1*, and *CXCL12*. Under licensed conditions, *VASH1* and *SOX9* were undetectable. Under unlicensed conditions, *CD274*, *IDO1*, *NFKBIA*, *NOS2*, and *PDGFA* were undetectable. We selected a broad spectrum of MSC(AT) transcripts initially but many of the undetectable genes are not commonly or are inconsistently expressed by MSCs. Other genes may have tissue of origin-dependent or context-dependent expression. All NanoString data has been deposited in NCBI's Gene Expression Omnibus (43) accessible through GEO Series accession number GSE212368.

Conditioned medium samples were analyzed for soluble factors using a custom 10-analyte LEGENDplex immunoassay (BioLegend) according to the manufacturer's instructions, and samples were run on a FACSCanto™ II flow cytometer (BD Biosciences, Franklin Lakes, USA). Values below the assay limit of detection were imputed as half of the lower limit of detection if >33% of samples were within range. IL-10, PIGF, and PD-L1 were undetectable in the samples tested. IL-1RA was undetectable in unlicensed samples only.

Pilot gene expression experiments were performed to i) examine gene expression in MSC(AT) cultured using the combination of 3D and hypoxic culture (3D-H), and ii) to evaluate effects of IL-6 treatment on MSC(AT) cultured under 2D-N conditions using the same IL-6 concentration and treatment duration as used for 3D-N conditions. Both sets of pilot experiments were performed under licensed conditions using the methods outlined above. After licensing, RNA was isolated from MSC(AT) by Trizol-chloroform extraction and cDNA was generated using SuperScript™ IV VILO™ Master Mix (Invitrogen, Waltham, USA). qPCR was run using custom primers (Suppl. Table 1, Invitrogen) and FastStart Universal SYBR Green Master Mix (Roche, Basel, Switzerland) on a QuantStudio™ 5 system (ThermoFisher). Results were normalized (ΔΔCT) against reference genes (*B2M* and *RPL13A*) and presented as fold-change values relative to 2D-N culture conditions.

In vitro MΦ polarization

Peripheral blood-derived $CD14^+$ monocytes were isolated from a leukopak (StemCell Technologies) by Ficoll density gradient separation and selection with $CD14^+$ magnetic beads as previously described (44). Cryopreserved monocytes were thawed and plated on 24-well plates at 100,000 cells/well and allowed to acclimate for 48 h in co-culture medium consisting of: 1 mM sodium pyruvate (Gibco), 1% penicillin-streptomycin (Gibco), 10% FBS (Wisent), and 10% low-glucose DMEM (Sigma) in RPMI medium (Gibco). Prior to co-culture, MSC (AT) were harvested from 2D-N, 2D-H, and 3D-N conditions, plated on 0.4 μm transwell inserts at 10,000 cells/insert in a separate 24-well plate, and allowed to attach for 2 h. The inserts were then transferred to MΦ wells and co-cultured for 20-24 h. Transwell inserts containing MSC(AT) were then removed, and lipopolysaccharide was spiked into wells at a final concentration of 2.5 ng/mL. After a 4 h incubation, MΦs (both adherent and in suspension) were collected and stored in Trizol (Roche) at -80°C. Conditioned medium was also collected and stored at -80°C.

Levels of TNFα in conditioned medium were measured by ELISA (R&D Systems, Minneapolis, USA) according to the manufacturer's instructions. To analyze MΦ gene expression, RNA was isolated by Trizol-chloroform extraction and cDNA

was generated using SuperScript™ IV VILO™ Master Mix (Invitrogen). qPCR was run using custom primers (Suppl. Table 1, Invitrogen) and FastStart Universal SYBR Green Master Mix (Roche) on a QuantStudio™ 5 system (ThermoFisher). Results were normalized (ΔΔCT) against reference genes (*ACTB*, *B2M*, and *TBP*) and presented as fold-change values relative to MΦ cultured without MSC(AT) (SOLO condition).

In vitro HUVEC tube formation

To prepare conditioned medium for the HUVEC tube formation assay, MSC(AT) were harvested from 2D-N, 2D-H, and 3D-N conditions, plated at 15,000 cells/cm^2 and 100,000 cells/mL of growth medium (no added HSA or exogenous cytokines), and incubated for 24 h in cell culture incubators. MSC(AT) harvested from all three CPP conditions were maintained under these conditions to prepare conditioned medium. To prepare unconditioned medium controls, growth medium was incubated on a cell culture plate for the same duration. Following the 24 h incubation period, the conditioned medium was collected, centrifuged (1,000 x g, 5 min), and the supernatant was frozen at -80°C for future use in the HUVEC tube formation assay.

Five to seven days prior to the tube formation assay, P4 HUVECs (Cat. CC2519, Lonza, Basel, Switzerland) were thawed and expanded in EGM™-2 (Lonza) according to the manufacturer's instructions. The HUVEC tube formation assay was performed based on previously published methods (38). 96-well plates were pre-coated with Cultrex Reduced Growth Factor Basement Membrane Extract, PathClear (R&D Systems) according to the manufacturer's instructions. HUVECs were harvested and plated on the coated plates at 42,500 cells/cm^2 in conditioned medium. The following medium formulations were used as controls: unconditioned medium, EGM™-2 medium (positive control), and basal medium without addition of growth factors/supplements (negative control). All wells were imaged 6 h after plating the cells using the EVOS XL Core Cell Imaging System (ThermoFisher) at 4X objective. The images were analyzed using the Angiogenesis Analyzer plugin in ImageJ (45).

Statistical analysis

Plots were created using GraphPad Prism 6.0 (La Jolla, USA) and JMP Pro 14 (Cary, USA) software. All statistical tests are specified in the figure captions. One- and two-way ANOVA, as well as simple linear regression was performed using GraphPad Prism software. Unbiased hierarchical clustering (Ward method), principal component (PC) analysis (default estimation method), and desirability profiling was performed using JMP software. Analysis of differential gene expression was performed in nSolver (NanoString) using single linear regressions for each covariate (*i.e.*, gene) with false discovery rate (FDR)-corrected p values calculated using the Benjamini-Yekutieli method (46). Data were considered statistically significant based on a threshold of $p<0.05$. For functional *in vitro* assays (MΦ polarization and HUVEC tube formation) where PC analysis was performed on the assay readouts, the PC1 score was taken as a 'composite functional score', based on previously published methods (14). For linear regression, analysis between functional PC1 scores and MSC(AT) characteristics (genes, soluble factors, and morphometric features), statistically significant ($p<0.05$) correlations are reported along with correlations with $0.05<p<0.1$ which were considered as near-significant. Normal residuals were checked to fulfill assumptions of linear regression, and parametric correlations were performed independently for each individual MSC(AT) characteristic that was measured.

Desirability profiling (47) was used as a tool for multiple response optimization that assigns individual responses a score from zero to one based on the range of data values, with zero representing an undesirable response, and one representing a highly desirable response. Minimization or maximization functions were assigned to each MSC(AT) characteristic (including genes, soluble factors, and morphological features) to indicate whether higher or lower values were desirable, based on outcomes from linear regression analyses with functional PC1 scores. Based on the regression analyses, all statistically significant ($p<0.05$) and near-significant ($p<0.1$) MSC(AT) characteristics were included in the desirability analysis. The R^2 values from the regression analyses were applied as weightings for each MSC(AT) characteristic.

Results

An *in vitro* assay matrix of readouts to identify putative CQAs

A matrix of *in vitro* readouts was used to investigate the responses of putative CQAs to varying donors and CPPs that were specifically selected for their known ability to enhance MSC immunomodulatory and angiogenic properties. The matrix consisted of multivariate morphometric measurements, gene expression, soluble factor analysis, and functional immunomodulatory and angiogenic readouts (Figure 1). The matrix of readouts demonstrated sensitivity to multiple sources of MSC(AT) variability, including variations in select CPPs, donor heterogeneity, and licensing with pro-inflammatory cytokines. Linear regression analyses were used to refine putative CQAs by evaluating correlations with anchor functional *in vitro* immunomodulatory and angiogenic outcomes. We further provided a range of values for assessing

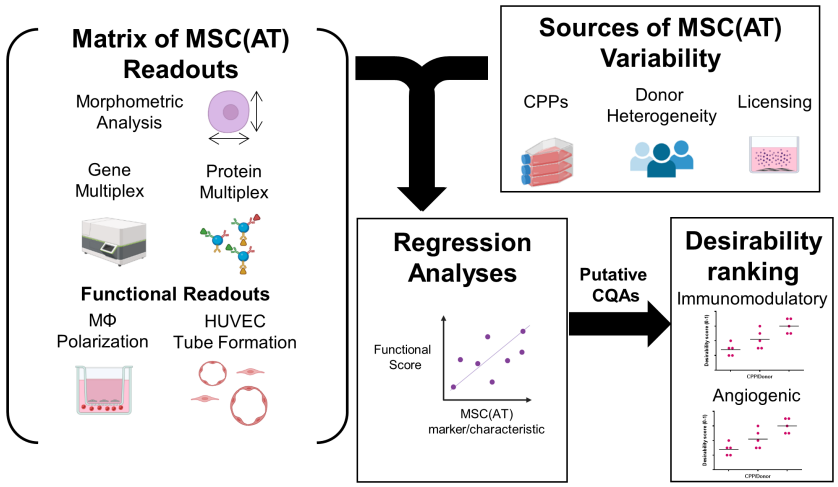

FIGURE 1
Schematic of experimental and statistical analyses to identify a putative matrix of critical quality attributes sensitive to changes in specific critical processing parameters that enhance MSC(AT) potency. The overarching aim of this study was to evaluate the response of putative critical quality attributes (CQAs) to variations in culture conditions, critical processing parameters (CPPs) selected for their known ability to enhance potency, and donor heterogeneity of MSC(AT). To do this, a matrix of assays consisting of morphometric analysis (of single cell suspensions), gene multiplex (58-gene panel), soluble factor analysis (10-analyte panel), *in vitro* monocyte/macrophage (MΦ) polarization (functional immunomodulatory assay), and *in vitro* human umbilical vein endothelial cell (HUVEC) tube formation assays (functional angiogenic assay) was applied. The matrix of MSC(AT) assays was sensitive to variations in CPPs (including 3D normoxic, 2D hypoxic, and 2D normoxic conditions), donor heterogeneity (N=5 human MSC(AT) donors), and to licensing with pro-inflammatory cytokines. Changes in the matrix of gene and protein expression profiles of MSC(AT), and morphological features correlated with functional immunomodulatory and angiogenic readouts by regression analyses to refine a panel of putative MSC(AT) CQAs. Desirability profiling of these putative CQAs allowed ranking of the effects of CPPs or donor heterogeneity on desired immunomodulatory or angiogenic properties.

basal MSC(AT) fitness range according to the significant and near-significant putative CQAs identified from the regression analyses. Desirability analysis was then applied to analyze the profile of putative CQAs and to assign empirical rankings for donors and CPP conditions that result in desirable MSC(AT) immunomodulatory and/or angiogenic functionality.

The CPPs investigated included 2D-N, 2D-H, and 3D-N culture conditions. These CPPs were chosen based on previous literature demonstrating that 3D and 2D hypoxic culture can enhance the immunomodulatory and angiogenic potency of MSCs (28, 29, 31, 32, 35). MSC(AT) cultured under 2D-N, 2D-H and 3D-N conditions satisfied surface marker expression criteria (42) and were $CD90^+CD73^+CD44^+CD13^+CD34^-CD31^-CD45^-$ (Figure S1A). Notably, CD105 appeared to be cleaved under enzymatic conditions required for dissociating 3D cell aggregates for flow cytometry analysis (Figure S1B). Western blot analysis verified CD105 expression by MSC(AT) cultured using 3D-N conditions, albeit at lower levels relative to 2D-N and 2D-H conditions (Figure S1C). MSC(AT) cultured under 2D-N and 2D-H conditions displayed a characteristic spindle-like morphology, while MSC(AT) cultured under 3D-N conditions formed cell aggregates of varying sizes (Figure S2A). Cell aggregates in the 3D-N condition had a median ferret diameter of 37.82 µm (range: 12.38 – 269.40 µm) and median circularity of 0.56 (range: 0.044 – 0.97). Morphometric measurements of MSC(AT) revealed differences in cell morphology with changes in CPP conditions. Analysis of single cell suspensions obtained from each culture condition demonstrated significantly reduced diameter and greater circularity of 3D-N MSC(AT) relative to 2D-N and 2D-H MSC(AT) (Figure S2B, C).

For gene expression and soluble factor analysis, 2D-N, 2D-H, and 3D-N MSC(AT) were subject to pro-inflammatory licensing conditions (with a cocktail of three pro-inflammatory cytokines, TNFα, IFNγ, and IL-1β to simulate a wide range of disease conditions) or cultured under unlicensed conditions in the absence of pro-inflammatory stimuli. The combination of 3D and hypoxic culture (3D-H) was investigated by gene expression analysis using an abbreviated panel of anti-inflammatory/angiogenic markers measured in two MSC(AT) donors (Figure S3) and demonstrated no significant benefit of combining these culture conditions. Thus, 3D-N was used as the select CPP in all subsequent experiments. The effects of IL-6 (used to support cell viability under the 3D-N culture condition) were also evaluated on MSC(AT) cultured under 2D-N culture conditions using the same cytokine concentration as used for the 3D-N culture method. An abbreviated panel of genes was selected using markers that were significantly differentially expressed in the 3D-N culture condition relative to 2D-N culture. Gene expression analysis revealed no significant effect

of IL-6 on 2D-N culture (Figure S4), suggesting that the 3D geometry was the major factor that primed the cells rather than IL-6.

Curated gene expression and soluble factor profiles are differentially sensitive to donor heterogeneity and select CPPs that enhance MSC potency

Gene expression analysis was performed using a curated panel of markers including predominantly immunomodulatory and angiogenic genes (data provided in Suppl. Tables 2, 3, 4, and 5). The panel was selected based on previous literature (11, 17, 48, 49) and our experience using MSC(M) in an osteoarthritis clinical trial (8). It was used to evaluate MSC(AT) fitness across multiple donors and while modulating select CPP conditions associated with enhanced immunomodulatory and angiogenic functionality. Unbiased hierarchical clustering analysis revealed that MSC(AT) gene expression profiles clustered according to both variations in CPP conditions and donor heterogeneity (Figures 2A, B). Under licensed conditions, CPP variations, specifically 3D-N configurations of culturing MSC(AT) clustered separately from 2D-N and 2D-H cultures for all but one donor (Donor 1) which clustered together regardless of CPP variations. For MSC(AT) cultured under 2D-N and 2D-H conditions, the gene expression profiles clustered together by donor rather than oxygen tension under licensed conditions. Interestingly, under unlicensed conditions, gene expression profiles clustered primarily by donor, regardless of variations in CPPs. Overall, variations in CPP conditions by changing culture geometry or oxygen tension and donor heterogeneity resulted in shifts in gene expression profiles dependent on pro-inflammatory licensing conditions or unlicensed conditions. For example, genes such as *HGF* (multifunctional growth factor) and *TNFAIP6* (anti-inflammatory gene encoding TSG6), were upregulated by 3D-N culture conditions relative to 2D-N culture conditions, under licensed conditions (Figure 2C). *NOS2* (encoding for inducible nitric oxide synthase, iNOS which may indicate cell stress or enhanced immunosuppressive functions for mouse, but not human MSCs (50)) and *PRG4* (lubricating proteoglycan with potential immunomodulatory functions (51, 52)) were also upregulated under these conditions. *ICAM1* (immunomodulatory marker), *PRG4*, and *TNFAIP6* were upregulated by 3D-N culture conditions relative to 2D-N under unlicensed conditions (Figure 2D). Furthermore, 2D-H culture conditions induced augmented expression of the immunomodulatory marker *PTGS2* relative to 2D-N culture conditions under unlicensed settings.

Levels of soluble factors in conditioned medium were queried using a curated sub-panel of immunomodulatory and angiogenic factors, based on significant results from the gene expression analysis (soluble factor data provided in Suppl. Tables 6, 7). Unbiased hierarchical clustering demonstrated that soluble factor profiles clustered based on both donor heterogeneity and variations in CPP conditions under licensed and unlicensed conditions (Figures 3A, B). Analysis of individual soluble factors was performed to evaluate the effects of CPP and donor heterogeneity on each soluble factor. Under licensed conditions, MSC(AT) cultured in 3D-N configurations expressed significantly higher levels of the multifunctional cytokine TGF-β relative to 2D-N, and significantly lower levels of the immunomodulatory factor soluble PD-L2 relative to 2D-H (Figure 3C). Furthermore, MSC(AT) cultured in 3D-N configurations expressed significantly higher levels of the growth factor HGF and the immunosuppressive factor IL-1RA relative to both 2D-N and 2D-H MSC(AT) under licensed conditions. Under unlicensed conditions, 2D-H and 3D-N MSC(AT) expressed significantly higher levels of TGF-β relative to 2D-N, while soluble PD-L2 was significantly upregulated by 2D-H relative to 3D-N MSC(AT) (Figure 3D). Expression of the angiogenic markers angiopoietin-1 (Ang-1) and VEGF showed statistically significant differences between donors, with Donor 3 expressing the highest levels of both factors under both licensed and unlicensed conditions (Figures 3C, D). Taken together, the curated panel of genes and soluble factors were differentially sensitive to donor heterogeneity and CPPs under licensed and unlicensed conditions. Interestingly, donor heterogeneity was masked under licensed conditions, and dominated under unlicensed conditions. Further, culturing MSC(AT) under 3D-N conditions rendered them with an elevated profile of anti-inflammatory/immunosuppressive genes (*HGF*, *TNFAIP6*, *PTGES*, *PTGS2*, *TLR2*, *NFKBIA*, *TGFB1*, *PRG4*, *IDO*, *ICAM1*, *TLR4*) and soluble factors (TGF-β, HGF, IL-1RA), corroborating previous reports that have investigated MSC culture in 3D formats (31, 32, 53).

MSC(AT)-mediated *in vitro* functional polarization of MΦ readouts are dependent on donor heterogeneity and CPPs

To further probe immunomodulatory properties of MSC (AT), an indirect co-culture assay was performed to evaluate functional MΦ polarization (Figure 4A). Alterations to CPP conditions by changing MSC(AT) culture configuration (3D-N) or oxygen tension (2D-H) significantly reduced levels of pro-inflammatory TNFα in conditioned medium relative to MΦs alone (Figure 4B), suggesting that these culture conditions enhanced anti-inflammatory functions of MSC(AT). Gene expression analysis of MΦs revealed statistically significant increased expression of inflammation-resolving MΦ markers (*CD206*, *HMOX1*, and *IL10*) in co-cultures with MSC(AT) in

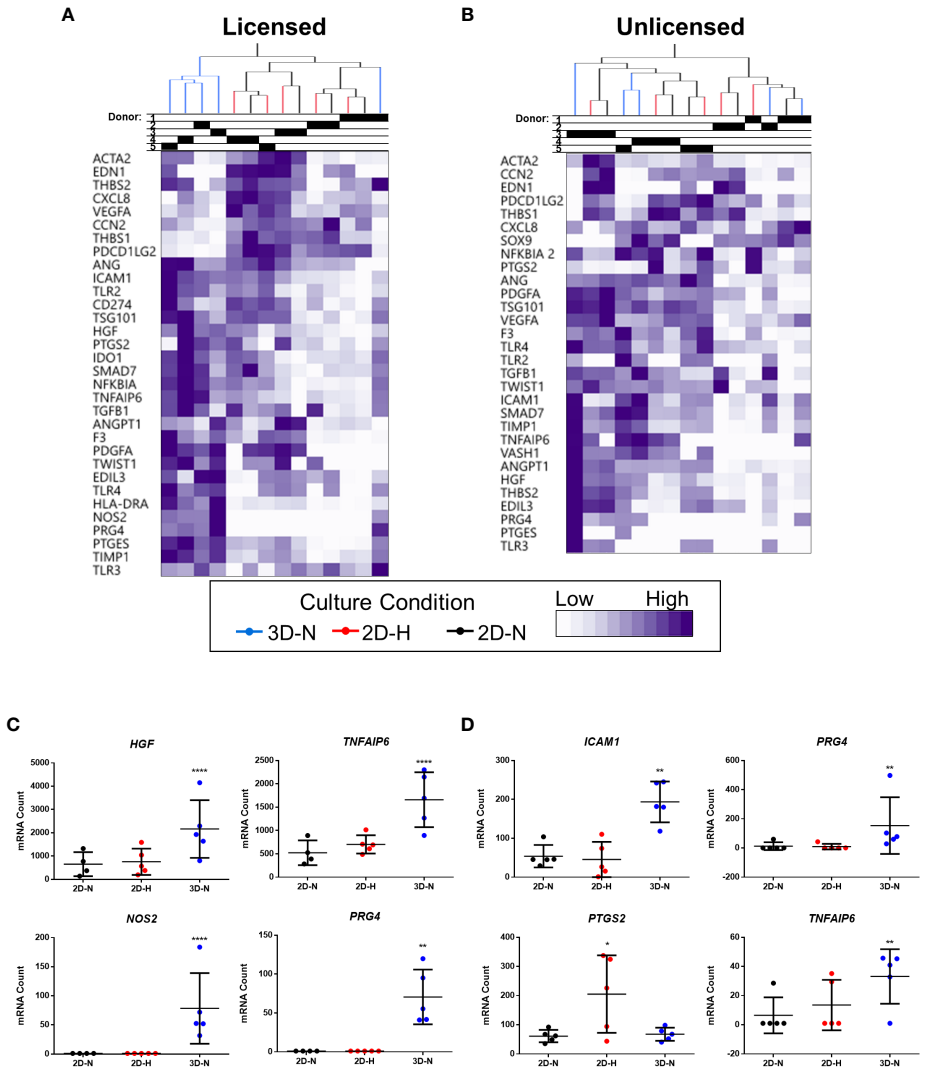

FIGURE 2
Curated gene expression panel was differentially sensitive to donor heterogeneity and select CPPs that enhance immunomodulatory and/or angiogenic potencies. A and B) Unbiased hierarchical clustering of normalized mRNA counts demonstrated clustering by CPPs (colour-coded dendrogram) and by donor (shaded regions in Donor chart indicate different donors) under both Licensed **(A)** and Unlicensed **(B)** conditions. C and D) Select genes were differentially expressed by modifying CPPs under Licensed **(C)** and Unlicensed **(D)** conditions. Multivariate linear regression, Benjamini-Yekutieli False Discovery Rate-corrected p values. *p<0.05, **p<0.01, ****p<0.0001 vs 2D-N. Horizontal bars: group mean, error bars: standard deviation. 3D-N, 3D Normoxic culture; 2D-N, 2D Normoxic culture; 2D-H, 2D Hypoxic culture. N=5 MSC(AT) donors, n=1 technical replicate due to high sensitivity of Nanostring measurements.

3D-N and 2D-H culture conditions relative to MΦ alone (Figure S5A). In addition, MSC(AT) cultured in 3D-N conditions significantly upregulated MΦ expression of *CD86* (pro-inflammatory) and *CD163* (inflammation-resolving), while 2D-N culture conditions significantly upregulated expression of *HMOX1* only. PC analysis was applied as an unbiased dimension reduction tool to evaluate the full gene expression panel and TNFα protein levels (Figure 4C, loading plots for PC1 and PC2 displayed in Figures S5B, C). Increased expression of *CD86*, *CD206*, *HMOX1*, and *STAB1* genes, and reduced expression of TNFα protein were the main contributors to higher scores along the PC1 axis (accounting for 35.7% of variation). Reduced expression of *CD274* and *HLADRA*, and increased expression of *CD163*, *IL12A*, and *TREM1* genes drove higher scores along the PC2 axis (accounting for 22.2% of variation).

To further probe the results of the PC analysis, we plotted individual PC1 and PC2 scores for each CPP and donor combination as these scores capture multivariate heterogeneity in a reduced, single dimension with PC1 capturing a larger

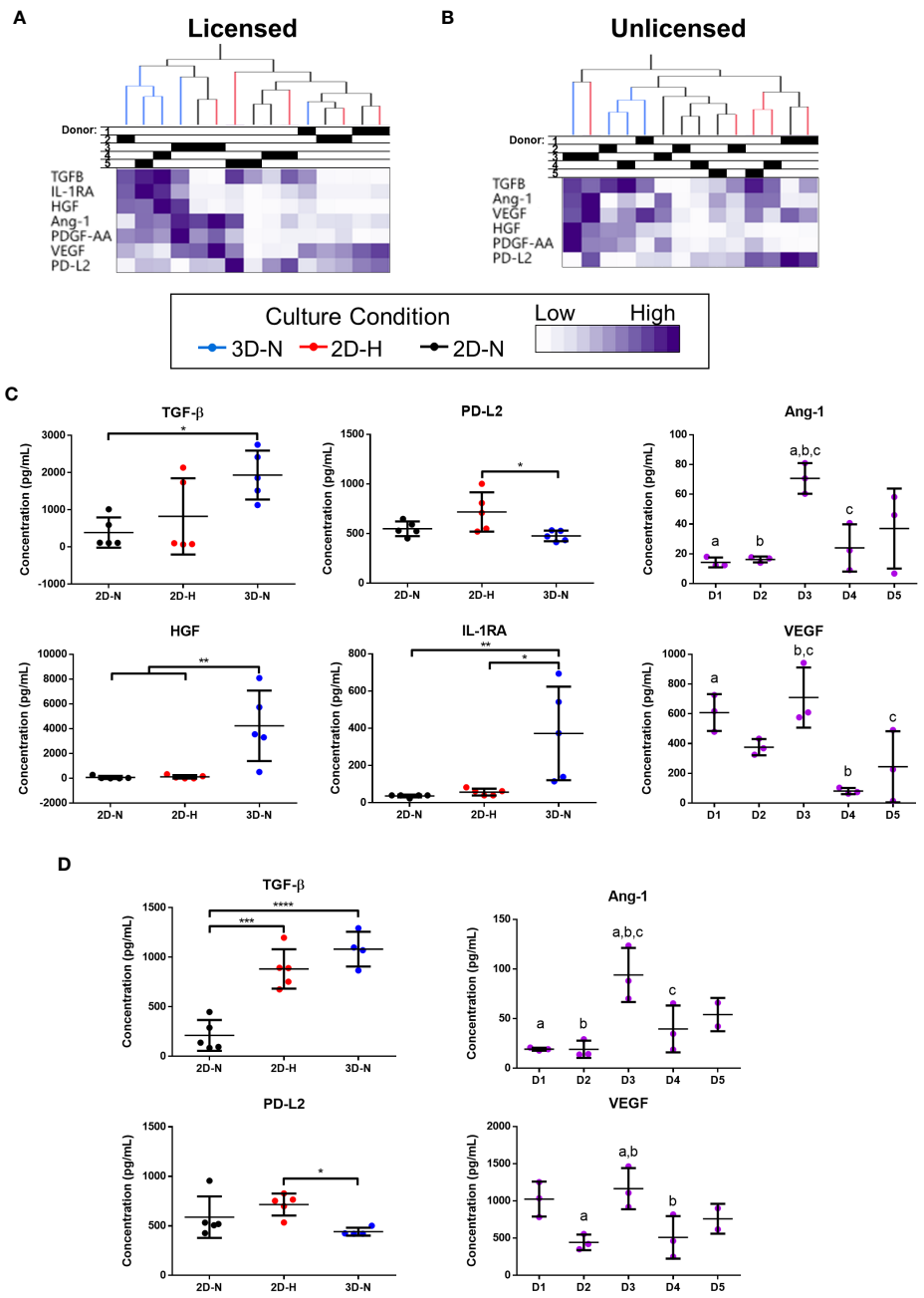

FIGURE 3
Curated anti-inflammatory and angiogenic soluble factors were differentially sensitive to donor heterogeneity and select CPPs that enhance immunomodulatory and/or angiogenic potencies. **(A, B)** Unbiased hierarchical clustering of soluble factors demonstrated clustering by CPPs and donor under Licensed **(A)** and Unlicensed **(B)** conditions. **(C, D)** Soluble factors with statistically significant differences between CPPs (left) or donors (right) are displayed for Licensed **(C)** and Unlicensed **(D)** conditions. One-way ANOVA, Tukey's *post-hoc* test. *p<0.05, **p<0.01, ***p<0.001, ****p<0.0001. Donors sharing same letter are significantly different (p<0.05). Horizontal bars: group mean, error bars: standard deviation. Data points represent mean of technical replicates for each donor and condition. 3D-N, 3D Normoxic culture; 2D-N, 2D Normoxic culture; 2D-H, 2D Hypoxic culture. N=5 MSC(AT) donors, n=2 technical replicates.

proportion of the total existing variation in the dataset relative to PC2. Analysis of individual PC1 scores demonstrated that separation along the PC1 axis was driven by co-culture with MSC(AT) as indicated by statistically significant differences in PC1 scores for MSC(AT) cultured under 2D-N, 2D-H, and 3D-N conditions relative to solo MΦ (positive control) without MSC (AT) (Figure 4D). Given that the PC1 axis accounted for differences in MΦ phenotypic marker profiles relative to

10.3389/fimmu.2022.972095

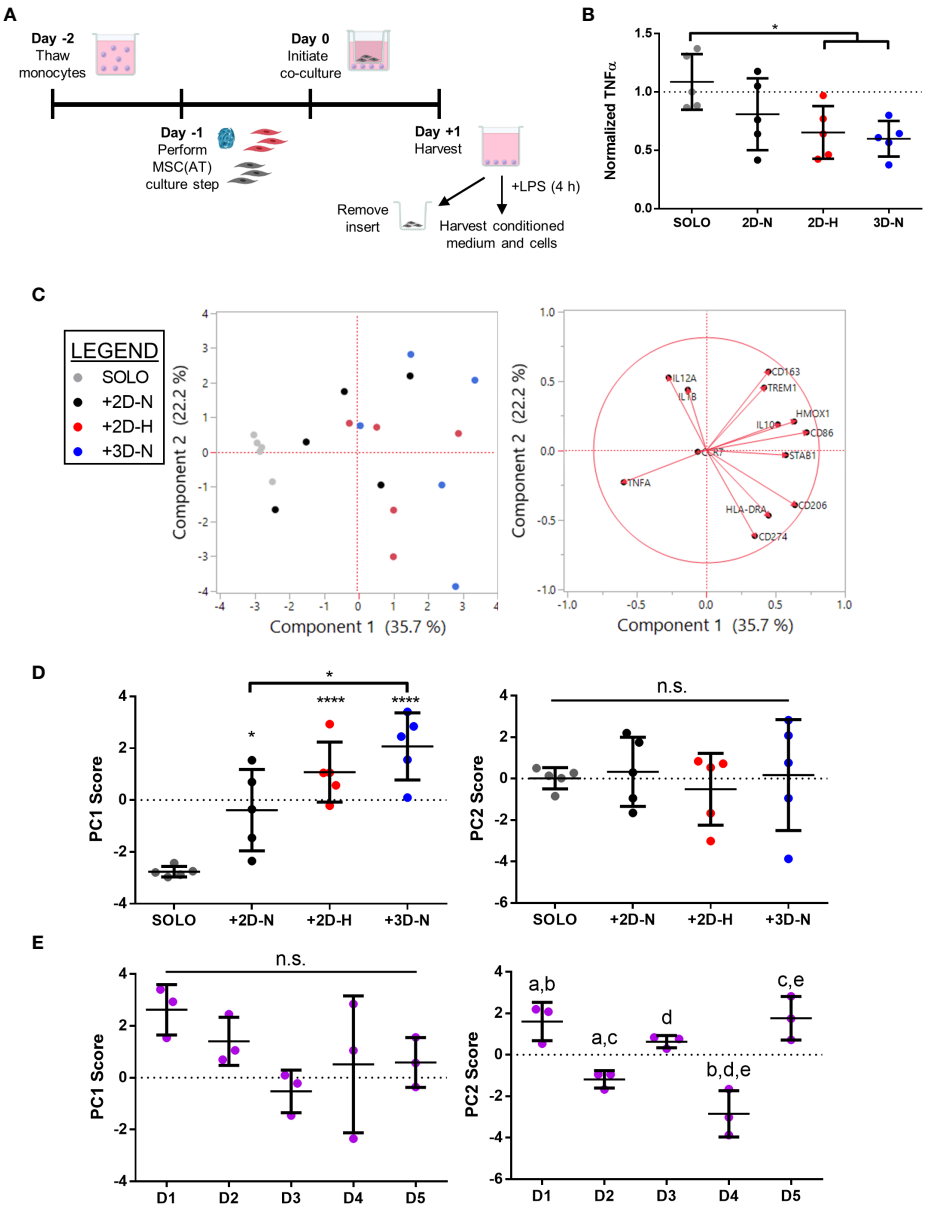

FIGURE 4
In vitro MSC(AT)-mediated functional polarization of MΦ was differentially sensitive to donor heterogeneity and select CPPs. **(A)** Schematic of indirect co-culture experiment. MSC(AT) (2D-N, 2D-H, or 3D-N culture conditions) were co-cultured with human peripheral blood-derived monocytes/macrophages (MΦ) for 24 h prior to removal of MSC(AT) and addition of lipopolysaccharide (LPS). **(B)** TNFα secretion, a surrogate marker for pro-inflammatory MΦs, showed significant reduction when co-cultured with 3D-N or 2D-H MSC(AT) compared to solo MΦs. One-way ANOVA, Tukey *post-hoc* test. *p<0.05. **(C)** Principal component (PC) analysis of median delta-delta Ct values of MΦ genes, indicative of pro-inflammatory (*CCR7*, *CD86*, *HLADRA*, *IL12A*, *IL1B*, *TREM1*) or pro-resolving (*CD163*, *CD206*, *HMOX1*, *IL10*, *CD274*, *STAB1*) status, and normalized TNFα levels from each donor and culture condition (left). The corresponding loading plot of eigenvectors for each marker (right) indicates the relative contribution of each factor to the PCs. **(D)** Principal component scores for PC1 and PC2 according to culture condition. PC1 scores were highest in the 3D-N co-culture condition. One-way ANOVA, Tukey *post-hoc* test. *p<0.05, ****p<0.0001 relative to MΦ SOLO condition or to groups indicated by brackets. **(E)** Principal component scores for PC1 and PC2 according to MSC(AT) donor heterogeneity. Statistically significant differences between groups were observed in PC2 scores and are indicated by groups sharing the same letter. One-way ANOVA, Tukey *post-hoc* test, p<0.01. N=5 MSC(AT) donors, n=3 technical replicates/condition. Horizontal bars: group mean, error bars: standard deviation. 3D-N, 3D Normoxic culture; 2D-N, 2D Normoxic culture; 2D-H, 2D Hypoxic culture; n.s., statistically non-significant.

positive control, PC1 scores were considered as a 'composite functional score' (14) for MSC(AT) immunomodulatory function. With the exception of *CD86* gene expression, higher scores along the PC1 axis were generally associated with greater inflammation-resolving MΦ polarization as evidenced by increased expression of *CD206*, *HMOX1*, and *STAB1*, along with reduced expression of TNFα protein. Using PC1 scores as an analytic, variations in CPP conditions resulted in differences in MSC(AT)-mediated MΦ polarization toward inflammation-resolving subtypes. Notably, MSC(AT) cultured in 3D-N configurations displayed the highest PC1 scores, and these were significantly different from 2D-N MSC(AT), suggesting that 3D-N MSC(AT) displayed a superior capacity to polarize MΦ phenotype toward inflammation-resolving subtypes. No significant differences in culture conditions were observed along the PC2 axis. Analysis of PC1 scores across individual donors showed no significant differences (Figure 4E); while not significant, Donor 1 displayed the highest PC1 scores suggesting that Donor 1 may have intrinsic improved immunomodulatory basal functionality, and Donor 3 displayed the lowest scores. In contrast, a significant effect of donor heterogeneity was observed along the PC2 axis. Given that PC2 scores represent changes in both pro-inflammatory and inflammation-resolving MΦ markers, these data suggest that donor heterogeneity dictates MSC(AT)-mediated polarization of MΦ toward mixed phenotypes.

In vitro MSC(AT)-mediated functional angiogenesis readouts are dependent on donor heterogeneity and CPPs

To evaluate the angiogenic functions of MSC(AT), the effects of MSC(AT) conditioned medium on HUVEC tube formation was explored (Figure 5A, Figure S6A). Recognizing that there is no standard quantitation method for HUVEC tube formation and that different measurements can yield different insights into *in vitro* angiogenesis (54), we employed the ImageJ Angiogenesis Analyzer plugin which provides twenty different types of measurements (45). PC analysis was applied to analyze all twenty parameters that profile tube formation image analyses (Figure 5B, loading plots for PC1 and PC2 displayed in Figure S6B, C). An increased number of nodes, number of junctions, and the total master segment length were the main contributors to higher scores along the PC1 axis (accounting for 69.2% of variation), indicative of greater angiogenesis. Increased total branches length and number of branches, along with reduced total mesh area drove higher scores along the PC2 axis (accounting for 14.3% of variation). Analysis of individual PC1 scores demonstrated that the positive control group (HUVECs cultured in pro-angiogenic medium) displayed significantly higher PC1 scores relative to the negative control (HUVECs cultured in basal medium), and to HUVECs cultured in conditioned medium derived from 2D-N or 3D-N MSC(AT) culture conditions (Figure 5C). As above, the PC1 scores were considered as a 'composite functional score' for MSC(AT) angiogenic functions given that higher scores along this axis reflected greater HUVEC tube formation. Surprisingly, conditioned medium derived from MSC(AT) cultured under 2D-H or 3D-N conditions did not elicit significant increases in HUVEC PC1 scores, and there were no significant differences between PC1 scores across MSC(AT) by varying CPP conditions. PC1 scores were instead driven by MSC(AT) donor differences (Figure 5D). Donors 1, 2, 3, and 5 all displayed statistically significant higher scores relative to Donor 4 indicative of greater angiogenic function. Analysis of PC2 scores similarly showed no significant effect of the conditioned medium from the different groups representing variability in culture conditions, or the controls on HUVEC tube formation profiles (Figure 5C). Some variation along the PC2 axis was driven by donor with Donors 1 and 3 displaying significantly higher PC2 scores relative to Donor 4 (Figure 5D).

To further analyze effects mediated by variations in donor and experimental batches, PC analysis was performed on *all* biological and technical replicates (Figure S7A) and PC1 scores were investigated for each donor (Figures S7B, C). Under this analysis, conditioned medium derived from MSC(AT) cultured under 2D-H conditions had the highest mean HUVEC PC1 scores for four out of five donors (Donor 2, 3, 4, and 5) compared to scores for the 2D-N and 3D-N conditions. Taken together, the data suggests that donor heterogeneity dominated over effects mediated by variations in CPPs in our analysis of angiogenic readouts. The net effect of CPPs on HUVEC tube formation was variable, donor-dependent, and in part driven by CPP conditions that favour angiogenesis.

Generating a matrix of putative MSC(AT) CQAs based on correlation of select genes, soluble factors, and morphological features with functional immunomodulation

The full set of gene and soluble factor expression profiles as well as morphological features measured for MSC(AT) were examined for correlations to composite functional (PC1) scores (indicative of inflammation-resolving MΦ polarization) generated for MSC(AT) immunomodulatory fitness. Under licensed conditions, MSC(AT) expression of *THBS1* (R^2 = 0.5481, p=0.0025, angiogenic gene), *CCN2* (R^2 = 0.3020, p=0.0418, encoding for the multifunctional growth factor), and *EDN1* (R^2 = 0.2854, p=0.0491, angiogenic gene) genes demonstrated significant ***inverse*** correlations with MΦ PC1 composite scores (Figure 6A, Table 2), suggesting that lower expression of these genes correlated with improved immunomodulatory MSC(AT) functionality. Correlations of

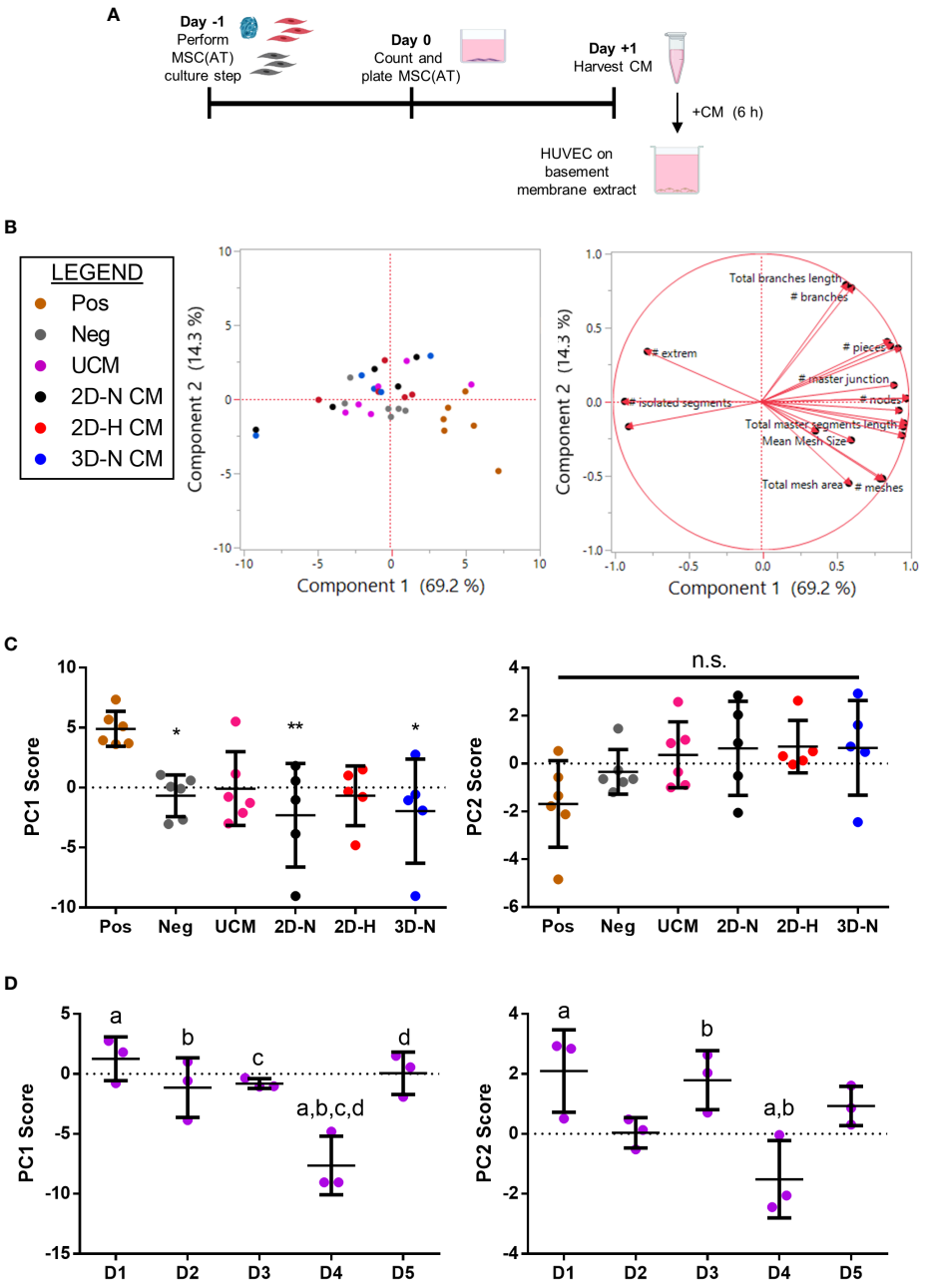

FIGURE 5
In vitro MSC(AT) mediated functional angiogenic HUVEC tube formation assay was differentially sensitive to donor heterogeneity and CPPs. **(A)** Schematic of experimental set-up for the tube formation assay. Conditioned medium (CM) was collected from MSC(AT) (2D-N, 2D-H, or 3D-N) after 24 h of incubation and added to HUVECs cultured on basement membrane extract for 6 h. **(B)** Principal component (PC) analysis of fold-change values (relative to negative control) of twenty HUVEC tube formation image analysis readouts (left). The corresponding loading plot of eigenvectors (right) indicates the relative contribution of each factor to the PCs. **(C)** Principal component scores for PC1 and PC2 according to culture condition. The positive control group (Pos; HUVECs cultured in pro-angiogenic medium) displayed significantly higher PC1 scores relative to the negative control (Neg; HUVECs cultured in basal medium), and to HUVECs cultured with conditioned medium derived from 2D-N or 3D-N MSC(AT) culture conditions. One-way ANOVA, Tukey *post-hoc* test. *p<0.05, **p<0.01 relative to positive control. **(D)** Principal component scores for PC1 and PC2 according to MSC(AT) donor heterogeneity. Statistically significant differences between donors were observed for PC1 and PC2 scores and are indicated by donors sharing the same letter. One-way ANOVA, Tukey *post-hoc* test, p<0.05. N=5 MSC(AT) donors, n=2-3 technical replicates/condition. Horizontal bars: group mean, error bars: standard deviation. HUVEC, human umbilical vein endothelial cell; Pos, positive control; Neg, negative control; UCM, unconditioned medium; 3D-N, 3D Normoxic culture; 2D-N, 2D Normoxic culture; 2D-H, 2D Hypoxic culture; CM, conditioned medium; n.s., statistically non-significant.

MΦ PC1 composite scores with *ACTA2*, *PDCD1LG2*, *TNFAIP6*, *ANGPT1*, and *CXCL8* were near-significant. Under unlicensed conditions, MSC(AT) expression of six genes (*CCN2*, *TSG101*, *THBS1*, *PDGFA*, *VEGFA*, and *EDIL3*) were significantly inversely correlated with MΦ PC1 composite scores, with *CCN2* (R^2 = 0.4934, p=0.0035), *TSG101* (R^2 = 0.4229, p=0.0087, negative growth regulator and regulator of vesicular trafficking), *THBS1* (R^2 = 0.3853, p=0.0135), and *PDGFA* (R^2 = 0.3754, p=0.0152) displaying the strongest correlations (Figure 6B, Table 2). Correlations of MΦ PC1 composite scores with *ACTA2*, TGF-β protein, *ANGPT1*, and *ANG* were near-significant. Interestingly, many of the statistically significant and near-significant correlations were inverse correlations and they predominantly consisted of angiogenic-associated genes (*THBS1, CCN2, EDN1, PDGFA*, *VEGFA*, *EDIL3*, *ANGPT1*, and *ANG*).

Analysis of morphological features of MSC(AT) single cell suspensions derived under varying CPP conditions and/or donors revealed that cell diameter was significantly inversely correlated with inflammation-resolving MΦ PC1 composite scores (Figure 6C, Table 2), suggesting that smaller cells exhibit greater immunomodulatory properties, concordant with observations by Klinker *et al.* (15). Correlation of MΦ PC1 composite scores with cell circularity was near-significant (Table 2). Taken together, the significant and near-significant correlations between MSC(AT) gene expression and morphometric features with MΦ pro-resolving polarization constituted a matrix of multivariate readouts that were considered as putative CQAs for informing MSC(AT) immunomodulatory fitness.

Generating a matrix of putative MSC(AT) CQAs based on correlation of select genes, soluble factors, and morphological features with functional angiogenesis

Linear regression analyses were also performed to investigate correlations of MSC(AT) markers with functional angiogenic HUVEC PC1 composite scores. A statistically significant ***positive*** correlation was found between HUVEC PC1 composite scores and levels of the pro-angiogenic factor VEGF in MSC(AT) conditioned medium measured under licensed conditions (R^2 = 0.3048, p=0.0328) (Figure 6D), while VEGF levels measured under unlicensed conditions showed a positive near-significant correlation (R^2 = 0.2416, p=0.0743) (Table 3). No significant or near-significant correlations to HUVEC PC1 scores were observed for the other measured soluble factors. Regression analyses of HUVEC PC1 scores with MSC(AT) genes revealed significant ***inverse*** correlations for *SMAD7* (R^2 = 0.4237, p=0.0117, inhibitor of TGF-β signaling), *HGF* (R^2 = 0.3807, p=0.0187), and *ANG* (R^2 = 0.3404, p=0.0285, pro-angiogenic marker) measured under licensed conditions (Figure 6E). Correlations of HUVEC PC1 composite scores with expression of *IDO1*, *TSG101*, and *CXCL8* were near-significant (Table 3). Under unlicensed conditions, expression of the chondrogenic marker *SOX9* (R^2 = 0. 2906, p=0.0381) was significantly ***inversely*** correlated with HUVEC PC1 scores (Table 3). Inverse correlations of HUVEC PC1 composite scores with expression of *TNFAIP6* were near-significant. No significant or near-significant correlations were observed between MSC(AT) cell diameter and circularity measurements with HUVEC PC1 composite scores. As above, the significant and near-significant correlations between expression levels of VEGF protein and the identified genes with HUVEC tube formation were considered as a matrix of multivariate readouts that served as putative CQAs for informing MSC (AT) angiogenic fitness.

Statistical rankings of the matrix of putative CQAs ranks different CPPs and donors for optimal MSC(AT) immunomodulation and angiogenic fitness

Desirability profiling was applied as an analytical tool using the matrix of putative CQAs to empirically rank CPP conditions and MSC(AT) donors that favour immunomodulation or angiogenic fitness. Putative CQAs were selected using a broader p value threshold of p<0.1 (near-significance) based on the regression analyses presented above. This p value threshold was selected to filter the large initial panels of genes and soluble factors (curated based on literature) through a pipeline with a still flexible threshold that allowed selection of a relatively broad array of putative CQAs for MSC(AT) immunomodulatory or angiogenic basal fitness. The genes and soluble factors (measured under either licensed or unlicensed conditions), as well as morphological features were assigned minimization or maximization functions in the desirability analysis based on whether the correlation to functional outcomes was positive or negative (Tables 2 and 3). For example, markers with negative correlations to inflammation-resolving MΦ or pro-angiogenic HUVEC PC1 composite scores (*i.e.*, lower expression of the marker correlated to greater immunomodulatory/angiogenic function) were assigned minimization functions so that lower expression of the marker corresponded to a higher immunomodulatory or angiogenic desirability score. Furthermore, the R^2 values were used as indicators of the amount of variation in the data explained by the model for each gene/soluble factor/morphological feature in correlation with either immunomodulatory or angiogenic functional outcomes. Thus, these values were applied as individual weightings for each gene, soluble factor, or morphological feature. For example, expression of *THBS1* by

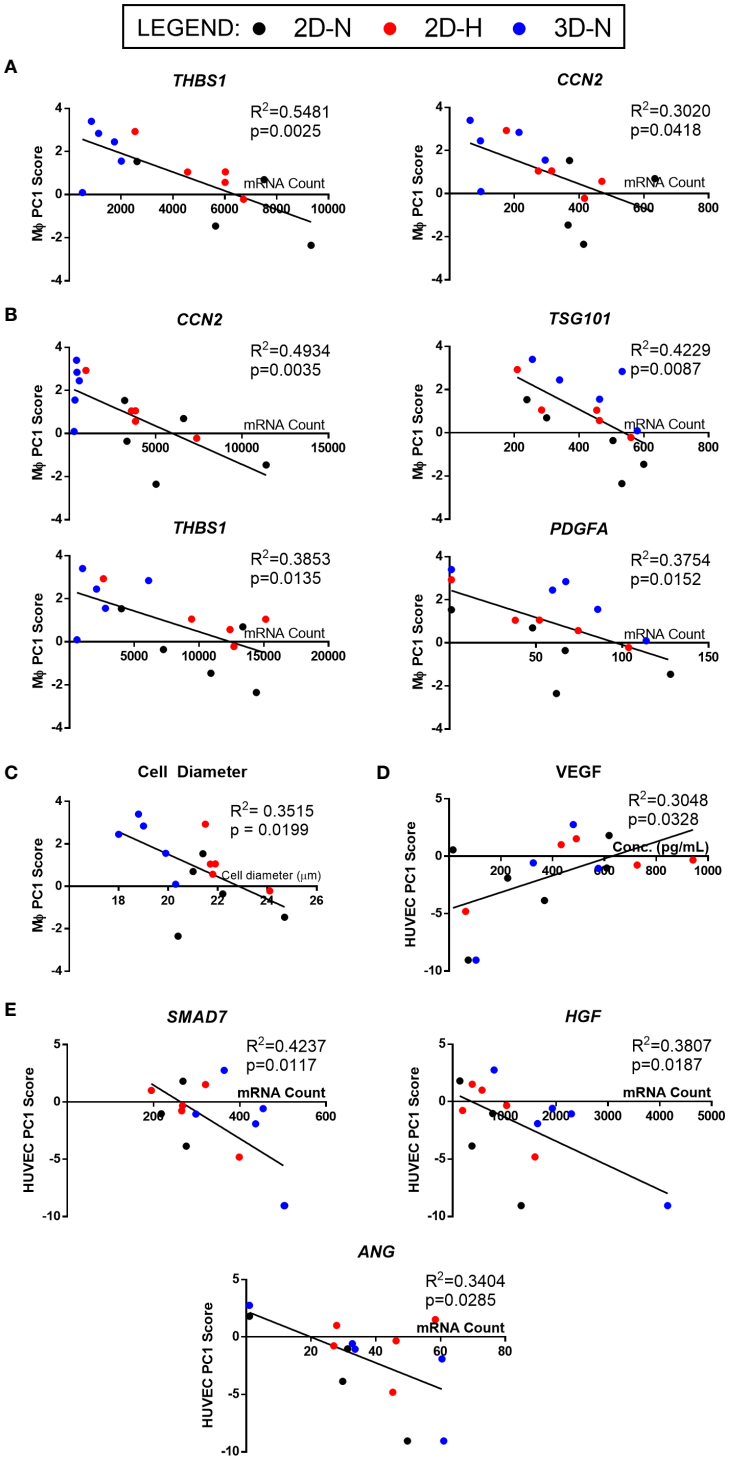

FIGURE 6
Linear regression analysis revealed genes, soluble factors, and morphological features that correlate with anchor functional assays to identify a putative matrix of CQAs for MSC(AT). **(A, B)** Inverse correlation between PC1 composite scores from MΦ polarization (Figure 4) and curated panels of MSC(AT) genes measured under Licensed **(A)** and Unlicensed **(B)** conditions. **(C)** Single cell diameter of MSC(AT) inversely correlated to MΦ polarization PC1 composite scores. **(D)** Positive correlation between HUVEC tube formation PC1 composite scores (Figure 5) and levels of VEGF protein in MSC(AT) conditioned medium under Licensed conditions. **(E)** Inverse correlation between HUVEC tube formation PC1 scores and curated panels of MSC(AT) genes measured under Licensed conditions. Only correlations with $R^2 \geq 0.3$ are shown. N=14-15. 3D-N, 3D Normoxic culture; 2D-N, 2D Normoxic culture; 2D-H, 2D Hypoxic culture.

licensed MSC(AT) correlated most strongly with inflammation-resolving MΦ PC1 composite scores (R^2 = 0.5481); the R^2 value was used as a relative weighting such that *THBS1* expression levels contributed more strongly to the overall desirability score relative to the other genes, soluble factors, and morphological features included in the analysis. Given that putative CQAs would require limits or ranges in order to be practically used, we provided a range of data outputs for each MSC(AT) readout (gene, soluble factor, and morphological feature) that correlated with immunomodulatory pro-resolving MΦ polarization or HUVEC tube formation (Tables 2 and 3). These values inform the upper and lower limits of the putative CQA matrix readouts corresponding to MSC(AT) immunomodulation (Table 2) or angiogenic fitness (Table 3).

Using the panels of MSC(AT) genes, soluble factors, and morphological features that correlated with inflammation-resolving MΦ PC1 scores (Licensed panel: *ACTA2*, *ANGPT1*, *CCN2*, *CXCL8*, *EDN1*, *PDCD1LG2*, *THBS1*, *TNFAIP6*; Unlicensed panel: *ACTA2*, *ANG*, *ANGPT1*, *CCN2*, *EDIL3*, *PDGFA*, TGF-β, *THBS1*, *TSG101*, *VEGFA*; Morphological features: cell diameter, cell circularity), desirability analysis revealed that MSC(AT) cultured under 3D-N configurations had significantly higher overall immunomodulatory desirability scores relative to 2D-H and 2D-N configurations (Figure 7A), further corroborating that 3D-N MSC(AT) displayed augmented immunomodulatory properties. No significant differences in overall immunomodulatory desirability scores could be detected between donors.

Similar desirability analyses were performed using the angiogenic markers that correlated with angiogenic HUVEC PC1 scores (Licensed panel: *SMAD7*, *HGF*, *ANG*, *IDO1*, *TSG101*, *CXCL8*, VEGF protein; Unlicensed panel: *SOX9*, *TNFAIP6*, VEGF protein). The analysis revealed that donor differences dominated over the desirability rankings with Donors 1, 2, and 3 displaying significantly higher scores relative to Donor 4 (Figure 7B), further suggesting that the effect of donor predominated over variations in CPP conditions when considering MSC(AT) angiogenic functionality. Donor 5 was excluded from the desirability analysis due to an incomplete dataset. No significant differences were observed for overall angiogenic desirability scores across variations in CPP conditions.

Altogether, using the matrix of putative CQAs that included MSC(AT) genes and soluble factors, morphological features, and immunomodulatory/angiogenic functional readouts, desirability analysis allowed us to empirically rank MSC(AT) immunomodulatory and angiogenic fitness across varying CPP conditions that enhance immunomodulation and angiogenic potency, and across MSC(AT) donors. The results showed that MSC(AT) cultured under 3D-N conditions displayed the highest

TABLE 2 Putative CQAs for MSC(AT) immunomodulatory fitness.

Marker/Characteristic	Licensed/Unlicensed	Gene/protein	Min/Max Function	Min value	Max value	p value	R^2 value
THBS1	Licensed	Gene	Min	296.30	1680.04	*0.0025	0.5481
CCN2	Unlicensed	Gene	Min	289.15	11393.39	*0.0035	0.4934
TSG101	Unlicensed	Gene	Min	209.22	599.97	*0.0087	0.4229
THBS1	Unlicensed	Gene	Min	575.38	15145.48	*0.0135	0.3853
PDGFA	Unlicensed	Gene	Min	1.00	127.95	*0.0152	0.3754
Cell Diameter	N/A	N/A	Min	18.00	24.70	*0.0199	0.3515
CCN2	Licensed	Gene	Min	63.40	634.06	*0.0418	0.302
VEGFA	Unlicensed	Gene	Min	214.27	894.31	*0.0378	0.2914
EDN1	Licensed	Gene	Min	1.00	65.27	*0.0491	0.2854
EDIL3	Unlicensed	Gene	Min	31.41	887.90	*0.0477	0.2689
ACTA2	Licensed	Gene	Min	54.88	201.10	0.0614	0.2619
PDCD1LG2	Licensed	Gene	Min	47.65	329.96	0.0628	0.2595
TNFAIP6	Licensed	Gene	Max	284.00	2300.07	0.0742	0.2417
ACTA2	Unlicensed	Gene	Min	78.54	3197.28	0.0736	0.2256
TGFβ	Unlicensed	Protein	Max	85.54	1292.81	0.0865	0.2251
ANGPT1	Licensed	Gene	Min	42.27	237.48	0.0868	0.2247
ANGPT1	Unlicensed	Gene	Min	27.79	327.12	0.0749	0.2238
CXCL8	Licensed	Gene	Min	25008.42	51553.32	0.0946	0.2154
ANG	Unlicensed	Gene	Min	25.10	88.99	0.0861	0.2096
Cell Circularity	N/A	N/A	Max	0.47	0.77	0.0981	0.1964

Summary of regression analyses between MΦ PC1 composite scores and MSC(AT) genes, soluble factors, and morphological features. Marker/Characteristic column indicates the gene or protein symbol, or morphological feature. Licensed/Unlicensed column indicates whether the factor was measured under licensed or unlicensed conditions. Min/Max Function column indicates whether minimization or maximation of the MSC(AT) characteristic was desirable based on positive or negative correlations in the linear regression analysis. Min value and Max value columns indicate the range of values measured across each gene (units: mRNA count), soluble factor (units: pg/mL), and morphological feature (units for cell diameter: microns, units for cell circularity: arbitrary). All significant (*p<0.05) and near-significant (p<0.1) correlations are displayed.

TABLE 3 Putative CQAs for MSC(AT) angiogenic fitness.

Marker/Characteristic	Licensed/Unlicensed	Gene/protein	Min/Max Function	Min value	Max value	p value	R^2 value
SMAD7	Licensed	Gene	Min	194.72	504.28	*0.0117	0.4237
HGF	Licensed	Gene	Min	139.8	4151.35	*0.0187	0.3807
ANG	Licensed	Gene	Min	1	61.01	*0.0285	0.3404
VEGF	Licensed	Protein	Max	15.2	942.15	*0.0328	0.3048
SOX9	Unlicensed	Gene	Min	1	61.46	*0.0381	0.2906
IDO1	Licensed	Gene	Min	4326.67	17824.17	0.0501	0.2832
VEGF	Unlicensed	Protein	Max	250.575	1463.65	0.0743	0.2416
TSG101	Licensed	Gene	Min	272.06	488.06	0.0744	0.2413
CXCL8	Licensed	Gene	Min	25008.42	51553.32	0.0879	0.2234
TNFAIP6	Unlicensed	Gene	Min	1	45.68	0.0809	0.216

Summary of regression analyses between HUVEC PC1 composite scores and MSC(AT) genes, soluble factors, and morphological features. Marker/Characteristic column indicates the gene or protein symbol, or morphological feature. Licensed/Unlicensed column indicates whether the factor was measured under licensed or unlicensed conditions. Min/Max Function column indicates whether minimization or maximation of the MSC(AT) characteristic was desirable based on positive or negative correlations in the linear regression analysis. Min value and Max value columns indicate the range of values measured across each gene (units: mRNA count) and soluble factor (units: pg/mL). All significant (*$p<0.05$) and near-significant correlations ($p<0.01$) are displayed.

overall immunomodulatory ranking, while specific adipose tissue donors had highest angiogenic desirability rankings.

Discussion

In the present study, we selected a matrix of putative quantitative CQAs with a range of minimum and maximum values that define MSC(AT) immunomodulatory and angiogenic basal fitness *in vitro* and are sensitive enough to detect variations in CPPs and donor heterogeneity. We generated putative CQAs based on statistically significant or near-significant correlations between MSC(AT) genes, soluble factors, and morphometric features and functional anchor *in vitro* readouts for immunomodulation (polarization of MΦs to pro-resolving subtypes) and angiogenic potency (network of tube formation with HUVECs). Importantly, the putative CQAs can empirically rank the relative immunomodulatory or angiogenic fitness of MSC(AT) across varying CPP conditions and donors to identify: i) optimal cell culture conditions, or ii) optimal MSC(AT) donors with desired functionality. Our approach is substantially more rigorous than use of surface identity markers which are frequently used as potential final product release criteria for MSCs therapeutics, despite clarifications made by the ISCT and the FDA (55, 56) and given that these surface markers are not sensitive to variations in donor or culture conditions (57). Our approach is also aligned with recommendations from the ISCT to characterize MSC fitness using a matrix of assay readouts (58, 59).

The CPP conditions we investigated had a pronounced effect on immunomodulatory fitness as measured by *in vitro* MSC (AT)-mediated MΦ polarization, with transient 3D-N conditions best augmenting MSC(AT) immunomodulatory basal functionality. We showed strong upregulated expression of immunomodulatory genes (*TNFAIP6*, *ICAM1*, and *PRG4*) and soluble factors (HGF, TGF-β, IL-1RA) by MSC(AT) cultured under 3D-N conditions. Our data also corroborates previous work that showed 3D MSC(M) spheroids promoted an inflammation-resolving macrophage phenotype *in vitro* and suppressed inflammation in a mouse model of peritonitis (31, 60). In contrast to our work using xeno-free 3D culture conditions, others have shown that 3D MSC(M) spheroids lose their ability to suppress pro-inflammatory macrophage activities *in vitro* when cultured using xeno-free medium (36). These differences may be attributed to different methods used for generating 3D cell aggregates. We also investigated the combination of 3D and hypoxic culture and found no additive effects using a targeted panel of both immunomodulatory and angiogenic genes. Based on this data, we evaluated 3D-N and 2D-H conditions separately recognizing that these are currently being explored as CPPs that enhance MSC(AT) fitness. Nevertheless, our methodological approach provides a platform for other investigators looking to evaluate and optimize different CPP conditions individually or in combinations using the provided range of quantitative CQAs.

MSC(AT) cultured under 2D-H conditions showed similar gene/soluble factor expression profiles relative to 2D-N conditions, with upregulation of only a few select immunomodulatory markers (*PTGS2* and PD-L2), and concordantly exhibited intermediate immunomodulatory functions. There is limited data on the immunomodulatory functions of MSCs cultured under hypoxic conditions, but

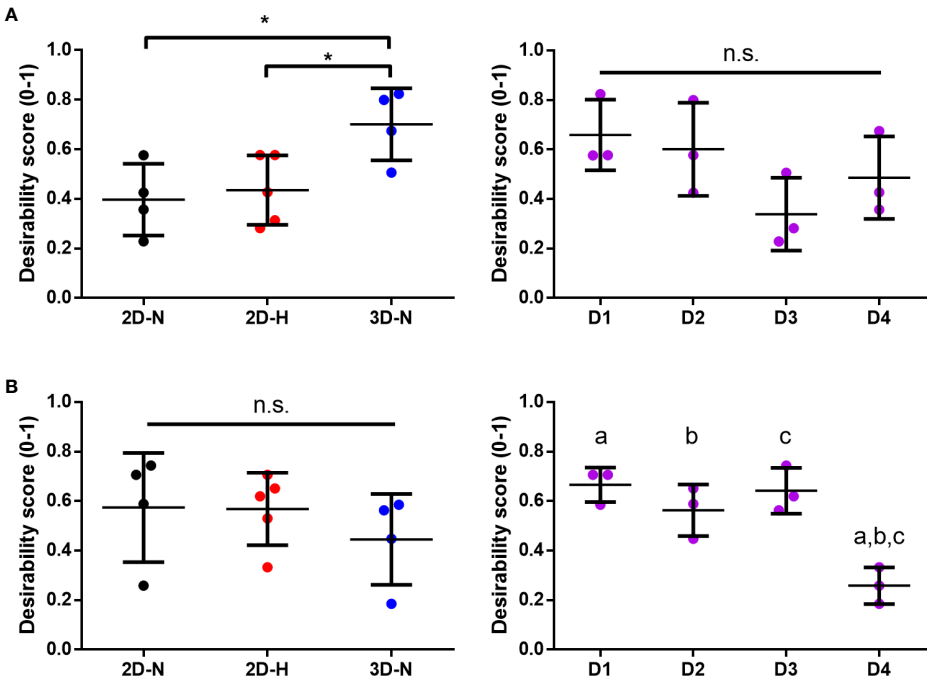

FIGURE 7
Statistical rankings of matrix of putative CQAs ranked different CPP conditions known to enhance MSC potency, and donors for optimal immunomodulation and angiogenic functionalities. Desirability analysis was performed on putative CQAs selected for evaluation of immunomodulatory **(A)** and angiogenic **(B)** functionalities. **(A)** Desirability profiling ranked 3D-N CPP conditions higher than 2D-H and 2D-N for overall immunomodulatory desirability scores, while scores were similar across donors. **(B)** Desirability profiling ranked Donors 1, 2, and 3 higher than Donor 4 for overall angiogenic desirability scores, while scores were similar across various CPPs. One-way ANOVA, Tukey *post-hoc* test. *p<0.05. Donors sharing same letter indicate statistically significant differences (p<0.05). Horizontal bars: group mean, error bars: standard deviation. 3D-N, 3D Normoxic culture; 2D-N, 2D Normoxic culture; 2D-H, 2D Hypoxic culture, n.s, non-significant.

previous work has shown that hypoxic culture can augment T cell inhibition mediated by rat MSC(M) (30) and human MSC (AT) (29). While varying CPP conditions exerted a greater effect on *in vitro* immunomodulation, increased expression of some pro-inflammatory MΦ markers was observed in co-cultures with MSC(AT) and this was partly donor-driven. Previous work has shown that MSCs can induce a mixed MΦ phenotype which may be important for augmenting MΦ microbicidal functions (61), and our work suggests an effect of donor heterogeneity on inducing these mixed MΦ phenotypes.

In contrast to results measuring immunomodulatory fitness, effects of donor heterogeneity predominated over effects of variations in CPPs in modulating angiogenic basal functionality of MSC(AT). This result is surprising given previous work that has shown augmented angiogenic functions of MSC(AT) cultured in 3D aggregates (32, 34), and extensive literature showing augmented angiogenic functions of MSC(AT) cultured under hypoxic conditions (27, 28, 35). Culture under 2D-H conditions augmented pro-angiogenic functions of MSC(AT) only for select donors. This discrepancy with prior literature could be related to the transient (16-20 h) incubations used for 3D/hypoxic priming. Furthermore, differences in the 3D culture method used in this study (e.g., culture using xeno-free medium), and a relatively high level of hypoxic oxygen tension (38 mmHg or approximately 5% O_2) could account for differences relative to previous work. Nonetheless, our data demonstrated a significant effect of donor heterogeneity and suggests that this predominates over variations in CPPs in dictating MSC (AT) basal angiogenic functionality. In future work, addition of specific pro-angiogenic factors (such as FGF-2 (17)) could be explored in conjunction with the CPP conditions in a strategy analogous to use of the pro-inflammatory licensing factors to induce additional expression of angiogenic genes/proteins.

The selection of *in vitro* functional MSC(AT) readouts were carefully chosen to anchor the matrix of multivariate read-outs and refine putative CQAs according to two therapeutically

relevant properties of MSCs: immunomodulation and angiogenesis. In terms of immunomodulatory functions, MSC (AT)-mediated MΦ polarization toward pro-resolving subtypes was evaluated, recognizing that MΦs represent primary effector cells for mediating MSC therapeutic functions in multiple diseases, including GVHD (9), colitis (62), and osteoarthritis (8). While effects of MSCs on T cells are more frequently employed as an *in vitro* readout to evaluate MSC immunomodulatory potency, this is not a gold standard as previous work has also demonstrated lack of correlation to clinical efficacy of MSC(M) in GVHD patients (10). Angiogenic functionality of MSC(AT), was measured using the widely-accepted HUVEC tube formation read-out, which recapitulates several aspects of *in vivo* angiogenesis including endothelial cell adhesion, migration, alignment, and formation of tubules (54). This assay has also been used to evaluate angiogenic functionality for clinical-grade MSCs (19, 38).

The functional *in vitro* read-outs were used as anchors in the putative CQA matrix allowing refinement of a putative set of 60 CQAs (48 genes of interest, 10 soluble factors, and 2 morphometric features) down to 20 CQAs that correlated to *in vitro* MΦ polarization, and 10 putative MSC(AT) CQAs that correlated to *in vitro* HUVEC tube formation. Interestingly, angiogenic genes measured under both licensed and unlicensed conditions negatively correlated with MΦ polarization toward inflammation-resolving subtypes. Conversely, increased expression of select immunomodulatory genes were also negatively correlated to greater *in vitro* HUVEC tube formation. This data suggests an inverse interplay between MSC(AT) immunomodulatory and angiogenic fitness and corroborates previous work by Boregowda *et al.* (17, 63). Our analysis supported the utility of previously reported MSC characteristics that correlate to immunomodulatory fitness – including T*NFAIP6* expression (encoding for TSG6) (8, 64, 65), *TGFB1* expression (8), and cell diameter (15)); and to angiogenic fitness, including increased VEGF expression (38). Furthermore, our results suggest that different CPP conditions or MSC(AT) donors should be selected/optimized for clinical applications depending on the target disease indication and desired therapeutic mechanism.

We applied desirability analysis to empirically rank the immunomodulatory or angiogenic basal fitness of each MSC (AT) donor or CPP condition. The results mirrored the functional assay outcomes, demonstrating a greater effect of CPPs on MSC(AT) immunomodulatory functions, and a greater effect of donor heterogeneity on angiogenic functions. Notably, we selected MSC(AT) characteristics (genes, soluble factors, and morphological features) for inclusion in the desirability analysis based on the strength of their correlations to the functional anchor assays, and we used the R^2 goodness-of-fit values as a relative "importance ranking" for each of the MSC(AT) characteristics. Thus, MSC(AT) characteristics with significant correlations to functional assay outcomes (lower p value and higher R^2 value) contributed to the overall desirability score to a larger extent compared to characteristics with near-significant correlations (higher p value and lower R^2 value). Based on these analytical methods, it is expected that the overall desirability rankings would closely match the results from the original functional assay outcomes as they were used to determine the relative strength of contributions to the overall desirability score calculations. Nonetheless, our empirical approach has utility in future studies where similar desirability analysis can be used as an unbiased tool to rank the immunomodulatory or angiogenic fitness of a given population of MSCs based on combinatorial analysis of a matrix of curated genes, soluble factors, and morphological features only. The same relative importance rankings for the set of putative CQAs could be applied, circumventing the need to conduct lengthy, non-high-throughput functional analyses. To our knowledge, this is the first reported application of desirability analysis for understanding MSC potency attributes.

In the present study, we used *in vitro* functional assays as surrogate read-outs for MSC(AT) immunomodulatory and angiogenic fitness. These analyses generated relatively broad panels of putative CQAs selected based on correlation analyses to *in vitro* functional readouts with a p value threshold set to $p<0.1$. We have, necessarily, termed the CQAs we evaluated here as "putative"; ultimately these putative CQAs can be narrowed down further and validated in clinical studies where specific MSC(AT) CQAs may be more or less relevant depending on the target disease and/or disease stage. To accelerate clinical translation of MSC products, there is a need for simple, robust, and reproducible potency readouts, which our panel of quantitative and correlative CQAs supply. Importantly, we used two *in vitro* functional readouts as surrogate anchors for clinical efficacy. Future studies may substitute disease-specific biomarkers as recommended by Krampera and Le Blanc (3) *in lieu* of the *in vitro* functional readouts; correlation of a refined list of MSC CQAs with changes in disease attributes would be the ultimate validation. In this vein, creation of registry databases that would allow logging of large datasets, including our proposed CQA matrix used to characterize MSC(AT), may be practical to allow different sponsors to query candidate CQAs in their respective clinical MSC products and examine correlations with disease-specific biomarker changes and thus therapeutic efficacy.

Variable clinical responses to MSC treatments can arise from several factors, including through heterogeneity in donor or CPP factors explored here, but also through *in vivo* interactions with host tissues (3, 5). While we are unable to capture host responses using the *in vitro* assays applied in this work, we argue that defining basal thresholds of MSC immunomodulatory and/or angiogenic fitness with defined ranges of quantitative CQAs enables a greater likelihood of eliciting stronger therapeutic effects, as hypothesized by the ISCT MSC Committee (66). MSC basal fitness levels are especially relevant to therapeutic potency for extravascular delivery where *in vivo* persistence allows for release of paracrine factors (66), compared to vascular delivery where efficacy may rely more on proclivity of MSCs to be rapidly cleared by host immune cells as evidenced in GVHD by Galleu *et al.* (9). Another limitation of our study design was the sourcing of MSC(AT) from patients with knee or hand osteoarthritis which was based on tissue availability in our research center. It should be noted that these MSCs satisfied minimal surface marker expression criteria for MSC(AT) (42), and the adipose tissue depots were located external to the affected joints from patients with mild to moderate osteoarthritis (KL grade 0-2). However, both local joint factors and systemic factors can contribute to the pathology of osteoarthritis (67), and thus we cannot discount potential effects on the isolated MSC(AT). Ultimately, our findings will need to be verified with additional MSC(AT) donors in the context of a registry of clinical studies to evaluate whether MSC (AT) with putative CQAs within the proposed ranges perform more effectively.

Taken together, our study provides a systematic, empirical approach to evaluate the effects of variations in CPPs, specifically those that can non-genetically enhance MSC immunomodulatory and/or angiogenic properties, and donor heterogeneity on MSC(AT) critical attributes. We established a matrix of putative, quantitative CQAs with a range of minimum and maximum values based on correlations of multivariate readouts of MSC(AT) cell morphology, gene expression, and soluble factor expression with functional readouts that served as an anchor in the analysis. We argue the relevance of these functional assays in determining CQAs for MSC(AT). Importantly, the empirical approach can be adapted and applied to future clinical studies where changes to disease-specific biomarkers may be substituted *in lieu* of *in vitro* functional readouts to serve as the anchor. Our putative CQA matrix empirically ranked the effects of CPPs or donor heterogeneity on desired immunomodulatory or angiogenic MSC(AT) basal fitness, and showed differential sensitivity to these variables, suggesting that a one-size-fits-all approach is not suitable for manufacturing MSC(AT). Ultimately, our analysis identified putative CQAs that may be used to prospectively screen potent MSC(AT) donors and select specific CPP conditions to enhance for desired MSC basal fitness ranges.

Data availability statement

The data presented in the study are deposited in the Gene Expression Omnibus repository, accession number GSE212368.

Ethics statement

The studies involving human participants were reviewed and approved by University Health Network. The patients/participants provided their written informed consent to participate in this study.

Author contributions

All authors contributed to conceptualization and design of the study. KR performed the experiments and analysed the data. The manuscript was drafted by KR and SV. All authors contributed to the article and approved the submitted version.

Funding

This research was funded by the Canadian Institutes of Health Research (CIHR) (PJT-166089), the Natural Sciences and Engineering Research Council of Canada (NSERC) (RGPIN-2018-05737), and an Ontario Institute for Regenerative Medicine (OIRM) New Ideas Grant awarded to SV. The work is in part supported by the Schroeder Arthritis Institute *via* the Toronto General and Western Hospital Foundation (University Health Network). Salary support for KR was provided by a Natural Sciences and Engineering Research Council (NSERC) Canada Graduate Scholarship, an Ontario Graduate Scholarship, and by the Arthritis Society (TGP-18-0206).

Acknowledgments

The authors would like to thank Dr. Heather Baltzer, Daniel Antflek, Kim Perry, Mary Nasim, and Luis Montoya for their assistance with adipose tissue acquisition. We would also like to acknowledge the work of Dr. Pamela Plant and Dr. Mozhgan Rasti for their technical assistance in running the NanoString gene expression and western blot experiments, respectively. The human umbilical vein endothelial cells used in this study were

kindly gifted by Dr. Edmond Young. Flow cytometry for LEGENDplex experiments was performed in the Toronto Western KDT-UHN Flow Cytometry Facility, with funding from the Canada Foundation for Innovation, and Toronto General and Western Hospital Foundation. Schematics for figures were created using BioRender.com.

Conflict of interest

SV declares 60% ownership in Regulatory Cell Therapy Consultants, Inc., a private regulatory consulting company.

The remaining authors declare that the research was conducted in the absence of any commercial or financial relationships that could be construed as a potential conflict of interest.

Publisher's note

Supplementary material

The Supplementary Material for this article can be found online at: https://www.frontiersin.org/articles/10.3389/fimmu.2022.972095/full#supplementary-material

References

1. Pittenger MF, Discher DE, Péault BM, Phinney DG, Hare JM, Caplan AI. Mesenchymal stem cell perspective: cell biology to clinical progress. *Regener Med* (2019) 4(1):1–15. doi: 10.1016/j.jcyt.2018.10.014

2. Robb KP, Fitzgerald JC, Barry F, Viswanathan S. Mesenchymal stromal cell therapy: progress in manufacturing and assessments of potency. *Cytotherapy* (2019) 21(3):289–306. doi: 10.1016/j.stem.2021.09.006

3. Krampera M, Le Blanc K. Mesenchymal stromal cells: Putative microenvironmental modulators become cell therapy. *Cell Stem Cell* (2021) 28 (10):1708–25. doi: 10.1016/j.stem.2018.05.004

4. Galipeau J, Sensébé L. Mesenchymal stromal cells: Clinical challenges and therapeutic opportunities. *Cell Stem Cell* (2018) 22(6):824–33. doi: 10.3389/fimmu.2019.01228

5. Weiss DJ, English K, Krasnodembskaya A, Isaza-Correa JM, Hawthorne IJ, Mahon BP. The necrobiology of mesenchymal stromal cells affects therapeutic efficacy. *Front Immunol* (2019) 10:1228. doi: 10.1038/srep46731

6. Liu S, De Castro LF, Jin P, Civini S, Ren J, Reems JA, et al. Manufacturing differences affect human bone marrow stromal cell characteristics and function: Comparison of production methods and products from multiple centers. *Sci Rep* (2017) 7(1):1–11. doi: 10.1186/s13287-019-1331-9

7. Czapla J, Matuszczak S, Kulik K, Wiśniewska E, Pilny E, Jarosz-Biej M, et al. The effect of culture media on large-scale expansion and characteristic of adipose tissue-derived mesenchymal stromal cells. *Stem Cell Res Ther* (2019) 10(1):235. doi: 10.1002/sctm.18-0183

8. Chahal J, Gómez-Aristizábal A, Shestopaloff K, Bhatt S, Chaboureau A, Fazio A, et al. Bone marrow mesenchymal stromal cells in patients with osteoarthritis results in overall improvement in pain and symptoms and reduces synovial inflammation. *Stem Cells Transl Med* (2019) 8(8):746–57. doi: 10.1126/scitranslmed.aam7828

9. Galleu A, Riffo-Vasquez Y, Trento C, Lomas C, Dolcetti L, Cheung TS, et al. Apoptosis in mesenchymal stromal cells induces *in vivo* recipient-mediated immunomodulation. *Sci Transl Med* (2017) 9(416):eaam7828. doi: 10.1016/j.bbmt.2011.07.023

10. von Bahr L, Sundberg B, Lönnies L, Sander B, Karbach H, Hägglund H, et al. Long-term complications, immunologic effects, and role of passage for outcome in mesenchymal stromal cell therapy. *Biol Blood Marrow Transplant* (2012) 18 (4):557–64. doi: 10.1016/j.celrep.2018.02.013

11. Chinnadurai R, Rajan D, Qayed M, Arafat D, Garcia M, Liu Y, et al. Potency analysis of mesenchymal stromal cells using a combinatorial assay matrix approach. *Cell Rep* (2018) 22(9):2504–17. doi: 10.1093/stcltm/szac050

12. Lipat AJ, Cottle C, Pirlot BM, Mitchell J, Pando B, Helmly B, et al. Chemokine assay matrix defines the potency of human bone marrow mesenchymal stromal cells. *Stem Cells Transl Med* (2022) 11(9):971–86. doi: 10.1002/stem.3035

13. Chinnadurai R, Rajakumar A, Schneider AJ, Bushman WA, Hematti P, Galipeau J. Potency analysis of mesenchymal stromal cells using a phospho-STAT matrix loop analytical approach. *Stem Cells* (2019) 37(8):1119–25. doi: 10.1016/j.jcyt.2021.08.002

14. Maughon TS, Shen X, Huang D, Michael AOA, Shockey WA, Andrews SH, et al. Metabolomics and cytokine profiling of mesenchymal stromal cells identify markers predictive of T-cell suppression. *Cytotherapy* (2022) 24 (2):137–48.

15. Klinker MW, Marklein RA, Lo Surdo JL, Wei C-HH, Bauer SR. Morphological features of IFN-gamma-stimulated mesenchymal stromal cells predict overall immunosuppressive capacity. *Proc Natl Acad Sci U.S.A.* (2017) 114(13):E2598–e2607. doi: 10.1002/bit.27974

16. Andrews SH, Klinker MW, Bauer SR, Marklein RA. Morphological landscapes from high content imaging reveal cytokine priming strategies that enhance mesenchymal stromal cell immunosuppression. *Biotechnol Bioeng* (2022) 119(2):361–75. doi: 10.1016/j.ebiom.2015.12.020

17. Boregowda SV, Krishnappa V, Haga CL, Ortiz LA, Phinney DG. A clinical indications prediction scale based on TWIST1 for human mesenchymal stem cells. *EBioMedicine* (2016) 4:62–73.

18. FDA Advisory Committee. *Oncologic drugs advisory committee. remestemcel-l for treatment of steroid refractory acute graft versus host disease in pediatric patients.* (2020). https://www.fda.gov/media/140996/download

19. Lehman N, Cutrone R, Raber A, Perry R, van't Hof W, Deans R, et al. Development of a surrogate angiogenic potency assay for clinical-grade stem cell production. *Cytotherapy* (2012) 14(8):994–1004. doi: 10.1016/j.scr.2008.07.007

20. Kuznetsov SA, Mankani MH, Bianco P, Robey PG. Enumeration of the colony-forming units-fibroblast from mouse and human bone marrow in normal and pathological conditions. *Stem Cell Res* (2009) 2(1):83–94. doi: 10.1016/j.jcyt.2013.01.218

21. Wang J, Liao L, Wang S, Tan J. Cell therapy with autologous mesenchymal stem cells-how the disease process impacts clinical considerations. *Cytotherapy* (2013) 15(8):893–904. doi: 10.1186/1741-7015-11-146

22. Siegel G, Kluba T, Hermanutz-Klein U, Bieback K, Northoff H, Schäfer R. Phenotype, donor age and gender affect function of human bone marrow-derived mesenchymal stromal cells. *BMC Med* (2013) 11(1):146. doi: 10.1038/s41551-018-0325-8

23. Yin JQ, Zhu J, Ankrum JA. Manufacturing of primed mesenchymal stromal cells for therapy. *Nat BioMed Eng* (2019) 3(2):90–104. doi: 10.3389/fimmu.2019.01112

24. Wilson A, Hodgson-Garms M, Frith JE, Genever P. Multiplicity of mesenchymal stromal cells: Finding the right route to therapy. *Front Immunol* (2019) 10:1112. doi: 10.1038/s41419-019-1583-4

25. Huang Y, Li Q, Zhang K, Hu M, Wang Y, Du L, et al. Single cell transcriptomic analysis of human mesenchymal stem cells reveals limited heterogeneity. *Cell Death Dis* (2019) 10(5):1–12. doi: 10.3389/fimmu.2022.917790

26. Wiese DM, Wood CA, Ford BN, Braid LR. Cytokine activation reveals tissue-imprinted gene profiles of mesenchymal stromal cells. *Front Immunol* (2022) 13:917790. doi: 10.3390/ijms18061320

27. Lee JH, Yoon YM, Lee SH. Hypoxic preconditioning promotes the bioactivities of mesenchymal stem cells via the HIF-1α-GRP78-Akt axis. *Int J Mol Sci* (2017) 18(6):1320.

28. Leroux L, Descamps B, Tojais NF, Seguy B, Oses P, Moreau C. Hypoxia preconditioned mesenchymal stem cells improve vascular and skeletal muscle fiber regeneration after ischemia through a Wnt4-dependent pathway. *Mol Ther*, (2010) 18(8):1545–52. doi: 10.1016/j.regen.2018.01.001

29. Wobma HM, Kanai M, Ma SP, Shih Y, Li HW, Duran-Struuck R, et al. Dual IFN-γ/hypoxia priming enhances immunosuppression of mesenchymal stromal cells through regulatory proteins and metabolic mechanisms. *J Immunol Regener Med* (2018), 1:45–56. doi: 10.1371/journal.pone.0193178

30. Kadle RL, Abdou SA, Villarreal-Ponce AP, Soares MA, Sultan DL, David JA, et al. Microenvironmental cues enhance mesenchymal stem cell-mediated immunomodulation and regulatory T-cell expansion. *PloS One* (2018) 13: e0193178. doi: 10.1073/pnas.1008117107

31. Bartosh TJ, Ylostalo JH, Mohammadipoor A, Bazhanov N, Coble K, Claypool K, et al. Aggregation of human mesenchymal stromal cells (MSCs) into 3D spheroids enhances their antiinflammatory properties. *Proc Natl Acad Sci U.S.A.* (2010) 107(31):13724–9. doi: 10.1155/2019/7486279

32. Miceli V, Pampalone M, Vella S, Carreca AP, Amico G, Conaldi PG. Comparison of immunosuppressive and angiogenic properties of human amnion-derived mesenchymal stem cells between 2D and 3D culture systems. *Stem Cells Int* (2019) 2019:7486279. doi: 10.3389/fimmu.2019.00018

33. Miranda JP, Camões SP, Gaspar MM, Rodrigues JS, Carvalheiro M, Bárcia RN, et al. The secretome derived from 3D-cultured umbilical cord tissue MSCs counteracts manifestations typifying rheumatoid arthritis. *Front Immunol* (2019) 10:18. doi: 10.5966/sctm.2013-0007

34. Cheng N-C, Chen S-Y, Li J-R, Young T-H. Short-term spheroid formation enhances the regenerative capacity of adipose-derived stem cells by promoting stemness, angiogenesis, and chemotaxis. . *Stem Cells Transl Med* (2013) 2(8):584–94. doi: 10.1634/stemcells.2007-0022

35. Potapova IA, Gaudette GR, Brink PR, Robinson RB, Rosen MR, Cohen IS, et al. Mesenchymal stem cells support migration, extracellular matrix invasion, proliferation, and survival of endothelial cells in vitro. *Stem Cells* (2007) 25 (7):1761–8. doi: 10.1016/j.jcyt.2013.09.004

36. Zimmermann JA, Mcdevitt TC. Pre-conditioning mesenchymal stromal cell spheroids for immunomodulatory paracrine factor secretion. *Cytotherapy* (2014) 16(3):331–45. doi: 10.1002/stem.3380

37. Galipeau J. Macrophages at the nexus of mesenchymal stromal cell potency: The emerging role of chemokine cooperativity. *Stem Cells* (2021) 39(9):1145–1154.

38. Thej C, Ramadasse B, Walvekar A, Majumdar AS, Balasubramanian S. Development of a surrogate potency assay to determine the angiogenic activity of stempeucel®, a pooled, ex-vivo expanded, allogeneic human bone marrow mesenchymal stromal cell product. *Stem Cell Res Ther* (2017) 8(1):47. doi: 10.1016/B978-0-12-802826-1.00001-5

39. Viswanathan S, Bhatt SJ, Gomez-Aristizabal A. Methods of culturing mesenchymal stromal cells. *World Intellectual Property Organ* (2017), WO2018053618A1.

40. Egger D, Schwedhelm I, Hansmann J, Kasper C. Hypoxic three-dimensional scaffold-free aggregate cultivation of mesenchymal stem cells in a stirred tank reactor. *Bioeng*, (2017) 4(2):47. doi: 10.1038/nmeth.2089

41. Schneider CA, Rasband WS, Eliceiri KW. NIH Image to ImageJ: 25 years of image analysis. *Nat Methods* (2012) 9(7):671–5. doi: 10.1016/j.jcyt.2013.02.006

42. Bourin P, Bunnell BA, Casteilla L, Dominici M, Katz AJ, March KL, et al. Stromal cells from the adipose tissue-derived stromal vascular fraction and culture expanded adipose tissue-derived stromal/stem cells: A joint statement of the international federation for adipose therapeutics and science (IFATS) and the international so. *Cytotherapy* (2013) 15(6):641–8. doi: 10.1093/nar/30.1.207

43. Edgar R, Domrachev M, Lash AE. Gene expression omnibus: NCBI gene expression and hybridization array data repository. *Nucleic Acids Res* (2002) 30 (1):207–10.

44. Gómez-Aristizábal A, Kim K-PP, Viswanathan S. A systematic study of the effect of different molecular weights of hyaluronic acid on mesenchymal stromal cell-mediated immunomodulation. *PloS One* (2016) 11(1):e0147868.

45. Carpentier G, Berndt S, Ferratge S, Rasband W, Cuendet M, Uzan G. Angiogenesis analyzer for ImageJ—a comparative morphometric analysis of "Endothelial Tube Formation Assay" and "Fibrin Bead Assay". *Sci Rep* (2020). 10:11568. doi: 10.1038/s41598-020-67289-8.

46. Benjamini Y, Yekutieli D. The control of the false discovery rate in multiple testing under dependency. *Ann Stat* (2001) 29(4):1165–88. doi: 10.1080/00224065.1980.11980968

47. Derringer G, Suich R. Simultaneous optimization of several response variables. *J Qual Technol* (1980) 12(4):214–9. doi: 10.1016/j.biomaterials.2018.03.027

48. Wobma HM, Tamargo MA, Goeta S, Brown LM, Duran-Struuck R, Vunjak-Novakovic G. The influence of hypoxia and IFN-γ on the proteome and metabolome of therapeutic mesenchymal stem cells. *Biomaterials* (2018) 167:226–34, 167. doi: 10.1093/bmb/ldt031

49. Watt SM, Gullo F, van der Garde M, Markeson D, Camicia R, Khoo CP, et al. The angiogenic properties of mesenchymal stem/stromal cells and their therapeutic potential. *Br Med Bull* (2013) 108:25–53. doi: 10.1002/stem.118

50. Ren G, Su J, Zhang L, Zhao X, Ling W, L'huillie A, et al. Species variation in the mechanisms of mesenchymal stem cell-mediated immunosuppression. *Stem Cells* (2009) 27(8):1954–62. doi: 10.3390/ijms22062838

51. Sekiya I, Katano H, Ozeki N. Characteristics of mscs in synovial fluid and mode of action of intra-articular injections of synovial mscs in knee osteoarthritis. *Int J Mol Sci* (2021) 22(6):1–13. doi: 10.1016/j.joca.2015.12.018

52. Ozeki N, Muneta T, Koga H, Nakagawa Y, Mizuno M, Tsuji K, et al. Not single but periodic injections of synovial mesenchymal stem cells maintain viable cells in knees and inhibit osteoarthritis progression in rats. *Osteoarthr Cartil* (2016) 24(6):1061–70. doi: 10.1038/s41598-017-09449-x

53. Ghazanfari R, Di Z, Li H, Ching Lim H, Soneji S, Scheding S. Human primary bone marrow mesenchymal stromal cells and their *in vitro* progenies display distinct transcriptional profile signatures. *Sci Rep* (2017) 7(1):1–10. doi: 10.1007/s10456-009-9146-4

54. Arnaoutova I, George J, Kleinman HK, Benton G. The endothelial cell tube formation assay on basement membrane turns 20: State of the science and the art. *Angiogenesis* (2009) 12(3):267–74.

55. Dominici M, Le Blanc K, Mueller I, Slaper-Cortenbach I, Marini FC, Krause DS, et al. Minimal criteria for defining multipotent mesenchymal stromal cells. the international society for cellular therapy position statement. *Cytotherapy* (2006) 8 (4):315–7. doi: 10.1016/j.stem.2014.01.013

56. Mendicino M, Bailey AM, Wonnacott K, Puri RK, Bauer SR. MSC-based product characterization for clinical trials: an FDA perspective. *Cell Stem Cell* (2014) 14:141–5. doi: 10.1038/s41598-021-83088-1

57. Bhat S, Viswanathan P, Chandanala S, Prasanna SJ, Seetharam RN. Expansion and characterization of bone marrow derived human mesenchymal stromal cells in serum-free conditions. *Sci Rep* (2021) 11(1):3403. doi: 10.1016/j.jcyt.2015.11.008

58. Galipeau J, Krampera M, Barrett J, Dazzi F, Deans RJ, DeBruijn J, et al. International society for cellular therapy perspective on immune functional assays for mesenchymal stromal cells as potency release criterion for advanced phase clinical trials. *Cytotherapy* (2016) 18:151–9. doi: 10.1016/j.jcyt.2019.08.002

59. Viswanathan S, Shi Y, Galipeau J, Krampera M, Leblanc K, Martin I, et al. Mesenchymal stem versus stromal cells: International society for cell & gene therapy (ISCT®) mesenchymal stromal cell committee position statement on nomenclature. *Cytotherapy* (2019) 21(10):1019–24. doi: 10.1016/j.jcyt.2014.07.010

60. Ylostalo JH, Bartosh TJ, Tiblow A, Prockop DJ. Unique characteristics of human mesenchymal stromal/progenitor cells pre-activated in 3-dimensional cultures under different conditions. *Cytotherapy* (2014) 16:1486–500. doi: 10.1183/13993003.02021-2017

61. Rabani R, Volchuk A, Jerkic M, Ormesher L, Garces-Ramirez L, Canton J, et al. Mesenchymal stem cells enhance NOX2-dependent reactive oxygen species production and bacterial killing in macrophages during sepsis. *Eur Respir J* (2018) 51(4):1702021. doi: 10.1016/j.celrep.2020.01.047

62. Giri J, Das R, Nylen E, Chinnadurai R, Galipeau J. CCL2 and CXCL12 derived from mesenchymal stromal cells cooperatively polarize IL-10+ tissue macrophages to mitigate gut injury. *Cell Rep* (2020) 30(6):1923–1934.e4. doi: 10.1016/S1465-3249(22)00135-9

63. Lee RH, Boregowda SV, Shigemoto-Kuroda T, Ortiz LA, Phinney DG. Mesenchymal Stem/Stromal cells: TWIST1 and TSG6 as potency biomarkers of human MSCs in pre-clinical disease models. *Cytotherapy* (2022), 24(5)S32.

64. Lee RH, Yu JM, Foskett AM, Peltier G, Reneau JC, Bazhanov N, et al. TSG-6 as a biomarker to predict efficacy of human mesenchymal stem/progenitor cells (hMSCs) in modulating sterile inflammation *in vivo*. *Proc Natl Acad Sci U.S.A.* (2014) 111:16766–71. doi: 10.1182/blood-2010-12-327353

65. Choi H, Lee RH, Bazhanov N, Oh JY, Prockop DJ. Anti-inflammatory protein TSG-6 secreted by activated MSCs attenuates zymosan-induced mouse peritonitis by decreasing TLR2/NF-κB signaling in resident macrophages. *Blood* (2011) 118:330–8. doi: 10.1016/j.jcyt.2020.11.007

66. Galipeau J, Krampera M, Leblanc K, Nolta JA, Phinney DG, Shi Y, et al. Mesenchymal stromal cell variables influencing clinical potency: the impact of viability, fitness, route of administration and host predisposition. *Cytotherapy* (2021) 23(5):368–72. doi: 10.1002/jcp.25716

67. Belluzzi E, El Hadi H, Granzotto M, Rossato M, Ramonda R, Macchi V, et al. Systemic and local adipose tissue in knee osteoarthritis. *J Cell Physiol* (2017) 232 (8):1971–8. doi: 10.1038/s41536-019-0083-6

frontiers | Frontiers in Immunology

TYPE Original Research
PUBLISHED 15 December 2022
DOI 10.3389/fimmu.2022.954984

OPEN ACCESS

EDITED BY
Raghavan Chinnadurai,
Mercer University, United States

REVIEWED BY
Ute Modlich,
Paul-Ehrlich-Institut (PEI), Germany
Rusan Ali Catar,
Charité Universitätsmedizin Berlin, Germany

*CORRESPONDENCE
Graça Almeida-Porada
galmeida@wakehealth.edu

†These authors share senior authorship

SPECIALTY SECTION
This article was submitted to Alloimmunity and Transplantation, a section of the journal Frontiers in Immunology

RECEIVED 27 May 2022
ACCEPTED 28 November 2022
PUBLISHED 15 December 2022

CITATION
Ramamurthy RM, Rodriguez M, Ainsworth HC, Shields J, Meares D, Bishop C, Farland A, Langefeld CD, Atala A, Doering CB, Spencer HT, Porada CD and Almeida-Porada G (2022) Comparison of different gene addition strategies to modify placental derived-mesenchymal stromal cells to produce FVIII. *Front. Immunol.* 13:954984. doi: 10.3389/fimmu.2022.954984

Comparison of different gene addition strategies to modify placental derived-mesenchymal stromal cells to produce FVIII

Ritu M. Ramamurthy[1], Martin Rodriguez[1], Hannah C. Ainsworth[2], Jordan Shields[3], Diane Meares[4], Colin Bishop[1], Andrew Farland[4], Carl D. Langefeld[2], Anthony Atala[1], Christopher B. Doering[3], H. Trent Spencer[3], Christopher D. Porada[1†] and Graça Almeida-Porada[1*†]

[1]Fetal Research and Therapy Program, Wake Forest Institute for Regenerative Medicine, Winston Salem, NC, United States, [2]Department of Biostatistics and Data Sciences Wake Forest School of Medicine, Winston Salem, NC, United States, [3]Department of Pediatrics, Aflac Cancer and Blood Disorders Center, Children's Healthcare of Atlanta, Emory University, Atlanta, GA, United States, [4]Department of Medicine, Hematology and Oncology, Wake Forest School of Medicine, Winston Salem, NC, United States

Introduction: Placenta-derived mesenchymal cells (PLCs) endogenously produce FVIII, which makes them ideally suited for cell-based fVIII gene delivery. We have previously reported that human PLCs can be efficiently modified with a lentiviral vector encoding a bioengineered, expression/secretion-optimized fVIII transgene (ET3) and durably produce clinically relevant levels of functionally active FVIII. The objective of the present study was to investigate whether CRISPR/Cas9 can be used to achieve location-specific insertion of a fVIII transgene into a genomic safe harbor, thereby eliminating the potential risks arising from the semi-random genomic integration inherent to lentiviral vectors. We hypothesized this approach would improve the safety of the PLC-based gene delivery platform and might also enhance the therapeutic effect by eliminating chromatin-related transgene silencing.

Methods: We used CRISPR/Cas9 to attempt to insert the bioengineered fVIII transgene "lcoET3" into the AAVS1 site of PLCs (CRISPR-lcoET3) and determined their subsequent levels of FVIII production, comparing results with this approach to those achieved using lentivector transduction (LV-lcoET3) and plasmid transfection (Plasmid-lcoET3). In addition, since liver-derived sinusoidal endothelial cells (LSECs) are the native site of FVIII production in the body, we also performed parallel studies in human (h)LSECs).

Results: PLCs and hLSECs can both be transduced (LV-lcoET3) with very high efficiency and produce high levels of biologically active FVIII. Surprisingly, both cell types were largely refractory to CRISPR/Cas9-mediated knockin of the lcoET3 fVIII transgene in the AAVS1 genome locus. However, successful insertion of an RFP reporter into this locus using an identical procedure

suggests the failure to achieve knockin of the lcoET3 expression cassette at this site is likely a function of its large size. Importantly, using plasmids, alone or to introduce the CRISPR/Cas9 "machinery", resulted in dramatic upregulation of TLR 3, TLR 7, and BiP in PLCs, compromising their unique immune-inertness.

Discussion: Although we did not achieve our primary objective, our results validate the utility of both PLCs and hLSECs as cell-based delivery vehicles for a fVIII transgene, and they highlight the hurdles that remain to be overcome before primary human cells can be gene-edited with sufficient efficiency for use in cell-based gene therapy to treat HA.

KEYWORDS

CRISPR/Cas, lentiviral (LV) vector, cell therapy, gene therapy, FVIII, hemophilia A, placental-derived mesenchymal stromal cells

Introduction

Hemophilia A (HA) is an X-linked inherited disorder caused by mutations in the gene encoding clotting factor 8 (FVIII), which results in defective/absent coagulation activity. The estimated frequency is 1 in 5000 live male births, and approximately 400,000 people live with HA worldwide (1). HA can be categorized into three degrees of severity depending on the levels of FVIII: severe (<1%), moderate (1-5%), and mild (6-30%). More than half (60%) the people diagnosed with HA are of the severe type (2). Severe HA is characterized by spontaneous bleeds, debilitating hemarthrosis, and life-threatening intracranial hemorrhages. Current treatments for HA primarily include regular infusions of FVIII protein twice a week for the duration of life. Not only is the treatment lifelong, but also expensive and not accessible to ~75% of HA patients (3). Currently, the lifetime cost estimate to treat a patient with HA is ~$20 million (4). Moreover, 30% of the patients who receive the treatment develop inhibitors against the infused protein, rendering the treatment ineffective (5).

Since HA is a monogenic disease, gene therapy represents a promising therapeutic approach for achieving lifelong phenotypic/clinical correction. To-date, over 3700 distinct mutations within the F8 gene have been identified in HA patients (6). Since the ideal therapy would be "universal" and benefit all HA patients, a "gene addition" approach to knock-in a functional fVIII transgene would be preferable to attempting to correct the mutation *via* gene-editing, which would require gRNA and homology arms specific to each patient's unique mutation. Currently, there are at least 10 ongoing "gene addition" clinical gene therapy trials for HA, with the majority using Adeno-associated virus (AAV) (7–9). While results to-date have been promising, major challenges such as immunologic barriers and the need for very high vector dose to achieve a clinically meaningful rate of transduction remain (7–13). In addition, the vast majority of AAV vector genomes remain episomal following transduction (14, 15), raising concerns over the duration of phenotypic correction that can be achieved with this approach. Recent data emerging from ongoing clinical trials showing that plasma FVIII levels are decreasing with time post-treatment validate this concern (10–13).

An attractive alternative to directly injecting viral vectors to achieve "gene addition" that is gaining momentum to achieve phenotypic correction of HA (16) is to genetically modify appropriate cells and to then use these engineered cells as vehicles to carry the therapeutic transgene. Such an approach allows the inclusion multiple safeguards during manufacturing that are not possible with direct vector injection, such as determination of vector copy number, quantitation of transgene expression, identification of genomic integration sites, and thorough tumorigenicity/toxicology testing. For such an approach to work for HA, the cellular vehicle must be carefully selected to ensure that the large and complex FVIII protein can be efficiently synthesized, post-translationally processed, and secreted without inducing cell stress response, while maintaining its procoagulant activity (17, 18).

Among the myriad putative cellular vehicles, one could consider, human placenta-derived mesenchymal stromal cells (PLCs) possess a host of unique biological and immunological properties that make them ideally-suited as an off-the-shelf product for cell-based therapies and for gene/drug delivery (19–21). One feature of particular relevance as a cellular platform for treating HA is that PLCs constitutively produce FVIII mRNA, protein, and procoagulant activity (22), establishing that they possess all the requisite machinery to produce, process, and secrete this complicated protein and

preserve its functionality. Moreover, PLCs also endogenously produce von Willebrand factor (vWF) (22), which serves as FVIII's carrier protein *in vivo*, dramatically prolonging its biological half-life (23–25), and preventing its uptake and presentation by antigen-presenting cells, thereby reducing its potential immunogenicity (26, 27). Based on these promising traits, we recently investigated the ability of human PLCs to serve as cellular vehicles for delivering a fVIII transgene. The complexity of the FVIII protein has always been a hurdle to developing gene therapy for HA (8, 28–30). However, the past decades have seen remarkable progress in bioengineering techniques, like codon optimization, that have been shown to enhance FVIII protein translation *in vitro* and in clinical trials (31, 32). We established that transducing PLCs with a lentiviral vector encoding a fVIII transgene that was >92% human, but which was codon optimized and bioengineered to include porcine sequence elements that have been shown to enhance post-translational processing and secretion of FVIII (22, 33–36) yielded clinically meaningful levels of secreted FVIII activity without triggering cellular stress or altering PLCs' inherently immune-inert state (22).

These prior studies with PLCs, and studies performed in other promising cell types, have collectively provided compelling evidence that efficient gene addition and long-term FVIII expression can be achieved following transduction with integrating vectors, such as those based upon murine retroviruses or lentiviruses (31, 34, 37–48). While we found no evidence of integration within or near oncogenes or tumor repressors in the lentiviral vector-transduced PLCs, we undertook the present studies to explore whether we could identify an even safer gene delivery approach, testing the hypothesis that using CRISPR/Cas9 to achieve site-specific insertion of an optimized fVIII transgene (lcoET3 (22, 22, 36, 49)) cassette into a genomic "safe harbor" would allow efficient gene addition, while avoiding the potential for insertional mutagenesis that is inherent to all integrating viral vectors (50–54). The specific genomic site we selected for this initial proof-of-concept was the AAVS1 site on chromosome 19, as integration into this site does not disrupt any essential genes, yet the site is transcriptionally active, ensuring inserted transgene cassettes are stably and robustly expressed (55). As liver sinusoid-derived endothelial cells (LSECs) are the natural producers of FVIII in the body (56) and are thus being explored as cellular platforms to treat HA (57), we also performed studies to ascertain whether it is possible to use CRISPR/Cas9 to efficiently mediate delivery of a fVIII transgene cassette into the AAVS1 locus in human (h) LSECs. With each cell type, we compare the success and efficiency of the CRISPR/Cas9-based approach to that achieved when the same fVIII transgene cassette was delivered *via* a lentiviral vector (LV-lcoET3) or transfection with a plasmid (Plasmid-lcoET3). We report that human PLCs and LSECs can both be efficiently transduced with lentiviral vectors encoding a bioengineered lcoET3 fVIII transgene and subsequently produce and secrete therapeutically relevant levels of FVIII procoagulant activity. Surprisingly, however, we found that both cell types appear to be largely refractory to CRISPR/Cas9-mediated knockin of the lcoET3 fVIII transgene in the AAVS1 genome locus. Nevertheless, the ability to successfully insert an RFP reporter into this locus using an identical procedure and donor template plasmid suggest the failure to achieve knockin of lcoET3 at this site is likely a function of the large size of the lcoET3 expression cassette. Interestingly, despite its inability to mediate integration of the lcoET3 cassette at the AAVS1 locus, the use of plasmid-based transfection to deliver the CRISPR/Cas9-based gene editing machinery to PLCs still upregulated expression of toll-like receptor (TLR) molecules TLR-3 and TLR-7, indicating that such manipulation may compromise the immune-inert properties that make these cells desirable as an off-the-shelf product, and highlighting the importance of selecting the appropriate delivery system if CRISPR/Cas9-edited human cells are ultimately to be used clinically.

Materials and methods

Isolation and culture of PLCs and hLSECs

Human placenta-derived mesenchymal stromal cells (PLCs) were isolated as previously described (22). In brief, as per the guidelines from the Office of Human Research Protection at Wake Forest University Health Sciences, human placentas were acquired from full-term deliveries. To isolate the placental stromal/stem cells, the tissue was minced, and enzymatic digestion was carried out, followed by culture in a 37°C humidified incubator with 5% CO_2 in placental cell growth media (PCGM), which consisted of α-minimum essential medium (α-MEM) supplemented with 15% fetal bovine serum (FBS), 19% AmnioMAX, 1% GlutaMAX, and 2.5 μg/mL gentamicin (Thermo Fisher Scientific, Waltham, MA). After 2-3 weeks of culture upon reaching 70-80% confluency, PLCs were passaged with TrypLE (Thermo Fisher Scientific, Waltham, MA) and positively selected for CD117/c-kit using c-kit selection microbeads (Miltenyi Biotec, Auburn, CA, USA) as per manufacturer's protocol. After c-kit selection, cells were seeded at a density of 3000-4000 cells/cm^2 and expanded in PCGM. Primary human liver sinusoid-derived endothelial cells (hLSECs) were purchased at Passage 2 from Lonza and cultured in endothelial growth medium 2 (EGM-2; Lonza, Walkersville, MD) using culture flasks coated with rat tail collagen 1 (Corning, Corning, NY) in a 37°C incubator with 5% CO_2.

Plasmid construction and synthesis

An AAVS1 transgene knock-in vector kit, consisting of the pCas-Guide-AAVS1 (GE100023) and pAAVS1-puro-DNR (GE100024) plasmids, was purchased from OriGene

Technologies, Inc. (Rockville, MD). A "cassette" containing the bioengineered fVIII transgene "lcoET3" under the transcriptional control of the constitutively active human EF1α promoter was cloned into the multiple cloning site (MCS) of the pAAVS1-puro-DNR plasmid using standard restriction enzyme digestion and ligation protocols and reagents (New England Biolabs/NEB, Ipswich, MA). lcoET3 is a liver-codon-optimized chimeric human/porcine fVIII transgene containing a designed to produce bioengineered fVIII with increased FVIII secretion efficiency and activity (22, 36). Both plasmids contain the ampicillin resistance gene. Therefore, they were transfected into competent *E. coli* cells (NEB) using heat shock, and the transformants were plated on LB agar plates containing ampicillin (100 μg/mL). Ampicillin-resistant colonies were plucked 24 hours later and inoculated into LB broth. Once the cultures were expanded, the plasmids from the *E. coli* were isolated using the Plasmid *Plus* Midi kit (Qiagen, Valencia, CA), and restriction enzyme digestion was performed followed by 2% agarose gel electrophoresis to verify the identity and integrity of the plasmid.

CRISPR/Cas9-mediated knock in of fVIII transgene and transfection with lcoET3 plasmid

To carry out CRISPR/Cas9-mediated gene addition of the EF1α-lcoET3 expression cassette into the AAVS1 locus, we utilized the AAVS1 Transgene Knockin kit (OriGene, Cat# GE100027), following the manufacturer's instructions (OriGene Technologies, Inc., Rockville, MD). In brief, PvuI/SpeI were used to cut the EF1α-lcoET3 expression cassette from the pLenti-EF1a-lcoET3 lentivector backbone plasmid. The excised cassette was then inserted into the pAAVS1-Puro-DNR donor template plasmid (OriGene, Cat# GE100024) using CloneEZ® PCR Cloning (Genscript USA, Inc., Piscataway, NJ) to directly insert the modified fragment into the right position while removing the existing CMV promoter. This entire custom cloning procedure was performed by GenScript USA, Inc. To achieve CRISPR/Cas9-mediated insertion of the EF1α-lcoET3 cassette at the AAVS1 site, hLSECs and PLCs were co-transfected with the pAAVS1-EF1α-lcoET3-Puro-DNR donor template plasmid (carrying the EF1α-lcoET3 expression cassette flanked by homology arms to the AAVS1 locus) and the pCas-Guide-AAVS1 plasmid encoding both the sgRNA to the AAVS1 site and Cas9 (OriGene Cat# GE100023) using Turbofectin 8.0 Transfection Reagent, following the manufacturer's instructions (OriGene Technologies, Inc.). Briefly, an appropriate number of PLCs/hLSECs were plated to achieve 50-70% confluency the next day. The following reagents were added in the specified order, mixing as indicated, to 250 μL of Opti-MEM I (Thermo Fisher Scientific, Waltham, MA) to prepare the transfection medium: 1 μg of pCas-Guide-AAVS1, vortex gently; 1 μg of pAAVS1-EF1α-lcoET3-Puro-DNR, vortex gently; and 6 μL of Turbofectin 8.0 (OriGene Technologies, Inc.), pipette gently to mix. The mixture was incubated at room temperature for 15 minutes. The media in the culture was replaced with fresh media, and the transfection medium was added dropwise. The culture flask was gently rocked back-and-forth to distribute the complex and was returned to the 37°C incubator with 5% C02. The cells were cultured for 3 weeks, passing as needed, to dilute out cells with the plasmids in episomal form. PLCs were then selected using puromycin (Gibco, Amarillo, TX). The appropriate puromycin concentration was determined based on a kill curve (0.4 μg/mL for PLCs). A similar procedure was carried out using the pAAVS1-EF1α-lcoET3-Puro-DNR plasmid alone, as a control for gene delivery efficiency arising from transient transfection alone.

Transduction with lentiviral vector encoding lcoET3

Cells were plated to reach 50-60% confluency the following day. Once confirming by microscopy that the cells were healthy, the media was removed and the cells were washed with QBSF-60 (Quality Biologicals, Gaithersburg, MD, USA). This was followed by transduction in QBSF-60 containing 8 μg/mL protamine sulfate (Fresenius Kabi, Lake Zurich, IL) and the third generation self-inactivating lentiviral vector encoding the lcoET3fVIII transgene under the transcriptional control of the constitutive human EF-1α promoter at an MOI (multiplicity of infection) of 7 (additional MOI of 7 after 4 h). After transduction, cells were washed and refed with fresh complete media and passaged three times before analyses were performed.

Determination of vector copy number

The provirus copy number per diploid human genome in lentivector-transduced (LV-lcoET3) cells was determined using the Lenti-X Provirus Quantitation Kit (Takara, Mountain View, CA) according to the manufacturer's protocol. Briefly, genomic DNA was isolated from transduced and non-transduced cells using the NucleoSpin Tissue kit (Takara, Mountain View, CA). Serial dilutions were made with genomic DNA, and qPCR amplification was carried out along with a standard curve derived from serial dilutions of calibrated provirus control template. The raw Ct values of the sample were correlated to the standard curve to determine the provirus copy number per cell. A correction coefficient was also incorporated to compensate for the different PCR sensitivities to amplifying provirus control template only vs. provirus sequence integrated in genomic DNA.

Flow cytometric analysis of cells for TLRs and ER stress molecules

Flow cytometric analysis of PLCs and hLSECs was performed using antibodies for TLR 3,4,7,8,9 (ab45093, ab11227, ab45097, ab58864, Abcam, Cambridge, UK [TLR 3,4,8,9] and IC5875P, R&D Systems [TLR 7]) and BiP/CHOP (Cell Signaling Technology, Danvers, MA). Intracellular staining was performed as per manufacturer's protocol using the Intracellular Flow Cytometry kit (Cell Signaling Technology, Danvers, MA) for TLR 3,7,8,9 and BiP/CHOP. Cells were directly stained and fixed for TLR 4. After processing, cells were analyzed using a BD Accuri C6 flow cytometer, and the data were analyzed using FlowJo Software (BD Biosciences, San Jose, CA). Cells treated with tunicamycin (1 µg/mL overnight for BiP and 2 µg/mL 8 h for CHOP) were used as positive control for ER stress.

Endpoint PCR to detect bioengineered fVIII in gene-modified cells

To determine whether the transgene was present in the gene-modified cells, genomic DNA was isolated post puromycin selection using the DNeasy Mini kit (Qiagen, Valencia, CA). The PCR reaction was carried out in a volume of 50 µL using 200 ng gDNA and primers specific for the lcoET3 fVIII transgene (forward: 5'-TTTCCGTCCTCAGCCGTCGC-3' and reverse: 5'-AGGACAGCTCCACAGCTCCCA-3'). gDNA from unmodified cells was used as a negative control in addition to a no-template water control. The cycle conditions were as follows: 1 cycle of initial denaturation at 94°C for 3 min, followed by 35 cycles of 94°C for 18 s, 60°C for 18 s, and 72°C for 30 s, and final extension at 72°C for 10 min (Platinum Blue Supermix, Invitrogen, Waltham, MA). Agarose (1%) gel electrophoresis was then carried out to visualize the PCR products.

RT-qPCR for assessing FVIII, RFP, and PPP1R12C mRNA expression

RNA was extracted from the cells using RNeasy Mini kit (Qiagen, Valencia, CA, USA). The concentration of RNA was measured using NanoDrop 2000 (Thermo Fisher Scientific, Wilmington, DE, USA), and the integrity of RNA was verified using RNA 6000 Nano kit and 2100 Bioanalyzer (Agilent, Santa Clara, CA, USA). gDNA contamination was eliminated using RQ1 RNase-free DNase (Promega, Madison, WI, USA), and RNA was converted to cDNA using the Omniscript RT kit (Qiagen, Valencia, CA, USA). RT-qPCR was then carried out to compare the expression of endogenous FVIII, exogenous lcoET3, and RFP between unmodified control, LV-lcoET3, plasmid-lcoET3, and CRISPR-lcoET3 cells. RT-qPCR was also performed to compare the expression of *PPP1R12C, the gene encoded by the AAVS1 locus, in PLCs, hLSECs, and human iPSC to assess the accessibility of this region to CRISPR/Cas9-mediated editing in each cell type.* The following sets of gene-specific primers were used for these studies:

lcoET3 transgene:
forward: 5'CTGGGCCCATCTGTGCTGTA-3'
reverse 5'-TCCAAGGTGGTCTTGGCCTG-3'

human FVIII B domain (lcoET3 is B domain-deleted):
forward 5'-TCTCCCGAAACCAGACTTGC-3'
reverse: 5'-GTTCCCTGAAGAAGGCTCCC-3')

human GAPDH (as the housekeeping gene for normalization):
forward 5'-CACTGCTGGGGAGTCCCTGC-3'
reverse 5'-GCACAGGGTACTTTATTGATGG-3'

RFP primer set #1 (Amplicon size = 92 bp):
forward 5'- TCC GAG GGC GAA GGC AAG -3'
reverse 5'- AGG ATG TCG AAG GCG AAG GG -3'

RFP primer set #2 (Amplicon size = 139 bp):
forward 5'- TCA TGT ACG GCA GCA AAG CC -3'
reverse 5'- GTG TCC TGG GTA GCG GTC A -3'

PPP1R12C:
forward 5'-GGCCTGCATTGATGAGAA-3'
reverse 5'-GAGGTACCTGGCGATATCTA-3'

The SYBR green–based TB Green Advantage Mastermix (Takara, Mountain View, CA), along with the primers (200 nM) and cDNA template (100 ng), was added to a MicroAmp Optical 96-well Reaction plate (Thermo Fisher Scientific, Waltham, MA). The PCR reaction was performed using the following settings: 1 cycle of initial denaturation at 95°C for 15 s, followed by 40 cycles of 95°C for 4 s, [60°C for 15 s and 72°C for 10 s, for lcoET3 and hFVIII] or [60°C for 1 minute, for *PPP1R12C* and RFP], and standard melt curve analysis, and the amplification was read using the Quant Studio 3 real-time PCR (Applied Biosystems, Waltham, MA).

Immunofluorescence microscopy for visualizing intracellular FVIII

Cells were grown on chamber slides (Thermo Fisher Scientific, Waltham, MA) to reach 60-70% confluency, and were then fixed

with 4% paraformaldehyde. Immunofluorescence staining for FVIII was performed by permeabilization with 0.2% Triton-X for 15 min, blocking with protein block (Dako, Santa Clara, CA) for 30 min at RT, and incubation at 4°C overnight with a mouse monoclonal anti-human FVIII primary antibody (ESH-8, Sekisui Diagnostics, Burlington, MA) at a dilution of 1:150. The slides were washed the following day and incubated with a goat anti-Mouse AlexaFluor® 594-conjugated secondary antibody (ab150116, Abcam, Cambridge, UK) at a dilution of 1:500. Finally, the nuclei were counterstained with DAPI (1:1000) and coverslips were mounted with ProLong Gold Antifade Mounting Medium (Thermo Fisher Scientific), followed by sealing with clear nail polish. The slides were imaged using either a Leica DM4000B or an Olympus BX63 fluorescence microscope. A control slide, stained with the secondary antibody only, was included to assess the degree of non-specific binding and determine the appropriate exposure settings for image acquisition.

Immunofluorescence microscopy for visualizing intracellular RFP

Cells (unmodified, transfected with pAAVS1-(CMV)-RFP-Puro-DNR, or edited with CRISPR/Cas9 to insert the CMV-RFP expression cassette into the AAVS1 locus) were grown on chamber slides (Thermo Fisher Scientific, Waltham, MA) to reach 60-70% confluency, and were then fixed with 4% paraformaldehyde. Immunofluorescence staining for RFP was performed by permeabilization with 0.2% Triton-X for 15 min, blocking with protein block (Dako, Santa Clara, CA) for 30 min at RT, and incubation at 4°C overnight with a rabbit polyclonal anti-RFP primary antibody (ab167453, Abcam, Cambridge, UK) at a dilution of 1:500. The slides were washed the following day and incubated with a goat anti-Rabbit AlexaFluor® 594-conjugated secondary antibody (A-11072, Thermo Fisher Scientific) at a dilution of 1:500. Finally, the nuclei were counterstained with DAPI (1:1000) and coverslips were mounted with ProLong Gold Antifade Mounting Medium (Thermo Fisher Scientific), followed by sealing with clear nail polish. The slides were imaged using a Leica DM4000B fluorescence microscope. A control slide, stained with the secondary antibody only, was included to assess the degree of non-specific binding and determine the appropriate exposure settings for image acquisition.

aPTT assay to quantify clotting activity of FVIII secreted into cell supernatants

Cells were plated to reach 30-40% confluency the next day. Media was replaced with phenol red-free PCGM/EGM-2 the following day. After 24 h of incubation, the media was collected, centrifuged to remove debris, aliquoted (after proper mixing), and stored at -80°C until they were sent out to perform aPTT (activated partial thromboplastin time) assays. These assays were performed by the Wake Forest Baptist Medical Center Special Hematology Laboratory according to standard clinical procedures, using a Top 300 CTS clinical coagulometer (Instrumentation Laboratories, Bedford, MA, USA). Cell counts were also performed and correlated with the aPTT results, enabling data to be presented as IU/24h/10^6cells.

WGS for assessing integration of lcoET3 fVIII transgene in the AAVS1 locus

Genomic DNA collected from cells was subjected to 2% agarose gel electrophoresis to verify integrity, and concentration was measured using the Qubit 3.0 Fluorometer (Thermo Fisher Scientific, Waltham, MA). Whole genome sequencing (WGS) was carried out with 40X coverage on DNBSEQ™ NGS technology platform by BGI Genomics (Shenzhen, Guangdong, China). The standard NCBI human reference genome GRCh38 (chromosome 19) was downloaded, and the 9 kb CRISPR sequence was inserted using AWK. The reference genome containing the intended insertion sequence was then used to map (FASTQC) the reads from WGS to ascertain whether the lcoET3 expression cassette had been successfully inserted into the AAVS1 locus.

Impact of gene delivery on cell viability

To assess the impact of each gene delivery platform/method on the viability of PLCs and hLSECs, viability of each cell population (n=3) was quantified at various time post-gene delivery using a NucleoCounter® NC-200™ (ChemoMetec, Denmark) or a Countess™ 3 (Invitrogen, Waltham, MA), following the protocols provided by the respective manufacturer.

Statistical analysis

All experimental results are presented as mean +/- the standard error of mean (SEM) with the number of replicates (n) indicated. GraphPad Prism 9 was used to perform all statistical analyses (one-way ANOVA followed by *post hoc* Tukey test), and p-value < 0.05 was considered to be statistically significant.

Results

A diagrammatic overview of the various gene delivery approaches tested in hese studies appears in Figure 1.

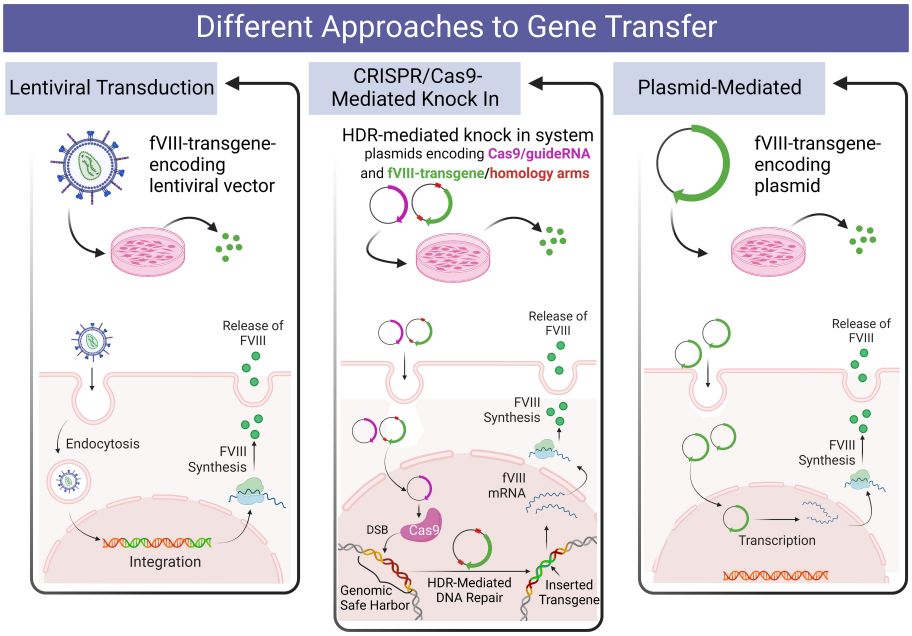

FIGURE 1
Diagrammatic overview of the design of the present studies comparing various methods of delivering a fVIII transgene to human PLCs and hLSECs.

CRISPR/Cas9 engineering using a dual-plasmid system

lcoET3 is a liver-codon-optimized (lco) bioengineered transgene that contains high-expression elements of porcine *F8* (ET3) (36). To achieve insertion of the lcoET3 transgene into the AAVS1 locus, PLCs (n = 5) and hLSECs (n = 3) were transfected with a dual-plasmid system (Figure S1) containing a Cas9/AAVS1 guide RNA-expressing plasmid and a donor plasmid into which the EF1α-lcoET3 expression cassette was commercially cloned (GenScript), between the left and right AAVS1 homologous "arm" sequences. The success of cloning was verified using restriction enzyme digestion (Figure S2).

Endpoint PCR confirms the presence of the lcoET3 transgene in gene-modified cells

Endpoint PCR using primers specific for lcoET3 was performed with genomic DNA isolated from gene-modified cells (LV-lcoET3, CRISPR-lcoET3, and Plasmid-lcoET3) and control (unmodified) cells that were passaged a minimum of 3 times prior to DNA isolation. The PCR products were run on a 1% agarose gel with a 100 bp ladder (New England Biolabs, Ipswich, MA). The lcoET3-specific primers yield a 395 bp amplicon. Figure 2 shows the correct amplicon is present in all gene-modified cells (PLCs: *n*=5, hLSECs: *n*=3), while no product was observed in the unmodified control (N) or the no-template/water control (W).

RT-qPCR detection of lcoET3 expression in gene-modified cells

In order to investigate whether the gene-modified PLCs and hLSECs were expressing lcoET3, the levels of the mRNAs lcoET3 and human GAPDH were quantified in CRISPR-modified, lentivector-transduced, plasmid-transfected, and unmodified cells (passaged a minimum of 3 times prior to RNA isolation) by RT-qPCR using the appropriate transcript-specific primers. The raw Ct values were normalized to GAPDH to obtain a ΔCt value, which was then compared with the negative control (unmodified cells) to obtain each sample's DΔCt value. The formula $2^{-\Delta\Delta Ct}$ was then used to represent the fold-change in expression of the different genes. All gene-modified PLCs (N=3 biological replicates; technical replicates: CRISPR-edited: *n*=5; lentivector-transduced: *n*=3; plasmid transfected: *n*=3) and hLSECs (N=3 biological replicates; technical replicates: CRISPR-edited: *n*=3; lentivector-transduced: *n*=3; plasmid transfected: *n*=3) exhibited detectable levels of lcoET3 mRNA that exceeded the minimal background amplification seen in the unmodified control group (*n*=4) in 4 independent experiments. However, only lentiviral transduction yielded levels of lcoET3 mRNA expression that were statistically elevated above the background seen in control unmodified PLCs and hLSECs. Indeed, the levels of lcoET3 mRNA expression achieved following

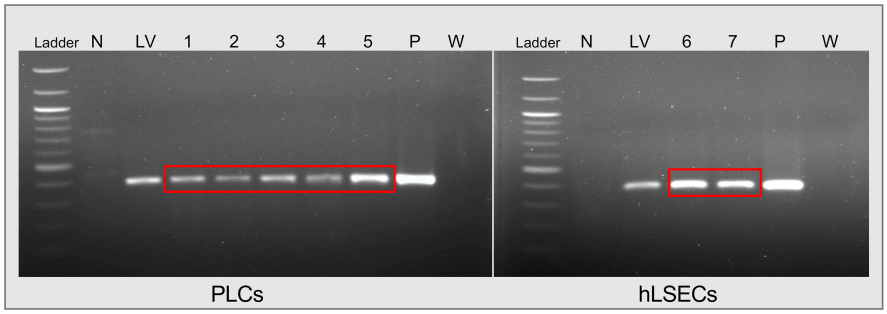

Ladder	100 bp (NEB)
N	Negative Control (Non-transduced)
LV	Positive Control 1 (Lentivirus-transduced)
P	Positive Control 2 (IcoET3 Plasmid only)
W	Water Control
1, 3, 6	Plasmid-IcoET3
2, 4, 5, 7	CRISPR-IcoET3

FIGURE 2
Verification of IcoET3 transgene DNA in gene-modified PLCs and hLSECs using PCR. DNA was extracted from control and gene-modified cells (3 passages after transduction/transfection) and subjected to PCR with primers designed to amplify a 395-bp region within the IcoET3 sequence. Agarose gel electrophoresis was then performed to visualize the size of the PCR products. Unmodified control cells and a reaction containing all constituents of the PCR except for template DNA (water/no-template) were used as negative controls while LV-IcoET3 cells and pure IcoET3 plasmid were used as positive controls.

lentivector transduction were quite robust, being ~5000-times and 800-times that seen in the CRISPR/Cas9-edited PLCs and hLSECs, respectively (Figures 3A, B).

To assess whether IcoET3 expression affected steady-state endogenous FVIII expression in PLCs and/or hLSECs, FVIII mRNA levels were compared between unmodified control and gene-modified cells (Figures 3C, D). No significant change in endogenous FVIII expression was observed after gene modification in either cell type, demonstrating that forced expression of a bioengineered fVIII transgene does not impact expression from the endogenous FVIII locus.

Evaluation of FVIII production and activity

After verifying the expression of IcoET3 FVIII mRNA, immunofluorescence microscopy was used to determine the

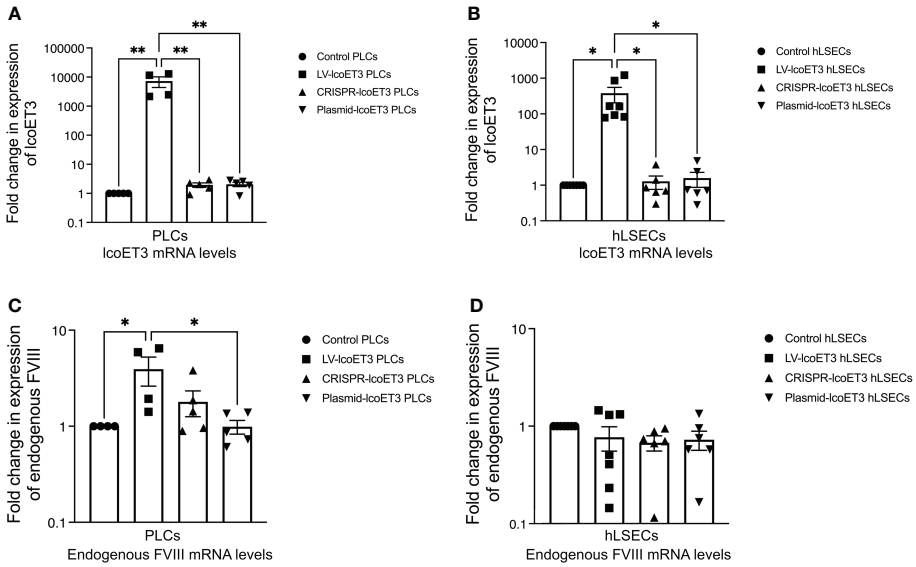

FIGURE 3
Detection of FVIII mRNA levels by RT-qPCR. Relative fold-change in expression of IcoET3 transgene **(A, B)** and endogenous FVIII mRNA **(C, D)** in gene-modified PLCs **(A, C)** and hLSECs **(B, D)** is presented in comparison to unmodified control after normalization to amplification of GAPDH in each respective sample. n = 5 for unmodified/control PLCs, n=4 for LV-IcoET3 PLCs, n = 5 for CRISPR-edited PLCs, n=5 for Plasmid-IcoET3-transfected PLCs; n = 6-8 for all hLSEC treatment groups. *p<0.05; **p<0.01.

presence and levels of lcoET3/FVIII protein in the gene-modified PLCs (Figure 4A) and hLSECs (Figure 4B). As can be seen in these figures, intracellular lcoET3/FVIII protein is readily detected in all groups compared to the negative control (secondary antibody alone), including the unmodified PLCs and hLSECs, both of which constitutively express endogenous FVIII. As was seen at the RNA level, no significant change was seen in the levels of lcoET3/FVIII protein in the CRISPR-edited or plasmid-transfected PLCs or hLSECs, but the lentivector-transduced group (LV-lcoET3) of both PLCs and hLSECs exhibited markedly enhanced levels of lcoET3/FVIII protein. The functionality of the secreted FVIII protein was then measured by performing an activated partial thromboplastin time (aPTT)-based one-stage coagulation assay on cell culture supernatants harvested from cells over the course of 24 h. The coagulation time in this assay is then translated into units of FVIII activity to determine the potential for these cells to correct the disease phenotype. The raw data from the aPTT assay was normalized to the volume of media collected and the cell number present in each sample to yield the final result presented as FVIII IU/10^6 cells/24 h. A significant increase ($p>0.05$) in FVIII activity was only observed in the lentivector-transduced (LV-lcoET3) groups of both cell types (N=3 biological replicates for PLCs and N=2 biological replicates for hLSECs; n=3 technical replicates for PLCs and n=9 technical replicates for hLSECs). In agreement with the RT-qPCR and immunofluorescence data, neither the PLCs (N=5 biological replicates) nor the hLSECs (N=3 biological replicates) that were gene-edited with CRISPR/Cas9 (n=12 technical replicates for PLCs and n=9 for hLSECs) or transfected with the lcoET3 plasmid (n=5 technical replicates for PLCs and n=9 for hLSECs) exhibited a statistically significant increase in FVIII activity over that of unmodified cells (N=3 biological replicates and n=5 technical replicates for PLCs; N=3 biological replicates and n=9 for hLSECs) (Figure 5).

Assessment of whether gene delivery alters viability of PLCs or hLSECs

We next investigated whether gene modification, *via* plasmid transfection, lentivector transduction, or CRISPR/Cas9-mediated editing, PLCs and hLSECs subjected to each gene modification (and unmodified as controls/reference) were analyzed using a NucleoCounter® NC-200™ or a Countess™ 3. No significant difference in viability was observed post gene transfer, irrespective of the method used for gene transfer (data not shown).

Assessment of whether gene delivery dysregulates innate immunity and/or stress molecules

We next investigated whether gene modification induced up-regulation of toll-like receptors (TLR), key molecules in the innate immune response to foreign genetic material (58–60). Flow cytometric analysis demonstrated that unmodified PLCs did not express detectable levels of TLR 3, 4, 7, 8, or 9. However, transfection of PLCs with either the lcoET3-expressing plasmid alone (Plasmid-lcoET3) or with the Cas9 + lcoET3-expressing

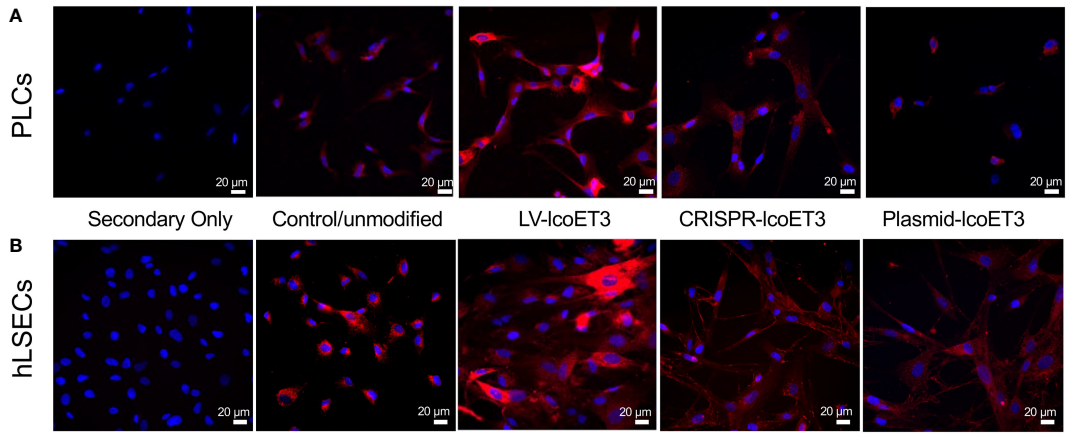

FIGURE 4
Representative images of immunofluorescence analysis of intracellular FVIII protein in unmodified and gene-modified PLCs and hLSECs. PLCs **(A)** and hLSECs **(B)** in each treatment group were stained with a primary antibody specific for FVIII that was then detected with an AlexaFluor® 594-conjugated secondary antibody (red) and nuclei were counterstained with DAPI (blue). Controls consisted of slides with unmodified PLCs and hLSECs stained identically and slides of each cell type stained with secondary antibody alone to establish levels of background fluorescence.

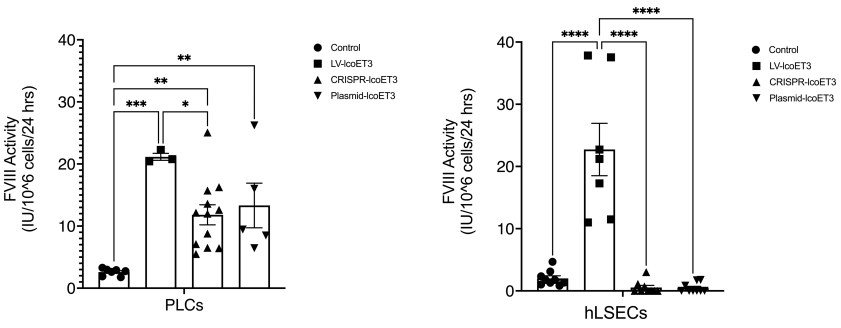

FIGURE 5
Evaluation of FVIII coagulation activity by activated partial thromboplastin time (aPTT) assay performed on 24h culture supernatants after normalization for cell number in each sample. Data are presented as the amount of functional FVIII in International Units (IU) being produced by 10^6 cells in 24h. (**A** – PLCs, **B** – hLSECs). n = 7 for unmodified/control PLCs, n = 3 for LV-lcoET3 PLCs, n = 12 for CRISPR-edited PLCs, and n = 5 for Plasmid-lcoET3-transfected PLCs; n = 7-9 for all hLSEC groups. *p<0.05; **p<0.01; ***p<0.001; ****p<0.0001.

plasmids (CRISPR-lcoET3) resulted in robust up-regulation of TLR 3 and TLR 7 in PLCs, such that > 65% of plasmid-transfected PLCs expressed TLR 3 and > 50% of plasmid-transfected PLCs expressed TLR 7 (Figure 6). Interestingly, transfection with the same plasmids did not elicit upregulation in any of the TLRs in hLSECs. In agreement with what we reported in prior studies with bone marrow-derived mesenchymal stromal cells (61), transduction of PLCs and hLSECs with lentiviral vectors did not induce expression of TLR molecules on a significant percentage of the modified cells (< 2%).

Since FVIII is a relatively large protein and can place significant stress on the endoplasmic reticulum (ER) and the downstream secretory pathway, we used flow cytometry to investigate whether there was an up-regulation in the unfolded protein response (UPR) sentinel chaperone BiP (binding immunoglobulin protein) and downstream signaling proapoptotic protein C/EBP homologous protein (CHOP) (17, 33, 62, 63). Tunicamycin-treated cells were used as positive controls. Compared to the unmodified control cells, the only groups that exhibited a significantly increased percentage of cells expressing BiP were the positive controls and the PLCs that were transfected with plasmids (CRISPR-lcoET3 and Plasmid-lcoET3) (Figure 7). With respect to CHOP, only the positive control group showed a significantly increased percentage of cells expressing this stress molecule. The percentages of cells expressing both BiP and CHOP were very low (<2%) in all other groups.

Whole genome sequencing to assess integration at AAVS1 site

Given that the RT-qPCR, immunofluorescence, and aPTT data did not suggest we had successfully inserted the EF1α-

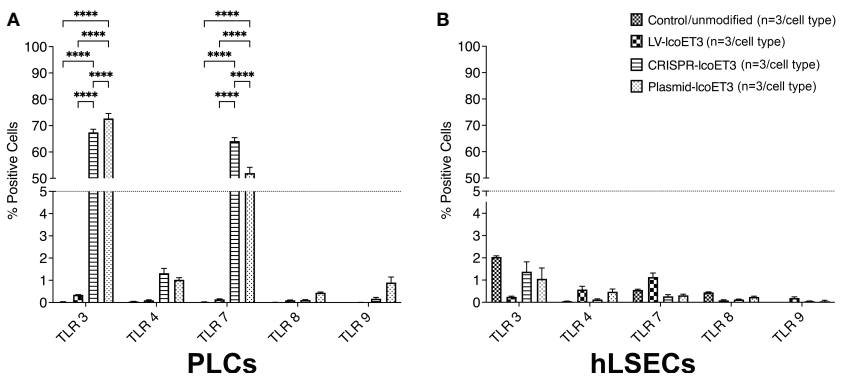

FIGURE 6
Flow cytometric analysis to quantify expression of Toll-like receptors (TLRs) on unmodified and gene-modified PLCs **(A)** and hLSECs **(B)**. n = 3/experimental group for each cell type. ****p<0.0001.

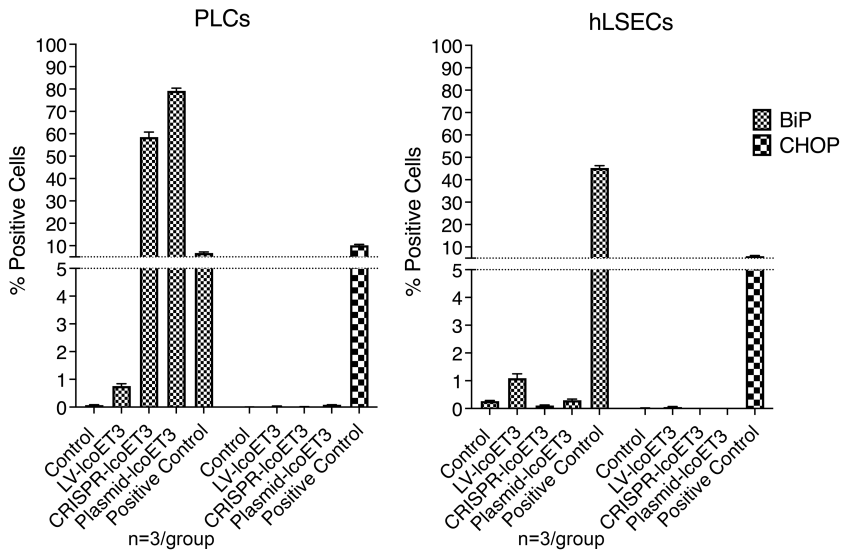

FIGURE 7
Flow cytometric analysis to quantify expression of ER stress molecules BiP and CHOP in unmodified and gene-modified PLCs (left panel) and hLSECs (right panel). Cells treated with tunicamycin were used as positive controls for ER stress. n=3/experimental group for each cell type.

lcoET3 expression cassette into the AAVS1 genomic locus, yet the endpoint PCR demonstrated the presence of DNA for the lcoET3 transgene within the CRISPR-edited PLCs that had been selected in puromycin, we next performed whole genome sequencing (WGS) on DNA from the putatively CRISPR-edited PLCs at 40x coverage and aligned the reads to a reference genome that had been modified *in silico* to contain the putative insertion at the AAVS1 site. As can be seen in Figure 8, these analyses did not demonstrate any significant coverage/alignments in this region, thus providing sequence-level proof for the apparent failure to successfully achieve CRISPR-mediated insertion of the EF1α-lcoET3 cassette at the AAVS1 locus in the PLCs.

Evaluation of whether the inaccessibility of the AAVS 1 locus and/or the size of the lcoET3 expression cassette are factors limiting CRISPR/Cas9-mediated gene editing in PLCS and hLSECs

As recent studies have shown that CRISPR/Cas9 can be used to introduce a GFP reporter into several different genetic loci (AAVS1 was not tested) in human mesenchymal stromal cells (MSC) (64), which are presumably similar to the mesenchymal PLCs used in the present studies, we performed studies to determine whether the accessibility/transcriptional activity of the AAVS1 genomic locus and/or the large size of the lcoET3 expression cassette might be responsible for the lack of CRISPR/Cas9-mediated insertion of the lcoET3 cassette into the AAVS1 locus of the PLCs and hLSECs. To address the first of these possibilities, we performed RT-qPCR on RNA isolated from human PLCs and hLSECs with primers specific to *PPP1R12C*, the gene encoded by the AAVS1 locus, comparing expression levels of this gene in these two cell types to that in human iPSCs, cells which are known to be highly amenable to CRISPR/Cas9-mediated gene knockin at the AAVS1 locus (65, 66). Relative levels of expression in each cell type were then calculated using the ΔCt method, with GAPDH serving as a reference. As can be seen in Figure 9, these studies revealed that the AAVS1 locus is significantly less accessible/transcriptionally active in both PLCs and hLSECs when compared to human iPSCs, providing a plausible explanation for why these cells might be more challenging to edit than iPSCs, but not explaining why they did not exhibit any editing.

Another factor which could be precluding editing at this locus in the PLCs and hLSECs is the size of the lcoET3 expression cassette being inserted. Indeed, prior studies in human umbilical cord-derived mesenchymal stromal cells (MSC - PLCs are mesenchymal in nature) showed that a donor vector encoding GFP mediated far more efficient CRISPR/Cas9-mediated editing at the AAVS1 site than the identical donor vector encoding the marginally larger sRAGE gene (67). Given the very large size of the lcoET3 expression cassette (~5,600 bp), we performed experiments to address whether the cassette size was playing a role in the observed lack of editing. Specifically, we attempted to insert a red fluorescence protein (RFP) expression cassette (< ¼ the size of the lcoET3 cassette) into the AAVS1 locus of PLCs and hLSECs using CRISPR/Cas9. To this end, we performed experiments

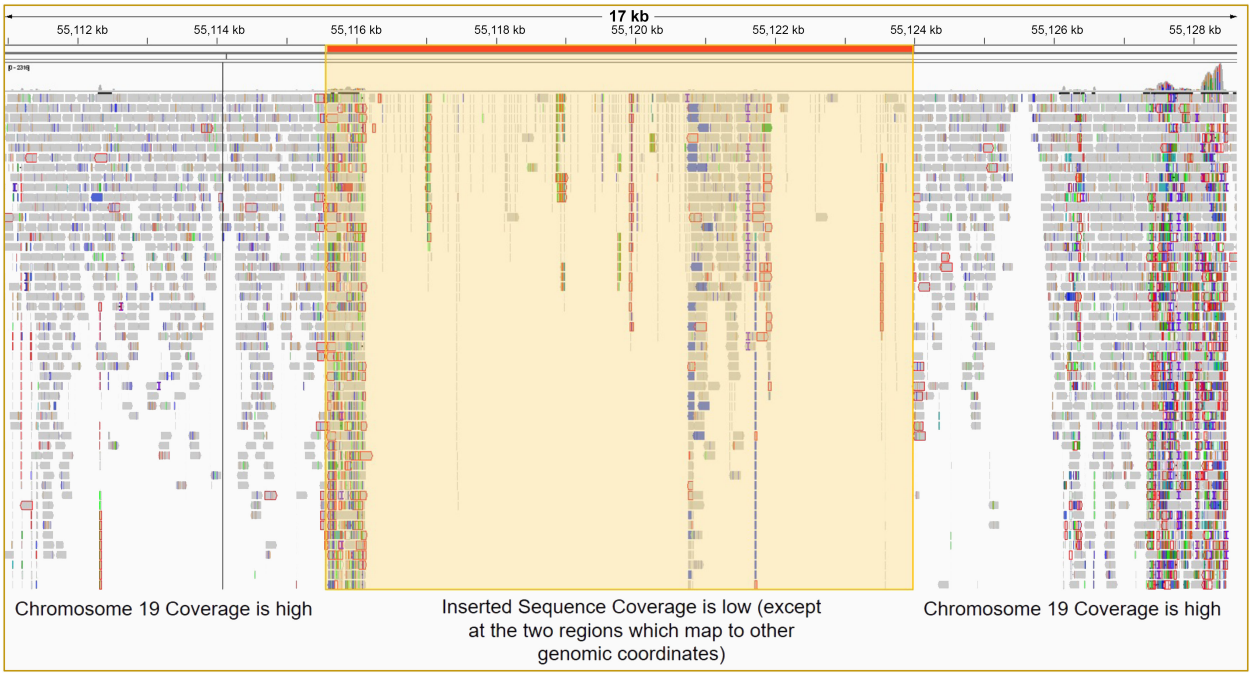

FIGURE 8
Whole genome sequencing (WGS) of PLCs to determine whether CRISPR/Cas9 editing led to successful insertion of the EF1α-lcoET3 expression cassette at the AAVS1 genomic locus. After ensuring DNA integrity, WGS was performed with 40X coverage using the DNBSEQ™ NGS platform, and the sequence reads were aligned to a standard reference human genome containing the inserted sequence at the desired locus.

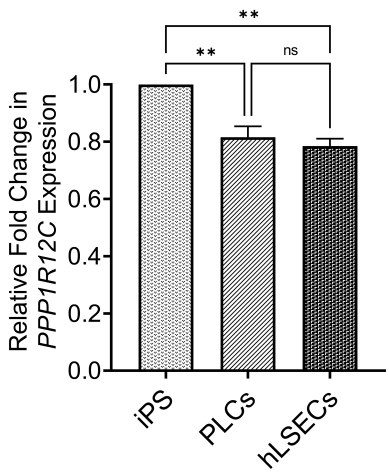

FIGURE 9
Graphical summary of expression levels of the *PPP1R12C* gene encoded by the AAVS1 locus to assess accessibility of locus for CRISPR/Cas9-mediated editing. RNA isolated from PLCs, hLSECs, and human iPSCs was subjected to RT-qPCR with primers specific to *PPP1R12C* and GAPDH as a reference. Relative fold-change in expression in PLCs and hLSECs is presented in comparison to human iPS cells after normalization with GAPDH as the housekeeping gene (n=3 for each cell type). Data are presented as mean plus/minus SEM; **p<0.01. ns, Not-significant.

identical to those detailed above, co-transfecting PLCs and hLSECs with the pCas-Guide-AAVS1 plasmid (encoding both the sgRNA to the AAVS1 site and Cas9) and the pAAVS1-RFP-Puro-DNR donor template plasmid (the identical donor template plasmid used to achieve insertion of the lcoET3 expression cassette, but the lcoET3 expression cassette was replaced with a much smaller expression cassette encoding RFP). As in the experiments with the lcoET3 cassette, each cell type was also transiently transfected with the pAAVS1-RFP-Puro-DNR donor template plasmid alone. At 72 hours post-transfection (for the transient transfection groups; *n*=3 technical replicates for each cell type) and after selection in puromycin (for the CRISPR/Cas9-edited groups; *n*=3 technical replicates for each cell type), cells were passed to chamber slides and analyzed by immunofluorescence with an antibody specific to RFP. As can be seen in Figure 10, both transiently transfected and CRISPR/Cas9-edited, puromycin-selected PLCs and hLSECs exhibited robust staining for RFP, while unmodified PLCs and hLSECs did not, confirming successful uptake of the plasmid into both cell types and verifying that both cell types can be edited at the AAVS1 locus *via* CRISPR/Cas9. To further confirm CRISPR/Cas9-mediated editing of PLCs and hLSECs, RNA was isolated from an aliquot of each cell type at the time of plating for immunofluorescence and RT-qPCR performed with primers specific for RFP. The resultant PCR products were then run

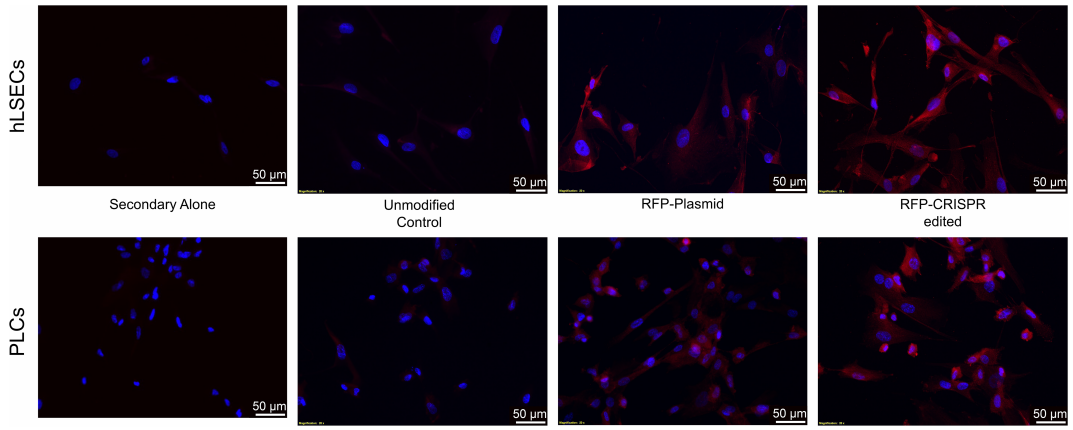

FIGURE 10
Immunofluorescence analysis of intracellular RFP protein in unmodified and gene-modified PLCs and hLSECs. PLCs (top panel) and hLSECs (bottom panel) in each experimental group were stained with a primary antibody for RFP that was then detected with an AlexaFluor® 594-conjugated secondary antibody (red) and nuclei were counterstained with DAPI (blue). Controls consisted of slides with unmodified PLCs and hLSECs stained identically (labeled "controls") and slides of each cell type stained with secondary antibody alone to establish levels of background fluorescence.

on an agarose gel and visualized with ethidium bromide. An image of the resultant gel appears in Figure 11, which clearly shows the correctly sized RFP amplicon in the puromycin-selected CRISPR/Cas9-edited PLCs and hLSECs, and its absence in both the unmodified and transiently transfected PLCs and hLSECs after 3 passages in culture. Collectively, these studies confirm hat the AAVS1 locus is a suitable target for gene knockin in both PLCs and hLSECs, and they support the conclusion that the large size of the lcoET3 expression cassette was likely the factor that precluded its knockin into this locus in PLCs and hLSECs.

Discussion

As a monogenic disease, HA is an ideal candidate for correction by gene therapy. While current clinical trials are employing direct injection of AAV-based vectors (7–13), the use of gene-modified cells as vehicles to accomplish gene "addition" has many advantages from a manufacturing standpoint, as it allows multiple safeguards to be added to the production process (57). In an effort to make cell-based gene therapy a clinical reality for HA, we and others have performed studies over the past decades to identify the ideal cell type for delivering a fVIII transgene and the optimal vector to introduce the fVIII transgene into the desired cell population (3, 22, 31, 34, 37–48). Previously, we demonstrated the advantages of using lentivector-transduced PLCs as the cellular vehicle for delivering a fVIII transgene (22, 68). The present study evaluated whether CRISPR/Cas9 could be used to deliver an EF1α-lcoET3 expression cassette into PLCs, with the hope of further enhancing safety by directing integration to the AAVS1 "safe harbor" genome locus, thereby eliminating the theoretical risk of insertional mutagenesis that is inherent to integrating vectors such as those based upon lentiviruses. Furthermore, as the AAVS1 site is thought to be a transcripionally active site with open chromatic structure and native insulators that can resist transgene silencing, it stood to reason that the use of CRISPR/Cas9 to introduce the EF1α-lcoET3 expression cassette into this site might also enhance the levels of expression of the fVIII transgene and thus improve therapeutic efficacy (55). As there are thousands of different mutations spanning the whole FVIII gene locus that can cause HA (69), the use of this "knock-in" approach to insert a functional fVIII transgene into the genome, rather than trying to correct a specific HA-causing mutation, was deemed to be far more practical, as it would yield a universal treatment that could be administered to all HA patients. PLCs were simultaneosuly modified with two common modes of gene delivery, lentivector transduction and transfection with lcoET3-expressing plasmid, and side-by-side comparisons performed to results obtained with CRISPR/Cas9 gene-editing.

Although a good deal of progress has been made using CRISPR/Cas9-mediated gene editing to correct hemophilia B (HB), only a few studies have reported using this approach to attempt to correct HA (70–79), due in large part to the difficulty of achieving CRISPR/Cas9-mediated knock-in of a transgene with the increased length and complexity of FVIII (80, 81). The studies published to-date using CRISPR/Cas9 to correct HA have employed iPSCs, which enables selection of clones that have been edited successfully, which can then be differentiated into the desired cell types, such as endothelial cells or mesenchymal stromal cells (MSC) that can then be transplanted to mediate

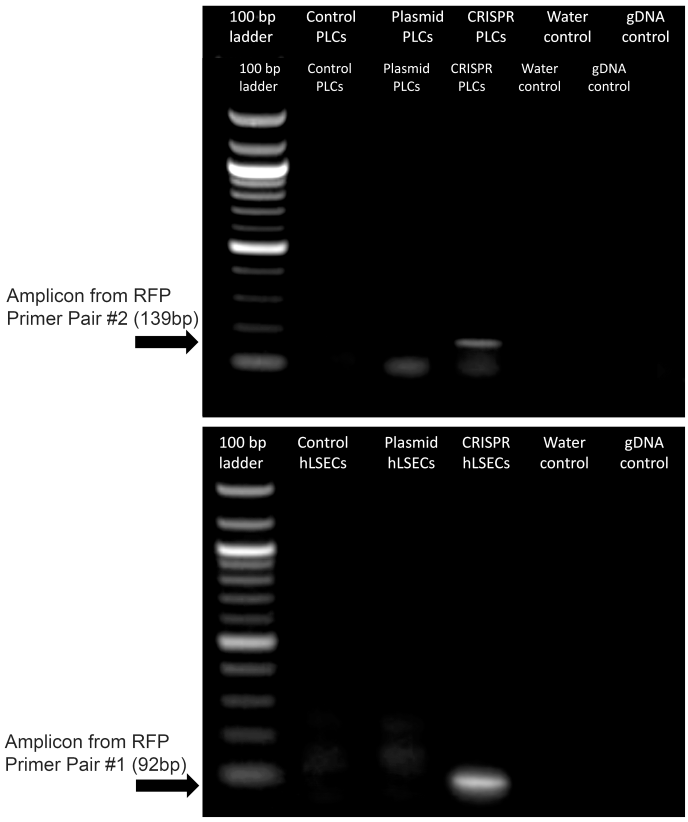

FIGURE 11
Expression of RFP in gene-modified PLCs and hLSECs by RT-qPCR. RNA was isolated from PLCs and hLSECs that were unmodified, transiently transfected with a plasmid encoding RFP, or had RFP permanently knocked-in *via* CRISPR/Cas9-mediated editing. RNA was isolated from the transfected cells after culture expansion and 3 passages and from the CRISPR/Cas9 edited cells following puromycin selection. RNA was then subjected to RT-qPCR and the resultant PCR products run on an agarose gel. Controls included no template/water and genomic DNA to confirm complete elimination of any contaminating gDNA by the RNase-free DNase step.

phenotypic correction (74–76, 82–87). The use of iPSC also has the added advantage of the ease with which these cells can be modified with genome-editing platforms, such as CRISPR/Cas9, that require induction of a doublestrand break (DSB) following by homologous recombination repair (HRR), a process that only occurs in actively dividing cells (88–92). The present study sought to determine whether it is possible to achieve similar success when the CRISPR/Cas9 system is used to insert a fVIII transgene cassette into a safe harbor in the genome of two primary, not iPSC-derived, cell types that are of direct clinical relevance to treating HA, human placental MSC (PLCs) (22) and human liver sinusoid-derived endothelial cells (hLSECs), the main cell type in the body responsible for synthesizing endogenous FVIII (93). In parallel, studies were performed using a lentivector and a plasmid to deliver this same cassette to PLCs and hLSECs to enable a side-by-side comparison of the efficacy of each approach.

The results reaffirm the potential of PLCs and hLSECs as cellular vehicles for delivering a fVIII transgene, showing both cell types can be transduced with a lentivector at high efficiency and subsequently express and secrete clinically meaningful levels of biologically active FVIII. Moreover, by using a bioengineered fVIII transgene (lcoET3) that contains elements from the porcine sequence that are known to facilitate ER trafficking (22, 33–36), these high levels of FVIII expression occur without induction of the stress response that can occur when misfolded FVIII accumulates in the ER (17, 33, 62, 63). This is an important finding, cells that are stressed as a result of over-expressing FVIII would not be predicted to engraft efficiently and survive long-term to provide sustained FVIII production and therapeutic effect. In addition, in similarity to what we previously reported in bone marrow-derived MSC (61), the use of lentivectors allows highly efficient gene delivery without evoking an innate immune response, as evidenced by the lack of expression of any of the TLRs in either PLCs or hLSECs following transduction with LV-lcoET3. Taken together, our results demonstrate that lentivector-mediated lcoET3 transgene delivery is a promising approach to engineer PLCs and hLSECs for cell-based fVIII delivery to treat HA.

In contrast to the results obtained with lentivector-mediated transduction, the transfection of plasmids designed to mediate the site-specific insertion of the EF1α-lcoET3 expression cassette into the AAVS1 genome locus *via* CRISPR/Cas9 revealed that primary human PLCs and LSECs are both highly refractory to such manipulation. Although endpoint PCR demonstrated the presence of DNA for the lcoET3 transgene in both cell types following attempts at gene-editing, neither cell type expressed appreciable levels of ET3 mRNA or protein, nor did they secrete significant levels of biologically active FVIII. Whole genome sequencing of PLCs followed by extensive bioinformatics analysis of the AAVS1 locus confirmed the absence of successful insertion of the EF1α-lcoET3 expression cassette at this site. The failure of CRISPR/Cas9 to mediate insertion of the EF1α-lcoET3 cassette is surprising given prior gene-editing successes by other groups with both FIX and FVIII (70–87) and prompted us to perform further studies to understand the factors responsible for the lack of successful knockin at the AAVS1 locus in the PLCs and hLSECs. The first factor we investigated for its possible role in the recalcitrance of PLCs to gene-editing was the site selected for gene insertion. While AAVS1 is considered to be a quintessential "safe harbor" locus, and has been used successfully in many studies, the accessibility of this locus in PLCs is unknown, and no gene expression data have been published that provide any hint as to whether the *PPP1R12C* gene encoded within the AAVS1 region is transcriptionally active in PLCs, or in MSC from any other tissue. Importantly, in a recent report (64) in which Cas9 was used to successfully insert PDGF-BB and VEGFA expression cassettes into MSC from bone marrow, adipose tissue, and umbilical cord blood, 3 different safe harbors were used for insertion, but not the AAVS1 site. To assess the basal transcriptional activity of this locus in PLCs and hLSECs when compared to iPSCs, which are highly amenable to gene knockin at this locus (65, 66), we performed RT-qPCR to quantitate expression of the *PPP1R12C*. These studies revealed significantly lower expression from this locus in PLCs and hLSECs, suggesting that the chromatin conformation in these cells may render them less amenable to CRISPR/Cas9-mediated knockin at this locus. Another contributing factor to the lack of gene editing in PLCs and hLSECs could be their markedly lower proliferative state when compared to the iPS cells that were employed in prior studies using CRISPR/Cas9 to knockin FIX or FVIII cassettes (70–87). Given that HRR only occurs in actively dividing cells (88–92), the PLCs and hLSECs used in the present study may not be ideally suited for HRR-mediated gene insertion, as their proliferation rate is markedly lower than that of iPS cells. This is especially true for the hLSECs, which exhibit very slow division kinetics and cannot be propagated for more than a couple of passages *in vitro* prior to senescing. The PLCs employed in the present study exhibit a phenotype and biological properties that closely resemble that of MSC from other tissues (3, 22, 68). It is noteworthy that prior studies have reported the downregulation of components of the DNA damage response (DDR) and HRR pathways in MSC with time in culture (94–96). As such, it is possible that the PLCs used in the present study, having been first cultured by explant, then selected for c-kit, and finally expanded for gene modification, no longer expressed sufficient levels of some of the key players in the HRR pathway required for efficient CRISPR/Cas9 gene-editing to occur.

Another key aspect that differs between the current report and prior studies in which MSCs were successfully edited with CRISPR/Cas9 (64, 67) is that the PDGF-BB, VEGFA, and GFP expression cassettes being inserted were substantially smaller than the EF1α-lcoET3 cassette employed in the present report. Prior studies have shown that it is far easier to achieve insertion of large inserts using NHEJ-mediated pathways than HRR (78). To ascertain whether the size of the EF1α-lcoET3 cassette played a role in the inability to achieve successful knockin at the AAVS1 locus in PLCs and hLSECs, we performed identical experiments using the same donor template, but replacing the EF1α-lcoET3 cassette with a much smaller CMV-RFP expression cassette. Both RT-qPCR and immunofluorescence data confirm that successful CRISPR/Cas9-mediated knockin of this smaller cassette can be achieved in both PLCs and hLSECs, supporting the conclusion that the large size of the EF1α-lcoET3 cassette was a major contributor to the apparent refractoriness of these cells to CRISPR/Cas9-mediated editing. One future avenue to explore would be to thoroughly characterize the PLCs and hLSECs with respect to their primary DNA repair pathways and/or to use cell cycle regulators such as Nocodazole and CCND1 (77) to induce specific pathways in an effort to improve the efficiency of CRISPR/Cas9-mediated knock-in of the very large EF1α-lcoET3 cassette into the AAVS1 locus of these cells.

It is also worth noting that the authors of the recent aforementioned MSC-editing study (64) used an AAV-based platform to deliver the gene-editing components, rather than transfection, as was employed in the present report. This likely improved efficiency of delivery of the gene-editing machinery. In addition, data presented herein demonstrate that the use of plasmids to deliver the CRISPR/Cas9 components led to dramatic up-regulation of TLR 3 and TLR 7 in PLCs, and it also triggered ER stress, as evidenced by upregulation of BiP. While the low levels of mRNA for the fVIII transgene argue that ER stress was not likely the cause of low secreted FVIII activity, the upregulation of ER stress is obviously not desirable, as it will likely negatively impact the viability and functionality of the PLCs, precluding their use in cell therapy. The upregulation of TLR 3 and TLR 7 by the plasmids would also likely compromise one of the key attributes of PLCs for use as an off-the-shelf therapy, namely, their state of relative immune-inertness, a conclusion supported by our recent report showing activation of PLCs leads to production of γ-IFN (68). As such, another lucrative avenue for future studies would be the redesign of the

plasmids to remove any bacterial sequences that might be serving as pathogen-associated molecular patterns (PAMPs) and be responsible for recognition by the TLRs within the PLCs.

In summary, PLCs and hLSECs transduced with a lentivector encoding a bioengineered, expression/secretion-optimized fVIII transgene exhibit durable and robust FVIII expression and clotting activity without triggering innate immunity or ER stress molecules. Although the primary objective of inserting the lcoET3 transgene cassette into the AAVS1 site in PLCs and hLSECs *via* CRISPR/Cas9 was not achieved, the results presented herein provide mechanistic insight into the factors that precluded knockin of this cassette at this locus in these two cell types, and they validate the utility of both cell types as delivery vehicles for a fVIII transgene. Moreover, these data highlight the hurdles that remain to be overcome before primary human cells can be gene-edited with sufficient efficiency and the then be expanded to clinically relevant numbers for use in cell-based gene therapy to treat HA.

Data availability statement

The original contributions presented in the study are included in the article/Supplementary Material. Further inquiries can be directed to the corresponding author.

Ethics statement

The studies involving human participants were reviewed and approved by Institutional Review Board. The patients/participants provided their written informed consent to participate in this study.

Author contributions

RR, MR, executed experiments, data analysis and interpretation; DM, AF, HCA, CL, CB provided technical expertise; CB, JS, and CB provided reagents; CBD, HTS, AA provided reagents and experimental feedback; RR drafted manuscript; GAP and CDP conception and experimental design, supervised experiments, wrote final version of the manuscript, and secured funding. All authors contributed to the article and approved the submitted version.

Funding

This work was supported by NIH, NHLBI, HL135853, HL148681 MR and GA-P are the recipients of a fellow/mentor HHMI Gilliam Graduate Fellowships grant.

Acknowledgments

We would like to thank Wake Forest Baptist Health Special Hematology Laboratory for their excellent technical support and the performance of FVIII testing, and the Wake Forest Institute for Regenerative Medicine Manufacturing Center for providing the PLCs used in these studies.

Conflict of interest

Authors CD and HS are co-founders of Expression Therapeutics, Inc. and own equity in the company. Dr. Denning is an employee of Expression Therapeutics, Inc. Expression Therapeutics licensed the intellectual property associated with the codon optimized ET3 transgene and HCB promoter. The terms of this arrangement have been reviewed and approved by Emory University in accordance with its conflict-of-interest policies.

The remaining authors declare that the research was conducted in the absence of any commercial or financial relationships that could be construed as a potential conflict of interest.

Publisher's note

Supplementary material

The Supplementary Material for this article can be found online at: https://www.frontiersin.org/articles/10.3389/fimmu.2022.954984/full#supplementary-material

References

1. Mehta P, Mehta P, Reddivari AKR. *Hemophilia*. Treasure Island (FL: StatPearls Publishing (2021). Available at: https://www.ncbi.nlm.nih.gov/books/NBK551607/.

2. Hemophilia a - an overview of symptoms, genetics, and treatments to help you understand hemophilia a. (2022). Available at: https://www.hemophilia.org/bleeding-disorders-a-z/types/hemophilia-a.

3. Stem C, Rodman C, Ramamurthy RM, George S, Meares D, Farland A, et al. Investigating optimal autologous cellular platforms for prenatal or perinatal factor VIII delivery to treat hemophilia a. *Front Cell Dev Biol* (2021) 9:678117. doi: 10.3389/fcell.2021.678117

4. Chen SL. Economic costs of hemophilia and the impact of prophylactic treatment on patient management. *Am J Manag Care* (2016) 22(5 Suppl):s126–33. doi: 10.3111/13696998.2015.1016228

5. Ragni MV. Hemophilia as a blueprint for gene therapy. *Science* (2021) 374 (6563):40–1. doi: 10.1126/science.abg0856

6. Castaman G, Matino D. Hemophilia a and b: Molecular and clinical similarities and differences. *Haematologica* (2019) 104(9):1702–9. doi: 10.3324/haematol.2019.221093

7. Batty P, Lillicrap D. Gene therapy for hemophilia: Current status and laboratory consequences. *Int J Lab Hematol* (2021) 43(Suppl 1):117–23. doi: 10.1111/ijlh.13605

8. High KA. Gene therapy for hemophilia: The clot thickens. *Hum Gene Ther* (2014) 25(11):915–22. doi: 10.1089/hum.2014.2541

9. High KA, George LA, Eyster ME, Sullivan SK, Ragni MV, Croteau SE, et al. A phase I/II trial of investigational spk-8011 in hemophilia a demonstrates durable expression and prevention of bleeds. *Blood* (2018) 132:487. doi: 10.1182/blood-2018-99-115495

10. George LA, Monahan PE, Eyster ME, Sullivan SK, Ragni MV, Croteau SE, et al. Multiyear factor VIII expression after AAV gene transfer for hemophilia a. *N Engl J Med* (2021) 385(21):1961–73. doi: 10.1056/NEJMoa2104205

11. Pasi KJ, Rangarajan S, Mitchell N, Lester W, Symington E, Madan B, et al. Multiyear follow-up of AAV5-hFVIII-SQ gene therapy for hemophilia a. *N Engl J Med* (2020) 382(1):29–40. doi: 10.1056/NEJMoa1908490

12. Rosen S, Tiefenbacher S, Robinson M, Huang M, Srimani J, Mackenzie D, et al. Activity of transgene-produced b-domain-deleted factor VIII in human plasma following AAV5 gene therapy. *Blood* (2020) 136(22):2524–34. doi: 10.1182/blood.2020005683

13. O'Mahony B, Mahlangu J, Peerlinck K, Wang J, Lowe G, Tan CW, et al. Health-related quality of life following valoctocogene roxaparvovec gene therapy for severe hemophilia a in the phase 3 trial GENEr8-1. *Blood* (2021) 138:4916a. doi: 10.1182/blood-2021-146021

14. Brommel CM, Cooney AL, Sinn PL. Adeno-associated virus-based gene therapy for lifelong correction of genetic disease. *Hum Gene Ther* (2020) 31(17-18):985–95. doi: 10.1089/hum.2020.138

15. Morgan J, Muntoni F. Changes in myonuclear number during postnatal growth - implications for AAV gene therapy for muscular dystrophy. *J Neuromuscul Dis* (2021) 8(s2):S317–24. doi: 10.3233/JND-210683

16. Porada CD, et al. Hemophilia a: An ideal disease to correct in utero. *Front Pharmacol* (2014) 5:276. doi: 10.3389/fphar.2014.00276

17. Zolotukhin I, et al. Potential for cellular stress response to hepatic factor VIII expression from AAV vector. *Mol Ther Methods Clin Dev* (2016) 3:16063. doi: 10.1038/mtm.2016.63

18. Kaufman RJ. Post-translational modifications required for coagulation factor secretion and function. *Thromb Haemost* (1998) 79(6):1068–79. doi: 10.1055/s-0037-1615018

19. Murphy SV, Atala A. Amniotic fluid and placental membranes: Unexpected sources of highly multipotent cells. *Semin Reprod Med* (2013) 31(1):62–8. doi: 10.1055/s-0032-1331799

20. Bonomi A, Silini A, Vertua E, Signoroni PB, Coccè V, Cavicchini L, et al. Human amniotic mesenchymal stromal cells (hAMSCs) as potential vehicles for drug delivery in cancer therapy: An *in vitro* study. *Stem Cell Res Ther* (2015) 6 (1):155. doi: 10.1186/s13287-015-0140-z

21. Magatti M, et al. The immunomodulatory properties of amniotic cells: The two sides of the coin. *Cell Transplant* (2018) 27(1):31–44. doi: 10.1177/0963689717742819

22. El-Akabawy N, Rodriguez M, Ramamurthy R, Rabah A, Trevisan B, Morsi A, et al. Defining the optimal FVIII transgene for placental cell-based gene therapy to treat hemophilia a. *Mol Ther Methods Clin Dev* (2020) 17:465–77. doi: 10.1016/j.omtm.2020.03.001

23. Rosenberg JB, Foster PA, Kaufman RJ, Vokac EA, Moussalli M, Kroner PA, et al. Intracellular trafficking of factor VIII to von willebrand factor storage granules. *J Clin Invest* (1998) 101(3):613–24. doi: 10.1172/JCI1250

24. Shi Q, et al. Targeting FVIII expression to endothelial cells regenerates a releasable pool of FVIII and restores hemostasis in a mouse model of hemophilia a. *Blood* (2010) 116(16):3049–57. doi: 10.1182/blood-2010-03-272419

25. Terraube V, O'Donnell JS, Jenkins PV. Factor VIII and von willebrand factor interaction: Biological, clinical and therapeutic importance. *Haemophilia* (2010) 16(1):3–13. doi: 10.1111/j.1365-2516.2009.02005.x

26. Kaveri SV, Dasgupta S, Andre S, Navarrete AM, Repessé Y, Wootla B, et al. Factor VIII inhibitors: Role of von willebrand factor on the uptake of factor VIII by dendritic cells. *Haemophilia* (2007) 13 Suppl 5:61–4. doi: 10.1111/j.1365-2516.2007.01575.x

27. Lacroix-Desmazes S, et al. The role of VWF in the immunogenicity of FVIII. *Thromb Res* (2008) 122 Suppl 2:S3–6. doi: 10.1016/S0049-3848(08)70002-1

28. High K. Gene transfer for hemophilia: can therapeutic efficacy in large animals be safely translated to patients? *J Thromb Haemost* (2005) 3(8):1682–91. doi: 10.1111/j.1538-7836.2005.01460.x

29. High KA. Gene transfer as an approach to treating hemophilia. *Semin Thromb Hemost* (2003) 29(1):107–20. doi: 10.1055/s-2003-37945

30. High KA. Gene therapy for haemophilia: a long and winding road. *J Thromb Haemost* (2011) 9 Suppl 1:2–11. doi: 10.1111/j.1538-7836.2011.04369.x

31. Brown HC, et al. Target-Cell-Directed bioengineering approaches for gene therapy of hemophilia a. *Mol Ther Methods Clin Dev* (2018) 9:57–69. doi: 10.1016/j.omtm.2018.01.004

32. McIntosh J, Lenting PJ, Rosales C, Lee D, Rabbanian S, Raj D, et al. Therapeutic levels of FVIII following a single peripheral vein administration of rAAV vector encoding a novel human factor VIII variant. *Blood* (2013) 121 (17):3335–44. doi: 10.1182/blood-2012-10-462200

33. Brown HC, Gangadharan B, Doering CB. Enhanced biosynthesis of coagulation factor VIII through diminished engagement of the unfolded protein response. *J Biol Chem* (2011) 286(27):24451–7. doi: 10.1074/jbc.M111.238758

34. Doering CB, Denning G, Dooriss K, Gangadharan B, Johnston JM, Kerstann KW, et al. Directed engineering of a high-expression chimeric transgene as a strategy for gene therapy of hemophilia a. *Mol Ther* (2009) 17(7):1145–54. doi: 10.1038/mt.2009.35

35. Doering CB, et al. Identification of porcine coagulation factor VIII domains responsible for high level expression *via* enhanced secretion. *J Biol Chem* (2004) 279(8):6546–52. doi: 10.1074/jbc.M312451200

36. Zakas PM, Brown HC, Knight K, Meeks SL, Spencer HT, Gaucher EA, et al. Enhancing the pharmaceutical properties of protein drugs by ancestral sequence reconstruction. *Nat Biotechnol* (2017) 35(1):35–7. doi: 10.1038/nbt.3677

37. Chuah MK, et al. Bone marrow stromal cells as targets for gene therapy of hemophilia a. *Hum Gene Ther* (1998) 9(3):353–65. doi: 10.1089/hum.1998.9.3-353

38. Chuah MK, Van Damme A, Zwinnen H, Goovaerts I, Vanslembrouck V, Collen D, et al. Long-term persistence of human bone marrow stromal cells transduced with factor VIII-retroviral vectors and transient production of therapeutic levels of human factor VIII in nonmyeloablated immunodeficient mice. *Hum Gene Ther* (2000) 11(5):729–38. doi: 10.1089/10430340050015626

39. Doering CB. Retroviral modification of mesenchymal stem cells for gene therapy of hemophilia. *Methods Mol Biol* (2008) 433:203–12. doi: 10.1007/978-1-59745-237-3_12

40. Doering CB, et al. Hematopoietic stem cells encoding porcine factor VIII induce pro-coagulant activity in hemophilia a mice with pre-existing factor VIII immunity. *Mol Ther* (2007) 15(6):1093–9. doi: 10.1038/sj.mt.6300146

41. Dooriss KL, Denning G, Gangadharan B, Javazon EH, McCarty DA, Spencer HT, et al. Comparison of factor VIII transgenes bioengineered for improved expression in gene therapy of hemophilia a. *Hum Gene Ther* (2009) 20 (5):465–78. doi: 10.1089/hum.2008.150

42. Gangadharan B, et al. High-level expression of porcine factor VIII from genetically modified bone marrow-derived stem cells. *Blood* (2006) 107(10):3859–64. doi: 10.1182/blood-2005-12-4961

43. Ide LM, et al. Hematopoietic stem-cell gene therapy of hemophilia a incorporating a porcine factor VIII transgene and nonmyeloablative conditioning regimens. *Blood* (2007) 110(8):2855–63. doi: 10.1182/blood-2007-04-082602

44. Ide LM, Iwakoshi NN, Gangadharan B, Jobe S, Moot R, McCarty D, et al. Functional aspects of factor VIII expression after transplantation of genetically-modified hematopoietic stem cells for hemophilia a. *J Gene Med* (2010) 12(4):333–44. doi: 10.1002/jgm.1442

45. Zakas PM, Spencer HT, Doering CB. Engineered hematopoietic stem cells as therapeutics for hemophilia a. *J Genet Syndr Gene Ther* (2011) 1(3):2410. doi: 10.4172/2157-7412.S1-003

46. Doering CB, Denning G, Shields JE, Fine EJ, Parker ET, Srivastava A, et al. Preclinical development of a hematopoietic stem and progenitor cell bioengineered factor VIII lentiviral vector gene therapy for hemophilia a. *Hum Gene Ther* (2018) 29(10):1183–201. doi: 10.1089/hum.2018.137

47. Johnston JM, et al. Generation of an optimized lentiviral vector encoding a high-expression factor VIII transgene for gene therapy of hemophilia a. *Gene Ther* (2013) 20(6):607–15. doi: 10.1038/gt.2012.76

48. Spencer HT, Denning G, Gautney RE, Dropulic B, Roy AJ, Baranyi L, et al. Lentiviral vector platform for production of bioengineered recombinant coagulation factor VIII. *Mol Ther* (2011) 19(2):302–9. doi: 10.1038/mt.2010.239

49. Brown HC, Wright JF, Zhou S, Lytle AM, Shields JE, Spencer HT, et al. Bioengineered coagulation factor VIII enables long-term correction of murine hemophilia a following liver-directed adeno-associated viral vector delivery. *Mol Ther Methods Clin Dev* (2014) 1:14036. doi: 10.1038/mtm.2014.36

50. Aiuti A, Roncarolo MG. Ten years of gene therapy for primary immune deficiencies. *Hematol Am Soc Hematol Educ Program* (2009) p:682–9. doi: 10.1182/asheducation-2009.1.682

51. Bauer G, Dao MA, Case SS, Meyerrose T, Wirthlin L, Zhou P, et al. In vivo biosafety model to assess the risk of adverse events from retroviral and lentiviral vectors. *Mol Ther* (2008) 16(7):1308–15. doi: 10.1038/mt.2008.93

52. Bokhoven M, Stephen SL, Knight S, Gevers EF, Robinson IC, Takeuchi Y, et al. Insertional gene activation by lentiviral and gammaretroviral vectors. *J Virol* (2009) 83(1):283–94. doi: 10.1128/JVI.01865-08

53. Howe SJ, Mansour MR, Schwarzwaelder K, Bartholomae C, Hubank M, Kempski H, et al. Insertional mutagenesis combined with acquired somatic mutations causes leukemogenesis following gene therapy of SCID-X1 patients. *J Clin Invest* (2008) 118(9):3143–50. doi: 10.1172/JCI35798

54. Williams DA, Thrasher AJ. Concise review: lessons learned from clinical trials of gene therapy in monogenic immunodeficiency diseases. *Stem Cells Transl Med* (2014) 3(5):636–42. doi: 10.5966/sctm.2013-0206

55. Ramachandra CJ, Shahbazi M, Kwang TW, Choudhury Y, Bak XY, Yang J, et al. Efficient recombinase-mediated cassette exchange at the AAVS1 locus in human embryonic stem cells using baculoviral vectors. *Nucleic Acids Res* (2011) 39 (16):e107. doi: 10.1093/nar/gkr409

56. Shahani T, Covens K, Lavend'homme R, Jazouli N, Sokal E, Peerlinck K, et al. Human liver sinusoidal endothelial cells but not hepatocytes contain factor VIII. *J Thromb Haemost* (2014) 12(1):36–42. doi: 10.1111/jth.12412

57. Fomin ME, Togarrati PP, Muench MO. Progress and challenges in the development of a cell-based therapy for hemophilia a. *J Thromb Haemost* (2014) 12 (12):1954–65. doi: 10.1111/jth.12750

58. Bessis N, GarciaCozar FJ, Boissier MC. Immune responses to gene therapy vectors: influence on vector function and effector mechanisms. *Gene Ther* (2004) 11 Suppl 1:S10–7. doi: 10.1038/sj.gt.3302364

59. Dow S. Liposome-nucleic acid immunotherapeutics. *Expert Opin Drug Delivery* (2008) 5(1):11–24. doi: 10.1517/17425247.5.1.11

60. Fejer G, et al. Adenovirus-triggered innate signalling pathways. *Eur J Microbiol Immunol (Bp)* (2011) 1(4):279–88. doi: 10.1556/EuJMI.1.2011.4.3

61. Boura JS, Vance M, Yin W, Madeira C, Lobato da Silva C, et al. Evaluation of gene delivery strategies to efficiently overexpress functional HLA-G on human bone marrow stromal cells. *Mol Ther Methods Clin Dev* (2014) 2014(1):14041. doi: 10.1038/mtm.2014.41

62. Lange AM, et al. Overexpression of factor VIII after AAV delivery is transiently associated with cellular stress in hemophilia a mice. *Mol Ther Methods Clin Dev* (2016) 3:16064. doi: 10.1038/mtm.2016.64

63. Malhotra JD, Miao H, Zhang K, Wolfson A, Pennathur S, Pipe SW, et al. Antioxidants reduce endoplasmic reticulum stress and improve protein secretion. *Proc Natl Acad Sci U.S.A.* (2008) 105(47):18525–30. doi: 10.1073/pnas.0809677105

64. Srifa W, Kosaric N, Amorin A, Jadi O, Park Y, Mantri S, et al. Cas9-AAV6-engineered human mesenchymal stromal cells improved cutaneous wound healing in diabetic mice. *Nat Commun* (2020) 11(1):2470. doi: 10.1038/s41467-020-16065-3

65. Stellon D, Tran MTN, Talbot J, Chear S, Khalid MKNM, Pébay A, et al. CRISPR/Cas-mediated knock-in of genetically encoded fluorescent biosensors into the AAVS1 locus of human-induced pluripotent stem cells. *Methods Mol Biol* (2022) 2549:379–98. doi: 10.1007/7651_2021_422

66. Gu J, et al. Targeting the AAVS1 site by CRISPR/Cas9 with an inducible transgene cassette for the neuronal differentiation of human pluripotent stem cells. *Methods Mol Biol* (2022) 2495:99–114. doi: 10.1007/978-1-0716-2301-5_6

67. Lee J, Bayarsaikhan D, Arivazhagan R, Park H, Lim B, Gwak P, et al. CRISPR/Cas9 edited sRAGE-MSCs protect neuronal death in parkinsons disease model. *Int J Stem Cells* (2019) 12(1):114–24. doi: 10.15283/ijsc18110

68. Trevisan B, Morsi A, Aleman J, Rodriguez M, Shields J, Meares D, et al. Effects of shear stress on production of FVIII and vWF in a cell-based therapeutic for hemophilia a. *Front Bioeng Biotechnol* (2021) 9:639070. doi: 10.3389/fbioe.2021.639070

69. Rodriguez M, Porada CD, Almeida-Porada G. Mechanistic insights into factor VIII immune tolerance induction *via* prenatal cell therapy in hemophilia a. *Curr Stem Cell Rep* (2019) 5(4):145–61. doi: 10.1007/s40778-019-00165-y

70. Nathwani AC, Tuddenham EG, Rangarajan S, Rosales C, McIntosh J, Linch DC, et al. Adenovirus-associated virus vector-mediated gene transfer in hemophilia b. *N Engl J Med* (2011) 365(25):2357–65. doi: 10.1056/NEJMoa1108046

71. Wang Q, Zhong X, Li Q, Su J, Liu Y, Mo L, et al. CRISPR-Cas9-Mediated *In vivo* gene integration at the albumin locus recovers hemostasis in neonatal and adult hemophilia b mice. *Mol Ther Methods Clin Dev* (2020) 18:520–31. doi: 10.1016/j.omtm.2020.06.025

72. Ramaswamy S, Tonnu N, Menon T, Lewis BM, Green KT, Wampler D, et al. Autologous and heterologous cell therapy for hemophilia b toward functional restoration of factor IX. *Cell Rep* (2018) 23(5):1565–80. doi: 10.1016/j.celrep.2018.03.121

73. Lyu C, Shen J, Wang R, Gu H, Zhang J, Xue F, et al. Targeted genome engineering in human induced pluripotent stem cells from patients with hemophilia b using the CRISPR-Cas9 system. *Stem Cell Res Ther* (2018) 9(1):92. doi: 10.1186/s13287-018-0839-8

74. Park CY, Kim DH, Son JS, Sung JJ, Lee J, Bae S, et al. Functional correction of Large factor VIII gene chromosomal inversions in hemophilia a patient-derived iPSCs using CRISPR-Cas9. *Cell Stem Cell* (2015) 17(2):213–20. doi: 10.1016/j.stem.2015.07.001

75. Sung JJ, et al. Restoration of FVIII expression by targeted gene insertion in the FVIII locus in hemophilia a patient-derived iPSCs. *Exp Mol Med* (2019) 51 (4):1–9. doi: 10.1038/s12276-019-0243-1

76. Park CY, et al. Universal correction of blood coagulation factor VIII in patient-derived induced pluripotent stem cells using CRISPR/Cas9. *Stem Cell Rep* (2019) 12(6):1242–9. doi: 10.1016/j.stemcr.2019.04.016

77. Zhang JP, Li XL, Li GH, Chen W, Arakaki C, Botimer GD, et al. Efficient precise knockin with a double cut HDR donor after CRISPR/Cas9-mediated double-stranded DNA cleavage. *Genome Biol* (2017) 18(1):35. doi: 10.1186/s13059-017-1164-8

78. Zhang JP, Cheng XX, Zhao M, Li GH, Xu J, Zhang F, et al. Curing hemophilia a by NHEJ-mediated ectopic F8 insertion in the mouse. *Genome Biol* (2019) 20(1):276. doi: 10.1186/s13059-019-1907-9

79. Chen H, Shi M, Gilam A, Zheng Q, Zhang Y, Afrikanova I, et al. Hemophilia a ameliorated in mice by CRISPR-based *in vivo* genome editing of human factor VIII. *Sci Rep* (2019) 9(1):16838. doi: 10.1038/s41598-019-53198-y

80. Miao HZ, Sirachainan N, Palmer L, Kucab P, Cunningham MA, Kaufman RJ, et al. Bioengineering of coagulation factor VIII for improved secretion. *Blood* (2004) 103(9):3412–9. doi: 10.1182/blood-2003-10-3591

81. Powell JS, Ragni MV, White GC 2nd, Lusher JM, Hillman-Wiseman C, Moon TE, et al. Phase 1 trial of FVIII gene transfer for severe hemophilia a using a retroviral construct administered by peripheral intravenous infusion. *Blood* (2003) 102(6):2038–45. doi: 10.1182/blood-2003-01-0167

82. Gage BK, et al. Therapeutic correction of hemophilia a by transplantation of hPSC-derived liver sinusoidal endothelial cell progenitors. *Cell Rep* (2022) 39 (1):110621. doi: 10.1016/j.celrep.2022.110621

83. Qiu L, et al. Restoration of FVIII function and phenotypic rescue in hemophilia a mice by transplantation of MSCs derived from F8-modified iPSCs. *Front Cell Dev Biol* (2021) 9:630353. doi: 10.3389/fcell.2021.630353

84. Wu Y, Hu Z, Li Z, Pang J, Feng M, Hu X, et al. *In situ* genetic correction of F8 intron 22 inversion in hemophilia a patient-specific iPSCs. *Sci Rep* (2016) 6:18865. doi: 10.1038/srep18865

85. Zhao J, et al. Ectopic expression of FVIII in HPCs and MSCs derived from hiPSCs with site-specific integration of ITGA2B promoter-driven BDDF8 gene in hemophilia a. *Int J Mol Sci* (2022) 23(2):623. doi: 10.3390/ijms23020623

86. Son JS, Park CY, Lee G, Park JY, Kim HJ, Kim G, et al. Therapeutic correction of hemophilia a using 2D endothelial cells and multicellular 3D organoids derived from CRISPR/Cas9-engineered patient iPSCs. *Biomaterials* (2022) 283:121429. doi: 10.1016/j.biomaterials.2022.121429

87. Sung JJ, et al. Generation of a gene edited hemophilia a patient-derived iPSC cell line, YCMi001-B-1, by targeted insertion of coagulation factor FVIII using CRISPR/Cas9. *Stem Cell Res* (2020) 48:101948. doi: 10.1016/j.scr.2020.101948

88. Han JP, Chang YJ, Song DW, Choi BS, Koo OJ, Yi SY, et al. High homology-directed repair using mitosis phase and nucleus localizing signal. *Int J Mol Sci* (2020) 21(11):3747. doi: 10.3390/ijms21113747

89. Sakamoto Y, Kokuta T, Teshigahara A, Iijima K, Kitao H, Takata M, et al. Mitotic cells can repair DNA double-strand breaks *via* a homology-directed pathway. *J Radiat Res* (2021) 62(1):25–33. doi: 10.1093/jrr/rraa095

90. van Essen M, Riepsaame J, Jacob J. CRISPR-cas gene perturbation and editing in human induced pluripotent stem cells. *CRISPR J* (2021) 4(5):634–55. doi: 10.1089/crispr.2021.0063

91. Wang L, Ye Z, Jang YY. Convergence of human pluripotent stem cell, organoid, and genome editing technologies. *Exp Biol Med (Maywood)* (2021) 246 (7):861–75. doi: 10.1177/1535370220985808

92. Yeh WH, et al. In vivo base editing of post-mitotic sensory cells. *Nat Commun* (2018) 9(1):2184. doi: 10.1038/s41467-018-04580-3

93. Fahs SA, et al. A conditional knockout mouse model reveals endothelial cells as the principal and possibly exclusive source of plasma factor VIII. *Blood* (2014) 123(24):3706–13. doi: 10.1182/blood-2014-02-555151

94. Bao X, Wang J, Zhou G, Aszodi A, Schönitzer V, Scherthan H, et al. Extended *in vitro* culture of primary human mesenchymal stem cells downregulates Brca1-related genes and impairs DNA double-strand break recognition. *FEBS Open Bio* (2020) 10(7):1238–50. doi: 10.1002/2211-5463.12867

95. Hare I, Gencheva M, Evans R, Fortney J, Piktel D, Vos JA, et al. *In vitro* expansion of bone marrow derived mesenchymal stem cells alters DNA double strand break repair of etoposide induced DNA damage. *Stem Cells Int 2016.* (2016), 2016:8270464. doi: 10.1155/2016/8270464

96. Hladik D, Höfig I, Oestreicher U, Beckers J, Matjanovski M, Bao X, et al. Long-term culture of mesenchymal stem cells impairs ATM-dependent recognition of DNA breaks and increases genetic instability. *Stem Cell Res Ther* (2019) 10(1):218. doi: 10.1186/s13287-019-1334-6

frontiers | Frontiers in Immunology

TYPE Original Research
PUBLISHED 26 January 2023
DOI 10.3389/fimmu.2023.1022676

OPEN ACCESS

EDITED BY
Raghavan Chinnadurai,
Mercer University, United States

REVIEWED BY
Paula Schiapparelli,
Mayo Clinic Florida, United States
Giuliana Minani Bertolino,
Université de Montpellier, France

*CORRESPONDENCE
Vivian Capilla-González
vivian.capilla@cabimer.es

†These authors have contributed equally to this work

‡These authors have contributed equally to this work

SPECIALTY SECTION
This article was submitted to Alloimmunity and Transplantation, a section of the journal Frontiers in Immunology

RECEIVED 18 August 2022
ACCEPTED 03 January 2023
PUBLISHED 26 January 2023

CITATION
Baliña-Sánchez C, Aguilera Y, Adán N, Sierra-Párraga JM, Olmedo-Moreno L, Panadero-Morón C, Cabello-Laureano R, Márquez-Vega C, Martín-Montalvo A and Capilla-González V (2023) Generation of mesenchymal stromal cells from urine-derived iPSCs of pediatric brain tumor patients.
Front. Immunol. 14:1022676.
doi: 10.3389/fimmu.2023.1022676

Generation of mesenchymal stromal cells from urine-derived iPSCs of pediatric brain tumor patients

Carmen Baliña-Sánchez[1†], Yolanda Aguilera[1†], Norma Adán[1‡], Jesús María Sierra-Párraga[1‡], Laura Olmedo-Moreno[1], Concepción Panadero-Morón[1], Rosa Cabello-Laureano[2], Catalina Márquez-Vega[3], Alejandro Martín-Montalvo[1,4] and Vivian Capilla-González[1*]

[1]Department of Regeneration and Cell Therapy, Andalusian Molecular Biology and Regenerative Medicine Centre (CABIMER)-CSIC-US-UPO, Seville, Spain, [2]Pediatric Surgery Service, Hospital Virgen del Rocio, Seville, Spain, [3]Pediatric Oncology Service, Hospital Virgen del Rocio, Seville, Spain, [4]Centro de Investigación Biomédica en Red de Diabetes y Enfermedades Metabólicas Asociadas (CIBERDEM), Madrid, Spain

Human induced pluripotent stem cells (iPSCs) provide a virtually inexhaustible source of starting material for next generation cell therapies, offering new opportunities for regenerative medicine. Among different cell sources for the generation of iPSCs, urine cells are clinically relevant since these cells can be repeatedly obtained by non-invasive methods from patients of any age and health condition. These attributes encourage patients to participate in preclinical and clinical research. In particular, the use of urine-derived iPSC products is a convenient strategy for children with brain tumors, which are medically fragile patients. Here, we investigate the feasibility of using urine samples as a source of somatic cells to generate iPSC lines from pediatric patients with brain tumors (BT-iPSC). Urinary epithelial cells were isolated and reprogrammed using non-integrative Sendai virus vectors harboring the Yamanaka factors *KLF4, OCT3/4, SOX2* and *C-MYC*. After reprogramming, BT-iPSC lines were subject to quality assessment and were compared to iPSCs obtained from urine samples of non-tumor pediatric patients (nonT-iPSC). We demonstrated that iPSCs can be successfully derived from a small volume of urine obtained from pediatric patients. Importantly, we showed that BT-iPSCs are equivalent to nonT-iPSCs in terms of morphology, pluripotency, and differentiation capacity into the three germ layers. In addition, both BT-iPSCs and nonT-iPSCs efficiently differentiated into functional mesenchymal stem/stromal cells (iMSC) with immunomodulatory properties. Therefore, this study provides an attractive approach to non-invasively generate personalized iMSC products intended for the treatment of children with brain tumors.

KEYWORDS

iPSC, mesenchymal stem/stromal cells (MSC), central nervous system cancer, children, cell therapy, cell reprogramming, oncology, cancer

Introduction

In 2006, there was a breakthrough in the field of regenerative medicine, when Takahashi and Yamanaka developed the technology to transform any somatic cell into a pluripotent stem cell. These reprogrammed cells, called induced Pluripotent Stem Cells (iPSCs), can be generated by ectopic expression of four transcription factors (i.e. OSKM factors): octamer binding transcription factor 3/4 (*OCT3/4*), sex determining region Y-box 2 (*SOX2*), Krüppel-line factor 4 (*KLF4*) and cellular-myelocytomatosis (*C-MYC*) (1, 2). Similar to embryonic stem cells, iPSCs have the ability to self-renew and differentiate into any specialized cell of the body. In addition, iPSCs have certain advantages over other stem cell types for cell-based therapies. Firstly, iPSCs avoid the ethical concerns about the use of embryos to generate pluripotent stem cells. Secondly, they provide a virtually unlimited supply of human cells, bringing the possibility of generating personalized cells for autologous treatment, preventing immune rejection. Importantly, iPSC technology allows the manufacturing of next generation cells, such as iPSC-derived mesenchymal stem/stromal cells (iMSCs), which have been shown to have increased therapeutic efficacy when compared to tissue-derived mesenchymal stem/stromal cells (MSCs) in pre-clinical studies (3–8). Thirdly, these cells can be harvested from easily accessible sources, such as skin, blood or urine. Particularly, urine-derived iPSCs are obtained by simple, pain-free methods, reducing the risk of adverse effects associated with invasive collection procedures. Therefore, urine offers an interesting option to collect cells repeatedly from patients of any age and under any medical condition, such as pediatric cancer patients (9–11).

Brain tumors are the most common solid tumor in children and represent the leading cause of pediatric cancer-related deaths. Latest advances in diagnosis and treatments have improved survival rates of children suffering brain tumors. However, adverse effects of cancer therapies are still affecting the health of many brain tumor survivors. For this reason, researchers are focusing on the development of new strategies aimed to reduce toxicity of cancer treatments. The majority of brain tumor patients that receive radiotherapy, one of the most common treatments for cancer (12), exhibit cognitive dysfunction, including deficits in learning, memory, language, attention and executive function (13). These neurological complications are frequently associated with radiation-induced damage to healthy brain tissue, such as neuroinflammation and cell death (12, 14–17). Despite the fact that neurocognitive sequelae of radiotherapy may occur in patients of any age, these adverse effects particularly affect pediatric patients because the developing brain is more sensitive to radiation.

Recent reports have demonstrated the neuroprotective effects of cell-based therapies to prevent neurological complications of radiotherapy, thus promoting a healthy cancer-free life (18–24). In particular, the administration of MSCs has been shown to efficiently rescue behavioral deficits in mice following cranial radiation, by reducing neuroinflammation and cell death (18, 22–24). However, the clinical translation of MSC-based therapies as a neuroprotective strategy is hampered by challenges related to manufacturing and cell availability. In this context, the use of iPSCs as an unlimited source of MSCs (i.e., iMSCs) emerges as an interesting option that enables large-scale production of cellular products for both autologous and allogenic therapies. Furthermore, iMSCs can generate from a single iPSC clone, thus reducing the heterogeneity acquired by tissue-derived MSCs (25–27). These attributes facilitate the obtaining of consistent and robust final products that could be used for the prevention of radiation-related neurological complications. However, the generation of iMSCs from brain tumor pediatric patients remains to be achieved.

In this study, we demonstrated that urine-derived epithelial cells (UDCs) is a feasible source to generate iPSCs from children with brain tumors following a non-invasive cell collection procedure. In addition, we show that iPSCs differentiate into functional iMSCs. To our knowledge, this is the first study involving brain tumor pediatric patients that successfully generate iMSCs. The establishment of iPSC lines offers a stable source of MSCs (i.e., iMSCs), boosting their clinical application in a variety of diseases, for both children and adults.

Methods

Obtaining of urine samples from pediatric patients

Urine samples were collected from pediatric patients (age <60 months old) at the Hospital Universitario Virgen del Rocío of Seville, after obtaining written informed consent. Samples with volumes ranging from 12 to 40 ml were collected in a sterile container, kept at 4° C, and processed within 1 hour. Urine obtained from brain tumor patients was collected prior to oncological treatment (e.g. surgery, radiotherapy or chemotherapy). Urine obtained from non-oncological patients was used as control samples (Table 1, Figure 1).

Isolation and expansion of UDCs

Urine was centrifuged at 400 × g for 10 min at room temperature. Cell pellets were washed with Dulbecco's phosphate buffered saline (DPBS), resuspended in isolation medium (DMEM/F-12 with 15mM HEPES, 10% fetal bovine serum (FBS), 1% non-essential amino acids, 10 ng/mL recombinant human EFG, 36 ng/mL hydrocortisone, 5 µg/mL recombinant human insulin, 500 ng/mL epinephrine, 5 µg/mL human holo-transferrin, 4 pg/mL triodo-L-thyronine, 434.4 µg/mL alanyl-glutamine, 100 µg/mL penicillin/streptomycin, 2.5 µg/mL amphotericin B and 0.1% rock inhibitor) and seeded in gelatin-coated plates. Half-medium changes were performed every day to avoid unnecessary cellular stress. Once the first colonies were observed (day 7-15), total medium was replaced. The first passage was performed when cells were approximately 30% confluent using trypsin (day 12-20). Then, UDCs were seeded at a density of 10.000 cells/cm^2 with a 1:1 mix of isolation medium and expansion media (i.e., isolation medium with reduced FBS concentration to 5% and antibiotic free). From passage 2, only expansion medium was used to boost UDC amplification prior to cell reprograming. UDCs were incubated at 37°C in a humidified atmosphere with 20% O_2 and 5% CO_2.

Reprogramming of UDCs into iPSCs

UDCs at passage below 5 were reprogrammed when cells reached a 30-60% confluency. To reduce the risk of genetic abnormalities, UDCs were reprogrammed to iPSCs using the non-integrative CytoTune™-iPS 2.0 Sendai Reprogramming Kit (Thermo Fisher, Waltham, MA, USA) (Figure 2A). After a 7-day period, transfected cells were transferred onto a matrigel-coated plate with mTeSR plus basal medium (STEMCELL Technologies, Grenoble, France) and allowed to grow in a humidified incubator with 37°C, 20% O_2 and 5% CO_2. After 5 days, iPSC colonies emerged. The first 4 passages were carried out mechanically to specifically select colonies with an iPSC morphology. Then, cell passages were performed using the ReLeSR reagent (STEMCELL Technologies), following the manufacturer's guidelines. iPSCs were expanded for full characterization and banking. All established cell lines will be deposited at the Banco Nacional de Líneas Celulares (BNLC) of the Institute of Health Carlos III, following the Spanish legislation.

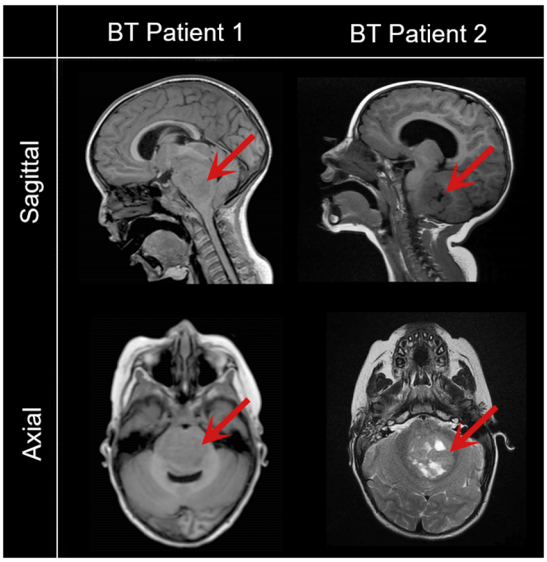

FIGURE 1
Representative magnetic resonance images of pediatric patients with brain tumors included in the study. Saggital and axial images reveal a low grade glioma (BT Patient 1, 43-month-old) and a metastatic brain tumor (BT Patient 2, 24-month-old). Red arrows point to the tumor.

Characterization of the generated iPSCs

Alkaline phosphatase staining

Alkaline phosphatase activity was evaluated in fixed iPSC colonies using the SIGMAFAST™ BCIP®/NBT kit (Sigma-Aldrich, St. Louis, MO, USA), following the manufacturer's guidelines. Stained iPSCs were visualized and imaged using an Olympus IX71 microscope equipped with an DPController and DPManager software (Center Valley, PA, USA).

Three lineage differentiation

For the differentiation of iPSCs into the three germ layers (endoderm, mesoderm and ectoderm), we used the specific induction media of the STEMdiff™ Trilineage Differentiation Kit (STEMCELL Technologies). According to the manufacturer's instructions, a 5-day period was required for endoderm and mesoderm differentiation, while ectoderm induction needed 7 days. Media was changed daily. Differentiated cells were harvested and used to isolate RNA for reverse transcriptase-polymerase chain reaction (RT-PCR) and to perform immunofluorescence assays.

Immunofluorescence staining

Cells were fixed with 4% paraformaldehyde (PFA), washed with phosphate buffered saline (PBS), incubated in blocking solution for 1 hour, and incubated with primary antibodies at 4°C overnight (see Supplemental Table 2 for antibodies information). Then, cells were washed and incubated with the appropriate secondary antibodies conjugated with fluorophores. Hoechst 33342 nucleic acid stain (Sigma-Aldrich) was used to detect cell nuclei. Fluorescence labeling was examined using an Olympus IX71 microscope equipped with DPController and DPManager software.

Molecular karyotyping

DNA from iPSCs was extracted using the DNeasy Blood and Tissue kit (QIAGEN, Gilden, Germany). Then, molecular karyotyping was performed with an Affymetrix CytoScan 750k Array (Affymetrix, Santa Clara, CA, USA) by trained experts of the Genome Core Facility of CABIMER to detect chromosomal variations (log2 ratio intensities and copy number). Data viewing and analysis was performed with the Affymetrix Chromosome Analysis Suite (ChAS) software, using the standard setting filters (400 kbp with a marker count of ≥50 for gains; 400 kbp with a marker count of ≥25 for losses) and compared to control data from the Database of Genomic Variants (DGV). The Online Mendelian Inheritance in Man (OMIM) database was used to study associations of genetic alterations with disease susceptibility. All samples and processes fulfilled the following

TABLE 1 Clinical characteristics of pediatric patients.

Patient	Age (months)	Sex	Diagnosis	Sample Volume (urine)	hPSCreg name	Sample ID*
nonT Patient 1	7	male	Inguinal hernia	12.6 mL	ESi089-A	nonT-iPSCs 1
nonT Patient 2	56	male	Cryptorchidism	13.6 mL	ESi090-A	nonT-iPSCs 2
BT Patient 1	43	female	Low grade Glioma	32 mL	ESi087-A	BT-iPSCs 1
BT Patient 2	24	female	Metastatic brain tumor	40 mL	ESi088-A	BT-iPSCs 2

* Sample ID relates to the name given to each iPSC line in this manuscript.

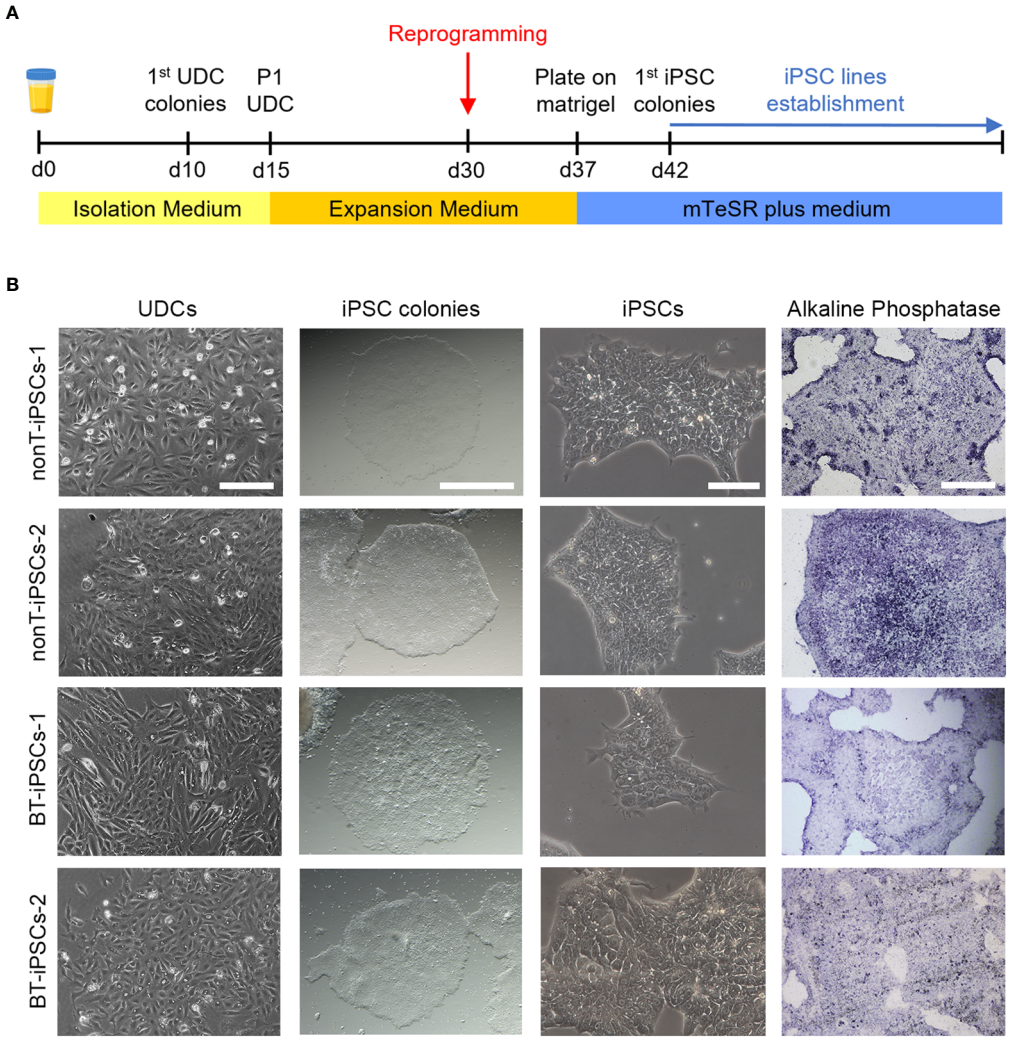

FIGURE 2
Isolation of UDCs and reprogramming process. **(A)** Schematic timeline of the process for isolation and expansion of UDCs and iPSC generation. **(B)** Microscope images showing the morphological aspect of cultured UDCs (scale bar 200 µm), iPSC colonies obtained after selective passaging post-reprogramming (scale bar 1 mm), iPSCs at higher magnifications (scale bar 100 µm) and alkaline phosphatase staining of iPSC colonies (scale bar 400 µm).

quality criteria: MAPD ≤ 0.25, Waviness SD ≤ 0.12 and SNPQC ≥15. Affymetrix data are deposited in Gene Expression Omnibus (GEO) database repository (accession number: GSE213813).

Fingerprinting

The identity of the established cell lines was analyzed by the cell line authentication service qGenomics (Barcelona, Spain). DNA analysis of the iPSCs and their parental UDCs was performed by genotyping the following human-specific short tandem repeat (STR) markers: *TH01*, *D21S11*, *D5S828*, *D13S317*, *D7S820*, *D16S539*, *CSF1PO*, *vWA* and *TPOX*. The combination of these nine genetic markers results in an allele profile with a random match probability of 1 in 2.9 x 10^9. A gender-specific marker (*AMEL*) was also analyzed to establish the presence of sex chromosomes, as well as a specific marker to detect the presence of murine sequences that could result from a possible cross-contamination of the cultured iPSCs with any independent culture of murine cells.

Differentiation of iPSCs into MSCs and characterization

Differentiation of iPSCs into iMSCs was induced with the STEMdiff™ Mesenchymal Progenitor Kit (STEMCELL Technologies), following the manufacturer's instructions. Briefly, iPSCs were differentiated into early mesoderm progenitor cells for four days. Then, cells were plated in animal component-free (ACF) precoated wells to derive early mesenchymal progenitor cells. By day 21, differentiated cells exhibited MSC phenotype that was verified by morphological analysis, flow cytometry and multilineage differentiation potential, based on previously published methodology (28, 29). For the flow cytometry study, the surface markers CD13, CD14, CD73, CD105, CD29, CD31, CD34, CD45, CD90 and HLA II were used (see Supplemental Table 2 for antibody information). Differentiation of iMSCs into adipocytes was performed using the MesenCult™ Adipogenic Differentiation Kit (STEMCELL

technologies). After 21 days, the presence of lipid droplets was determined by staining the cells with Oil red O (Sigma-Aldrich) after fixation with 4% PFA for 5 minutes. Differentiation of iMSCs into osteoblasts was performed using the MesenCult™ Osteogenic Differentiation Kit (STEMCELL technologies). After 15 days, the presence of osteoblasts was determined by staining the cells with Alizarin Red S sodium salt (Alfa Aesar, Haverhill, MA, USA), after fixation with 4% PFA for 5 minutes. Differentiation of iMSCs into chondrocytes was performed using the MesenCult™-ACF Chondrogenic Differentiation kit (STEMCELL technologies). After 21 days, cell pellets were fixed overnight with 4% PFA, paraffin-embedded and sectioned with a microtome (Leica RM 2255) to 5 µm thickness. Then, sections were stained with Alcian-Blue solution (Sigma-Aldrich). Images were visualized with an Olympus IX71 microscope and a Nikon ECLIPSE Si microscope.

Inflammatory cytokines secreted by iMSCs

Culture medium was collected after 48 hours of cell growth to analyze cytokines secreted by iMSCs. Interleukin 8 (IL-8), interleukin 12p70 (IL-12p70), monocyte chemoattractant protein-1 (MCP-1, also named CCL2), platelet-derived growth factor BB (PDGF-BB) and tumor necrosis factor alpha (TNFα) were examined using the Quantibody Human Inflammation Array-3 (Raybiotech, Inc., Norcross, GA, USA), according to the manufacturer´s protocol. Fluorescence signals were detected at 532 nm by a laser scanner (Axon GenePix; Molecular Devices, Sunny-vale, CA, USA).

iMSC priming

Cells were incubated during 48 hours with (primed iMSC) or without (non-primed iMSC) an inflammatory cytokine mixture containing recombinant human TNFα (10 ng/mL) and recombinant human Interferon gamma (IFNγ; 10 ng/mL) in DMEM supplemented with 15% FBS. For gene expression analysis, a set of cells was thoroughly washed after priming to remove these cytokines and collected for RNA isolation either inmediatly or 48 hours after priming. For secretome generation, another set of cells was thoroughly washed after priming and then fresh culture medium was added. After a 48 hours period, conditioned medium (CM) was collected and stored at -80° until use.

RNA extraction and RT-PCR

Total RNA was isolated from cultured cells with the Easy-Blue™ kit (iNtRON Biotechnology, Inc., Seongnam, Korea). cDNA was obtained from 1 µg of total RNA using the iScript cDNA synthesis kit (Bio-Rad Laboratories, Hercules, CA, USA). Conventional RT-PCR was used to evaluate the expression of pluripotency- and differentiation-associated genes using the primers described in Supplemental Table 1. The clearance of the Sendai virus (SeV) vector and the OSKM reprogramming factors was also confirmed by conventional RT-PCR. Agarose gel electrophoresis was used to resolve PCR products. Presence of mycoplasma was analyzed using the commercial kit Venor GeM (Minerva Biolabs GmbH, Berlin, Germany). For quantitative RT-PCR (RT-qPCR), the iTaq Universal SYBR Green Supermix (Bio-Rad Laboratories) was used following the manufacturer guidelines, using a total volume of 10 µL and 50 ng of cDNA per reaction, in triplicates. RT-qPCR was performed using a ViiA™ 7 Real-Time PCR System (Applied Biosystems, Foster City, CA, USA) and analyzed with the ViiA™ 7 Software (Applied Biosystems), using the standard instrument protocol. The expression of immunomodulatory genes was studied using the primers described in Supplemental Table 1 and the relative gene expression was normalized using TATA box binding protein (TBP) as the housekeeping gene. Data was collected from three independent experiments.

iMSC and PBMC cocultures

Peripheral blood mononuclear cells (PBMCs) from two donors with different blood types were purchased from STEMCELL Technologies (Cat# 70025.2). PBMCs were thawed and cultured overnight in RPMI medium supplemnted with 10% FBS, 1% penicillin/streptomycin, and 1% L-glutamine to allow resumption of metabolism, as suggested by the manufacturer. ImmunoCult™ Human CD3/CD28 T Cell Activator reagent (Cat# 10971, STEMCELL Technologies) was used to stimulate PBMCs, following the manufacturer's instructions (25 µl of reagent per ml of medium). For direct cocultures, $1{\cdot}10^5$ activated PBMCs were added to cultured iMSCs at different ratios (PBMC:iMSC of 2:1, 4:1, 8:1, 16:1) in a 96 well plate for 5 days (30). For indirect cocultures, $1{\cdot}10^5$ activated PBMCs were incubated for 72h either in RPMI or in a combination of RPMI and CM from primed/non-primed iMSC (volume ration RPMI : RPMI:CM of 1:1) in a 96 well plate. The CM was generated from $1{\cdot}10^6$ iMSCs cultured for 2 days in 10 ml of medium. To study the proliferation of CD3+ T cell, PBMCs were labelled with the cell division tracker 5-chloromethylfluorescein diacetate (C7025, Thermo Fisher) and then subjected to flow cytometry (31). To evaluate the proliferation of CD4+ and CD8+ T cell subpopulations, a Ki-67 proliferation test was performed following the manufacturer´s protocol (32).

Flow cytometry

Cultured cells were harvested and incubated for 20 minutes with the appropriated primary antibodies in the dark at room temperature (see Supplemental Table 2 for antibody information). For Ki-67 staining, cells were fixed and permeabilized with ethanol at -20° C for 2 hours before incubation with primary antibody. After primary antibody incubation, cells were washed with PBS, centrifuged at 2000 rpm for 5 minutes and analyzed using an LSRFortessa X-20 flow cytometer (BD Biosciences, San Diego, CA, USA) and the BD FACSDiva software (BD Biosciences).

Determination of superoxide dismutase activity

The antioxidant action of the iMSC secretome was measured by the Superoxide Dismutase (SOD) Activity Assay Kit (Cayman

Chemical, Ann Arbor, MI, USA). Samples were assayed according to the manufacturer's instructions. Absorbance was measured at 450 nm using a Varioskan Flash microplate reader (Thermo Electron, Vantaa, Finland). Units of SOD activity were calculated from a standard curve using purified bovine erythrocyte SOD enzyme. All measurements were performed in duplicate.

Statistical analysis

Data expressed as mean ± SEM was analyzed using the GraphPad Prism 8 software (GraphPad Software Inc., San Diego, CA). Parametric ANOVA followed by a Tukey´s or Dunnett's *post-hoc* test was performed to compare more than two experimental groups. Comparison between two experimental groups were performed with Student's t-test. All differences were considered significant at a P value <0.05.

Results

UDCs from children with brain tumors can be successfully cultured and reprogrammed into iPSCs

The isolation of epithelial cells was carried out from urine samples of four pediatric patients, two with brain tumors (BT patients) and two with non-tumor conditions (nonT patients) (Figure 1, Table 1). Adherent UDCs were observed during the first week of culture, showing spindle-shaped or round-shaped morphologies. First UDC colonies emerged on day 11 and, then, UDCs were expanded for a maximum of 5 passages to assure enough material for reprogramming (Figure 2).

To generate iPSCs, we used the non-integrative Sendai viral vectors to reduce the risk of genetic abnormalities in the generated cell lines (Figure 2A). The reprogramming efficiency was similar in all patient-derived samples. At day 7 post-reprogramming, colonies with typical iPSC morphology (i.e. dense, roundly shaped colonies with sharp edges, containing small cells with a high nucleus-to-cytoplasm ratio) were selected and manually picked to achieve highest culture purity. Alkaline phosphatase activity staining confirmed the identification of pluripotent iPSC colonies (Figure 2B). Passaged iPSCs were seeded onto matrigel-coated plates and expanded for full characterization.

To further validate the identity of the generated cell lines, gene expression of pluripotency markers was evaluated. RT-PCR analysis evidences that, in contrast to UDCs, iPSC colonies from BT patients and nonT patients had a robust expression of the key pluripotency genes *OCT3/4, SOX2, NANOG* and *TERT* (Figure 3A). We also evaluated the expression of pluripotency markers at protein level by immunofluorescence, using the intracellular marker OCT3/4 and the surface markers SSEA4, TRA-1-60 and TRA-1-81. Cultured iPSCs stained positive for all the markers assessed, confirming their pluripotency (Figure 3B).

Multilineage differentiation potential was confirmed in patient-derived iPSCs

To further demonstrate the pluripotency of iPSCs, tri-lineage differentiation was performed using specific induction media. Reprogrammed cells efficiently differentiated into endodermal,

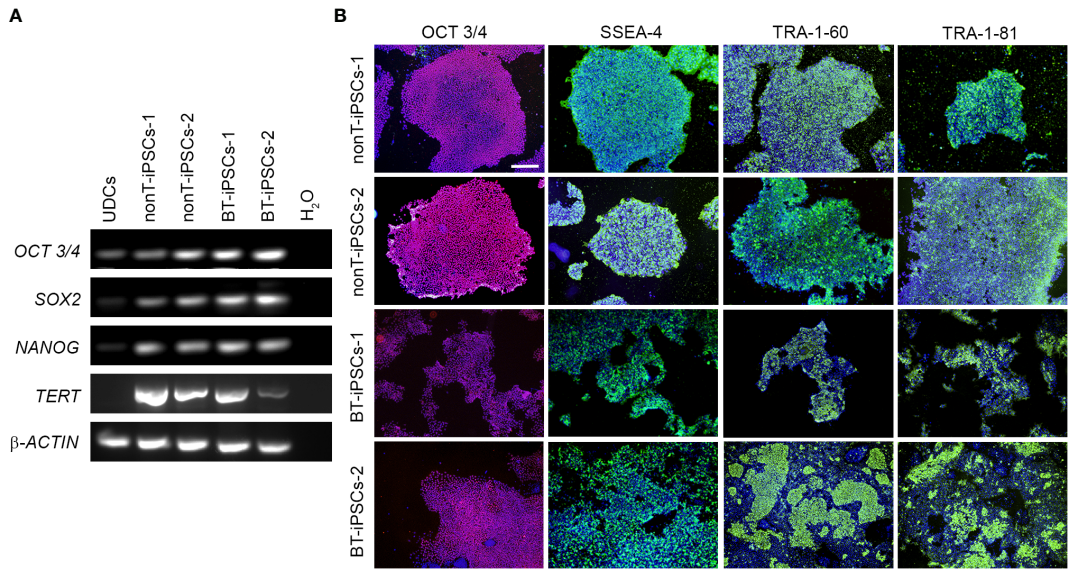

FIGURE 3
Analysis of the pluripotency markers in the generated iPSC lines. **(A)** RT-PCR analysis of the expression of pluripotency-associated genes. Note that all iPSC lines highly express *OCT3/4, SOX2, NANOG* and *TERT*, while UDCs do not. **(B)** Immunofluorescence staining showing the presence of pluripotency markers OCT3/4 (magenta), SSEA-4 (green), TRA-1-60 (green) and TRA-1-81 (green) in the iPSCs. Nuclei were counterstained with Hoechst 33342 (blue). Scale bar 100 μm.

mesodermal and ectodermal lineage cells. The differentiation potential of the generated iPSCs was confirmed through expression of specific genes for endoderm (*SOX17, FOXA2*), mesoderm (*CXCR4, BRACH*) and ectoderm (*NGN3*) (Figure 4A). In addition, differentiated iPSCs were assessed for immunofluorescence using AFP (endoderm marker), SMA (mesoderm marker) and Nestin (ectoderm marker) (Figure 4B). Both RT-PCR and immunofluorescence results denoted similar tri-lineage differentiation potential in all patient-derived iPSC lines.

Authentication, molecular karyotyping, virus clearance and mycoplasma testing of established iPSC

DNA fingerprinting analysis indicates that iPSCs from BT and nonT patients shared identity with their parental UDCs, demonstrating that we generated four new iPSC lines (Figure 5A). The safety of the reprogramming method was evaluated by molecular karyotyping, which evidences minimal chromosomal abnormalities (<1.1% for autosomes) in all urine-derived iPSCs, based on Log2 ratio and copy number (Figure 5B). Importantly, genomic alterations related to tumorigenesis were absent in the iPSCs from brain tumor pediatric patients (Supplemental Table 3). Finally, the absence of exogenous reprogramming vectors and mycoplasma contamination was verified in the generated iPSC lines by negative PCR (Figures 5C, D). These results support that the production of iPSCs from pediatric patients with brain tumors may be suitable for clinical applications.

Differentiation of iPSCs into iMSCs

In order to determine whether iPSCs can serve as a platform to obtain next generation MSCs, we used specific induction media to generate iMSCs (Figure 6A). During the course of the protocol, iPSCs from BT and nonT patients acquired a fibroblast-like morphology (Figure 6B). By day 21, differentiated iPSCs expressed typical MSC markers, such as CD13, CD29, CD73, CD90 and CD105, while they lacked the expression of CD14, CD31, CD34, CD45, and HLA-II (Figure 6C, Supplemental Figure 1). In addition, the absence of undifferentiated cells (i.e. iPSCs) was confirmed by the lack of expression of TRA-1-60 and SSEA4, supporting successful differentiation of iPSCs into MSCs (Supplemental Figure 2). iMSC identity was further confirmed based on their multilineage differentiation potential. Both BT and nonT patient-derived iMSC possessed the ability to differentiate into adipocytes, osteocytes and chondrocytes, as demonstrated by the positive staining for Oil Red O, Alizarin Red S and Alcian Blue, respectively (Figure 6D, Supplementary Figure 1). These data demonstrate that urine-derived iPSCs from pediatric patients can be efficiently differentiated into iMSCs, irrespective of brain tumor diagnosis.

Immunomodulatory potential of the generated iMSCs

To evaluate the immunomodulatory phenotype of the generated iMSCs, we examined the secretion of immunoregulatory cytokines in the media of cultured cells. We analyzed the presence of IL-8, IL-

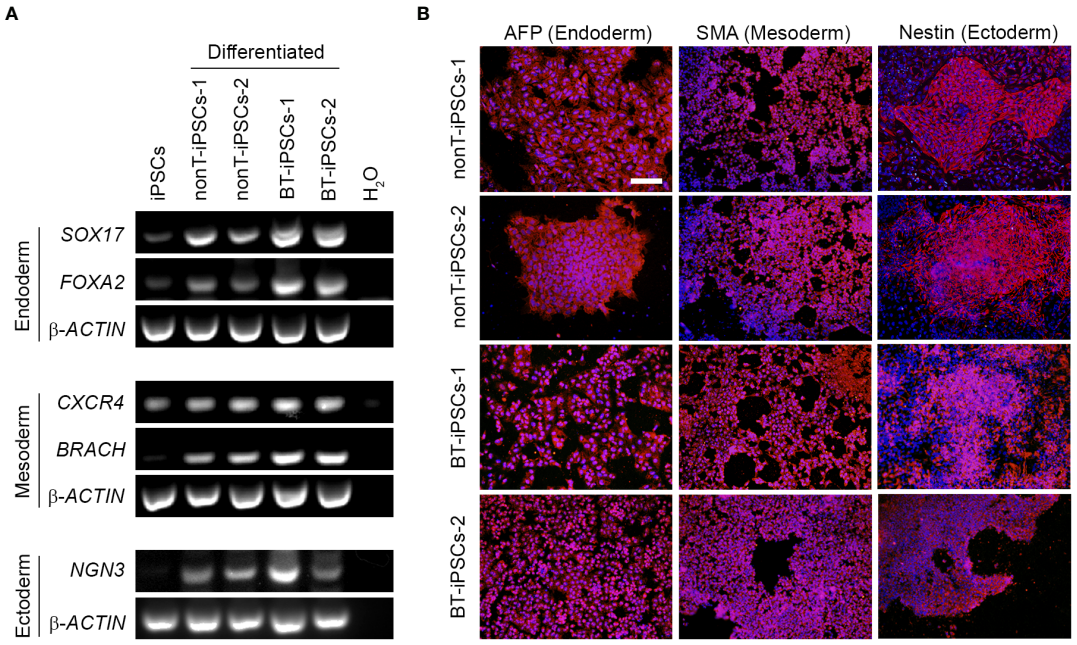

FIGURE 4
Analysis of the differentiation capacity of the generated iPSCs into the three embryonic layers. **(A)** RT-PCR analysis showing the expression of specific differentiation markers, including markers for endoderm (*SOX17* and *FOXA2*), mesoderm (*CXCR4* and *BRACH*) and ectoderm (*NGN3*). Note that differentiated iPSCs highly express all the trilineage differentiation markers, while undifferentiated iPSCs do not. **(B)** Immunofluorescence staining showing the presence of alfa-fetoprotein (AFP) for endoderm, Smooth Muscle Actin (SMA) for mesoderm and Nestin for ectoderm in the differentiated iPSCs. Nuclei were counterstained with Hoechst 33342. Scale bar 50 μm.

A

STR LOCUS	OBSERVED ALLELES IN EACH SAMPLE							
	nonT patient 1		nonT patient 2		BT patient 1		BT patient 2	
	UDC	iPSC	UDC	iPSC	UDC	iPSC	UDC	iPSC
TH01	7,8	7,8	8,9	8,9	6	6	9,9.3	9,9.3
D21S11	31.2,32.2	31.2,32.2	30	30	31	31	32.2,33.2	32.2,33.2
D5S818	11,12	11,12	10,11	10,11	13	13	13	13
D13S317	8,11	8,11	8,11	8,11	11,13	11,13	8	8
D7S820	8,9	8,9	8,12	8,12	9,11	9,11	8,13	8,13
D16S539	10,13	10,13	11,14	11,14	11	11	11,12	11,12
CSF1PO	10,11	10,11	11,12	11,12	10,12	10,12	9,10	9,10
vWA	14,19	14,19	17,18	17,18	16,17	16,17	15,18	15,18
TPOX	8,11	8,11	9,11	9,11	8	8	8	8
AMEL	X,Y	X,Y	X,Y	X,Y	X	X	X	X
Percent match (UDC vs iPSC)	100		100		100		100	

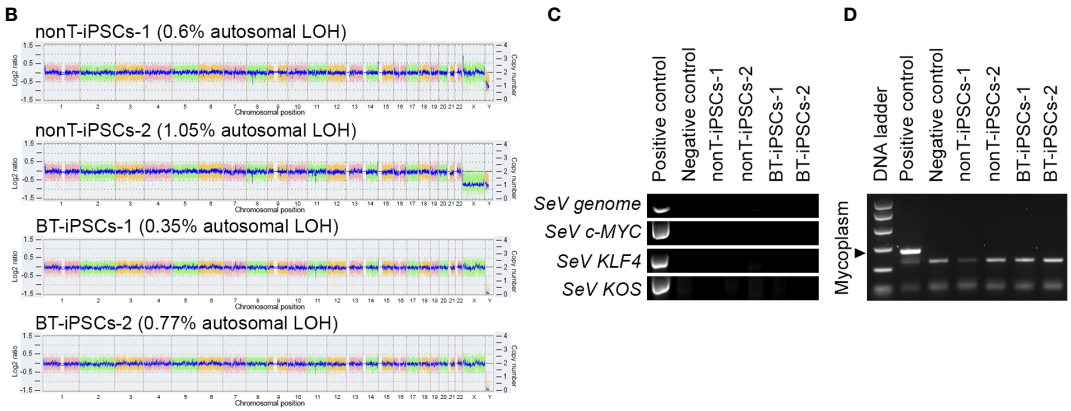

FIGURE 5
Authentication, molecular karyotyping, virus clearance and mycoplasma testing of established iPSCs. **(A)** DNA fingerprint analysis showing that the allele pattern in the iPSCs generated is 100% concordant with the patients' UDCs and it is not concordant with any commercial cell line whose genotype is posted in public databases. The STR locations studied were: *TH01, D21S11, D5S818, D13S317, D7S820, D16S539, CSF1PO, vWA, TPOX* and *AMEL*. The percentage of matching between iPSCs and their parental UDCs is indicated for each sample. **(B)** Whole genome view of the iPSC lines which displays all somatic and sex chromosomes in one frame. The smooth signal plot (right y-axis) is the smoothing of the Log2 ratios (left y-axis), which depict the signal intensities of probes on the microarray and represents the number of copies of each chromosome. The pink, green and yellow colors represent the raw signal for each individual chromosome probe, and the blue signal represents the normalized probe signal, used to identify copy number and any aberrations. The percentage of autosomal loss of heterozygosity (LOH) is indicated for each cell line. **(C)** RT-PCR analysis showing the absence of expression of Sendai virus (SeV) genome and OSKM transgenes in the established iPSC lines. UDCs served as negative control and recently transfected iPSCs served as positive control. **(D)** PCR test for mycoplasma detection, showing the absence of contamination in cultured iPSC lines.

12p70, MCP-1, PDGF-BB and TNFα and observed that all the iMSCs secrete at least two of the analyzed cytokines (Figure 7A). Then, we assessed the capacity of iMSCs to reduce T cell proliferation using activated PBMCs from different donors, in both direct and indirect cocultures (Figures 7B, C). We showed that the generated iMSCs cultured in direct contact with PBMCs inhibited CD3+ T cell proliferation in the PBMC of the two donors tested (Figure 7B). In addition, we also determined that the proliferation of CD3+ T cells was diminished by the secretome of BT-iMSC and nonT-iMSC, with an overall similar trend in both CD4+ and CD8+ T cell subsets (Figure 7C). Despite the fact that comparison of iMSCs with adipose tissue-derived MSCs (adMSCs) was not the focus of this study, we would like to mention that the secretome of iMSCs exhibited higher capacity to decrease CD3+ T cell proliferation and showed enhanced antioxidant capacity when compared to adMSCs (Supplemental Figures 3A-C). Furthermore, the secretome of primed iMSCs was used to interrogate the immunomodulatory plasticity of MSCs after stimulation with inflammatory cytokines (33, 34). We found that cell priming with TNFα and IFNγ modulated the immunomodulatory potential of iMSC secretome, showing in several instances a predisposition to dampen the inhibition of T cell proliferation when compared to the CM of non-primed iMSCs (Figure 7C). These results demonstrated that urine-derived iPSCs from BT and nonT patients are a viable source to obtain iMSCs with immunomodulatory properties.

In order to investigate how the priming with inflammatory cytokines regulates BT-iMSC immunomodulation, we examined themRNA levels of several immunomodulatory genes, including TNFa, TGFb, IL-6, IL-1b, IDO and COX2, in BT-iMSCs. While an overall increase of these factors was found immediately after cell priming (Figure 7D), the expression of the immunomodulatory genes tested reverted to basal levels after 48 hours of priming, with minimal residual effects on IL-6 expression in primed cells (Figure 7E). These data suggest that a transient upregulation of immunomodulatory genes in iMSCs is sufficient to improve their immunomodulatory secretome.

Discussion

Reprogramming somatic cells into iPSCs has emerged as an innovative strategy to improve manufacturing of cellular products for regenerative medicine. Among the different somatic cell types,

10.3389/fimmu.2023.1022676

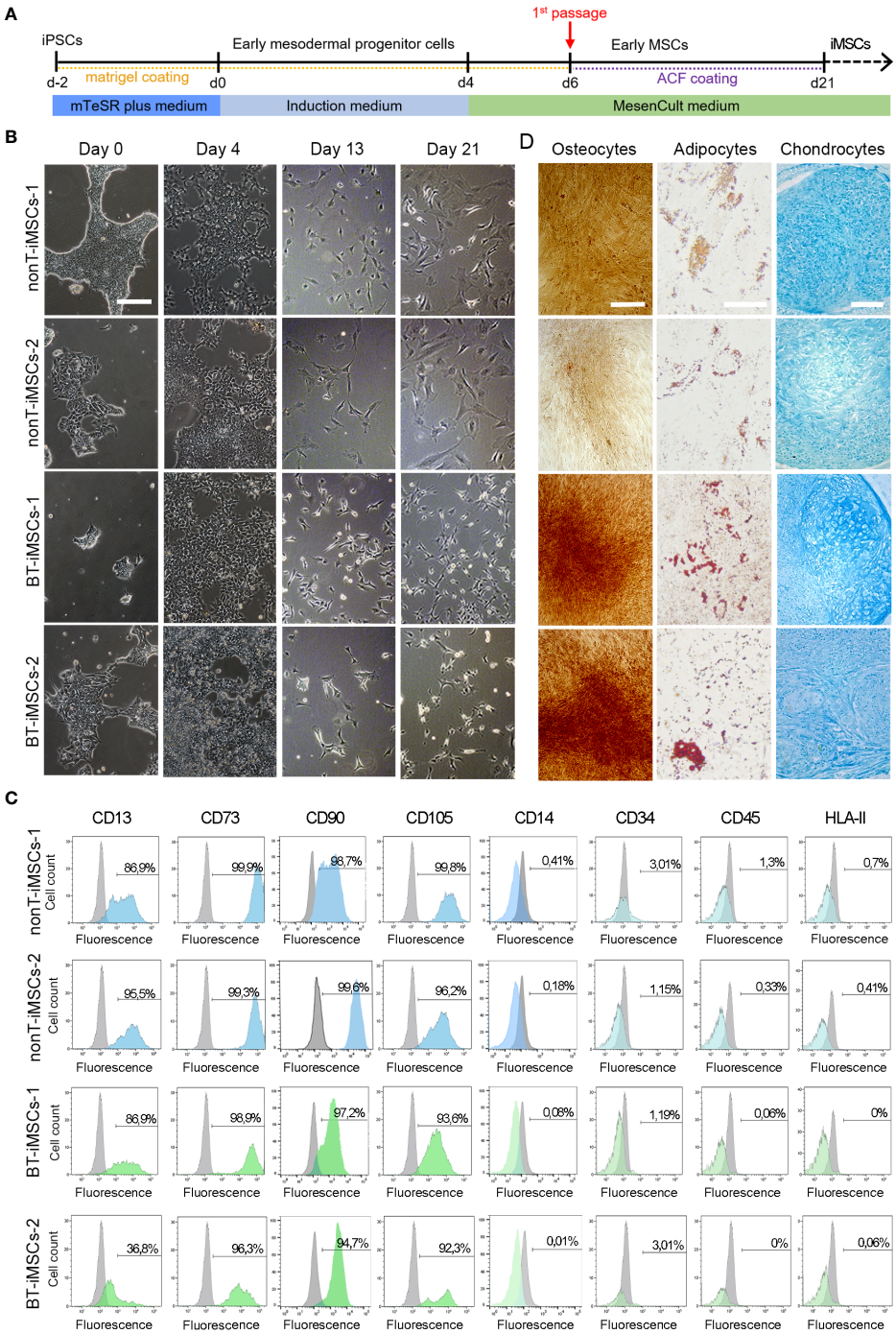

FIGURE 6
Directed differentiation of iPSCs towards iMSCs. **(A)** Schematic timeline of the process for differentiation into iMSCs. **(B)** Microscope images showing the morphological aspect of differentiated iMSCs over time (scale bar 100 µm). **(C)** Flow cytometry analysis of differentiated iMSCs showing that cells were positive for the MSC-specific markers CD13, CD73, CD90 and CD105, whereas they were negative for CD14, CD34, CD45, and HLA-II. **(D)** Representative images of the differentiated iMSCs into osteocytes (scale bar 100µm), adipocytes (scale bar 50µm) and chondrocytes (scale bar 100µm) identified by Alizarin Red, Oil Red O and Alcian Blue staining, respectively.

UDCs represent a convenient source of iPSCs for personalized cell therapies, particularly for those patients with a severe disability affecting their health. Among medically fragile patients, children with cancer are at a high risk of frailty due to the progression of the disease and to the side effects of cancer treatments. For instance, brain tumor pediatric patients experience multiple neurological complications, including deficits in learning, memory, language, attention and processing speed, even after overcoming the illness (35). These debilitating conditions impede in many cases their participation in clinical trials, which is a major challenge for the translation of pediatric cancer research into clinical practice. Unlike solid biopsies, urine collection represents an easy, safe, pain-free and inexpensive way of obtaining large quantities of somatic cells to engineer cell-based therapeutics for a variety of diseases (11, 36, 37).

10.3389/fimmu.2023.1022676

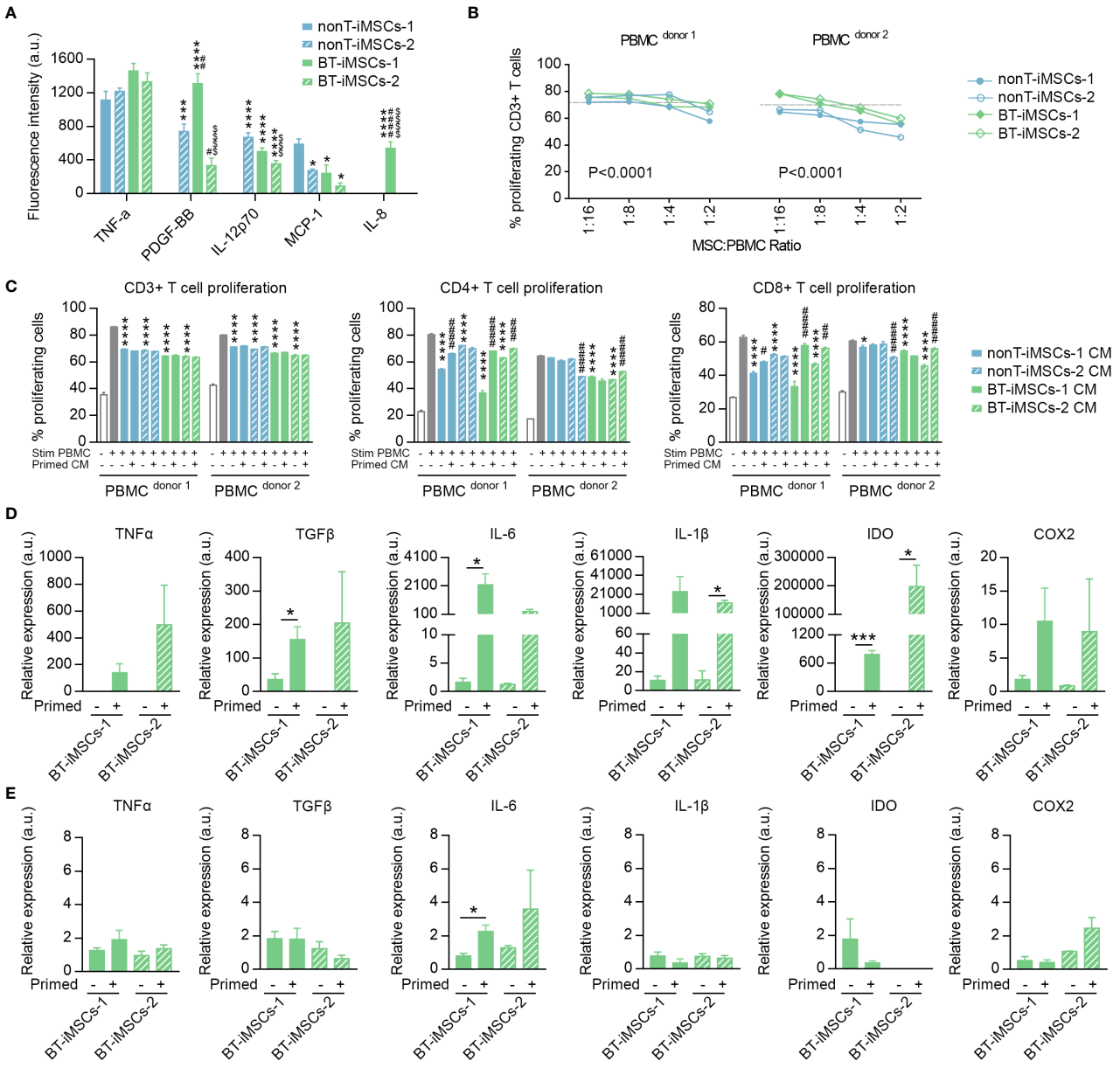

FIGURE 7
Immunomodulatory potential of the generated iMSCs. **(A)** Bar graph showing the fluorescence intensity for inflammatory cytokines secreted by iMSCs determined by ELISA. **(B)** Inhibitory effect of iMSCs on CD3+ T cell proliferation after 5 days co-culture. Dashed line indicates the % of proliferation for CD3+ T cells without iMSCs. **(C)** Bar graphs showing the percentage of $CD3^+$, $CD4^+$ and $CD8^+$ proliferating T cells in response to the secretome of primed or non-primed iMSCs. Of note, the secretome was collected 48 hours after priming. **(D)** Bar graphs showing the expression levels of immunomodulatory genes analyzed by RT-qPCR in primed and non-primed iMSCs derived from BT patients. Of note, the RNA was isolated immediately after priming. **(E)** Bar graphs showing the expression levels of immunomodulatory genes analyzed by RT-qPCR in primed and non-primed iMSCs derived from BT patients. Of note, the RNA was isolated 48 hours after priming. Data are represented as mean ± SEM. The absence of bar in any graph indicates undetected levels of the specific parameters assessed. For **(A)**; *p*0.05, ***p<0.001, ****p<0.0001 compared to nonT-iMSCs-2; $^{\#}$p<0.05, $^{\#\#}$p<0.01, $^{\#\#\#\#}$p<0.0001 compared to nonT-iMSCs-1; $$$p<0.001, $$$$p<0.0001 compared to BT-iMSCs-1. One-way ANOVA. For **(B)**; P value refers to dose effects. Two-way ANOVA. For **(C)**; *p<0.05, ****p<0.0001 compared to stimulated PBMC cultured in regular growth medium. $^{\#}$p<0.05, $^{\#\#}$p<0.01, $^{\#\#\#}$p<0.001, $^{\#\#\#\#}$p<0.0001 compared to their primed counterparts. One-way ANOVA. For **(D–E)**; *p<0.05, ***p<0.001. Student's t-test.

Here we report for the first time the generation of two iPSC lines from UDCs of children with brain tumors. Our results demonstrated that iPSCs can be obtained from small volumes of urine (12-40 ml range), allowing the generation of patient-specific cellular products for therapeutic use, without the need for invasive biopsies. The use of non-invasive sampling methods could increase the number of patients that can benefit from cell therapies, irrespective of their medical condition. Importantly, we used the non-integrative Sendai viral vectors, thus reducing the risk of generating genetic alterations. All these important aspects represent a decisive boost for personalized medicine in the field of childhood cancer. The application of an iPSC-based therapy using autologous cells will prevent an immune response, as the host will recognize the transplanted cell products as their own. In a recent study, personalized iPSC-derived dopamine progenitor cells were successfully applied in a patient with Parkinson's disease, who exhibited clinical improvements and

survived without the need for immunosuppression (38). This evidences that, in contrast to allogeneic cell products, patient-specific cells may be safe in terms of immunoreaction. Therefore, the use of iPSC technology might represent a feasible manner to generate safe and cost-effective cell-based products.

All patient-derived UDCs in this study were successfully reprogrammed into iPSCs, which underwent exhaustive characterization by assessing their pluripotency and multilineage differentiation potential. In addition, we tested iPSC identity, karyotype, virus clearance and mycoplasma contamination, basic quality attributes that are required for cell banking. The storage of high-quality iPSCs allows for clinical application under autologous and allogenic conditions, but also provides researchers the opportunity to conduct iPSC-based studies when they are unable to generate iPSCs in their own labs. In addition to cell-based therapies, banked iPSCs can serve as an effective tool for other applications, including drug discovery and disease modeling (39–42). Although the establishment of iPSC banks has gained recognition, technical challenges remain, such as efficient cryopreservation and storage (43, 44). Researchers are making constant efforts to develop optimal methods that robustly support the use of these cells in fundamental, preclinical and clinical research.

In addition to efficient cell reprograming, we demonstrated for the first time that urine-derived iPSCs from brain tumor patients differentiate into iMSCs. Previous research has established that iMSCs possess remarkable advantages over MSCs derived from organs or tissues (27). Among these advantages, iMSCs originate from an infinite cell source (i.e. iPSCs), thus overcoming the availability limitation for the manufacturing process (45). Moreover, while tissue-derived MSCs possess high heterogeneity that may interfere with their therapeutic effects (25), iMSCs are theoretically more homogeneous because they can generate from a single iPSC clone (26, 27). Consequently, iMSCs may yield more consistent and reproducible results, even when different batches of iMSCs are used. In this context, several reports have demonstrated that iMSCs, including urine-derived iMSCs, show increased therapeutic efficacy in experimental models of disease (3–8, 46). For instance, intra-myocardial administration of iMSCs provided better regenerative effects compared with bone marrow MSCs in a rodent model of myocardial infarction (6). Similarly, the intracranial delivery of iMSCs promoted more robust neuroprotective effects than umbilical cord-derived MSCs in a hypoxic–ischemic rat model (5). A comparative study showed that iMSCs differentiated from the urine of a healthy volunteer exhibited superior wound-healing properties than umbilical cord MSCs (8). Interestingly, iMSCs have been suggested to be safer than bone marrow-derived MSCs in cancer treatment, since they are less prone to promote epithelial–mesenchymal transition, invasion, stemness and growth of cancer cells (47). In a separated study, iMSCs obtained from aged individuals acquired a rejuvenation-associated gene signature, which may be associated with a greater proliferation and differentiation capacity than native MSCs (48). In our study, we demonstrated that iMSCs possess immunomodulatory capacity, supporting their therapeutic application for the treatment of inflammatory processes, such as those induced by radiotherapy (18, 49). This opens new avenues for the generation of more efficient MSC-based therapies in pediatric regenerative medicine. As a major limitation, our study was performed with a reduced number of samples, which prevented from conducting a robust comparative study. Further research will help to elucidate whether the therapeutic properties of BT-iMSCs are equivalent to those of nonT-iMSCs, or even to tissue derived MSCs.

In conclusion, iPSC-based therapies are making steady progress, with more than 100 ongoing or completed clinical trials for several diseases, including neurological diseases, cardiomyopathy or cancer. Interestingly, 40% of these studies include the participation of children, which evidence the value of this sophisticated iPSC technology in the field of pediatric research. Despite the booming advancement on iPSC-derived products, such as iMSCs, a number of hurdles still have to be overcome to exploit their clinical application (50). Among their limitations, safety is the main concern when transplanting iPSC-derived cells, since any residual iPSCs may result in the formation of teratomas (51). For this reason, the development of efficient methods for iPSC differentiation is a crucial step prior to application, in both preclinical and clinical studies. Our research represents a step forward in the development of patient-specific products based on iPSC systems for the treatment of several diseases, which could be applied not only in pediatric patients, but also in adults.

Data availability statement

The original contributions presented in the study are included in the article/Supplementary Materials, further inquiries can be directed to the corresponding author/s.

Ethics statement

The studies involving human participants were reviewed and approved by the Institutional Review Board (or Ethics Committee) of "Secretaría General de Investigación, Desarrollo e Innovación en Salud of Junta de Andalucia (protocol code PR-03-2020, approved on March 2nd 2021)" and the "Consejo Interministerial de Organismos Modificados Genéticamente (protocol code A/ES/21/03, approved on March 2nd 2021)". Written informed consent to participate in this study was provided by the participants' legal guardian/next of kin.

Author contributions

CB-S, YA, JMS-P and VC-G contributed to conception and design of the study. CM-V and RC-L collected human samples and provided magnetic resonances images of patients. CB-S, YA, NA, JMS-P, LO-M and CP-M performed the experiments. CB-S, YA, JMS-P and VC-G analyzed the data. VC-G and CB-S wrote the manuscript and prepared figures. JMS-P and AM-M contributed to data interpretation and wrote sections of the manuscript. All authors contributed to manuscript revision, read, and approved the submitted version.

Funding

This research was funded by the Institute of Health Carlos III, cofounded by Fondos FEDER (CP19/00046 and PI20/00341 to VC-

G), the Asociación Pablo Ugarte (+VIDA project to VC-G), the Asociación Española Contra el Cancer (IDEAS20051CAPI to VCG), the Consejería de Transformación Económica, Industria, Conocimiento y Universidades of Junta de Andalucia, co-funded by Fondos FEDER (PY20/00481 to VC-G and PY20/00480 to AM-M) and the Spanish Ministry of Science and Innovation (PID2021-123965OB-I00 to AM-M). LO-M receives the support of the Spanish Ministry of Universities (FPU19/04703). JMS-P is supported by the Consejería de Transformación Económica, Industria, Conocimiento y Universidades of Junta de Andalucia, co-funded by Fondos FEDER (POSTDOC/21/00424).

Acknowledgments

We are extremely grateful to all the donors and their families who have taken part in this study. In addition, we would like to thank the members of the Pediatric Oncology team who provided continuous support throughout the project.

Conflict of interest

The authors declare that the research was conducted in the absence of any commercial or financial relationships that could be construed as a potential conflict of interest.

Publisher's note

Supplementary material

The Supplementary Material for this article can be found online at: https://www.frontiersin.org/articles/10.3389/fimmu.2023.1022676/full#supplementary-material

References

1. Takahashi K, Tanabe K, Ohnuki M, Narita M, Ichisaka T, Tomoda K, et al. Induction of pluripotent stem cells from adult human fibroblasts by defined factors. *Cell* (2007) 131:861–72. doi: 10.1016/j.cell.2007.11.019

2. Takahashi K, Yamanaka S. Induction of pluripotent stem cells from mouse embryonic and adult fibroblast cultures by defined factors. *Cell* (2006) 126:663–76. doi: 10.1016/j.cell.2006.07.024

3. Lian Q, Zhang Y, Zhang J, Zhang HK, Wu X, Zhang Y, et al. Functional mesenchymal stem cells derived from human induced pluripotent stem cells attenuate limb ischemia in mice. *Circulation* (2010) 121:1113–23. doi: 10.1161/CIRCULATIONAHA.109.898312

4. Sun YQ, Zhang Y, Li X, Deng MX, Gao WX, Yao Y, et al. Insensitivity of human iPS cells-derived mesenchymal stem cells to interferon-gamma-induced HLA expression potentiates repair efficiency of hind limb ischemia in immune humanized NOD scid gamma mice. *Stem Cells* (2015) 33:3452–67. doi: 10.1002/stem.2094

5. Huang J, Kin Pong U, Yang F, Ji Z, Lin J, Weng Z, et al. Human pluripotent stem cell-derived ectomesenchymal stromal cells promote more robust functional recovery than umbilical cord-derived mesenchymal stromal cells after hypoxic-ischaemic brain damage. *Theranostics* (2022) 12:143–66. doi: 10.7150/thno.57234

6. Thavapalachandran S, Le TYL, Romanazzo S, Rashid FN, Ogawa M, Kilian KA, et al. Pluripotent stem cell-derived mesenchymal stromal cells improve cardiac function and vascularity after myocardial infarction. *Cytotherapy* (2021) 23:1074–84. doi: 10.1016/j.jcyt.2021.07.016

7. Liang X, Lin F, Ding Y, Zhang Y, Li M, Zhou X, et al. Conditioned medium from induced pluripotent stem cell-derived mesenchymal stem cells accelerates cutaneous wound healing through enhanced angiogenesis. *Stem Cell Res Ther* (2021) 12:295. doi: 10.1186/s13287-021-02366-x

8. Rajasingh S, Sigamani V, Selvam V, Gurusamy N, Kirankumar S, Vasanthan J, et al. Comparative analysis of human induced pluripotent stem cell-derived mesenchymal stem cells and umbilical cord mesenchymal stem cells. *J Cell Mol Med* (2021) 25:8904–19. doi: 10.1111/jcmm.16851

9. Pavathuparambil Abdul Manaph N, Al-Hawwas M, Bobrovskaya L, Coates PT, Zhou XF. Urine-derived cells for human cell therapy. *Stem Cell Res Ther* (2018) 9:189. doi: 10.1186/s13287-018-0932-z

10. Zhou T, Benda C, Duzinger S, Huang Y, Li X, Li Y, et al. Generation of induced pluripotent stem cells from urine. *J Am Soc Nephrol* (2011) 22:1221–8. doi: 10.1681/ASN.2011010106

11. Mulder J, Sharmin S, Chow T, Rodrigues DC, Hildebrandt MR, D'Cruz R, et al. Generation of infant- and pediatric-derived urinary induced pluripotent stem cells competent to form kidney organoids. *Pediatr Res* (2020) 87:647–55. doi: 10.1038/s41390-019-0618-y

12. Capilla-Gonzalez V, Bonsu JM, Redmond KJ, Garcia-Verdugo JM, Quinones-Hinojosa A. Implications of irradiating the subventricular zone stem cell niche. *Stem Cell Res* (2016) 16:387–96. doi: 10.1016/j.scr.2016.02.031

13. Ali FS, Hussain MR, Gutierrez C, Demireva P, Ballester LY, Zhu JJ, et al. Cognitive disability in adult patients with brain tumors. *Cancer Treat Rev* (2018) 65:33–40. doi: 10.1016/j.ctrv.2018.02.007

14. Capilla-Gonzalez V, Guerrero-Cazares H, Bonsu JM, Gonzalez-Perez O, Achanta P, Wong J, et al. The subventricular zone is able to respond to a demyelinating lesion after localized radiation. *Stem Cells* (2014) 32:59–69. doi: 10.1002/stem.1519

15. Dong X, Luo M, Huang G, Zhang J, Tong F, Cheng Y, et al. Relationship between irradiation-induced neuro-inflammatory environments and impaired cognitive function in the developing brain of mice. *Int J Radiat Biol* (2015) 91:224–39. doi: 10.3109/09553002.2014.988895

16. Suckert T, Beyreuther E, Muller J, Azadegan B, Meinhardt M, Raschke F, et al. Late side effects in normal mouse brain tissue after proton irradiation. *Front Oncol* (2020) 10:598360. doi: 10.3389/fonc.2020.598360

17. Beera KG, Li YQ, Dazai J, Stewart J, Egan S, Ahmed M, et al. Altered brain morphology after focal radiation reveals impact of off-target effects: implications for white matter development and neurogenesis. *Neuro-oncology* (2018) 20:788–98. doi: 10.1093/neuonc/nox211

18. Soria B, Martin-Montalvo A, Aguilera Y, Mellado-Damas N, Lopez-Beas J, Herrera-Herrera I, et al. Human mesenchymal stem cells prevent neurological complications of radiotherapy. *Front Cell Neurosci* (2019) 13:204. doi: 10.3389/fncel.2019.00204

19. Piao J, Major T, Auyeung G, Policarpio E, Menon J, Droms L, et al. Human embryonic stem cell-derived oligodendrocyte progenitors remyelinate the brain and rescue behavioral deficits following radiation. *Cell Stem Cell* (2015) 16:198–210. doi: 10.1016/j.stem.2015.01.004

20. Acharya MM, Rosi S, Jopson T, Limoli CL. Human neural stem cell transplantation provides long-term restoration of neuronal plasticity in the irradiated hippocampus. *Cell Transplant* (2015) 24:691–702. doi: 10.3727/096368914X684600

21. Huang X, Li M, Zhou D, Deng Z, Guo J, Huang H. Endothelial progenitor cell transplantation restores vascular injury in mice after whole-brain irradiation. *Brain Res* (2020) 1746:147005. doi: 10.1016/j.brainres.2020.147005

22. Wang G, Ren X, Yan H, Gui Y, Guo Z, Song J, et al. Neuroprotective effects of umbilical cord-derived mesenchymal stem cells on radiation-induced brain injury in mice. *Ann Clin Lab Sci* (2020) 50:57–64.

23. Liao H, Wang H, Rong X, Li E, Xu RH, Peng Y. Mesenchymal stem cells attenuate radiation-induced brain injury by inhibiting microglia pyroptosis. *BioMed Res Int* (2017) 2017:1948985. doi: 10.1155/2017/1948985

24. Wang GH, Liu Y, Wu XB, Lu Y, Liu J, Qin YR, et al. Neuroprotective effects of human umbilical cord-derived mesenchymal stromal cells combined with nimodipine against radiation-induced brain injury through inhibition of apoptosis. *Cytotherapy* (2016) 18:53–64. doi: 10.1016/j.jcyt.2015.10.006

25. Olmedo-Moreno L, Aguilera Y, Balina-Sanchez C, Martin-Montalvo A, Capilla-Gonzalez V. Heterogeneity of *In vitro* expanded mesenchymal stromal cells and strategies to improve their therapeutic actions. *Pharmaceutics* (2022) 14:1112. doi: 10.3390/pharmaceutics14051112

26. Wruck W, Graffmann N, Spitzhorn LS, Adjaye J. Human induced pluripotent stem cell-derived mesenchymal stem cells acquire rejuvenation and reduced heterogeneity. *Front Cell Dev Biol* (2021) 9:717772. doi: 10.3389/fcell.2021.717772

27. Zhang J, Chen M, Liao J, Chang C, Liu Y, Padhiar AA, et al. Induced pluripotent stem cell-derived mesenchymal stem cells hold lower heterogeneity and great promise in biological research and clinical applications. *Front Cell Dev Biol* (2021) 9:716907. doi: 10.3389/fcell.2021.716907

28. Capilla-Gonzalez V, Lopez-Beas J, Escacena N, Aguilera Y, de la Cuesta A, Ruiz-Salmeron R, et al. PDGF restores the defective phenotype of adipose-derived mesenchymal stromal cells from diabetic patients. *Mol Ther* (2018) 26:2696–709. doi: 10.1016/j.ymthe.2018.08.011

29. Aguilera Y, Mellado-Damas N, Olmedo-Moreno L, Lopez V, Panadero-Moron C, Benito M, et al. Preclinical safety evaluation of intranasally delivered human mesenchymal stem cells in juvenile mice. *Cancers* (2021) 13:1169. doi: 10.3390/cancers13051169

30. Porter AP, Pirlot BM, Dyer K, Uwazie CC, Nguyen J, Turner C, et al. Conglomeration of T and b cell matrix responses determines the potency of human bone marrow mesenchymal stromal cells. *Stem Cells* (2022) 40:1134–48. doi: 10.1093/stmcls/sxac064

31. Cerezo M, Guemiri R, Druillennec S, Girault I, Malka-Mahieu H, Shen S, et al. Translational control of tumor immune escape *via* the eIF4F-STAT1-PD-L1 axis in melanoma. *Nat Med* (2018) 24:1877–86. doi: 10.1038/s41591-018-0217-1

32. Lipat AJ, Cottle C, Pirlot BM, Mitchell J, Pando B, Helmly B, et al. Chemokine assay matrix defines the potency of human bone marrow mesenchymal stromal cells. *Stem Cells Trans Med* (2022) 11:971–86. doi: 10.1093/stcltm/szac050

33. Chinnadurai R, Copland IB, Garcia MA, Petersen CT, Lewis CN, Waller EK, et al. Cryopreserved mesenchymal stromal cells are susceptible to T-cell mediated apoptosis which is partly rescued by IFNgamma licensing. *Stem Cells* (2016) 34:2429–42. doi: 10.1002/stem.2415

34. Yin JQ, Zhu J, Ankrum JA. Manufacturing of primed mesenchymal stromal cells for therapy. *Nat Biomed Eng* (2019) 3:90–104. doi: 10.1038/s41551-018-0325-8

35. Monje M, Fisher PG. Neurological complications following treatment of children with brain tumors. *J Pediatr Rehabil Med* (2011) 4:31–6. doi: 10.3233/PRM-2011-0150

36. Steinle H, Weber M, Behring A, Mau-Holzmann U, von Ohle C, Popov AF, et al. Reprogramming of urine-derived renal epithelial cells into iPSCs using srRNA and consecutive differentiation into beating cardiomyocytes. *Mol Ther Nucleic Acids* (2019) 17:907–21. doi: 10.1016/j.omtn.2019.07.016

37. Lin VJT, Hu J, Zolekar A, Yan LJ, Wang YC. Urine sample-derived cerebral organoids suitable for studying neurodevelopment and pharmacological responses. *Front Cell Dev Biol* (2020) 8:304. doi: 10.3389/fcell.2020.00304

38. Schweitzer JS, Song B, Herrington TM, Park TY, Lee N, Ko S, et al. Personalized iPSC-derived dopamine progenitor cells for parkinson's disease. *New Engl J Med* (2020) 382:1926–32. doi: 10.1056/NEJMoa1915872

39. Yang X, Liu Y, Zhou T, Zhang H, Dong R, Li Y, et al. An induced pluripotent stem cells line (SDQLCHi014-a) derived from urine cells of a patient with ASD and hyperactivity carrying a 303kb *de novo* deletion at chr3p26.1 implicating GRM7 gene. *Stem Cell Res* (2019) 41:101635. doi: 10.1016/j.scr.2019.101635

40. Guo X, Qian R, Shan X, Yang L, Chen H, Ding Y, et al. Generation of a human induced pluripotent stem cell line (WMUi021-a) from a gitelman syndrome patient carrying a SLC12A3 gene mutation (c.179C > T). *Stem Cell Res* (2021) 53:102280. doi: 10.1016/j.scr.2021.102280

41. Xu J, Wang Y, He J, Xia W, Zou Y, Ruan W, et al. Generation of a human charcot-Marie-Tooth disease type 1B (CMT1B) iPSC line, ZJUCHi001-a, with a mutation of c.292C>T in MPZ. *Stem Cell Res* (2019) 35:101407. doi: 10.1016/j.scr.2019.101407

42. Cao Y, Xu J, Wen J, Ma X, Liu F, Li Y, et al. Generation of a urine-derived ips cell line from a patient with a ventricular septal defect and heart failure and the robust differentiation of these cells to cardiomyocytes *via* small molecules. *Cell Physiol Biochem* (2018) 50:538–51. doi: 10.1159/000494167

43. Cottle C, Porter AP, Lipat A, Turner-Lyles C, Nguyen J, Moll G, et al. Impact of cryopreservation and freeze-thawing on therapeutic properties of mesenchymal Stromal/Stem cells and other common cellular therapeutics. *Curr Stem Cell Rep* (2022) 8:72–92. doi: 10.1007/s40778-022-00212-1

44. Huang CY, Liu CL, Ting CY, Chiu YT, Cheng YC, Nicholson MW, et al. Human iPSC banking: barriers and opportunities. *J Biomed Sci* (2019) 26:87. doi: 10.1186/s12929-019-0578-x

45. Robb KP, Fitzgerald JC, Barry F, Viswanathan S. Mesenchymal stromal cell therapy: progress in manufacturing and assessments of potency. *Cytotherapy* (2019) 21:289–306. doi: 10.1016/j.jcyt.2018.10.014

46. Gao WX, Sun YQ, Shi J, Li CL, Fang SB, Wang D, et al. Effects of mesenchymal stem cells from human induced pluripotent stem cells on differentiation, maturation, and function of dendritic cells. *Stem Cell Res Ther* (2017) 8:48. doi: 10.1186/s13287-017-0499-0

47. Zhao Q, Gregory CA, Lee RH, Reger RL, Qin L, Hai B, et al. MSCs derived from iPSCs with a modified protocol are tumor-tropic but have much less potential to promote tumors than bone marrow MSCs. *Proc Natl Acad Sci United States America* (2015) 112:530–5. doi: 10.1073/pnas.1423008112

48. Spitzhorn LS, Megges M, Wruck W, Rahman MS, Otte J, Degistirici O, et al. Human iPSC-derived MSCs (iMSCs) from aged individuals acquire a rejuvenation signature. *Stem Cell Res Ther* (2019) 10:100. doi: 10.1186/s13287-019-1209-x

49. Hwang SY, Jung JS, Kim TH, Lim SJ, Oh ES, Kim JY, et al. Ionizing radiation induces astrocyte gliosis through microglia activation. *Neurobiol Dis* (2006) 21:457–67. doi: 10.1016/j.nbd.2005.08.006

50. Yamanaka S. Pluripotent stem cell-based cell therapy-promise and challenges. *Cell Stem Cell* (2020) 27:523–31. doi: 10.1016/j.stem.2020.09.014

51. Gutierrez-Aranda I, Ramos-Mejia V, Bueno C, Munoz-Lopez M, Real PJ, Macia A, et al. Human induced pluripotent stem cells develop teratoma more efficiently and faster than human embryonic stem cells regardless the site of injection. *Stem Cells* (2010) 28:1568–70. doi: 10.1002/stem.471

frontiers | Frontiers in Immunology

TYPE Original Research
PUBLISHED 16 February 2023
DOI 10.3389/fimmu.2023.1078551

OPEN ACCESS

EDITED BY
Guido Moll,
Charité Universitätsmedizin Berlin,
Germany

REVIEWED BY
Magdiel Pérez-Cruz,
Stanford University, United States
Behnam Sadeghi,
Karolinska Institutet (KI), Sweden

*CORRESPONDENCE
Alexander Hackel
alexandermaximilian.hackel@uksh.de

†PRESENT ADDRESS
Alexander Hackel,
Rheumatology and Clinical Immunology,
University Hospital Luebeck, Lübeck,
Germany

SPECIALTY SECTION
This article was submitted to
Alloimmunity and Transplantation,
a section of the journal
Frontiers in Immunology

RECEIVED 24 October 2022
ACCEPTED 09 January 2023
PUBLISHED 16 February 2023

CITATION
Hackel A, Vollmer S, Bruderek K, Lang S and Brandau S (2023) Immunological priming of mesenchymal stromal/stem cells and their extracellular vesicles augments their therapeutic benefits in experimental graft-versus-host disease *via* engagement of PD-1 ligands.
Front. Immunol. 14:1078551.
doi: 10.3389/fimmu.2023.1078551

Immunological priming of mesenchymal stromal/stem cells and their extracellular vesicles augments their therapeutic benefits in experimental graft-versus-host disease *via* engagement of PD-1 ligands

Alexander Hackel*†, Sebastian Vollmer, Kirsten Bruderek, Stephan Lang and Sven Brandau

Department of Otorhinolaryngology, University Hospital Essen, University Duisburg-Essen, Essen, Germany

Mesenchymal stromal cells (MSCs) and their extracellular vesicles (EVs) exert profound anti-inflammatory and regenerative effects in inflammation and tissue damage, which makes them an attractive tool for cellular therapies. In this study we have assessed the inducible immunoregulatory properties of MSCs and their EVs upon stimulation with different combinations of cytokines. First, we found that MSCs primed with IFN-γ, TNF-α and IL-1β, upregulate the expression of PD-1 ligands, as crucial mediators of their immunomodulatory activity. Further, primed MSCs and MSC-EVs, compared to unstimulated MSCs and MSC-EVs, had increased immunosuppressive effects on activated T cells and mediated an enhanced induction of regulatory T cells, in a PD-1 dependent manner. Importantly, EVs derived from primed MSCs reduced the clinical score and prolonged the survival of mice in a model of graft-versus-host disease. These effects could be reversed *in vitro* and *in vivo* by adding neutralizing antibodies directed against PD-L1 and PD-L2 to both, MSCs and their EVs. In conclusion, our data reveal a priming strategy that potentiates the immunoregulatory function of MSCs and their EVs. This concept also provides new opportunities to improve the clinical applicability and efficiency of cellular or EV-based therapeutic MSC products.

KEYWORDS

mesenchymal stromal/stem cells (MSCs), graft-versus-host disease (GVHD), immunomodulation, extracellular vesicles (EVs), regulatory T cells (Tregs), cytokine priming, programmed death ligand system (PD-1 and PD-L1)

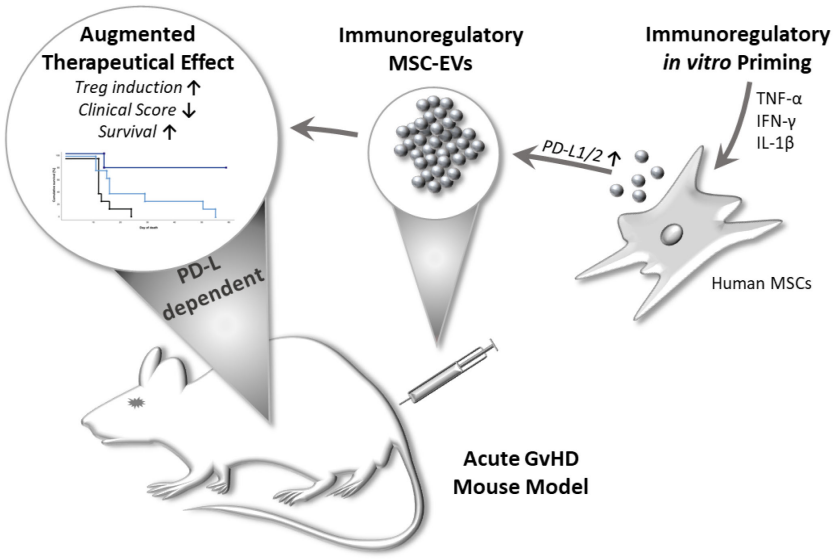

GRAPHICAL ABSTRACT
Multi-cytokine priming combined with subsequent screening of immune responding MSCs, improved MSC-EVs immunomodulatory activity in a PD-1 dependent manner. Primed MSC-EVs demonstrated immunosuppressive effects on activated T cells and mediated an enhanced induction of regulatory T cells. Importantly, primed MSC-EVs reduced disease severity and prolonged survival in a mouse model of acute graftversus-host disease (GvHD). These effects could be reversed by adding neutralizing antibodies directed against PD-Ls to MSC-EVs.

Introduction

Mesenchymal stromal/stem cells (MSCs) are non-hematopoietic, fibroblast-like progenitor cells, capable of differentiating into different mesenchymal tissue lineages, such as chondrocytes, osteoblasts and adipocytes (1–4). They are defined by their plastic adherence, the expression of a set of characteristic cell surface markers, but absence of endothelial and hematopoietic cell surface antigens, and their multilineage differentiation capacity (1, 5–7). Originally identified in the bone marrow, they have now been isolated from many vascularized tissue sources and body fluids (8–13). Considering their broad immunoregulatory capacity towards the innate and adaptive immune system, MSCs are in the focus as a novel therapeutic approach in many inflammation-related diseases (14–17).

MSCs display their multifaceted immunomodulatory properties *via* both, cell-contact-dependent direct mechanisms and contact-independent paracrine mechanisms, including the induction of anti-inflammatory dendritic cells (DCs) and Tregs (18–22). While initial studies have indicated that MSCs are capable of migrating to areas of tissue damage, more recent studies suggest that MSCs often do not reach these sites, but rather accumulate in the lung and spleen and are rapidly cleared from the system (11–13, 23–25). Thus, immunomodulation exerted by MSCs is strongly associated with paracrine mechanisms, e.g. extracellular vesicles (EVs) are suggested as potential mediators of their therapeutic effects (26–28).

EVs contain a multitude of bio- and immuno-active molecules, such as cytokines, nucleic acids, and other proteins, which in part resemble a comparable molecular spectrum to their parental cells of origin (29, 30). Regarding their immunoregulatory activity, MSC-derived EVs exert comparable therapeutic effects akin to the MSCs themselves (26, 31, 32). Compared to their parental cells and conventional MSC-based therapy, the use of MSC-EVs represent a more easy-to-handle sterile therapeutic tool, whose application also minimizes any risks for patients (11–13, 26, 33).

The receptor programmed cell death 1 (PD-1) system is a crucial component in the regulation and activation of T cells, as demonstrated by the enhanced susceptibility of PD-1 knockout mice to autoimmune diseases (34, 35) and its role in GvHD mice models (36–38). The expression of PD-1 ligand 1 (PD-L1) is reported on non-hematopoietic cells, like MSCs, but also on hematopoietic cells, while PD-1 ligand 2 (PD-L2)-expression is typically found on antigen-presenting cells (APCs), but it is also found to be expressed by MSCs (37, 39, 40). Previous reports have suggested the presence of PD-L1 within EVs and as soluble 'free' entities, and in addition as part of soluble cell membrane particles (37, 41, 42).

A big challenge in MSC and EV therapy is to overcome the considerable variations in therapeutic efficiency observed between different donor and manufacturing batches (43). Variations in culture conditions, differences in donor and tissue origin, but also variations in isolation and culture procedures can alter the epigenetic profile of MSCs, thus providing a challenge to generate immunoregulatory MSCs/EVs with consistent properties (44). MSC biology itself may provide some important cues to generate higher degree of reproducibility. Indeed, exposure to an inflammatory environment is necessary to fully activate MSCs immunoregulatory function to a more robust level of homogeneity (45, 46).

In our previous studies, assessing the immune response of MSCs to stimulations with multiple cytokines (47), we have identified an optimal proinflammatory cytokine stimulation approach for MSCs to be employed prior to their therapeutic application, for generating fully activated MSCs and MSC-EVs with an increased and robust immunoregulatory capacity. Building on our previous studies (46,

48), we here used tissue-specific MSCs derived from two different sources, nasal mucosa and human bone marrow, to evaluate their immunomodulatory features and the underlying mechanism in an *in vivo* mouse model.

Ultimately, this method may provide a more efficient and robust therapeutic approach to better standardize MSC/EV-based therapy of inflammation-related diseases.

Methods

Study approval, isolation and culture of MSCs

The use of human samples was approved by the ethics committee of the medical faculty of the University Duisburg-Essen. Nasal mucosa MSCs, further referred to as "MSCs" in this study, were obtained from the inferior nasal concha of healthy individuals (age 30-70 years) at the Department of Othorhinolaryngology, University Hospital Essen (Essen, Germany). The isolation, culture of MSCs and evaluation of differentiation potential were conducted as described before (8). MSCs were cultured in DMEM/RPMI-1640 high glucose (50%/50% v/v), supplemented with 2mM L-Glutamine, 100 IU/ml penicillin, 100 mg/ml streptomycin (all ThermoFisher Scientific, Karlsruhe, Germany) and 10% (v/v) heat-inactivated FCS (Merck/Biochrom, Berlin, Germany). All MSCs used in experiments were between passages 3-6.

Bone marrow MSCs further referred to as "bmMSCs" were kindly provided by Bernd Giebel from the Institute of Transfusion Medicine, University Hospital Essen, Germany, registered as "MSC 41.5". BmMSCs were originally isolated from bone marrow aspirates of healthy individuals after informed consent as described before (26) and acquisition was approved by the ethics committee of the medical faculty of the University Duisburg-Essen. Phenotyping of bmMSCs used in the study was conducted in line with ISCT minimal criteria for MSCs (6), by evaluating cell-surface marker expression with flow cytometry and trilineage differentiation to validate multipotent differentiation capacity of MSCs (8). Experiments with bmMSCS were conducted within passage 4-6. BmMSCs were cultured in DMEM low glucose (PAN Biotech, Aidenbach, Germany), supplemented with 10% platelet lysate (kindly provided by the Institute of Transfusion Medicine, University Hospital Essen), 100 U/mL penicillin-streptomycin-glutamine and 5 IU/mL Heparin (Ratiopharm, Ulm, Germany).

Multi cytokine-priming of MSCs and bmMSCs

Cytokine-priming of MSCs and bmMSCs was based on a previously established concept (47). In brief, MSCs and bmMSCs were stimulated in culture medium, with IFN-γ (1000 U/ml; PeproTech, Hamburg, Germany) and TNF-α (1000 U/ml; Miltenyi, Bergisch Gladbach, Germany) in the present or absence of IL-1β (10 ng/ml; Miltenyi) for 24 h at 37°C, 5% CO_2. Afterwards, cells were washed twice with PBS, and incubated in culture medium for additional 48 h. Subsequently, MSCs were either processed directly for FACS analysis, co-culture experiments or administered in mouse GvHD models.

Flow cytometric analysis

Following antibodies were used for MSC characterization: CD29-PE (clone MAR4), CD45-V500 (clone HI30, both BD Bioscience, Heidelberg, Germany), CD31-APC-eFlour780 (clone WM59), CD73-PerCP-eFlour710 (clone AD2, both ThermoFisher scientific), CD34-FITC (clone 581), CD90-Brilliant Violet 421 (clone 5E10) and CD105-Pe-Cy7 (clone 43A3, all BioLegend, Koblenz, Germany). After stimulation with IFN-γ/TNF-α +/- IL-1β cells were stained with CD54-APC (clone HA58), CD274-PerCP-eFlour710 (PD-L1, clone MIH1, all ThermoFisher scientific) and CD273-PE-Vio770 (PD-L2, clone MIH18, Miltenyi). Cells were analysed using FACSCanto II flow cytometer and BD FACS Diva Software 8.0. (BD Bioscience).

Isolation and size characterization of extracellular vesicles from MSCs and bmMSCs

For isolation of MSCs and bmMSCs EVs, cells were cultured and stimulated with IFN-γ/TNF-α +/- IL-1β as described above in Nunc™ High Cell Factory™. Cell culture supernatants were collected and EVs were purified by differential centrifugations and polyethylene glycol (PEG) precipitation as recently described (49). EV isolated from culture medium of $4*10^7$ MSCs or bmMSCs that had been conditioned for 48 h were defined as 1 EV unit. MSC-EV size and particle concentration were determined by using nanoparticle tracking analysis by ZetaView (Particle Metrix, Meerbusch, Germany) (49, 50). ZetaView was calibrated with a polystyrene bead standard of 100 nm (ThermoFisher Scientific). Loaded samples were recorded by video at 11 positions, repeated 5 times. Further settings were Sensitivity: 75, shutter: 75, minimum brightness: 20, minimum size: 5, maximum size: 20 and median value: 20.

Transmission electron microscopy of extracellular vesicles

Transmission electron microscopy of extracellular vesicles was executed in the department of Physical Chemistry, Faculty of Chemistry, University Duisburg-Essen, Essen, Germany. The MSC-EV preparations were diluted 1:10 (1 EV-unit/ml in 10 mM HEPES, 0.9% NaCl) and subjected to a formvar-coated copper grid. The samples were further incubated with a staining solution of 0.75% Uranyl formate, 6 mM NaOH and dried at room temperature. MSC-EV samples were analysed with a ZEISS EM910 at 120 kV.

SDS-PAGE and Western blot analysis

For SDS-PAGE, supernatants and corresponding EV preparations were incubated with SDS sample buffer (pH 6.8, 50

mM Tris, 4% glycerine, 0.8% SDS, 0.04% bromphenol blue and with or without 1.6% β-mercaptoethanol) as described before (49). Samples were further analysed by wet immunoblotting on nitrocellulose membranes (GE Healthcare) and staining with following antibodies: mouse anti-human CD9 (VJ1, kindly provided by Francisco Sanchez-Madrid), mouse anti-human CD81 (JS-81, BD-Bioscience), rabbit anti-human/mouse/rat HSP70/HSPA1A (R&D Systems, Abingdon, United Kingdom), rabbit anti-human Flotillin-1 (Sigma-Aldrich, St. Loius, USA) and rabbit anti-human CD274 (PD-L1, Pro-Sci-Inc., Poway, USA). Goat anti-rabbit IgG and goat anti-mouse IgG (both HRP-conjugated, Cell Signaling Technology, Danvers, MA, USA) were used as secondary antibodies.

$CD3^+$ T cell proliferation assay

$CD3^+$ T cells of healthy donors were isolated from peripheral blood mononuclear cells after density-gradient centrifugation *via* positive selection using human $CD3^+$ MicroBeads (Miltenyi) according to the manufacturer's instructions. After isolation, T cells were labelled with 10 mmol/l Cell Proliferation Dye eFluor 450 (CPDye405) according to the manufacturer's instructions (ThermoFisher Scientifc). To assess the effect of MSC cells on $CD3^+$ T cells, cells were co-cultured in MSC culture medium (see above) with a T-cell:MSC ratio of 2:1 ($0.5*10^5$ $CD3^+$: $0.25*10^5$ MSCs) at 37°C, 5% CO^2. To study the influence of EVs from stimulated MSCs on T cell proliferation, $0,5*10^5$ $CD3^+$ T cells were cultured in the present or absence of 30 µL isolated EV preparations. T cell proliferation was induced by adding tetrameric antibody-complex ImmunoCult™ Human CD2/CD3/CD28 (StemCell Technologies, Grenoble, France). CPDye405 intensity was analysed by flow cytometry after 4 days of proliferation. Proliferation index calculation is based on dye dilution and was calculated with ModFit LT 3.3 (Verity Software House) according to an algorithm provided by the software. The index of the non-proliferated fraction was subtracted, and the index of T cells without MSCs was set as 100%. The proliferation index is the sum of the cells in all generations divided by the computed number of original parent cells theoretically present at the start of the experiment. The proliferation index thus reflects the increase in cell number in the culture over the course of the experiment.

$CD3^+$ Tregs induction assay

After isolation by CD3 microbeads (see above), $CD3^+$ T cells were stimulated with MSC or bmMSC preparations, in the respective culture medium (see above). Treg assay was performed in a 96-well round-bottom plate coated with antibodies against CD3 (10 µg/ml, clone OKT-3; ThermoFisher scientific) and CD28 (2 µg/ml, clone 28.2; Beckman Coulter) for T cell-activation. To assess the effect of MSC cells on $CD3^+$ T cells, cells were co-cultured in a T-cell:MSC ratio of 2:1 ($0.5*10^5$ $CD3^+$: $0.25*10^5$ MSCs) at 37°C, 5% CO^2 To test effects of EVs isolated from stimulated MSC, $0,5*10^5$ $CD3^+$ T cells were cultured in the present or absence of 30 µl EV preparations. After 3 days of culture $CD3^+$ T cells were stained with CD4-APC-Cy7 (clone RPA-T4), CD25-APC (clone NM-A251, both BD-Bioscience), CD127-PE-Cy7 (eBioRDR5, ThermoFisher scientific), and intracellular with FoxP3-FITC (ECH101, both ThermoFisher scientific). Tregs induction were determined with marker expression of $CD4^+$ $CD127^{dim}$ $CD25^+$ $FOXP3^+$ of total $CD4^+$. Cells were analysed with BD FACSCanto II using BD FACS DIVA 8.01 software (BD Biosciences).

GvHD mouse model

Female BalbALB/c and C57BL/6 mice (12-14 weeks old) were purchased from Charles River Laboratory or Janvier Laboratory, were housed in a pathogen-free facility of the University Hospital Essen and treated with water containing antibiotics (0,11 g/l Neomycin, Ampicillin, Vancomycin and Metronidazole). All animal procedures were performed in accordance with the international guidelines for good laboratory practice and the institutional guidelines of the University Hospital Essen, approved by the animal welfare committees of North Rhine Westphalia. MHC-mismatched murine HSCT model of GvHD was generated by transplanting CD90.2 depleted bone marrow cells (bm cells) from female C57BL/6 donor-mice into female Balb/c recipient-mice, previously total body irradiated with a dose of 8 Gy (50, 51). The recipient female BALB/c mice were reconstituted with $5*10^6$ bm cells from C57BL/6 mice and $0.5*10^6$ naïve $CD4^+$ spleen cells were used to induce GvHD pathology. For CD90.2 depletion of total bone marrow cells after isolation from femur and tibia of C57BL/6 mice, negative selection mouse CD90.2 cell isolation Kit (Miltenyi, Bergisch Gladbach, Germany) according to the manufacturer's instructions was used. Naïve $CD4^+$ spleen cells were isolated from total spleen after erythrocyte depletion with ammonium-chloride-potassium buffer and subsequent negative selection using mouse naïve $CD4^+$ T cell isolation Kit (Miltenyi) according to the manufacturer's instructions. The clinical symptoms of GvHD were assessed with a clinical scoring system (Supplementary Table S1). In long-term experiments, mice were kept until day 58 after HSCT to analyse long-term clinical follow up and to record survival curves. In short-term experiment, mice were sacrificed on day 11 after HSCT and the frequency of Tregs in the circulation was determined. Treatment was performed by intravenous injection of 0.03 EV units per mice for three consecutive days or by a single treatment with $5*10^6$ MSC per mice, starting as soon mice regained weight at day 7 or 8 after BMT. Mice were sacrificed when the respective criteria as set out in the institutional and governmental animal welfare guidelines were reached (Supplement Table). For neutralizing PD-1 ligands in EV preparations, MSC-EVs were pre-incubated for 30 minutes with inhibitory antibodies against CD274 (PD-L1, clone 29E.2A3, BioLegend) (2ug/ml) and CD273 (PD-L2, MIH18, BioLegend) (2µg/ml). To determine non-specific effects of inhibitory antibodies, isotype controls were used at the same concentrations as the specific antibodies. Unbound antibodies were removed by 100-kDa molecular weight cut-off (Vivaspin®, Sartorius, Göttingen, Germany) centrifugal polyether sulfone membrane ultrafiltration before intravenous injection of EV preparations. Mice were sacrificed when the respective criteria as set out in the institutional and governmental animal welfare guidelines were reached. Animals that died from radiation disease or due to failed engraftment of bone marrow of C57BL/6 donor mice were excluded from experiments.

Mice that had to be sacrificed during the experiment due to clinical scoring were continuously recorded with a score of 10.

Swiss roll colon analysis

In order to analyse the colon histology of groups within the short-term GvHD model, we employed a previously published technique referred as "Swiss roll" (52). In brief, directly after sacrifice of mice feces were removed by flushing with PBS. The colon was rolled up on a wooden stick to be subsequently fixed in 4% formalin. The fixed preparations were embedded in paraffin for subsequent cutting in 5 µm sections by microtome. Sections were stained with hematoxylin and eosin (HE) and analysed by light microscopy.

Analysis of blood samples

Blood samples were taken from donor C57BL/6 mice at day 1 and from recipient Balb/c mice on day 11 after irradiation. Mice were anaesthetized with isoflurane, blood was drawn from retro-orbital venous and collected in EDTA-tubes and subjected to flow cytometry analysis. Notably, it was not feasible to collect a sufficient quantity of blood samples from every mouse for further analysis, caused by the severe pathology of the GvHD mouse model.

Statistical analysis

All data are shown as means as center value and errors bars (+/-) SD or SEM as indicated. Data were analysed by paired parametric t-test or by one-way analysis of variance (ANOVA) with Tukey's multiple comparison test. Kaplan–Meier curves were analysed with Gehan-Breslow-Wilcoxon to compare survival between treatment groups. Data are presented as p-values of $p < 0.05$ (*), $p < 0.01$ (**), $p < 0.001$ (***) or $p < 0.0001$ (****) were considered statistically significant.

Results

Enhanced induction of Tregs by primed MSC and their EVs is mediated by PD-1 Ligands *in vitro*

The MSCs used in the study were characterized in a standarized procedure and daily routine in our lab according to ISCT criteria (6) (Figures 1A, B). Crucial for our study is the immunomodulatory priming of MSCs, which was previously shown to mediate MSCs immunoregulatory activity and specific cell surface markers (45, 46, 53).

In our previous work we observed that during triple cytokine priming by TNF-α, IL-1β and IFN-γ, the cytokine IL-1β further augmented the well-established immunoregulatory activity of MSCs induced by TNF-α/IFN-γ (47). Based on previous studies, we decided to test for PD-l ligand expression of cytokine primed MSCs, as these surface proteins have been described to be crucial for MSCs' immunoregulatory activity towards T cells (37, 54). We analysed MSCs of different donors with respect to their responsiveness to strong triple-cytokine priming (With 1000 U/ml of TNF-α/IFN-γ and 10ng/ml IL-1β). This response we compared to the well-established dual stimulation with TNF-α and IFN-γ (each 1000 U/ml) (55).

Interestingly, we found two response patterns of MSCs. First, MSCs compiled in Figures 1C–E (representative FACS histograms shown in Figure S1A) demonstrated a substantial increase in protein expression after triple-cytokine priming compared to the dual priming with TNF-α/IFN-γ alone. These MSCs were considered "full-responders". In turn, MSCs which were not additionally activated by triple cytokine priming (TNF-α/IFN-γ and IL-1β) and/or showed lower expression of marker proteins in general, were considered as incompletely responsive (Figures 1F–H). Further *in vitro* and *in vivo* experiments were conducted with full responder MSC preparations.

For validation of MSCs immunoregulatory capacity, we tested the same MSC preparations shown in Figures 1C–E and in addition their derived EVs in different immune-functional *in vitro* read-outs based on $CD3^+$ T lymphocytes (Figures 2A–F). Addition of triple-primed MSC or EVs showed the strongest potential to reduce T cell proliferation (Figures 2C, D) and to induce Tregs (Figures 2E, F) in CD3 T cell culture assays.

Multi-cytokine priming increased PD-L1 and PD-L2 expression in full responder (Figures 1A–C). As these proteins have shown strong immunoregulatory activity towards T lymphocytes (34, 35), as proof of concept, we inhibited the function of PD-L1 and PD-L2 on MSCs and EVs by neutralizing antibodies and analysed effects on T lymphocyte proliferation and induction of Tregs. Interestingly, we could showed that PDL blockade restored $CD3^+$ T lymphocyte proliferation in co-culture systems with MSC (Figures 3A, B). Triple-cytokine stimulated MSCs (Figure 3C) and their EVs (Figure 3D) strongly augmented induction of Tregs in our *in vitro* system. This induction of Tregs was strongly reduced in the presence of inhibitory antibodies to PD-1 ligands. Interestingly, the Treg induction by unstimulated and dual TNF-α/IFN-γ stimulated MSCs and their EVs was hardly abrogated after PD-L inhibition. Thus, our results support the notion that Treg induction is largely dependent on PD-1/PDL1/2 interaction.

EVs from immunologically primed MSCs ameliorate murine experimental GvHD

In order to test the therapeutic potential and applicability of the immunologically optimized triple primed MSCs and their EVs, defined by our functional *in vitro* experiments (Figures 1–3), we utilized a model of experimental murine GvHD. We conducted the following *in vivo* experiments with full responder MSCs after triple-priming compared to unstimulated MSCs and PBS control.

In this model, GvHD is generated by transplanting CD90.2-depleted bone marrow cells (BM cells) from female C57BL/6 donor-mice into female Balb/c recipient-mice, previously irradiated with a total dose of 8 Gy. The recipient female Balb/c mice were reconstituted with BM cells from C57BL/6 mice and with naïve $CD4^+$ spleen cells to induce GvHD pathology (51). Groups were treated with MSC-EVs (one injection per day for three consecutive days) or with a single injection of MSCs. Triple-primed MSCs showed an activated

10.3389/fimmu.2023.1078551

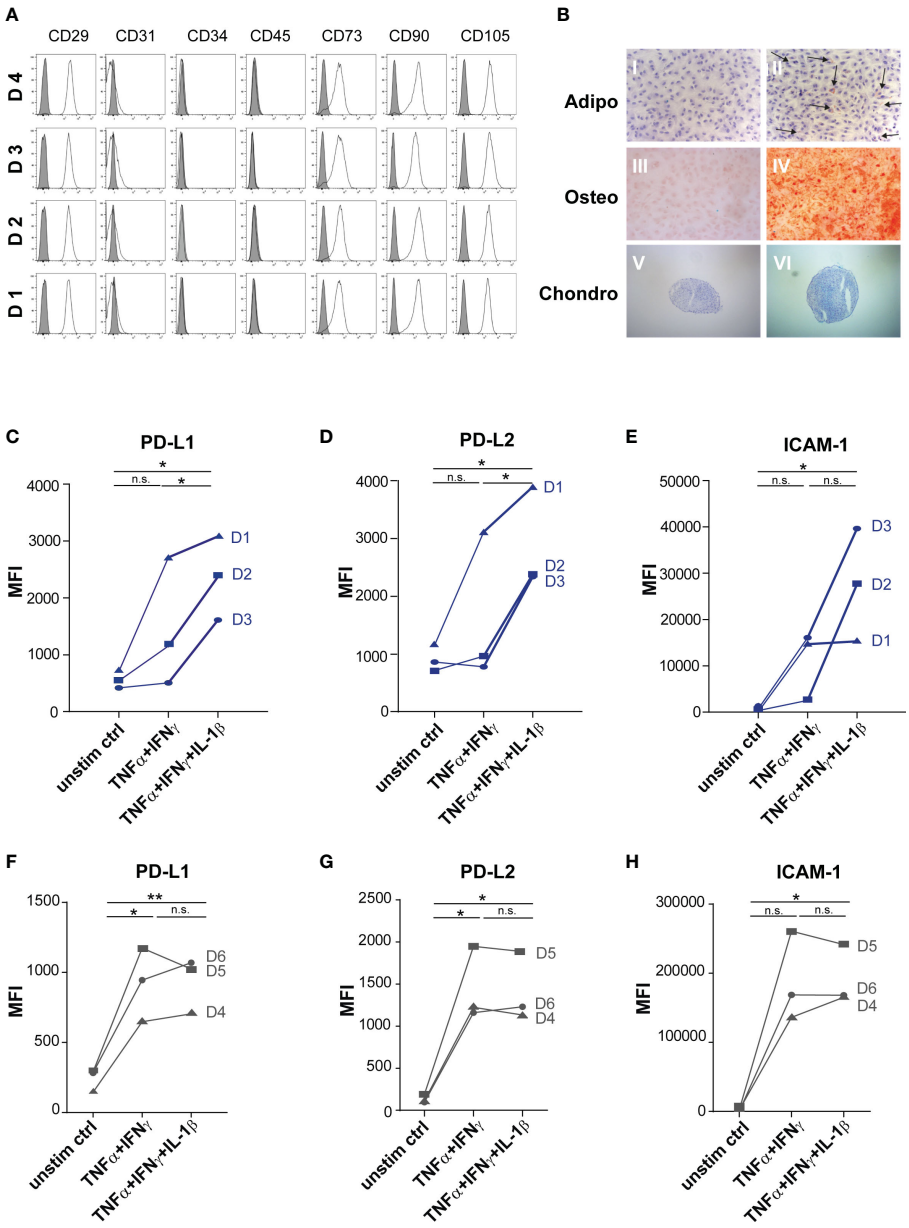

FIGURE 1
Priming with TNFα, IFNγ and IL-1β significantly increased expression of immuno- modulatory surface proteins of distinct MSCs. **(A+B)** Routine phenotyping after isolation in 2nd passage. **(A)** Flow cytometry analysis of MSCs. Data are shown as an overlay histogram: isotype control (gray) and specific cell-surface markers (white). Cells were labelled with antibodies against CD29, CD31, CD34, CD45, CD73, CD90, and CD105. Dead cells were excluded by live/dead staining. Representative experiments of MSCs used in this study. **(B)** Trilineage differentiation of MSCs. (I+II) Adipogenic differentiation after 14 days of cultivation with standard culture medium or adipogenic induction medium, sudan III staining (arrow: fat vacuoles); nuclei staining with hematoxylin. (III+IV) Osteogenic differentiation after 21 days of cultivation with standard culture medium or osteogenic induction medium, alizarin red staining. (V+VI) Chondrogenic differentiation after 21 days of cultivation in cultivation with standard culture medium or chondrogenic induction medium, alician blue staining. Representative results from MSCs used in the study. **(C–H)** MSCs were stimulated by TNFα (1000 U) and IFNγ (1000 U) or by TNFα (1000 U) and IFNγ (1000 U) in combination with IL-1β (10ng/ml). **(C+F)** PD-L1, **(D+G)** PD-L2, **(E+H)** ICAM-1 expression were measured by flow cytometry, fluorescence mean intensity (MFI): Marker expression minus isotype. **(C-E)** "Full responder" MSCs show further immunoactivating PD-1 ligand expression after triple-priming (D1-D3, in blue) compared to **(F–H)**, (D4-D6). Paired t-test was used to test statistical significance ($p < 0.05$ considered as significant), data are means (n=3). Data are shown as individual MSC donors. ns, not significant.

phenotype (*in vitro*) and, when injected as whole cells, had a lethal effect on mice directly after intravenous injection, most likely caused by the embolization of lung vessels by this highly activated MSCs.

Thus, in this first set of experiments we compared unstimulated MSCs versus MSC-EVs, and EVs from un-primed versus primed MSCs for the other part (Figure 4). From all treatments tested, EVs derived from triple-primed MSCs showed the most beneficial effect in a time course of up to 58 days observation time. At the end of the observation time, we observed a significantly decreased clinical GvHD score, shown with the significant lower slope, after application of triple-primed MSC-EVs compared to all other treatment groups (Figure 4).

Additionally, also the overall survival was substantially increased in the group treated with triple primed MSC-EVs (data not shown). Of note, compared to PBS control, the un-primed/resting MSCs

10.3389/fimmu.2023.1078551

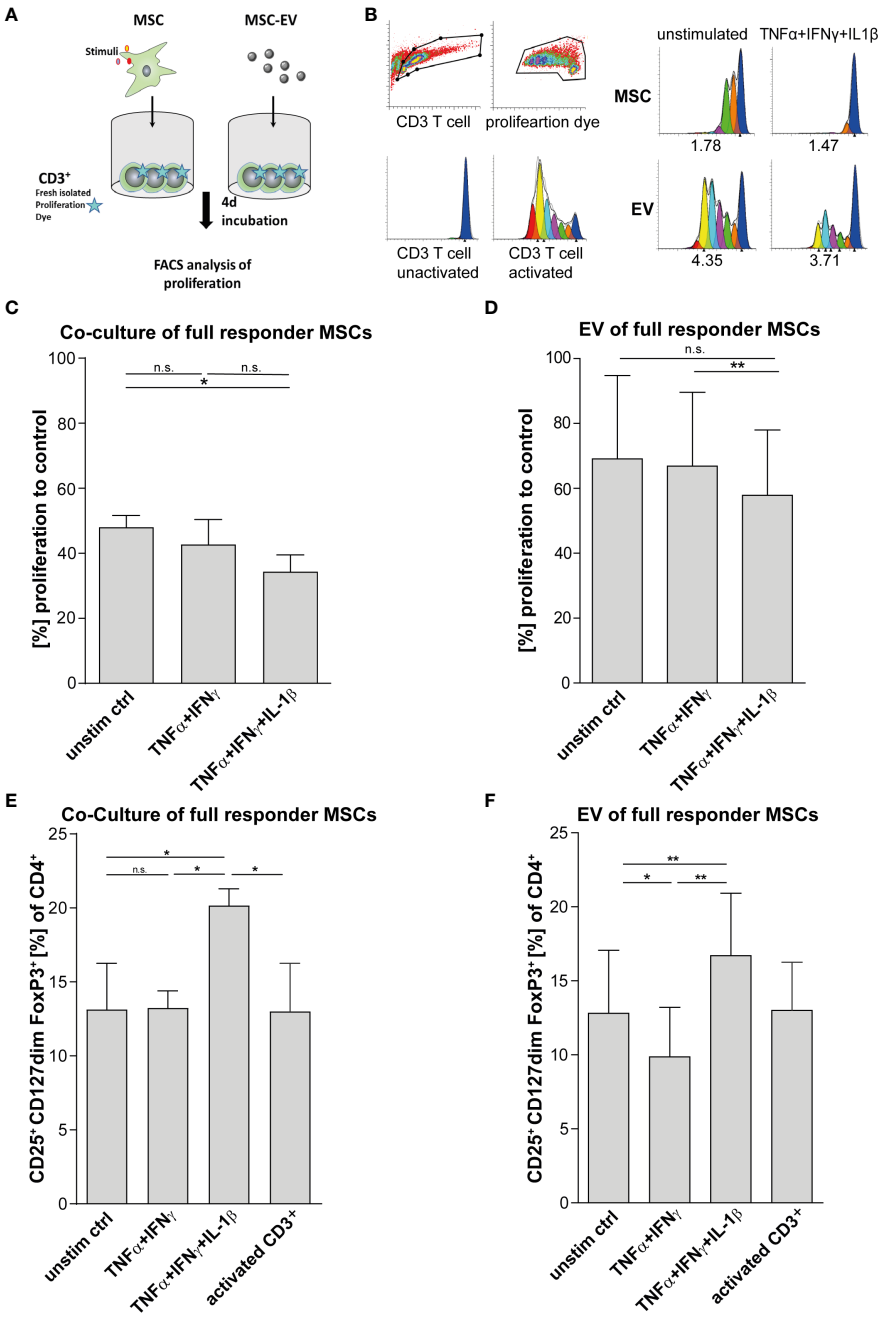

FIGURE 2
T cell effector function is strongly suppressed *via* direct cell-cell contact and by MSC-EVs after TNFα, IFNγ and IL-1β priming. **(A)** Schematic overview of $CD3^+$ proliferation assay. MSCs were primed for 24h by TNFα/IFNγ or by TNFα/IFNγ in combination with IL-1β, cells were washed and cultured in media for additional 48h. For Tcell proliferation assay, $CD3^+$ repsonder cells were stimulated with T cell-activating tetrameric antibody-complex CD2/CD3/CD28 and incubated for 4d in the present or absence of different conditioned MSC preparations. **(B)** $CD3^+$ proliferation measured *via* dilution of proliferation dye by flow cytometry and proliferation index as indicated below was calculated *via* Modfit software. **(C)** Co-culture of $0.5*10^5$ $CD3^+$ and $0.25*10^5$ full responder MSCs ($CD3^+$ n = 3), **(D)** $0.5*10^5$ $CD3^+$ incubated with EVs isolated from conditioned media of full responder MSCs (MSC-EV n=3; $CD3^+$ n=3). Paired t-test was used to test statistical significance ($P < 0.05$ considered as significant), data are shown as center value: mean; error bars: SD. **(E, F)** For Treg induction assays, MSCs were primed for 24h with TNFα and IFNγ or TNFα, IFNγ and IL-1β SN, cells were washed and additionally incubated in media for additional 48h. Freshly islolated $CD3^+$ T cells were incubated for 3d with different MSC preperations. T cells were activated with plate bound antibodies CD3 (1mg/mL) and CD28 (2µg/mL). **(E)** Co-culture of $0.5*10^5$ $CD3^+$ T cells and $0.25*10^5$ MSCs selected for subsequent *in vivo* assays ($CD3^+$ n = 3). **(F)** $0.5*10^5$ $CD3^+$ T cells incubated with EV isolated from conditioned media of full responder MSCs (MSC-EV n = 3; $CD3^+$ n = 3). Frequency of Tregs was detected by flow cytometry with MFI marker expression of $CD4^+$ $CD127^{dim}$ $CD25^+$ $FOXP3^+$ of total $CD4^+$. Paired t-test was used to test statistical significance ($p < 0.05$ considered as significant). Data are shown as center value: mean; error bars: SD. ns, not significant.

(cells) showed a transient decrease in the clinical score directly after treatment (Figure 4; at days 8-20). In our priming set-up, only effects of triple-primed MSC-EVs and not primed MSCs (cells) could be analysed as mentioned before.

Next, we considered that PD-L1 and PD-L2 are involved in down-regulating T cell effector function mediating a beneficial therapeutic effect *in vivo*, based on our *in vitro* experiments (compare Figure 3). To test this, we treated one group with triple-primed MSC-EVs that were pre-

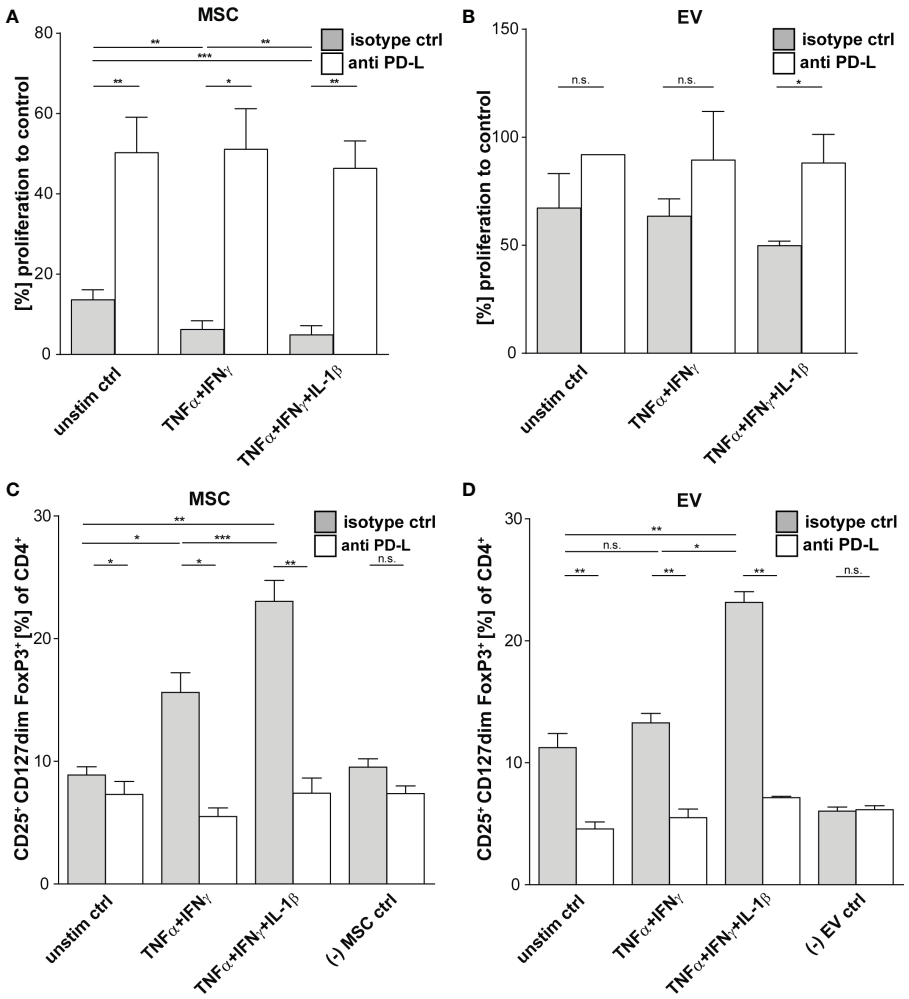

FIGURE 3
Suppression of $CD3^+$ T Cells by primed MSCs/MSC-EVs is mediated by PD-1 Ligands. $CD3^+$ isolated from healthy donors were incubated with MSCs/MSC-EVs primed by TNFα and IFNγ or by TNFα and IFNγ in combination with IL-1β and with inhibitory antibodies against PD-L1 (2μg/ml) and PD-L2 (2μg/ml) or isotype control (mIgG1/2a). **(A, B)** $CD3^+$ proliferation measured *via* proliferation dye by flow cytometry. $CD3^+$ T cells cultured with **(A)** primed MSC or **(B)** MSC-EVs. **(C, D)** Tregs were determined with MFI marker expression of $CD4^+$ $CD127^{dim}$ $CD25^+$ $FOXP3^+$ of total $CD4^+$ by flow cytometry. $CD3^+$ T cells were cultured with **(C)** MSCs or **(D)** incubated with MSC-EVs. Paired t-test was used to test statistical significance ($p < 0.05$ considered as significant), MSC, n = 3. Data are shown as center value: mean; error bars: SD. ns, not significant.

incubated with antibodies directed against PD-L1 and PD-L2 before injection. The second group received primed MSC-EVs pre-incubated with the corresponding isotypes and the control group was treated with PBS + isotype. The unbound antibodies were then removed by 100-kDa molecular weight cut-off (MWCO) centrifugal polyether sulfone membrane ultrafiltration before intravenous injection.

In accordance with the previous results, treatment with EVs generated from triple- primed MSCs decreased the clinical score long term (Figure 5A). Similar results were obtained when Kaplan-Meier survival analysis was applied (Figure 5B). Importantly, the neutralization of PD-1 ligands by blocking antibodies largely abrogated the therapeutic effect (Figures 5A, B) suggesting that upregulation of PD-1 ligands substantially contributes to the enhanced therapeutic efficacy of EVs generated from triple-primed MSCs.

In published work, many MSC-based cellular therapies rely on MSCs isolated from bone marrow. Therefore, in a subsequent experiment we aimed to translate our findings based on triple-primed nasal mucosa MSC-EVs to MSC-EVs derived from bone marrow. The bmMSC-EV preparation showed a strong Treg induction *in vitro* which could be significantly enhanced by triple-priming of bmMSCs (Figure 6A). Neutralizing antibodies against PD-1 ligands led to significant decrease of Treg induction (Figure 6A). In a final series we tested bmMSC-EVs in a short-term GvHD model. Such short-term model enabled us to avoid early death of mice, high clinical scores and offered the possibility to obtain tissue material and peripheral blood from all experimental animals for full comparative analysis between experimental groups.

Using this approach, we found that triple-primed bmMSC-EVs show a similar beneficial therapeutic effect to MSC-EVs from nasal mucosa (Figures 6B, C), thus demonstrating that this mechanism is conserved for MSCs isolated from different adult tissue reservoirs. These data demonstrate that immunological priming augments therapeutic efficacy of MSC-EVs from different tissue sources.

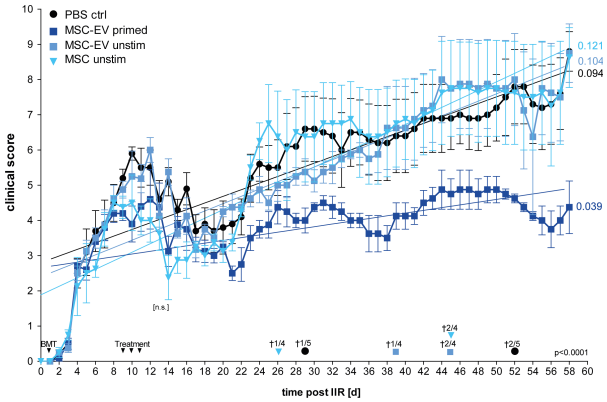

FIGURE 4
Primed MSC-EVs show long-term beneficial therapeutic effects compared to unprimed MSCs. Balb/c mice were lethally irradiated (day 0) and injected with CD90.2 depleted bone marrow cells and naïve CD4 cells from C57BL/6J mice to induce GvHD (day 1). Treatment with MSC-EVs were performed at day 9, 10 and 11. MSC cells were injected at day 9. Time flowchart of clinical score. Day of deaths and remaining mice per group as indicated. Numbers at the end of linear regressions indicate the slope. P value indicates statistical differences between the groups, [n.s.] on day 13, indicates no significant difference between the groups two days after last treatment, One-way ANOVA with Tukey's multiple comparison test was used to test statistical significance. Data is shown as center value: mean error bars: SEM.

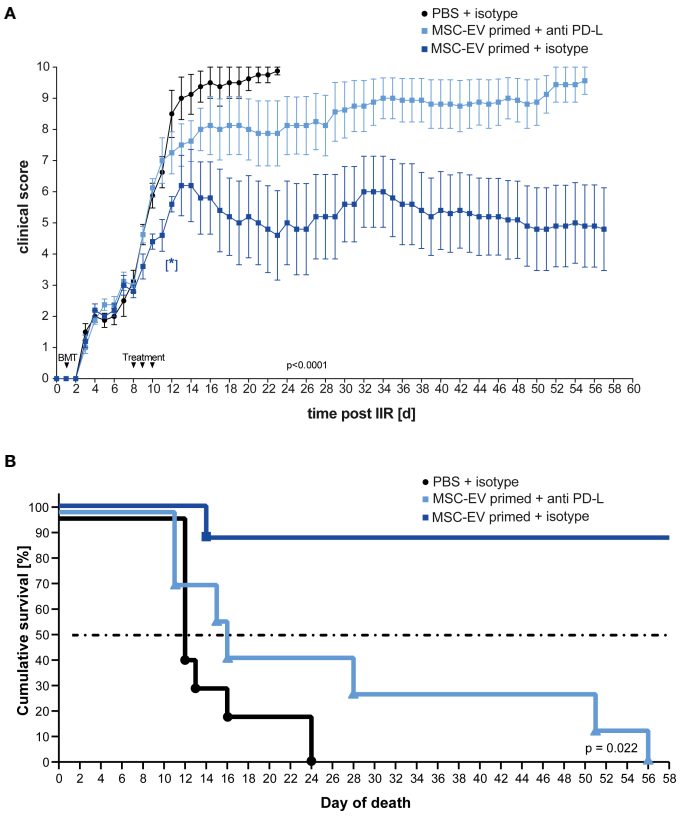

FIGURE 5
Inhibition of PD-Ligands on primed MSC-EVs abrogates beneficial therapeutic effects. Balb/c mice were lethally irradiated (day 0) and injected with CD90.2 depleted bone marrow cells and naïve CD4 cells from C57BL/6J mice to induce GvHD (day 1) and treated with MSC-EVs of unstimulated MSCs or TNFα, IFNγ and IL-1β stimulated MSCs at day 8, 9 and 10 with primed MSC-EVs pre-incubated with inhibitory PD-1 ligand antibodies or isotype control. **(A)** Time flowchart of clinical score. Data is shown as center value: mean; error bars: SEM. P value indicates statistical differences between the groups until day 24, analysed by linear regression. [*] Indicates p=0,026 significant difference between triple-primed+isotype MSC-EV treated and PBS +isotype treated group two days after last treatment on day 12. **(B)** Kaplan Meier survival curve. n = 8; MSC-EV stimulated + anti-PD-L antibody n = 8; MSC-EV stimulated + isotype control, n = 5. P-value indicates statistical difference for survival between treatment groups, Gehan-Breslow-Wilcoxon test was used to test statistical significance.

10.3389/fimmu.2023.1078551

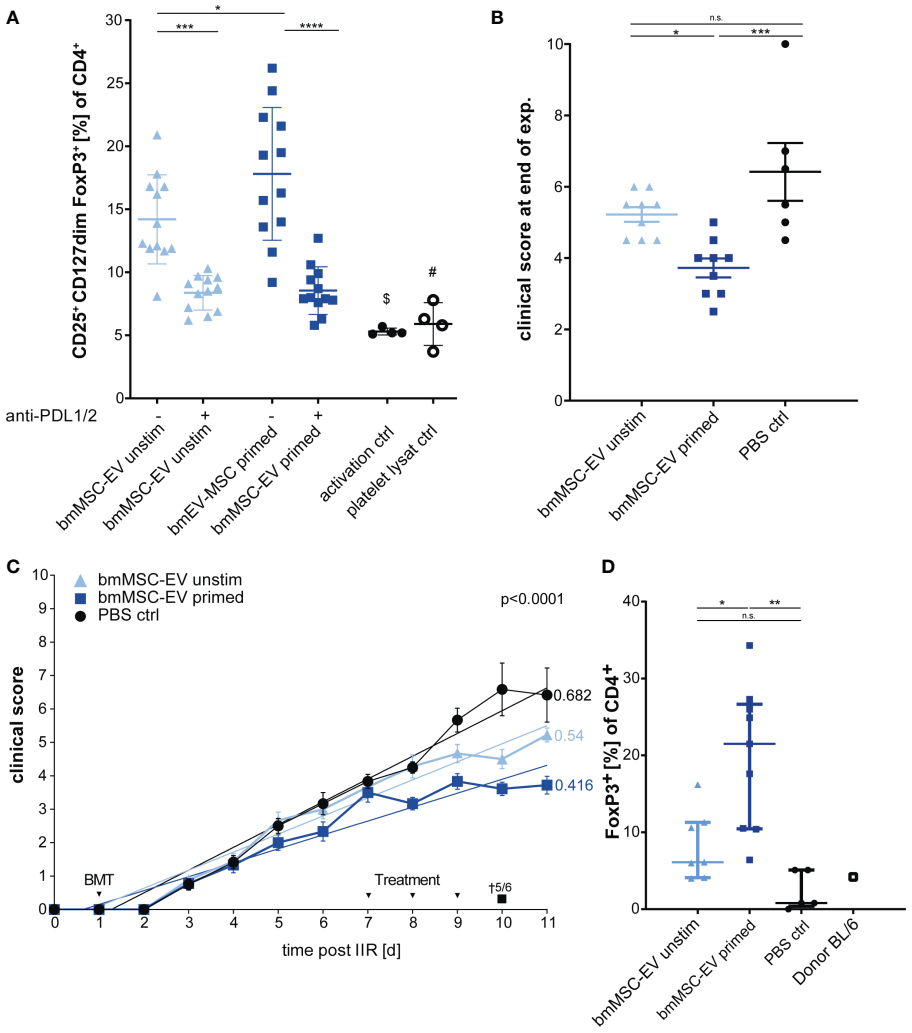

FIGURE 6
Therapeutic effects can be confirmed with EVs from bone marrow MSCs (bmMSCs). **(A)** Treg induction assay. $CD3^+$ T cells isolated from healthy donors were incubated with EVs of unstimulated bmMSCs or TNFα, IFNγ and IL-1β primed bmMSCs. Assay was performed in the presence of inhibitory antibodies against PD-L1 (2µg/ml) and PD-L2 (2µg/ml) or isotype control (mIgG1/2a). Frequency of Tregs were determined by MFI marker expression of $CD4^+$ CD127dim $CD25^+$ $FOXP3^+$ of total $CD4^+$ by flow cytometry. $CD3^+$ T cells from 4 different donors were tested with 3 different independently cultured and precipitated EV preparations of bmMSC 41.5 batch. Mixed reaction (REML) test was used to test statistical significance, ($) P= n.s., (#) P=0,0248. **(B–D)** Balb/c mice were lethally irradiated (day 0) and injected with CD90.2 depleted bone marrow cells and naïve CD4 cells from C57BL/6J mice to induce GvHD (day 1) and treated with bmMSC-EVs at day 7, 8 and 9. **(B)** Clinical score at day 11 of experiment. One-way ANOVA with Tukey's multiple comparison test was used to test statistical significance. Data is shown as center value: mean; error bars: SD. **(C)** Time flowchart of clinical score. Data is shown as center value: mean; error bars: SEM. Values on linear regressions indicate the slope. P value indicates statistical differences between the groups analysed by linear regression. **(B, C)** Combined data from two independent animal experiments; bmMSC-EVs unstimulated, n = 9; bmMSC-EV primed, n = 9; PBS control, n = 6. **(D)** Percentage of $CD4^+$ $FOXP3^+$ Tregs in whole blood after sacrifice. Mice with insufficient blood for further processing are excluded. One-way ANOVA with Tukey's multiple comparison test was used to test statistical significance. Data is shown as center value: mean; error bars: SD. bmMSC-EVs unstimulated, n = 7; bmMSC-EVs primed, n = 9; PBS control, n = 5. ns, not significant.

Interestingly, and despite clear differences of clinical scores in treatment groups, the gut pathology as analysed by swiss roll technology, was not affected by MSC-therapy (Supplement Figure S3).

In addition, the short-term model enabled us to analyse the $CD4^+$ $FoxP3^+$ T lymphocytes in mice blood after scarification at the end of experiment by flow cytometry. The group treated with triple-primed bmMSC-EVs demonstrated the strongest induction of Tregs followed by the unprimed bmMSC-EVs (Figure 6D). Tregs might be key cells in maintaining the therapeutic effect in primed bmMSC-EV treated group.

Discussion

MSC-EVs often recapitulate the immunoregulatory properties of their "parent" cells (20, 26, 27, 38). However, EVs lack the full ability of their parental cells to respond to external signals and thus can only deliver signals and effector molecules already present in their membrane or lumen when generated from their cell of origin (29). Due to the rather short survival time of MSCs in the host (3, 11–13, 23, 24), it is also questionable whether MSCs always receive sufficient priming signals for full immune activation. Against this background, we wanted to develop new priming protocols that robustly enhance

the immunoregulatory capacity of MSC-EVs ante partum/prior to therapeutic application. In order to generate "immune enhanced" MSCs, we established a triple-cytokine priming protocol, which enhanced the expression of immunoregulatory proteins associated with MSC's migration and T lymphocyte suppressor function *via* the PD-1 pathway.

The heterogeneity of MSC therapeutic efficiency, caused by differences in donor and tissue origin as well as isolation and culture procedures, makes it challenging to produce immunoregulatory MSCs with reproducible properties (3, 4, 11–13, 17). Neither searching for surrogate markers to predict MSCs immunoregulatory capacity nor producing immortalized MSCs has led to production of MSC-EVs with robust and reproducible immunoregulatory properties (56). Importantly, within this study we demonstrate that in particular triple-cytokine priming and pre-testing of MSC-EV preparations improve their immunoregulatory properties and can partly overcome MSC heterogeneity and that of their EVs. Nevertheless, as stated and demonstrated by Kordelas et al., the recipient-specific response to primed MSC-EVs has to be elucidated and is of crucial importance (48). Interestingly, we were able to demonstrate that EVs from triple-primed mucosal tissue and bone marrow MSCs significantly increased Treg induction *in vitro* and showed the strongest therapeutic capacity *in vivo*.

Pro-inflammatory stimulation of MSCs has been previously reported to increase PD-1 ligand expression and results in an enhanced suppression of T cell effector function (40, 41, 45, 55, 57, 58). It has also been demonstrated that PD-L1 and PD-L2 function in unison to immune regulate T cells and promote Tregs induction (37, 59). Here, we demonstrate that EVs derived from triple-primed MSCs provide an enhanced clinical outcome in a murine GvHD model, and that this therapeutic effect is at least partly mediated by PD-1 ligands. Our data also support a crucial role of PD-1 ligands on MSCs and MSC-EVs in mediating Treg induction. Of note, TGF-β is abundantly found on EVs and has also shown to immune regulate T cell effector function by inducing Tregs (32). Interestingly, in work related to this study, we found a significant upregulation of TGF-β secretion by MSCs primed by the same multi-cytokine combination used within this study (47).

Stimulation of MSCs lead to enhanced expression of adhesion molecules and to changes in cellular morphology (53, 60). These changes may pose significant risks and side effects especially during intravenous application in the course of cellular therapy (61). In our study, the application of stimulated MSCs also showed a lethal outcome directly after injection in 4 of 5 mice in our GvHD model (data not shown, Figure 4), most likely caused by the embolization of lung vessels by highly activated MSCs (11–13, 17). Fatal embolism was described for transfused human decidual stromal cells before in a likely GvHD mouse model (62). These considerations suggest that MSC-EVs may represent a safer and more feasible therapeutic option to prevent therapy-related death (26, 27, 33, 61). Both, in MSC- and MSC-EV-therapy for severe steroid-refractory acute GvHD, the risk for pneumonia-related and mould infection-related death is increased. However, it remains unclear whether these infections owing to the immune-suppressive effect of the steroid therapy, to the immune-regulatory effect of MSCs/MSC-EVs or occurring simply by stochastic risk due to the prolonged survival of patients treated with MSCs/MSC-EVs *per se* (48, 61, 63).

Conclusion

In this report, we tested dual and triple pro-inflammatory stimulation of MSCs to robustly increase the immunoregulatory properties and in turn to reduce the functional heterogeneity of the parental MSCs and their derived EVs and to study the underlying mechanisms of action in a well-established preclinical GvHD *in vivo* model. Importantly, triple-primed MSCs and their EVs, displayed enhanced therapeutic efficiency, in a PD-1 ligand dependent manner.

Data availability statement

The original contributions presented in the study are included in the article/Supplementary Material. Further inquiries can be directed to the corresponding author.

Ethics statement

The use of human samples was approved by the ethics committee of the medical faculty of the University Duisburg-Essen. The patients/participants provided their written informed consent to participate in this study. All animal procedures were performed in accordance with the international guidelines for good laboratory practice and the institutional guidelines of the University Hospital Essen approved by the animal welfare committees of North Rhine Westphalia.

Author contributions

SB, SL, and AH contributed to conception and design of the study. AH, SV, and KB performed the experiments, AH, SV, and SB performed the statistical analysis. AH wrote the first draft of the manuscript. SB and KB wrote sections of the manuscript. All authors contributed to the article and approved the submitted version.

Funding

This project was partly supported by the European Union under the programme "Investition in unsere Zukunft, Europäische Fonds für regionale Entwicklung", by the EFRE.NRW programme (European Regional Development Fund 2014-2020, FKZ-EFRE: EFRE-0800401) and by SEVRIT: "Produktion und Qualitätssicherung von Stammzell-abgeleiteten Extrazellulären Vesikeln für neuartige regenerative und immunmodulierende Therapieansätze".

Acknowledgments

We thank Petra Altenhoff (Department of Otorhinolaryngology, University Duisburg-Essen) for technical support. We thank the

Giebelgroup (Institute of Transfusion Medicine, University Duisburg-Essen) and Verena Börger for support during EVisolation and characterization as well as bmMSC culture, Kirschning group (Institute of Medical Microbiology, University Duisburg-Essen) and Rabea JuliaMadel for contributing to the animal experiments and Schlücker group (Department of Physical Chemistry, Faculty of Chemistry, University Duisburg-Essen) for help with EV characterization by TEM.

Conflict of interest

The authors declare that the research was conducted in the absence of any commercial or financial relationships that could be construed as a potential conflict of interest.

Publisher's note

Supplementary material

The Supplementary Material for this article can be found online at: https://www.frontiersin.org/articles/10.3389/fimmu.2023.1078551/full#supplementary-material

References

1. Pittenger MF, Discher DE, Péault BM, Phinney DG, Hare JM, Caplan AI. Mesenchymal stem cell perspective: Cell biology to clinical progress. *NPJ Regenerative Med* (2019) 4:22. doi: 10.1038/s41536-019-0083-6

2. Viswanathan S, Shi Y, Galipeau J, Krampera M, Leblanc K, Martin I, et al. Mesenchymal stem versus stromal cells: International society for cell & gene therapy (ISCT) mesenchymal stromal cell committee position statement on nomenclature. *Cytotherapy* (2019) 21:1019–24. doi: 10.1016/j.jcyt.2019.08.002

3. Moll G, Hoogduijn MJ, Ankrum JA. Editorial: Safety, efficacy and mechanisms of action of mesenchymal stem cell therapies. *Front Immunol* (2020) 11:243. doi: 10.3389/fimmu.2020.00243

4. Capilla-González V, Herranz-Pérez V, Sarabia-Estrada R, Kadri N, Moll G. Editorial: Mesenchymal stromal cell therapy for regenerative medicine. *Front Cell Neurosci 16* (2022). doi: 10.3389/fncel.2022.932281

5. Horwitz EM, Le Blanc K, Dominici M, Mueller I, Slaper-Cortenbach I, Marini FC, et al. Clarification of the nomenclature for MSC: The international society for cellular therapy position statement. *Cytotherapy* (2005) 7:393–5. doi: 10.1080/14653240500319234

6. Dominici M, Le Blanc K, Mueller I, Slaper-Cortenbach I, Marini F, Krause D, et al. Minimal criteria for defining multipotent mesenchymal stromal cells. *Int Soc Cell Ther position statement. Cytotherapy* (2006) 8:315–7. doi: 10.1080/14653240600855905

7. Pittenger MF, Mackay AM, Beck SC, Jaiswal RK, Douglas R, Mosca JD, et al. Multilineage potential of adult human mesenchymal stem cells. *Science* (1999) 284:143–7. doi: 10.1126/science.284.5411.143

8. Jakob M, Hemeda H, Janeschik S, Bootz F, Rotter N, Lang S, et al. Human nasal mucosa contains tissue-resident immunologically responsive mesenchymal stromal cells. *Stem Cells Dev* (2010) 19:635–44. doi: 10.1089/scd.2009.0245

9. Kim YJ, Yoo SM, Park HH, Lim HJ, Kim YL, Lee S, et al. Exosomes derived from human umbilical cord blood mesenchymal stem cells stimulates rejuvenation of human skin. *Biochem Biophys Res Commun* (2017) 493:1102–8. doi: 10.1016/j.bbrc.2017.09.056

10. Gregoire-Gauthier J, Selleri S, Fontaine F, Dieng MM, Patey N, Despars G, et al. Therapeutic efficacy of cord blood-derived mesenchymal stromal cells for the prevention of acute graft-versus-host disease in a xenogenic mouse model. *Stem Cells Dev* (2012) 21:1616–26. doi: 10.1089/scd.2011.0413

11. Moll G, Ankrum JA, Kamhieh-Milz J, Bieback K, Ringden O, Volk HD, et al. Intravascular mesenchymal Stromal/Stem cell therapy product diversification: Time for new clinical guidelines. *Trends Mol Med* (2019) 25:149–63. doi: 10.1016/j.molmed.2018.12.006

12. Moll G, Ankrum JA, Olson SD, Nolta JA. Improved MSC minimal criteria to maximize patient safety: A call to embrace tissue factor and hemocompatibility assessment of MSC products. *Stem Cells Trans Med* (2022) 11:2–13. doi: 10.1093/stcltm/szab005

13. Cottle C, Porter AP, Lipat A, Turner-Lyles C, Nguyen J, Moll G, et al. Impact of cryopreservation and freeze-thawing on therapeutic properties of mesenchymal Stromal/Stem cells and other common cellular therapeutics. *Curr Stem Cell Rep* (2022) 8:72–92. doi: 10.1007/s40778-022-00212-1

14. Sherman LS, Shaker M, Mariotti V, Rameshwar P. Mesenchymal stromal/stem cells in drug therapy: New perspective. *Cytotherapy* (2017) 19:19–27. doi: 10.1016/j.jcyt.2016.09.007

15. Pedrosa M, Gomes J, Laranjeira P, Duarte C, Pedreiro S, Antunes B, et al. Immunomodulatory effect of human bone marrow-derived mesenchymal stromal/stem cells on peripheral blood T cells from rheumatoid arthritis patients. *J Tissue Eng regenerative Med* (2019). doi: 10.1002/term.2958

16. Liu L, Wong CW, Han M, Farhoodi HP, Liu G, Liu Y, et al. Meta-analysis of preclinical studies of mesenchymal stromal cells to treat rheumatoid arthritis. *EBioMedicine* (2019). doi: 10.1016/j.ebiom.2019.08.073

17. Ringdén O, Moll G, Gustafsson B, Sadeghi B. Mesenchymal stromal cells for enhancing hematopoietic engraftment and treatment of graft-versus-Host disease, hemorrhages and acute respiratory distress syndrome frontiers in immunology. (2022). doi: 10.3389/fimmu.2022.839844

18. Zhang W, Ge W, Li C, You S, Liao L, Han Q, et al. Effects of mesenchymal stem cells on differentiation, maturation, and function of human monocyte-derived dendritic cells. *Stem Cells Dev* (2004) 13:263–71. doi: 10.1089/154732804323099190

19. Lu Z, Chang W, Meng S, Xu X, Xie J, Guo F, et al. Mesenchymal stem cells induce dendritic cell immune tolerance *via* paracrine hepatocyte growth factor to alleviate acute lung injury. *Stem Cell Res Ther* (2019) 10:372. doi: 10.1186/s13287-019-1488-2

20. Luz-Crawford P, Kurte M, Bravo-Alegría J, Contreras R, Nova-Lamperti E, Tejedor G, et al. Mesenchymal stem cells generate a CD4+CD25+Foxp3+ regulatory T cell population during the differentiation process of Th1 and Th17 cells. *Stem Cell Res Ther* (2013) 4:65. doi: 10.1186/scrt216

21. Franquesa M, Mensah FK, Huizinga R, Strini T, Boon L, Lombardo E, et al. Human adipose tissue-derived mesenchymal stem cells abrogate plasmablast formation and induce regulatory b cells independently of T helper cells. *Stem Cells* (2015) 33:880–91. doi: 10.1002/stem.1881

22. Zhang Y, Ge XH, Guo XJ, Guan SB, Li XM, Gu W, et al. Bone marrow mesenchymal stem cells inhibit the function of dendritic cells by secreting galectin-1. *BioMed Res Int* (2017) 2017:3248605. doi: 10.1155/2017/3248605

23. Schrepfer S, Deuse T, Reichenspurner H, Fischbein MP, Robbins RC, Pelletier MP. Stem cell transplantation: The lung barrier. *Transplant Proc* (2007) 39:573–6. doi: 10.1016/j.transproceed.2006.12.019

24. Zhu XY, Urbieta-Caceres V, Krier JD, Textor SC, Lerman A, Lerman LO. Mesenchymal stem cells and endothelial progenitor cells decrease renal injury in experimental swine renal artery stenosis through different mechanisms. *Stem Cells* (2013) 31:117–25. doi: 10.1002/stem.1263

25. Duijvestein M, Wildenberg ME, Welling MM, Hennink S, Molendijk I, van Zuylen VL, et al. Pretreatment with interferon-gamma enhances the therapeutic activity of mesenchymal stromal cells in animal models of colitis. *Stem Cells* (2011) 29:1549–58. doi: 10.1002/stem.698

26. Kordelas L, Rebmann V, Ludwig AK, Radtke S, Ruesing J, Doeppner TR, et al. MSC-derived exosomes: A novel tool to treat therapy-refractory graft-versus-host disease. *Leukemia* (2014) 28:970–3. doi: 10.1038/leu.2014.41

27. Blazquez R, Sanchez-Margallo FM, de la Rosa O, Dalemans W, Alvarez V, Tarazona R, et al. Immunomodulatory potential of human adipose mesenchymal stem cells derived exosomes on *in vitro* stimulated T cells. *Front Immunol* (2014) 5:556. doi: 10.3389/fimmu.2014.00556

28. Harrell CR, Jovicic N, Djonov V, Arsenijevic N, Volarevic V. Mesenchymal stem cell-derived exosomes and other extracellular vesicles as new remedies in the therapy of inflammatory diseases. *Cells 8* (2019). doi: 10.3390/cells8121605

29. Yanez-Mo M, Siljander PR, Andreu Z, Zavec AB, Borras FE, Buzas EI, et al. Biological properties of extracellular vesicles and their physiological functions. *J Extracell Vesicles* (2015) 4:27066. doi: 10.3402/jev.v4.27066

30. Fierabracci A, Del Fattore A, Luciano R, Muraca M, Teti A, Muraca M. Recent advances in mesenchymal stem cell immunomodulation: The role of microvesicles. *Cell Transplant* (2015) 24:133–49. doi: 10.3727/096368913X675728

31. Wang L, Gu Z, Zhao X, Yang N, Wang F, Deng A, et al. Extracellular vesicles released from human umbilical cord-derived mesenchymal stromal cells prevent life-

threatening acute graft-Versus-Host disease in a mouse model of allogeneic hematopoietic stem cell transplantation. *Stem Cells Dev* (2016) 25:1874–83. doi: 10.1089/scd.2016.0107

32. Alvarez V, Sanchez-Margallo FM, Macias-Garcia B, Gomez-Serrano M, Jorge I, Vazquez J, et al. The immunomodulatory activity of extracellular vesicles derived from endometrial mesenchymal stem cells on CD4+ T cells is partially mediated by TGFbeta. *J Tissue Eng Regener Med* (2018) 12:2088–98. doi: 10.1002/term.2743

33. Borger V, Bremer M, Ferrer-Tur R, Gockeln L, Stambouli O, Becic A, et al. Mesenchymal Stem/Stromal cell-derived extracellular vesicles and their potential as novel immunomodulatory therapeutic agents. *Int J Mol Sci 18* (2017). doi: 10.3390/ijms18071450

34. Salama AD, Chitnis T, Imitola J, Ansari MJ, Akiba H, Tushima F, et al. Critical role of the programmed death-1 (PD-1) pathway in regulation of experimental autoimmune encephalomyelitis. *J Exp Med* (2003) 198:71–8. doi: 10.1084/jem.20022119

35. Nishimura H, Minato N, Nakano T, Honjo T. Immunological studies on PD-1 deficient mice: Implication of PD-1 as a negative regulator for b cell responses. *Int Immunol* (1998) 10:1563–72. doi: 10.1093/intimm/10.10.1563

36. Fujiwara H, Maeda Y, Kobayashi K, Nishimori H, Matsuoka K, Fujii N, et al. Programmed death-1 pathway in host tissues ameliorates Th17/Th1-mediated experimental chronic graft-versus-host disease. *J Immunol* (2014) 193:2565–73. doi: 10.4049/jimmunol.1400954

37. Davies LC, Heldring N, Kadri N, Le Blanc K. Mesenchymal stromal cell secretion of programmed death-1 ligands regulates T cell mediated immunosuppression. *Stem Cells* (2017) 35:766–76. doi: 10.1002/stem.2509

38. Tobin LM, Healy ME, English K, Mahon BP. Human mesenchymal stem cells suppress donor CD4(+) T cell proliferation and reduce pathology in a humanized mouse model of acute graft-versus-host disease. *Clin Exp Immunol* (2013) 172:333–48. doi: 10.1111/cei.12056

39. Yamazaki T, Akiba H, Iwai H, Matsuda H, Aoki M, Tanno Y, et al. Expression of programmed death 1 ligands by murine T cells and APC. *J Immunol* (2002) 169:5538–45. doi: 10.4049/jimmunol.169.10.5538

40. Chinnadurai R, Copland IB, Patel SR, Galipeau J. IDO-independent suppression of T cell effector function by IFN-gamma-licensed human mesenchymal stromal cells. *J Immunol* (2014) 192:1491–501. doi: 10.4049/jimmunol.1301828

41. Chen G, Huang AC, Zhang W, Zhang G, Wu M, Xu W, et al. Exosomal PD-L1 contributes to immunosuppression and is associated with anti-PD-1 response. *Nature* (2018) 560:382–6. doi: 10.1038/s41586-018-0392-8

42. Goncalves FDC, Luk F, Korevaar SS, Bouzid R, Paz AH, Lopez-Iglesias C, et al. Membrane particles generated from mesenchymal stromal cells modulate immune responses by selective targeting of pro-inflammatory monocytes. *Sci Rep* (2017) 7:12100. doi: 10.1038/s41598-017-12121-z

43. Moll G, Jitschin R, von Bahr L, Rasmusson-Duprez I, Sundberg B, Lonnies L, et al. Mesenchymal stromal cells engage complement and complement receptor bearing innate effector cells to modulate immune responses. *PloS One* (2011) 6:e21703. doi: 10.1371/journal.pone.0021703

44. Costa LA, Eiro N, Fraile M, Gonzalez LO, Saá J, Garcia-Portabella P, et al. Functional heterogeneity of mesenchymal stem cells from natural niches to culture conditions: Implications for further clinical uses. *Cell Mol Life Sci* (2021) 78:447–67. doi: 10.1007/s00018-020-03600-0

45. Liang C, Jiang E, Yao J, Wang M, Chen S, Zhou Z, et al. Interferon-gamma mediates the immunosuppression of bone marrow mesenchymal stem cells on T-lymphocytes in vitro. *Hematology* (2018) 23:44–9. doi: 10.1080/10245332.2017.1333245

46. Petri RM, Hackel A, Hahnel K, Dumitru CA, Bruderek K, Flohe SB, et al. Activated tissue-resident mesenchymal stromal cells regulate natural killer cell immune and tissue-regenerative function. *Stem Cell Rep* (2017) 9:985–98. doi: 10.1016/j.stemcr.2017.06.020

47. Hackel A, Aksamit A, Bruderek K, Lang S, Brandau S. TNF-α and IL-1β sensitize human MSC for IFN-γ signaling and enhance neutrophil recruitment. *Eur J Immunol* (2021) 51:319–30. doi: 10.1002/eji.201948336

48. Kordelas L, Schwich E, Dittrich R, Horn PA, Beelen DW, Borger V, et al. Individual immune-modulatory capabilities of MSC-derived extracellular vesicle (EV) preparations and recipient-dependent responsiveness. *Int J Mol Sci 20* (2019). doi: 10.3390/ijms20071642

49. Ludwig AK, De Miroschedji K, Doeppner TR, Borger V, Ruesing J, Rebmann V, et al. Precipitation with polyethylene glycol followed by washing and pelleting by ultracentrifugation enriches extracellular vesicles from tissue culture supernatants in small and large scales. *J Extracell Vesicles* (2018) 7:1528109. doi: 10.1080/20013078.2018.1528109

50. Anderson BE, McNiff J, Yan J, Doyle H, Mamula M, Shlomchik MJ, et al. Memory CD4+ T cells do not induce graft-versus-host disease. *J Clin Invest* (2003) 112:101–8. doi: 10.1172/JCI17601

51. Riesner K, Kalupa M, Shi Y, Elezkurtaj S, Penack O. A preclinical acute GVHD mouse model based on chemotherapy conditioning and MHC-matched transplantation. *Bone marrow Transplant* (2016) 51:410–7. doi: 10.1038/bmt.2015.279

52. Moolenbeek C, Ruitenberg EJ. The "Swiss roll": A simple technique for histological studies of the rodent intestine. *Lab Anim* (1981) 15:57–9. doi: 10.1258/002367781780958577

53. Barrachina L, Remacha AR, Romero A, Vazquez FJ, Albareda J, Prades M, et al. Effect of inflammatory environment on equine bone marrow derived mesenchymal stem cells immunogenicity and immunomodulatory properties. *Vet Immunol Immunopathol* (2016) 171:57–65. doi: 10.1016/j.vetimm.2016.02.007

54. Kronsteiner B, Wolbank S, Peterbauer A, Hackl C, Redl H, van Griensven M, et al. Human mesenchymal stem cells from adipose tissue and amnion influence T-cells depending on stimulation method and presence of other immune cells. *Stem Cells Dev* (2011) 20:2115–26. doi: 10.1089/scd.2011.0031

55. Li H, Wang W, Wang G, Hou Y, Xu F, Liu R, et al. Interferon-gamma and tumor necrosis factor-alpha promote the ability of human placenta-derived mesenchymal stromal cells to express programmed death ligand-2 and induce the differentiation of CD4(+)interleukin-10(+) and CD8(+)interleukin-10(+)Treg subsets. *Cytotherapy* (2015) 17:1560–71. doi: 10.1016/j.jcyt.2015.07.018

56. Phinney DG. Functional heterogeneity of mesenchymal stem cells: Implications for cell therapy. *J Cell Biochem* (2012) 113:2806–12. doi: 10.1002/jcb.24166

57. Wobma HM, Kanai M, Ma SP, Shih Y, Li HW, Duran-Struuck R, et al. Dual IFN-gamma/hypoxia priming enhances immunosuppression of mesenchymal stromal cells through regulatory proteins and metabolic mechanisms. *J Immunol Regener Med* (2018) 1:45–56. doi: 10.1016/j.regen.2018.01.001

58. Zhang Q, Fu L, Liang Y, Guo Z, Wang L, Ma C, et al. Exosomes originating from MSCs stimulated with TGF-beta and IFN-gamma promote treg differentiation. *J Cell Physiol* (2018) 233:6832–40. doi: 10.1002/jcp.26436

59. Francisco LM, Salinas VH, Brown KE, Vanguri VK, Freeman GJ, Kuchroo VK, et al. PD-L1 regulates the development, maintenance, and function of induced regulatory T cells. *J Exp Med* (2009) 206:3015–29. doi: 10.1084/jem.20090847

60. Wen L, Zhu M, Madigan MC, You J, King NJ, Billson FA, et al. Immunomodulatory effects of bone marrow-derived mesenchymal stem cells on pro-inflammatory cytokine-stimulated human corneal epithelial cells. *PloS One* (2014) 9:e101841. doi: 10.1371/journal.pone.0101841

61. Forslow U, Blennow O, LeBlanc K, Ringden O, Gustafsson B, Mattsson J, et al. Treatment with mesenchymal stromal cells is a risk factor for pneumonia-related death after allogeneic hematopoietic stem cell transplantation. *Eur J Haematol* (2012) 89:220–7. doi: 10.1111/j.1600-0609.2012.01824.x

62. Sadeghi B, Heshmati Y, Khoein B, Kaipe H, Uzunel M, Walfridsson J, et al. Xeno-immunosuppressive properties of human decidual stromal cells in mouse models of alloreactivity *in vitro* and *in vivo*. *Cytotherapy* (2015) 17:1732–45. doi: 10.1016/j.jcyt.2015.09.001

63. Xu F, Fei Z, Dai H, Xu J, Fan Q, Shen S, et al. Mesenchymal stem cell-derived extracellular vesicles with high PD-L1 expression for autoimmune diseases treatment. *Adv Mater* (2022) 34:e2106265. doi: 10.1002/adma.202106265

Frontiers in Immunology

Explores novel approaches and diagnoses to treat immune disorders.

The official journal of the International Union of Immunological Societies (IUIS) and the most cited in its field, leading the way for research across basic, translational and clinical immunology.

Discover the latest Research Topics

See more →

Frontiers

Avenue du Tribunal-Fédéral 34
1005 Lausanne, Switzerland
frontiersin.org

Contact us

+41 (0)21 510 17 00
frontiersin.org/about/contact